

Binary Stars in Dwarf Spheroidal Galaxies

by

Meghin Elise Spencer

A dissertation submitted in partial fulfillment
of the requirements for the degree of
Doctor of Philosophy
(Astronomy and Astrophysics)
in The University of Michigan
2017

Doctoral Committee:

Professor Mario L. Mateo, Chair
Professor Eric F. Bell
Professor Dragan Huterer
Lecturer Sarah R. Loebman
Professor Monica Valluri

© Meghin E. Spencer 2017
All Rights Reserved

meghins@umich.edu

ORCID ID:0000-0003-1240-1939

ACKNOWLEDGMENTS

As I reflect on the last five years of my time in grad school, I am reminded now more than ever that it takes a village to raise a grad student. Countless people have helped make this journey possible, and I would like to highlight some of the ones who played a particularly influential role in that process.

First and foremost, I want to thank my research advisor, Mario Mateo. I arrived in Michigan without a plan of who I would work with or what I would research. Mario filled that gap perfectly, and reiterated time and time again that the research you do depends on where the data take you. (Although, it did take a solid three years before we finally figured out that the data really wanted us to research binary stars.) Throughout my five years at UMich, Mario gave me both the space to explore my own research questions and the guidance necessary to keep me from going astray. Despite the fact that my dissertation required no further observations, he graciously allowed me to go on 11 observing runs during which I was crowned as a jefe for his spectrograph M2FS. This also afforded me the opportunity to gain invaluable experience at a telescope and make connections with astronomers from all around the world. Above all else, I am most grateful for his receptiveness to my left field request to simultaneously change my dissertation topic and complete my final two years of school remotely. He had faith in me to remain diligent to my research outside of an academic setting and the patience to deal with time zones and technical difficulties over Skype. It has been fun playing softball (something at which he will always be better) and plugging plates (something at which I am arguably faster)

alongside Mario. I have learned many life lessons from him and feel confident that I can use these skills in my future endeavors.

I am also very grateful to the four other members of my thesis committee, who also stuck with me when I changed my dissertation topic. Their comments and criticisms have greatly improved this work. They have been a great influence to me in other realms of grad school. I have fond memories of building galaxies out of M&M's and sprinkles on my first day of grad school in Eric's class, and I really enjoyed teaching astronomy summer camp side by side with Monica and Dragan. I extend a special thank you to Sarah who helped me publish my very first paper—a project which receives a mere sentence of recognition in this dissertation—and for mentoring me through my entire graduate school career. She was a great audience for listening to many of my practice talks and provided the computing power necessary to carry out my simulations. I will miss eating chocolate while sitting on the chaise lounge in her office and discussing everything from science and teaching to children's songs and cartoon shows.

I am thankful to my fellow grad students at Michigan and colleagues elsewhere in the world who have supported me along this journey. I had a great time kayaking down the Huron River, birding the arboretum, camping in the Upper Peninsula, sledding at the golf course, and playing intramural battleship in Ann Arbor with many of these grad students. Specific thanks must be given to Jeb Bailey, who was the best academic brother I could have asked for; to Marina Kounkel, who partook in many thought-provoking conversations with me while commuting on Bus 36 and over Skype; and to Hui Li who was a fantastic office mate during my second and final year of having a real office. A number of colleagues have also helped me on this journey. I thank Jon Miller for reiterating the benefits of pursuing a PhD; Matt Walker for patiently answering all of my emails, even the ones that required hours of work on his end; and Ed Olszewski for livening up many of my observing runs with unforgettable

stories, and for enduring my late-night craziness.

This research would not have been possible without the encouragement from my lifelong best friends: the Buddy Ol' Pals. My highest gratitude is extended to Stephanie Brereton for encouraging me to stick with it and navigate my own path toward my career goals; to Kasey Eck for reminding me that I wrote 200+ pages on dwarf butts (more scientifically known as dwarf galaxy posterior probability distributions); to Aubrey Steingraber for informing me that no dissertation is a success without using the word “paucity” (look for it) and for reading a draft of this dissertation; and to Jessica Hartman for genuinely caring about my work even if she didn't have a clue what it meant.

Last but not least, I want to acknowledge the love and support offered to me by my family. To my mom, Shelli Spencer, thank you for sending me care packages and checking in with me on a regular basis to ensure that your little train stayed on the tracks. To my dad, Brian Spencer, thank you for sparking my interest in science and astronomy at such a young age. To my brother, Andrew Spencer, thank you for keeping it real. To my grandpa, Gene Spencer, I would say this: “now you finally have a Dr. Spencer in the family. Neat stuff!” And lastly I give thanks to my husband, Aaron Beckner, for always being there for me, even when he was 2,000 miles away on the other side of the country. Aaron, your unconditional love and belief in my abilities has meant the world. We both set our sights high; mine to the stars and yours to the skies.

TABLE OF CONTENTS

ACKNOWLEDGMENTS	ii
LIST OF FIGURES	viii
LIST OF TABLES	xi
LIST OF APPENDICES	xii
ABSTRACT	xiii
CHAPTER	
I. Introduction	1
1.1 Denizens of the Outer Galactic Halo	1
1.1.1 Star Formation	2
1.1.2 Galaxy Formation	2
1.1.3 Dwarf Galaxies and Dark Matter	4
1.2 Binary Stars in Dwarf Galaxies	6
1.2.1 Binaries in Ultra-Faints	8
1.2.2 The Radial Velocity Equation	9
1.2.3 Methods for Determining Binary Fraction	11
1.3 Dissertation Objectives and Structure	15
II. A Multi-Epoch Kinematic Study of Leo II	20
2.1 Introduction	20
2.2 Observations and Data Processing	22
2.2.1 Photometry	22
2.2.2 Spectroscopy	25
2.2.3 Velocity Measures	26
2.2.4 Quality Control	30
2.3 Kinematic and Chemical Analysis	32
2.3.1 Defining Membership	32

2.3.2	Kinematic Features	36
2.3.3	Chemical Features	42
2.4	Summary and Conclusions	50
III. The Binary Fraction in Leo II		52
3.1	Introduction	52
3.2	Radial Velocities	53
3.2.1	Velocity variability	58
3.3	Methodology	61
3.3.1	Binary Orbital Parameters	63
3.3.2	Method for Determining Binary Fraction	68
3.3.3	Likelihood	70
3.3.4	Characterizing the PPDs	73
3.4	Binary Fraction in Leo II	74
3.4.1	Other Considerations: Heterogeneity	79
3.4.2	Other Considerations: Velocity Errors	80
3.4.3	Consequences for Ultra-faints	82
3.5	Summary and Conclusions	83
IV. The Binary Fractions in Draco and Ursa Minor		87
4.1	Introduction	87
4.2	Velocity Data	89
4.2.1	Data Sets	90
4.2.2	Sample Definition	92
4.2.3	Correcting Systematic Offsets	97
4.2.4	Velocity Uncertainty	98
4.2.5	Summary of Velocity Data	102
4.3	Methodology	103
4.3.1	Binary Parameters	106
4.3.2	Monte Carlo Simulations	112
4.3.3	Bayesian Technique	114
4.3.4	Repeatability	118
4.4	Results	118
4.4.1	Binary Fractions Among Dwarfs	125
4.5	Conclusions	138
V. Summary and Conclusions		142
5.1	Velocities are a Multi-Purpose Tool	142
5.2	Binary Fractions in Classical dSphs	144
5.3	The Effect of Binaries in Ultra-faints	148
5.4	Future Work	151
5.4.1	The Value of Additional Kinematic Data	151

5.4.2	Improving the Error Model	151
5.4.3	Determining the Period Distribution	153
5.4.4	Alternative Definitions of β	153
5.4.5	Moving Forward: More Data is the Key	154
APPENDICES		156
BIBLIOGRAPHY		285

LIST OF FIGURES

Figure		
1.1	Radial velocities caused by binaries	7
1.2	Geometry of a binary orbit	18
1.3	Sample velocity curves	19
2.1	Image of Leo II spectroscopic targets on the sky	23
2.2	Leo II color-magnitude diagram	24
2.3	fxcor method of extracting velocities from spectra	28
2.4	Comparison of velocity extraction techniques.	29
2.5	Velocity quality criteria from Bayesian technique	31
2.6	Velocity histogram for Leo II	33
2.7	Metallicity histogram of Leo II	35
2.8	Velocity dispersion profiles of Leo II	38
2.9	Rotation signature of Leo II	39
2.10	Velocity vs. radius for Leo II	41
2.11	Metallicity comparison between other published works	43
2.12	Metallicity distribution function of Leo II	45
2.13	Metallicity gradient of Leo II	47

2.14	Chemodynamic features in Leo II	49
3.1	Histograms of Leo II radial velocity errors	55
3.2	Summary of Leo II dataset	57
3.3	Velocity comparison between datasets for Leo II	59
3.4	χ^2 histogram for Leo II	60
3.5	Stars with velocity variability in Leo II	62
3.6	Binary parameter distributions used for Leo II MC simulations . . .	65
3.7	Procedure for determining the likelihood	71
3.8	Characterizing the posterior probability distributions	75
3.9	Posteriors for binary fraction in Leo II	77
3.10	Limits of smaller datasets	81
3.11	Effects of binaries on observed velocity dispersion of mock dSphs . .	84
4.1	Histogram of Draco velocities	95
4.2	Histogram of Ursa Minor velocities	96
4.3	Velocity comparison between Draco datasets	99
4.4	Velocity comparison between Ursa Minor datasets	100
4.5	χ^2 histograms for Draco and Ursa Minor	101
4.6	Summary of Draco dataset	104
4.7	Summary of Ursa Minor dataset	105
4.8	Binary parameter distributions for Draco and Ursa Minor MC simu- lations	111
4.9	Procedure for determining likelihood in Draco and Ursa Minor . . .	115
4.10	Binary fraction in Draco-like mock galaxies	119

4.11	Posteriors for binary fraction in Draco	121
4.12	Posteriors for binary fraction in Ursa Minor	122
4.13	Preferred binary parameter distributions	124
4.14	Posteriors for seven dwarfs: Dra, UMi, LeoII, Car, For, Scl, Sex . . .	130
4.15	Probability of a constant binary fraction	133
4.16	Probability of binary fraction being within a sliding range	135
4.17	Binary fraction vs. absolute magnitude, velocity dispersion, and star formation history	139
5.1	Effects of binaries on observed velocity dispersion in mock ultra-faints	149
5.2	Effect of binaries on Reticulum II	152
A.1	Geometry for derivation of radial velocity equation	159
B.1	Cumulative $P(\chi^2, \kappa)$ for three mock galaxies	166
B.2	Velocity error correction for mock Galaxy 1	169
B.3	Velocity error correction for mock Galaxy 2	170
B.4	Velocity error correction for mock Galaxy 3	171
B.5	Cumulative $P(\chi^2, \kappa)$ for Fornax	172
C.1	Probability mass functions of toy model	174
C.2	Joint probability mass function of toy model	175
C.3	Probability of various events occurring in toy model	177

LIST OF TABLES

Table

1.1	Multi-epoch binary analyses in dwarf galaxies	13
2.1	Hectochelle observations of Leo II fields	26
3.1	Papers with radial velocity data in Leo II	58
3.2	Median and credible intervals of PPDs for Leo II	78
4.1	Papers with radial velocity data in Draco and Ursa Minor	92
4.2	Median and credible intervals of PPDs for Draco and Ursa Minor	126
4.3	Quantities used to derive a_{max} in seven dSphs	127
4.4	Binary fractions for seven dSphs	128
4.5	Photometric and structural properties of classical dSphs	136
4.6	Spectroscopic and mass properties of classical dSphs	137
D.1	Photometric properties of candidate Leo II members	182
E.1	Spectroscopic properties of stars in the direction of Leo II	196
F.1	Velocities of RGB stars in Leo II	209
G.1	Velocities of RGB stars in Draco	226
H.1	Velocities of RGB stars in Ursa Minor	260

LIST OF APPENDICES

Appendix

A.	The Orbital Radial Velocity Equation	157
	Derivation	157
	Glossary of Variables	162
B.	Correcting Velocity Error Measurements	164
C.	The Probability of f being “The Same” for All dSphs	173
	Toy Model for Probability	173
	Application to Binary Fraction Probability	179
	Glossary of Variables	180
D.	Photometry of Stars in the Direction of Leo II	182
E.	Spectroscopic Properties of Leo II Stars	195
F.	Velocities of Stars in Leo II	209
G.	Velocities of Stars in Draco	226
H.	Velocities of Stars in Ursa Minor	260

ABSTRACT

Dwarf spheroidal galaxies (dSphs) are the smallest, most numerous, and among the oldest galaxies in the Universe. Since their discovery in the 1930’s, dSphs have provided insights into ancient stellar populations, galaxy formation, and early Universe star formation. Beginning in the 1980’s, spectroscopy revealed anomalous stellar kinematics within dSph galaxies, which is typically interpreted as considerable amounts of dark matter (DM) existing in these systems. One kinematic effect that could mimic DM arises from the orbital motions of binary stars; however, subsequent work found that binaries alone could not account for the anomalous kinematics within the larger dSph galaxies. The recent discovery of a new class of dSphs called “ultra-faints” has reignited the issues of binaries due to the intrinsically low velocity dispersions in these systems. Motivated by the need to better understand the extent of binary contamination in ultra-faints, this dissertation draws upon both recent and archival data in brighter dSphs to determine updated kinematic properties and to provide a fresh look at the binary fraction within dSphs.

The spectroscopic data used in this dissertation comes from many different telescopes and instruments, spans 2–3 decades in time, and concerns three dSphs: Leo II, Draco, and Ursa Minor. For Leo II, our analysis included a new study of the galaxy’s internal kinematics, finding among other results, (a) the V-band mass-to-light ratio is 15.2 ± 5.5 , (b) no signs of internal rotation, and (c) suggestive evidence of kinematic substructure related to metallicity. The full kinematic datasets for all three dwarfs were used to characterize the likely binary fraction of each galaxy under the assumption that velocity fluctuations for individual stars with multiple observations

were due to binaries. The process we followed was to first generate Monte Carlo simulations of the observations, whereby binary fraction was varied. Then we performed a Bayesian analysis that compared the simulations with the data to discern the most likely binary fraction in each dSph. We explored various mass ratio, eccentricity, and period distributions throughout the simulations. We also applied our method to preexisting data in Carina, Fornax, Sculptor, and Sextans to yield a homogeneous measurement of binary fraction in seven dwarfs—the largest sample to date. The probability that the binary fraction is the same (i.e., exists within a range of fractions spanning 20%) amongst these dwarfs is $< 1\%$. We generally found no significant correlations between binary fraction and other galactic properties, though we cannot rule out a weak dependence with star-formation history.

Given the variability of binary fraction that we inferred between galaxies, we modeled the effects of binaries on the global kinematics of mock dwarf galaxies as a function of binary fraction. We simulated different intrinsic dispersions for dwarfs, sample sizes, number of observations, and size of velocity errors. Unless the binary fraction is low ($< 10\%$), binaries will have a non-negligible effect on the observed velocity dispersion of ultra-faints. Recent observations do show cases where binaries have a significant effect. We illustrate that this can be partially mitigated by numerous observations, removing obvious velocity variables, and averaging the remaining stars in the velocity dispersion calculation. The results of this work illustrate that multi-epoch radial velocity measurements of additional stars will be necessary to better understand binary fractions, binary parameter distributions, and the role binaries have in distorting the inferred global kinematics of the smallest galaxies.

CHAPTER I

Introduction

1.1 Denizens of the Outer Galactic Halo

The halo of the Milky Way (MW) is home to the most abundant type of galaxy in the universe. These so called dwarf galaxies stand apart from their more massive counterparts—spiral and elliptical galaxies—in terms of their size, luminosity, and stellar content, and from their sub-galactic neighbors—globular clusters—in terms of their stellar metallicity distribution and dark matter content.

Dwarf spheroidal galaxies (dSphs) span a wide range of properties from the more luminous “classical” dSphs to the recently discovered “ultra-faint” dSphs. They have half-light radii between $\sim 30 < r_h < 700$ pc, total mass between $\sim 2 \times 10^5 M_\odot$ and $1 \times 10^8 M_\odot$, mean metallicities between $-1.0 < [Fe/H] < -2.8$, and luminosities between $\sim 1 \times 10^2 L_\odot$ and $1 \times 10^7 L_\odot$, and (Mateo, 1998; McConnachie, 2012). Although dwarfs are optically insignificant, they have proven to be quite remarkable in many ways. This unique class of object has shed light on complex topics including early star formation, galaxy formation on both large and small scales, and the nature of dark matter.

1.1.1 Star Formation

Dwarf galaxies, specifically dwarf spheroidal galaxies (dSphs), are dominated by stars having low metallicities. Coupling this with the presence of very evolved stars (e.g., RR Lyrae and horizontal branch stars) has led to the widely accepted fact that dSphs are composed—always at least in part—of ancient stars, making them the oldest types of galaxies and, by extension, among the first to form (Mateo, 1998). As such, they provide unique and comparatively nearby windows to the earliest era of star formation in the Universe and to star formation in shallow potentials.

For example, dSphs exhibit a spread in $[\text{Fe}/\text{H}]$ metallicity, indicating that they are massive enough to retain metals ejected by supernovae, and that they experienced extended star formation that enabled them to form multiple generations of stars (Willman & Strader, 2012; Weisz et al., 2014). Additionally, the scatter of r -process elements at low metallicity indicates that the oldest stars in these systems enriched faster than stars in the MW halo, or that the r -process is less common or less efficient in dSphs (Tolstoy et al., 2009). A nearly linear relation between luminosity and metallicity reveals a systematic behavior between integrated star formation histories of individual galaxies and their baryon content, with brighter galaxies having higher average metallicity (Kirby et al., 2013). In addition, there is a relation between luminosity and metallicity spread, suggesting longer periods of star formation for more luminous dwarfs (Kirby et al., 2011). Furthermore, it has been shown that the faintest dwarfs may have undergone very little chemical evolution since the time of their formation, making them nearly identical to the first galaxies (Frebel et al., 2010).

1.1.2 Galaxy Formation

Galaxy formation theories call for hierarchical buildup, whereby smaller galaxies are incorporated into larger galaxies over time (Searle & Zinn, 1978). The discovery

of stellar streams extending from tidally disrupted dwarf galaxies has substantiated this hypothesis (Helmi et al., 1999; Belokurov et al., 2006). As such, dwarf galaxies are thought to be local analogs to the building blocks of large galaxies. By studying dwarf galaxies we can therefore hope to learn about how the stellar (and dark) halo grew via accretion into the structure and stellar population that we see today.

The internal properties of individual dwarfs can also reveal illuminating peculiarities suggestive of complex dynamical evolutionary processes. In cases such as Fornax (Battaglia et al., 2006), Sculptor (Battaglia et al., 2008), and Sextans (Battaglia et al., 2011), there is a segregation between high and low-metallicity stars, the latter of which have faster velocity dispersions and preferentially exist at larger projected radii (Walker et al., 2015b). Sculptor also shows evidence of uniform rotation (Battaglia et al., 2008). Carina and Ursa Minor contain stars beyond their tidal radius (Muñoz et al., 2005, 2006b). An ever-increasing knowledge of dSph internal kinematics is revealing that nearly all dSphs exhibit some sort of kinematic peculiarity, and so it is important to revisit older dwarfs as additional velocity data becomes available to search for such features. Galaxy formation theories must be able to account for the diversity found in dwarfs. The features and variations within dwarfs both complicate and help refine the interpretation of how dwarfs evolve and their role in the evolution of larger structures.

The application of dwarfs to questions in other subfields of galactic astronomy are numerous. For example, the number and luminosity function of dwarfs within the MW halo can put constraints on cosmological models (Moore et al., 1999; Klypin et al., 1999); the systemic velocities and proper motions of dwarfs and associated tidal streams can be used as dynamical tracers for revealing the underlying mass distribution of the MW halo (Watkins et al., 2010; Law & Majewski, 2010); and the large fraction of dark to baryonic matter coupled with the lack of star formation within dSphs makes them ideal places to search for gamma ray signatures of dark

matter particle annihilations that would put restrictions on the particle cross-section (Ackermann et al., 2011; Geringer-Sameth et al., 2015).

1.1.3 Dwarf Galaxies and Dark Matter

Perhaps the most intriguing way that dSphs have contributed to our understanding of galaxies arose with their internal kinematics. Their velocity dispersions are much larger ($2 < \sigma_v < 12 \text{ km s}^{-1}$) than what is expected for purely baryonic systems. Pairing this with their large half-light radii yields V-band mass-to-light ratios that range from as little as 5 to as large as 5000 (McConnachie, 2012). For reference, globular clusters have mass-to-light ratios around 2 (Strader et al., 2011; Kimmig et al., 2015). The larger values of dSphs imply that either Newtonian mechanics does not properly describe dSphs, that all dSphs are being observed at a special time when they are being disrupted by the Milky Way, or that dSphs are dominated by dark matter. If we assume the latter, then dwarf galaxies are also the darkest objects known to associate with baryons, with dark matter constituting more than 99% of the mass in the faintest of these galaxies.

The first evidence to support this interpretation for dSphs came in the early 1980's with the first velocity dispersion measurement of a dSph. Using spectroscopic radial velocities of only three stars in Draco, Aaronson (1983) reported a velocity dispersion of 6.5 km s^{-1} . The implication was that Draco appeared to have a mass-to-light ratio of around 30, considerably larger than the mass-to-light ratios of globular clusters, despite their seemingly very similar stellar populations. At the time, however, there were five additional mechanisms that could potentially account for Draco's large velocity dispersion without invoking dark matter or Modified Newtonian Dynamics (MOND). They were small number statistics, poor velocity precision, stellar atmospheric jitter, galactic tides, and binary stars (Aaronson, 1983; Cohen, 1983; McClure, 1984).

The concern over small number statistics was quickly eliminated as the number of observed stars per dSph increased from three to several hundred. Improved resolution in newer spectrographs allows velocity measurements with 1–2 km s⁻¹ precision, making it possible to extract the dispersions in ultra-faints which are only a few km s⁻¹. The advent of better spectrographs also allowed observation of fainter K-giants, which exhibit far less atmospheric jitter than brighter carbon stars (Mayor et al., 1984; Seitzer & Frogel, 1985). Ruling out these three mechanisms was fairly straight forward. The remaining two have proved more difficult.

One explanation was that Draco was being tidally disrupted by the Milky Way. This idea held ground because velocity dispersion is only a good estimator of mass if the galaxy is in dynamic equilibrium. This seemed plausible since Draco is the closest of the classical dSph galaxies to the Milky Way. However, with the addition of radial velocity data from other dSphs — Sculptor (Armandroff & Da Costa, 1986), Ursa Minor (Aaronson & Olszewski, 1987; Armandroff et al., 1995; Olszewski et al., 1995), Fornax (Mateo et al., 1991), Carina (Mateo et al., 1993), Sextans (Suntzeff et al., 1993; Hargreaves et al., 1994a), Leo II (Vogt et al., 1995), and Leo I (Mateo, 1998) — it became apparent that most dwarfs, regardless of their proximity to the Milky Way, exhibited large velocity dispersions without evidence for streaming motions. In addition, some simulations predicted that a perigalactic passage would leave behind a velocity gradient larger than the velocity dispersion (Piatek & Pryor, 1995; Pryor, 1996), a feature not seen in any of the known dwarfs at the time (and still rare among subsequently discovered systems). This initially seemed to rule out the explanation of tides, but other simulations have shown that the fast stellar kinematics of dSphs might be produced through repeated tidal shaping of a more massive progenitor by the Milky Way (Kroupa, 1997; Klessen & Kroupa, 1998). The remnants of these interactions do not always exhibit tidal tails and when observed at the right time along the right orbit they can produce dwarf galaxies equivalent to what is observed

(Casas et al., 2012).

1.2 Binary Stars in Dwarf Galaxies

Another means for producing large internal motions of dSphs was through radial velocity variations caused by binary stars. The orbital motion of one star around another in the center of mass frame of the binary system will impose an additional radial velocity component. The velocity that is observed is thus no longer a reflection of the star's motion within the potential of a dwarf galaxy, but rather a combination of the motion within the binary and the motion within the dwarf. While the velocities of some stars will shift inward toward the systemic velocity of the dwarf, others will move outward into the tail of the velocity distribution, causing a net increase in the width of the distribution and thus an increase in the observed velocity dispersion.

Most of the radial velocities contributed by binary stars will be much smaller than the error bars and have a negligible effect on the velocity dispersion due to either long periods or unfavorable viewing angles. However, there is still a significant portion of binaries that can contribute velocities of a few km s^{-1} , and some that have upwards of 10 km s^{-1} . The latter are identifiable by taking repeat observations and can be removed from the sample. It is the cases with orbital radial velocity components of a few km s^{-1} that are both difficult to find and have large enough velocities to inflate the velocity dispersion.

As an example, we show histograms in Figure 1.1 of the orbital radial velocity that a primary star would exhibit within a binary system, v_b . We considered 10^5 binary systems. For each binary, we drew the parameters describing the orbit (e.g., period, eccentricity, inclination, etc; see Section 1.2.2) from distributions listed in Duquennoy & Mayor (1991) and assumed measurement errors of 1 km s^{-1} . 43% of the stars have v_b 's less than 1 km s^{-1} , 53% of them have $1 < v_b < 10 \text{ km s}^{-1}$, and 4% of them have v_b 's greater than 10 km s^{-1} . Binaries with short periods and high mass ratios

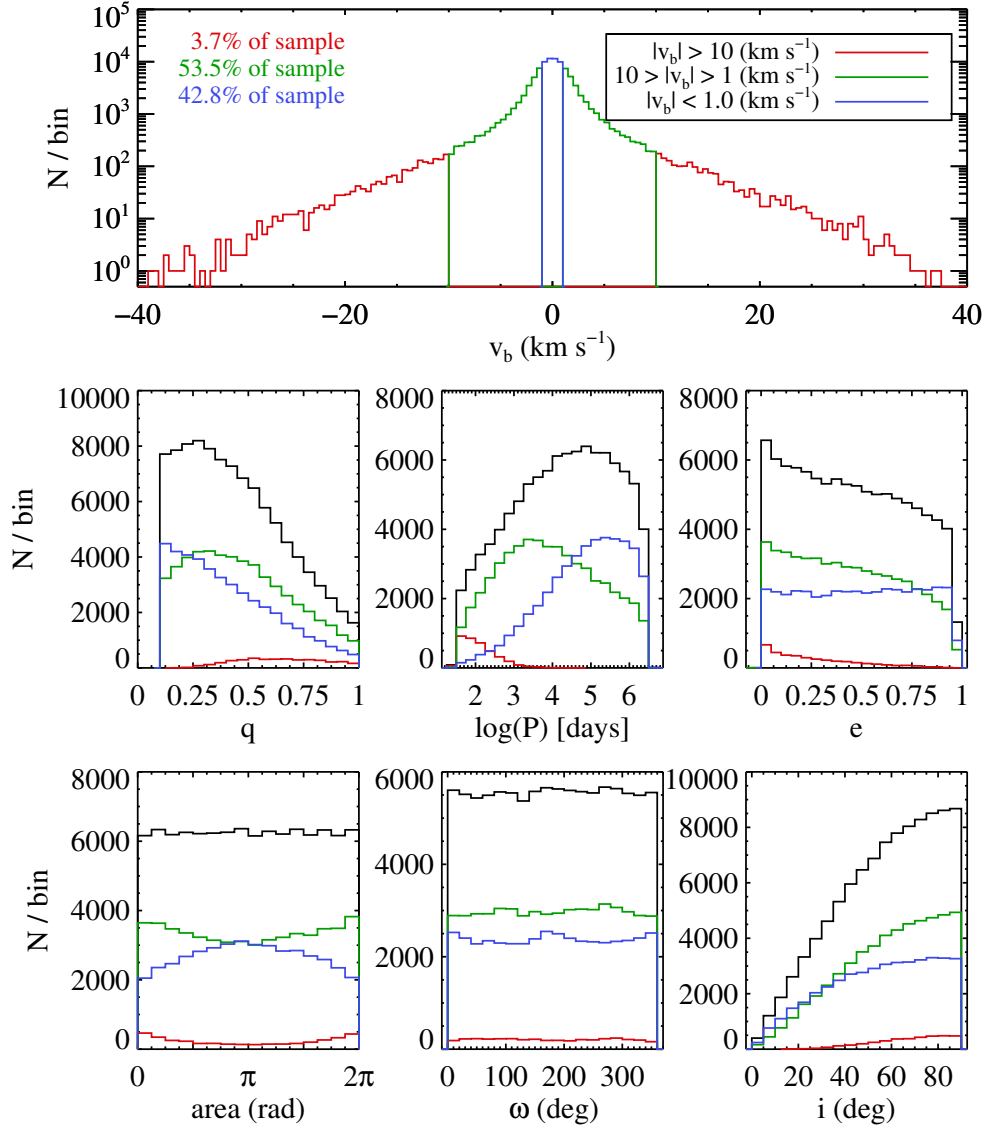


Figure 1.1 Top: histogram of the orbital radial velocity of a primary star in a binary system. 10^5 random combinations of binary parameters are shown. Bottom six panels: probability density distributions of binary parameters that determine the orbital radial velocity of a binary star. See Section 1.2.2 for further information on these parameters. Colors indicate sub samples of v_b with red having the largest v_b and blue having the smallest v_b ; black lines show the entire sample.

contribute the largest radial velocities. As we will see in Chapters IV and V, a dwarf with a sample of 60 stars and an intrinsic dispersion of 1 km s^{-1} can exhibit a velocity dispersion that is inflated by up to a factor of four, assuming period and mass ratio distributions from Duquennoy & Mayor (1991). The amount that binaries can inflate the velocity dispersion by depends largely on the fraction of stars in binaries, the number of stars in the sample, and the orbital parameters of binaries, namely period and mass ratio. As a result, it is tricky to correct these inflated velocity dispersions. However, simulations can be used to predict the inflationary effect on the velocity dispersion, given certain assumptions about the binary population.

Repeat observations of Draco stars showed that binaries contributed very little to the high velocity dispersion (Aaronson & Olszewski, 1987; Olszewski et al., 1995), and Monte Carlo simulations of binaries predicted the same results (Hargreaves et al., 1996a; Olszewski et al., 1996). Furthermore, studies of Ursa Minor (Olszewski et al., 1995), Sculptor (Queloz et al., 1995), and Leo II (Koch et al., 2007b) saw indistinguishable changes in dispersions measured from one epoch of velocity data versus multiple epochs, which was sufficient to rule out binaries as the cause for large dispersions. All in all, the addition of more and better velocity measures mitigated most of the skepticism surrounding these large velocity dispersions in regards to dark matter. As such, it is now widely accepted that dSphs are some of the most dark matter dominated objects in the Universe.

1.2.1 Binaries in Ultra-Faints

Some of the aforementioned issues, such as small number statistics and galactic tides, resurfaced with the discovery of ultra-faint dwarf galaxies in 2005, the most prominent of these being binary stars. Ultra-faints have dispersions closer to the $2\text{-}4 \text{ km s}^{-1}$ that can be contributed by binaries, making them more susceptible to velocity dispersion inflation. Recent work by Dabringhausen et al. (2016) has verified

that binaries affect the inferred properties of ultra-faints to a greater extent than their more massive counterparts. It was also shown by McConnell & Côté (2010) that there is a $\gtrsim 20\%$ chance that the intrinsic velocity dispersions of many ultra-faints (e.g., Segue 1, Segue 2, Willman 1, Bootes II, Leo IV, Leo V, and Hercules) are actually $\sim 0.2 \text{ km s}^{-1}$ like globular clusters, but the presence of binaries has increased the observed dispersions to a few km s^{-1} . While this is an extreme scenario, the fact that binary stars can drastically impact the velocity dispersion of ultra-faints cannot be ruled out.

For the galaxy Bootes I, Koposov et al. (2011) repeatedly took spectra of the same stars 15 times over the course of one month and discarded any stars that showed velocity variability. As a result, they found that the stars in Bootes I could be fit by a single population having a velocity dispersion of $4.6_{-0.6}^{+0.8} \text{ km s}^{-1}$, as opposed to previous single-epoch velocity dispersion measurements of $6.6 \pm 2.3 \text{ km s}^{-1}$ (Muñoz et al., 2006a) and $6.5_{-1.4}^{+2.0} \text{ km s}^{-1}$ (Martin et al., 2007). While this is a significant step in the right direction, simply removing the velocity variables does not remove all the binaries, as there can be stars with orbital periods much longer than the observation cadence. In Segue 1, Simon et al. (2011) not only removed obvious velocity variables to get a dispersion of $3.9 \pm 0.8 \text{ km s}^{-1}$, but they also corrected for binaries that were non-variable on the timescale of their observations, finding a slightly lower dispersion of $3.7_{-1.1}^{+1.4} \text{ km s}^{-1}$ (Simon et al., 2011; Martinez et al., 2011). For comparison, the single-epoch velocity dispersion was measured at $4.3 \pm 1.2 \text{ km s}^{-1}$ (Geha et al., 2009).

1.2.2 The Radial Velocity Equation

At the heart of any kinematic binary analysis that wishes to correct the velocity dispersion for the effects of binaries is the orbital radial velocity equation. It describes the radial velocity component of a star in orbit around another body as measured by an observer. While there are always seven parameters in this equation, it should

be noted that there are several different versions of this equation depending on the definition of such parameters. The version of the orbital radial velocity equation that I use is written as

$$v_{r,orb} = \frac{q \sin i}{\sqrt{1 - e^2}} \left(\frac{2\pi G m_1}{P(1 + q)^2} \right)^{1/3} (\cos(\theta + \omega) + e \cos \omega). \quad (1.1)$$

A derivation of this equation can be found in Appendix A. G is the gravitational constant. The definitions for the other parameters are as follows:

- m_1 : mass of primary star. Star 1 is the more massive of the two stars.
- q : mass ratio. This is defined as $q = m_2/m_1$, where m_2 is the mass of the less massive star. It is defined so that q cannot be larger than 1.
- P : period of the system. This is the time it takes for a star to complete a full orbit. The period of Star 1 is the same as the period of Star 2.
- e : eccentricity. It is defined as $\sqrt{1 - b^2/a^2}$, where a is the semi-major axis and b is the semi-minor axis. The eccentricity of a circle is 0, and the eccentricity of an unbound orbit is > 1 , such as a parabola.
- i : angle of inclination. This is the angle that orbital plan makes with the plane of the sky. We define it such that $i = 0^\circ$ is a face-on orientation and $i = 90^\circ$ is an edge on orientation. This angle is depicted in Figure 1.2.
- θ : true anomaly. This is the angle between the line connecting the periastron to the focus and the focus to the star. It is shown in Figure 1.2 as the angle between the solid and red dashed lines.
- ω : argument of periastron. This angle is between the line connecting the ascending node to the focus and the focus to the periastron. The ascending node

is the point where the star moves up through the plane of the sky toward the observer. Both of these are labeled in Figure 1.2.

Another parameter that does not directly appear in Equation 1.1 but is useful in other regards is the semi-major axis, a , which is half the distance between periastron and apastron. This can be related to P using Kepler’s Third Law: $a^3 = P^2 G(m_1 + m_2)/4\pi^2$. The semi-major axis in this equation refers to that of the binary system. a is the sum of $a_1 + a_2$, where a_1 is the semi-major axis for the orbit of Star 1 and a_2 is the semi-major axis for the orbit of Star 2.

To illustrate how the binary orbital parameters interact, Figure 1.3 shows how the line of sight velocity of the primary star varies with time. The left panels vary the mass ratio over $q = \{0.1, 0.5, 1\}$; the middle panels vary eccentricity over $e = \{0, 0.5, 0.9\}$; and the right panels vary the argument of periastron over $\omega = \{0, 45, 90\}$. For every case, the mass of the primary has been set to $0.8 M_\odot$, the period is 100 years, and the inclination is 90° . From this it is clear that the mass ratio (along with the period) affect the amplitude of the velocity as expected. The eccentricity affects the amplitude to some degree but has a much more marked affect on the shape of the sinusoid. Pairing a non-zero eccentricity with the argument of periastron can lead to highly asymmetric velocity curves.

1.2.3 Methods for Determining Binary Fraction

Several methods have been devised to determine the binary fraction—the fraction of apparently single stars that are actually binaries—and to correct the velocity dispersion for inflation caused by binaries. The details of the most notable methods are summarized in Table 1.1. Early attempts required assumptions about the binary fraction (Mateo et al., 1993; Suntzeff et al., 1993; Vogt et al., 1995; Hargreaves et al., 1996a), while more recent techniques have implemented a Bayesian process to bypass these assumptions (Minor et al., 2010; Martinez et al., 2011; Cottaar et al., 2012).

Others focused their effort on determining the binary fraction and explored velocity dispersion as a secondary result (Olszewski et al., 1996; Minor, 2013). The only commonality between all of these studies is the general use of Monte Carlo simulations to generate mock radial velocities via Equation 1.1. The Monte Carlo velocities are then used to calculate some statistic that represents the number of stars with excessively large velocity variability. Variables in the simulations are changed until the statistic obtained by the simulations matches the statistic seen in the observational data. Each method has benefits and detriments when compared to the others, so no single method is the best.

The first method in Table 1.1 is Olszewski et al. (1996). For their test statistic, they considered something called the “discovery fraction”, which is the fraction of observed stars that have large velocity variances when compared to the measurement errors. They varied the binary fraction in the Monte Carlo simulations in an attempt to reproduce the observed discovery fraction. They used multi-epoch velocity data for Draco and Ursa Minor (Armandroff et al., 1995) and the mass ratio and period distributions from Duquennoy & Mayor (1991). The binary fraction for stars with periods around 1 year came out to be 0.2-0.3, which is 3-5 times larger than what is found in the solar neighborhood. When they considered periods without upper or lower boundaries, the binary fraction they expected was 1.4-2.8. While their unique definition of binary fraction did allow for values greater than one (due to triple-systems counting as two binaries), such large binary fractions were still unrealistic. Nevertheless, this provided the groundwork for future attempts at constraining the binary fraction.

Soon after, Hargreaves et al. (1996a) published a complementary work that focused on the effect of binaries on velocity dispersion. They created a statistic called “threshold velocity” that dictated the minimum change in velocity that a star would need to undergo in order to be identified as a binary, and defined the statistic as

Table 1.1 Multi-Epoch Binary Analyses in dwarf galaxies

Feature	Olszewski et al. (1996)	Hargreaves et al. (1996a)
Primary focus (f or σ)	binary fraction	velocity dispersion
Number of epochs allowed	> 1	> 1
Statistic to measure f	single value ($P(\chi^2)$)	single value ($3\sqrt{2}\sigma_{err}$)
q distributions considered ^a	DM91	DM91, KTG93, M93
P distributions considered ^a	DM91	DM91, M93
Incorporates error model	no	no
Incorporates membership likelihood	no	no
Galaxies analyzed	Dra, UMi	Dra, UMi, Scl
Related paper(s)	none	none
Notable feature	First detailed study	Many choices for q, P
Conclusion	$f_{dSphs} > f_{Sol.Neighbor.}$	σ not caused by binaries
Feature	Minor et al. (2010)	Martinez et al. (2011)
Primary focus (f or σ)	both	velocity dispersion
Number of epochs allowed	2	> 2
Statistic to measure f	single value (Δv)	single value (Δv)
q distributions considered ^a	DM91	DM91
P distributions considered ^a	DM91, log-normal w/ variable μ, σ	log-normal w/ variable μ, σ
Incorporates error model	yes	yes
Incorporates membership likelihood	no	yes
Galaxies analyzed	Car, For, Scl, Sex	Segue 1
Related binary paper(s)	Minor (2013)	Simon et al. (2011)
Notable feature	error model	assumption of f not required
Conclusion	Car \neq For,Scl,Sex; binaries little effect on $\sigma > 4\text{km s}^{-1}$ gals.	σ insensitive to P; Segue 1 is DM dominated
Feature	This Work	
Primary focus (f or σ)	both	
Number of epochs allowed	> 1	
Statistic to measure f	distribution of values (β)	
q Distributions Considered ^a	DM91, R10	
P Distributions Considered ^a	DM91, FM92, MK11	
Incorporates error model	no	
Incorporates membership likelihood	no	
Galaxies analyzed	Leo II, Dra, UMi	
Related binary paper(s)	Spencer et al. (2017b), Ch. IV	
Notable feature	statistic	
Conclusion	f likely different amongst dSphs; binaries can cause big σ_{obs} in $\sigma_{int} < 4\text{km s}^{-1}$ gals.	

^aDM91 = Duquennoy & Mayor (1991), FM92 = Fischer & Marcy (1992), M93 = Mateo et al. (1993), KTG93 = Kroupa et al. (1993), R10 = Raghavan et al. (2010), MK11 = Marks & Kroupa (2011)

$3\sqrt{2}\sigma_{err}$. They sought to reproduce the number of stars exceeding their threshold velocity via Monte Carlo simulations of radial velocity. They explored several new period and mass ratio distributions and tested binary fractions of 0.25, 0.5, 0.75, and 1. Their goal was not to determine the binary fraction, but rather to explore the magnitude of velocity dispersion inflation that could be induced by binaries. Ultimately they found that the dispersions caused by binaries were small compared to the total velocity dispersion. To produce larger dispersions, the binary parameter distributions would need to be more heavily weighted toward shorter periods and higher mass secondaries. Such distributions have not been observed in the solar neighborhood so if binaries are at the heart of the velocity dispersion then it is unlikely that they exhibit period and mass ratio distributions similar to the solar neighborhood.

An improved method (Minor et al., 2010) was developed to determine the binary fraction by way of a “threshold fraction”, which was defined as the fraction of stars with an observed change in velocity greater than a certain value after some time interval. This procedure was vastly improved by incorporating a model of the velocity uncertainties into the measurement and by using a Bayesian approach. It resulted in posterior probability distributions of the binary fraction, which made it easier to grasp the range of allowable binary fractions. They also attempted to simultaneously constrain the binary fraction and the shape of the period distribution. Unfortunately this method found a degeneracy between the two parameters that could only be broken with a sample of > 2000 stars that have velocity uncertainties of $< 0.5 \text{ km s}^{-1}$ with four or more epochs. The method was applied to MMFS/Magellan data in Carina, Fornax, Sculptor, and Sextans (Walker et al., 2009a) with the primary goal of determining the binary fraction (Minor, 2013). They concluded that Carina exhibited a much lower binary fraction than the other three dSphs. In addition they found that the threshold fraction was tightly correlated with the dispersion caused by binaries and so the velocity dispersion could be corrected in this way. This allowed them

to determine that dSphs with intrinsic dispersions $> 4 \text{ km s}^{-1}$ cannot have their observed velocity dispersions inflated by more than 30%.

Martinez et al. (2011) expanded on the work by Minor et al. (2010). Their modification allowed for more than two epochs of data in the definition of threshold fraction and included a term to model the likelihood of stellar membership. It also aimed to constrain structural parameters of a dwarf including the half-light radius and the slope of the stellar profile. They applied the method to Segue 1 (Simon et al., 2011; Martinez et al., 2011). Due to the degeneracy discovered in Minor et al. (2010), and an additional discovery that velocity dispersion is insensitive to the period distribution, they could correct the velocity dispersion without needing to know either of these. The main result of this method was a robust technique to correct velocity dispersion for large sample sizes, with at best, weak constraints on the actual binary fraction.

1.3 Dissertation Objectives and Structure

Regardless of the method used, there is still some uncertainty in the corrected velocity dispersion when the binary fraction is not well known. The goal of this dissertation is to use extant data to determine the binary fractions in classical dSph galaxies, in part so that more precise corrections can be applied to the velocity dispersions of ultra-faints. Along the way, I have also made comparisons between the binary fraction in dSphs and in the solar neighborhood; considered whether or not the dSphs all have the same binary fraction; investigated potential correlations between binary fraction and other galactic properties; and explored the possibility of constraining the period and/or mass ratio distribution from detailed comparisons of the data to modeled binary populations. In doing so, I have developed yet another method of finding the binary fraction that considers the shape of the entire velocity distribution. This contrasts with all previous methods that only aimed to reproduce

the number of stars exceeding some velocity variability limit (Olszewski et al., 1996; Hargreaves et al., 1996a; Minor et al., 2010; Martinez et al., 2011). I also use 2-11 epochs of data per dwarf rather than just one (Cottaar et al., 2012).

There are two key difficulties in determining a binary fraction in dwarf galaxies. First is the inherent uncertainty in the binary parameters, specifically mass ratio, period, and eccentricity. One attempt at determining the period distribution (Minor, 2013) showed that it is extremely difficult to put constraints on the shape of the period distribution for periods greater than 10 years when velocity measurement errors are $\gtrsim 1.7 \text{ km s}^{-1}$. Along those same lines, Martinez et al. (2011) found a strong degeneracy between the period distribution and binary fraction. The method that I employ does not attempt to constrain the parameters, but as we will see, it does favor some combinations of binary parameters over others.

The second difficulty applies more specifically to ultra-faints. It is not currently feasible to determine the binary fraction in ultra-faints due to the lack of extensive multi-epoch velocity measurements (although there are some exceptions such as Segue 1, which has 50+ stars with multi-epoch observations). Classical dSphs, on the other hand, have been accumulating spectroscopic observations for over 30 years. If the binary fraction is constant across all dwarfs, one need only determine the binary fraction for the more accessible classical dwarfs. On the other hand, if the binary fraction varies then there must be some physical mechanism that drives it. Perhaps by understanding the binary fraction in classical dSphs we can infer the binary fraction in ultra-faints, be it a constant or variable value. We will begin to address this question in our analysis but note that our results are not yet definitive.

Taking all this together, the specific goal of this dissertation is to measure the binary fractions in three classical dSphs. We selected Leo II, Draco, and Ursa Minor because they have large amounts of velocity data and have not been studied in detail for over 10 years. We also reanalyzed data in Carina, Fornax, Sculptor, and Sextans

to provide a consistent framework to compare the binary fractions between all seven of these galaxies.

This dissertation is composed of two published papers and one paper in preparation. The first, “A multi-epoch kinematic study of the remote dwarf spheroidal galaxy Leo II” (Spencer et al., 2017a), comprises Chapter II. It focuses on the kinematic and chemical features of Leo II by use of a new spectroscopic dataset from the Multiple Mirror Telescope. The second paper, entitled “The binary fraction of stars in dwarf galaxies: the case of Leo II” (Spencer et al., 2017b), describes the Bayesian technique that I use to measure the binary fraction in Leo II. It makes up Chapter III. The third paper, found in Chapter IV, has not yet undergone the submission/publication process. It improves upon the Bayesian technique and applies the new method to Draco and Ursa Minor.

Up until now, the papers that mention binaries within Leo II, Draco, or Ursa Minor merely conclude that binaries play a very small role in increasing the velocity dispersion. There has been only one paper that describes a quantitative binary fraction, but it is for the combined stars from Draco and Ursa Minor (Olszewski et al., 1995). My papers and this dissertation report individual values for binary fraction in these three dwarfs for the first time.

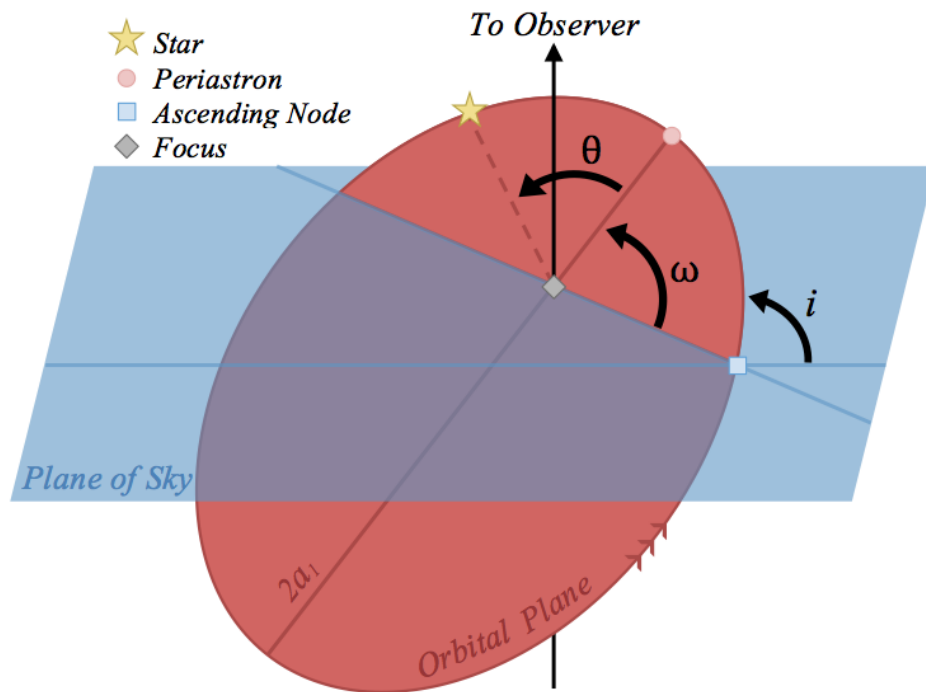


Figure 1.2 The geometry of a binary orbit. i is the angle of inclination, θ is the true anomaly, and ω is the argument of periastron.

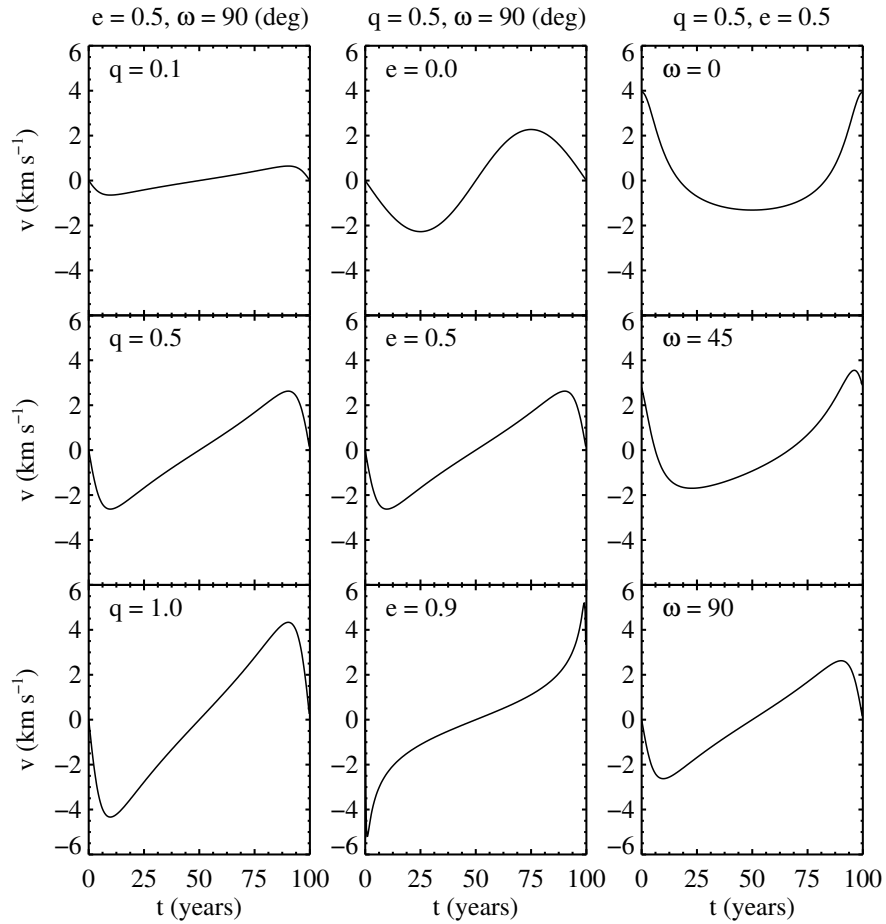


Figure 1.3 Radial velocity of the binary systems vs. time. In all panels the mass of the primary is $0.8 M_{\odot}$, the period is 100 years, and the inclination is 90° . The left column varies the mass ratio while keeping eccentricity and argument of periastron constant, which are labeled at the top of the figure. The center column varies eccentricity but keeps mass ratio and argument of periastron constant. The right column varies the argument of periastron but keeps the mass ratio and eccentricity constant.

CHAPTER II

A Multi-Epoch Kinematic Study of Leo II

2.1 Introduction

A detailed analysis on most of the classical dwarfs of the Milky Way (MW) has already been completed by collaborators (see, Walker, 2007). This included Leo I (Mateo et al., 2008), Carina, Fornax, Sculptor, Sextans (Walker et al., 2009b), and Draco (Walker et al., 2015b). Far less time has been spent on Leo II, the farthest classical MW dSph, which is located at a distance of 233 ± 15 kpc from the Galaxy. Most dSphs are found near the MW, but Leo II instead occupies a region of space that is dominated by star-forming dwarf irregular galaxies (see, for example, Mateo, 1998). Because of its large distance, it has been questioned whether or not Leo II is gravitationally bound to the Milky Way (Demers & Harris, 1983). Based on its radial velocity and dSph morphology, it is reasonable to consider Leo II an MW satellite (McConnachie, 2012, their Figure 2), but when taking into account the small galactocentric radial velocity component (Lépine et al., 2011; Piatek et al., 2016) and lack of evidence for tidal disruption (Koch et al., 2007b), it seems possible that Leo II has evolved in relative isolation within the Local Group at apocenter.

Since its discovery (Harrington & Wilson, 1950), Leo II has been the focus of many photometric studies. What started as only a few dozen individually detectable stars has evolved into massive studies of thousands of stars (see, for example, Bellazzini

et al., 2005; Coleman et al., 2007; Komiyama et al., 2007; Gullieuszik et al., 2008). From these massive space-based and ground-based surveys, it has been concluded that Leo II has undergone little to no star formation in the last ~ 7 Gyr (Mighell & Rich, 1996); red clump stars are more centrally concentrated than blue horizontal branch stars (Bellazzini et al., 2005); a mixture of stellar populations exists in the center of the galaxy while an older, more homogeneous population exists at larger radii (Komiyama et al., 2007); and some minor isophotal twisting is present but there is no dynamical evidence for tidal distortion (Coleman et al., 2007).

Due to the relatively large distance of Leo II from the MW, far fewer stars have been observed spectroscopically than photometrically. The first velocity measurements of only two very luminous red giant stars were published by Suntzeff et al. (1986), and shortly after came a study with five carbon stars (Zaritsky et al., 1989). A more extensive study was carried out by Vogt et al. (1995, hereafter V95), which included 31 red giant branch members. Based on this dataset they found the bulk radial motion of the dwarf to be 76.0 ± 1.3 km s $^{-1}$ and the velocity dispersion to be 6.7 ± 1.1 km s $^{-1}$. Furthermore they noted that the mass-to-light ratio in the V-band was 11.1 ± 3.8 , suggesting that the galaxy was embedded in a massive dark matter halo with mass of $9 \times 10^6 M_{\odot}$, similar to the known halo masses of other dwarfs (Mateo et al., 1993), and consistent with more recent findings that the smallest dark matter halos are similar in mass (Strigari et al., 2008; Walker et al., 2009a). Since then, Koch et al. (2007b, hereafter K07b) expanded upon the kinematic data of Leo II, observing 200 stars and concluding that 171 of them were members. The precision of the individual velocity measurements was worse than V95 by about 1 km s $^{-1}$, but with over five times more stars, they improved the precision of the systemic velocity measurement to 79.1 ± 0.6 km s $^{-1}$ and the dispersion to 6.6 ± 0.7 km s $^{-1}$. They found no velocity gradient, velocity asymmetry, or signs of rotation, and therefore concluded that the galaxy has not been affected by tides. Bosler et al. (2007) obtained

low-resolution spectra of 74 Leo II stars for the purpose of better understanding the chemical composition but lacked the necessary precision to report velocity measurements to better than $\sim 50 \text{ km s}^{-1}$. More recently, Kirby et al. (2010) targeted 394 red giant branch stars in the direction of Leo II and determined that 258 of them were members based on radial velocities. In a follow-up paper (Kirby et al., 2011, hereafter K11), they focused on chemical abundances and notably derived a metallicity gradient of $-4.26 \pm 0.31 \text{ dex deg}^{-1}$ in Leo II, which stood in contrast to the negligible slope found by Koch et al. (2007a) for 52 stars.

In this chapter we present new spectroscopic data with high precision from a large sample of red giant branch stars in Leo II. Details of our observing strategy, data reduction, and velocity extraction methods are found in Section 2.2. Section 2.3.2 provides a kinematic analysis of the stars while Section 2.3.3 focuses on the chemistry of the stars. Section 2.4 contains concluding remarks and a summary of our findings.

2.2 Observations and Data Processing

2.2.1 Photometry

We used the 90prime imager (Williams et al., 2004) on the 2.3 meter Bok telescope at Steward Observatory in Arizona to collect photometry of Leo II. Stars were observed in the Washington *M* and *I* filters during 2006 February. Data were processed in the usual way: subtracting an average bias frame, dividing by a normalized twilight flat-field, and adding repeated observations to remove cosmic rays.

After processing, we used the DoPHOT software (Schechter et al., 1993) to get positions and magnitudes for objects in the images. The algorithm works by first fitting a user-supplied guess of the FWHM to all bright sources in the frame. After finding most of the obvious stars, it recalculates the FWHM and recomputes the

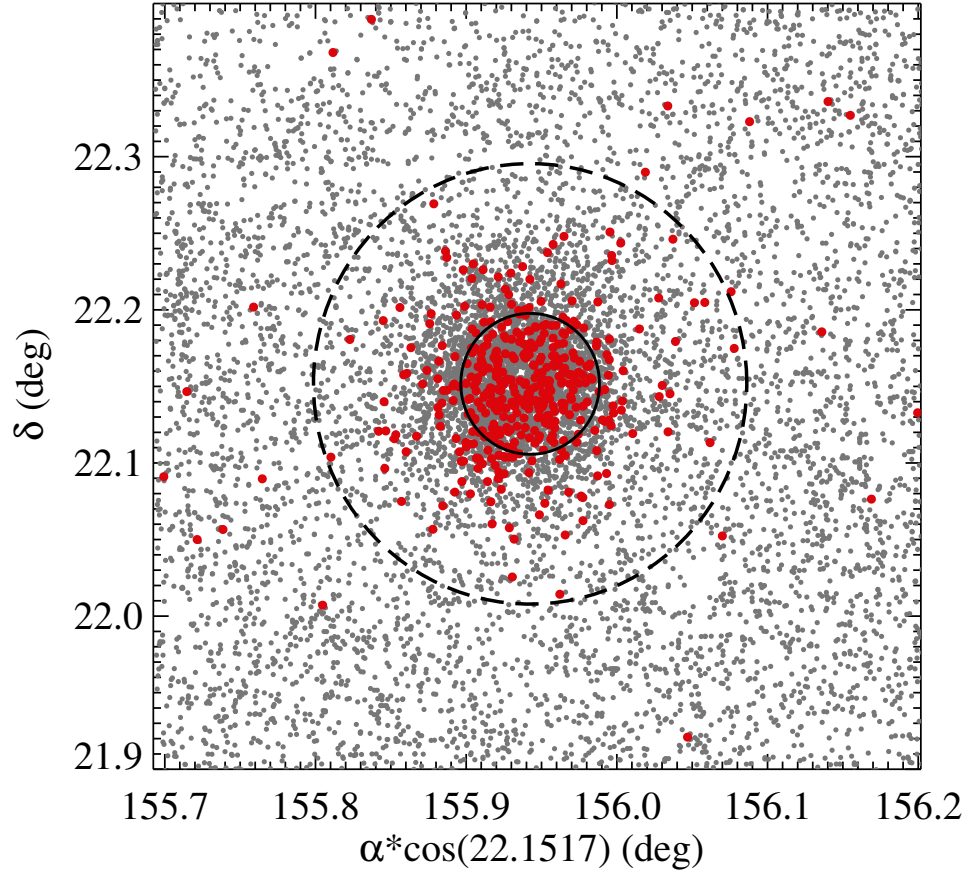


Figure 2.1 Right ascension vs. declination of the targets observed photometrically. Stars highlighted in red were selected for spectroscopic followup based on the color-magnitude diagram in Figure 2.2. The core and tidal radii from Komiyama et al. (2007) are shown as black solid and dashed lines, respectively.

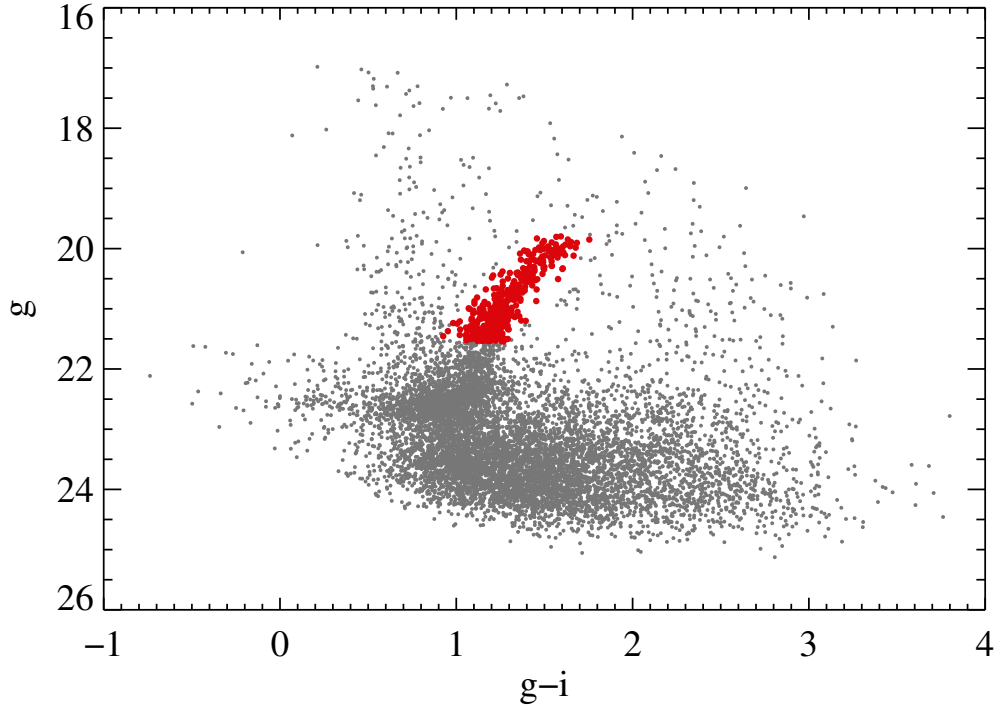


Figure 2.2 Color-magnitude diagram of objects in the direction of Leo II. The filters are Sloan g and i . Giant stars selected for spectroscopic follow-up are shown in red.

brightness of each target. The magnitudes are recorded into a file along with the pixel coordinates and a set of χ^2 values for an assumed profile of a single-star, multiple-star, or galaxy.

We calibrated these instrumental M and I magnitudes by transposing them to apparent Sloan g and i magnitudes. Approximately half of the stars in our sample were listed in SDSS, so we used those stars to fit a three-term function relating the SDSS magnitudes, our magnitudes, and a color term. The best fitting transformations were $i = I + 0.88(M - I) + 7.52$ and $g = M - 1.11(M - I) + 8.52$. Table D.1 in the appendices lists the celestial coordinates and these apparent magnitudes for stars that were targeted for spectroscopic followup. Figure 2.1 shows all of the stars on the sky that we measured apparent magnitudes for. The red points are stars that we targeted for spectroscopic followup. They were selected on the basis of having g magnitudes brighter than 21.55 and being confined within the red giant branch of the

color magnitude diagram in Figure 2.2.

2.2.2 Spectroscopy

Spectroscopic observations were obtained with the Multiple Mirror Telescope (MMT) using Hectochelle, a multi-fiber, single-order echelle spectrograph (Szentgyorgyi et al., 1998). The instrument can target up to 244 objects within a 1 degree field, and has an operational spectral range between 3800 and 9000 Å. We used the RV31 filter for our observations, which isolates the spectral region spanning between ~ 5150 and 5300 Å and contains the Mg I and Mg b features. Spectra were taken on five different runs between 2006 and 2013. Table 2.2.2 summarizes the observed fields, dates of observation, heliocentric Julian dates, exposure times, and number of exposures.

Processing of the raw images was done with IRAF. The steps are identical to those in Mateo et al. (2008), but are briefly repeated here. The overscan region was subtracted from all images, and then trimmed out. Hectochelle has two amplifiers for each of its two CCDs, so data from the amplifiers for both CCDs were combined. Multiple exposures for each pointing were also combined to form a single, deeper image for each pointing, as listed in Table 2.2.2. In doing so, cosmic rays could be simultaneously removed by a sigma clipping algorithm.

The fibers at the focal surface of the spectrograph collimator are staggered to allow for tighter packing, and thus the spectra need to be extracted before further reductions. Locations of the individual spectra on the CCD were traced by quartz lamp spectra that were taken after each science exposure. The quartz traces were allowed to shift en masse to align with the data. These shifted traces were used to extract science and calibration spectra. A fifth-order polynomial was used to produce a wavelength solution based on 30-40 ThAr emission lines. Relative fiber throughputs were determined from twilight observations, because fibers were not evenly illumi-

Table 2.1. Hectochelle observations of Leo II fields

Field	α_{J2000}^a (hh:mm:ss.ss)	δ_{J2000} (dd:mm:ss.ss)	UT Date (yyyy mmm dd)	HJD ^b (days)	N_{exp}^c	Exp. Time ^d (s)
LeoII-01	11:13:25.41	+22:08:57.60	2006 Apr 25	2453850.67	3	8100
LeoII-02	11:13:25.41	+22:08:57.61	2007 Apr 22	2454212.79	2	5400
LeoII-03	11:13:25.84	+22:08:33.61	2008 Feb 26	2454522.72	3	7200
LeoII-04	11:13:23.68	+22:08:03.61	2008 Mar 01	2454526.82	3	7200
LeoII-05	11:13:32.61	+22:10:42.62	2011 Jan 20	2455591.92	5	12000
LeoII-06	11:13:29.57	+22:04:06.84	2011 Feb 05	2455597.96	4	9600
LeoII-07	11:13:32.29	+22:10:48.62	2011 Feb 07	2455599.81	2	4800
LeoII-08	11:13:25.74	+22:08:39.12	2013 Feb 17	2456340.93	4	2700
LeoII-09	11:13:03.47	+22:05:57.38	2013 Feb 18	2456341.94	3	2700

^aCentral coordinates of field.

^bAt beginning of first sub-exposure.

^cNumber of sub-exposures.

^dExposure time summed over all sub-exposures.

nated by the quartz lamp. The throughputs were then divided out. Lastly, sky spectra were recorded by unassigned fibers and combined to produce a master sky spectrum for each pointing, which was then subtracted from the science spectra. There were anywhere from 40 to 60 sky spectra in each pointing. This resulted in a set of 1,921 wavelength-calibrated, one-dimensional spectra with a resolution of 0.1 Å/pix ($R \sim 25,000$).

2.2.3 Velocity Measures

Most of our past papers analyzing Hectochelle data used `fxcor` — a Fourier cross-correlation routine in IRAF — to generate velocities from these spectra. We have subsequently begun to use a new approach (Walker et al., 2015b) that fits a library of synthetic spectra in order to estimate velocities as well as effective temperatures, surface gravities and metallicities. Since part of our analysis requires long-baseline observations, we want to be certain that there are no systematic velocity differences between methods. Therefore, we carried out our velocity measurements with both procedures to compare results quantitatively.

The `fxcor` routine performs a Fourier cross-correlation between a template spec-

trum, which serves as the velocity zero-point, and a science spectrum. The template that we used consists of coadded spectra acquired for various radial velocity standards with Hectochelle and is the same template used by Mateo et al. (2008); the co-added spectrum has $S/N > 350$. Figure 2.3 illustrates the input and output of `fxcor`. The top and middle panels of Figure 2.3 show a sample science spectrum and the template spectrum, respectively. The bottom panel shows the cross correlation function, where the pixel shift at the highest peak corresponds to the redshift of the spectrum. The pixel shift is converted to a shift in wavelength, and thus a radial velocity.

We refer the reader to Walker et al. (2015b) for a complete description of our newer Bayesian method. Briefly, we obtain simultaneous estimates of radial velocity, effective temperature, surface gravity, and metallicity by fitting a library of smoothed, synthetic stellar spectra to each Hectochelle spectrum in pixel space. Following Walker et al. (2015b), we use the library provided by Lee et al. (2008a,b), which was used to estimate stellar parameters for the SEGUE. The library is computed over a regular grid of T_{eff} , $\log g$ and $[\text{Fe}/\text{H}]$, and assumes a piecewise-linear relationship between $[\text{Fe}/\text{H}]$ and $[\alpha/\text{Fe}]$. We use the software package MultiNest (Feroz & Hobson, 2008; Feroz et al., 2009) to sample parameter space and to sample the posterior probability distribution function (PDF) of our 15-dimensional model. For each parameter, we summarize the marginalized 1D PDF by recording the mean, variance, skewness, and kurtosis. Following Walker et al. (2015b), we use the skewness and kurtosis of the velocity distribution to reject poor-quality observations (see Section 2.2.4).

Our Leo II targets were each observed between one and seven times, giving us multiple measurements per star, often over many epochs. In total, we observed 727 spectra for 336 stars in the direction of Leo II.

We compare the velocity results from the two methods in Figure 2.4. Error bars are not shown so as to increase plot readability; the median error for the `fxcor` method is 2.8 km s^{-1} , and that for the Bayesian analysis method is 2.0 km s^{-1} . We fit a line

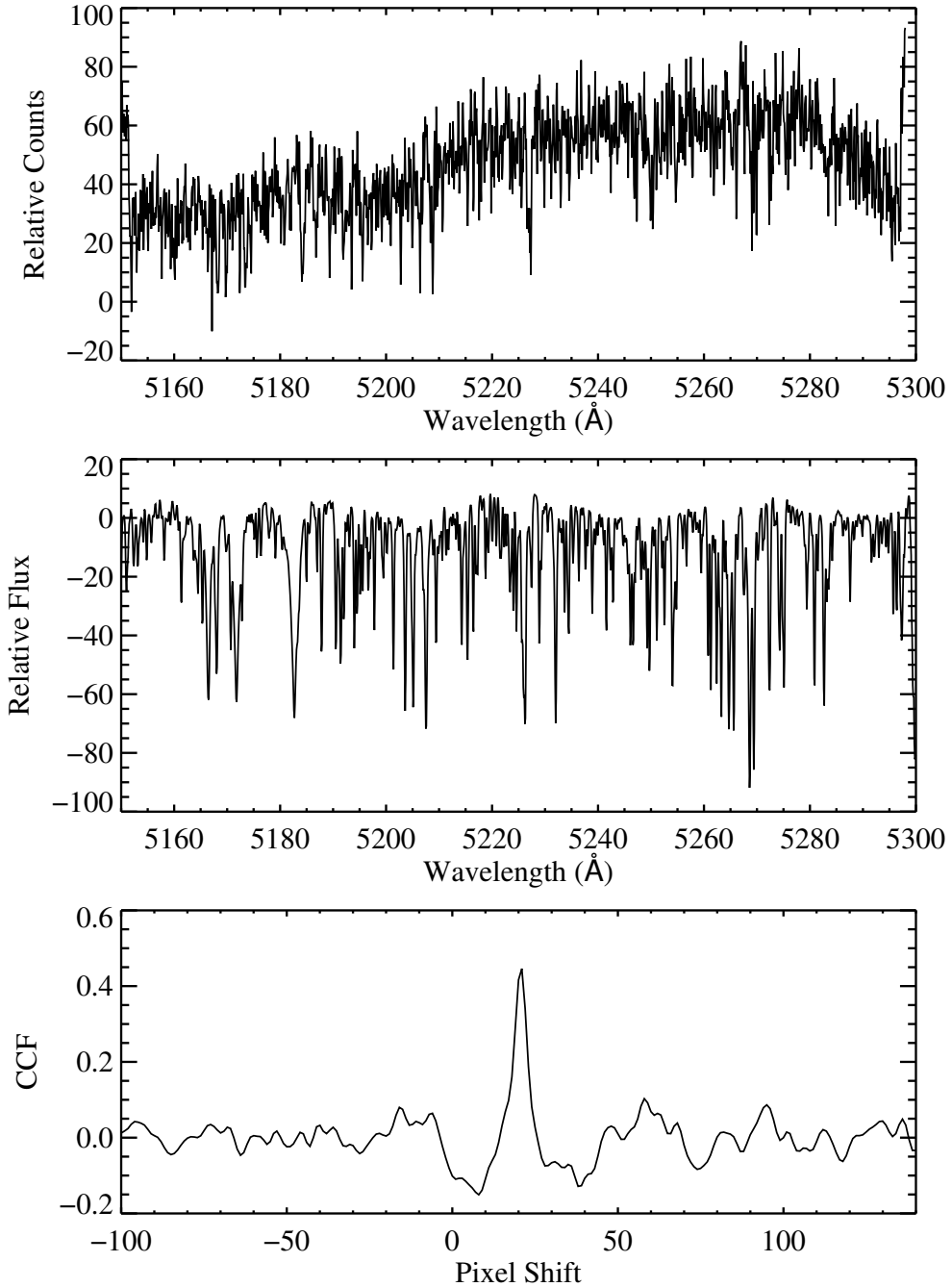


Figure 2.3 Top: sample spectrum of one of our science targets. Middle: template spectrum used in `fxcor`, an IRAF task that performs a Fourier cross-correlation between a science spectrum and a template spectrum to determine a radial velocity. Bottom: Cross-correlation function between the two spectra. The peak corresponds to the best shift between the two spectra and indicates the radial velocity for the science target.

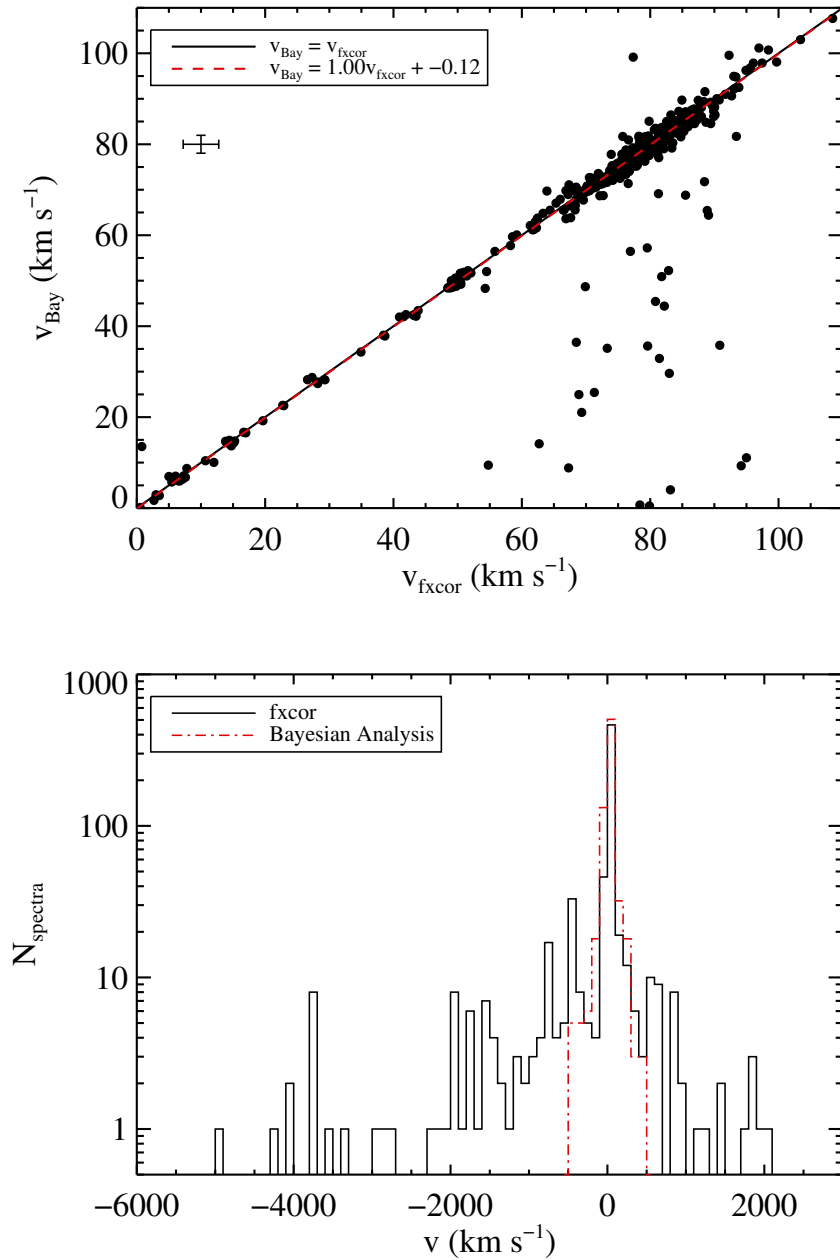


Figure 2.4 Top: velocity measures extracted via Bayesian analysis plotted against velocity measures extracted by fxcor. Each dot represents a measure from a spectrum, so there may be multiple points per star. The median velocity error is 2.77 km s^{-1} for fxcor and 1.97 km s^{-1} for Bayesian analysis; this is represented by the symbol in the top left. The black solid line marks the one-to-one line where the two measurements are exactly the same; the red, dashed line traces the best fit to the data when the slope has been set equal to one. The black and red lines overlap almost perfectly. Bottom: number of spectra with a given velocity measure from fxcor (black, solid line) and Bayesian analysis (red, dash-dotted line).

with slope equal to unity and identify a very slight systematic offset of 0.13 km s^{-1} . This offset is well within the combined errors so we have chosen to apply no corrections to either set of velocity measurements. We choose to use the Bayesian approach for all further analysis because it extracts stellar atmospheric parameters and also has a more straightforward and self-consistent estimate of the errors.

2.2.4 Quality Control

Since we are ultimately interested in recovering the velocity dispersion of Leo II and measuring the velocity variability of its stars, we must be particularly careful in identifying and excising low-quality data from the sample. Shown in Figure 2.5 are the velocity errors, σ_v , plotted against the skewness, S_v , and kurtosis, K_v , of the error distribution returned in the Bayesian analysis. In each panel, the points cluster in two groups, with good measures occupying the left side of the plot where error distributions are relatively narrow and Gaussian. For consistency, we adopt the same quality criteria as Walker et al. (2015b). Thus, measurements used in the analysis of this chapter have $\sigma_v < 5 \text{ km s}^{-1}$, $-1.0 < S_v < 1.0$, and $-1.0 < K_v < 1.0$. Of the 336 stars observed with MMT, 222 had velocity measures that met these criteria.

With the remaining velocity measurements, we combined any observations taken over multiple epochs to arrive at one average velocity per star, which is useful for determining membership. Velocities were weighted by the inverse of their variances and are expressed as $v = \sum \frac{v_i}{\sigma_i^2} / \sum \frac{1}{\sigma_i^2}$. Similarly, the error measurements were combined such that $\sigma = (\sum \frac{1}{\sigma_i^2})^{-1/2}$. Other spectral quantities and their errors were averaged in the same way, including $[\text{Fe}/\text{H}]$, $\log(g)$, and T_{eff} . Up to seven different epochs of observations contributed to these average measurements. The averages are reported in Table E.1 of the appendices and individual measures that went into these averages are listed immediately below the corresponding average. The columns are as follows: (1-2) celestial coordinates, (3) heliocentric Julian date, (4) heliocentric radial veloc-

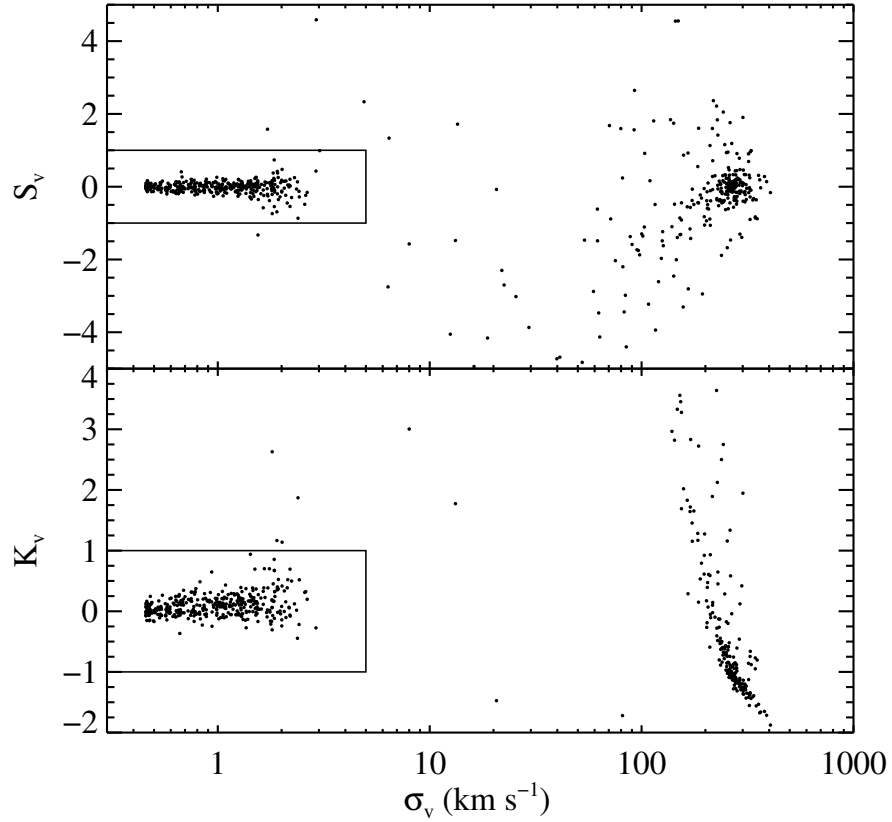


Figure 2.5 Skewness (top) and kurtosis (bottom) vs. standard deviation of the posterior probability distribution functions for radial velocity. The posteriors were obtained through a Bayesian analysis of the spectra. Measurements outside the black boxes are discarded as low quality and are not used for further analysis. The boundaries for the quality cuts are adopted from Walker et al. (2015b).

ity and error, (5) effective temperature and error, (6) surface gravity and error, (7) metallicity and error, (8) the number of observations that went into the calculation of the average measurements, and (9) the star’s membership status (see Section 2.3.1).

2.3 Kinematic and Chemical Analysis

2.3.1 Defining Membership

To separate stellar members from nonmembers we first employed a simple velocity cut. Figure 2.6 shows a histogram of the averaged velocity measures, so that there is one data point per star. We fit a three-parameter Gaussian to the histogram of the form $f(v) = a_0 \exp\left(-\frac{(v-a_1)^2}{2a_2^2}\right)$. The best fit parameters were $a_0=30.6$, $a_1=78.9$ km s⁻¹, and $a_2=7.2$ km s⁻¹. Stars with radial velocities that fall within 3σ of the center (within the range $57.3 < v < 100.5$ km s⁻¹) were taken to be likely members of Leo II, while stars outside this range were assumed to be foreground Milky Way halo stars. This boundary is marked as two vertical dotted lines in Figure 2.6. Employing this cut yielded 186 velocity members of Leo II.

There is expected to be a small number of apparent member stars that are actually halo stars with projected positions and velocities matching those of Leo II. We quantified this fraction by using the Besançon models of the MW halo (Robin et al., 2003). The models provide synthetic stellar evolutionary and dynamic populations that are expected to exist in a queried region of the Milky Way. We produced a kinematic sample of $\sim 25,000$ stars along the line of sight toward Leo II according to the model. We then computed a generalized histogram, whereby each star is represented by a Gaussian curve with unit area, centered on the listed Besançon velocity and having a standard deviation equal to the median of the weighted MMT velocity errors (0.94 km s⁻¹). The $\sim 25,000$ Gaussians were summed up to produce a single smooth distribution. A generalized histogram was also produced for our 222 stars with ob-

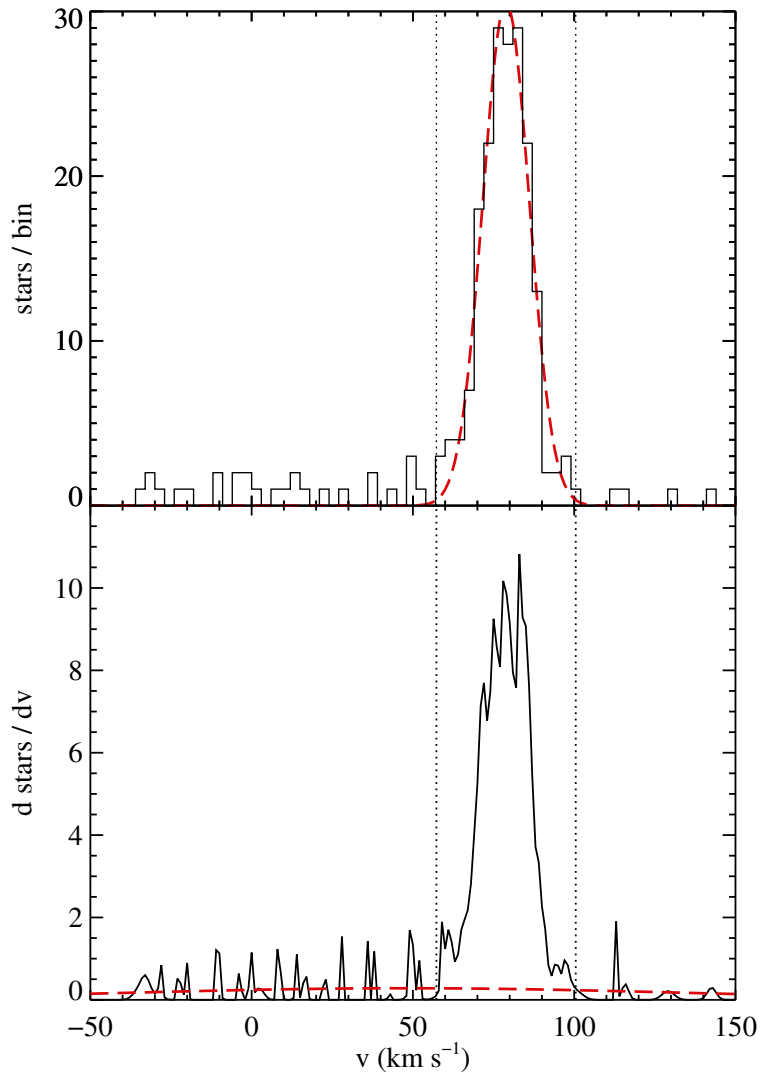


Figure 2.6 Top: the numbers of stars in each velocity bin are shown in solid black. The Gaussian fit to the histogram is plotted as a red dashed line. The center and standard deviation of the Gaussian are 78.9 km s^{-1} and 7.2 km s^{-1} respectively. Stars within 3σ of the center velocity are considered to be velocity members; this boundary is marked by the vertical dotted lines. Bottom: each star is represented by a Gaussian distribution with unit area and the sum of these Gaussians is the solid black line. The red dashed line is a distribution of $\sim 25,000$ stars from Robin et al. (2003), scaled such that the integrated area represented by stars with velocities between -50 and 50 km/s is equal to the area of the stars from our data in the same range. The area under the red dashed curve between the Leo II velocity boundaries is 11.3 , suggesting there should be 11 foreground stars.

served radial velocities, but using the velocity errors as the standard deviations. We normalized the Besançon distribution by requiring the area under the curve in the range $-50 < v < 50 \text{ km s}^{-1}$ —the typical velocity range of Milky Way foreground stars—to be equal to the area occupied by our observed stars within the same region. This normalized distribution of model MW halo stars is shown as a red dashed line in the lower panel of Figure 2.6; the generalized Gaussian histogram for our observed stars is marked by a black solid line. By integrating the red distribution over the velocity range of accepted Leo II membership, we estimated that there should be 11 halo stars with velocities and positions similar to those of Leo II.

As a result of this contamination, we choose to apply one more cut on the data based on stellar surface gravities. As can be seen in Figure 2.7, the majority of stars that were flagged as nonmembers according to radial velocities also have high surface gravities. This is expected since the stars we targeted should be on the red giant branch if they are members of Leo II, but will be dwarfs if they are foreground Milky Way stars. Therefore, our final requirement for a star to be considered a member is that it has $\log(g) \leq 4$. This removes 11 stars from the sample, which is equal to the expected contamination from the Besançon model (Robin et al., 2003) that we generated.

Utilizing these cuts in velocity and surface gravity ($57.3 < v < 100.5 \text{ km s}^{-1}$ and $\log(g) \leq 4$), we have a total sample of 175 member stars. This is the set of stars that we will use for the kinematic and chemical analyses in this chapter.

We compared our velocities with others published in V95, K07b, and K11 (obtained via private communication). There were 22, 94, and 94 stars that were observed in both the respective studies and ours. The offsets between our data and previous studies were 0.84 km s^{-1} for V95, 0.66 km s^{-1} for K07b, and 0.61 km s^{-1} for K11. All of these offsets are smaller than the median errors of the datasets, suggesting good agreement between studies. More details on this comparison can be found in Chapter

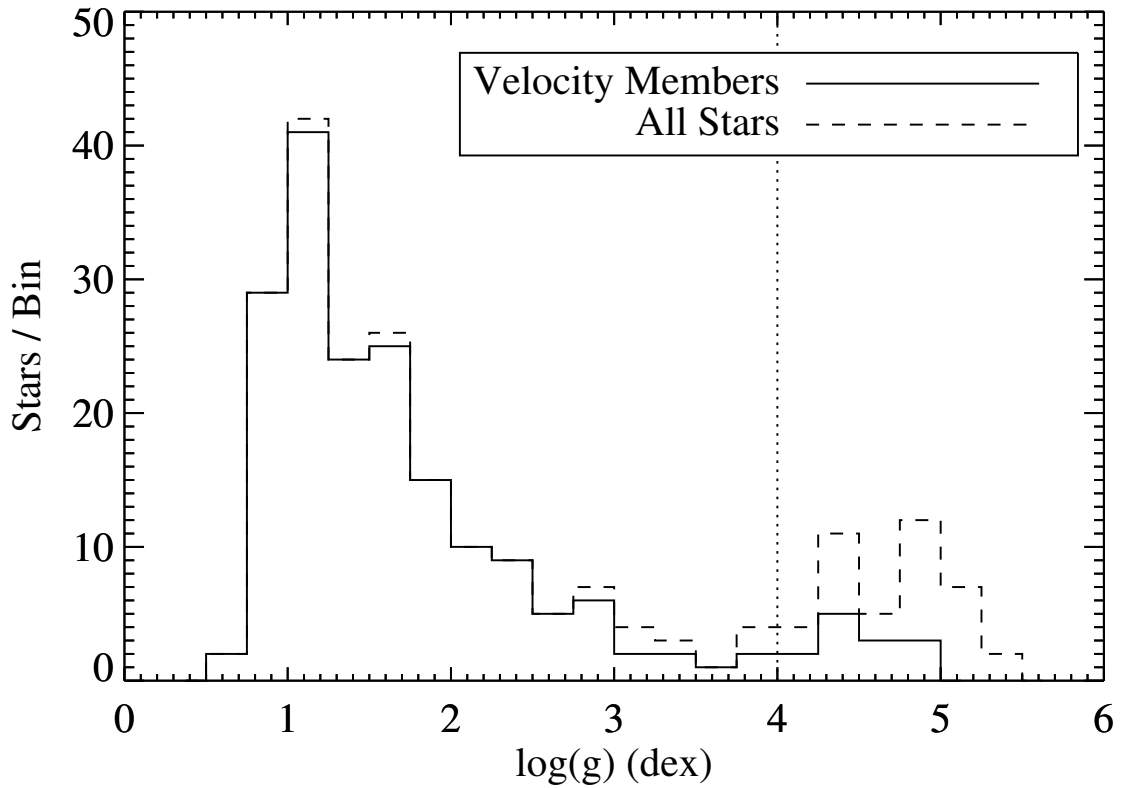


Figure 2.7 The number of stars per $\log(g)$ bin of width 0.25 dex is plotted for all stars (dashed line) and for only velocity members (solid line). Most stars that are velocity nonmembers have high surface gravities, as expected for MW halo stars. For this reason we consider all stars with $\log(g) > 4$ to be nonmembers.

III.

2.3.2 Kinematic Features

The systemic velocity and velocity dispersion of Leo II were calculated following the method of maximum likelihood laid out by Walker et al. (2006). The observed quantities are found by maximizing the natural logarithm of the joint probability function of the two being drawn from Gaussian distributions. Following the notation of Walker et al. (2006),

$$\ln(p) = -\frac{1}{2} \sum_{i=1}^N \ln(\delta_i^2 + \sigma_p^2) - \frac{1}{2} \sum_{i=1}^N \frac{(v_i - \langle v \rangle)^2}{(\delta_i^2 + \sigma_p^2)} - \frac{N}{2} \ln(2\pi). \quad (2.1)$$

Here, $\langle v \rangle$ is the systemic velocity and σ_p is the velocity dispersion. v_i and δ_i are the radial velocity and corresponding error for star i selected from a total of $N = 175$ stars. Errors were calculated through a covariance matrix with the variances of $\langle v \rangle$ and σ_p as the diagonal elements. Further details can be found in Walker et al. (2006). This yielded a systemic velocity of $78.5 \pm 0.6 \text{ km s}^{-1}$ and a velocity dispersion of $7.4 \pm 0.4 \text{ km s}^{-1}$ over the full tidal radius of the dwarf. Both of these measurements agree with the best fit values of the Gaussian in Section 2.3.1 to within 1σ . Our systemic velocity falls comfortably between those from V95 and K07b, which are $76.0 \pm 1.3 \text{ km s}^{-1}$ and $79.1 \pm 0.6 \text{ km s}^{-1}$, respectively. The velocity dispersion is also consistent within 1σ of both V95 ($6.7 \pm 1.1 \text{ km s}^{-1}$) and K07b ($6.6 \pm 0.7 \text{ km s}^{-1}$). The weighted average between these three measures is $78.5 \pm 0.4 \text{ km s}^{-1}$ for the systemic velocity and $7.2 \pm 0.3 \text{ km s}^{-1}$ for the velocity dispersion.

We produced three velocity dispersion profiles with 13, 19, or 25 stars per bin in projected radius. The dispersions for the stars within the bins were found by a similar method as described above except we set the systemic velocity equal to the value calculated using all Leo II member stars, which was 78.5 km s^{-1} . These profiles

can be seen in Figure 2.8. The error bars in the radial direction are the standard deviations of the radii in those bins. Errors in the velocity dispersion were found using the same method described above with the covariance matrix. We fit a flat line and a sloped line to each of the velocity dispersion profiles, which are plotted as a dotted line and a dashed line respectively. The reduced χ^2 between these lines and the data are listed in the top right corners of the plots. In all cases, the data are fit equally well by a flat line and a sloped line. Additionally, the error bars on the sloped lines are large enough such that the sloped lines are indistinguishable from a constant dispersion at the 1σ level. Therefore we conclude that the velocity dispersion remains flat at all radii regardless of bin size. These results are in good agreement with K07b who also found a flat profile.

The velocity dispersion can be used to produce a simple mass estimate for Leo II. We used the estimator in Equation 10 of Walker et al. (2009b), which reduces to $M(r_{\text{half}}) = 2.5r_{\text{half}}\sigma^2/G$ when evaluated at the half-light radius. This method assumes that the stars are distributed as a Plummer sphere and have an isotropic velocity distribution with constant dispersion, both of which are reasonable for Leo II. We used $r_{\text{half}} = 176 \pm 42$ pc (McConnachie, 2012) and found $M(r_{\text{half}}) = (5.6 \pm 1.4) \times 10^6 M_{\odot}$. Dividing this mass estimate by half of the total luminosity ($(7.4 \pm 2.0) \times 10^5 L_{\odot}$, Coleman et al., 2007) yields a mass-to-light ratio of $(M/L)_V = 15.2 \pm 5.5$ in solar units, consistent with previous results.

With this sample we can test for signatures of ordered rotation within the dwarf. To do this, we sliced the dwarf in half and computed the difference between the average velocities for each of the two halves. The position angle, θ , of the bisecting line was rotated through 360° , with 0° marking the meridian through the center of Leo II. A sinusoidal pattern is distinguishable as seen in the top panel of Figure 2.9, and it was fitted with $\langle v \rangle = a_1 \sin(\theta + a_2)$, where $a_1 = 1.55$ km s $^{-1}$ (amplitude) and $a_2 = 167.1^\circ$ (phase).

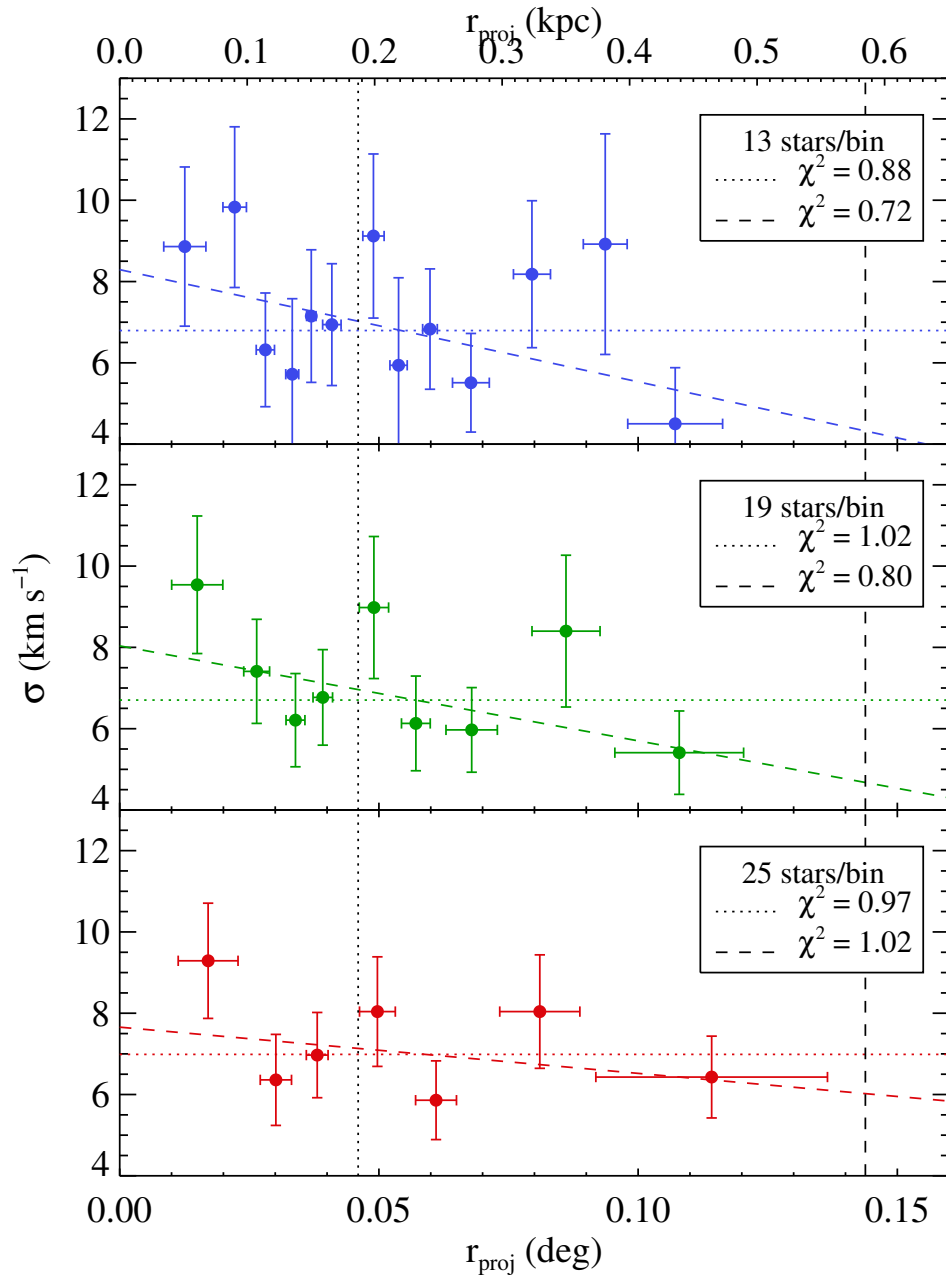


Figure 2.8 The velocity dispersion profile is plotted using three different bin sizes: 12 stars per bin (top), 19 stars per bin (middle), 25 stars per bin (bottom). Errors in the radial direction are the standard deviations of the projected radii for stars in each bin; errors in the velocity dispersion come from the covariance matrix discussed in Section 2.3.2. Black vertical dotted and dashed lines are the core and tidal radii respectively. We fit a flat (dotted) and sloped (dashed) line to each of the profiles. The reduced χ^2 values of the fits are indicated in the plot legends.

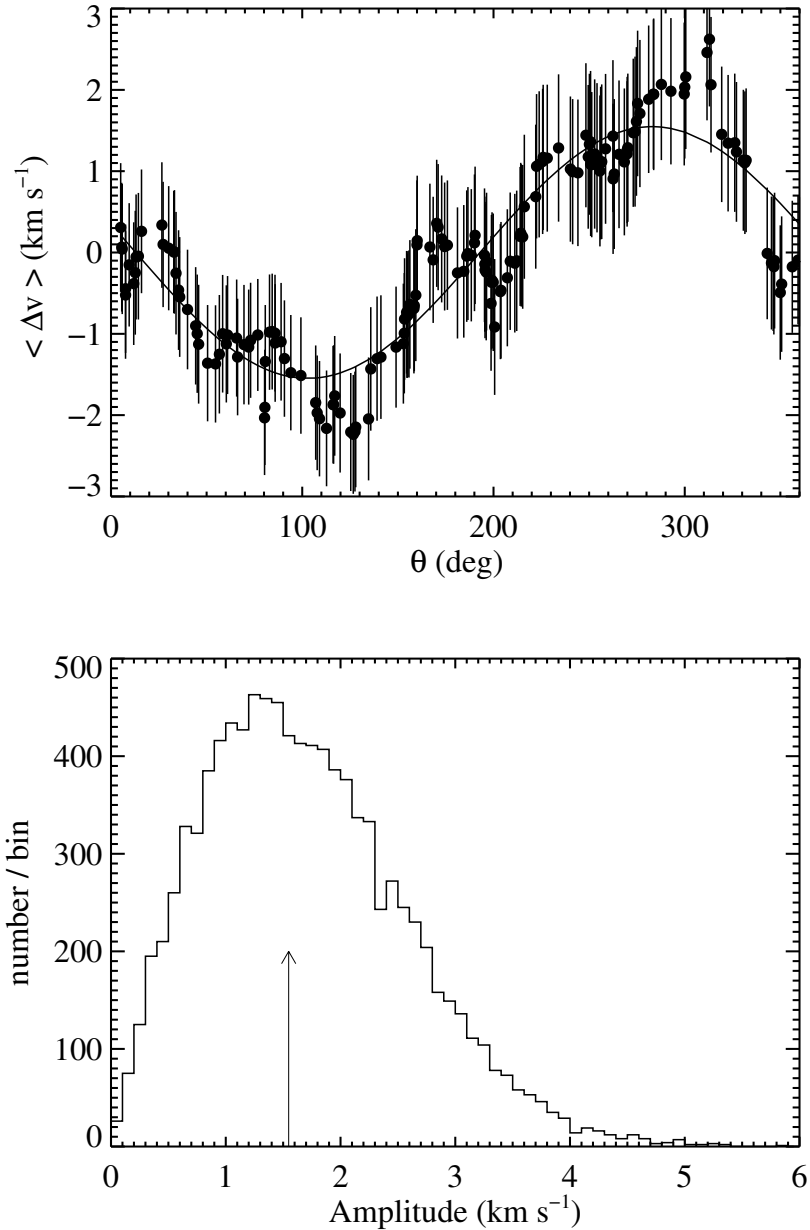


Figure 2.9 Top: the difference between the average velocity of stars on either side of a bisecting line plotted against the position angle of that line. 0° is north; 90° is east. The vertical error bar is treated as the standard deviation of the stellar velocities divided by the square root of half the number of stars. The solid line is the best fit sinusoid to the trend and has an amplitude of 1.55 km s^{-1} . Bottom: we completed 10^4 Monte Carlo realizations and performed the same rotation analysis on them. The amplitudes of these simulations are plotted as a histogram. The vertical arrow marks the location of the amplitude that we recovered for Leo II. Amplitudes larger than this are expected to be present in 52% of non-rotating systems, therefore there is no statistically significant evidence for uniform rotation in Leo II.

To determine the likelihood that a 1.55 km s^{-1} signal could be produced by chance, we generated 10,000 Monte Carlo simulations with stellar positions equal to those of our observations and velocities drawn from a Gaussian having standard deviation equal to the velocity dispersion of Leo II. The bottom panel of Figure 2.9 is a histogram of the amplitudes from these simulations. 52% of the trials have amplitudes larger than what we find in Leo II, thus the signal we find is only significant at a 0.64σ confidence level. From this we conclude that Leo II has no statistically significant, ordered rotation. K07b recovered a slightly stronger signal with an amplitude of $\sim 2 \text{ km s}^{-1}$ and a position angle at 16.5° . They ran similar Monte Carlo tests and found that 87% of the tests had an amplitude greater than 2 km s^{-1} with a highly variable position angle for the peak velocity signal. Thus our conclusion matches that of K07b.

We also completed a test to identify whether any stars clumped in 3D (right ascension, declination, radial velocity) phase space, because such features might indicate a more interesting merger history for Leo II (Coleman et al., 2004; Assmann et al., 2013). We considered the similarity of velocities between stars and their nearest neighbors. For each star we counted how many of its neighbors within a given radius had velocities similar to that star. We considered radii between 10 and 50 arcsec and velocities within 0.5 to 2 km s^{-1} of the central star. To understand if the number of stars in each iteration was significant, we randomly reassigned the velocities to different spatial positions 10,000 times and completed the same exercise. In all cases, no signatures of clumping were found at statistically significant levels.

Having no rotation, clumps, or otherwise interesting kinematic substructure, the only remaining dynamic peculiarity that we find in Leo II is one star located beyond the tidal radius, as can be seen in Figure 2.10. The separation of this star from the center of the dwarf is 1.3 times the tidal radius. A couple other stars are located near the tidal radius, but only one is positioned at least 3σ beyond that boundary. The velocity ($v = 83.0 \text{ km s}^{-1}$), surface gravity ($\log(g) = 1.03 \text{ dex}$), and metallicity

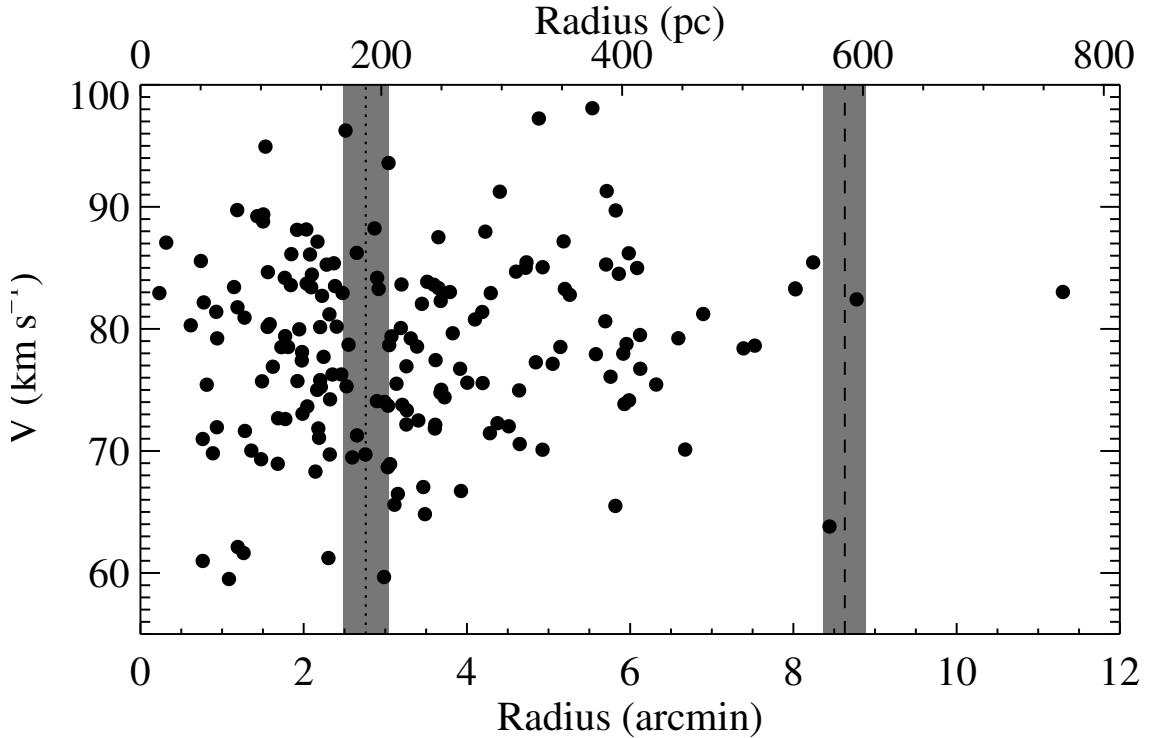


Figure 2.10 Stellar radial velocity versus projected radius from the dSph center. The King core and tidal radii are plotted as vertical dotted and dashed lines respectively. Values for the radii are taken from Komiyama et al. (2007). Errors on these measurements are shown as gray shaded bars. Several stars are found near the tidal radius, but only one is located well beyond this limit. The upper x-axis scale in parsecs is based on a distance of 233 kpc (Bellazzini et al., 2005).

($[\text{Fe}/\text{H}] = -1.66$ dex) of this star are all very close to the mean values for the dwarf. While photometric studies have found stellar overdensities beyond the tidal radius (Komiyama et al., 2007), this is the first extratidal star with kinematic evidence supporting its membership. Our star and the four-star photometric clump found in Komiyama et al. (2007) are separated by ~ 5 arcmin but are both located ~ 11 arcmin from the center on the western side of the dwarf.

The existence of tidal stars in other dwarfs like Ursa Minor (Muñoz et al., 2005) and Carina (Muñoz et al., 2006b) has been attributed to tidal disruption from the Milky Way. The interpretation for the tidal star in Leo II is slightly different because

the dwarf galaxy is located so far away; it is likely encountering the inner parts of the MW dark matter halo for the first time (Lépine et al., 2011) and would not yet exhibit such features. Recent evidence suggests that Leo II is falling into the Milky Way in a tidal stream of satellites comprising Leo IV, Leo V, Crater, and Crater 2 (Torrealba et al., 2016). The positions of both our star and the photometric clump are not aligned with the great circle that connects all five satellites, ruling out the notion that they were caused by streaming motion. Instead, it seems plausible that our star and the clump in Komiyama et al. (2007) are remnants of the interactions between these satellites prior to their disruption. The best interpretation for the four-star cluster in Komiyama et al. (2007) was that a small globular cluster merged with Leo II, which would fit with this scenario. Future studies of Leo II may wish to obtain velocities for stars beyond the tidal radius for more conclusive evidence regarding the nature of these features.

2.3.3 Chemical Features

[Fe/H] stellar metallicities were reported in both K07b and K11. Many of our stars also exist in those papers, so we completed a quick comparison to see if there were any major differences between them. In the top panel of Figure 2.11, we plot [Fe/H] from K07b against our own data. The offset between them is 0.38 dex—as large as the mean scatter—so no real correlation between them can be identified. Since the spectral resolution of their study was less than ours, this result is not surprising. The comparison with K11 is much better for low metallicities, with an offset of only 0.11 dex, but their distribution saturates at $[\text{Fe}/\text{H}] \approx -1$ while ours extends to higher metallicity.

We inspected our spectra of these high-metallicity stars and found that the sky subtraction was poor, leading to some absorption features having negative flux. As a result, these metallicity measurements got pushed to larger values. We identify 13

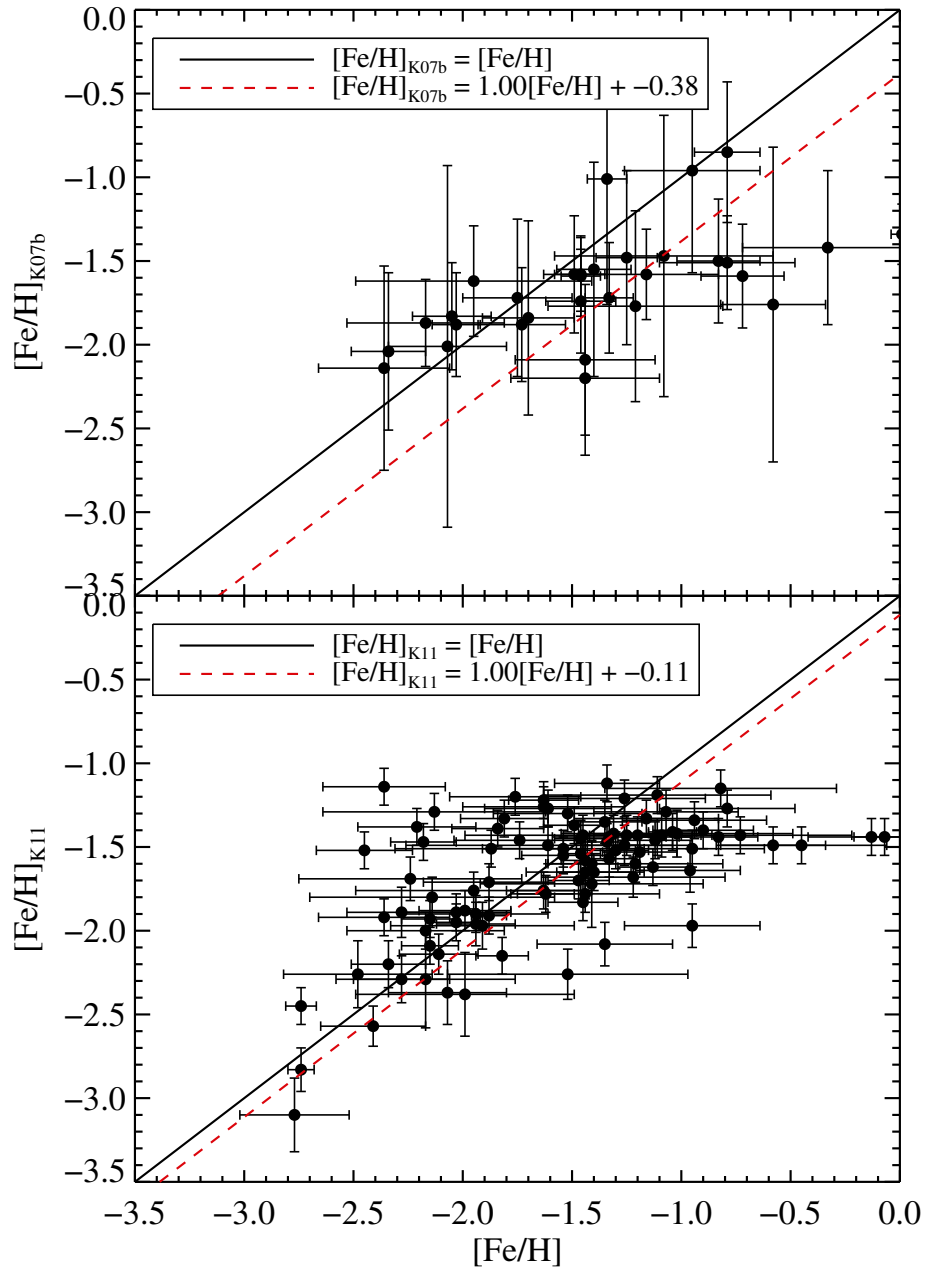


Figure 2.11 A comparison between our $[\text{Fe}/\text{H}]$ measures and those from K07b (top panel) and K11 (bottom panel). Not all stars listed in K07b have published metallicities. The black lines are where stars would fall if there were perfect agreement between the studies. The red lines are the best fits to the data with slope set equal to 1.

such stars in our sample that have metallicities larger than -0.7 dex and remove them for the remaining chemical analysis.

In Figure 2.12 we plot the metallicity distribution function (MDF) for our data and a separate one for K11 as a comparison. These two datasets have similar spatial distributions and thus we might expect the MDF to be comparable for our stars and those in K11. The mean metallicity weighted by the measurement uncertainties in our data is $\langle[\text{Fe}/\text{H}]\rangle = -1.70 \pm 0.02$ dex. The standard deviation uncorrected for measurement errors is 0.48 dex. Correcting for measurement uncertainties as done by K11 instead yields a width of 0.40 dex. The skewness of the distribution is -0.27, which indicates a low-metallicity tail. The (excess) kurtosis is -0.67, which means the MDF is less peaked than a normal distribution. Many of these MDF characterizations are discrepant from the ones published by K11, who report a mean metallicity of $\langle[\text{Fe}/\text{H}]\rangle = -1.62 \pm 0.01$ dex. Their standard deviation and spread corrected for measurement uncertainties are 0.42 and 0.37 dex, and their skewness and kurtosis are -1.11 and 1.10 respectively, implying that our MDF is slightly wider, less peaked, and has a shorter low-metallicity tail than the MDF in K11. All of these features can be seen in Figure 2.12.

Metallicity gradients have been found in about half the classical dSphs of the MW, with the slope in Leo II being the steepest (K11). On the other hand, K07b reports no such gradient for Leo II. In Figure 2.13 we plot the metallicity versus radius of the stars in our sample, once again excluding the 13 stars with erroneous high-metallicity measurements. We fit a flat and sloped line to the data and find that neither provides a very good fit, with reduced χ^2 values of 7.6 and 6.3 respectively. The Pearson correlation coefficient between radius and metallicity is -0.22. Spearman's rank correlation coefficient is -0.17. These coefficients can range from -1 to 1, with values near the endpoints signifying a monotonically decreasing or increasing trend and a value of 0 indicating no correlation in radius and metallicity.

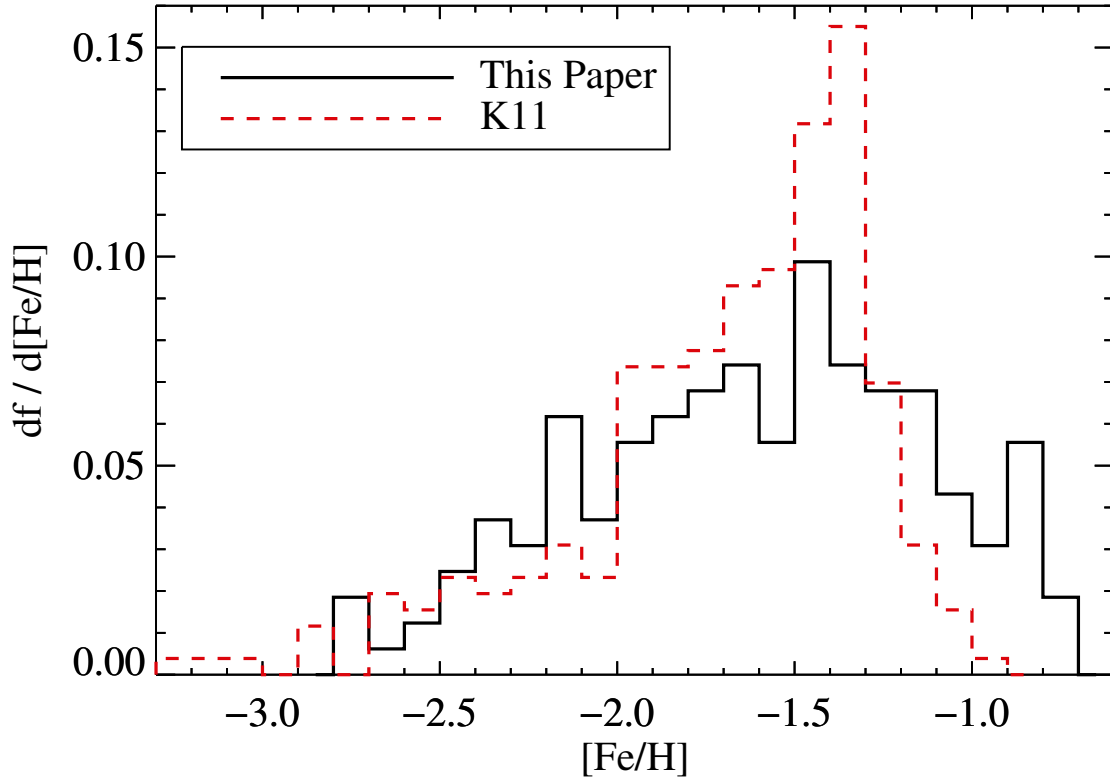


Figure 2.12 Metallicity distribution function of Leo II members with $[\text{Fe}/\text{H}]$ measurements in our dataset (black) and from K11 (red dashed). The true number of stars per bin can be recovered by multiplying the values on the y-axis by the number of stars in the sample (162 for solid black or 258 for red dashed).

Both of the coefficients are near zero, indicating that there is a lot of scatter in the data caused by either large measurement errors or by the absence of a metallicity gradient. We considered the significance of the coefficients by randomly reassigning metallicity measurements to different radius measurements in 10^4 permutations and then recalculating the coefficients. The p -value from this resampling is 0.002 for the Pearson correlation coefficient and 0.018 for Spearman's rank correlation coefficient, thus ruling out the null hypothesis that radius and metallicity are not monotonically correlated. We therefore conclude that there is likely a metallicity gradient but the large measurement errors make it difficult to produce a linear relation that is a good fit to the data.

The metallicity gradient listed in K11 was determined by the slope of a two-parameter best fit line; even though our sloped line is a poor fit to the data, we continue with the analysis to provide a side-by-side comparison of our metallicities and those in K11. The best fitting sloped line to our data yielded a gradient of -5.85 ± 0.39 dex deg $^{-1}$, or -1.53 ± 0.10 dex kpc $^{-1}$ using a distance of 233 kpc (Bellazzini et al., 2005). This slope is somewhat steeper than the metallicity gradient published by K11, who found -4.26 ± 0.31 dex deg $^{-1}$ (-1.11 ± 0.08 dex kpc $^{-1}$, for a distance of 219 kpc). Regardless of the discrepancy between the slope measurements, both indicate that there is a steep metallicity gradient with metal-rich stars clustering toward the center of the galaxy. The existence of a metallicity gradient agrees with the photometric findings that red clump stars are more centrally clustered than blue horizontal branch stars (Bellazzini et al., 2005). This connection arises because high- and low-metallicity red giant branch stars are, respectively, the progenitors for red clump and blue horizontal branch stars.

The tendency for high-metallicity stars to be in a colder, less extended distribution than the low-metallicity stars is seen in many resolved dwarfs: for example, Fornax (Battaglia et al., 2006), Sculptor (Battaglia et al., 2008), and Sextans (Battaglia et al.,

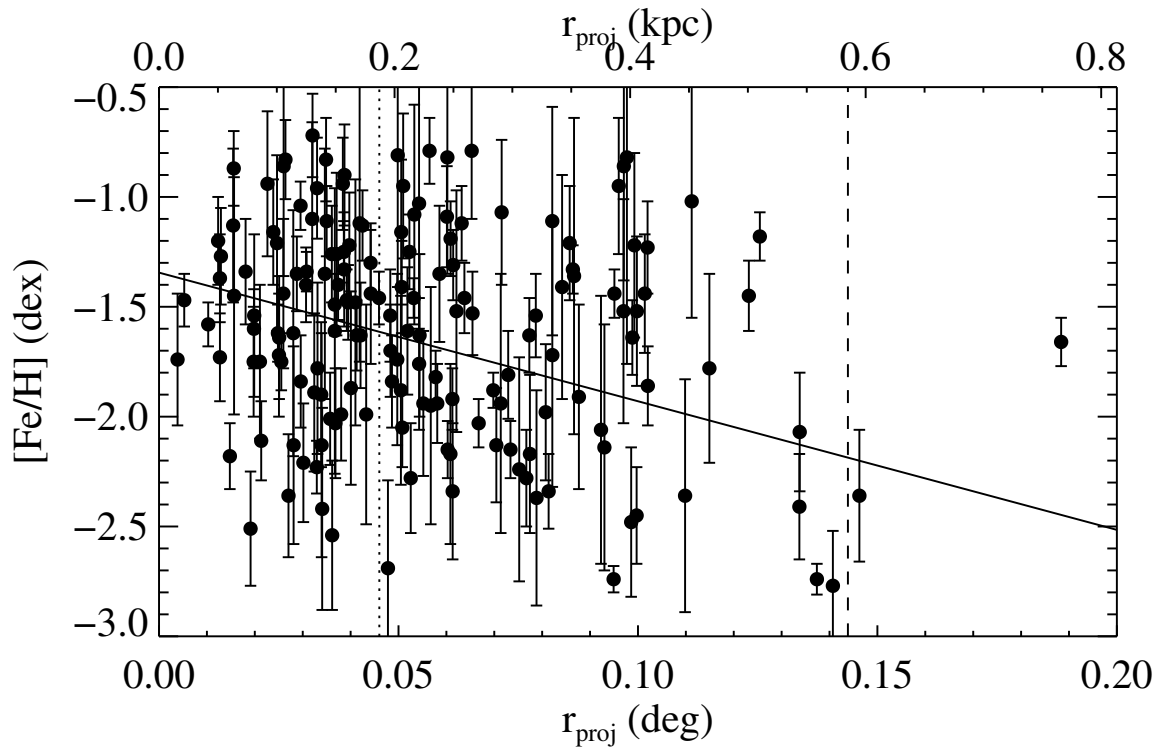


Figure 2.13 The metallicities of the member stars are plotted against their separations from the dSph center. Core and tidal radii are shown as vertical dotted and dashed lines, respectively. The solid black line is the best fitting linear function to the data and has a slope (metallicity gradient) of $-5.85 \pm 0.39 \text{ dex deg}^{-1}$, or $-1.53 \pm 0.10 \text{ dex kpc}^{-1}$ assuming a distance of 233 kpc (Bellazzini et al., 2005).

2011). We explored the possibility that Leo II might also show different chemodynamic populations by first splitting the stars into two groups by the $[\text{Fe}/\text{H}]$ mean, such that high-metallicity stars have $[\text{Fe}/\text{H}] > -1.7$ and low-metallicity stars have $[\text{Fe}/\text{H}] < -1.7$. Then we plotted the velocity dispersion profiles for these selections, which can be seen in Figure 2.14. The dispersion for the low-metallicity stars (blue points) is always larger than the dispersion for the high-metallicity stars (red points), but given the large error bars, the two profiles are consistent with being the same. We also calculated the overall dispersion for each of the two supposed populations. The high-metallicity stars have a velocity dispersion of $7.04 \pm 0.54 \text{ km s}^{-1}$ and the low-metallicity stars have a dispersion of $8.13 \pm 0.74 \text{ km s}^{-1}$. Once again, we find that the values suggest the high-metallicity stars are kinematically colder, but when the errors are considered it is only a 1.2σ detection.

As one final test, we allowed the value of the split between high and low metallicity to vary from $[\text{Fe}/\text{H}] = -2.2 \text{ dex}$ to $[\text{Fe}/\text{H}] = -1.1 \text{ dex}$ in steps of 0.05 dex , as opposed to fixing it at the mean of -1.7 dex . In all but one case, the high-metallicity dispersion was less than the low-metallicity dispersion, but the error bars made the results not significant beyond 1.6σ at the most. Furthermore, we tried removing any stars with metallicities within 0.1 dex of the split value, as these stars might dampen the signal. The results were the same as before, though with slightly less significance. Taking all of the evidence together, it seems possible that there might be a slight chemodynamic bifurcation whereby high-metallicity stars have a larger velocity dispersion than low-metallicity stars due to the fact that this was repeatedly the trend in our data. Nevertheless, our large error bars caused by sample size and measurement error make it impossible to state this claim with more than $\sim 1\sigma$ confidence. A larger sample of stars with individual velocity precisions $\lesssim 2 \text{ km s}^{-1}$ will be needed to explore the question of multiple chemical populations in Leo II definitively.

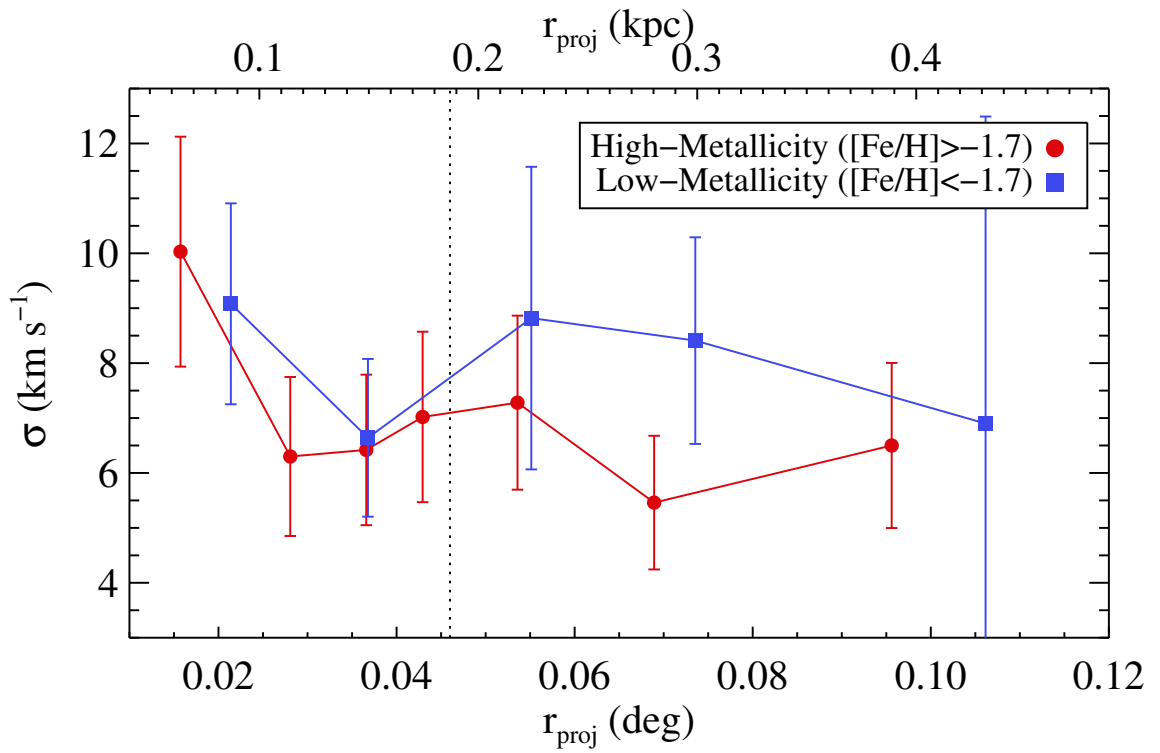


Figure 2.14 The velocity dispersion profiles for high-metallicity stars (red circles, $[\text{Fe}/\text{H}] > -1.70$) and low-metallicity stars (blue squares, $[\text{Fe}/\text{H}] < -1.70$). There are 13 stars in each bin. The core radius is shown by a vertical dotted line.

2.4 Summary and Conclusions

In total we spectroscopically observed 336 stars within Leo II and determined that 175 of them are members based on radial velocities ($57.3 < v_{\text{mem}} < 100.5 \text{ km s}^{-1}$) and surface gravities ($\log(g)_{\text{mem}} \leq 4$). Many of the observed stars extend beyond the tidal radius of the dwarf into regions not previously studied by other publications, but only one of these extratidal stars is a member according to our constraints. Other than this one star, there are no signs of tidal disruption or rotation in the dwarf. By maximizing the likelihood that the velocities of these stars were drawn from a normal distribution, we determined that the systemic velocity of the dwarf is $78.5 \pm 0.6 \text{ km s}^{-1}$, and its velocity dispersion is $7.4 \pm 0.4 \text{ km s}^{-1}$. The velocity dispersion profile is consistent with being flat even when using three different bin sizes, suggesting that Leo II is embedded in a massive dark matter halo that extends well beyond the tidal radius. Using the mass estimator from Walker et al. (2009b), we determined the corresponding mass for Leo II to be $M(r_{\text{half}}) = 5.6 \pm 1.4 \times 10^6 M_{\odot}$ and its mass-to-light ratio to be $(M/L)_V = 15.2 \pm 5.5$ in solar units.

The mean metallicity of the member stars is $\langle [\text{Fe}/\text{H}] \rangle = -1.70 \pm 0.02 \text{ dex}$, which is only slightly higher than average for dSphs of the MW. The shape of the metallicity distribution function is wider, less peaked, and has a shorter low-metallicity tail than the MDF reported in K11. Additionally, we found that Leo II has a steep metallicity gradient of $-5.85 \pm 0.39 \text{ dex deg}^{-1}$ ($-1.53 \pm 0.10 \text{ dex kpc}^{-1}$). Lastly we used three tests to look for differences in the dynamics of high- and low-metallicity stars. In all cases, the results had low signal but were consistent with a model that has correlated metallicities and kinematics.

The dataset that we have compiled adds eight epochs of observation between the years 2006 and 2013 for stars in Leo II. Fifty of these stars were observed on more than one occasion, with the maximum number of repeat observations being five. Combining our MMT data with the data from V95, K07b, and K11, there are 372

stars that are likely members of Leo II and 196 stars with repeat observations. Given the wealth of temporal radial velocity measurements, it is now possible to determine the binary fraction of stars in Leo II and evaluate the impact that these stars have on the measured velocity dispersion. The proposed analysis is carried out in Spencer et al. (2017b), which is the next chapter of this dissertation.

CHAPTER III

The Binary Fraction in Leo II

3.1 Introduction

Within the solar neighborhood, there are approximately one to two times as many binary star systems as single stars (Duquennoy & Mayor, 1991; Raghavan et al., 2010). The presence of binary systems is also expected within dwarf galaxies, but the quantity is largely unknown. If the fraction is similar to the solar neighborhood, then the additional radial velocity components of the binary systems can inflate the observed velocity dispersion in some dSphs, which can impact inferences that draw upon the kinematics, such as mass estimates. This effect can be corrected if the attributes of the binary population—including binary fraction and orbital parameter distributions like period, mass ratio, and eccentricity—are well measured. Measurements of the binary populations are also helpful in predicting the frequency of type Ia supernova and in putting constraints on star formation processes in dSphs.

A recent, detailed binary analysis has been performed on Carina, Fornax, Sculptor, and Sextans (Minor, 2013), but not for the remaining Milky Way dSphs, Draco, Ursa Minor, Leo I, and Leo II. In this chapter, we turn our attention to Leo II. Relatively few spectroscopic observations have been taken for this dwarf galaxy due to its large distance away from the Milky Way (233 ± 15 kpc, Bellazzini et al., 2005). Spencer et al. (2017a) significantly expanded upon preexisting data by adding radial velocities from

MMT/Hectochelle for 175 member stars over the course of eight years with as many as five observational epochs per star. Combining this with other studies (Vogt et al., 1995; Koch et al., 2007b; Kirby et al., 2010) now makes it possible to perform an extensive analysis on the binary fraction in Leo II.

This chapter is organized as follows. In Section 3.2 we introduce the dataset for Leo II. In Section 3.3 we describe the methodology for determining the binary fraction of a dwarf galaxy. Section 3.4 contains the results for Leo II and Section 3.4.3 quantifies the implications for ultra-faints. The summary and conclusions are in Section 3.5.

3.2 Radial Velocities

We use radial velocity data from four studies, which are summarized in Table 3.2. The first set comprises 31 red giant branch (RGB) stars with a median radial velocity error of 3 km s^{-1} (Vogt et al., 1995, hereafter V95). It contains the first spectroscopic observations of RGB stars in Leo II, and remained the only kinematic dataset for over a decade. The second study, by Koch et al. (2007b, hereafter KK07), consists of radial velocities for 171 member stars. KK07 published average velocities taken during three epochs between 2003 and 2004. Velocity measures that are averaged over more than a few days (as in KK07) will damp out the velocity changes caused by binaries. Instead, we used the unpublished single-epoch velocity measures, which were taken on the three dates listed in KK07. We have included these velocities in Table F.1 of the appendices. The drawback of using the non-averaged velocities in KK07 is that the error bars can be very large (up to $\sim 140 \text{ km s}^{-1}$). We chose to exclude KK07 measurements with errors larger than 35 km s^{-1} or measurements with the square of the velocity deviation from the mean over the square of the velocity error, $(v_i - \bar{v})^2/\sigma_i^2$, larger than three. This removed 20 measurements from the two epochs in 2003 and leaves us with a median velocity error of 2.8 km s^{-1} for the

remaining sample.

The third dataset comes from Kirby et al. (2010, hereafter, KG10). They used Keck/DEIMOS to obtain medium resolution spectroscopy for the purpose of chemical abundance measurements, but also extracted radial velocities to help identify member stars. This was done by cross-correlating the red half of each spectrum with a set of template spectra from Simon & Geha (2007). The cross-correlation peak from the best fitting spectrum was adopted as the velocity. Velocity errors were calculated by resampling the spectrum 1000 times with different noise realizations. The error was the quadrature sum of the systematic error floor (2.2 km s^{-1} , Simon & Geha, 2007) and the standard deviation of the 1000 velocity trials. These measurements were not published in KG10, so we include them in Table F.1. Additional details of the observations can be found in KG10. This dataset contains one epoch of velocities for 258 stars with a median error of 2.3 km s^{-1} .

The fourth and final dataset is published in Spencer et al. (2017a, hereafter, S17a), which contains radial velocities for 175 member stars. Fifty of these have two or more observations, which were taken over the course of eight years with Hectochelle (Szentgyorgyi et al., 1998) on the Multiple Mirror Telescope. This dataset contains five epochs between the years 2006 and 2013. The median error for these velocities is 1.1 km s^{-1} . Histograms of the error bars for each of these four studies are shown in Figure 3.1.

We note that Bosler et al. (2007) reported velocities for 74 stars, but since their focus was on stellar chemistry rather than kinematics and their radial velocity errors are $\sim 50 \text{ km s}^{-1}$, the data are not precise enough for us to use in this study.

Taking these four datasets together, the total number of unique RGB stars with multiple observations in Leo II is 196. In Figure 3.2, we plot some useful quantities to help summarize this larger dataset. The top panel shows the number of observations per star, with the maximum being seven observations. The middle panel has the

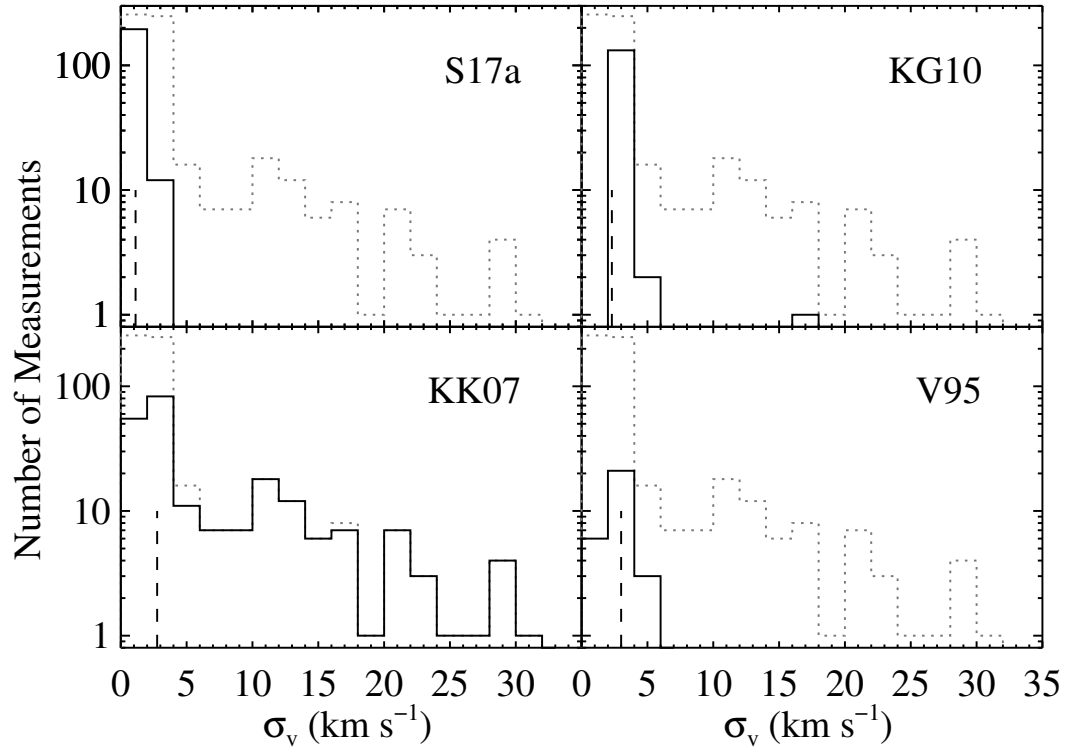


Figure 3.1 Histograms of the radial velocity errors for each of the four datasets are shown as solid black lines. Vertical black dashed lines show the median error for each of the four datasets. The gray dotted line is the histogram of the velocity errors for the combined data set. Only measurements for stars with more than one observation are plotted (i.e., the measurements in Table F.1).

maximum time baseline for each star. This ranges from 11 days to nearly 19 years. Finally the bottom panel shows the number of observations taken per year. The years are labeled with the study that contributed to them. In total, we have 596 independent velocity measurements. Table 3.2 summarizes the systemic velocity, velocity dispersion, median velocity error, number of stars, and number of epochs contained in each of the four studies.

Table F.1 in the appendices lists the measurements that we used in this study. Column 1 is an id number that we assign to each unique star. Column 2 is the number of observations for that star. Columns 3 and 4 contain the coordinates. Column 5 lists the Heliocentric Julian date when the observations were made. Column 6 has the radial velocity and uncertainty after adjusting for any systematic offsets (see the next paragraph). Column 7 lists the relevant paper. Measurements from V95 and S17a have been previously published, whereas measurements referencing KK07 and KG10 have not. Only stars that had more than one observation are included in the table.

As a consequence of combining data from different spectroscopic surveys, we needed to identify if there were any systematic offsets present between the studies. Figure 3.3 shows average velocities from S17a plotted against the average velocities reported in V95, KK07, and KG10 when stars existed in both catalogs. For each comparison, we fit a line weighted on the ordinate errors and set the slope equal to one. Stars with velocities that disagreed by more than 10 km s^{-1} were excluded from the fit because their large velocity variations are not likely to be caused by systematic offsets. Such stars pulled the fit lines away from the main group of stars, especially since they all had small error bars, as was found by inspection. The seven stars that fall into this category are plotted as open triangles. Finally, we took the resulting y -intercept of the best-fit line as the systematic offset between the external datasets and our dataset in S17a. We subtracted these corrections, such that the correspond-

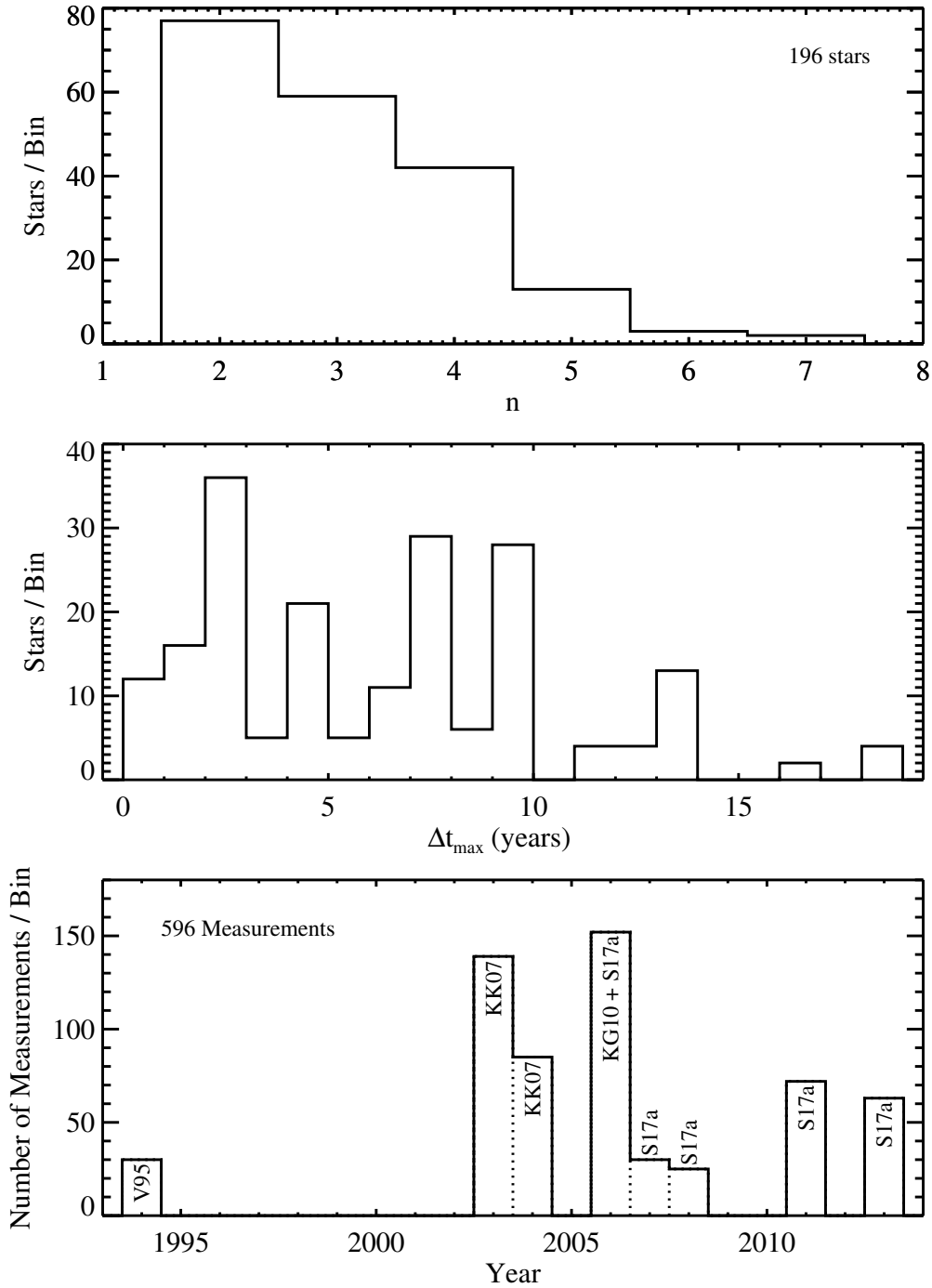


Figure 3.2 Top: number of observations per star for the 196 stars in the sample. Middle: longest time separation between measurements per star. Bottom: number of velocity measurements per year for the 596 measurements in the sample. Bins are labeled with the paper that contributed those measurements.

Table 3.1. Papers with radial velocity data in Leo II

Measure	S17a	KG10	KK07	V95
Systemic Velocity (km s ⁻¹)	78.3±0.6	Not Reported	79.1±0.6	76±1.3
Velocity Dispersion (km s ⁻¹)	7.4±0.4	Not Reported	6.6 ±0.7	6.7±1.1
Median Velocity Error (km s ⁻¹)	1.1	2.3	2.8	3.0
Number of Stars	175	258	171	31
Number of Epochs	5	1	3	1

ing velocities follow the form $v_{\text{study_corrected}} = v_{\text{study}} - \text{offset}$. The offset values are -0.84 km s⁻¹ for V95, 0.66 km s⁻¹ for KK07, and 0.61 km s⁻¹ for KG10.

3.2.1 Velocity variability

Although the goal of this chapter is to determine the binary fraction of the galaxy, we can also use our dataset to single out individual stars that are binary candidates. These stars will show velocity variability that cannot be accounted for by the velocity measurement uncertainties.

For each star with multiple observations, we calculated the reduced chi squared statistic as

$$\chi_{\kappa}^2 = \frac{1}{\kappa} \sum_i^n \left(\frac{v_i - \langle v \rangle}{\sigma_i} \right)^2, \quad (3.1)$$

where v_i is a single velocity measurement, $\langle v \rangle$ is the average weighted velocity of the star, σ_i is the corresponding velocity measurement error, $\kappa = n - 1$ is the number of degrees of freedom, and n is the number of observations per star¹. For reference, the number of stars with a given n is plotted in the top panel of Figure 3.2. The probability of exceeding χ_{κ}^2 is $P(\chi^2, \kappa)$. A histogram of these probabilities is shown in Figure 3.4. If no binaries are present, then this distribution should be uniform over all probabilities, which equates to about two stars per bin. Alternatively, if binaries are present, they would cause a spike in the number of stars with low $P(\chi^2, \kappa)$ (i.e., the

¹Although this definition of χ^2 is atypical, it is valid notation because it considers the variance of random normal deviates, that is to say, each v_i is normally distributed about its mean value $\langle v \rangle$. It then follows that our assumption about the uniform shape of $P(\chi^2, \kappa)$ is also valid.

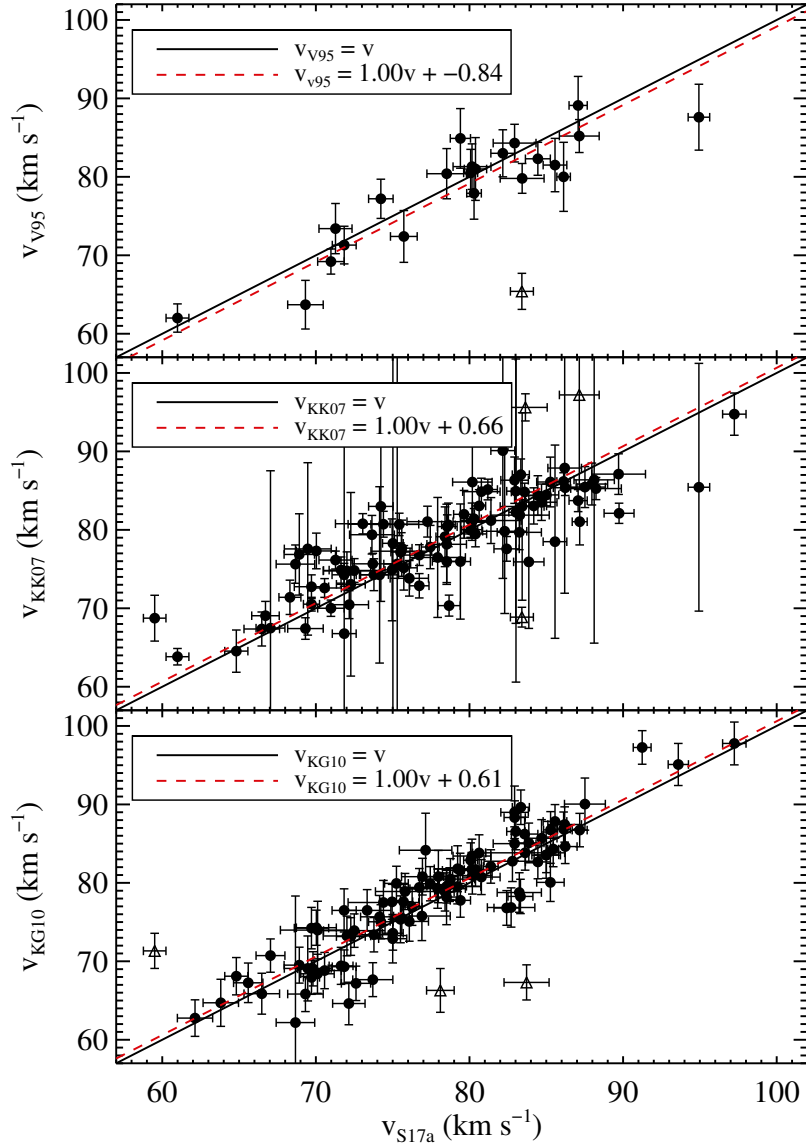


Figure 3.3 Radial velocities measured by S17a versus velocities measured by other papers. Top: V95 had 23 stars that overlapped with our survey. Middle: KK07 had 97 overlapping stars. Bottom: KG10 had 97 overlapping stars. The solid black line indicates where stars would be if the measurements perfectly matched. The dashed red line indicates the best fit to the data after setting the slope equal to 1. Stars that had different velocities by more than 10 km s^{-1} were not included in the fit, and are shown by open triangles. The y -intercept of this line is the systematic offset between the datasets and was subtracted from the respective datasets.

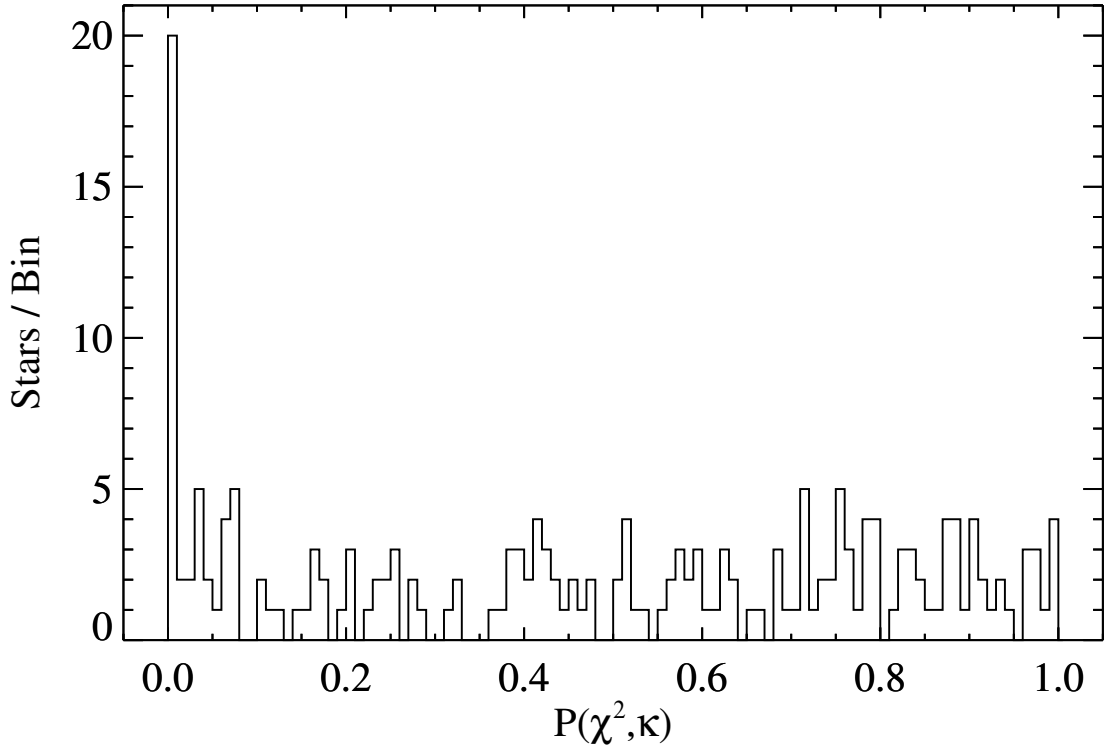


Figure 3.4 Probability of exceeding χ_κ^2 for each star. Stars that are likely binaries will have $P(\chi^2, \kappa) < 0.01$. 20 stars fall into this region and the expectation is only 2.

stars with high values of χ^2). The latter case is precisely what we see in Figure 3.4. The bin with $P(\chi^2, \kappa) < 0.01$ contains 20 stars rather than the null hypothesis of two stars. Most of these 20 stars have only two observations (though some have three or four), so we do not have enough temporal data to map out the orbits. It is therefore impossible to say which of the stars would fall in this low $P(\chi^2, \kappa)$ range naturally and which would have been moved into this bin as the result of binary motion.

The amplitude of the velocity variability for these stars is illustrated in the top two panels of Figure 3.5. A sample of nine stars that do not fall into this category, and thus have small velocity variability, are shown in the bottom panel as a comparison. The figure is essentially a glorified table; the difference between the weighted mean velocity of a star and its individual velocity measurements is plotted along the y-axis,

and the x-axis simply serves as a way to separate one observation from another. Stars are distinguished by vertical gray dashed lines. Along the top edge of each panel, we list the probability corresponding to each star. For the first two panels, we listed the logarithm of $P(\chi^2, \kappa)$ because some of these probabilities are very small, but in the last panel it is simply $P(\chi^2, \kappa)$. The small number of observations per star limits our ability to constrain the binary properties or to draw velocity curves, hence our reason for not plotting time along the x-axis.

The number of stars in the bin $P(\chi^2, \kappa) < 0.01$ can be used to derive the lower limit for the binary fraction. If all 20 of the stars are binaries, then the fraction would be 0.10. Given the variation in the number of stars per bin in the histogram, (i.e. 0 to 5) it is also plausible that only 15 of them are binaries, which produces a binary fraction of 0.08. We adopt the smaller of these as the minimum binary fraction for Leo II.

3.3 Methodology

The method we use to find the binary fraction is to first generate a series of radial velocity Monte Carlo simulations that have the same velocity uncertainties and temporal observations as our real data. Then we use Bayesian analysis to compare the simulations to the data and ultimately determine which binary fraction can best reproduce the observed velocities in Leo II.

In Section 3.3.1, we describe the seven binary orbital parameters that contribute to the radial velocity component of binary motion. In Section 3.3.2, we list the steps in the Monte Carlo simulations and explain how we can use an observable—called β —to perform Bayesian analysis. Section 3.3.3 gives the details of the Bayesian analysis, and Section 3.3.4 shows how we extract the binary fraction from the posterior probability distribution.

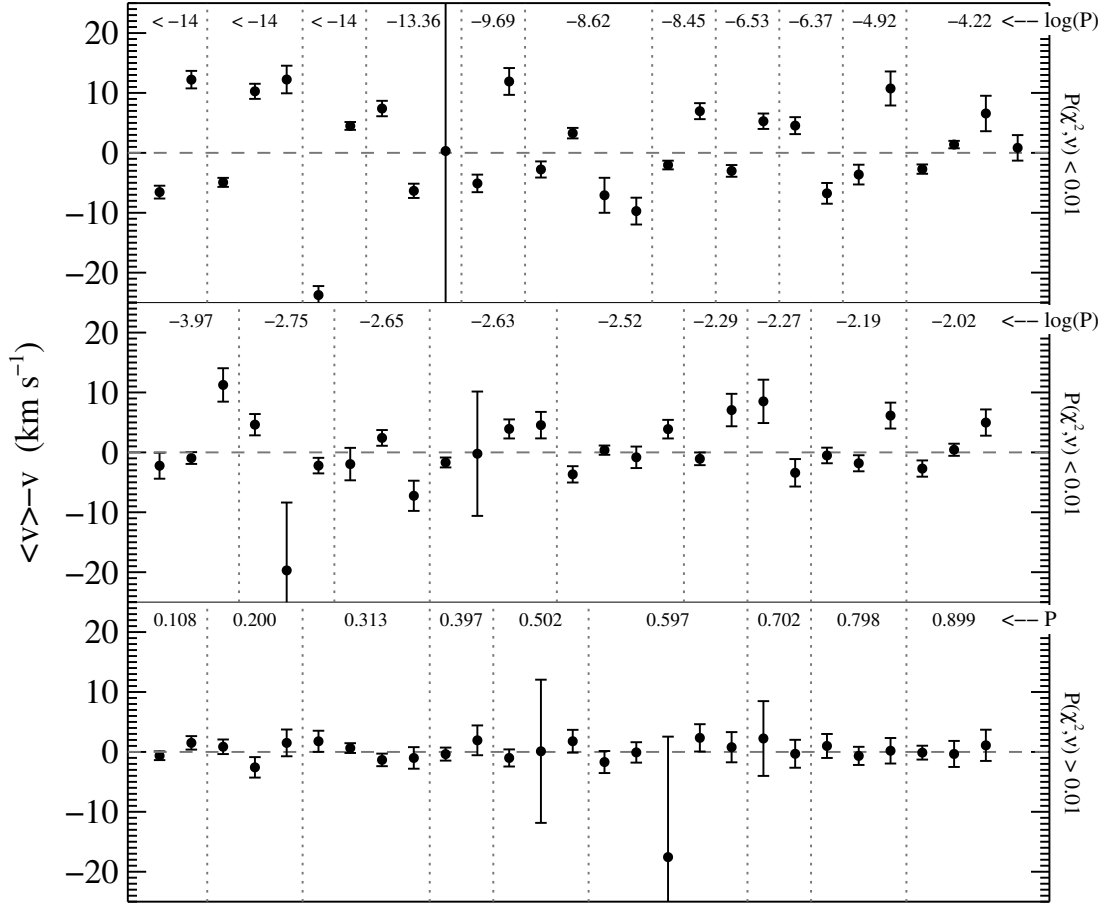


Figure 3.5 Mean velocity for a star minus the individual velocity measures of that star. Observations are evenly spaced along the x-axis, and vertical gray dashed lines separate the velocities from one star to another. The top two panels of the plot show the 20 stars with $P(\chi^2, \nu) < 0.01$, and the bottom panel shows 9 stars with $P(\chi^2, \nu) > 0.01$ for comparison. $\log P(\chi^2, \nu)$ for each star is listed at the top of the upper two panels and $P(\chi^2, \nu)$ is listed at the top of the last panel.

3.3.1 Binary Orbital Parameters

We start by writing the observed radial velocity associated with the orbital motion of a binary star, which can be expressed as

$$v_{r,orb} = \frac{q \sin i}{\sqrt{1 - e^2}} \left(\frac{2\pi G m_1}{P(1 + q)^2} \right)^{1/3} (\cos(\theta + \omega) + e \cos \omega) \quad (3.2)$$

(for a detailed derivation of this equation, see Appendix A). Note that this equation gives velocity relative to the system center of mass, which is what we observe. The seven parameters that characterize the orbital radial velocity are the mass of the primary (m_1), mass ratio (q), eccentricity (e), period (P), true anomaly (θ), angle of inclination (i), and argument of periastron (ω). Some are intrinsic to the system (m_1 , q , e , P), and others depend on the observational circumstances (θ , i , ω). A diagram of the parameter distributions used in this analysis is shown in Figure 3.6.

For the intrinsic parameters, we have adopted the distributions from Duquennoy & Mayor (1991) and Raghavan et al. (2010), which are both based on Sun-like stars in the solar neighborhood. We have selected these distributions over the options in other papers (e.g., Fischer & Marcy, 1992; Reid & Gizis, 1997; Marks & Kroupa, 2011) so that we can perform a side by side comparison between our results and those of Minor (2013). Furthermore, the distributions in these two papers for mass ratio and eccentricity are quite different, allowing use to get a sense of how big of a role they play in our analysis of the binary fraction. The lack of knowledge on the actual distributions for red giant stars in dSphs is the largest limiting factor in constraining the binary fraction in Leo II. Due to this shortcoming, additional distributions should be explored in subsequent analyses, especially those with different period distributions, as we will see in Section 3.4.

One exception to the distributions is m_1 , which we fix at $m_1 = 0.8 M_\odot$. Our primary stars are all red giants and thus must have a mass around this value (Hargreaves

et al., 1996a).

Next is the distribution of the mass ratio between binary stars, which is defined as $q = m_2/m_1$. The variable m_1 is the mass of the visible star and m_2 is the mass of the secondary star. We assumed the secondary star must be a non-remnant, non-giant star and must therefore have a mass $\leq m_1$. It then follows that $q \leq 1$. We set the minimum mass ratio equal to $q_{min} = 0.1$, such that the smallest companion is a hydrogen-burning object. The distribution for q from Duquennoy & Mayor (1991) takes the form

$$\frac{dN}{dq} \propto \exp\left(-\frac{(q - \mu_q)^2}{2\sigma_q^2}\right), \quad (3.3)$$

where $\mu_q = 0.23$ and $\sigma_q = 0.42$. Alternatively, Raghavan et al. (2010) finds a flat mass ratio distribution such that $\frac{dN}{dq} \propto const.$ Both of these distributions are plotted in panel A of Figure 3.6 and will be considered in this analysis.

We take the period distribution from Duquennoy & Mayor (1991), which has the log-normal form

$$\frac{dN}{d\log P} \propto \exp\left(-\frac{(\log P - \mu_{\log P})^2}{2\sigma_{\log P}^2}\right). \quad (3.4)$$

For periods measured in days, $\mu_{\log P} = 4.8$ and $\sigma_{\log P} = 2.3$. Raghavan et al. (2010) finds a similar distribution but with $\mu_{\log P} = 5.03$ and $\sigma_{\log P} = 2.28$. Since these two distributions are very similar, we choose to use the parameterization from Duquennoy & Mayor (1991). The minimum period possible for a binary corresponds to the minimum semi-major axis of the system, which is when the two stars are orbiting such that their surfaces are just out of contact. In our case, the primary is a red giant so the separation can be estimated as the radius of the larger star. Using a surface gravity of 10 cm s^{-2} and a mass of $0.8 M_\odot$ yields a radius of $a_{min} = 0.21 \text{ AU}$. When $q = 0.1$, this corresponds to a period of $\log P_{min} = 1.57$ (or 37.4 days), and when $q = 1.0$ this is $\log P_{min} = 1.44$ (or 27.8 days). These minima are plotted as the left two vertical lines in panel B of Figure 3.6. For the maximum semi-major axis (and

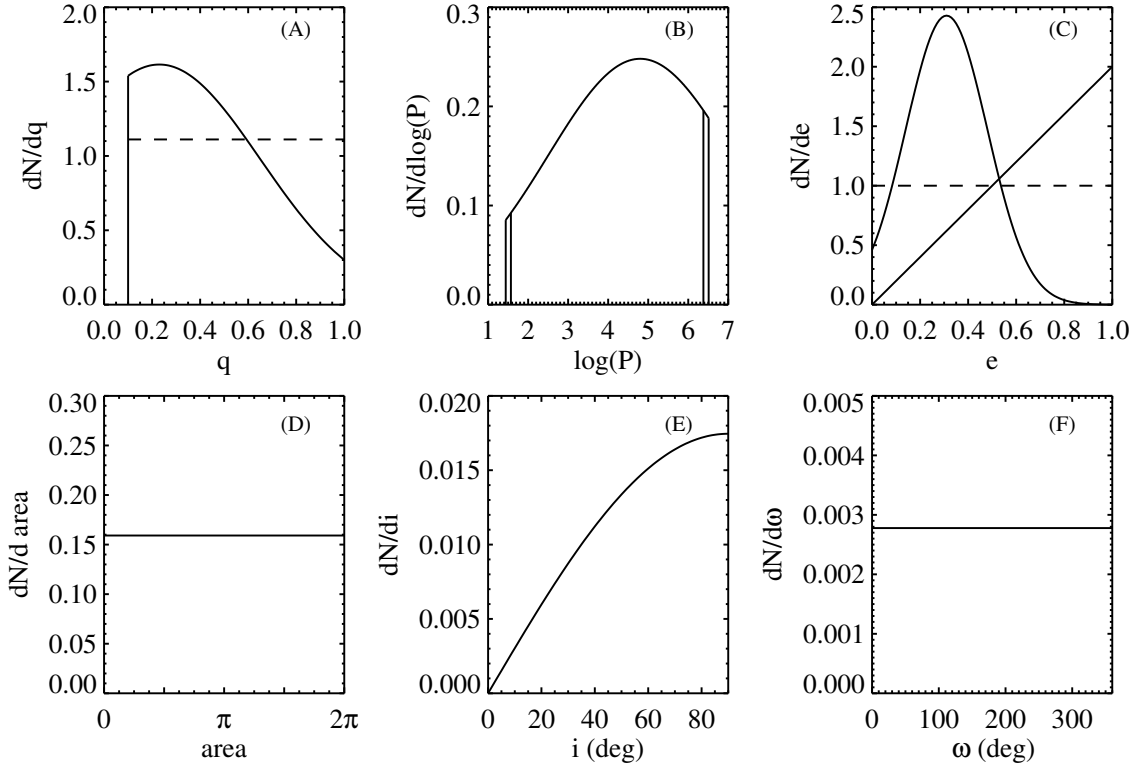


Figure 3.6 Probability distribution functions for six of the binary parameters: mass ratio (A), period (B), eccentricity (C), area swept out since pericenter at time of first observation (D), inclination (E), and argument of periastron (F). Panels A and C show the distributions from Duquennoy & Mayor (1991) as solid lines and the distributions from Raghavan et al. (2010) as dashed lines. The eccentricity distribution in Panel C from Duquennoy & Mayor (1991) depends on the period. The normally distributed function is for $\log P < 3$ and the linear function is for $\log P > 3$.

thus maximum period), we solve for the impact parameter of a star traveling through Leo II, such that $a_{max} = (\pi v t n)^{-1/2}$. $v = 7.4 \text{ km s}^{-1}$ is the velocity dispersion (S17a) and $t = 9 \times 10^9$ years is the average age of the main population of stars (Mighell & Rich, 1996). Assuming an average star has mass $0.4 M_\odot$ and $(L/L_\odot) = (M/M_\odot)^4$, then the average luminosity is $0.025 L_\odot$. The central luminosity density of Leo II is $I_0 = 0.029 L_\odot \text{ pc}^{-3}$ (Mateo, 1998), and so the volume that one star occupies is 0.88 pc^3 . The number density is then $n = 1.14 \text{ stars pc}^{-3}$. (For comparison, the number density of the solar neighborhood is about $0.13 \text{ stars pc}^{-3}$, Chabrier, 2001). This produces a maximum semi-major axis of 412 au. Once again, when $q = 0.1$, this corresponds to a period of $\log P_{min} = 6.51 \log(\text{days})$, and when $q = 1.0$ this is $\log P_{min} = 6.38 \log(\text{days})$. These maxima are plotted as the right two vertical lines in panel B of Figure 3.6.

The last intrinsic parameter is eccentricity, which has perhaps the least certain distribution of all. In principle, this parameter can range from 0 to 1, but in practice the upper limit is often times smaller due to the constraints placed on period and mass ratio. The maximum eccentricity that keeps the stars from colliding is $e_{max} = 1 - (a_{min}/a)$, where a is the semi-major axis that corresponds to P and q from above. Duquennoy & Mayor (1991) found that the eccentricity distribution is a piecewise function that depends on period in such a way that

$$\frac{dN}{de} \propto \begin{cases} \exp\left(-\frac{(e-\mu_e)^2}{2\sigma_e^2}\right) & \text{if } 1.08 < \log P < 3 \\ 2e & \text{if } \log P > 3. \end{cases} \quad (3.5)$$

The shape of the first function was only based on 16 stars, so Duquennoy & Mayor (1991) do not list parameter values. However, since we required a quantitative distribution, we took the mean $\mu_e = 0.31$ and standard deviation $\sigma_e = 0.17$ of these stars for the parameters of this distribution. On the other hand, Raghavan et al. (2010) claimed that the eccentricities for all stars with $\log P > 1.08$ followed a single flat

distribution: $\frac{dN}{de} \propto \text{const.}$ Both studies agreed that the eccentricity for binaries with $\log P < 1.08$ would be 0 (circular) due to tidal interactions between the stars, but since we estimated the minimum period for red giants in Leo II to be $\log P_{min} = 1.44$, we do not need to include this case in our analysis.

The fifth parameter, θ , is the angle between lines connecting the periastron to the focus and the focus to the star (see, Figure 1.2). This is called the true anomaly, and it is simply telling us the phase of the star within its orbit. Periastron is at $\theta = 0^\circ$ (or 360°) and apastron is at $\theta = 180^\circ$. All other angles representing locations between these points are dependent on the eccentricity. Due to its dependence on eccentricity, the probability density distribution for θ does not have an analytic solution². Instead, we pick the star's location within its orbit from the area swept out since periastron, and normalize it such that the area is 0 (or 2π) at periastron and π at apastron. From Kepler's Second Law, we know that equal areas are swept out in equal times, and thus

$$\frac{dN}{d \text{ area}} = \text{const.} \quad (3.6)$$

Due to the way we have normalized it, this area is also known as the mean anomaly. We can then numerically solve for the true anomaly using the mean anomaly and the eccentricity. It is important to note that the mean anomaly for the first observation of the star can be drawn at random from Equation 3.6, but all subsequent mean anomalies that correspond to additional observations of a star are defined as $\text{area} = \text{area}_1 + (2\pi\Delta t/P)$, where Δt is the time elapsed since the first observation.

The final two parameters concern the orientation of the system relative to our line of sight. The first of these is the angle of inclination, i , between our line of sight and the normal to the orbital plane. The probability distribution of the inclination angle is given by

$$\frac{dN}{di} \propto \sin(i) \quad (3.7)$$

²Once exception is the circular case where $e = 0$, then $dN/d\theta = \text{const.}$

where i ranges from 0° (face on) to 90° (edge on).

Last is the argument of periastron, which defines the angle of the ascending node of the orbit relative to the periastron point; this orientation is random and so ω takes on the simple form

$$\frac{dN}{d\omega} \propto \text{const.} \quad (3.8)$$

where ω ranges from 0° to 360° . Figure 3.6 plots the distributions for all six of these parameters.

With ideal observing conditions (i.e. $a = 0$, $i = 90$ and $\omega = 0$), a circular orbit ($e = 0$), and a short period ($\log P_{min} = 1.46$), the maximum change in velocity for a mass ratio of 1 and 0.1 is 81 km s^{-1} and 12 km s^{-1} respectively. For a long period ($\log P_{max} = 6.39$) these values decrease to 1.8 km s^{-1} and 0.27 km s^{-1} . In practice, long-period binaries with these parameters will exhibit a change in velocity of around $10^{-4} \text{ km s}^{-1}$ over a 19 year baseline.

3.3.2 Method for Determining Binary Fraction

In the simulations that follow, we define the binary fraction, f , as the fraction of RGB stars that have a less massive (or equally massive) binary companion. The binary fraction ranges from 0 to 1. Given the parameter distributions in Section 3.3.1, the velocity measurement errors from the observations, and the Heliocentric Julian dates from the observations, model data were generated via Monte Carlo simulations as follows.

1. For a star in Leo II that has multiple observations, we selected it to be a binary or non-binary according to the binary fraction, f , under consideration.
2. If the star was determined to be a binary, we then selected a set of binary parameters from the distributions in Eqs. 3.3-3.8.
3. Then we calculated the orbital radial velocities of that star at all epochs when it

was actually observed. These velocities were calculated from Eq. 3.2 using the parameters chosen in Step 2. For a non-binary star, the orbital radial velocity was taken to be 0 km s^{-1} .

4. For both binary and non-binaries, Gaussian deviates with standard deviation equal to the observational errors of the corresponding star and epoch were calculated and added to the velocity of the star determined in Step 3. (In our analysis, we only cared about the change in velocity of the star over time, so we did not add additional radial velocity components from the motion of Leo II or the velocity dispersion since these are constant over the timescale of our observations.)
5. Steps 1-4 were repeated for all 196 stars in Leo II.
6. Steps 1-5 were repeated η times to improve statistical certainty. For our case, we carried out $\eta = 10,000$ trials per simulation.
7. Steps 1-6 were repeated for different binary fractions, from 0 to 1 in increments of 0.01.

As a means of using our kinematic dataset of Leo II to determine the galaxy's binary fraction, we calculated the following statistic as a measure of the binary frequency of stars in the sample:

$$\beta = \frac{|v_m - v_n|}{\sqrt{\sigma_m^2 + \sigma_n^2}}. \quad (3.9)$$

In this relation, v is velocity, σ is the corresponding velocity error, and the subscripts indicate different observations for a single star³. The number of β calculations per

³We also tried defining β as $\frac{|v_m - \langle v \rangle|}{\sqrt{\sigma_m^2 + \sigma_{\langle v \rangle}^2}}$, where $\langle v \rangle$ is the average velocity of the star and $\sigma_{\langle v \rangle}$ is the corresponding uncertainty. In one definition, we treated $\langle v \rangle$ and $\sigma_{\langle v \rangle}$ as the straight average and error; in a second definition, we considered them to be the weighted average and error. Both cases yielded similar results on the binary fraction. The first definition found a binary fraction

star is equal to $n(n-1)/2$, where n is the number of observations for that star. Since n ranges from 2 to 7 in our sample, the number of β 's ranges from 2 to 21, and considering the distribution of n in Figure 3.2, the total number of β 's is 723. When β is computed from radial velocities in the observational data, we call it β_{obs} ; when β is computed from radial velocities in the model data, we call it β_{mod} .

A comparison between the distributions of β_{obs} and β_{mod} was then made using Bayesian analysis. The probability of Leo II having a binary fraction, f , given the data, D , and a set of models, M , is

$$P(f|D, M) = \frac{P(D|f, M)P(f|M)}{P(D|M)}. \quad (3.10)$$

The variables D and M will be defined in the next subsection. The prior probability of the binary fraction in question, $P(f|M)$, is assumed to be uniform because there are no independent constraints on the binary fraction. The likelihood of the data given the models, $P(D|M)$, is a normalizing factor, which we selected such that the integral of the posterior is unity. Therefore, the posterior probability distribution, $P(f|D, M)$, is directly proportional to the likelihood, $P(D|f, M)$.

3.3.3 Likelihood

Since calculating the likelihood is the most crucial part of the analysis, we include Figure 3.7 which illustrates two of the major steps in determining the likelihood and denotes key variables. In the top panel, we separated the β 's into six bins sorted by increasing β . The data D is the number of β_{obs} values in each bin x , and is shown as a red dashed line. For clarity and consistency, we redefine this as $N(x)_{obs}$. A similar histogram can be made for a set of β_{mod} and is shown as a blue solid line. The number of β_{mod} values in each bin x is defined as $N(x)_{mod}$. We plotted only one that was different by only $\sim 2\%$ while the second differed by 8%. These agree at the 0.5σ level. Furthermore, the width of the credible intervals differed by only 2%–4 %.

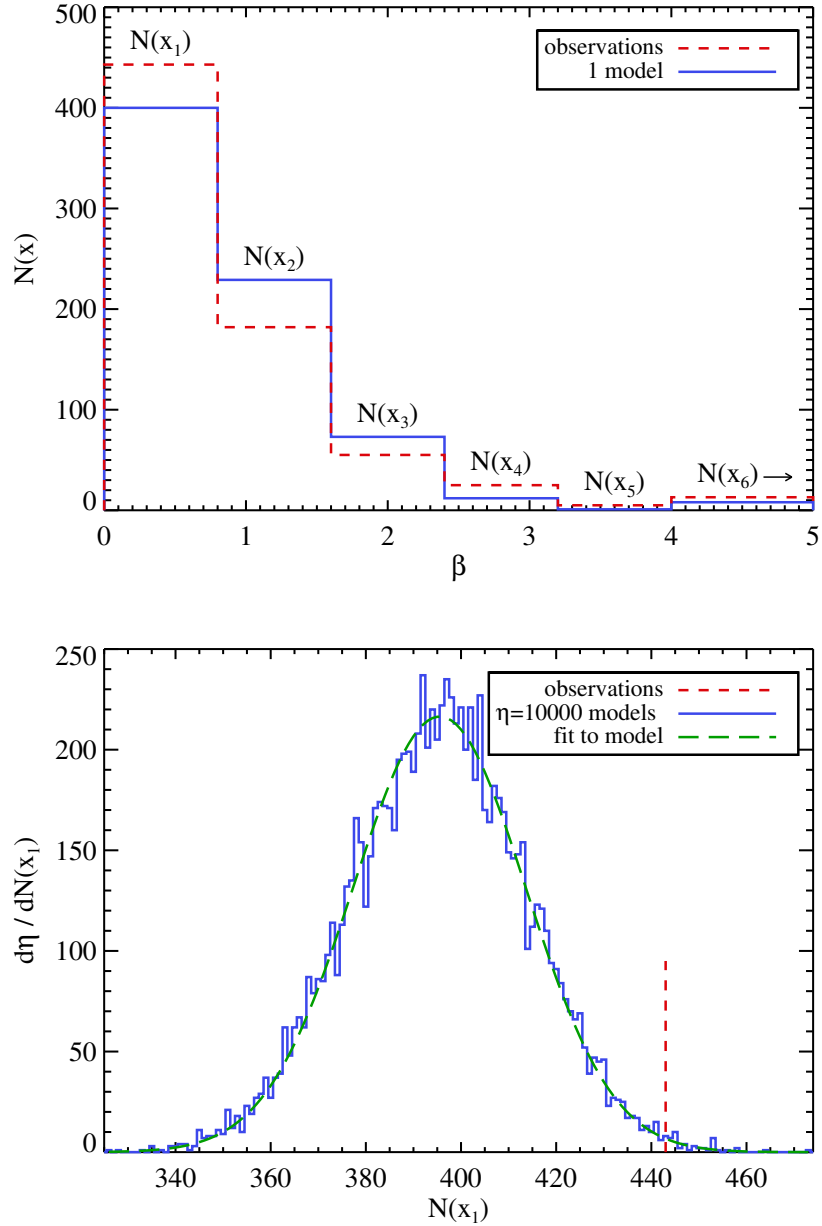


Figure 3.7 Top: histograms of β_{obs} (red dashed line) and β_{mod} (blue solid line). One histogram of β_{mod} is generated for each of the $\eta = 10,000$ Monte Carlo simulations, but for readability we only show one of these. Bottom: the number of β_{mod} that fall into bin one, $N(x_1)$, for each of the η simulations is shown as the blue solid line. We mark the value in bin one for β_{obs} as a vertical red dashed line. The models are fit using Equation 3.11, which is shown as a green dashed line. This green line is then normalized and used as a probability density function to extract the probability of the observed galaxy being represented by this set of models for a given binary fraction. The process is repeated for all bins and all binary fractions to produce a PPD.

histogram of β_{mod} for readability, but there are actually η in total since we performed η Monte Carlo simulations for a given f , where η was 10,000. The results in Figure 3.7 correspond to the distribution of β 's for the model in which the binary fraction, f , is 0.3 and the mass ratio and eccentricity distributions were constant.

The histogram bins are defined such that there are five between $0 < \beta \leq 4$ with widths of 0.8, and a sixth bin that includes all $\beta > 4$. The $\beta = 4$ limit reflects the fact that for $f = 0$ (no binaries), we observed in our models very few instances where β is this large. Placing this division at smaller β would make it increasingly difficult to distinguish between $f = 0$ and $f \neq 0$. On the other hand, selecting a larger division would yield poorly populated bins since the vast majority of β 's are < 4 even in cases with $f = 1$, and would yield noisier results. Although much of the information on the binary fraction is contained within $\beta < 4$, the number of β 's existing beyond this division is useful for ruling out (or confirming) small binary fractions because these cases would produce few large values of β . As a reference, less than 0.01% of β 's exist in the last bin for the case of $f = 0$ and there are less than 4% β 's in this bin for $f = 1$. For this reason, we collect all large β 's into a final bin to represent the tail of the β distribution.

The bin width matters very little as long as the β division is reasonably small, as in our case. Too large of a bin size will flatten the posterior, making it harder to distinguish f from neighboring values of f , while too small of a bin size will produce a noisy posterior. We selected 0.8 because both of these effects were minimal for that value.

It should be noted that the bin width and division for the last bin can be changed somewhat before the aforementioned effects begin to take place. For example, we found that if we held the cutoff limit at 4, then we could drop the bin size down to 0.2 or increase it to 1.0 without seeing any statistically significant effects on the posterior. Alternatively, if we held the bin size at 0.8, we could change the cutoff

value between 2.4 and 6.4 without it impacting the results.

In the bottom panel of Figure 3.7, we have plotted $N(x_1)_{obs}$ and $N(x_1)_{mod}$. This is a single value for the observations so it is shown as a red dashed mark. For the models, there are η values for this statistic (and $\eta = 10,000$ in our case), so the resulting probability distribution function is plotted as a solid blue histogram. The probability density function that best fits $N(x_1)_{mod}$ over all six bins takes the form of a skewed-normal distribution such that

$$\phi(N(x)|\mu, \sigma, \gamma) = \frac{1}{\sigma} \sqrt{\frac{2}{\pi}} \exp \frac{-(N(x) - \mu)^2}{2\sigma^2} \times \int_{-\infty}^{\gamma(N(x)-\mu)/\sigma} \exp \frac{-z^2}{2} dz. \quad (3.11)$$

Here μ is the location, σ is the scale, γ is the skewness, and z is a dummy variable. We performed a Levenberg–Marquardt least-squares fit of Equation 3.11 on $N(x_1)_{mod}$, allowing all three parameters — location μ , scale σ , and skewness γ — to vary. The best fit with parameters μ_{mod} , σ_{mod} , and γ_{mod} is plotted in Figure 3.7 as a green long-dashed line and serves as the model M for bin x_1 .

For a single bin x_1 , the likelihood that the data $N(x_1)_{obs}$ are given by the model $\phi(N(x_1)_{mod}|\mu_{mod}, \sigma_{mod}, \gamma_{mod})$ and a binary fraction f is $\phi(N(x_1)_{obs}|\mu_{mod}, \sigma_{mod}, \gamma_{mod})$. The likelihood using all six bins is the product of the six individual likelihoods. Therefore, we can rewrite Equation 3.10 as

$$P(f|D, M) \propto \prod_{x=x_1}^{x_6} \phi(N(x)_{obs}|\mu_{mod}, \sigma_{mod}, \gamma_{mod}). \quad (3.12)$$

This is the the posterior probability for f , which can be repeated over all f to find the posterior probability distribution (PPD).

3.3.4 Characterizing the PPDs

To find the PPD statistic that best correlates with the binary fraction, we generated 11 sets of 200 mock galaxies with binary fractions between 0 and 1 in increments

of 0.1, yielding 2200 galaxies in total. These galaxies have the same number of stars, number of observations per star, velocity errors, and observing cadences as our Leo II data. They are essentially just single Monte Carlo realizations and thus were generated using the same method as the simulations (see Steps 1-5 above).

We added up PPDs with the same assigned binary fraction to get a summed master PPD for each of the 11 binary fractions that we tested. These are shown in the top panel of Figure 3.8. The mean, median, and mode of these master PPDs are plotted against the true binary fractions in the bottom panel of Figure 3.8. The black line is the one-to-one line for which a statistic should follow if it perfectly matches the binary fraction that created it. The mean is the blue dashed line, the median is the green dash-dotted line, and the mode is the red dotted line. The mode underestimates the binary fraction for $f \leq 0.4$ but greatly overestimates it for $f \geq 0.8$. The mean, on the other hand, overestimates the binary fraction for $f \leq 0.6$ and underestimates it for $f \geq 0.8$. The median behaves in a way similar to the mean, but with a smaller bias of only a few percent. Therefore, we choose to use the median of the PPD as an indicator for the binary fraction of Leo II.

3.4 Binary Fraction in Leo II

Since we used two mass ratio distributions (normal in Equation 3.3 and constant) and two eccentricity distributions (piecewise in Equation 3.5 and constant), we have four different parameter combinations. The PPDs for these four sets of parameters of Leo II are shown in Figure 3.9. Median values range from 0.30 (constant q , constant e) to 0.34 (normal q , piecewise e). The medians are indicated with vertical green dashed lines in the PPDs in the top panel of Figure 3.9 or a green dot in the bottom panel. The 68.2% credible intervals are shown by blue dashed lines or blue squares, and the 95.4% credible intervals are shown by red dashed lines or red triangles. Values for the medians and credible intervals are given in Table 3.2. Our highest estimate

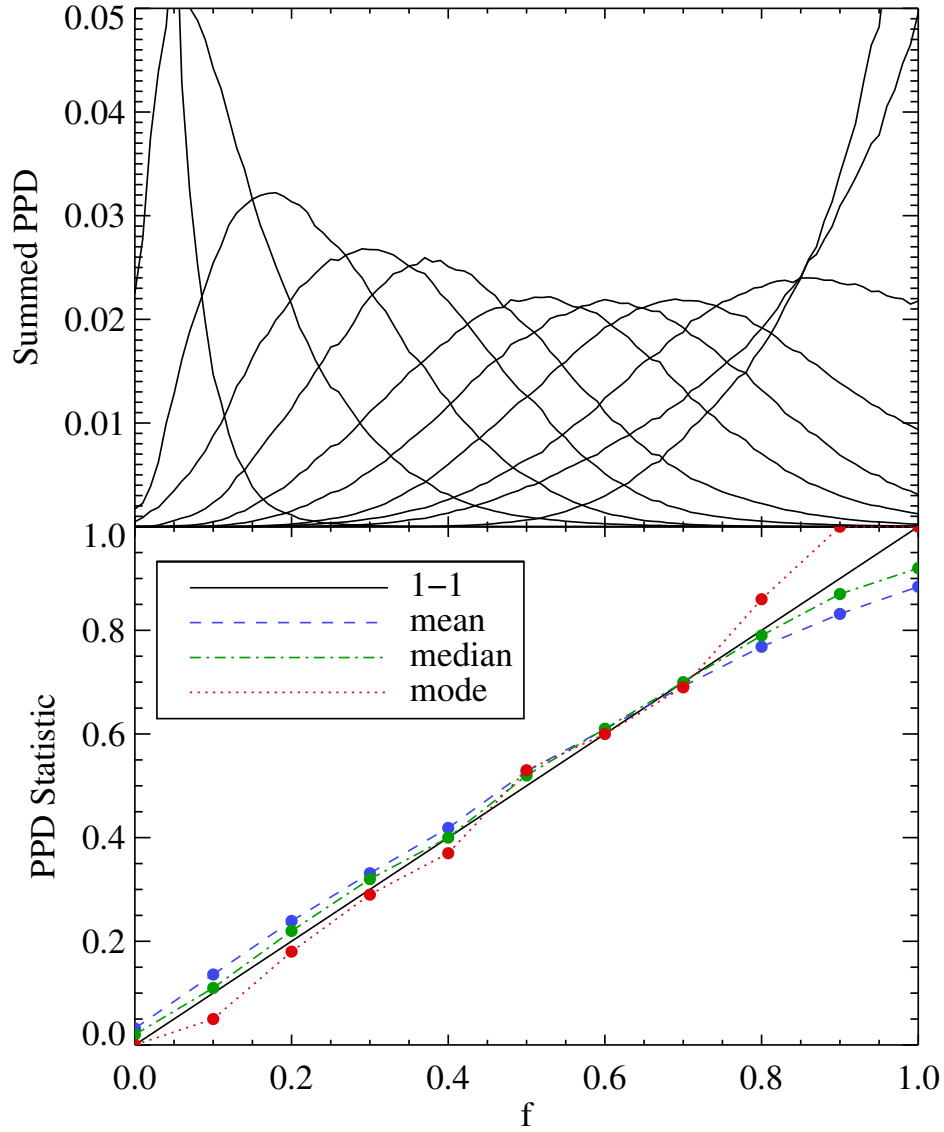


Figure 3.8 Top: the PPDs of 200 mock galaxies with equal binary fractions were totaled to make eleven normalized curves. Bottom: the mean, median, and mode of the summed PPDs are plotted against the intrinsic binary fraction of the set of 200 mock galaxies. The mode (red dotted line) is biased toward lower binary fractions for $f \leq 0.4$, whereas the mean (blue dashed line) is slightly biased toward higher binary fractions for $f \leq 0.6$. The median (green dash-dotted line) is very slightly biased in the same direction as the mean, but with a magnitude less than 3%, it does the best job of reproducing the intrinsic binary fraction of the mock galaxies, and we therefore select as the statistical estimator for f .

for the binary fraction of Leo II is $0.34_{-0.11}^{+0.11}$ for normal q and piecewise e ; the lowest estimate is $0.30_{-0.10}^{+0.09}$ for constant q and constant e . Binary fractions above 0.63 or below 0.11 are strongly ruled out with $> 99\%$ confidence regardless of the parameter distribution combinations.

Our use of multiple mass ratio and eccentricity distributions also allows us to determine two ways in which these affect the PPD. First, the PPD is very insensitive to the eccentricity distribution. The medians of posteriors that used a constant eccentricity distribution are larger than the medians of posteriors that used a piecewise eccentricity distribution by only 0.01. This result is illustrated by the fact that the cumulative PPDs group into nearly indistinguishable pairs in the bottom panel of Figure 3.9. Second, the mass ratio distribution plays a larger role in shaping the posterior than the eccentricity, though the effects are still minor. Posteriors that were built from a piecewise mass ratio distribution had medians that were 0.03–0.04 larger than posteriors with a constant mass ratio distribution. In intermediate stages of this analysis, we also considered a larger value for $\log P_{max}$ of 9.95 based on a static estimate, and found that this parameter could cause the median of the PPDs to increase by 0.10–0.12. We later discarded this value of $\log P_{max}$ as being unrealistically large, but would like to point out that the period distribution seems to have the biggest impact on the PPD. Our conclusions on the parameter distribution sensitivity are similar to those of Minor et al. (2010) who found that the the posterior is also very sensitive to the position μ_p and width σ_p values in the period function.

In the solar neighborhood, the binary fraction for main sequence stars is estimated to range from around 2/3 for F7-G9 type stars (Duquennoy & Mayor, 1991) to 0.50 ± 0.04 for F6-G2 type stars and 0.41 ± 0.03 for G2-K3 type stars (Raghavan et al., 2010). While some parameter distribution combinations provide better agreement than others, the values that we find for Leo II match the results from Raghavan et al. (2010) within 1-2 σ . Although, the agreement between Leo II and the solar

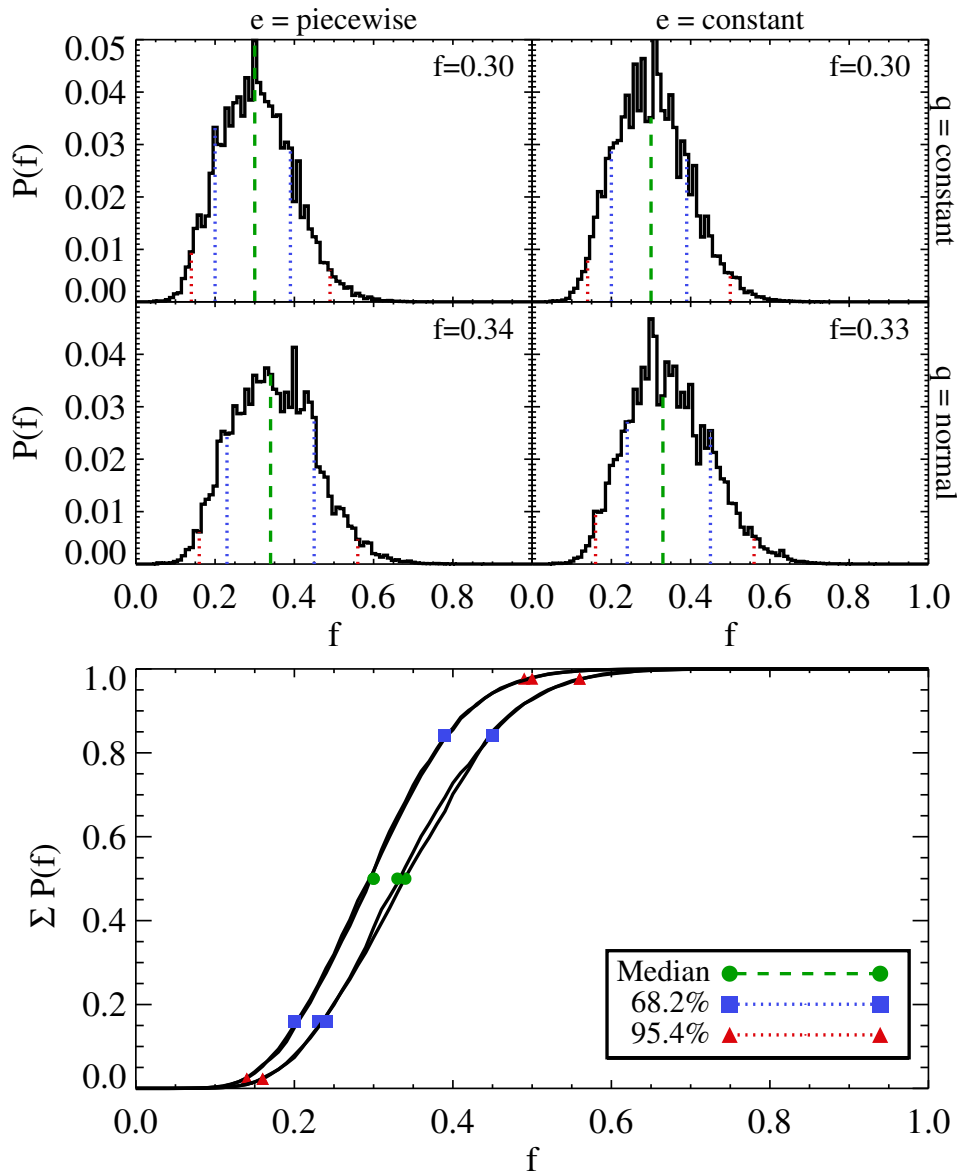


Figure 3.9 Top: the posterior probability distributions of Leo II for four different combinations of the mass ratio and eccentricity distributions. The x-axis is binary fraction and y-axis is the probability that Leo II has that binary fraction. The median of the distribution is shown as a green dashed line, and is what we adopt as the binary fraction of Leo II. The 68% credible interval is between the two vertical blue dotted lines and the 95% credible interval is between the red dotted lines. These values are listed in Table 3.2. Bottom: the cumulative posterior probability distributions. The 68% and 95% credible intervals are repeated here and marked by blue squares and red triangles, respectively. The medians are the green circles.

Table 3.2. Median and credible intervals of PPDs for Leo II

q distribution	e distribution	median (f)	68.2% interval	95.4% interval
normal	piecewise	0.34	0.23-0.45	0.16-0.56
normal	constant	0.33	0.24-0.45	0.16-0.56
constant	piecewise	0.30	0.20-0.39	0.14-0.49
constant	constant	0.30	0.20-0.39	0.14-0.50

neighborhood is not necessarily expected. One set of simulations predicted that dwarf galaxies should have larger binary fractions than the MW disk stars (Marks & Kroupa, 2011).

Minor (2013) reports the binary fraction in four MW dwarf spheroidals using data taken on Michigan/MIKE Fiber System at the Magellan/Clay telescope with ~ 1 year baselines (Walker et al., 2009a). Taking a similar but slightly different approach, they found the probability that each individual star was a binary and used likelihood analysis to extrapolate the overall binary fractions for the galaxies. Fornax, Sculptor, and Sextans all had similar fractions of $0.44_{-0.12}^{+0.26}$, $0.59_{-0.16}^{+0.24}$, and $0.69_{-0.23}^{+0.19}$, respectively, while Carina fell significantly below the others with a fraction of $0.14_{-0.05}^{+0.28}$ (Minor, 2013). Given our highest and lowest estimates, Leo II seems to bridge the gap between the three galaxies with higher f and the one with lower f . Other studies that comment on dwarf binary fractions discuss the fraction of stars that have velocity changes inconsistent with the velocity errors (i.e., KK07), or binary fractions over a shorter period range (see, for example, Olszewski et al., 1996). Because these are not global properties, we do not draw comparisons between them here.

Past kinematic studies of Leo II have concluded that the presence of binaries does not inflate the observed velocity dispersion by an appreciable amount (V95; KK07). Although our binary fraction is larger than what was assumed in these studies, it does not change the conclusion: binaries cannot under typical circumstances artificially increase the true velocity dispersion of Leo II even when based on single-epoch kinematic measurements. We support this statement with a quick simulation using

the equations and methods discussed in Sections 3.3.1 and 3.3.2. For a mock galaxy with an intrinsic velocity dispersion of 7.4 km s^{-1} and single-epoch observations for 196 stars (values equal to Leo II), the velocity dispersion will be increased by an average of 0.3 km s^{-1} . If the radial velocities are averaged over two epochs having a one year baseline, the dispersion is inflated by only 0.15 km s^{-1} . The length of the baseline does impact this effect, and an interval of 1–2 years has been found to be the optimal choice (Minor et al., 2010). To further reduce the inflation, three or more epochs are required. Thus, in an era of multi-epoch observations with long baselines, it becomes safe to ignore the effects of binaries in Leo II and other similar classical dwarf spheroidals that have several hundred spectroscopically observed stars and velocity dispersions greater than $\sim 4 \text{ km s}^{-1}$.

3.4.1 Other Considerations: Heterogeneity

We also considered what effects, if any, the heterogeneity between the four datasets might have on the predicted binary fraction. Based on the case for constant eccentricity and mass ratio distributions, we assumed that the binary fraction for Leo II should always come out to be $0.30_{-0.09}^{+0.10}$ regardless of which subset of velocity data is used in the analysis. The binary fraction estimated with only data from S17a is $0.63_{-0.22}^{+0.20}$, whereas data from KK07 finds $0.13_{-0.10}^{+0.29}$. Both of these values are within the errors of the binary fraction found using the entire dataset, as is true for every other combination of data. Since the credible intervals on these numbers are so large, it could be possible for nearly any binary fraction to be consistent with 0.30. Therefore, we also ran Monte Carlo simulations to determine the probability that Leo II has a binary fraction of 0.30, but that the S17a/KK07 datasets individually predict it will be 0.63/0.13. The results of these simulations are shown in Figure 3.10, with S17a on the left and KK07 on the right. The top panels are composed of 11 histograms that each summarize the extrapolated binary fractions for 200 Monte Carlo galaxies

with true binary fractions described by the color of the lines. The median of each of these histograms is plotted in the bottom panels; small and large error bars represent the ranges that 68% or 95% of the galaxies occupy respectively. If the binary fraction for these two subsets is in fact 0.30, then we should expect data with the same structure as S17a to recover binary fractions between 0.17 and 0.56 68% of the time, or between 0.09 and 0.80 95% of the time; for KK07 data we should expect binary fractions between 0.11 and 0.30 68% of the time. The fact that S17a data and KK07 data found a wide range of binary fractions is thus expected. As long as the datasets are placed on the same velocity standard (as was done in Section 3.2), there is no danger in mixing studies that have different velocity errors or different times elapsed between observations.

One additional feature in the bottom right panel is that the slope of the dashed line is shallower than the solid line, implying that some datasets, such as KK07, can have a significant bias toward higher or lower binary fractions. In this case, the particular combination of small baselines, few repeat observations, and few stars lead to a set of β 's that did a poor job of constraining the binary fraction. Including other datasets will increase the number and range of β 's, thereby improving both the precision and accuracy of the binary fraction estimate.

3.4.2 Other Considerations: Velocity Errors

This entire analysis has been completed using only three pieces of data: radial velocity, radial velocity uncertainty, and time of observation. There is very little error in the time of observation, and we have removed any errors in velocity to the best of our abilities by subtracting systematic offsets. However, it is more difficult to detect any errors in the velocity uncertainties.

To better understand how over- or under-reported velocity uncertainties could affect our results, we created two more Monte Carlo simulations with velocity errors

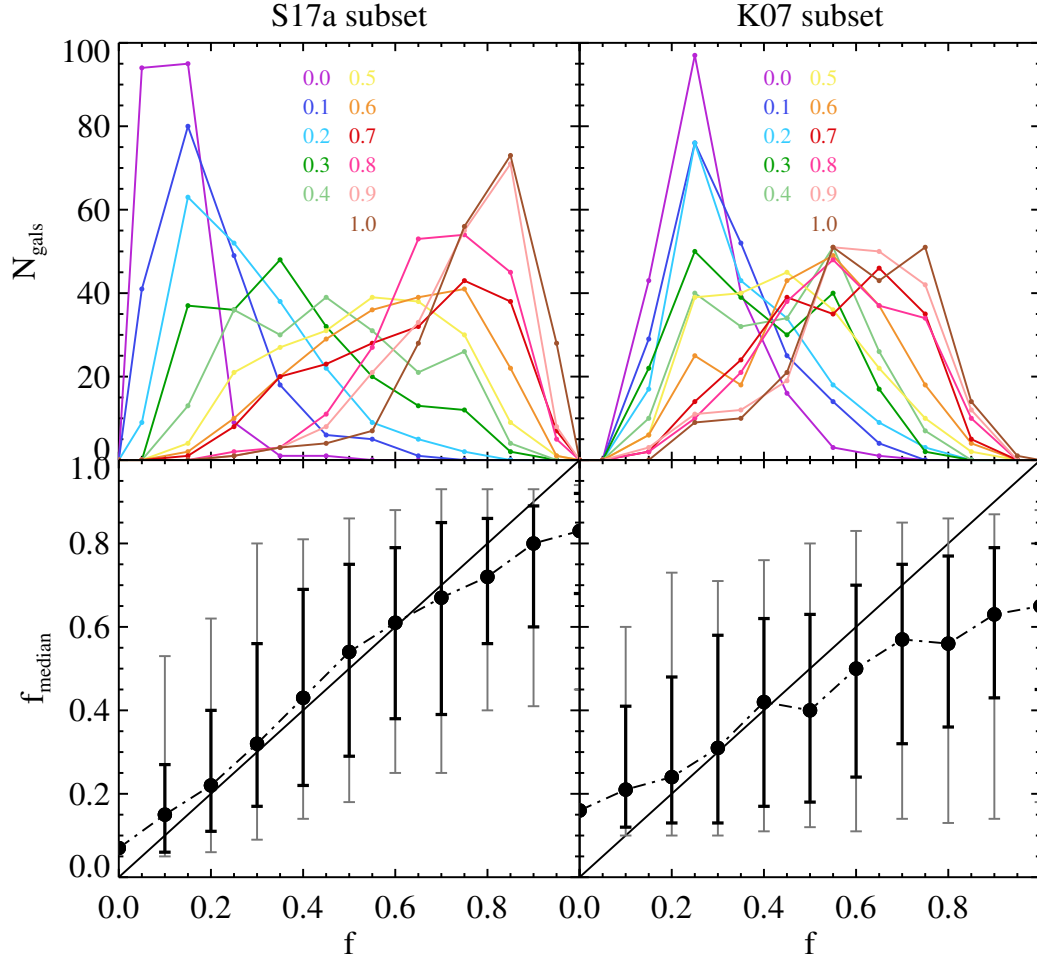


Figure 3.10 Top: histograms of the binary fractions found for 200 mock galaxies with the actual binary fraction indicated by line color. For readability, they are drawn as points centered on bins with widths 0.1 connected by lines rather than traditional histogram stair-steps. Bottom: the median of each histogram is shown as a dot with 68% and 95% of all values falling within the small and large error bars respectively. If the analysis did a perfect job of recovering the binary fraction, then the dots would fall along the solid one-to-one line. Plots on the left were made using only data from S17a and plots on the right were made using only data from KK07.

either twice or half as large. In the first case, the PPD shows sharp spikes at a variety of binary fractions. The large errors mask any changes in velocity caused by binaries, making it impossible to tease out a binary fraction. Since we are seeing a much cleaner PPD for Leo II, we feel reassured that our velocity errors are not overestimated.

For the second case, the PPD does not have an unnatural shape. Instead, it yields a high probability that the binary fraction is 1. If any of the velocity uncertainties are underestimated it will push our binary fraction toward higher values. The change happens gradually. When the errors are only 10% smaller, the binary fraction still works out to be $0.43_{-0.10}^{+0.09}$. This case is harder to rule out; however the distribution of $P(\chi^2, \kappa)$ in Figure 3.4 can help. When the errors are underestimated, the stars will cluster toward low $P(\chi^2, \kappa)$. Alternatively, when the errors are overestimated, the stars will cluster toward high $P(\chi^2, \kappa)$. Even in the case of 10% smaller errors, stars begin to overpopulate the second to lowest bin. Our distribution is flat and shows no overpopulated bins (with the exception of the lowest bin being caused by binaries), so we are reasonably confident that the velocity uncertainties used in this analysis are representative of the formal errors. Moving forward, we would like to emphasize the critical importance of robust error determination when exploring precision dynamics of dwarf galaxies.

3.4.3 Consequences for Ultra-faints

As we have seen, binaries do not affect the velocity dispersion of Leo II and other classical dwarfs (Hargreaves et al., 1996a; Olszewski et al., 1996). More recently, the problem has reemerged due to the possibility of binaries artificially inflating the dispersions of ultra-faint systems. In these cases, the dispersions appear to be < 4 km s⁻¹, considerably smaller than in classical systems. To illustrate the severity of this issue, we completed yet another set of Monte Carlo simulations to explore the amplitude of this effect. We computed the observed velocity dispersion of six mock

galaxies having intrinsic dispersions of 0.5, 1, 2, 4, 8, and 12 km s⁻¹. Each galaxy contained 100 stars with single-epoch observations and velocity measurement errors of 1 km s⁻¹. The results are shown in Figure 3.11. For galaxies with large intrinsic dispersions (red and orange lines in the figure), even binary fractions of 1 increase the observed dispersion by very little. On the other hand, galaxies with intrinsic dispersions of 0.5 to 2 km s⁻¹ (black, purple, and blue lines) can have their observed dispersion inflated by a factor of 2–8 from a binary fraction of 1, or a factor of 1.5–4 for a more realistic binary fraction of 0.3. It is not likely that binaries are the sole contributors to the high velocity dispersions (and thus mass-to-light ratios) present in ultra-faints (McConnachie & Côté, 2010), but even if the binary fractions are only ~ 0.3 , like what we find in Leo II, then they can play a non-negligible role in inflating the velocity dispersion. Furthermore, the stars typically observed in ultra-faints are subgiants or main sequence stars rather than RGBs. These types of stars allow tighter binary orbits with shorter periods, which would increase the effects of binaries as well.

3.5 Summary and Conclusions

Multiple observations of several stars over many epochs made it possible to detect changes in radial velocities due to the presence of binaries. Coupling our data from S17a with V95, KK07, and KG10 yields a total of 196 unique stars with two to seven observations between 1994 and 2013; the longest baseline for a single star was 19 years. 8 to 10% of the stars have a small (e.g., less than 0.01) probability of exceeding their χ^2 , indicating that the change in velocity over time is significant and cannot be attributed to measurement errors. This corresponds to the detectable binary fraction in our sample. This value depends strongly on the baseline and number of observations per star and is therefore not a global property.

To find the overall binary fraction for red giants in Leo II, we generated a suite of Monte Carlo simulations that sample from the seven binary parameters that define the

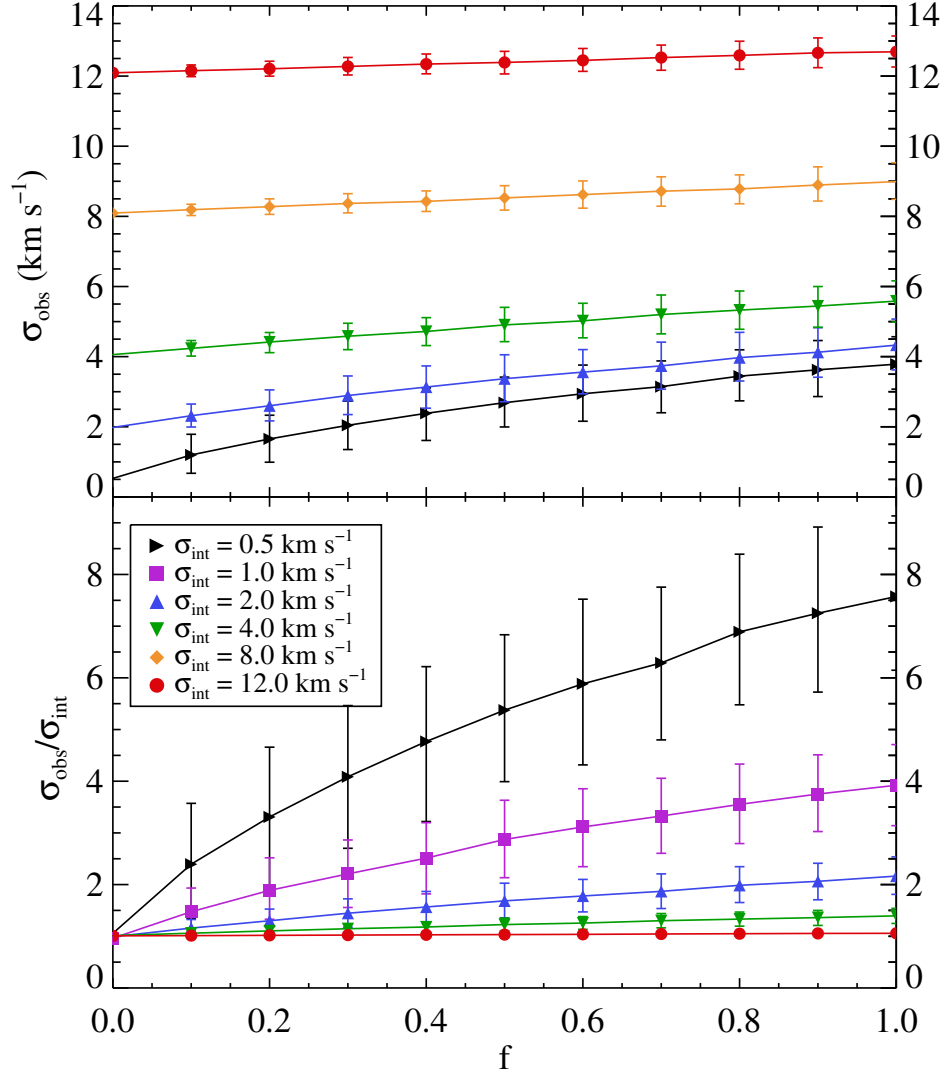


Figure 3.11 Top: the observed velocity dispersion vs. binary fraction. Bottom: the ratio of observed to intrinsic velocity dispersion vs. binary fraction. Six mock galaxies are considered, each containing 100 stars with single-epoch observations and 1 km s^{-1} velocity uncertainties. The intrinsic dispersions are 0.5 km s^{-1} (black right-facing triangles), 1 km s^{-1} (purple squares), 2 km s^{-1} (blue upward triangles), 4 km s^{-1} (green downward triangles), 8 km s^{-1} (orange diamonds), and 12 km s^{-1} (red circles). As the binary fraction increases, so does the observed velocity dispersion. This effect is minimal for galaxies with high intrinsic dispersions, but for galaxies with low intrinsic dispersions, the observed dispersion can be 1.5–4 times that of the intrinsic dispersion for $f \sim 0.3$. Models were generated using a normal mass ratio distribution and a piecewise eccentricity distribution.

orbital radial velocity for a binary star. We considered two mass ratio and eccentricity distributions, yielding four combinations of parameters. Using Bayesian analysis, we compared the simulations to the combined dataset and determined that the binary fraction for Leo II is around 0.30–0.34. The lowest recovered binary fraction was for a constant mass ratio distribution and a constant eccentricity distribution, which returned $f = 0.30_{-0.10}^{+0.09}$ for a 68% credible interval and $_{-0.16}^{+0.20}$ for a 95% credible interval. The highest binary fraction was for a normal mass ratio distribution and piecewise eccentricity distribution, which returned $f = 0.34_{-0.11}^{+0.11}$ for a 68% credible interval and $_{-0.22}^{+0.18}$ for a 95% credible interval. The results of all four simulations are listed in Table 3.2. Regardless of the parameter distributions, we can rule out binary fractions greater than 0.63 or less than 0.11 with 99% confidence. Owing to the fact that the velocity dispersion of Leo II is large and our dataset is composed of stars with multiple observations, the effect of binaries on the velocity dispersion is negligible.

While large systems like Leo II are little affected by binaries, these stars may play a bigger role in ultra-faints, particularly in cases of single or few observations. In our simulations, we found that dwarfs with low intrinsic velocity dispersions of 0.5–2 km s⁻¹ could be observed to have dispersions 1.5–4 times larger than in actuality, given a binary fraction of 0.3. This effect further magnifies due to the extreme faintness of ultra-faints; the only way to increase kinematic samples in individual systems is to observe fainter stars, even down to the main sequence when feasible. In doing so, the period range and thus velocity amplitudes of binaries compared to larger red giant stars will increase. This has two important implications. First, it will be difficult to ever directly measure binary frequencies in ultra-faints. Second, the effects of binaries are necessarily amplified in ultra-faints not only because of their small dispersions, but also due to the increased impact binaries have on altering the velocities in the types of stars that need to be observed.

Multi-epoch observations of ultra-faints are worth pursuing to directly explore

their binary frequencies. Since it will be a while before the sample sizes of ultra-faints become large enough to accurately determine binary fractions on a case by case basis, an interim solution might be to correct the velocity dispersions using known binary fractions in brighter dSphs. The current results for dwarfs in the south use data that only span one year, but it will soon become possible to expand the analysis for Fornax, Sculptor, Sextans, and Carina as observations continue. Data for dwarfs in the north are already quite extensive so we plan to apply our method of determining the binary fraction to Draco and Ursa Minor. Combining our three galaxies with the four in Minor (2013) will give us a better picture of what the average binary fraction for dSphs is and if there are any dependencies on other galactic properties.

CHAPTER IV

The Binary Fractions in Draco and Ursa Minor

4.1 Introduction

The dwarf spheroidal galaxies Draco and Ursa Minor were the first such systems for which resolved, internal velocity dispersions were obtained (Aaronson, 1983). A key factor in this development was the relative proximity of the galaxies (~ 76 kpc, Bellazzini et al., 2002; Bonanos et al., 2004) and the moderate number of red giant targets. Even with low signal-to-noise data, it was possible to obtain precision radial velocities for these stars and discern velocity dispersions of $\sim 9 \text{ km s}^{-1}$ (Hargreaves et al., 1994b; Olszewski et al., 1995; Armandroff et al., 1995). These apparently large velocity dispersions pointed toward dark matter, but they also implicated binary stars.

Over time, the role of binary stars on velocity dispersion of dSphs was addressed. By combining all of the available velocity data, Olszewski et al. (1996) had access to 118 stars with multi-epoch measurements between Draco and Ursa Minor. They created Monte Carlo simulations to make the first prediction of the binary fraction in these galaxies. They reported the frequency to be 0.2-0.3 per decade of period in the vicinity of periods of one year, which is 3-5 times larger than what is found in the solar neighborhood.

A similar analysis was completed by Hargreaves et al. (1996a), with the addition

of Sextans data. They additionally varied the orbital parameter distributions to understand the effect binaries might have on the velocity dispersion. They concluded that velocity dispersion could only be significantly altered if the binary parameters were different from the Solar Neighborhood. Specifically, the periods in the galaxies would need to be shorted and the mass ratios would need to be larger compared to stars near the Sun.

At the turn of the 21st century, a new spectroscopic survey of Draco was conducted for the purpose of studying the details of its dark matter halo by way of a velocity dispersion profile (Kleyna et al., 2002). The multi-epoch nature of their data in combination with past observations from Armandroff et al. (1995) allowed them to interpret the binary fraction. They tested the binary fractions 0.2, 0.5, and 0.8. Contrary to Olszewski et al. (1996), the binary fraction that best fit the data was 0.5, consistent with the Solar Neighborhood. It was clear that Draco and Ursa Minor (and other classical dSphs) had abnormally high internal dispersions compared to the Newtonian expectation, but that binaries were not the cause.

Over the past 15 years, a number of new high-precision velocities have been obtained of large samples of stars in Draco and Ursa Minor. This offers an opportunity to revisit the question of the binary populations in these galaxies. While it is still unlikely that binaries will significantly alter our view of the dark matter content of classical dSphs such as Draco and Ursa Minor, the discovery of ultra-faints has resurrected the issue. Ultra-faints have exhibited much smaller dispersions, and while they are still believed to be dark matter dominated, the role of binaries might be significant in these cases. In this chapter, we aim to better constrain the binary fractions in both Draco and Ursa Minor. We will then use this result to estimate the binary fraction in ultra-faints and provide examples on the severity of the effect for ultra-faints.

This chapter is organized as follows. In Section 4.2 we introduce the velocity data for Draco and Ursa Minor, and the steps taken to prepare the data for a binary

analysis. Section 4.3 outlines the methods used in evaluating the binary fraction, including a discussion of binary orbital parameters, our Monte Carlo simulations, the Bayesian technique, and the reliability of the process as applied to mock galaxies. In Section 4.4 we report the results. These include the binary fractions for Draco and Ursa Minor, the possibility of there being one binary fraction across all dSphs, correlations between binary fraction and other galactic properties, and the potential for constraining the period distribution. Finally we summarize the conclusions in Section 4.5.

4.2 Velocity Data

Our analysis aims to define the binary fractions in Draco and Ursa Minor via the presence of velocity variability amongst the stars. Data must meet several criteria to be used in this analysis.

- The stars must be red giants. We make simplifications later about the mass and period distributions for binary stars by assuming that the primaries are red giants. The same assumptions would not be true for main sequence, horizontal branch, or asymptotic giant branch stars.
- The stars must be members of the dSphs. Binaries are found in both dSphs and the MW halo, but the frequency with which they are found is not necessarily the same. Since we aim to find the binary fraction specifically within dSphs, we do not want MW halo stars to skew the results.
- The velocities cannot be averaged over multiple epochs. Doing so would conceal the signatures of velocity variability, which are key in our method of determining the binary fraction.
- The velocity errors must reflect the measurement uncertainty. As we will see in

Section 4.2.4, poorly determined errors can increase or decrease the significance of velocity variation, and thereby lead to incorrect measurements of the binary fraction.

- The stars must have multi-epoch observations. Velocity variability is identified as a function of time, so we require multiple observations.

There are six datasets for Draco and Ursa Minor that meet our criteria. These are summarized in Table 4.1. Column 1 lists the paper order as it appears in Section 4.2.1, column 2 lists the reference paper, column 3 lists the dataset abbreviation, column 4 lists the number of stars in the dataset that adhere to the first four of the above criteria, column 5 lists the median velocity error of those stars, column 6 lists the years when the observations were taken, column 7 lists the number of stars from the dataset that we use in this analysis, and column 8 lists the velocity offset that we apply to put the stars on the same velocity standard. In this section we will first introduce the datasets (Section 4.2.1) and then describe the ways in which we trimmed them to meet our requirements (Sections 4.2.2–4.2.4).

4.2.1 Data Sets

The first dataset is Olszewski et al. (1995, hereafter O95). Using the echelle spectrograph on the Multiple Mirror Telescope, they measured velocities every year between 1982 and 1991. They collected data for 24 stars in Draco and 18 stars in Ursa Minor.

The second dataset (Armandroff et al., 1995, hereafter A95) was obtained with the Hydra multi-fiber positioner and the Bench Spectrograph on the KPNO 4-meter telescope. They observed many of the same stars as O95 in both Draco and Ursa Minor during the years 1992 to 1994. The sample expanded greatly to include 91 stars in Draco and 94 in Ursa Minor.

The third dataset was split into two papers, with Kleyna et al. (2002, hereafter K02) focusing on Draco and Kleyna et al. (2003, hereafter K03) focusing on Ursa Minor. They used the AF2/WYFFOS fiber-fed spectrograph on the William Herschel Telescope during the year 2000 for Draco and 2002 for Ursa Minor.

The fourth dataset (Wilkinson et al., 2004, hereafter W04) is a followup to the previous K02 and K03 data, using the same instrument and telescope. They took measurements in the year 2003 to compose a second epoch of data for about a third of the Kleyna stars in Draco and about one half of the Kleyna stars in Ursa Minor.

The fifth set of data was described in Kirby et al. (2010, hereafter K10). They observed stars in both dwarfs during 2009 and additional stars in Ursa Minor in 2010 using Keck/DEIMOS. Each star only received a single epoch of observations, but many of the stars appeared in other datasets making them useful to our research. These velocities were not published in the aforementioned paper and have been kindly provided by the author.

The sixth dataset for Draco is Walker et al. (2015b, hereafter W15) and for Ursa Minor is Walker et al. (2017, hereafter W17). They observed consecutively between the years 2006 to 2011 on the MMT telescope using Hectochelle.

There were three other studies with radial velocities of red giants in Draco and/or Ursa Minor but these failed to meet one or more of the criteria listed in Section 4.2. Jardel et al. (2013) observed 13 stars in Draco during a single epoch, but only one star exists in the other datasets. This sample does not appreciably add to the size of the combined data or expand the temporal information. It would also be impossible to put it on the same velocity standard as the other data given the minimal overlap. (This step is described in Section 4.2.3).

Muñoz et al. (2005) used Keck HIRES to obtain average radial velocities of 52 stars in Ursa Minor over two epochs separated by 2 years. These were later supplemented with additional observations of both Ursa Minor and Draco. The individual velocities

Table 4.1. Papers with radial velocity data in Draco and Ursa Minor

Paper number	Paper	Abbreviation	Nstars criteria	median σ_v (km s ⁻¹)	years	Nstars usable	v_{offset} (km s ⁻¹)
Draco							
1	citetolszewski1995	O95	20	1.8	1982-1991	20	-0.41
2	Armandroff et al. (1995)	A95	86	4.2	1992-1994	75	-0.41
3	Kleyna et al. (2002)	K02	158	1.7	2000	140	-0.17
4	Wilkinson et al. (2004)	W04	114	2.5	2003	96	-0.17
5	Kirby et al. (2010)	K10	305	2.5	2009	123	0.21
6	Walker et al. (2015b)	W15	414	0.9	2006-2011	292	0.0
Ursa Minor							
1	Olszewski et al. (1995)	O95	16	1.9	1983-1989	16	0.06
2	Armandroff et al. (1995)	A95	90	4.3	1992-1994	88	0.06
3	Kleyna et al. (2003)	K03	64	5.1	2002	58	-1.07
4	Wilkinson et al. (2004)	W04	146	2.9	2003	112	-1.07
5	Kirby et al. (2010)	K10	336	2.4	2009-2010	136	-0.24
6	Walker et al. (2017)	W17	404	1.0	2008-2011	250	0.0

were not published nor available from the authors, and so these data could not be used in our analysis.

Lastly, Hargreaves et al. (1994b) and Hargreaves et al. (1996b) published velocity data for Ursa Minor and Draco, respectively. It was found in Armandroff et al. (1995) that the velocity errors of these data were systematically underestimated by about 15%, an effect likely caused by poor sky subtraction. Due to the inadequate treatment of the velocity errors, we have chosen to exclude this dataset from our analysis.

4.2.2 Sample Definition

Each dataset was trimmed to match the needs of this analysis, as described in Section 4.2. For O95 and A95 we removed four or five carbon stars, as we are only concerned with red giant branch stars here.

The K02, K03, and W04 datasets contained stars both in the dSphs and in the MW foreground. We removed the halo stars on the basis of radial velocity. Normally, a wide cut in velocity risks including MW members while a narrow cut risks excluding dSph binaries. However, the location of the cut turned out not to matter much in this case because most of the stars just inside or just outside this limit were discarded

later because they only had one epoch of observations, even after combining with the other datasets. The membership criteria that we used were $-330 < v_{mem} < -250$ km s⁻¹ for Draco and $-300 < v_{mem} < -200$ km s⁻¹ for Ursa Minor. There is likely still some contamination from the Milky Way but we expect this to only be a couple stars. The effect of such contamination on our results will be negligible.

For K10, measurements with velocity errors larger than 10 km s⁻¹ were discarded. Velocity nonmembers were present in the Draco data so we removed likely foreground stars that had velocities less than -320 km s⁻¹ or greater than -265 km s⁻¹. These limits are the same as what we applied to the W15 dataset, which is described below.

W15 and W17 contained a larger datasets and probed fainter stars so they incurred many more non-members than the other studies. For this reason, we spent extra care separating the members from the non-members.

We started by taking the average radial velocity and surface gravity for each star. In the top panels of Figures 4.1 (Draco) and 4.2 (Ursa Minor), we plot Gaussian kernel density estimates of the radial velocities in black. This was done by adding together for each star a Gaussian with area equal to unity, location equal to the average radial velocity ($v = \Sigma \frac{v_i}{\sigma_i} / \Sigma \frac{1}{\sigma_i}$), and width equal to the weighted velocity uncertainty ($\sigma = (\Sigma \frac{1}{\sigma_i^2})^{-1/2}$). There is a sharp peak around -290 km s⁻¹ for Draco and at -250 km s⁻¹ for Ursa Minor, and a wide bump of Milky Way foreground stars that have slower radial velocities. For illustrative purposes we generated a Besançon model, which simulates the kinematics of Milky Way stars along the line of sight to each of the dwarfs. We generated another Gaussian kernel density estimate for the Besançon stars and set the width of each kernel equal to the median weighted velocity error of the dwarf under consideration. This value was 0.6 km s⁻¹ for both dwarfs. We normalized the Besançon model such that the area under the curve between $-200 < v < -20$ km s⁻¹ for Draco (or $-160 < v < -20$ km s⁻¹ for Ursa Minor) was equal to the area under the black line over the same range. The model is shown as a blue line in Figures

4.1 and 4.2. In the middle panels of Figure 4.1–4.2 we also plot regular histograms of the radial velocities. It is clear from both of these representations that there will be contamination from the Milky Way. The Besançon models confirm the expectation that for such faint stars, most of the MW contaminants are main sequence stars, which have significantly higher surface gravities. W15 and W17 measured surface gravity, so we have adopted a cutoff at $\log g = 4.0$ to separate nonmember main sequence stars ($\log g \geq 4.0$) from possible Draco/Ursa minor member red giant and sub-giant stars ($\log g < 4.0$).

We then determined the radial velocity cuts that we should use by simultaneously deriving the systemic velocity and velocity dispersion of the dwarfs from the culled samples. The velocity dispersion and systemic velocity are found by a method of maximum likelihood described in Walker et al. (2006), which assumes that velocities are drawn from a Gaussian distribution. We need to start with a guess for the velocity boundaries. We fit a Gaussian distribution to the middle panels of Figures 4.1 and 4.2. The standard deviation of this fit is multiplied by three to provide a 3σ velocity cut. Then we use the stars within this velocity range to calculate the velocity dispersion and systemic velocity. The resulting velocity dispersion can be used to make new 3σ velocity boundaries. Then we repeat the process of calculating the velocity dispersion and systemic velocity until it converged on an answer within 0.1 km s^{-1} . This took 3-4 iterations.

The resulting membership criteria for Draco were $-319.4 < v < -265.2 \text{ km s}^{-1}$ and $\log(g) < 4.0$. The systemic velocity for Draco is $-292.3 \pm 0.4 \text{ km s}^{-1}$ with a velocity dispersion of $9.0 \pm 0.3 \text{ km s}^{-1}$. Previously reported average, median, or systemic velocities are $-293.3 \pm 1.0 \text{ km s}^{-1}$ (A95), $-293.8_{-2.7}^{+2.6} \text{ km s}^{-1}$ (Hargreaves et al., 1996b), and $-290.7_{-0.6}^{+1.2} \text{ km s}^{-1}$ (W04), all of which agree with our findings. The velocity dispersion has been reported as 10.7 ± 0.9 or 8.5 ± 0.7 depending on the inclusion of one peculiar star (A95), $8.2 \pm 1.3 \text{ km s}^{-1}$ (O95), $10.5_{-1.7}^{+2.2} \text{ km s}^{-1}$ (Hargreaves et al.,

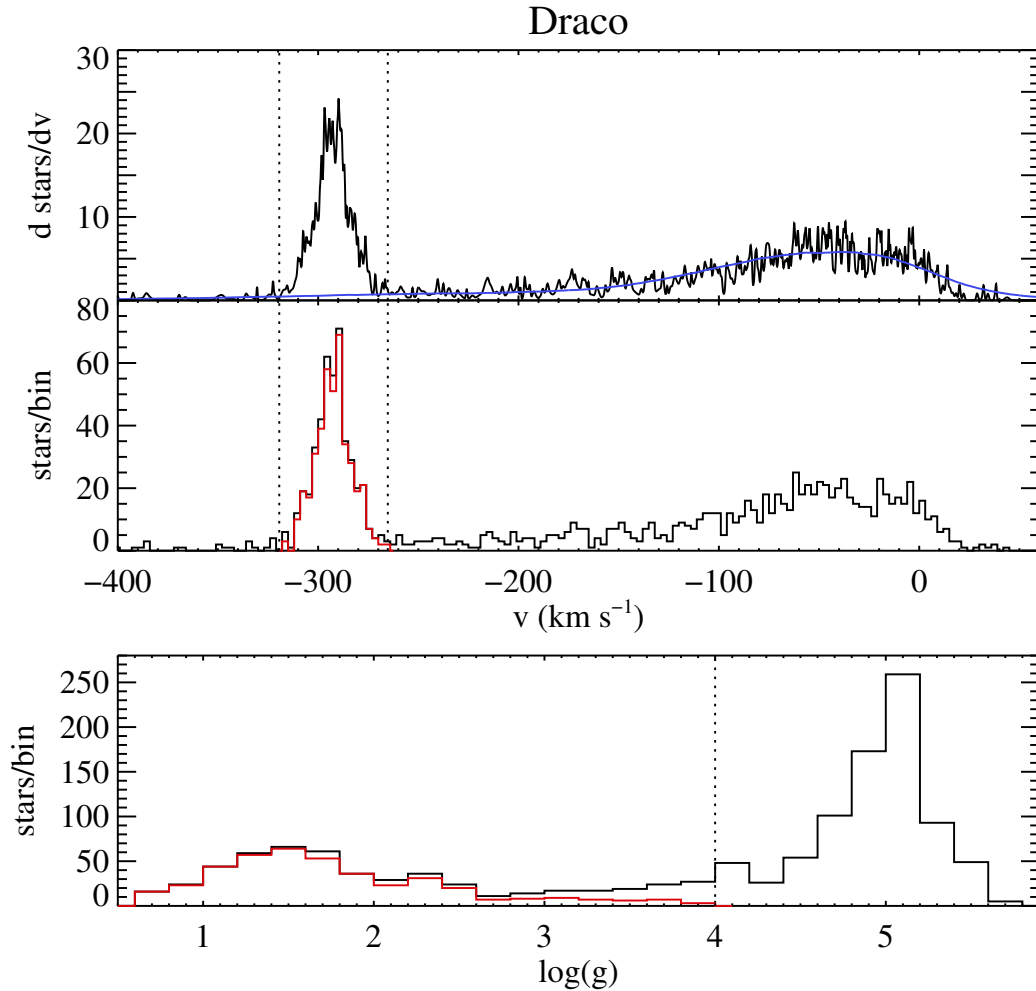


Figure 4.1 Top: Gaussian kernel density estimates of radial velocity from the W15 dataset (black) and from a Besançon model of MW foreground stars (blue). Middle: histogram of the average radial velocities in W15. The red line is the histogram of the final member selection. Vertical dotted lines demarcate the velocity boundary for membership. Bottom: histogram of the surface gravities in W15. The red line shows the histogram for the final member selection. The vertical dotted line shows the membership cut in surface gravity.

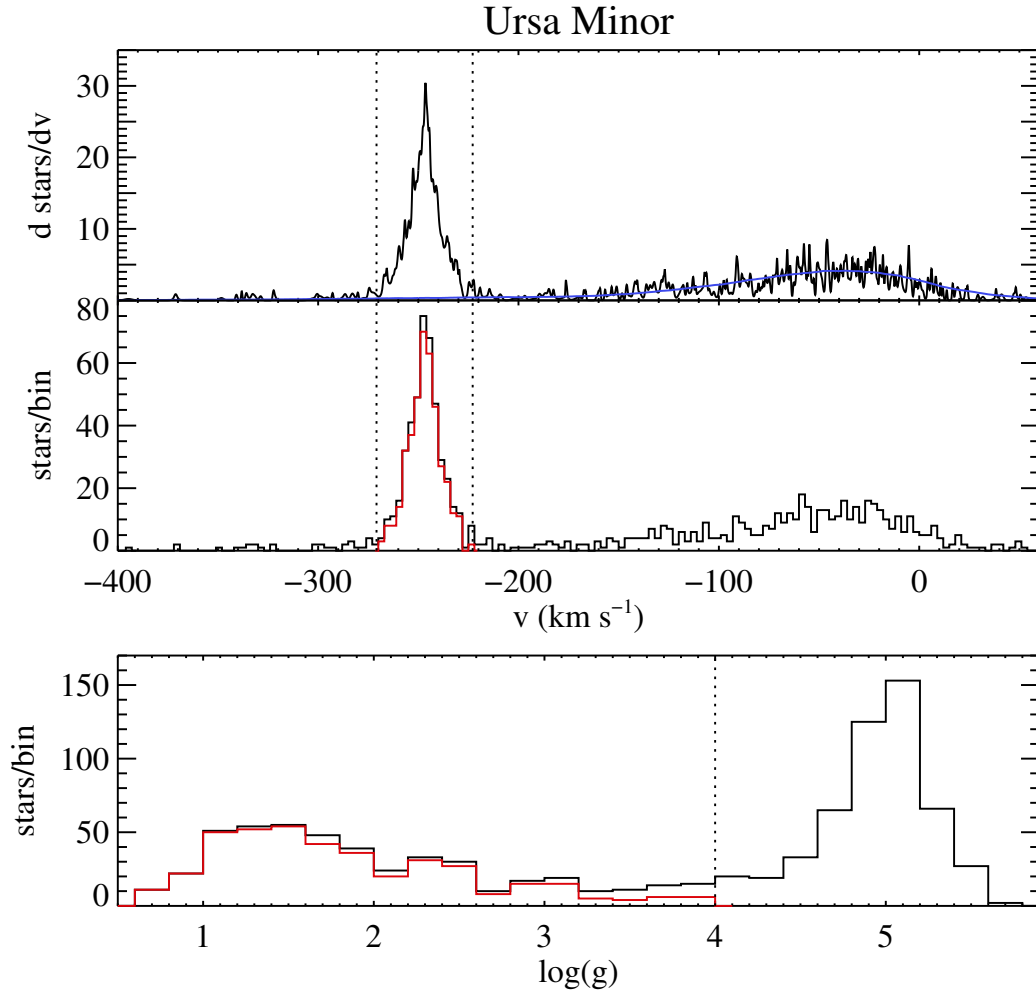


Figure 4.2 Top: Gaussian kernel density estimates of radial velocity from the W17 dataset (black) and from a Besançon model of MW foreground stars (blue). Middle: histogram of the average radial velocities in W17. The red line is the histogram of the final member selection. Vertical dotted lines demarcate the velocity boundary for membership. Bottom: histogram of the surface gravities in W17. The red line shows the histogram for the final member selection. The vertical dotted line shows the membership cut in surface gravity.

1996b), and $9.1 \pm 1.2 \text{ km s}^{-1}$ (McConnachie, 2012). Our measurements are in good agreement with the literature, especially given the large range of reported values.

For Ursa Minor the criteria were $-270.9 < v < -222.9 \text{ km s}^{-1}$ and $\log(g) < 4.0$. The systemic velocity for Ursa Minor is $-246.9 \pm 0.4 \text{ km s}^{-1}$ with a velocity dispersion of $8.0 \pm 0.3 \text{ km s}^{-1}$. The average velocity was previously found to be $-247.2 \pm 1.0 \text{ km s}^{-1}$ (A95), $-249.2 \pm 1.5 \text{ km s}^{-1}$ (Hargreaves et al., 1994b), and $-245.2_{-0.6}^{+1.0} \text{ km s}^{-1}$ (W04). Our measurement falls between these values. The velocity dispersion was listed as 10.4 ± 0.9 or $8.8 \pm 0.8 \text{ km s}^{-1}$ depending on inclusion of peculiar stars (A95), $10.5 \pm 2.0 \text{ km s}^{-1}$ (O95), 8.8 km s^{-1} (K03), and $9.5 \pm 1.2 \text{ km s}^{-1}$ (McConnachie, 2012). Our velocity dispersion is lower than all the other measurements, but the agreement is still within 1.3σ for all but one case. Several studies have found that the kinematics of Ursa Minor are better fit by a two component model (Kleyna et al., 2003; Wilkinson et al., 2004). We do not explore more complicated dynamical models because the velocity distribution in Figure 4.2 appears to be sufficiently Gaussian, and thus the method we used to determine membership should be valid.

4.2.3 Correcting Systematic Offsets

Because we have incorporated data from a variety of different sources, it is likely that there are systematic offsets between the datasets. We have chosen W15 as the reference to which all the distributions will be shifted for Draco, and W17 as the reference for Ursa Minor. In Figures 4.3 (Draco) and 4.4 (Ursa Minor) we plot velocities from W15 or W17 along the x-axis and velocities from the other studies along the y-axis when stars exist in both catalogs. The black solid represents perfect mean agreement. The red dashed line indicates the best fitting line with slope equal to 1. The y-intercept of the line indicates the offset between W15 or W17 and others. We correct the velocities such that $v_{study_corrected} = v_{study} - v_{offset}$. Two outlier stars in K10 were not used in the fit for Draco, and they are shown as open triangles in

the bottom panel of Figure 4.3.

A95 found that an offset of 1.59 km s^{-1} existed between their data and that of O95. We add the same offset to the A95 data and plot the combined dataset in the top panel to perform a comparison with W15 and W17. This was necessary because only a couple stars were observed in common between the Walker and Olszewski data, making it impossible to perform the necessary comparison otherwise.

K02, K03, and W04 are also included in the same panel because the methods of observation and velocity extraction were identical and they showed no signs of zero-point offsets between observing runs.

In Draco the offsets are -0.17 km s^{-1} for K02 and W04, -0.41 km s^{-1} for O95 and A95, and 0.21 km s^{-1} for K10. In Ursa Minor the offsets are -1.07 km s^{-1} for K03 and W04, 0.06 km s^{-1} for O95 and A95, and -0.24 km s^{-1} for K10.

4.2.4 Velocity Uncertainty

A crucial element of this analysis is having accurate radial velocity errors. Underestimated errors will inflate the binary fraction while overestimated errors will decrease it. To determine if the errors are an accurate representation of the scatter in the velocity data, we use the χ_κ^2 statistic defined as

$$\chi_\kappa^2 = \frac{1}{\kappa} \sum_i^n \left(\frac{v_i - \langle v \rangle}{\sigma_i} \right)^2, \quad (4.1)$$

where $\kappa = n - 1$ is the number of degrees of freedom, and n is the number of observations per star. The probability of exceeding χ_κ^2 is $P(\chi^2, \kappa)$. In Figure 4.5 we plot histograms of $P(\chi^2, \kappa)$ under the assumption that all stars are velocity non-variables. If the errors are accurate and there are no intrinsic velocity variables with resolvable Δv 's, then the distribution should be flat. If the errors are over/underestimated and there are no stars with resolved Δv 's, the histograms would be biased toward

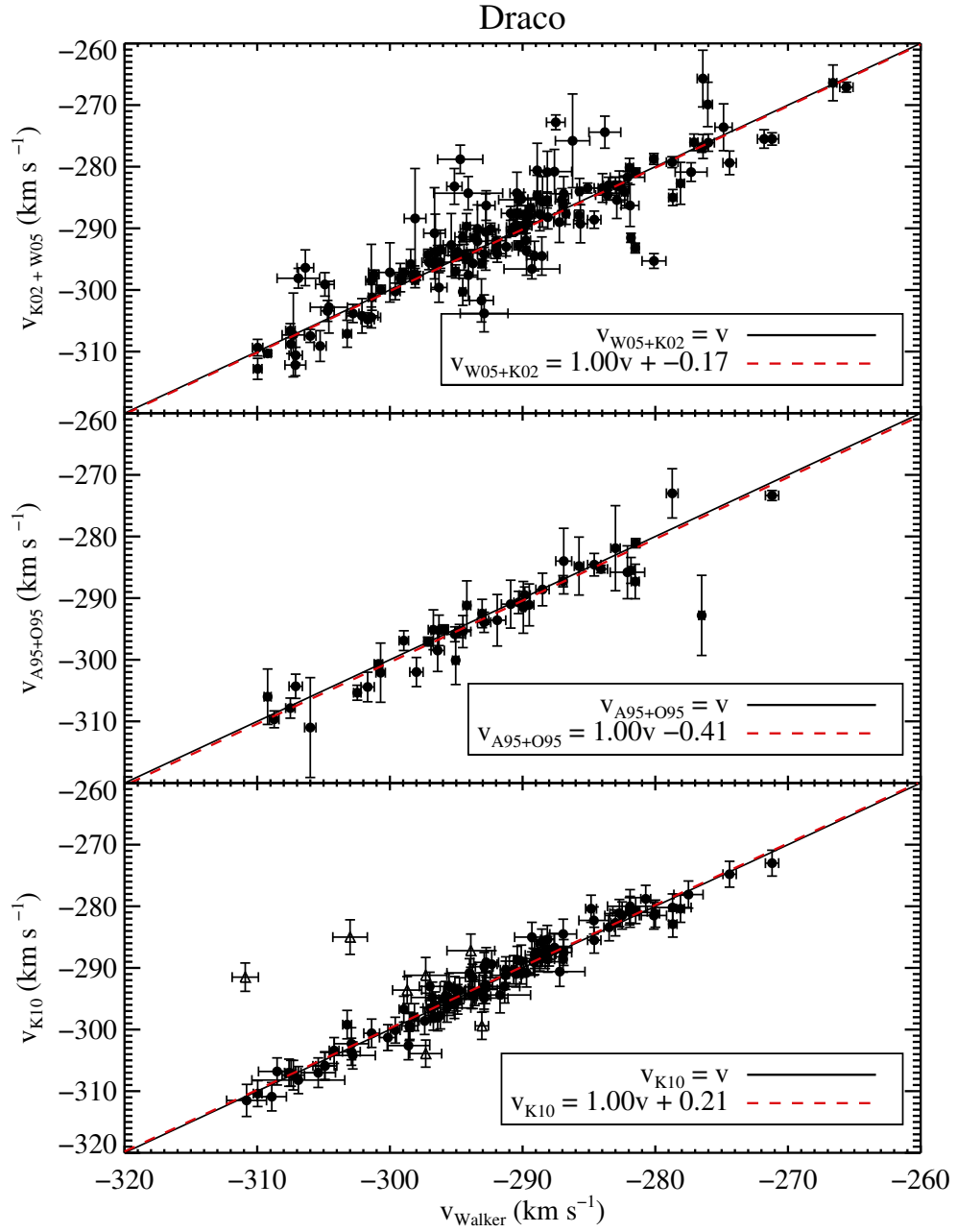


Figure 4.3 Comparison of literature velocities to those of W15 for Draco. The solid black line is where stars should fall if they have perfect agreement across studies and the red dashed line shows the best-fit line with slope set equal to 1. The offset that is applied to each data set is the y-intercept of the red dashed line.

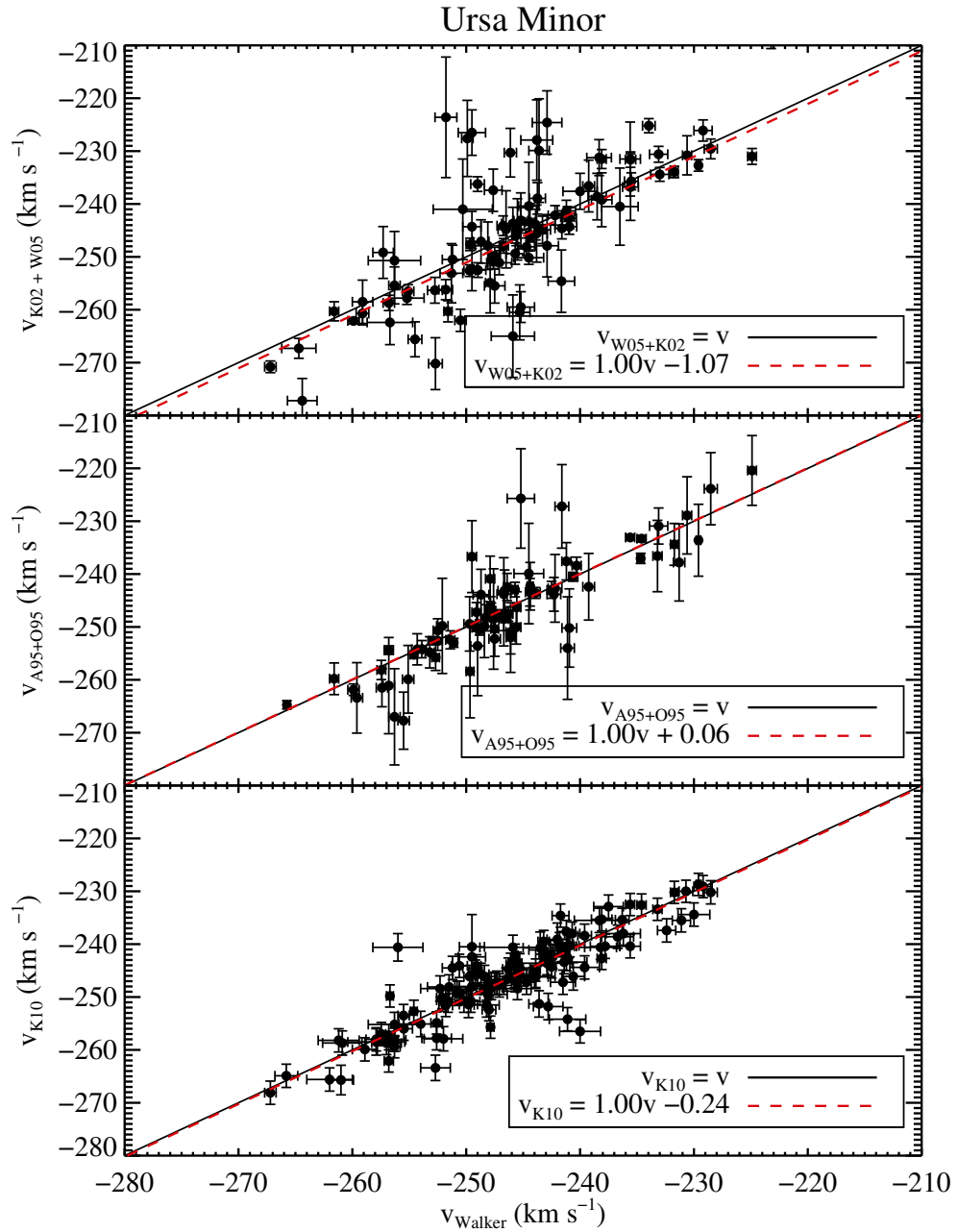


Figure 4.4 Comparison of literature velocities to those of W17 for Ursa Minor. The solid black line is where stars should fall if they have perfect agreement across studies and the red dashed line shows the best-fit line with slope set equal to 1. The offset that is applied to each data set is the y-intercept of the red dashed line.

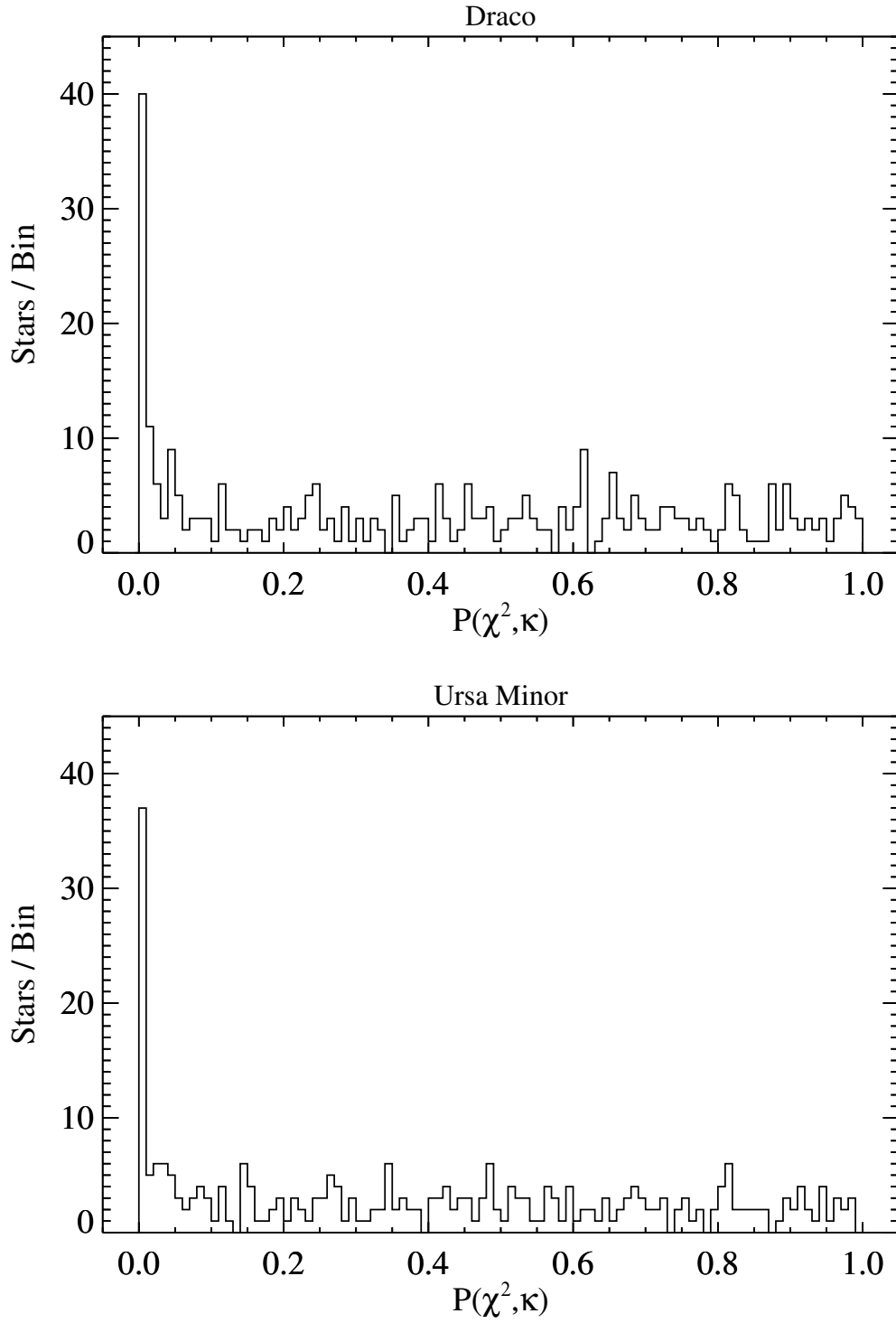


Figure 4.5 Probability of exceeding χ^2 . Top panel is Draco and bottom panel is Ursa Minor.

higher/lower P values. If binaries exist with Δv 's comparable to the observational errors and the errors are well-determined, then the lowest bin, $0 < P(\chi^2, \kappa) < 0.01$, would be enhanced relative to the mean χ^2 value.

As a test of the precision of our error estimates and the existence of binaries, we have fit two lines to the histograms in Figure 4.5; one line has a fixed slope of zero and the other has a variable non-zero slope. In Draco the flat line had a y-intercept of 2.96 ± 0.15 , and the expectation was 3.03 (calculated as the number of stars with $P(\chi^2, \kappa) > 0.01$ divided by 99 bins). The slope in the second line had a 1σ error bar as large as the value, indicating that it is consistent with being flat. The good agreement of the line being flat indicates that the velocity errors in Draco accurately represent the data. In Ursa Minor the results are very similar. The flat line had a y-intercept of 2.47 ± 0.14 , and the expectation was 2.49. Once again the slope of the second line had errors as large as the value. We draw the same conclusion for Ursa Minor as Draco: the velocity errors are not over- or underestimated.

4.2.5 Summary of Velocity Data

In Draco there are 692 unique stars, 341 of which have multiple observations. There are a total of 1204 velocity measurements for the subset of stars with multiple observations. These data are listed in Table G.1 of the appendices. In Ursa Minor there are 680 unique stars. 284 of them have multiple observations. There are a total of 875 measurements for the stars with multiple observations, which are listed in Table H.1.

Some important aspects of these velocity data are highlighted in Figure 4.6 for Draco and Figure 4.7 for Ursa Minor. In the top panel we plot a histogram of the number of observations per star, n . The maximum number of observations in Draco is 11 and in Ursa Minor the maximum is 10. The middle panel is a histogram of the amount of time elapsed between the first observation and the last observation for

each star. Both dwarfs have a handful of stars with baselines as long as 25 years. Finally the bottom panel is a histogram of the number of measurements taken per year. The bins are labeled with the study that produced the measurements.

4.3 Methodology

The definition of binary fraction is notoriously slippery, having slightly different definitions amongst different studies and often taking on other names such as companion frequency, multiplicity frequency, multiplicity rate, etc. (see, for example, Olszewski et al., 1996; Duchêne & Kraus, 2013). In the present study, we consider two stars that are gravitationally bound to one another to be a binary system. We define the binary fraction, f , to be the fraction of all apparently single stars that turn out to be binary systems based, in our case, on their velocity variability. We do not consider photometric binaries because the remoteness of the systems makes these hard to detect, though wide binaries do exist in dSphs (e.g., Peñarrubia et al., 2016). The constituent stars of a binary system do not get double counted by this definition of the binary fraction. This definition is sufficient for our study because we are considering only binary systems containing red giants, which are unlikely to pair with similar stars due to their comparatively short lifetimes.

The goal of this study is to determine the binary fractions of the stellar populations comprising the Draco and Ursa Minor dSph galaxies. The method for determining the binary fraction that we adopt in this chapter is similar to that described in Chapter III, but with some changes. The primary steps of the process involve defining the binary fraction (Section 4.3.1), running Monte Carlo simulations of the velocity variability (Section 4.3.2), performing a Bayesian analysis on the data and simulations (Section 4.3.3), and extracting a binary fraction from the posterior (Section 4.3.4).

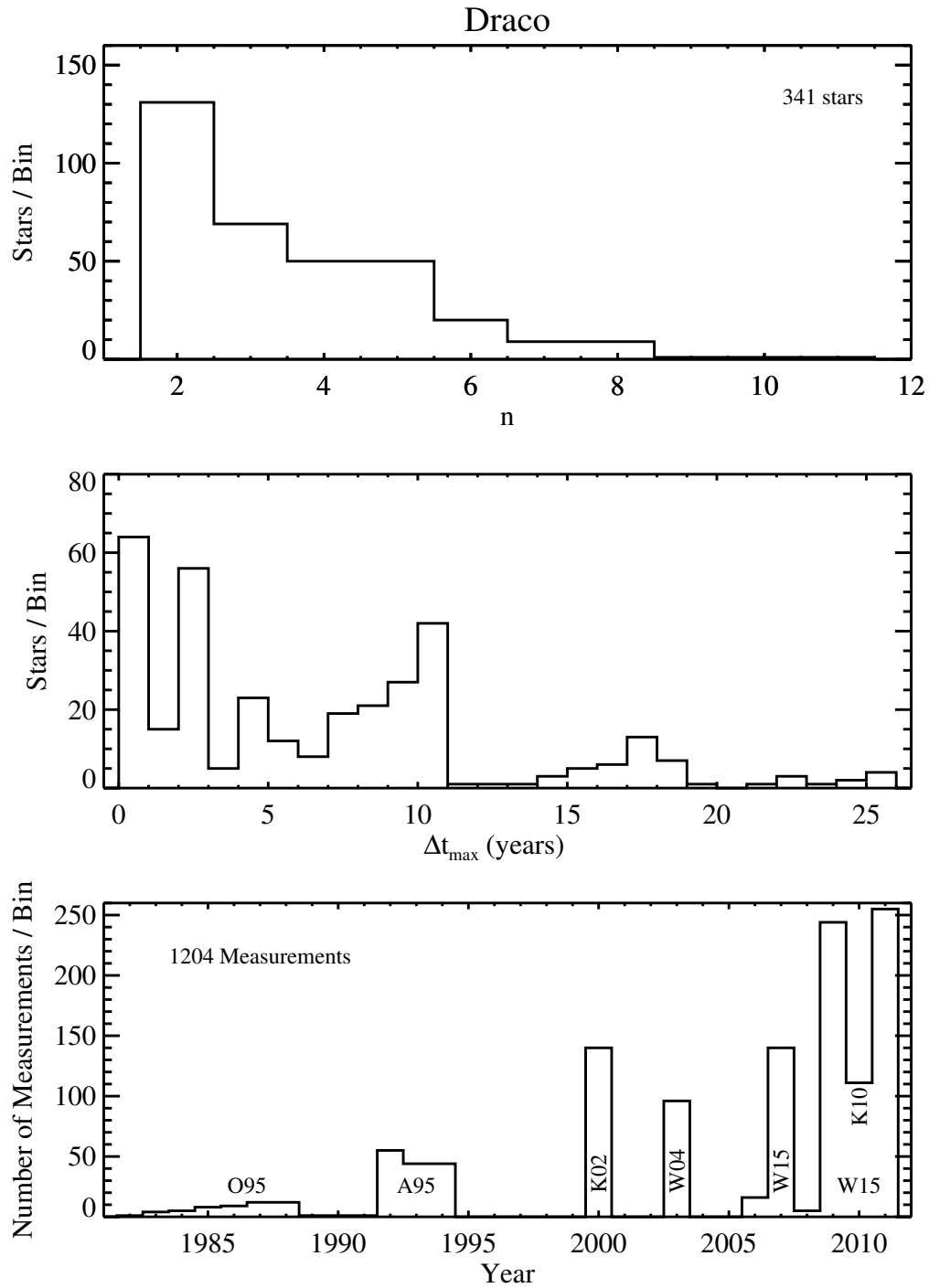


Figure 4.6 Summary of Draco data. Top: histogram of number of observations per star. Middle: histogram of maximum time baseline length per star. Bottom: histogram of number of measurements taken per year. Bins are labeled with the paper that produced the measurements.

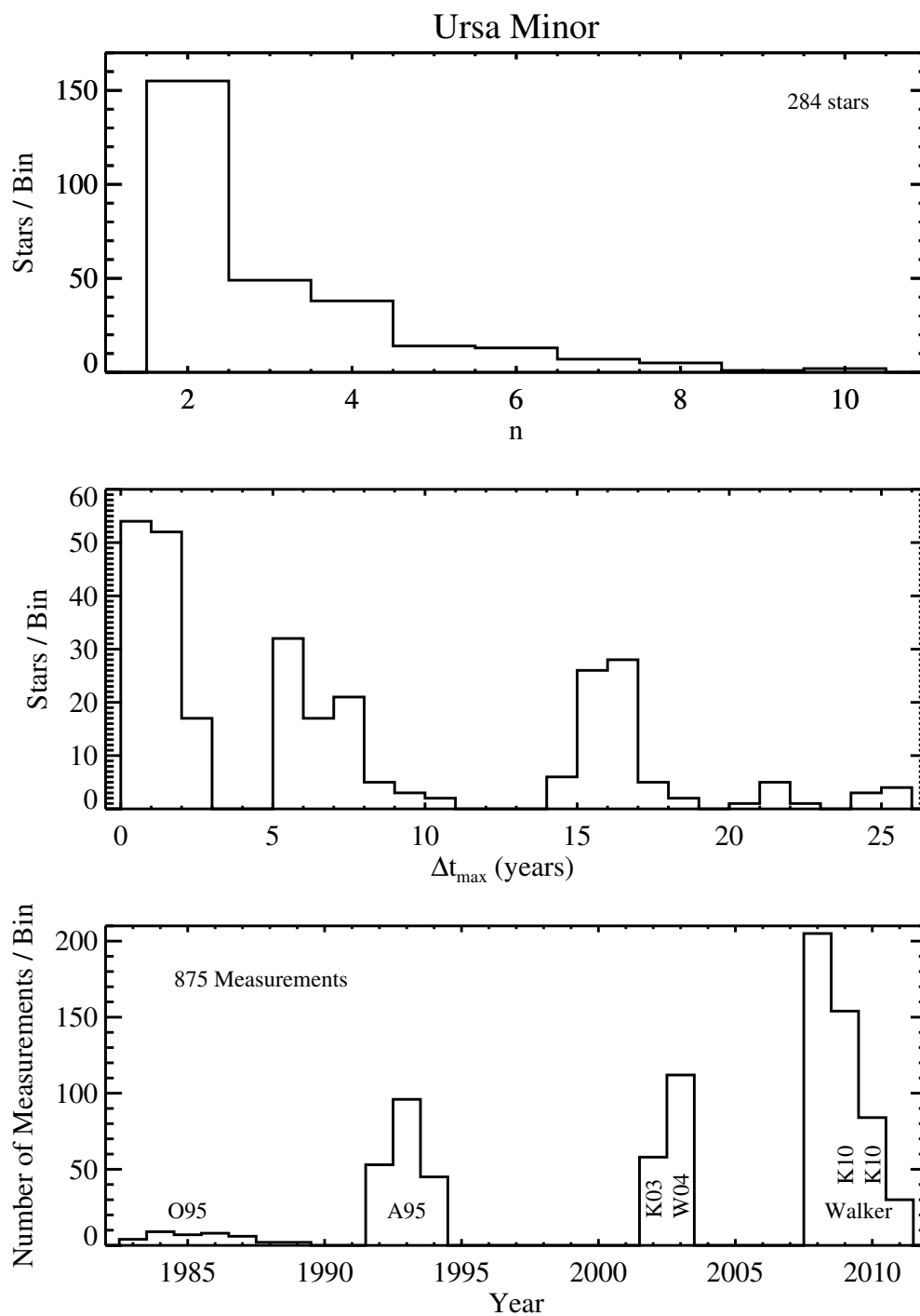


Figure 4.7 Same as Figure 4.6 but for Ursa Minor. Top: histogram of number of observations per star. Middle: histogram of maximum time baseline length per star. Bottom: histogram of number of measurements taken per year. Bins are labeled with the paper that produced the measurements.

4.3.1 Binary Parameters

Like the methodology described in Chapter 3.3.1, there are seven parameters that go into determining the orbital radial velocity of a binary. They are mass of the primary (m_1), mass ratio (q), period (P), eccentricity (e), true anomaly (θ), inclination (i), and argument of periastron (ω). The first four parameters are intrinsic to the system and three reflect the geometry of the system with respect to the observer. The equation that relates these parameters to the orbital radial velocity is

$$v_{r,orb} = \frac{q \sin i}{\sqrt{1 - e^2}} \left(\frac{2\pi G m_1}{P(1 + q)^2} \right)^{1/3} (\cos(\theta + \omega) + e \cos \omega). \quad (4.2)$$

For a derivation and additional details of this equation see Appendix A.

The mass of the primary, m_1 , can be set at a fixed value of $m_1 = 0.8 M_\odot$ because all of the stars in our sample are extremely old and are located along the red giant branch. All of the other parameters will vary from binary to binary. Mass ratio, period, and eccentricity are somewhat dependent on one another, so they will be drawn in the same order every time to ensure that the dependencies are preserved.

In this study, the second parameter, mass ratio, is defined as $q = m_2/m_1$, where m_1 is the primary red giant star and m_2 is the secondary star. We assume that the secondary is non-giant. We select the minimum mass ratio to be $q_{\min} = 0.1$. This requires the secondary companion to be a hydrogen-burning star with a mass of at least $0.08 M_\odot$. The maximum allowed value that we select for the mass ratio is $q_{\max} = 1$. This means that the secondary cannot have a mass larger than the red giant star that we observed.

We selected two mass ratio distributions to investigate in our simulations. The first is a normal distribution from Duquennoy & Mayor (1991), which is described by

$$\frac{dN}{dq} \propto \exp\left(-\frac{(q - \mu_q)^2}{2\sigma_q^2}\right). \quad (4.3)$$

The parameters that they found to best describe their data were $\sigma_q 0.42$ and $\mu_q = 0.23$. The second distribution,

$$\frac{dN}{dq} = \text{const}, \quad (4.4)$$

is constant across all mass ratios. This was used in Raghavan et al. (2010), as well as many other papers. The two distributions are plotted in Panel A of Figure 4.8.

As we shall see below, the period distribution has the largest effect on the binary fraction (Minor, 2013; Spencer et al., 2017b). For this reason, we consider three different period distributions to get a better understanding of the range of allowable binary fractions. This also allows us to rule out very high or very low binary fractions. Most studies have found a log-normal form provides the best fit to the, so we will select this form and change the parameters in the equation. The notation for this period distribution is

$$\frac{dN}{d \log P} \propto \exp \left(- \frac{(\log P - \mu_{\log P})^2}{2\sigma_{\log P}^2} \right), \quad (4.5)$$

where $\mu_{\log P}$ is the center of the distribution and $\sigma_{\log P}$ is the width. The period is expressed in units of $\log(\text{days})$. In addition to fixing the functional form, we also fix the second parameter $\sigma_{\log P}$ at $2.3 \log(\text{days})$ (Duquennoy & Mayor, 1991). This makes it easier to discern the effect that $\mu_{\log P}$ has on the inferred binary fraction. We first select $\mu_{\log P} = 4.8$ (Duquennoy & Mayor, 1991). This value was found by Duquennoy & Mayor (1991) to provide the best fit to F7 to G9 type stars in the Solar Neighborhood. A larger study by Raghavan et al. (2010) recovered $\mu_{\log P} = 5.03$ from their sample of F6 to G2 type stars. Because these two values are so similar, we opted to only use the first prescription.

The second parameter we considered is for K and M-dwarf stars (Fischer & Marcy, 1992). They found that the peak in $\log P$ occurred at much lower values between 3.5 to 4.9. We selected the smaller value for $\mu_{\log P}$ because this provided a distribution

that was more discrepant from the one defined above.

The third period distribution is theoretical in nature and comes from Marks & Kroupa (2011). They explored how the shape of the period distribution for main sequence stars might change with respect to spectral type, birth cluster clump size, and star formation rate. We selected their solution for a dwarf irregular galaxy in their Figure 9. This distribution is not log-normal, but instead is skewed toward higher periods. We fit a log-normal to their distribution and find that $\mu_{\log P} = 5.8$ does the best job of reproducing it, and so we adopt this for the last value of $\mu_{\log P}$.

The minimum and maximum binary periods expected for red giants in Draco and Ursa Minor can be constrained by considering the semi-major axes, a , compatible with these stars in such environments. The minimum semi-major axis occurs when the stellar surfaces are just out of contact. The primary star is a red giant with a radius much larger than the secondary, so we estimate a_{min} as the radius of the primary. Assuming a mass of $0.8 M_{\odot}$ and a surface gravity of about $10,000 \text{ cm s}^{-1}$, the radius works out to be about 0.21 AU. Using Kepler’s Third Law this corresponds to a period of $\log P_{min} = 1.57$ for a mass ratio of 0.1 or $\log P_{min} = 1.44$ for a mass ratio of 1.

The maximum semi-major axis is the maximum extent that a binary can reach before the gravitational force from its partner is less than that of neighboring stars in the galaxy. If we consider the gravitational unbinding of a binary due to the encounter with another star to be a “collision”, then the minimum semi-major axis can be thought of as the cross-section in the equation for mean free path. This yields the equation $a_{max} = (\pi\sigma_v tn)^{-1/2}$, where σ_v is velocity dispersion, t is the average age of the stars, and n is the number density of the stars. We calculate the number density by converting central luminosity density to mass density with the assumptions that a star has an average mass of $0.4 M_{\odot}$ and that $L/L_{\odot} \propto (M/M_{\odot})^4$. For Draco, we used 9.0 km s^{-1} as the velocity dispersion (Section 4.2.2), 10 Gyr as the average age

(Aparicio et al., 2001), and $0.008 L_{\odot} \text{ pc}^3$ as the central luminosity density (Mateo, 1998). For Ursa Minor, we used 8.0 km s^{-1} as the velocity dispersion (Section 4.2.2), 10 Gyr as the average age (Carrera et al., 2002), and $0.006 L_{\odot} \text{ pc}^3$ as the central luminosity density (Mateo, 1998). This places $\log P_{max}$ between 6.71 and 6.84 log days for Draco, and between 6.83 and 6.96 log days for Ursa Minor, depending on the mass ratio. These three period distributions and the limits are shown graphically in Panel B of Figure 4.8.

As we shall see below, eccentricity only has a small (1%) effect on the observed binary fraction (Minor et al., 2010; Spencer et al., 2017b), therefore we select a single distribution for this parameter. We used the one from Raghavan et al. (2010).

$$\frac{dN}{de} \propto \text{const.} \quad (4.6)$$

Another choice would have been a thermal distribution (i.e., $dN/de = 2e$), but it has been shown by Duchêne & Kraus (2013) that binary main sequence stars with periods greater than 100 days do not follow this trend. We note that binaries with short periods (on the order of 10 to 20 days) will have circular orbits. However, we do not need to include this condition because binaries with such short periods would have been destroyed as the primary ascended the red giant branch (Iben & Livio, 1993; Nie et al., 2012).

The eccentricity can range from 0 to 1, but in many cases the maximum value must be lower to prevent the stars from colliding as can happen with certain combinations of P and q . This limit is set by $e_{max} = 1 - (a_{min}/a)$, where a is the solution for the semi-major axis from Kepler's Third Law, given q and P from above.

The true anomaly, θ , is the angle between the lines connecting the periastron to the focus and the focus to the location of the star along its orbit. It dictates where the star is in its orbit. This angle is dependent on the eccentricity and period in such

a way that it has no analytical solution. Instead, we define a distribution for the area swept out by the star since it passed periastron. Kepler's Second Law states that within a gravitationally bound binary system, the radius vector of each component will sweep out an equal area in a given amount of time relative to the position of the other star. This can be written as

$$\frac{dN}{dA} = \text{const.} \quad (4.7)$$

By normalizing the area, A , so that periastron corresponds to 0 or 2π and apastron corresponds to π , we can redefine area as the mean anomaly. The true anomaly can then be numerically solved for using the mean anomaly and the eccentricity. Once the area at the time of the first observation is selected, the location of the star in its orbit at all later times can be described by $A = A_1 + (2\pi\Delta t/P)$, where Δt is the time elapsed since the first observation.

Inclination, i , is the angle between the observer's line of sight and the normal to orbital plane of the system. It ranges from 0 (face on) to 90 degrees (edge on) and has the form

$$\frac{dN}{dI} \propto \sin(i). \quad (4.8)$$

Finally, the argument of periastron, ω , is the angle between the ascending node of the orbit and the periastron point. It ranges from 0° to 360° . All values have an equal probability of occurring so we can write the distribution as

$$\frac{dN}{d\omega} = \text{const.} \quad (4.9)$$

The distributions of all the parameters described in this section are plotted in Figure 4.8.

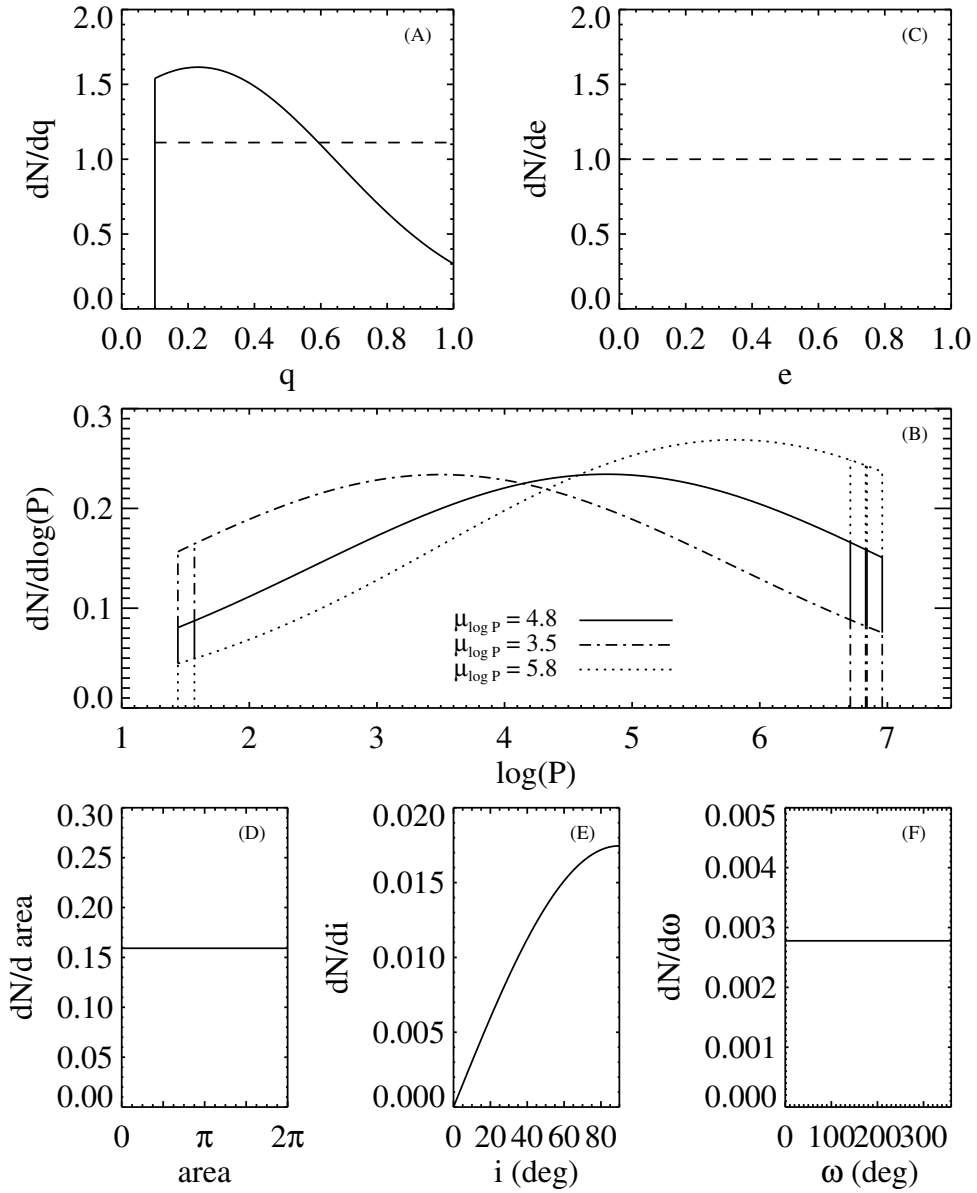


Figure 4.8 The binary parameter distributions used in our simulations. Panels A, B, and C are based on observations or theory from Duquennoy & Mayor (1991) (solid lines), Raghavan et al. (2010) (dashed lines), Marks & Kroupa (2011) (dotted line), and Fischer & Marcy (1992) (dot-dashed line). Vertical lines in Panel B indicate the range in the upper and lower boundaries caused by the mass ratio. Panels D, E, and F are based on observational geometry.

4.3.2 Monte Carlo Simulations

The purpose of the Monte Carlo (MC) simulations produced for this study is to generate a set of radial velocities that would be expected for a given binary fraction and compare those velocities with our observed radial velocities. The set of MC simulations that most resembles the data will tell us what the binary fraction is, under the assumptions of the simulations and given the binary parameter distributions described in Section 4.3.1. We have chosen to perform our analysis on the entire set of velocity data simultaneously for a given dwarf galaxy—Draco or Ursa Minor—rather than considering the binarity of each individual star, as has been done by others (Minor et al., 2010; Martinez et al., 2011; Cottaar & Hénault-Brunet, 2014).

Since we are only concerned with velocity variability, the mean motion of each star within the potential of a dwarf galaxy is irrelevant for this part of the analysis. We consider the change in velocity by defining a statistic as

$$\beta = \frac{|v_i - v_j|}{\sqrt{\sigma_i^2 + \sigma_j^2}}, \quad (4.10)$$

where v is the radial velocity and σ is the corresponding uncertainty in velocity. The subscripts i and j denote different observations of the same star. Stars with more observations will have more β 's and thus provide better leverage on the binary fraction. The number of β 's per star goes as $n(n - 1)/2$, where n is the number of observations per star.

The collection of β 's for a dSph is what we aim to reproduce with MC simulations. Our simulations employ data from the observational catalogs of Draco and Ursa Minor—radial velocity uncertainty, and the Julian date of each radial velocity measurement—along with the binary fraction, binary parameter distributions, and parameter limits described in Section 4.3.1. With these data and parameter inputs, we carry out the following steps to generate MC simulations of β , using binary frac-

tion, f , as the primary variable:

1. While going through each star in the input datasets for Draco or Ursa Minor, we randomly assign the star as a member of a binary system based on the binary fraction, f , being tested.
2. If the star is a binary according to Step 1, then we randomly select a value for each of the seven binary parameters according to the distributions described by Equations 4.3–4.9. If the star is not a binary, this step is skipped.
3. We then calculate the radial velocity for the star. If the star is a binary, this value comes from Equation 4.2. If the star is not a binary, this value is 0 km s^{-1} . (Zero signifies that the star has no velocity variation induced by a binary.)
4. We then resample the velocity from step 3 by adding a Gaussian deviate with standard deviation equal to the velocity uncertainty for that observation.
5. Steps 3-4 are repeated n times, where n is the number of observations for that star. All binary parameters from Step 2 are kept the same for an individual star except for the true anomaly, θ . This parameter is advanced by an amount corresponding to Δt , as described in the paragraph surrounding Equation 4.7.
6. We then calculate the β 's for that star by using Equation 4.10.
7. Steps 1-6 are repeated for all stars in a given galaxy's database. (There were 341 stars in Draco and 284 in Ursa Minor.)
8. Steps 1-7 are repeated η times. Unless noted, we typically adopted $\eta = 10^4$.
9. If a range of binary fractions was being investigated, we then repeated Steps 1-8 for each binary fraction under consideration. In most cases, we tested binary fractions from 0 to 1 in increments of 0.01.

4.3.3 Bayesian Technique

Next we compare the “base distribution”—the distribution of β values from the observations, β_{obs} —with the distributions of β 's from the MC simulations, β_{mod} . Our aim is to determine the probability that the base distribution can be reproduced by β_{mod} , given a certain binary fraction, f . One way to address this is through a Bayesian analysis. To begin, we can write Bayes' Theorem as

$$P(f|D, M) = \frac{P(D|f, M)P(f|M)}{P(D|M)}, \quad (4.11)$$

where the data, D , is β_{obs} from the observations and the model, M , is β_{mod} from the MC simulations. $P(f|M)$ is the prior and contains any previous knowledge that we might have had on the binary fraction before we began the analysis. This term is set equal to 1 because we have no prior constraints on f . The denominator, $P(D|M)$, is a normalization factor that we select such that the integral of the posterior, $P(f|D, M)$, is equal to unity. These two simplifications mean that the posterior is directly proportional to the likelihood of the data being produced by a given binary fraction and set of models, $P(D|f, M)$.

Deriving the equation for likelihood is somewhat complicated so we include Figure 4.9 to help illustrate the process for the case of $f = 0.5$. We start by placing the β 's into bins according to their value. In the top panel of Figure 4.9 we show this ordering as a red dashed histogram for β_{obs} . A similar histogram for β_{mod} is shown as a solid black line. We only show one of these to enhance readability, but there are in fact $\eta = 10^4$ of these histograms. We then define the number of β_{obs} in bin x as $N(x)_{obs}$. This is represented by the vertical red dashed line in the second panel of Figure 4.9 for the first bin. The number of β_{mod} in a given bin, x , for a certain simulation number, $j = \{0, 1, 2 \dots \eta\}$, is $N(x|j)_{mod}$. The histogram for $N(x_1|j)_{mod}$ is shown as a black solid line in the second panel of Figure 4.9.

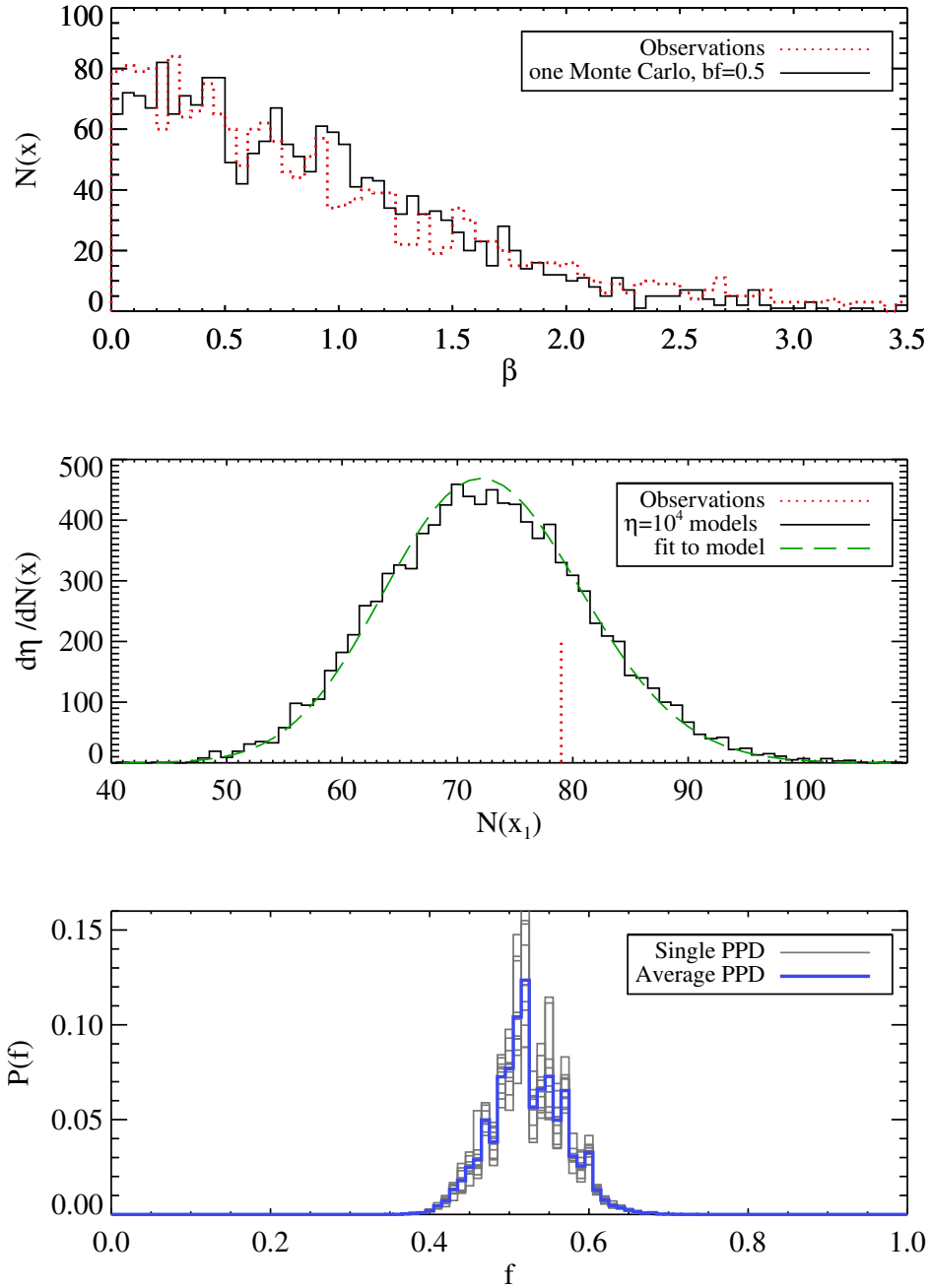


Figure 4.9 Top: Histogram of β_{obs} is shown as red dotted line. For readability we plot only one histogram of a single Monte Carlo simulation with $f = 0.5$, which is shown by the black solid line. Middle: A histogram of the number of β_{mod} in bin 1. The $\eta = 10^4$ MC models are fit with a green long-dashed line. The vertical red dashed line marks the number of β_{obs} in the bin. Bottom: PPDs for a single bin size are shown in gray. The normalized sum of these is shown in blue. These particular PPDs are for Draco with a normal mass distribution and a log-normal period distribution located at $\mu_{\log P} = 4.8$.

One could, in theory, use the histogram of $N(x = 1|j)_{mod}$ as the probability mass function to compute a likelihood. However, this would yield a very noisy posterior. Instead it is best to use a smooth function for the probability mass function. We have found that a Poisson function does a good job of reproducing $N(x|j)_{mod}$, which can be written as

$$\phi(N(x)|\mu_x) = \frac{\mu_x^{N(x)} \exp(-\mu_x)}{N(x)!}. \quad (4.12)$$

There is only one parameter in this distribution, μ_x , the average number of β_{mod} in the bin x , ($\mu_x = (1/\eta) \sum_{j=1}^{\eta} N(x|j)_{mod}$). In cases where μ_x was greater than 100, the equation became numerically unstable so we approximated it as a Gaussian with location μ_x and standard deviation equal to $\sqrt{\mu_x}$. We plot the corresponding Poisson function for the first bin, $\phi(N(x_1)|\mu_1)$, as a green long dashed line in the second panel of figure 4.9.

The likelihood for a single bin is then Equation 4.12 evaluated at $N(x)_{obs}$. This can easily be extrapolated to the likelihood over all bins by taking the product of the likelihoods from each bin. Recalling that the posterior is proportional to the likelihood, we finally arrive at

$$P(f|D, M) \propto \prod_x \phi(N(x)_{obs}|\mu_x). \quad (4.13)$$

We repeated this calculation over all f and normalized it such that $\sum_{f=0}^{f=1} P(f|D, M) = 1$.

There are two key parameters that we have yet to discuss that play a role in the posterior. They are bin size and number of bins. The bin size must be smaller than the largest β for a given f . This limit is set by the $f = 0$ case and works out to be about 2.5. If the bin size is larger than this value then the probabilities for $f = 0$ and other small f will be indistinguishable. In addition, $N(x|j)_{mod}$ is only well fit by a Poisson when the bin size is sim less than 0.05. Bin sizes larger than 0.05 but smaller

than 2.5 can still recover the binary fraction, but a skewed normal must be used in place of a Poisson (Spencer et al., 2017b).

The number of bins must be large enough to encapsulate all of the β 's, both observed and modeled. The largest values of β_{mod} are usually around 90, which equates to about 2000 bins. Additional bins that reach beyond the maximum value of β have no effect on the posterior, so it is always better to have too many bins than too few.

Because the Poisson distribution only has one well defined parameter, it is computationally fast to calculate the posterior. As such we have decided to solve for the posterior using 11 different bin sizes between 0.044 and 0.058. Then we add up all of the resulting posteriors and divide by 11 to normalize it once again. The final result is a posterior that is slightly less noisy. In the bottom panel of Figure 4.9 we plot the 11 individual posteriors in black, and the averaged posterior in red. We take the median of the posterior to be the binary fraction because this was shown shown in Chapter III to best reproduce the binary fraction in mock galaxies.

A final note worth mentioning is that while this method is similar to that in Chapter III, there are two key changes. The first is that we use a much smaller bin size, and continue binning up to the largest value of β . The previous method only used a total of 6 bins and lumped all β 's larger than 4 into one bin. One consequence of this was that we needed to fit a skewed normal function to $N(x|j)_{mod}$ rather than the much simpler Poisson that we have used here. Secondly, our earlier method in Chapter III used only one bin size to find the posterior, whereas we have taken the average of 11 here. Without this addition, the posteriors from Chapter III could shift a few percent to the right or left as a result of the wide binning. As we will see in Section 4.4, both methods produce the same binary fraction for Leo II. However, the variability of binary fraction with bin size seen in our earlier analysis (Chapter III) becomes negligible using our new methodology.

4.3.4 Repeatability

To ensure that our method produces accurate and unbiased results, we applied it to a series of test cases where the binary fraction was known. We considered 500 Monte Carlo realizations for 11 binary fractions evenly spaced from $f = 0$ to $f = 1$. These mock galaxies were based on the velocity errors and observation times from the Draco dataset. In all cases, we adopted a Gaussian mass ratio distribution (Equation 4.3) and a log-normal period distribution centered on $\mu_{\log P} = 4.3$. In Figure 4.10 we plot the difference between the observed binary fraction that our method recovered and the intrinsic binary fraction that was programmed into the galaxy. Black dots indicate the median observed binary fraction from the 500 mock galaxies. The error bars indicate the range that includes 68% of the galaxies. The horizontal dotted line is what we expect for an unbiased result, and it is indeed what we find for the majority of the mock galaxies. The only exception is the case where $f = 1$, and presumably other very high binary fractions ($f \gtrsim 0.9$), and the binary fraction is consistently underestimated by a few percent. Since it is physically unlikely for the binary fraction of an old stellar population to be near 1 (Goodwin et al., 2007, and references therein), this bias at high values is not a significant problem for realistic cases.

4.4 Results

Six combinations of mass ratio and period distributions were used to generate six complete sets of MC simulations, and consequently six posterior probability distributions (PPDs) of the binary fraction for each dSph. Certain clear correlations arise for specific adopted parameters. For example, the smallest f in both Draco and Ursa Minor is found with a constant mass ratio distribution and a log-normal period distribution with a location of $\mu_{\log P} = 3.5$ and a width of $\sigma_{\log P} = 2.3$. The largest

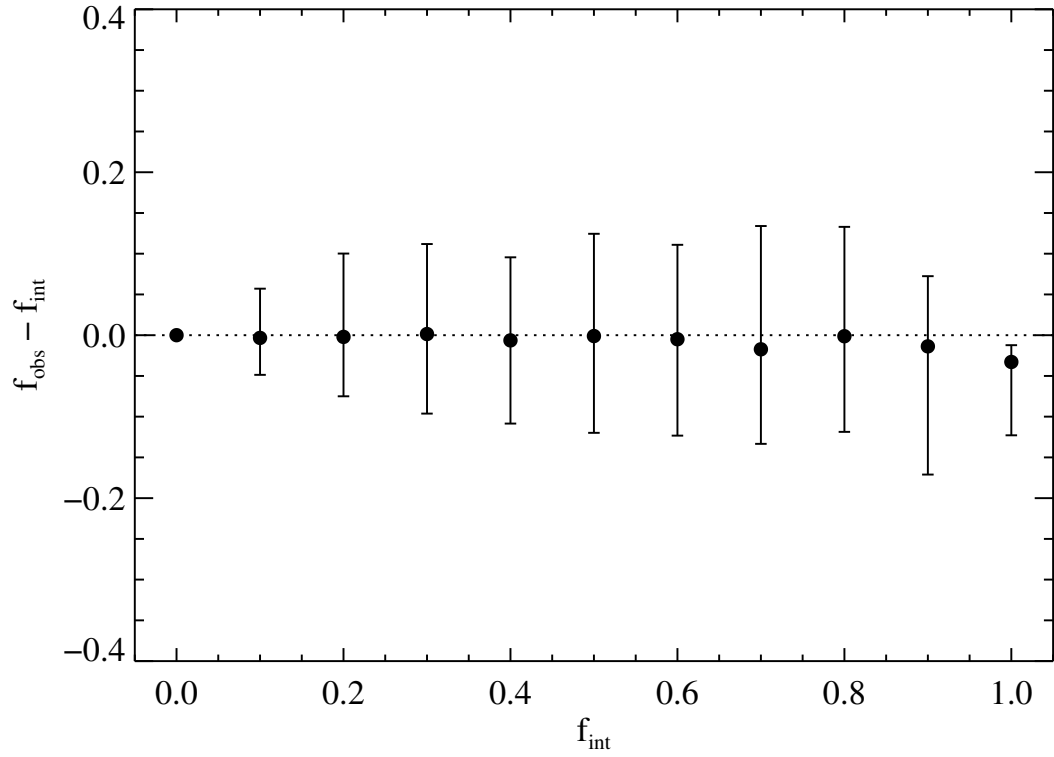


Figure 4.10 The median observed binary fraction, f_{obs} , for 500 mock Draco-like galaxies is plotted against the intrinsic binary fraction, f_{int} . The horizontal dotted line is where the observed binary fraction perfectly matches the intrinsic binary fraction. Error bars show the range of observed binary fractions that 68% of all mock galaxies fell between.

binary fraction for both galaxies corresponds to a normal mass ratio distribution and a log-normal period distribution with $\mu_{\log P} = 5.8$. The smallest and largest binary fractions found in Draco are $0.29_{-0.03}^{+0.03}$ and $0.69_{-0.06}^{+0.07}$. For Ursa Minor the binary fraction ranges from $0.45_{-0.05}^{+0.05}$ to $0.96_{-0.06}^{+0.03}$. Even though the binary fractions vary considerably with the binary orbital parameters, we can still rule out $f > 0.86$ and $f < 0.22$ in Draco with 99% confidence. Similarly, binary fractions below 0.32 can be ruled out with 99% confidence in Ursa Minor. It should be noted that while these limits do depend on binary orbital parameters, it is not likely that the binary fraction will be beyond these limits because we specifically chose parameter distributions that explored the largest range of observed parameters. A full summary of the PPDs is provided in Table 4.2.

In Figures 4.11 and 4.12 we plot all of the PPDs for Draco and Ursa Minor respectively. The top row shows the posteriors with a normal mass ratio distribution (Duquennoy & Mayor, 1991) and the middle row has a constant mass ratio distribution (Raghavan et al., 2010). The left column uses a log-normal period centered at $\mu_{\log P} = 4.8$ (Duquennoy & Mayor, 1991), the middle column is centered at $\mu_{\log P} = 3.5$ (Fischer & Marcy, 1992), and right column is centered at $\mu_{\log P} = 5.8$ (Marks & Kroupa, 2011). As expected, the binary fraction is larger for higher values of $\mu_{\log P}$. Changes to the period distribution also have the largest effect on the posterior. Increasing $\mu_{\log P}$ from 0.35 to 0.58 increases the binary fraction by about 30% for Draco and about 40% for Ursa Minor. Alternatively the mass ratio distribution can only change the resulting binary fraction by 5-10% for a given period distribution.

One interesting thing of note is that the distribution of β_{obs} from the data never fully matched the distributions of β_{mod} from the simulations. (This discrepancy was much more pronounced in Leo II, a dSph that we consider in the next section, than for Draco or Ursa Minor.) This suggests that the binary parameter combinations that we used do not reflect the actual parameters found in the dwarfs. Although beyond

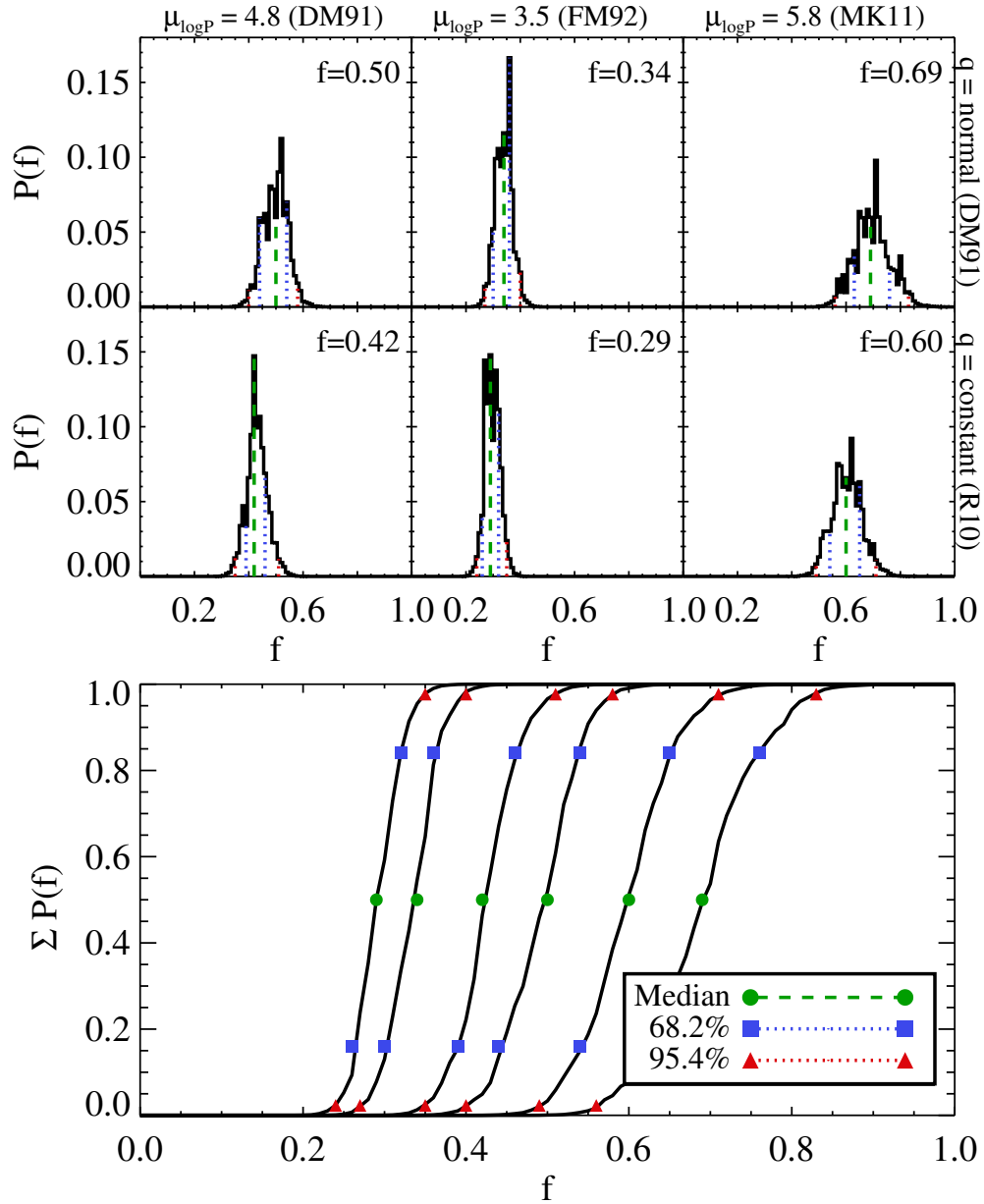


Figure 4.11 Top panels are PPDs and bottom panels are cumulative PPDs for Draco. The parameters used in the simulations are listed on the top and right axes of the PPDs. DM91=Duquennoy & Mayor (1991), FM92 = Fischer & Marcy (1992), R10 = Raghavan et al. (2010), MK11 = Marks & Kroupa (2011).

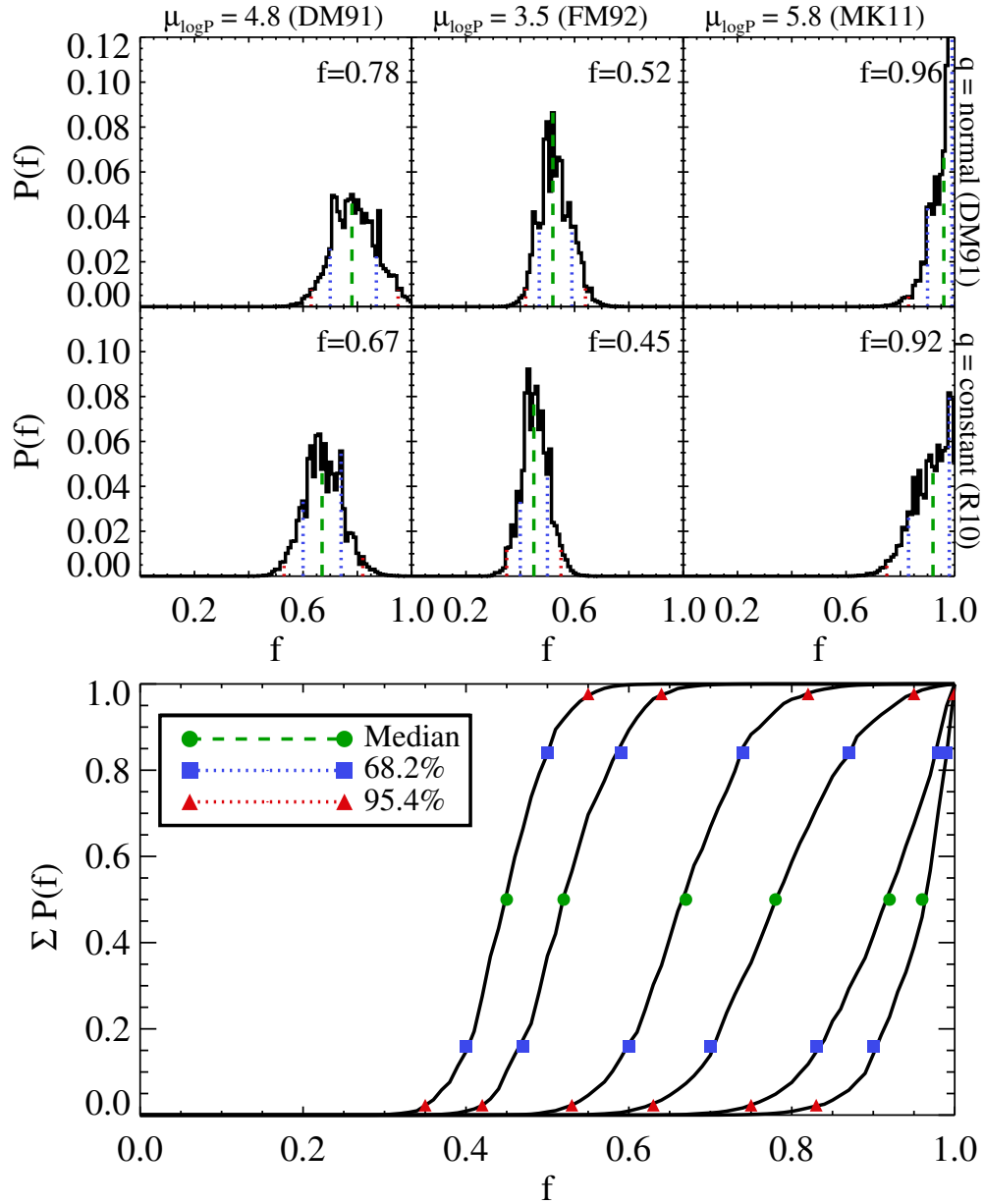


Figure 4.12 Same as Figure 4.11 but for Ursa Minor. Top panels are PPDs and bottom panels are cumulative PPDs. The parameters used in the simulations are listed on the top and right axes of the PPDs. DM91=Duquennoy & Mayor (1991), FM92 = Fischer & Marcy (1992), R10 = Raghavan et al. (2010), MK11 = Marks & Kroupa (2011).

the scope of this work, it seems possible that some constraints could be put on the mass ratio and period distributions by considering the shape of the β distributions. The best we can do here is comment on which of the six parameter sets provides the best fit to the data.

We repeat the Bayesian analysis from Section 4.3.2 that was used to generate the PPDs in Figures 4.11 and 4.12, with one adjustment. We normalize the posterior such that the sum of all six PPDs for each of the models is equal to one, rather than the sum of each individual PPD being equal to one. Because these are relative probabilities, their values have no physical meaning, but comparisons between models can be used to say which model is more likely and by how much. In Figure 4.13, the relative probability for each of the six models over all values of f is shown as a solid line; the relative probability over the 68% credible interval is shown as a dashed line. Parameter distributions are listed above each bar in the figure.

In all cases, the models with the Duquennoy & Mayor (1991) mass ratio distribution were more likely than the models with the Raghavan et al. (2010) mass ratio distribution for a given period distribution. For a given mass ratio distribution, the models with $\mu_{\log P} = 3.5$ (as in Fischer & Marcy (1992)) always had the lowest probability. The set of parameters that best reproduced the data in Draco was the Duquennoy & Mayor (1991) mass ratio distribution and a period distribution with $\mu_{\log P} = 5.8$, which corresponded to a binary fraction of $0.69^{+0.07}_{-0.06}$. For Ursa Minor the parameters were the Duquennoy & Mayor (1991) mass ratio distribution and Duquennoy & Mayor (1991) period distribution ($\mu_{\log P} = 4.8$), which had a binary fraction of $0.78^{+0.09}_{-0.08}$. The three best fitting models—Duquennoy & Mayor (1991) mass ratio distribution with either $\mu_{\log P} = 4.8$ or $\mu_{\log P} = 5.8$, and Raghavan et al. (2010) mass ratio distribution with $\mu_{\log P} = 5.8$ —are the same for both dwarfs. While we cannot comment on the absolute parameters of the mass ratio and period distributions, we can say that the Duquennoy & Mayor (1991) mass ratio distribution is preferred over

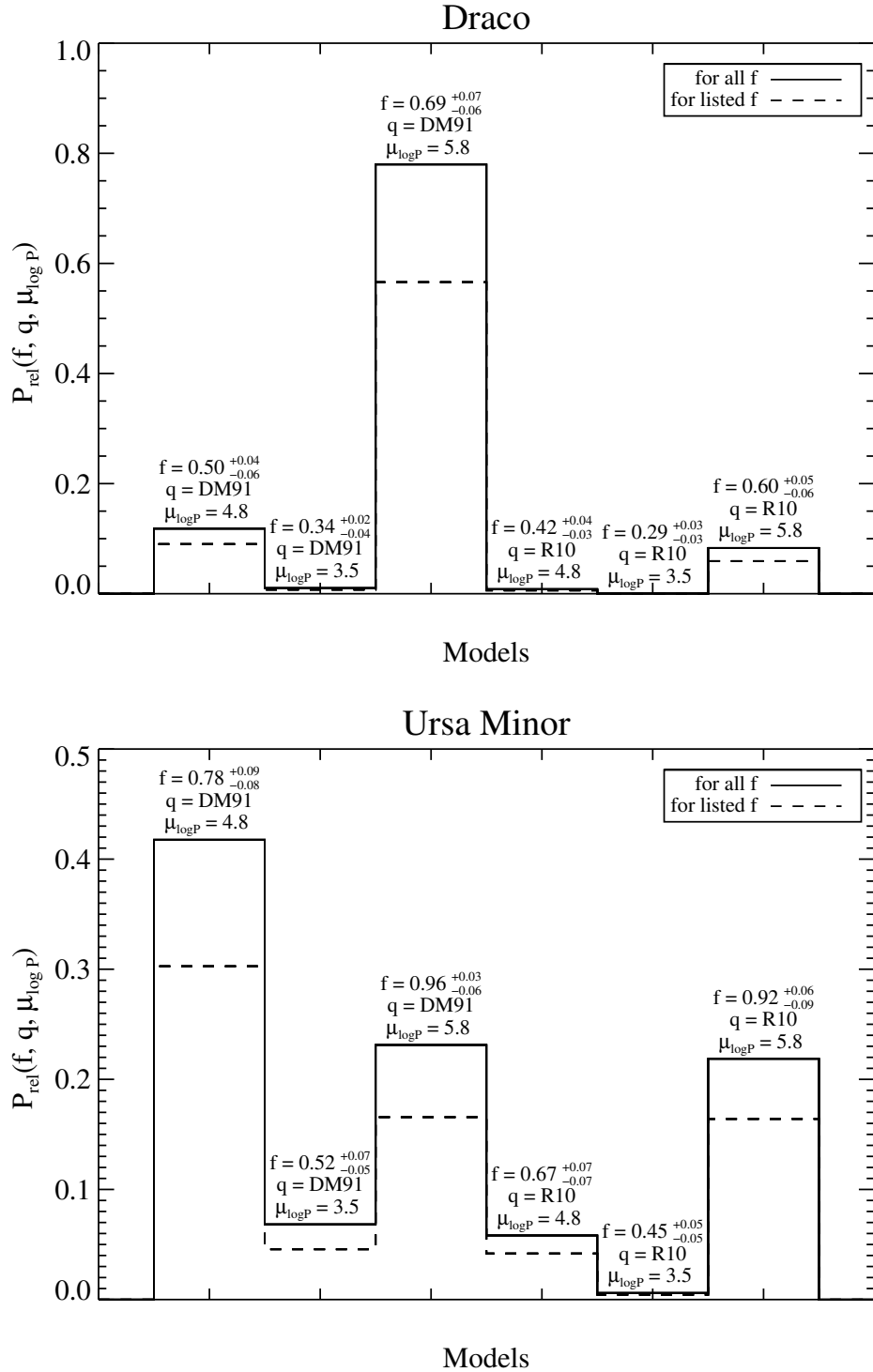


Figure 4.13 Relative probability of a model fitting the data. Model parameters are indicated above each bar. Bars are normalized so that the sum is equal to 1. Solid lines compare the relative probabilities of the PPDs over all values of f ($0 \leq f \leq 1$) and dashed lines are for the values of f within the 68% credible intervals (listed above each bar). The top panel is Draco and the bottom panel is Ursa Minor.

the Raghavan et al. (2010) distribution, and that the period distribution peaks towards longer periods. A more continuous exploration of the parameter distributions should yield better constraints on the period and mass ratio distributions. Since the Duquennoy & Mayor (1991) parameter distributions are preferred by Ursa Minor and are more commonly found in other binary literature works, we use those parameters in the discussion below.

4.4.1 Binary Fractions Among Dwarfs

Binary fractions for Carina, Fornax, Sculptor, and Sextans have previously been reported by Minor (2013) based on MMFS/Magellan data from Walker et al. (2009a). These data spanned about 1 year and had 2–4 repeat observations. Due to the limits on n and Δt_{max} , that dataset was not ideal for a binary fraction analysis, but it still proved suitable to produce broad PPDs that ruled out some binary fractions. Given these results, it was natural to consider combining them with our results for Draco, Ursa Minor, and Leo II (Chapter III) to explore the behavior of the binary fraction across the more luminous MW dSph systems. However, there are some differences between our methods and those in Minor (2013) that make a simple combination of results problematic and potentially misleading. For example, they used a different eccentricity distribution, applied an error model to their analysis, and performed the Bayesian analysis on a star by star basis rather than as a dataset, all in contrast to the approach we describe here. Since a comparison still seems desirable, we chose to apply our methodology to the MMFS/Magellan data used by Minor (2013) to ensure consistency among binary fraction calculations.

The MMFS/Magellan dataset contains both member and nonmember stars of their respective dwarf galaxies (Walker et al., 2009a). We chose to select stars as members if they were within three times the velocity dispersion of the systemic velocity. The velocity dispersions and systemic velocities that we derived using the method from

Table 4.2. Median and credible intervals of PPDs for Draco and Ursa Minor

Galaxy	q distribution	$\sigma_{\log P}$ (log days)	$\mu_{\log P}$ (log days)	e distribution	median (f)	68.2% interval	95.4% interval
Draco	normal (DM91)	2.3 (DM91)	4.8 (DM91)	constant (R10)	0.50	0.44-0.54	0.40-0.58
Draco	normal (DM91)	2.3 (DM91)	3.5 (FM92)	constant (R10)	0.34	0.30-0.36	0.27-0.40
Draco	normal (DM91)	2.3 (DM91)	5.8 (MK11)	constant (R10)	0.69	0.63-0.76	0.56-0.83
Draco	constant (R10)	2.3 (DM91)	4.8 (DM91)	constant (R10)	0.42	0.39-0.46	0.35-0.51
Draco	constant (R10)	2.3 (DM91)	3.5 (FM92)	constant (R10)	0.29	0.26-0.32	0.24-0.35
Draco	constant (R10)	2.3 (DM91)	5.8 (MK11)	constant (R10)	0.60	0.54-0.65	0.49-0.71
Ursa Minor	normal (DM91)	2.3 (DM91)	4.8 (DM91)	constant (R10)	0.78	0.70-0.87	0.63-0.95
Ursa Minor	normal (DM91)	2.3 (DM91)	3.5 (FM92)	constant (R10)	0.52	0.47-0.59	0.42-0.64
Ursa Minor	normal (DM91)	2.3 (DM91)	5.8 (MK11)	constant (R10)	0.96	0.90-0.99	0.83-1.00
Ursa Minor	constant (R10)	2.3 (DM91)	4.8 (DM91)	constant (R10)	0.67	0.60-0.74	0.53-0.82
Ursa Minor	constant (R10)	2.3 (DM91)	3.5 (FM92)	constant (R10)	0.45	0.40-0.50	0.35-0.55
Ursa Minor	constant (R10)	2.3 (DM91)	5.8 (MK11)	constant (R10)	0.92	0.83-0.98	0.75-1.00

Note. —

DM91 = Duquennoy & Mayor (1991),

FM92 = Fischer & Marcy (1992),

R10 = Raghavan et al. (2010),

MK11 = Marks & Kroupa (2011).

Table 4.3. Quantities used to derive a_{max} in seven dSphs

Galaxy	v_{sys}^a (km s^{-1})	σ^b (km s^{-1})	Source of Data ^c	I_0^d ($L_{\odot} \text{pc}^{-3}$)
Draco	-292.3 ± 0.4	9.0 ± 0.3	Walker et al. (2015b)	0.008
Ursa Minor	-246.9 ± 0.4	8.0 ± 0.3	Walker et al. (2017)	0.006
Leo II	78.5 ± 0.6	7.4 ± 0.4	Spencer et al. (2017a)	0.029
Carina	223.0 ± 0.3	6.4 ± 0.3	Walker et al. (2009a)	0.006
Fornax	54.9 ± 0.2	11.8 ± 0.2	Walker et al. (2009a)	0.018
Sculptor	111.3 ± 0.2	8.4 ± 0.1	Walker et al. (2009a)	0.055
Sextans	224.0 ± 0.4	8.2 ± 0.4	Walker et al. (2009a)	0.002

^aSystemic velocity

^bVelocity dispersion

^cSource for velocity data that we used to determine the systemic velocity and velocity dispersion.

^dCentral luminosity density from Mateo (1998).

Section 4.2.2 are listed in Table 4.3. These velocity dispersions were also used in conjunction with the luminosity densities from Mateo (1998) to derive a_{max} . The results of our simulations, assuming a normal mass ratio distribution and log-normal period distribution with $\mu_{\log P} = 4.8$ (i.e., parameters equivalent to those in the top left panels of Figures 4.11-4.12), agree very well with those from Minor (2013) in three of the four cases. Our binary fractions for Carina, Fornax, Sculptor, and Sextans are $0.20_{-0.13}^{+0.09}$, $0.87_{-0.09}^{+0.12}$, $0.58_{-0.17}^{+0.15}$, and $0.71_{-0.14}^{+0.15}$ respectively¹. Those from Minor (2013) are $0.14_{-0.05}^{+0.28}$, $0.44_{-0.12}^{+0.26}$, $0.59_{-0.16}^{+0.24}$, and $0.69_{-0.23}^{+0.19}$. These binary fraction results are displayed in Table 4.4.

The discrepancy between values for Fornax is almost certainly due to the treatment of the velocity errors. Minor (2013) estimated that the velocity errors on Fornax were under-reported by a factor of 55%. We can also see that the histogram of $P(\chi^2, \kappa)$ for Fornax exhibits some strange behavior. The number of stars per bin are not uniformly biased toward low P , as one would expect for a systematic underestimate of the velocity errors. Rather, there are some bins in the middle of the distribution

¹Assuming that the reported velocity error measurements are accurate. Systematically overestimated errors would lead to an underestimated binary fraction, whereas underestimated errors would lead to an overestimated binary fraction. See Appendix B.

Table 4.4. Binary fractions for seven dSphs

Galaxy	f	f_{ref}	Ref.
Draco	$0.50^{+0.05}_{-0.04}$	-	-
Ursa Minor	$0.78^{+0.08}_{-0.09}$	-	-
Leo II	$0.36^{+0.07}_{-0.08}$	$0.33^{+0.12}_{-0.09}$	Spencer et al. (2017b)
Carina	$0.20^{+0.09}_{-0.13}$	$0.14^{+0.28}_{-0.05}$	Minor (2013)
Fornax	$0.87^{+0.12}_{-0.09}$	$0.44^{+0.26}_{-0.12}$	Minor (2013)
Sculptor	$0.58^{+0.15}_{-0.17}$	$0.59^{+0.24}_{-0.16}$	Minor (2013)
Sextans	$0.71^{+0.15}_{-0.14}$	$0.69^{+0.19}_{-0.23}$	Minor (2013)

that contain more values than expected by Poisson errors. Since we are not set up to treat improperly reported velocity errors in our simulations, it is not surprising that our results are very different from what was previously reported. We ran two additional simulations in which we applied a constant corrective factor to the velocity errors. In the first case we multiplied the errors by a factor of 1.55 to match the estimates from Minor (2013), which yielded a binary fraction of $0.22^{+0.11}_{-0.09}$. In the second case we multiplied by a factor of 1.15 because we found this provided the best correction to our $P(\chi^2)$ histogram (see, Appendix B). It yielded a binary fraction of $0.61^{+0.15}_{-0.13}$.

It is curious that Minor (2013) finds such a large discrepancy between the reported velocity errors (Walker et al., 2009a) and their own velocity error estimates for Fornax but not for the other dwarfs, because all of the data were taken on the same instrument and often during the same run. An alternative to the Fornax errors being largely overestimated is that Fornax actually has a large binary fraction. Binary fraction and velocity errors are somewhat hard to disentangle. If the errors have been underestimated then the binary fraction will appear large; if the binary fraction is large then the errors will appear to be underestimated. The best way to determine velocity errors in the context of binaries is on a nightly basis by comparing the measurements from multiple exposures. Or if that is not possible, then using exposures taken over the course of a couple nights should suffice. Velocities observed

over such short timescales should not have any significant velocity variability caused by binaries and should represent the observational errors.

For archival velocity data that has only a single epoch, we have outlined a process for determining correction factors to velocity measurement errors in Appendix B, whereby different correction factors are applied for different epochs. This exercise was completed to illustrate the effects of incorrectly reported velocity errors on the inferred binary fraction. We do not implement the full routine in our simulations of Fornax because a) it becomes quite complicated for more than two epochs, b) we find no compelling evidence that the errors are misreported in such a way that the binary fraction would be grossly inaccurate, and c) because we see no reason why Fornax should have such inaccurate errors while the other three MMFS/Magellan dwarfs do not.

A binary fraction for Leo II was reported in Chapter III, but since the method in that chapter was slightly different than the one here, we chose to run a new set of MC simulations for Leo II as well. We used the normal mass ratio distribution and log-normal period distribution with $\mu_{\log P} = 4.8$, as was done for Carina, Fornax, Sculptor, and Sextans. The binary fraction for Leo II came out to be $0.36^{+0.07}_{-0.08}$, in good agreement with the previous results. The posteriors for all seven dwarfs are plotted in Figure 4.14, and the binary fractions are listed in Table 4.4.

The posteriors cover a large range of binary fractions, however their distributions are wide and all overlap around 0.55–0.60. This overlap region is small, suggesting that binary fraction is not a constant property across all dwarfs. Nevertheless, it is still valuable to determine the probability that the binary fraction is the same, and if it is the same, what value it takes on.

For the purpose of this discussion, we define “the same” as all the binary fractions being within some specified range. The width, w , of that range can be any value, but we chose to focus on $w = 0.1$ and $w = 0.2$. These were selected because the 68%

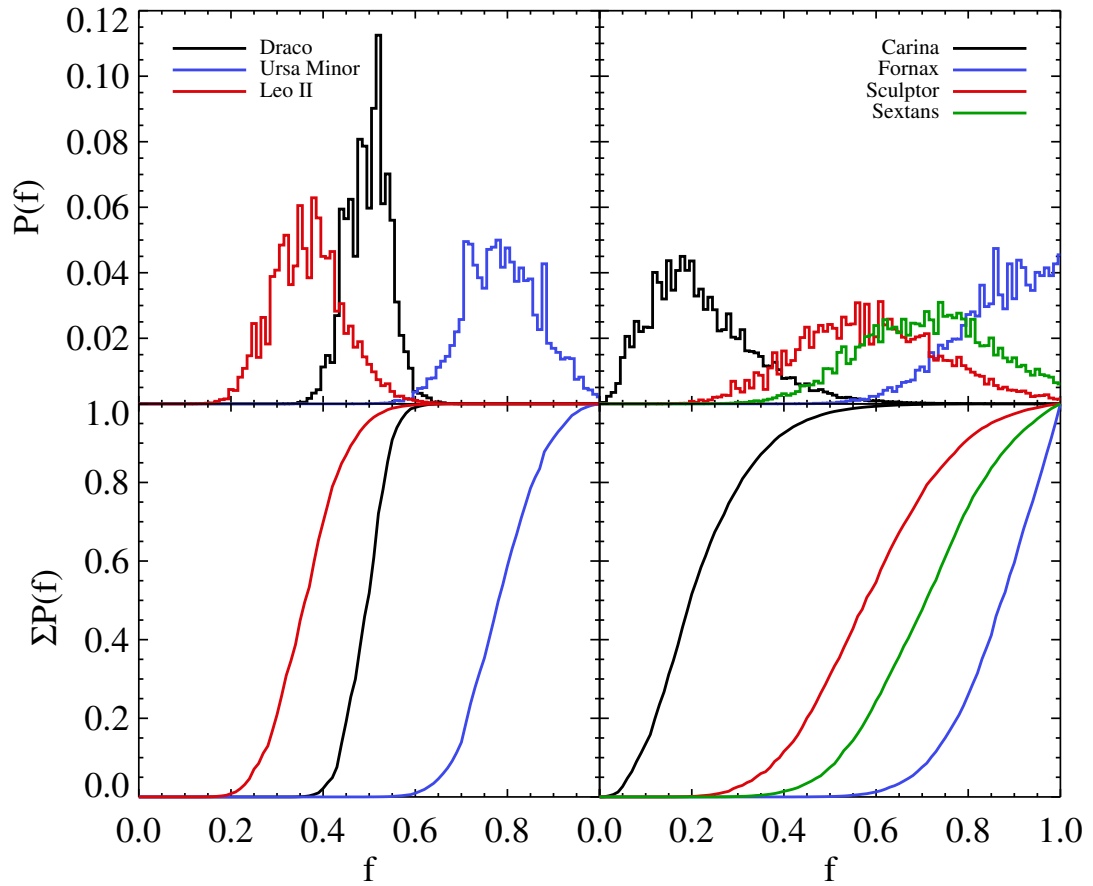


Figure 4.14 Top: PPDs for seven dwarfs using a normal mass ratio distribution and a log-normal period distribution centered on $\mu_{\log P} = 4.8$. Bottom: cumulative distributions of the posterior.

credible interval for Draco was ≈ 0.1 , and for Ursa Minor, Leo II, Carina, and Fornax it was ≈ 0.2 .

We can calculate the 7-dimensional joint probability that all the dwarfs have a binary fraction within some width, w , centered on some binary fraction f_g . (For example, the probability that all the dwarfs have a binary fraction between 0.4 to 0.6 would be the case where $f_g = 0.5$ and $w = 0.2$.) First we take the sum of the PPD for a single dSph over the range $(f_g - w/2)$ to $(f_g + w/2)$. This can be written as

$$P_d(w, f_g) = \sum_{f=f_g-w/2}^{f_g+w/2} P_d(f),$$

which yields the probability that the binary fraction for the dwarf, d , is within the specified range, w , centered on some binary fraction, f_g . Since we have normalized $P_d(f)$ such that the a sum over all f is equal to 1.0, this term will always be < 1 .

To find the probability that the binary fraction is within the range w centered on f_g for all the dwarfs, we need only take the product of the sums over over d . Assuming the PPDs are independent, this is given by

$$P(w, f_g) = \prod_d P_d(w, f_g) = \prod_d \left(\sum_{f=f_g-w/2}^{f_g+w/2} P_d(f) \right), \quad (4.14)$$

where d is the set of dwarfs, $d = \{\text{Draco, Ursa Minor, Leo II, Carina, Fornax, Sculptor, Sextans}\}$, and $P_d(f)$ is the PPD corresponding to that dwarf. We plot this probability as a function of f_g in Figure 4.15, with $w = 0.1$ occupying the left two panels and $w = 0.2$ in the right two panels. Since our posterior for Fornax is likely biased toward large values of f , we do this for the sample of seven dwarfs (top two panels), and for a sub-sample that excludes Fornax (bottom two panels). Due to the formulation of Equation 4.14, there are only values of $P(w, f_g)$ between $0.05 \leq f_g \leq 0.95$ for $w = 0.1$, and between $0.1 \leq f_g \leq 0.9$ for $w = 0.2$. (For example, if we selected $f_g = 0$

and $w = 0.1$ then the lower limit on the sum in Equation 4.14 would be $f = -0.05$, which is not a physically possible value for the binary fraction.)

The foremost feature of Figure 4.15 is the extremely small probabilities along the y-axes, which range from 10^{-9} – 10^{-5} . These values imply that it is unlikely for the binary fraction to be “the same” (i.e., within a 20% range) for the dSphs considered here. This concept will be given additional attention later in this section when we introduce another form of the probability equation.

The maximum probability for the seven-galaxy sample occurs at $f_g = 0.57$ for $w = 0.1$ and $f_g = 0.58$ for $w = 0.2$. This means that if these dSphs have binary fractions within 0.1 (0.2) of each other this is most likely to occur in the range $0.52 \leq f \leq 0.62$ ($0.48 \leq f \leq 0.68$). For the six-galaxy sample, the maximum probability occurs at $f_g = 0.53$ ($f_g = 0.54$) for $w = 0.1$ ($w = 0.2$). This means that if these dSphs have binary fractions within a range of 0.1 (0.2) then it is most likely to occur when $0.48 \leq f \leq 0.58$ ($0.44 \leq f \leq 0.64$).

The range of binary fractions for the sample of seven galaxies spans higher values than the sample of six galaxies because our analysis finds a large binary fraction for Fornax. As a result, Fornax imposes a lower limit on f_g . When Fornax is removed then f_g can shift toward lower values, but is still limited by Ursa Minor. On the other end, Carina and Leo II impose an upper limit on f_g .

The sample excluding Fornax has higher—though still very small—probabilities of the binary fraction being the same, as can be seen by the y-axis labels in Figure 4.15. This is once again because our analysis finds a large binary fraction for Fornax. The probability of Fornax having $f < 0.6$ is only 1%, and when such small numbers get multiplied through Equation 4.14 the result is very small probabilities. These probabilities are about two orders of magnitude smaller than the probabilities that exclude Fornax. To summarize, the inclusion of Fornax 1) pulls f_g toward higher values, and 2) decreases the probability that f could be the same for all dwarfs.

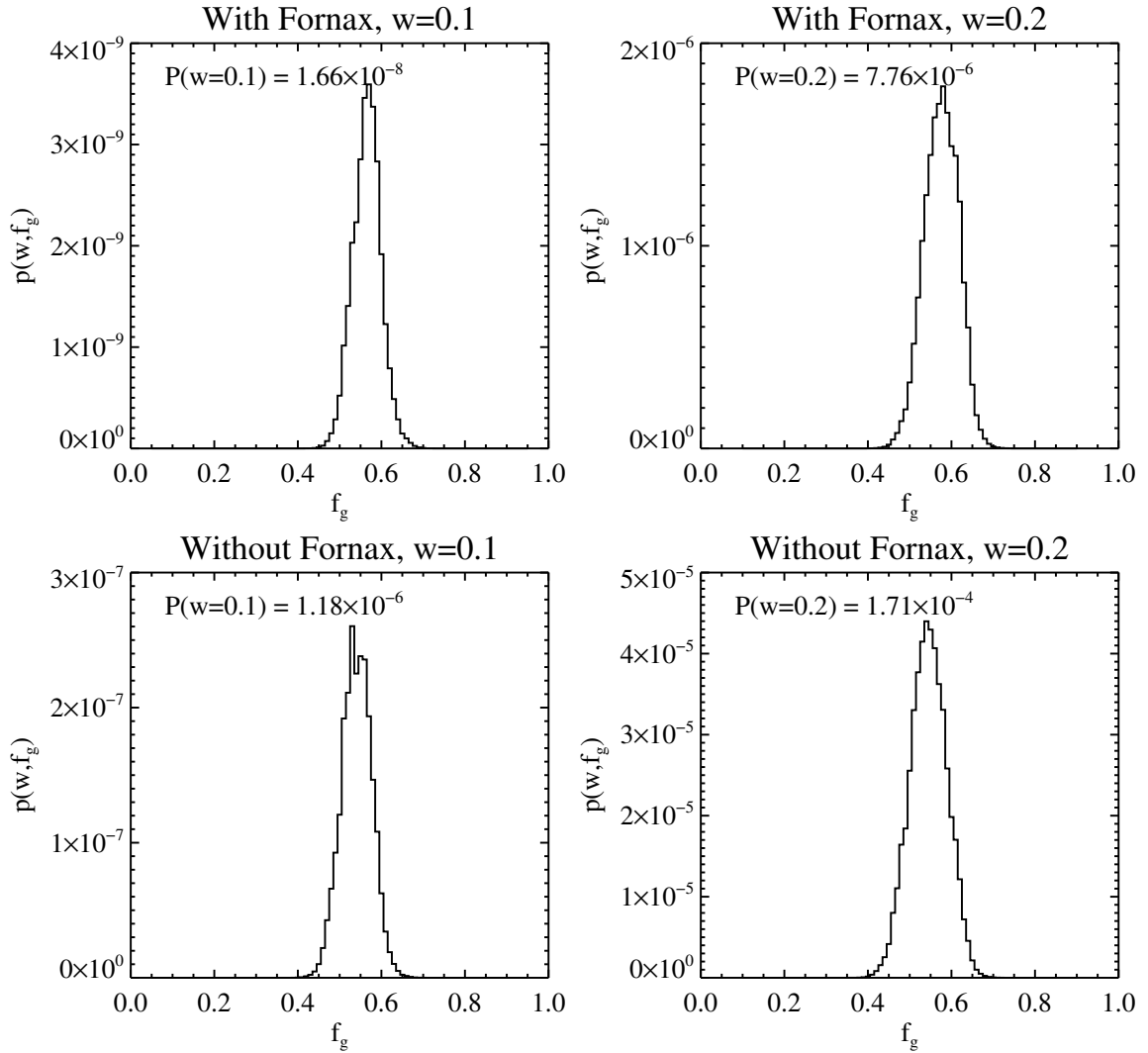


Figure 4.15 The probability that the binary fraction for all galaxies exists within a finite range, w , that is centered on f_g , as described by Equation 4.14. The left two panels use $w = 0.1$ and the right two use $w = 0.2$. The top two panels include seven galaxies and the bottom two include six galaxies. The total probability that binary fraction exists within some width w regardless of f_g is printed in the top left corner of each panel, and is defined in Equation 4.15. This figure was made under the assumptions that the period and mass ratio distributions take the forms described in Duquennoy & Mayor (1991).

Regardless of whether or not Fornax is included, the probability that the binary fraction for all the dwarfs is “the same” in these intervals is extremely small.

We now turn to a new question: how large must w be for the probability of f being “the same” to become appreciable? We tackle this by summing $P(w, f_g)$ over all f_g and exploring a continuous choice of w . The probability that all the dwarfs have a binary fraction within some range, w , centered on any value of f_g can be expressed as

$$P(w) = \prod_d \left(\sum_{f=0}^w P_d(f) \right) + \sum_{f_g=0.01+w/2}^{1-w/2} \left(\prod_d \left(\sum_{f=f_g-w/2}^{f_g+w/2} P_d(f) \right) - \prod_d \left(\sum_{f=f_g-w/2}^{f_g+w/2-0.01} P_d(f) \right) \right) \quad (4.15)$$

The last product term is subtracted to prevent some probabilities from being counted more than once. See Appendix C for a derivation.

Figure 4.16 plots this probability as a function of w . The set of seven galaxies is shown by the black solid line and the set of six galaxies is shown by the blue dashed line. The probability of the six-galaxy sample becomes greater than 1% around $w = 0.3$. For the seven-galaxy sample this transition occurs around $w = 0.4$. This means that the binary fractions of the galaxies do not all begin to occur within some specified range until that range has a width of at least 0.3–0.4 in f . This is larger than the credible intervals of most of the PPDs (as in Table 4.4), so an alternative interpretation is that the binary fractions should no longer be considered “the same” when w is this large. Rather, the binary fractions are spread over some range of values with a width of at least 0.3–0.4.

We produced variations of Figure 4.16 for different period and mass ratio distributions and found that the Fischer & Marcy (1992) distribution could bring this turning point down to as low as $w = 0.2$. Regardless of the inclusion of Fornax or binary parameter distributions, there is a $< 1\%$ chance that the binary fractions for

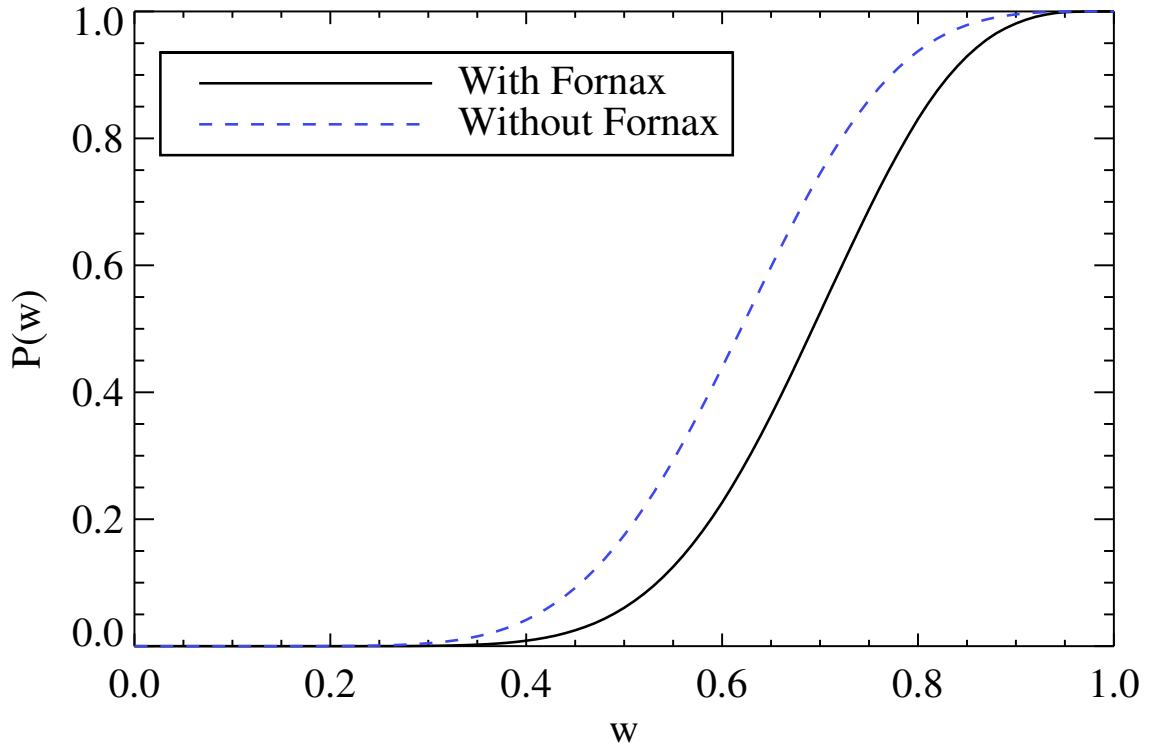


Figure 4.16 The probability that the binary fractions of dSphs exist within a specified range with width w . The solid black line includes 7 galaxies; the dashed blue line includes six galaxies. The dwarfs do not occupy the same range of f until that range is widened to about 0.3 or 0.4. This figure was made under the assumptions that the period and mass ratio distributions take the forms described in Duquennoy & Mayor (1991).

Table 4.5. Photometric and structural properties of classical dSphs

Dwarf	Distance ^a (kpc)	M_v ^a (mag)	surf bright ^a (mag arcsec ⁻²)	ellipticity ^a	r_{half} ^a (pc)	L_v ^b $10^6 L_\odot$	lum density ^b ($L_\odot \text{pc}^{-3}$)
Draco	76	-8.8±0.3	25.0±0.2	0.31±0.02	221±19	0.26	0.008
Ursa Minor	78	-8.8±0.5	26.0±0.5	0.56±0.05	181±27	0.29	0.006
Leo II	236	-9.8±0.3	24.2±0.3	0.13±0.05	176±42	0.58	0.029
Leo I	258	-12.0±0.3	22.6±0.3	0.21±0.03	251±27	4.79	0.092
Carina	107	-9.1±0.5	25.5±0.5	0.33±0.05	250±39	0.43	0.006
Fornax	149	-13.4±0.3	23.3±0.3	0.30±0.01	710±77	15.5	0.018
Sculptor	86	-11.1±0.5	23.5±0.5	0.32±0.03	283±45	2.15	0.055
Sextans	89	-9.3±0.5	27.1±0.5	0.35±0.05	695±44	0.5	0.002

^aValues taken from McConnachie (2012)

^bValues taken from Mateo (1998)

the considered dSphs all exist within some range of f with width 0.2. Ultimately, we find that it is highly unlikely that the binary fraction is constant across dwarf spheroidal galaxies.

Assuming that binary fraction varies amongst dwarfs, we examined whether it is dependent on any galactic properties. The properties we considered were distance from the Milky Way (McConnachie, 2012), absolute magnitude (McConnachie, 2012), surface brightness (Mateo, 1998), luminosity density (Mateo, 1998), mass density (Mateo, 1998), total mass within half light radius (Walker et al., 2009b), velocity dispersion (McConnachie, 2012), half light radius (Mateo, 1998), ellipticity (McConnachie, 2012), mean metallicity (Kirby et al., 2011), time to form 50% of the stellar mass (Weisz et al., 2014), and time to form 95% of the stellar mass (Weisz et al., 2014). Tables 4.4.1 and 4.4.1 list the values for the properties for the eight classical dSphs. We compare these properties to the binary fractions of Draco, Ursa Minor, and Leo II that were calculated in this chapter, and to the binary fractions of Carina, Fornax, Sculptor, and Sextans in Minor (2013).

Figure 4.17 shows four of the parameters plotted against binary fraction. Most cases yield scatterplots, such as absolute magnitude (top left panel). The three parameters that exhibited the most promising correlations with binary fraction are velocity

Table 4.6. Spectroscopic and mass properties of classical dSphs

Dwarf	σ^a km s ⁻¹	$M_{dyn}(\leq r_{half})^a$ $10^6 M_\odot$	mass density ^b (M_\odot pc ⁻³)	mean [Fe/H] ^a (dex)
Draco	9.1±1.2	11	0.46	-1.93±0.01
Ursa Minor	9.5±1.2	9.5	0.35	-2.13±0.01
Leo II	7.4±0.4	4.6	0.29	-1.62±0.01
Leo I	9.2±1.4	12	0.28	-1.43±0.01
Carina	6.6±1.2	6.3	0.17	-1.72±0.01
Fornax	11.7±0.9	56	0.086	-0.99±0.01
Sculptor	9.2±1.4	14	0.60	-1.68±0.01
Sextans	7.9±1.2	25	0.065	-1.93±0.01

^aValues taken from McConnachie (2012).

^bValues taken from Mateo (1998).

dispersion (top right panel), time since forming 50% of the stellar mass (bottom left panel), and time since forming 95% of the stellar mass (bottom right panel). The loose trends that we find are that binary fraction roughly increases with velocity dispersion, and that galaxies that formed more of their stars early on have higher binary fractions than those with a more extended star formation history.

Recall that one of the underlying purposes of this research is to see if binaries can alter our view of ultra-faints. The implication of the first trend is that ultra-faints would have low binary fractions. As a consequence their velocity dispersions would have very minor inflation due to binaries. This seems unlikely given the cases of Bootes I (Koposov et al., 2011) and Segue 1 (Simon et al., 2011), which did have 0.5-2 km s⁻¹ velocity dispersion corrections due to binaries. We fit a flat and sloped line to the data and find they both poorly represent the data with reduced chi square values of 3.9 and 3.6 respectively.

Marks & Kroupa (2011) used simulations to predict that the binary fraction should be larger for lower star formation rates. We use the time to form 50 or 95% of the stellar mass as a proxy for star formation rate and find the opposite – binary fraction is higher for fast star formation rates. This discrepancy could be caused by possible invalid assumptions in the models by Marks & Kroupa (2011) (i.e., that all stars are

start as members of binary systems), or small number statistics and large error bars on our findings. Once again we performed a flat and sloped fit to the data. The reduced chi square goodness of fit statistics for the time to form 50%(95%) were 7.0 (12.8) and 3.7 (7.2) for the flat and sloped lines respectively. The fits poorly represent the data but in both cases the sloped case does a much better job than the flat case. Either way, the quality and quantity of the data are not sufficient to discern any meaningful trends.

It has been suggested that a more densely populated star forming region should have a larger binary fraction (Kounkel et al., 2016). We do not see this reflected in the mass density or luminosity density of the dwarfs, but this is likely because the properties we have access to do not translate to the density of progenitor star-forming regions.

4.5 Conclusions

Velocity data for Draco and Ursa Minor has been accumulating since the early 1980s (O95; A95; K02; K03; W04; K10; W15; W17). We identified, collected, and combined the available data to produce the largest multi-epoch dataset of radial velocities in both dwarfs. While many of these datasets have been used in previous studies to achieve a myriad of kinematic results, all of them required additional culling before we could use them for our purposes. The most involved process was for the W15 and W17 data, which entailed a maximum likelihood estimation of the velocity dispersion and systemic velocity that could be used for membership identification.

This extensive velocity data made it possible for us to explore the binary fractions in Draco and Ursa Minor. We generated MC simulations of the data and used a Bayesian technique that was pioneered in Spencer et al. (2017b) and improved upon in this work to explore the binary fractions in Draco and Ursa Minor. By testing six different binary orbital parameter combinations for mass ratio and period, we

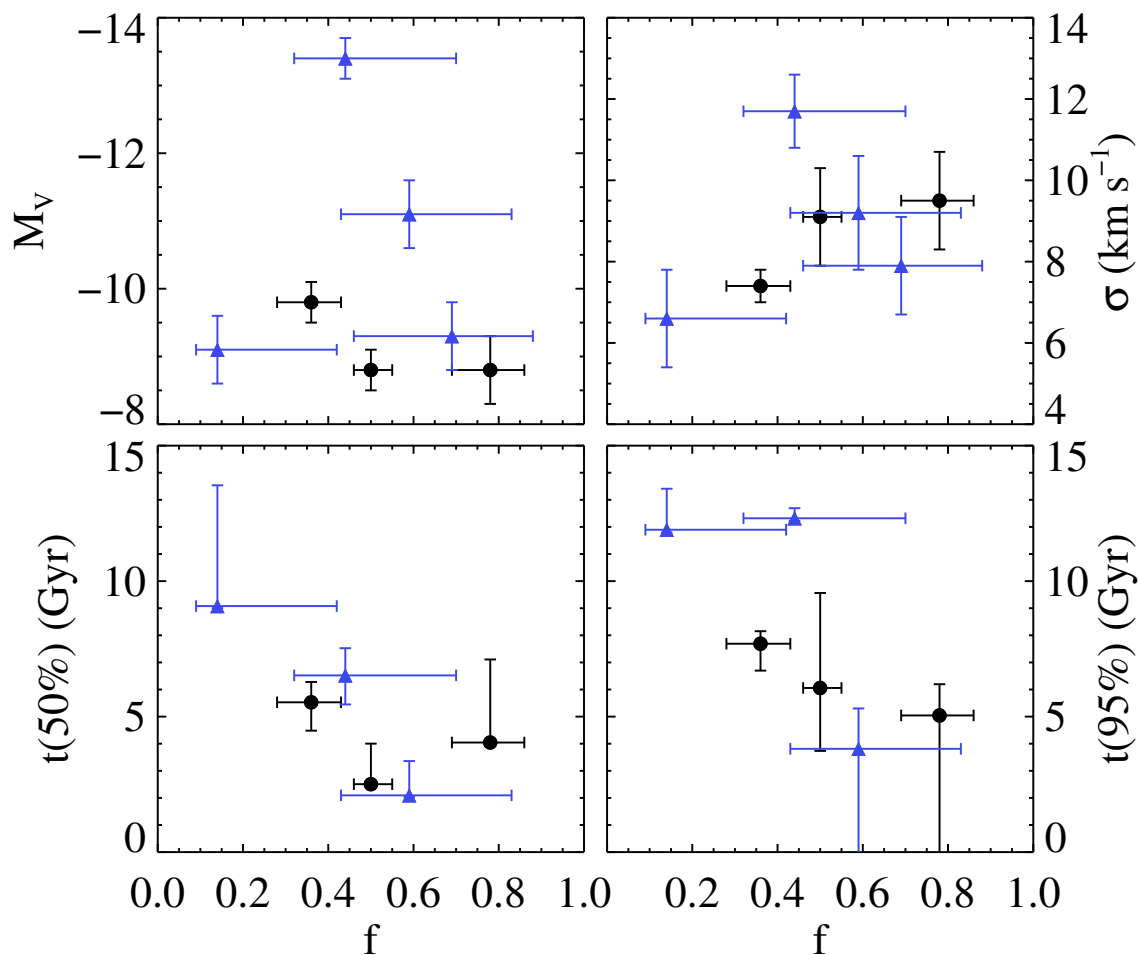


Figure 4.17 Binary fraction, f , is plotted against four other properties of the galaxies: absolute magnitude (top left), velocity dispersion (top right), lookback time when half of the stars were formed (bottom left), lookback time when 95% of the stars were formed (bottom right). Galaxies with f calculated in this chapter are shown as black circles and galaxies with f calculated in Minor (2013) are shown as blue triangles.

conclude that the binary fraction for Draco is between $0.29_{-0.03}^{+0.03}$ – $0.69_{-0.06}^{+0.07}$, and the binary fraction for Ursa Minor is between $0.45_{-0.05}^{+0.05}$ – $0.96_{-0.06}^{+0.03}$. The most commonly used period and mass ratio distributions come from Duquennoy & Mayor (1991), which yielded binary fractions of $0.50_{-0.06}^{+0.04}$ and $0.78_{-0.09}^{+0.08}$ in Draco and Ursa Minor respectively.

Changes to the shape of the period distribution had the largest effect on the posterior of the binary fraction, causing it to vary by as much as 30-50%. The values we tested for the period distribution were inspired by observations of F–M type stars (Duquennoy & Mayor, 1991; Fischer & Marcy, 1992) and simulations of stars in dwarf irregular galaxies (Marks & Kroupa, 2011). The mass ratio distributions that we tested only produced binary fractions that varied by 4-11%. Future work towards refining these distributions should focus more on the period distribution because it plays a larger role in determining the binary fraction. We found that the Duquennoy & Mayor (1991) mass ratio distribution always did a better job of reproducing the data than the Raghavan et al. (2010) distribution for a given period distribution. Period distributions peaking at $\mu_{\log P=4.8}$ or $\mu_{\log P=5.8}$ were always preferred over a distribution peaking at shorter periods ($\mu_{\log P=3.5}$).

Finally, we explored whether binary fraction is constant among dSphs by expanding our sample of two dwarfs to include Leo II, Carina, Fornax, Sculptor, and Sextans. We calculated the binary fraction for the additional dwarfs in the same way as was done for Draco and Ursa Minor, using velocity data from Chapter III for Leo II and from Walker et al. (2009a) for Carina, Fornax, Sculptor, and Sextans. The probability that the binary fraction is constant (i.e., exists within a range of f with width of 0.2 for all dwarfs) is $< 1\%$, regardless of the inclusion of Fornax or the combination of period and mass ratio distributions. Because this probability was so low, we considered how binary fraction may vary with a variety of dSph properties. The strongest trend we found was that binary fraction was larger for dSphs that formed

50 or 95% of their stars faster. However, the reduced χ^2 of the best fitting sloped lines were 3.7 or 7.2 for the time to form 50% and 95% of stars respectively, so the evidence does not strongly favor the correlation. Incorporating additional data for Carina, Fornax, Sculptor, and Sextans from other sources would allow for a better determination of their binary fractions and should yield cleaner trends with binary fraction if such trends exist.

CHAPTER V

Summary and Conclusions

5.1 Velocities are a Multi-Purpose Tool

The first 50 years of study on dwarf spheroidals relied exclusively on photometry. It wasn't until the 1980's that precision spectroscopy became observationally practical, thereby unlocking a whole new avenue for scientific study of the smallest yet most numerous type of galaxy. Radial velocities are typically the easiest spectroscopic measurement possible, even with low signal-to-noise data, and they present a myriad of uses for dSphs. Among these are the ability to determine membership, systemic velocity, proper motion, velocity dispersion, dSph total mass, velocity dispersion profile, bulk rotation, tidal streaming, and presence of binaries. However, without good precision, none of these lines of analysis are possible; as we shall see, the internal, streaming, and binary motions in dSphs manifest themselves on scales of a few km s^{-1} , so precisions of 1-2 km s^{-1} are required to reliably carry out these analyses.

One of the primary uses for radial velocities is to identify stellar membership of a dwarf, a process that I have completed for Draco, Ursa Minor (Section 4.2.2), and Leo II (Section 2.3.1). For our MMT data, this removed 47 out of 222 stars as Milky Way interlopers that otherwise looked like Leo II stars in regards to their positions, magnitudes, and colors. The percentage of nonmember stars in Draco was 74%, and

in Ursa Minor it was 58%. Although the exercise is somewhat dull, it is a crucial step as MW foreground contaminants can drastically alter later kinematic results.

Radial velocities also allow for the determination of systemic velocity. We did this using a maximum likelihood technique for Leo II, Draco, and Ursa Minor, finding values that agreed with others published in the literature. A useful application of systemic velocity is to treat dwarf satellites as dynamical tracers to estimate the mass of their host galaxy (Bahcall & Tremaine, 1981; Little & Tremaine, 1987). This has been done for the Milky Way (Zaritsky et al., 1989; Watkins et al., 2010), Andromeda (Evans et al., 2003; Watkins et al., 2010), and several other galaxies outside the Local Group (for example, NGC4259, Spencer et al. (2014), M87 Oldham & Auger (2016)). Proper motions of dSphs enhance these mass estimates by adding two vectors to the 6-D phase space, but such velocities typically take a couple of decades to observe in MW dSphs. A faster approach is to infer proper motion from a gradient in radial velocity across a dwarf (Kaplinghat & Strigari, 2008), as has been done for Carina, Fornax, Sculptor, and Sextans (Walker et al., 2008).

More importantly, radial velocities can be used to get velocity dispersion. The dispersions derived in this work were $7.4 \pm 0.4 \text{ km s}^{-1}$ for Leo II, $9.0 \pm 0.3 \text{ km s}^{-1}$ for Draco, and $8.0 \pm 0.3 \text{ km s}^{-1}$ for Ursa Minor. Combining this with the half-light radius yields a mass estimate. We used the estimator from Walker et al. (2009b) on Leo II to get a mass of $5.6 \pm 1.4 \times 10^6 M_{\odot}$ contained within the half-light radius. The mass-to-light ratio is straightforward to calculate if the luminosity is known. In Leo II this ratio was 15.2 ± 5.5 . We determined that binaries cannot inflate Leo II's velocity dispersion by more than 0.3 km s^{-1} for single epoch observations or 0.15 km s^{-1} for 2-epoch observations. It is clear that binaries are not the cause for the large mass-to-light ratio. While we did find one star beyond the tidal radius of Leo II, it is not likely that tides have had such a large effect as to inflate Leo II's dispersion from the non-dark matter expectation of $\sim 2 \text{ km s}^{-1}$ to the observed 7.4 km s^{-1} .

Therefore we conclude that Leo II is embedded in a massive dark matter halo.

With the addition of stellar position, another set of analyses is possible. The velocity dispersion profile shows how velocity dispersion varies with projected radius. In Leo II it remained flat out to the tidal radius of the dwarf, indicating that the dark matter extended to large radii. It allows for the identification of stars existing beyond the tidal radius, which we found one of in Leo II. Uniform rotation can also be examined. While we did find a sinusoidal signature in Leo II, it had a low amplitude and only 0.64σ significance. Signatures like this have also been attributed to the motion of the dwarf in the plane of the sky (Walker et al., 2006). Lastly the combination of velocities and positions can identify the presence of kinematic clumps, but no significant clumps were found in Leo II.

Chemical abundances, such as $[\text{Fe}/\text{H}]$ metallicity, are another spectroscopic quantity that can add to the depth of an analysis. On their own, they can be used to determine the metallicity distribution function, as we have done for Leo II. Pairing them with stellar positions reveals whether or not metallicity varies as a function of radius. In Leo II we found a metallicity gradient of $-1.53 \pm 0.10 \text{ dex kpc}^{-1}$. Combining the power of both velocities and kinematics allows the chemodynamics of to be studied. In Leo II we found loose evidence for high-metallicity ($[Fe/H] > -1.7$) stars having a lower velocity dispersion than low metallicity stars.

5.2 Binary Fractions in Classical dSphs

Since the start of spectroscopic observations of individual stars in dSphs, it had been long suspected (McClure, 1984), and later confirmed (Aaronson & Olszewski, 1987), that binaries are present in these galaxies. The effects of binaries on dSphs were first investigated for Carina (Mateo et al., 1993), Sextans (Suntzeff et al., 1993), and Leo II (Vogt et al., 1995) but were forced to adopt poorly-constrained binary fractions in their analyses. The first attempt at a quantitative estimation of the binary fraction

was carried out by Olszewski et al. (1996) using combined data for Draco and Ursa Minor, but the final result remained highly uncertain. The lack of extensive multi-epoch velocity data made it difficult to improve precision on the binary fraction on individual systems. Nonetheless, dozens of studies were conducted throughout the 1980s-1990s and it became clear that the role of binaries, regardless of the actual binary fraction, had a negligible effect on inflating the observed dispersions of $\sim 7\text{--}10 \text{ km s}^{-1}$ in classical dSphs. Only well after the initial excitement over binaries had faded did a more rigorous estimation of the binary fractions for Carina, Fornax, Sculptor, and Sextans become available (Minor, 2013).

The discovery of ultra-faints has reopened the issues relating to binaries in both bright and faint dSphs for two reasons. Firstly, ultra-faints exhibit small velocity dispersions of $2\text{--}4 \text{ km s}^{-1}$, making them more susceptible to inflation by binaries. Simulations have shown that the velocity dispersions of some dwarfs, such as Leo IV and Segue II, have a $> 20\%$ probability of being almost entirely due to binary stars. The implications of this would be that these dwarfs would move from being some of the darkest dSphs to having much smaller amounts of dark matter. Along the same lines, Minor et al. (2010) showed by way of simulations that dwarfs having velocity dispersions smaller than about 4 km s^{-1} were in danger of contamination by binaries.

Secondly, it will be nearly impossible to determine binary fractions in individual ultra-faints any time soon due to the paucity of stellar radial velocities within these galaxies. They contain few stars bright enough for precision radial velocities to be obtained, and only a handful of cases have received a second epoch of observations. An alternative to determining binary fraction on a case by case basis in ultra-faints is to study it in classical dSphs, which have the necessary data to perform such research; if the binary fraction is found to be the same amongst classical dSphs then that value can be applied to ultra-faints. Alternatively, if binary fraction varies amongst classical dSphs, it might be possible to correlate binary fraction with other observable

properties and extrapolate the binary fraction for ultra-faints. With this in mind, we chose to expand the sample of known binary fractions in classical dSphs by drawing upon several decades of archival velocity data in Leo II, Draco, and Ursa Minor.

The largest inhibiting factor in binary fraction analysis for classical dSphs is the lack of knowledge on the eccentricity, mass ratio, and period distributions for RGB stars in dSphs. By exploring different options for these distributions, we have found that the shape of the eccentricity distribution has very little ($\sim 1\%$) effect on the binary fraction. The same cannot be said for the other two distributions. We have tested the normal mass ratio distribution from Duquennoy & Mayor (1991) and the flat mass ratio distribution from Raghavan et al. (2010). For the period distribution we used the log-normal form from Duquennoy & Mayor (1991) with width $\sigma_{\log P} = 2.3$ and changed the position parameter, $\mu_{\log P}$. We tested $\mu_{\log P} = 4.8$ (Duquennoy & Mayor, 1991), $\mu_{\log P} = 3.5$ (Fischer & Marcy, 1992), and $\mu_{\log P} = 5.8$, which most closely resembled the simulated period distribution for dwarf galaxies in Marks & Kroupa (2011). Period distributions that were centered toward higher $\log P$ yielded larger binary fractions, as expected. The normal mass ratio distribution yielded larger binary fractions than the constant distribution. Going forward, these distributions, especially the period distribution, will be the most critical in further refining the estimates for binary fraction in classical dwarfs.

Some work has been done to simultaneously determine the period distribution and the binary fraction (Minor, 2013; Martinez et al., 2011), but these attempts found a degeneracy between the two variables that requires more than 2000 stars to break. We performed a KS test between the data and the models and found that Draco is best fit by a flat mass ratio distribution and a log-normal period distribution with $\mu_{\log P} = 5.8$, whereas Ursa Minor preferred a normal mass ratio distribution and a period distribution with $\mu_{\log P} = 4.8$. Since we only tested six combinations of mass ratio and period it is difficult to say whether this variation reflects physical differences

between the dwarfs or is a result of the degeneracy. Either way it would be worthwhile to explore the parameter space of the period distribution to see if our Bayesian method can chip away at the period-binary fraction degeneracy more effectively than previous methods.

While our focus was on Leo II, Draco, and Ursa Minor, we also considered Carina, Fornax, Sculptor, and Sextans for the purpose of understanding how, if at all, binary fraction varies amongst dSphs. For the latter four dSphs, we used the MMFS velocity data from Walker et al. (2009a). We were able to recover the same binary fractions reported in Minor (2013) for Carina, Sculptor, and Sextans, but not for Fornax. This is almost certainly due to underestimated velocity errors. Minor (2013) incorporated a model that corrected the errors in their analysis, so the binary fraction they derive for Fornax is more reliable than what we found. Therefore we used our posteriors from all but Fornax and find that the probability of the binary fraction being the same amongst the six dwarfs is $< 1\%$ regardless of the period and mass ratio distributions. We conclude that it is highly likely that the binary fraction varies between dwarf galaxies.

Given the unlikely outcome of the binary fraction being constant, we combine our three binary fractions with the four from Minor (2013) to search for any correlations between binary fraction and other properties. The strongest correlation we find is that binary fraction increases for dSphs that formed more of their stars in shorter periods of time. This roughly translates to high star formation rates in dSphs with large binary fractions. The trend is opposite of one theory, which predicts that higher star formation rates should yield larger cluster mass; clusters with larger masses are generally denser, and dense regions are expected to produce lower binary fractions (Marks & Kroupa, 2011). On the other hand, it has been found that denser regions in the Orion Molecular Clouds exhibit higher binary fractions (Kounkel et al., 2016), which agrees with our findings.

5.3 The Effect of Binaries in Ultra-faints

As noted above, binaries can have, and have had, a strong effect on inferred dispersions in ultra-faints. This has been seen in Segue 1 (Simon et al., 2011), Triangulum II (Kirby et al., 2017), and in unpublished velocity data for Tucana IV (private communication with M. Walker). In Chapter III, we explored how binaries could affect generic dwarf galaxies with intrinsic dispersions ranging from 0.5 to 12 km s⁻¹. These test galaxies had single-epoch measurements for 100 stars and velocity uncertainties of 1 km s⁻¹. If the binary fraction is 0.5 then the observed velocity dispersion can be inflated by a factor of 3 for intrinsic dispersion of 1 km s⁻¹ or by a factor of 5 for intrinsic dispersions of 0.5 km s⁻¹. The maximum inflation—corresponding to $f = 1$ —is a factor of 4 for the 1 km s⁻¹ galaxy and a factor of 7.5 for the 0.5 km s⁻¹ galaxy.

Since most ultra-faints do not have 100 spectroscopically measured stars, we conducted the same experiment but for galaxies containing 20 or 60 stars. We also wanted to see how adding in a second and third epoch of observations separated by 1 year would change the results. And finally, we raised the velocity uncertainty from 1 km s⁻¹ to 2 km s⁻¹ (though this had little to no effect on the dispersions). In all cases we considered intrinsic velocity dispersions of 0.5, 1, 2, and 4 km s⁻¹ as these resemble ultra-faints. The period and mass-ratio distributions were taken from Duquennoy & Mayor (1991) and the eccentricity distribution from Raghavan et al. (2010). Figure 5.1 shows the results.

For samples containing more stars, the range of values that the observed dispersion can take on narrowed and the increase in velocity dispersion is slightly more pronounced. For example, the $\sigma_{int} = 2$ km s⁻¹ galaxy was observed at 4.2 km s⁻¹ for the 60 star case and at 3.8 km s⁻¹ for 20 star case assuming a binary fraction of 1. As binary fraction decreases, this difference decreases as well. When $f = 0.5$, the $\sigma_{int} = 2$ km s⁻¹ 60 star galaxy displayed a velocity dispersion of 3.0 km s⁻¹ whereas the 20 star galaxy showed 2.8 km s⁻¹. Increasing the number of repeat observations

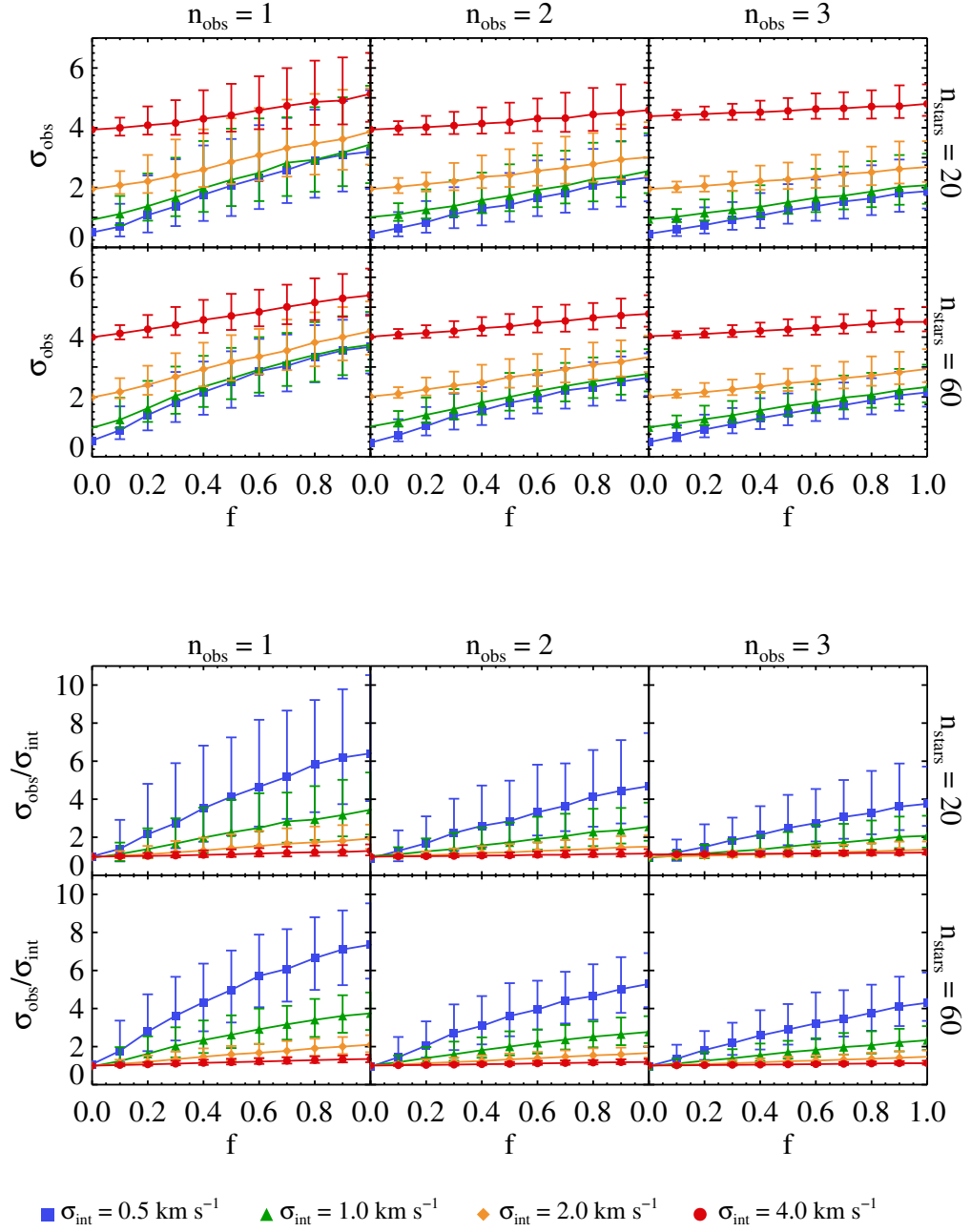


Figure 5.1 The top six panels plot observed velocity dispersion versus binary fraction and the bottom six panels plot the ratio of observed to intrinsic dispersion versus binary fraction. The number of observations and number of stars is displayed along the top and right axes. The intrinsic dispersions are 0.5 km s^{-1} (blue squares), 1 km s^{-1} (green triangles), 2 km s^{-1} (orange diamonds), and 4 km s^{-1} (red circles).

also minimizes this difference.

When we added more epochs, the ratio of observed to intrinsic dispersion decreased, as expected. The observed dispersion in the 20 star, $\sigma_{int} = 0.5 \text{ km s}^{-1}$, single-epoch simulations was larger by a factor of 4 for $f = 0.5$ and a factor of 6.5 for $f = 1$. When a second epoch was added, these factors decrease to approximately 3 and 4.5; the third epoch decreases them further to 2.5 and 4. Adding additional epochs of observations helps diminish the inflationary effect caused by binaries, but it does not eliminate it, especially for galaxies with with large binary fractions and intrinsic dispersions $\leq 2 \text{ km s}^{-1}$. In these cases additional modeling work must be done to correct the observed velocity dispersion.

One real life example of the effects on binaries in ultra-faints is Reticulum II. Radial velocities were measured for 17 stars and it was found to have a velocity dispersion of $3.6_{-0.7}^{+1.0} \text{ km s}^{-1}$ (Walker et al., 2015a) or $3.3 \pm 0.7 \text{ km s}^{-1}$ (Simon et al., 2015). Using the same 17 stars, we derived a velocity dispersion of 3.4 km s^{-1} . Given a certain binary fraction, we calculated what the intrinsic dispersion would need to be if the observed dispersion was 3.4 km s^{-1} . This is plotted as the solid line in Figure 5.2. We assumed the Duquennoy & Mayor (1991) mass ratio and period distributions, and the Raghavan et al. (2010) distribution for eccentricity. If the binary fraction is around 0.6 then binaries would be inflating the dispersion by 1 km s^{-1} . This would correspond to a M/L ratio 2 times smaller. Then we simulated a second set of observations taken 1 year later for each of the 17 stars. The average velocity over the two epochs was used to calculate the dispersion and the results is the dashed line in Figure 5.2. In this case the observed velocity dispersion would only be inflated by 0.6 km s^{-1} assuming $f = 0.6$ and the mass-to-light ratio would only be 1.5 times smaller. The mass-to-light ratio for Reticulum II was reported as 470 (Walker et al., 2015a; Simon et al., 2015), so a factor of 1.5 to 2 makes a significant difference in this measurement. The inflation caused by binaries can clearly be suppressed with

a second epoch of velocities, motivating the crucial need for repeat observations in ultra-faint dSphs.

5.4 Future Work

5.4.1 The Value of Additional Kinematic Data

A detailed binary analysis had been completed for Leo II, Draco, and Ursa Minor in this work. Carina, Fornax, Sculptor, and Sextans were considered in Minor (2013). The only remaining classical dSph with decades old velocities is Leo I. Binary analysis should be done for Leo I to finish the set of classical dSphs. The addition of an eighth dwarf to the sample would help define the loose trends between binary fraction and star formation history. Furthermore, old velocity data exists for Carina, Fornax, Sculptor, and Sextans. This could be folded into the MMFS data used in Minor (2013) to fine tune the binary fractions in those galaxies. Lastly, new data with lower velocity errors can and should be taken to improve upon the binary fractions measured in all of these dSphs.

5.4.2 Improving the Error Model

The Bayesian method that we use varies from those described in Minor et al. (2010) and Martinez et al. (2011). We are able to utilize an unlimited number of epochs into our analysis whereas they are limited to 2 or 3. As such we are able to reduce the errors on our binary fractions. On the other hand, they incorporated a velocity error model into their simulations. The impact of this feature on the resulting binary fraction is large. This was obvious in Fornax, which had a median velocity error that was under-reported by 55%. Using the same MMFS data, we found a binary fraction of $0.87_{-0.09}^{+0.12}$ but they found a binary fraction of $0.44_{-0.12}^{+0.26}$. Since the errors are incorrectly reported for only some of the stars, we cannot simply multiply

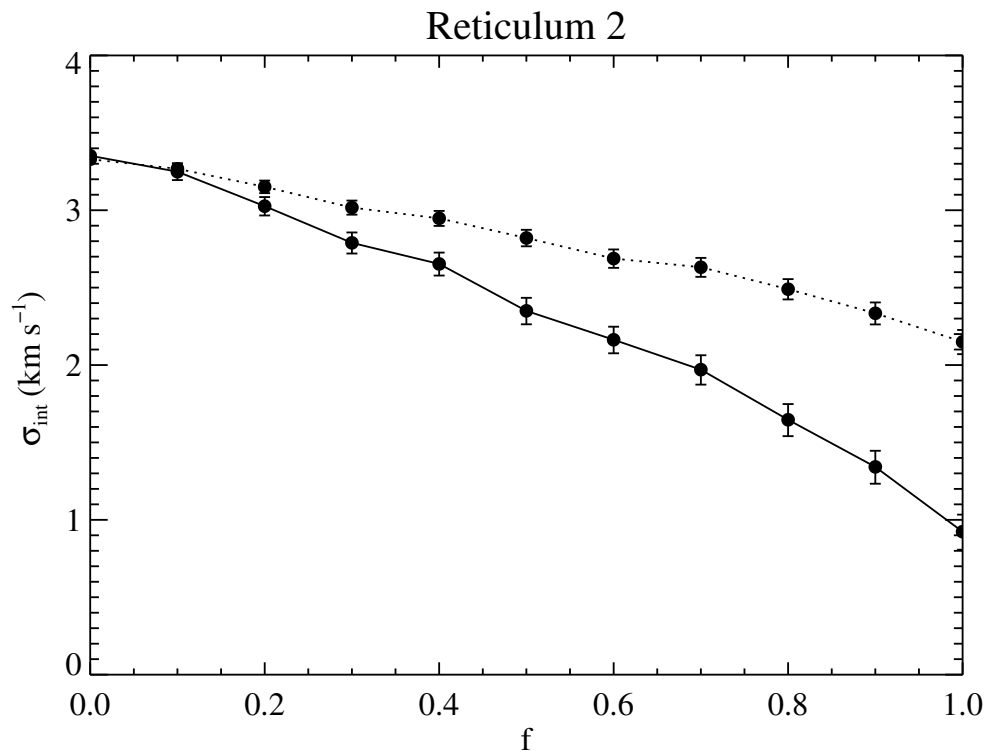


Figure 5.2 The intrinsic dispersion of Reticulum 2 is plotted against binary fraction, given an observed velocity dispersion of 3.3 km s^{-1} . The solid line includes single-epoch velocities for 17 stars. The dashed line incorporates a second epoch of simulated observations taken exactly 1 year later.

all the velocity errors by a single factor. (Doing so yielded $f = 0.22_{-0.09}^{+0.11}$.) Cases like this necessitate a more detailed treatment of the velocity errors, and our current method has no way of correcting these. Our method would benefit greatly from the addition of an error treatment model.

5.4.3 Determining the Period Distribution

Three period distributions were tested on Draco and Ursa Minor. All of them were log-normal in form, having a set width of $\sigma_{\log P} = 2.3$ but variable locations. We were able to say which of these best reproduced the distribution of β_{obs} by way of a KS test. While this was not an extensive search of the parameter space, we were able to say whether a log-normal period distribution centered at low ($\mu_{\log P} = 3.5$), medium ($\mu_{\log P} = 4.8$), or high ($\mu_{\log P} = 5.8$) values best reproduced the data. The work by Minor (2013) spent more effort on constraining $\mu_{\log P}$ and $\sigma_{\log P}$. In the process they found a degeneracy between the period distribution and binary fraction. One key aspect of their simulations is that they were trying to constrain period using only the threshold fraction, which is a single value for each simulation. Our method, on the other hand, makes use of an entire distribution of β 's. This additional information might suffice to decrease the degeneracy, or possibly even break it. Therefore, a more detailed study of the period (and mass ratio) distribution with our method is something to consider. This is especially important because a poorly defined period distribution amongst red giants in dSphs is the largest inhibiting factor in determining the binary fraction.

5.4.4 Alternative Definitions of β

We used one definition of β throughout this research. We did not explore other options extensively because our definition was able to reproduce the intrinsic binary fraction in mock galaxies. That being said, we did briefly explore the outcome of

defining β as $\frac{|v_m - \langle v \rangle|}{\sqrt{\sigma_m^2 + \sigma_{\langle v \rangle}^2}}$, where $\langle v \rangle$ is the average velocity of the star and $\sigma_{\langle v \rangle}$ is the corresponding uncertainty. We defined $\langle v \rangle$ and $\sigma_{\langle v \rangle}$ as the unweighted average and error in one consideration and in another we used the weighted average and error. The resulting posteriors yielded binary fractions similar to that of our primary β in Leo II, differing by 2% or 8%, but had a narrower shape by 2-4%. This new definition yields fewer β 's, which means it will require less time to generate and run a Bayesian analysis on the models. While we only tested alternative definitions of β on one galaxy, it could potentially yield smaller error bars on the binary fraction. Furthermore a new definition for β could be more sensitive to the period distribution, making the shape of the period distribution easier to discern. Other statistics in place of β may prove useful as well. Future consideration of such statistics using more extensive datasets is certainly warranted.

5.4.5 Moving Forward: More Data is the Key

The impacts of binaries on the velocity dispersions of dSphs have the potential to be very significant. Accounting for binaries can drastically alter our view of dark matter in these systems, thereby impacting galaxy formation and evolution models as well as dark matter formulations. While larger telescopes and more sensitive instruments are needed to make progress on some fronts, there is still plenty that can be done now with current technology.

- *Binary parameter distributions of red giants:* As we have shown, the period distribution has the largest effect on the observed binary fraction. Observations of a couple thousand stars in a single dwarf should be sufficient to reveal the shape of the period distribution, and so, more observations of additional stars should be taken in classical dSphs to reach this limit. It would also be advantageous to observe binary red giants within the solar neighborhood in hopes of constructing their period and mass ratio distributions, because these are the type star most

commonly observed in dSphs. While these distributions might still be different from what is present in dSphs, they would likely provide a better foundation than the currently used distributions for main sequence stars.

- *Multi-epoch observations in ultra-faints:* Multi-epoch radial velocities are absolutely necessary when calculating the velocity dispersion of ultra-faints. They can reveal velocity variables, which should be removed from the sample unless a full orbit can be obtained. Observations of this nature can also be averaged to dampen the effects of less obvious binaries (as demonstrated in Reticulum 2). Extreme caution should be exercised when publishing or reading about single-epoch velocity dispersions. The best way to improve upon kinematic research in ultra-faints is to obtain multi-epoch radial velocities of more stars.
- *Multi-epoch observations in classical dSphs:* Even for classical dwarfs whose velocity dispersions are barely affected by binaries, it is important to obtain multiple epochs so that the binary fraction can be measured in each system. Given that there is likely variation in binary fraction amongst classical dwarfs, each system should be treated on a case by case basis. If a trend with other observational properties exists, then we need to know the binary fraction for as many systems as possible to identify correlations. All of this can be achieved by taking more observations in more dwarfs.

We have presented results for binary fractions in seven classical dwarfs. While this has been a significant step forward within the field of dSph binary populations, there is still much that needs to be done. Future research should aim to use all available velocity data and to continue taking more observations, both of new stars and of previously measured stars.

APPENDICES

APPENDIX A

The Orbital Radial Velocity Equation

The orbital radial velocity equation can be expressed in many different forms, and the geometry of the problem can be somewhat confusing. Therefore, we have completed a derivation of the equation used in this dissertation to avoid any confusion. A glossary of the variables used in this derivation can be found in Section A.2.

A.1 Derivation

First we will write down some basic ellipse geometry that will be helpful throughout the derivation. The length of the line connecting a point along an ellipse to its focus is

$$r = \frac{a(1 - e^2)}{1 + e \cos \theta}, \quad (\text{A.1})$$

where a is the semi-major axis, e is the eccentricity, and θ is the angle between periastron, focus, and point along the ellipse. For the purposes of this derivation, the “point along the ellipse” is the location of the star. Figure A.1 helps illustrate some of this geometry, like r and θ . The semi-minor axis expressed in terms of the

semi-major axis and eccentricity is given by

$$b = a\sqrt{1 - e^2}. \quad (\text{A.2})$$

The area of a slice of the ellipse between one angle, θ_1 , and another angle, θ_2 , can be expressed as

$$A_{\text{slice}} = \int_{\theta_1}^{\theta_2} \frac{1}{2} r^2 d\theta. \quad (\text{A.3})$$

The total area of an ellipse is given by

$$A = \pi ab. \quad (\text{A.4})$$

To begin, we need to find an expression for the position vector along the line of sight, z . This can be done by considering the geometry in Figure A.1. There are two triangles that can be used to define z , and both of these are shown in the figure. The first leads to the equation $\sin i = z/l$, and the second gives us $\sin \phi = l/r$, where i is the angle of inclination, l is a length segment along the perimeter of the ellipse, ϕ is $180^\circ - (\theta + \omega)$, and ω is the argument of periastron. Combining these and simplifying gives us

$$\begin{aligned} z &= r \sin \phi \sin i \\ &= r \sin(\theta + \omega) \sin i. \end{aligned} \quad (\text{A.5})$$

The radial velocity equation will be the time derivative of this, $v_{r,orb} = \frac{dz}{dt}$. The values ω and i do not change with time. Therefore the time derivative of z is

$$\frac{dz}{dt} = \sin i \left(\frac{dr}{dt} \sin(\theta + \omega) + r \frac{d\theta}{dt} \cos(\theta + \omega) \right). \quad (\text{A.6})$$

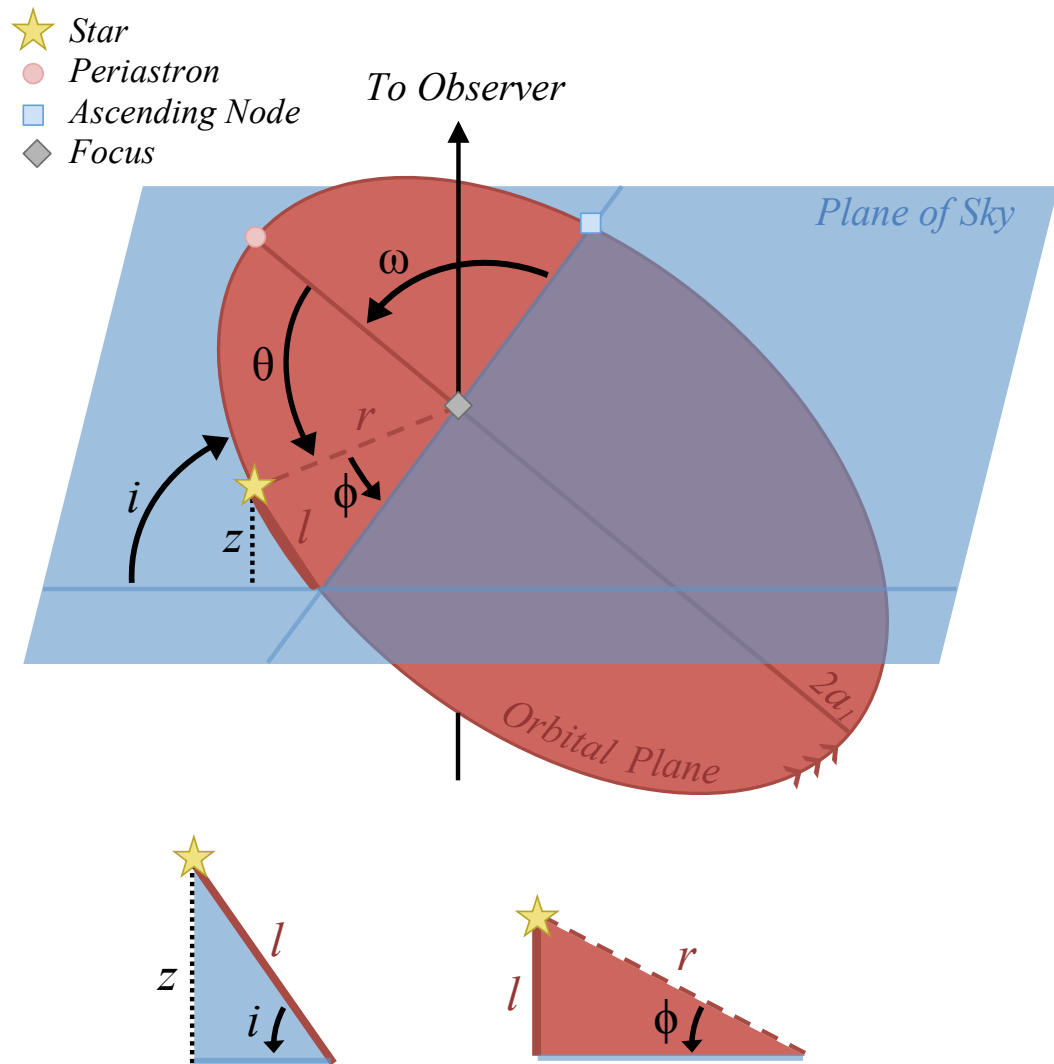


Figure A.1 Geometry of a binary orbit. The two triangles are used in the derivation of z in Equation A.5.

To find dr/dt we take the derivative of Equation A.1 and get

$$\frac{dr}{dt} = \frac{re \sin \theta}{1 + e \cos \theta} \frac{d\theta}{dt}. \quad (\text{A.7})$$

To find $d\theta/dt$ we take the derivative of Equation A.3 and get

$$\frac{dA}{dt} = \frac{1}{2} r^2 \frac{d\theta}{dt}. \quad (\text{A.8})$$

Substituting $dA/dt = A/P$, where P is the period, and plugging in Equations A.1, A.2, and A.4 we have

$$\begin{aligned} \frac{d\theta}{dt} &= 2 \frac{dA}{dt} \frac{1}{r^2} \\ &= 2 \frac{A}{Pr^2} \\ &= 2 \frac{(\pi a(a\sqrt{1-e^2})) (1 + e \cos \theta)^2}{P a^2(1-e^2)^2} \\ &= \frac{2\pi(1 + e \cos \theta)^2}{P(1-e^2)^{3/2}}. \end{aligned} \quad (\text{A.9})$$

It is useful at this point to also write the expression

$$r \frac{d\theta}{dt} = \frac{2\pi a(1 + e \cos \theta)}{P\sqrt{1-e^2}}. \quad (\text{A.10})$$

Substituting Equations A.7 and A.10 into Equation A.6 we have

$$\begin{aligned}
\frac{dz}{dt} &= \sin i \left(\frac{e \sin \theta}{1 + e \cos \theta} \frac{rd\theta}{dt} \sin(\theta + \omega) + \frac{rd\theta}{dt} \cos(\theta + \omega) \right) \\
&= \sin i \frac{2\pi a(1 + e \cos \theta)}{P\sqrt{1 - e^2}} \left(\frac{e \sin \theta \sin(\theta + \omega)}{1 + e \cos \theta} + \cos(\theta + \omega) \right) \\
&= \frac{\sin i 2\pi a(1 + e \cos \theta)}{P\sqrt{1 - e^2}} \left(e \sin \theta \sin(\theta + \omega) + \cos(\theta + \omega) + e \cos \theta \cos(\theta + \omega) \right).
\end{aligned} \tag{A.11}$$

The right portion enclosed in parentheses can be simplified using several trigonometric identities and is more neatly written as

$$\frac{dz}{dt} = \frac{2\pi a}{P\sqrt{1 - e^2}} \sin i (\cos(\theta + \omega) + e \cos \omega). \tag{A.12}$$

The velocity that we care about is the velocity of Star 1. Thus, the semi-major axis in Equation A.12 refers to a_1 . However, a_1 is not a parameter with a known distribution function, like what we will need in Chapters III and IV. So we must instead express it in terms of P and q .

To do this, we start with Newton's form of Kepler's Third Law

$$a^3 = \frac{P^2 G(m_1 + m_2)}{4\pi^2}, \tag{A.13}$$

which gives a for the system. Using the definitions $a = a_1 + a_2$, $q = m_1/m_2$, and the equation for center of mass, $m_1 a_1 = m_2 a_2$, we can write

$$a_1 = \frac{qa}{1 + q}. \tag{A.14}$$

Plugging in Kepler's Third Law we have

$$a_1 = \left(\frac{q}{1+q} \frac{P^2 G(m_1 + m_2)}{4\pi^2} \right)^{1/3} \quad (\text{A.15})$$

Finally, inserting Equation A.15 into Equation A.12 and simplifying, we arrive at the radial velocity equation:

$$v_{r,orb} = \frac{q \sin i}{\sqrt{1-e^2}} \left(\frac{2\pi G m_1}{P(1+q)^2} \right)^{1/3} (\cos(\theta + \omega) + e \cos \omega). \quad (\text{A.16})$$

A.2 Glossary of Variables

The variables used in this derivation are:

- a = semi-major axis
- b = semi-minor axis
- P = period
- e = eccentricity
- q = mass ratio
- m_1 = mass of star 1
- m_2 = mass of star 2
- a_1 = semi-major axis of star 1's orbit
- a_2 = semi-major axis of star 2's orbit
- θ = true anomaly
- ω = argument of periastron
- i = angle of inclination

- A = area of ellipse
- t = time
- r = length between the focus and the star
- z = position vector along the line of sight
- l = length of the side of a triangle in Figure A.1
- $v_{r_{orb}}$ = orbital radial velocity of primary star

APPENDIX B

Correcting Velocity Error Measurements

Velocity errors would ideally be determined by the variance between velocities extracted from multiple exposures over the course of a couple nights. This was not possible for much of the archival data used in this analysis so we outline one potential method for correcting velocity errors if they are believed to be over- or underestimated. We find no evidence of our velocity errors being incorrect, so we do not apply this correction. Rather, we use it to explore the severity with which incorrect velocity errors can affect the inferred binary fraction.

In order to determine whether errors might be incorrect, we plot the cumulative distribution of $P(\chi^2, \kappa)$ (see, Equation 4.1). If there are no binaries, the slope of this distribution should be equal to one. If there are binaries, then the distribution will grow rapidly where $P(\chi^2, \kappa) < 0.01$. In that case, the slope of the cumulative distribution that excludes values of $P(\chi^2) < 0.01$ should be equal to one. Examples of this are shown in Figure B.1. If the slope is not near one, then the velocity errors are likely incorrect. One caveat to these trends is the case where a subset of errors is underestimated while another subset of errors is overestimated. The net effect of this configuration could be a cumulative $P(\chi^2, \kappa)$ with a slope of one, and thus appear as though the errors were properly reported. These cases are impossible to correct with

the proposed method, which is why it is crucial to get multiple observations of each star over the course of a couple nights to accurately measure the velocity errors in the first place.

The process to rectify incorrect velocity errors starts by assuming that the velocity errors for stars observed during a given epoch will all be mis-reported by some multiplicative factor. This factor is assumed to be the same for all stars observed during a given epoch, but it can vary between epochs. If this factor is 1, then the velocity errors are accurate.

For each epoch, the velocity errors are multiplied by a range of factors. Each combination of multiplicative factors will yield a different cumulative distribution for $P(\chi^2, \kappa)$. The combination of factors that does the best job of correcting the slope of the cumulative distribution should be adopted and used in the Monte Carlo simulations of binary fraction. This process becomes computationally expensive for many epochs, and so we do not apply it to any of our data. Furthermore, the three dwarfs that we focused on (Leo II, Draco, and Ursa Minor) do not show any obvious deviations from the expected cumulative distribution for $P(\chi^2, \kappa)$.

Instead, we show the viability of the method in the case of three mock galaxies and recommend that it be used in future analyses if the slope of the $P(\chi^2, \kappa)$ distribution clearly deviates from one. The mock galaxies that we generated had two epochs of observations separated by four years for 200 stars, and had binary fractions of 0.50. Galaxy 1 had errors that were underestimated by a factor of 0.6 for epoch one and 0.8 for epoch two. Galaxy 2 had errors that were underestimated by a factor of 0.7 for both epochs. Galaxy 3 had errors that were overestimated by a factor of 1.2 for epoch 1 and underestimated by a factor of 0.7 for epoch 2.

In Figures B.2-B.4 we show the binary fraction for these galaxies with uncorrected errors and with corrected errors. The top panels show the posterior probability distributions of the binary fraction for uncorrected errors (blue), perfectly corrected errors

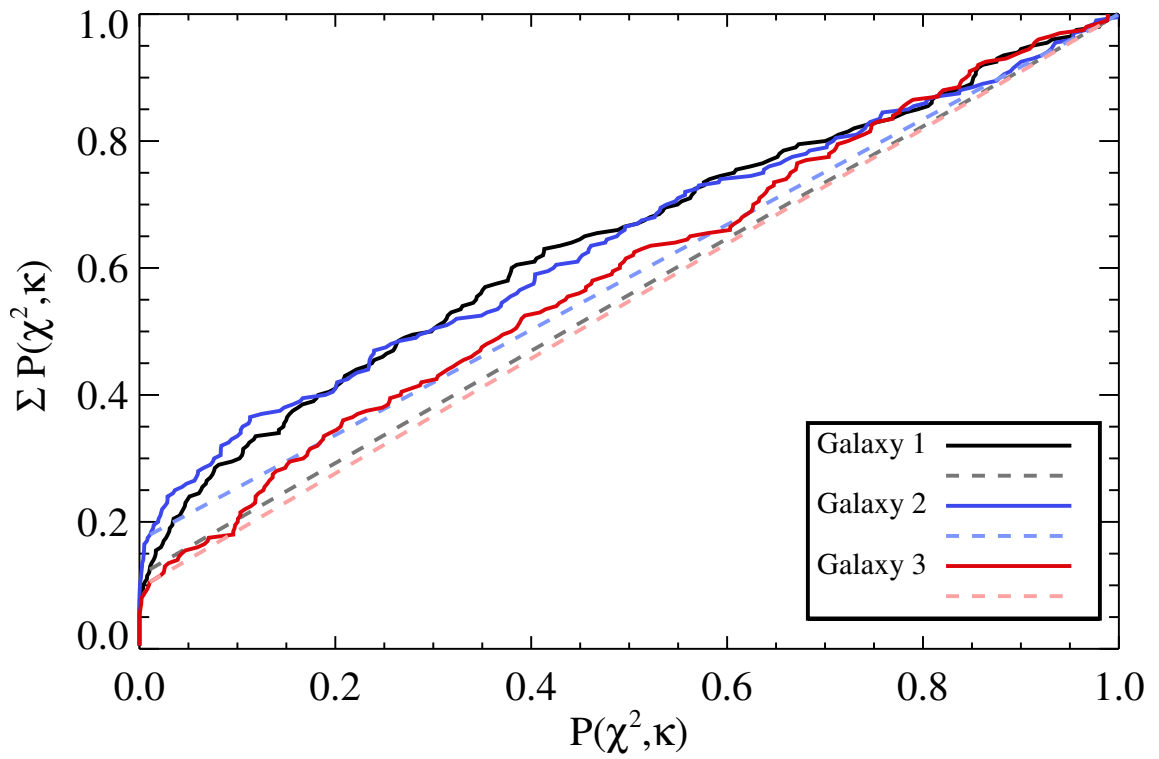


Figure B.1 Cumulative distribution of $P(\chi^2, \kappa)$ for three mock galaxies. Dashed lines show expected slope if error measurements are correct. The cumulative distributions for Galaxy 1 and Galaxy 2 deviate more from the expectation than Galaxy 3.

(black), and errors corrected via our method of forcing the slope of $P(\chi^2, \kappa)$ to one. We found that there were many combinations of multiplicative factors that yielded equally good corrections to the binary fraction and they all resulted in statistically equal posteriors. The middle panels of Figures B.2-B.4 show the cumulative posteriors. The bottom panel shows the medians of the posteriors. The gray histogram shows the posterior medians for 200 realizations of the mock galaxy in question. In almost all cases the applied corrections yield binary fractions within 1σ of the true binary fraction.

If the errors are strongly misestimated in the same direction—as is the case for Galaxy 1 and Galaxy 2—then applying a multiplicative correction to each epoch will correct the observed binary fraction to within 1σ of the true value. If some of the errors are overestimated while others are underestimated—like for Galaxy 3—then applying a correction can yield no significant change in the binary fraction, and might actually lead to binary fractions that deviate more from the true binary fraction. As seen in Figure B.1, Galaxy 3 deviated from a slope of one by less than Galaxies 1 and 2. It then follows that the binary fraction with uncorrected errors for Galaxy 3 is closer to the truth than the binary fractions with uncorrected errors for Galaxies 1 and 2. Therefore, we conclude that our method of correcting velocity errors is only useful if the slope of $P(\chi^2, \kappa)$ is obviously discrepant from one, which is most likely to occur when the velocity errors are misestimated in the same direction. If the slope of $P(\chi^2, \kappa)$ is not equal to one, then the resulting binary fraction with uncorrected errors will probably be significantly different from what is inferred (see, Figures B.3 and B.4).

The cumulative distributions of $P(\chi^2, \kappa)$ of our three galaxies (Leo II, Draco, Ursa Minor) and of the four galaxies in Minor (2013) (Carina, Fornax, Sculptor, and Sextans) do not deviate from the expected distribution by enough for this sort of error correction to be warranted. (Although, it is still possible that all of the galaxies

have incorrect errors but that the $P(\chi^2, \kappa)$ distributions are still flat, similar to what is seen in Galaxy 3. This is a case that we are unable to correct with our method.) Even Fornax, the galaxy that Minor (2013) claimed had a median error that was underestimated by a factor of 0.55, did not exhibit large deviations in $P(\chi^2, \kappa)$ from the expectation like what is seen in mock Galaxies 1 and 2 (see, Figure B.5). If the errors for Fornax were to be corrected by assuming the same multiplicative factor over all epochs, then the method that we describe above finds that the errors might only be underestimated by a factor of 0.87 rather than 0.55. The $P(\chi^2, \kappa)$ histograms with these factors implemented are shown in Figure B.5. We report the binary fraction results from applying both our correction and that of Minor (2013) in Section 4.4.1, but find no compelling evidence that either of these are necessary because a) the slope of the cumulative $P(\chi^2, \kappa)$ distribution is near one and b) Fornax was observed in an identical way to the other MMFS galaxies, so there is no obvious reason why one dataset would have such a large error misestimation while the other three do not.

From this exercise, we can conclude that errors that have been misestimated in the same direction will yield $P(\chi^2, \kappa)$ distributions with slopes not equal to one. Such deviations can lead to wildly inaccurate binary fractions. For example, Galaxies 1 and 2 showed binary fractions of 0.76 and 0.87, respectively, when their true fractions were 0.50. If the slope appears to be equal to one, then either the errors are correct or the errors are misestimated in a more complicated way that our method cannot easily fix. In these cases, it is crucial to make sure the errors are reported accurately in the first place. This should be done while at the telescope by observing the same stars over the course of a couple nights and using the measured variation to express the velocity error.

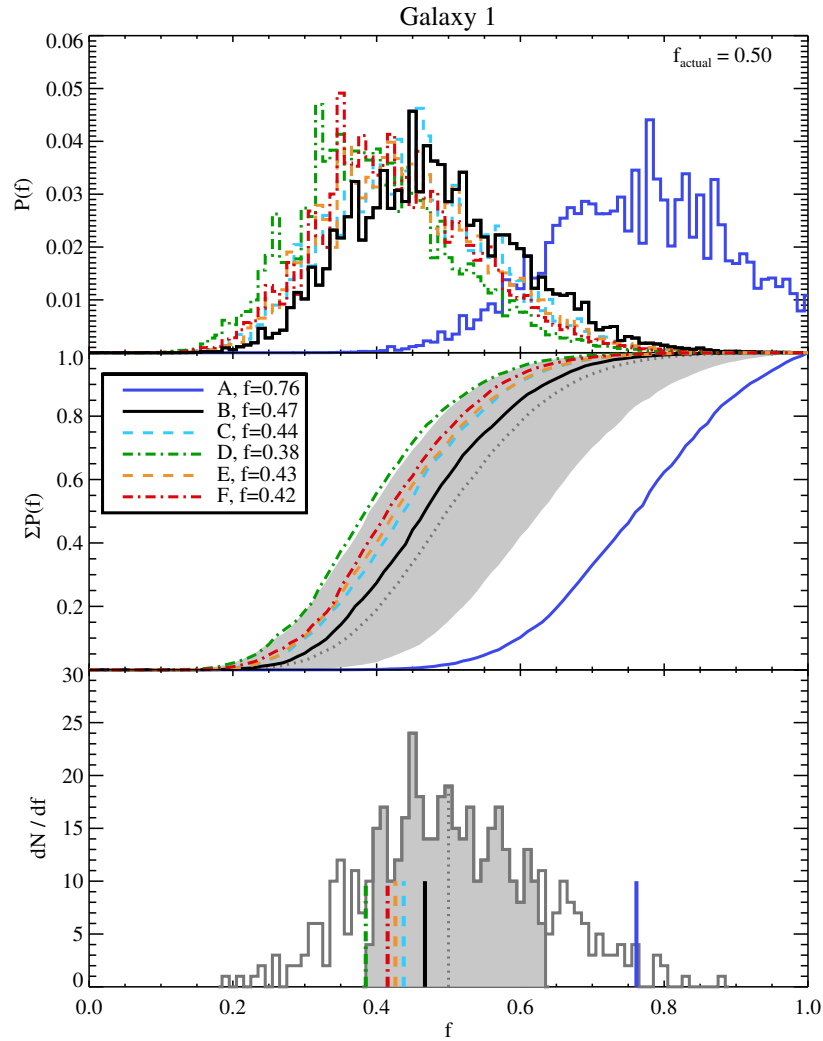


Figure B.2 Simulation results for a mock galaxy (Galaxy 1) with 200 stars, two epochs, and a binary fraction of 0.5. Top: Posterior probability distributions. Middle: Cumulative PPDs. Bottom: histogram of binary fraction in 200 mock galaxies with vertical lines denoting the binary fractions from MC simulations. Colors correspond to different error model corrections. Black: results for galaxy with correct velocity error measurements. Blue: results for galaxy with incorrect error measurements. (First epoch underestimated by a factor of 0.6 and second epoch underestimated by a factor of 0.8.) We applied the best correction to the errors assuming (C) a single multiplicative factor, cyan, (D) only the first epoch needed to be corrected, green, (E) only the second epoch needed to be corrected, orange, and (F) a different multiplicative factor for each epoch, red. Gray shaded region shows the space occupied by 68% of 200 mock galaxies.

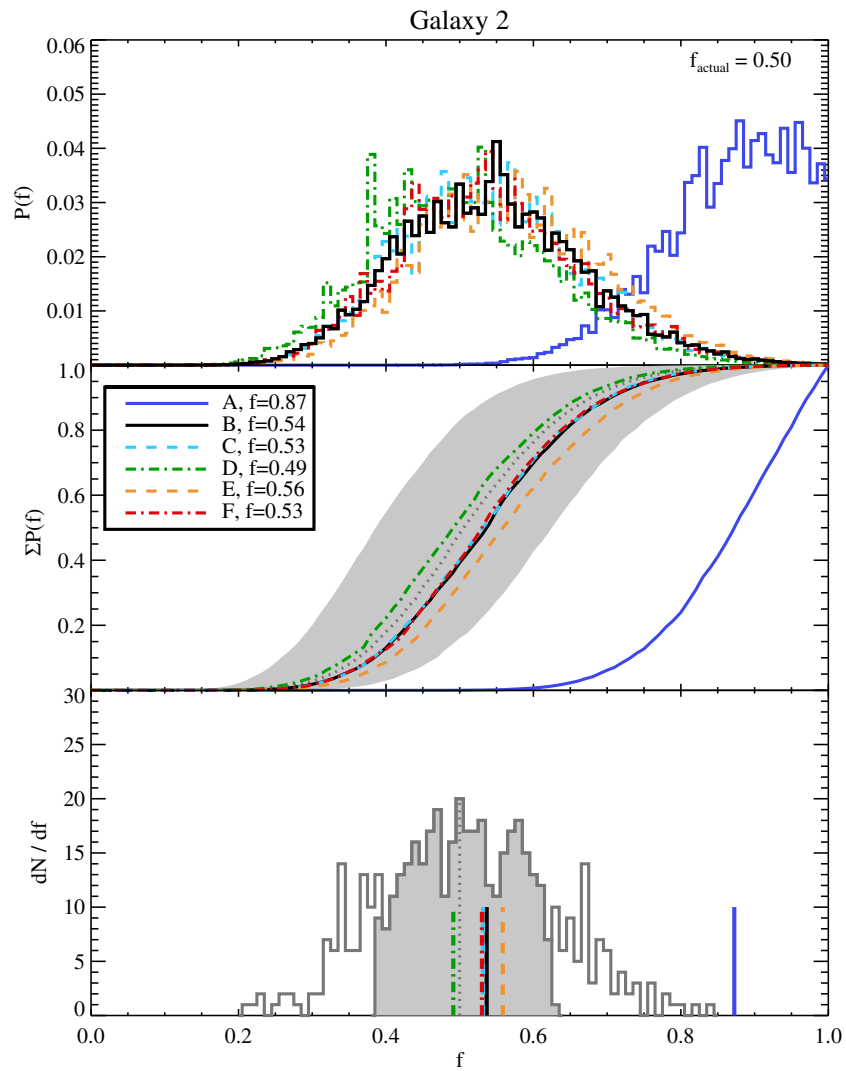


Figure B.3 Same as Figure B.2 but with both epoch having errors underestimated by a factor of 0.7 (Galaxy 2).

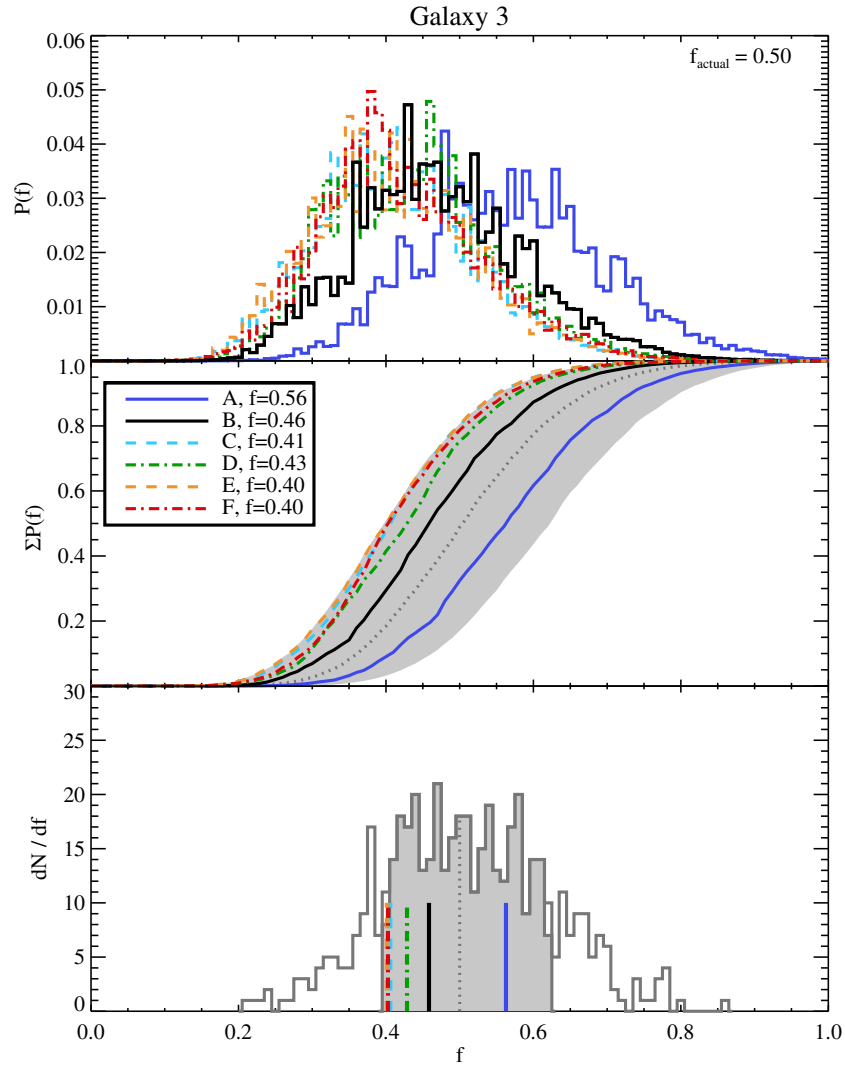


Figure B.4 Same as Figure B.2 but with the first epoch having errors overestimated by a factor of 1.2 and the second epoch having errors underestimated by a factor of 0.7 (Galaxy 3).

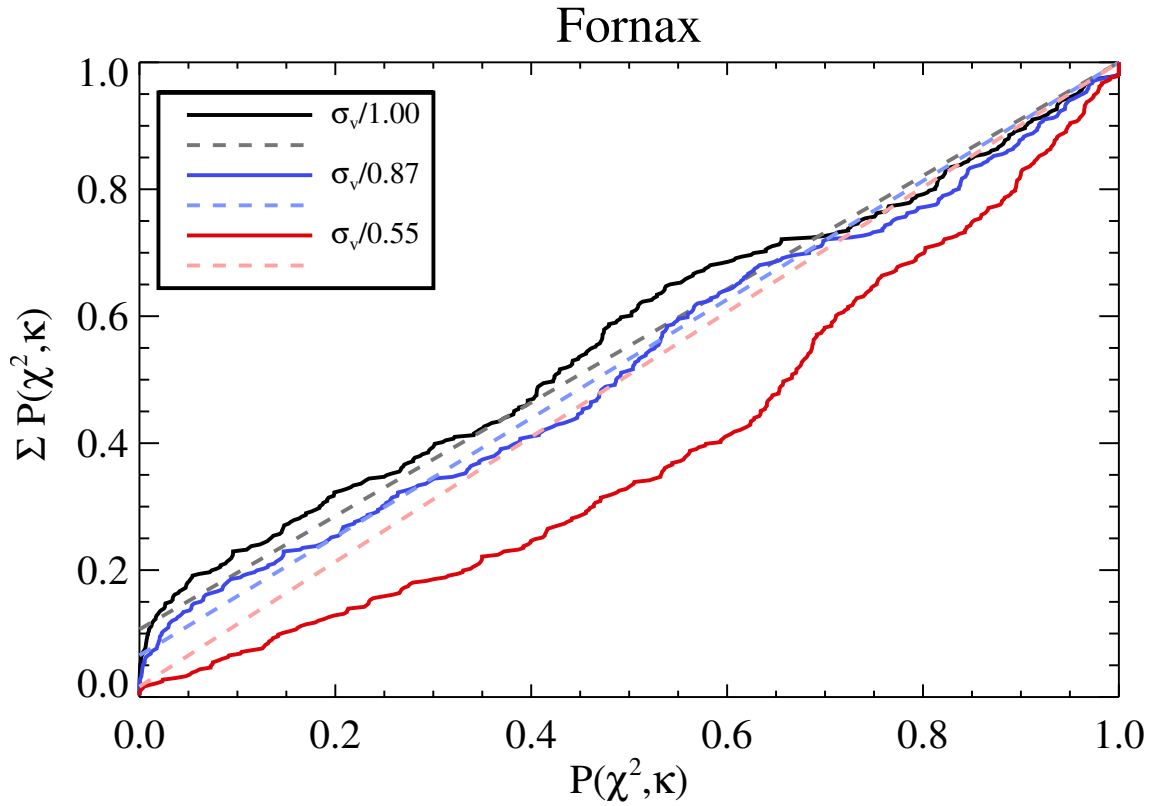


Figure B.5 Cumulative $P(\chi^2, \kappa)$ histograms for Fornax. Solid lines show the histogram and dashed lines show the expectation. Black is uncorrected velocity errors, blue is the best error correction that we find using our method in Appendix B, and red is the median error deviation that Minor (2013) finds. The slope of the uncorrected histogram (black) is very close to the expectation so error corrections taking the form described here are not necessary.

APPENDIX C

The Probability of f being “The Same” for All dSphs

Equation 4.15 describes the probability that all dSphs have a binary fraction within some specified width in f . It was designed to help answer the question: is the binary fraction the same amongst the brighter dSphs? While the equation is built from simple concepts (i.e., the multiplication rule of probability for independent events and the unit measure axiom), the formulation is rather complex. The difficulty comes in determining which marginal probabilities need to be multiplied and which need to be added. To best describe the derivation of Equation 4.15, we start by introducing a toy model for joint probabilities (Section C.1) and then generalize that model to answer the above question and arrive at the final equation (Section C.2).

C.1 Toy Model for Probability

For our toy model, we will consider two bags, A and B , that each contain 10 tiles. Every tile has a number written on it, ranging from 1–5. The probability of drawing a tile with a given number from bag A , $P(A)$, is shown in the top panel of Figure C.1, and the probability of drawing a tile with a given number from bag B ,

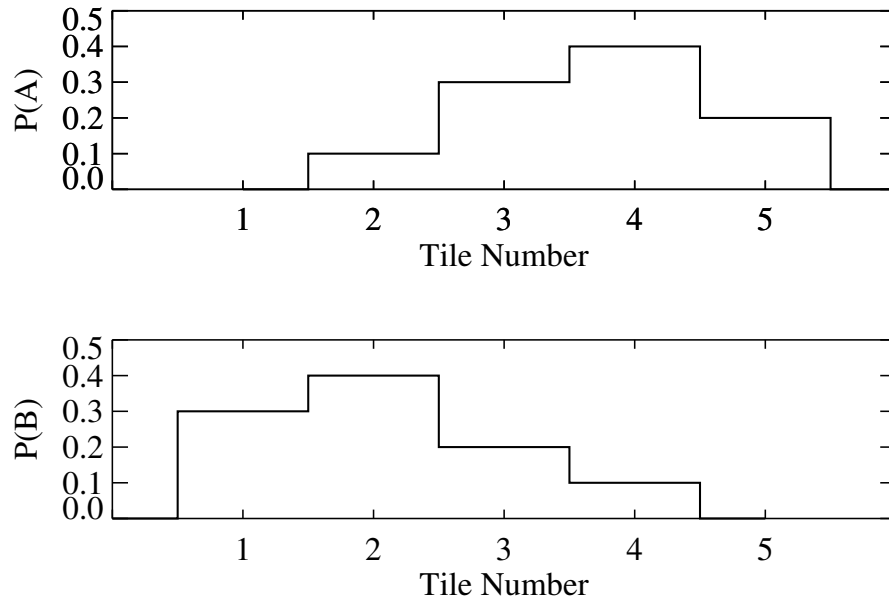


Figure C.1 Probability mass functions of drawing a tile with a given number on it from bag A (top) and bag B (bottom).

$P(B)$, is shown in the bottom panel. These are known as independent probability mass functions because the outcome of drawing from bag A has no effect on the outcome from bag B , and vice versa. For example, the probability of drawing a tile with the number 5 on it from bag A will always be 0.2, regardless of what was drawn from bag B . $P(A)$ and $P(B)$ are also called marginal probabilities because they are not conditional on any other event. Note that $\sum P(A) = 1$ and $\sum P(B) = 1$. This is known as the unit measure axiom, which states that the probability of an entire sample space is equal to 1.

The joint probability of A and B is the probability of two events occurring at the same time. It is written as $P(A \cap B)$, and when the two events are independent it is the product of the two events: $P(A \cap B) = P(A) * P(B)$. One example might be the probability that a 2-tile is drawn from bag A and a 3-tile is drawn from bag B , which is $0.1 * 0.2 = 0.02$. The joint probability distribution is the product of all possible combinations of the outcomes of A and B . This is shown in the top left panel of

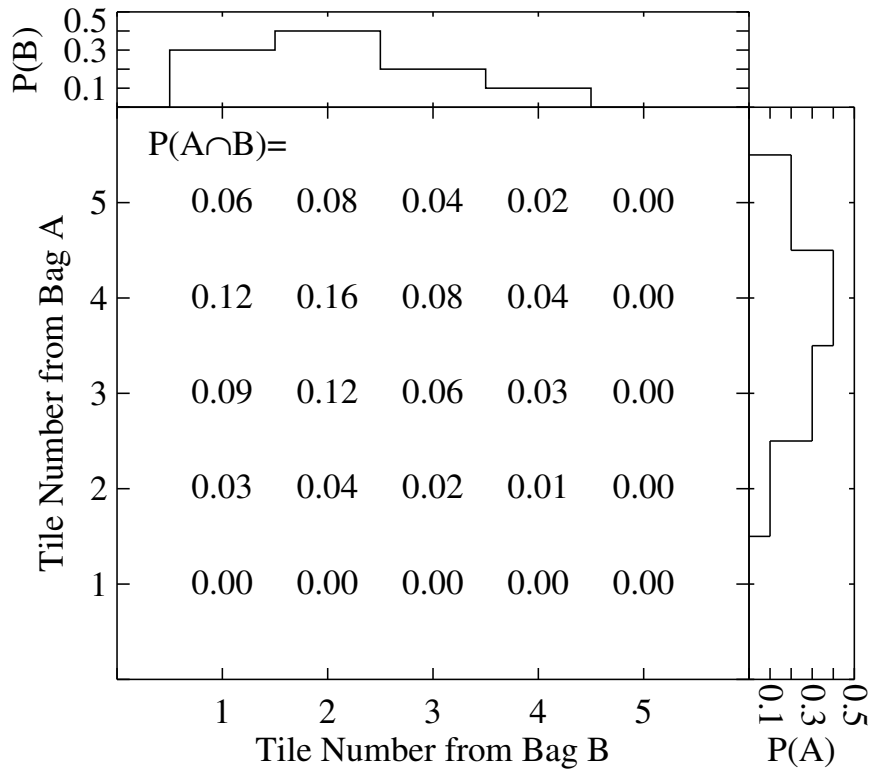


Figure C.2 Joint probability mass function, $P(A \cap B)$, of drawing a tile with a given number on it from bag A and a tile with a given number on it from bag B . The marginal probability mass functions, $P(A)$ and $P(B)$, are shown as histograms along the top and right of the figure.

Figure C.3. The sum of the joint probability distribution is equal to 1, a consequence of the unit measure axiom.

Many different questions can be answered using a joint probability distribution, three of which will help us eventually arrive at Equation 4.15. Firstly, we can ask what the probability of one set of events or another set of events occurring is. An example might be the probability that a 2-tile is drawn from bag A and a 3-tile is drawn from bag B , OR a 3-tile is drawn from bag A and a 4-tile is drawn from bag

B. The resulting probability is

$$\begin{aligned} P(A = 2 \cap B = 3) + P(A = 3 \cap B = 4) &= (0.1 * 0.2) + (0.3 * 0.1) \\ &= 0.05. \end{aligned} \tag{C.1}$$

This is illustrated in the top right panel of Figure C.3.

A second question might be, what is the probability of one of a range of events occurring for *A* and another from a range of events occurring for *B*. An example of this would be a tile between 1–3 being drawn from bag *A* and a tile between 2–4 being drawn from bag *B*. A diagram of this joint probability is shown in the bottom left panel of Figure C.3. The resulting probability is

$$\begin{aligned} P(A = [1 : 3] \cap B = [2 : 4]) &= \sum_{a=1}^{a=3} P(A = a) * \sum_{b=2}^{b=4} P(B = b) \\ &= (0.0 + 0.1 + 0.3) * (0.4 + 0.2 + 0.1) \\ &= 0.28. \end{aligned} \tag{C.2}$$

As can be seen, questions of this form are answered by a combination of addition and multiplication of probabilities. At the heart of this arithmetic, we are simply adding up the joint probability located at each intersection. For more complicated scenarios such as having many more numbers on the tiles, or having more than two bags to draw from, adding up the joint probabilities will not be straightforward and we must rely on the arithmetic formulas.

We are now ready to take on the final question: what is the probability that the tile drawn from bag *A* and the tile drawn from bag *B* will be separated in value by some small amount, say, 3. Once again, we draw the joint probability in the bottom right panel of Figure C.3. As can be seen, there are some intersections that occur more than once (e.g., $A = 3 \cap B = 2$, $A = 3 \cap B = 3$, etc.), and we must be careful not to add them more than once.

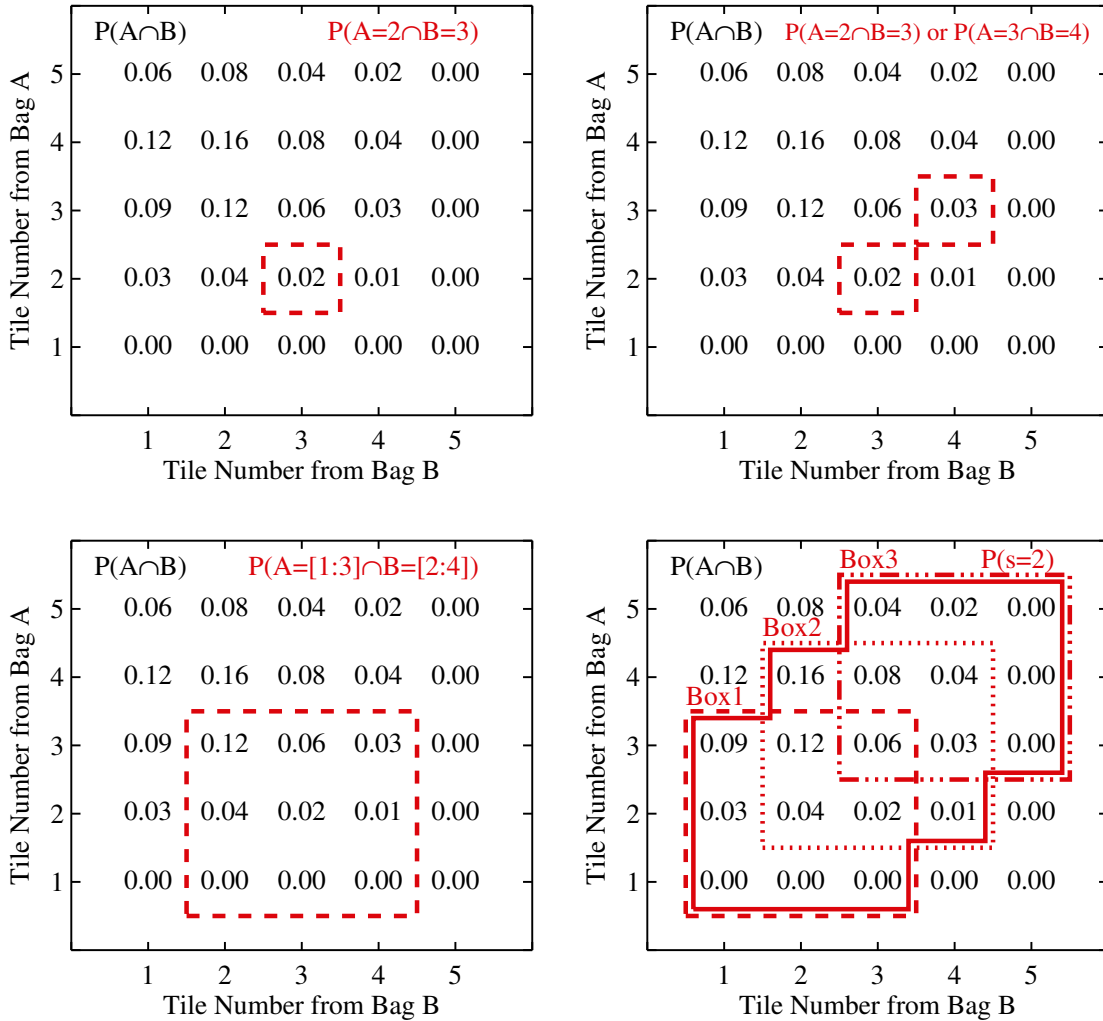


Figure C.3 Joint probability mass function is shown in black. Red denotes the following conditional probabilities. Top left: probability of a 2 being drawn from bag A and a 3 being drawn from bag B . Top right: probability of a 2 being drawn from bag A and a 3 being drawn from bag B , OR probability of a 3 being drawn from bag A and a 4 being drawn from bag B . Bottom left: probability of a 1, 2, or 3 being drawn from bag A and a 2, 3, or 4 being drawn from bag B . Bottom right: probability that the numbers drawn from bags A and B are within 2 of one another.

We will start with the probability within Box 1. This is much like the previous problem and can be written as

$$\begin{aligned}
P(\text{Box1}) &= P(A = [1 : 3] \cap B = [1 : 3]) \\
&= \sum_{a=1}^{a=3} P(A = a) * \sum_{b=1}^{b=3} P(B = b) \\
&= 0.4 * 0.9 \\
&= 0.36.
\end{aligned} \tag{C.3}$$

Box 2 has some new values in it, but the four probabilities in the bottom left corner have already been included in Box 1. Thus we can write the new probability contained within Box 2 as

$$\begin{aligned}
P(\text{Box2}) &= P(A = [2 : 4] \cap B = [2 : 4]) - P(A = [2 : 3] \cap B = [2 : 3]) \\
&= \left(\sum_{a=2}^{a=4} P(A = a) * \sum_{b=2}^{b=4} P(B = b) \right) - \left(\sum_{a=2}^{a=3} P(A = a) * \sum_{b=2}^{b=3} P(B = b) \right) \\
&= 0.56 - 0.24 \\
&= 0.32.
\end{aligned} \tag{C.4}$$

Box 3 much the same as Box 2:

$$\begin{aligned}
P(\text{Box3}) &= P(A = [3 : 5] \cap B = [3 : 5]) - P(A = [3 : 4] \cap B = [3 : 4]) \\
&= \left(\sum_{a=3}^{a=5} P(A = a) * \sum_{b=3}^{b=5} P(B = b) \right) - \left(\sum_{a=3}^{a=4} P(A = a) * \sum_{b=3}^{b=4} P(B = b) \right) \\
&= 0.27 - 0.21 \\
&= 0.06.
\end{aligned} \tag{C.5}$$

Taking all this together, the probability that the tile drawn from bag A and the tile drawn from bag B will be separated in value by 2 or less is

$$\begin{aligned}
P(s = 2) &= P(\text{Box1}) + P(\text{Box2}) + P(\text{Box3}) \\
&= 0.32 + 0.36 + 0.06 \\
&= 0.74
\end{aligned} \tag{C.6}$$

Recalling that the equations for probabilities contained in each box were a combination of products of sums, the formulation can be generalized further for additional bags ($X = A, B, C, D, E, \dots$), additional tile numbers ($x = 1, 2, 3, 4, 5, 6, 7, 8, \dots$), and different selections of the separation amount ($s = 2, 3, 4, 5, \dots$) as

$$\begin{aligned}
P(s) &= \prod_X \left(\sum_{x=1}^{1+s} P_X(x) \right) + \\
&\quad \sum_{x_i=2}^s \left(\prod_X \left(\sum_{x=x_i}^{x_i+s} P_X(x) \right) - \prod_X \left(\sum_{x=x_i}^{x_i+s-1} P_X(x) \right) \right)
\end{aligned} \tag{C.7}$$

The first term covers the probability in Box 1 and the second term covers the probabilities in all other boxes.

C.2 Application to Binary Fraction Probability

Equation C.7 is what we applied to our binary fraction question. Instead of bags, we had dwarf galaxies, d ; for the tile numbers we used binary fractions, f ; and in place of tile separations we had binary fraction separations, w . If we rewrite Equation C.7 with these substitutions, we have

$$\begin{aligned}
P(w) &= \prod_d \left(\sum_{f=0}^w P_d(f) \right) + \\
&\quad \sum_{f_i=0.01}^w \left(\prod_d \left(\sum_{f=f_i}^{f_i+w} P_d(f) \right) - \prod_d \left(\sum_{f=f_i}^{f_i+w-0.01} P_d(f) \right) \right)
\end{aligned} \tag{C.8}$$

This is nearly the same as Equation 4.15. The final step in completing the derivation is to change variables to have the separation intervals centered on a binary fraction, f_g , where $f_g = f_i + (w/2)$. Finally we arrive at Equation 4.15:

$$P(w) = \prod_d \left(\sum_{f=0}^w P_d(f) \right) + \sum_{f_g=0.01+w/2}^{1-w/2} \left(\prod_d \left(\sum_{f=f_g-w/2}^{f_g+w/2} P_d(f) \right) - \prod_d \left(\sum_{f=f_g-w/2}^{f_g+w/2-0.01} P_d(f) \right) \right) \quad (\text{C.9})$$

$P(w)$ gives us the probability that all the dwarf galaxies have a binary fraction within some specified range of f having a width of w and being centered on f_g . We can increase or decrease w depending on what we want our definition of “the same” to be, but we usually adopted $w = 0.1$ or $w = 0.2$.

C.3 Glossary of Variables

Variables from the toy model:

- A = bag of tiles
- B = bag of tiles
- X = general variable for a bag of tiles; $X = \{A, B, C, D, \dots\}$
- a = outcome of drawing a tile from bag A
- b = outcome of drawing a tile from bag B
- x = general outcome of drawing a tile from bag X
- x_i = tile number at lower edge of separation interval
- s = separation between the value of a tile from bag A and the value of a tile from bag B
- $P(A)$ = probability mass function for drawing a tile from bag A

- $P(B)$ = probability mass function for drawing a tile from bag B
- $P(A \cap B)$ = joint probability of a tile being drawn from bag A and a tile being drawn from bag B

Variables from the application to binary fraction:

- d = list of dwarf galaxies: {Draco, Ursa Minor, Leo II, Carina, Fornax, Sculptor, Sextans }
- w = width of range in f
- f = binary fraction
- f_g = binary fraction at the center of the width, w
- f_i = binary fraction at lower edge of width interval
- $P_d(f)$ = probability of the dwarf d having the binary fraction f ; PPD for the dwarf d
- $P(w, f_g)$ = probability of binary fraction of all d being within a given width w centered on a specified binary fraction f_g
- $P(w)$ = probability of binary fraction of all d being within a given width w

APPENDIX D

Photometry of Stars in the Direction of Leo II

There were nearly 10,000 stars in the direction of Leo II for which we obtained photometry. In this appendix we include only the 439 stars appearing along the red giant branch that were targeted for spectroscopic followup. We converted our instrumental Washington M and I magnitudes to apparent SDSS g and i magnitudes using a transformation described in Section 2.2.1. Column 1 lists the right ascension; column 2 lists the declination; column 3 lists the g magnitude; and column 4 lists the i magnitude.

Table D.1: Photometric properties of candidate Leo II members

α_{J2000}	δ_{J2000}	g	i
(hh:mm:ss.ss)	(dd:mm:ss.ss)	(mag)	(mag)
11:13:22.98	22:09:22.80	18.20±0.03	19.80±0.03
11:13:13.89	22:08:50.30	18.24±0.03	19.81±0.03
11:13:25.73	22:01:31.90	18.10±0.05	19.85±0.04
11:13:03.54	22:11:34.60	18.22±0.03	19.85±0.03
11:14:03.90	22:10:29.30	18.37±0.03	19.83±0.03
11:13:22.26	22:03:36.70	18.38±0.03	19.87±0.03
11:13:28.76	22:13:11.90	18.24±0.04	19.89±0.03
11:13:31.10	22:06:30.30	18.22±0.04	19.91±0.03
11:13:25.48	22:13:26.30	18.36±0.03	19.90±0.03
11:13:20.82	22:08:34.60	18.42±0.03	19.91±0.03

Table D.1: Continued; Photometric Properties of Candidate Leo II Members

α_{J2000} (hh:mm:ss.ss)	δ_{J2000} (dd:mm:ss.ss)	g (mag)	i (mag)
11:13:34.75	22:09:42.60	18.31±0.04	19.93±0.03
11:13:40.44	22:12:18.50	18.37±0.03	19.93±0.03
11:13:22.73	22:08:09.40	18.31±0.04	19.95±0.03
11:13:23.39	22:08:54.50	18.31±0.04	19.96±0.03
11:13:24.48	22:06:13.50	18.36±0.04	19.97±0.03
11:13:18.54	22:04:47.30	18.44±0.03	19.96±0.03
11:13:23.64	22:06:43.10	18.31±0.04	19.98±0.03
11:13:19.26	22:07:41.70	18.51±0.03	19.98±0.03
11:13:21.92	22:12:06.60	18.43±0.03	20.00±0.03
11:13:32.06	22:07:29.90	18.41±0.03	20.00±0.03
11:13:32.06	22:08:58.70	18.43±0.03	20.00±0.03
11:13:25.92	22:08:59.00	18.44±0.04	20.01±0.03
11:13:25.69	22:06:37.80	18.51±0.03	20.00±0.03
11:13:26.57	22:07:26.40	18.48±0.03	20.01±0.03
11:13:23.43	22:07:17.30	18.44±0.03	20.01±0.03
11:13:27.69	22:10:13.20	18.53±0.03	20.01±0.03
11:13:19.80	22:09:20.50	18.47±0.03	20.03±0.03
11:13:34.45	22:11:42.70	18.48±0.03	20.03±0.03
11:13:27.70	22:10:39.90	18.55±0.03	20.03±0.03
11:13:13.15	22:07:52.70	18.58±0.03	20.02±0.03
11:13:30.74	22:10:51.30	18.51±0.03	20.04±0.03
11:13:28.87	22:08:53.40	18.65±0.03	20.03±0.03
11:13:41.24	22:07:41.30	18.45±0.03	20.06±0.03
11:13:32.65	22:07:04.80	18.65±0.03	20.04±0.03
11:13:36.37	22:09:23.80	18.64±0.03	20.05±0.03
11:13:39.47	22:09:16.90	18.49±0.03	20.08±0.03
11:13:19.84	22:09:46.10	18.51±0.03	20.09±0.03
11:13:28.69	22:06:59.20	18.49±0.03	20.11±0.03
11:13:33.88	22:06:08.20	18.54±0.03	20.10±0.03
11:13:21.37	22:10:37.90	18.72±0.03	20.08±0.03
11:14:35.44	22:07:58.00	18.45±0.04	20.12±0.03
11:13:23.84	22:05:32.80	18.66±0.03	20.09±0.03
11:13:37.82	22:09:27.40	18.56±0.03	20.11±0.03
11:13:30.85	22:08:11.60	18.68±0.03	20.09±0.03
11:13:30.27	22:06:57.60	18.61±0.03	20.11±0.03
11:13:29.67	22:06:46.50	18.65±0.03	20.13±0.03
11:13:31.78	22:14:14.50	18.60±0.03	20.14±0.03

Table D.1: Continued; Photometric Properties of Candidate Leo II Members

α_{J2000} (hh:mm:ss.ss)	δ_{J2000} (dd:mm:ss.ss)	g (mag)	i (mag)
11:13:37.10	22:07:07.50	18.57±0.03	20.15±0.03
11:13:12.92	22:09:17.90	18.61±0.03	20.14±0.03
11:13:37.12	22:09:33.30	18.73±0.03	20.15±0.03
11:13:22.25	22:08:54.20	18.70±0.03	20.18±0.03
11:13:31.33	22:04:25.10	18.70±0.03	20.20±0.03
11:13:52.47	22:19:59.20	18.82±0.03	20.18±0.03
11:13:22.18	22:06:10.30	18.75±0.03	20.19±0.03
11:13:59.75	22:06:47.80	18.67±0.03	20.21±0.03
11:13:26.52	22:11:07.60	18.76±0.03	20.21±0.03
11:13:16.15	22:11:47.30	18.74±0.03	20.21±0.03
11:13:24.06	22:09:02.80	18.80±0.03	20.21±0.03
11:13:20.86	22:11:30.90	18.81±0.03	20.21±0.03
11:13:53.36	22:14:46.00	18.81±0.03	20.21±0.03
11:13:13.13	22:09:59.20	18.73±0.03	20.23±0.03
11:13:29.61	22:08:57.80	18.74±0.03	20.23±0.03
11:13:29.46	22:09:49.60	18.76±0.04	20.24±0.03
11:13:31.01	22:11:22.10	18.77±0.03	20.26±0.03
11:13:23.26	22:10:05.40	18.74±0.03	20.28±0.03
11:13:23.03	22:10:22.80	18.75±0.03	20.29±0.03
11:13:29.58	22:07:16.10	18.87±0.03	20.29±0.03
11:13:19.00	22:13:47.80	18.80±0.03	20.30±0.03
11:13:25.22	22:03:27.50	18.86±0.03	20.31±0.03
11:13:06.68	22:04:29.60	18.72±0.03	20.33±0.03
11:13:31.21	22:08:24.70	18.83±0.03	20.32±0.03
11:13:23.98	22:08:29.50	18.74±0.04	20.34±0.03
11:13:25.11	22:12:35.60	18.95±0.03	20.33±0.03
11:13:20.92	22:08:38.90	18.90±0.03	20.34±0.03
11:13:35.55	22:09:06.30	18.85±0.03	20.35±0.03
11:13:33.09	22:07:37.70	18.95±0.03	20.34±0.03
11:13:34.51	22:08:09.90	18.93±0.03	20.37±0.03
11:13:28.78	22:08:47.20	18.97±0.03	20.37±0.03
11:14:03.36	22:12:42.60	18.97±0.03	20.37±0.03
11:13:20.61	22:07:15.00	18.99±0.03	20.39±0.03
11:13:27.87	22:08:15.40	19.12±0.03	20.38±0.03
11:13:25.58	22:07:44.20	18.97±0.03	20.40±0.03
11:13:17.53	22:12:08.30	19.00±0.03	20.40±0.03
11:13:22.79	22:05:54.50	19.05±0.03	20.40±0.03

Table D.1: Continued; Photometric Properties of Candidate Leo II Members

α_{J2000} (hh:mm:ss.ss)	δ_{J2000} (dd:mm:ss.ss)	g (mag)	i (mag)
11:13:30.98	22:08:44.80	18.93±0.03	20.42±0.03
11:13:26.09	22:10:05.10	19.06±0.03	20.40±0.03
11:13:27.87	22:08:29.60	19.06±0.03	20.41±0.03
11:13:30.88	22:09:32.80	19.10±0.03	20.40±0.03
11:13:31.67	22:07:46.80	19.04±0.03	20.42±0.03
11:13:17.80	22:09:06.80	18.99±0.03	20.43±0.03
11:13:28.45	22:08:43.40	19.01±0.03	20.44±0.03
11:13:27.92	22:12:00.10	19.03±0.03	20.43±0.03
11:13:16.55	22:08:59.10	19.09±0.03	20.44±0.03
11:13:15.53	22:09:01.00	19.18±0.03	20.43±0.03
11:13:31.68	22:09:44.90	19.08±0.03	20.46±0.03
11:13:31.59	22:08:34.30	19.24±0.03	20.45±0.03
11:13:36.03	22:12:20.90	19.04±0.03	20.48±0.03
11:13:32.06	22:09:13.60	19.05±0.03	20.48±0.03
11:13:19.82	22:05:47.20	19.08±0.03	20.48±0.03
11:13:29.35	22:09:50.40	18.93±0.04	20.51±0.04
11:13:34.54	22:10:41.10	19.05±0.03	20.51±0.03
11:13:38.52	22:09:47.40	19.28±0.03	20.48±0.03
11:13:42.73	22:07:27.70	19.13±0.03	20.50±0.03
11:12:54.54	22:06:13.70	19.20±0.03	20.50±0.03
11:13:01.51	22:23:22.80	19.12±0.04	20.51±0.04
11:13:13.37	22:07:26.10	19.08±0.03	20.52±0.03
11:13:22.66	22:06:58.10	19.10±0.03	20.53±0.03
11:13:32.14	22:09:11.90	19.13±0.03	20.54±0.03
11:13:21.48	22:05:16.20	19.16±0.03	20.54±0.03
11:13:22.05	22:04:28.80	19.21±0.03	20.54±0.03
11:13:41.94	22:05:35.30	19.16±0.03	20.56±0.03
11:13:24.84	22:09:17.10	19.28±0.03	20.55±0.03
11:13:23.64	22:07:07.30	19.27±0.03	20.59±0.03
11:14:27.49	22:04:35.00	19.24±0.03	20.60±0.03
11:13:34.31	22:09:11.70	19.27±0.03	20.60±0.03
11:13:32.48	22:11:23.00	19.18±0.03	20.61±0.03
11:13:24.75	22:07:23.60	19.25±0.03	20.60±0.03
11:13:05.70	22:07:06.20	19.25±0.03	20.64±0.03
11:13:17.84	22:06:37.80	19.36±0.03	20.62±0.03
11:13:21.63	22:09:42.80	19.29±0.03	20.64±0.03
11:13:37.89	22:03:44.40	19.33±0.03	20.64±0.03

Table D.1: Continued; Photometric Properties of Candidate Leo II Members

α_{J2000} (hh:mm:ss.ss)	δ_{J2000} (dd:mm:ss.ss)	g (mag)	i (mag)
11:13:35.44	22:04:51.50	19.34±0.03	20.66±0.03
11:13:33.26	22:11:23.60	19.29±0.03	20.67±0.03
11:14:37.23	22:14:56.30	19.22±0.04	20.68±0.03
11:12:42.74	22:05:22.70	19.43±0.03	20.66±0.03
11:13:16.96	22:06:03.70	19.45±0.03	20.66±0.03
11:13:36.18	22:10:18.80	19.33±0.03	20.68±0.03
11:13:34.62	22:14:52.60	19.34±0.03	20.68±0.03
11:13:35.87	22:09:27.80	19.34±0.03	20.69±0.03
11:13:40.67	22:08:46.90	19.42±0.03	20.68±0.03
11:13:23.22	22:09:50.50	19.31±0.03	20.70±0.03
11:13:22.00	22:08:39.50	19.40±0.03	20.69±0.03
11:12:57.79	22:10:50.30	19.35±0.03	20.70±0.03
11:13:35.77	22:11:14.30	19.51±0.03	20.68±0.03
11:13:34.18	22:06:29.20	19.38±0.03	20.70±0.03
11:13:25.73	22:10:11.90	19.35±0.03	20.71±0.03
11:13:35.04	22:11:34.90	19.39±0.03	20.71±0.03
11:13:18.29	22:06:44.90	19.37±0.03	20.72±0.03
11:13:21.69	22:07:02.50	19.36±0.03	20.73±0.03
11:13:22.88	22:09:35.40	19.38±0.03	20.73±0.03
11:13:26.77	22:08:24.90	19.41±0.03	20.73±0.03
11:13:41.62	22:07:37.80	19.42±0.03	20.74±0.03
11:13:24.09	22:09:33.70	19.41±0.03	20.74±0.03
11:13:27.82	22:10:16.20	19.47±0.03	20.74±0.03
11:13:19.88	22:08:22.70	19.50±0.03	20.74±0.03
11:13:24.89	22:07:20.40	19.50±0.03	20.74±0.03
11:13:38.03	22:11:17.50	19.49±0.03	20.75±0.03
11:13:33.67	22:10:39.30	19.43±0.03	20.77±0.03
11:13:24.15	22:08:10.40	19.49±0.03	20.76±0.03
11:13:24.34	22:05:34.50	19.50±0.03	20.76±0.03
11:13:42.82	22:14:07.80	19.43±0.03	20.78±0.03
11:13:18.22	22:08:29.40	19.45±0.03	20.78±0.03
11:13:29.66	22:11:20.20	19.51±0.03	20.77±0.03
11:13:32.76	22:10:53.50	19.48±0.03	20.78±0.03
11:13:28.53	22:08:17.40	19.43±0.03	20.78±0.03
11:13:27.91	22:10:08.70	19.48±0.03	20.78±0.03
11:13:20.44	22:08:09.50	19.56±0.03	20.77±0.03
11:13:25.61	22:12:12.80	19.53±0.03	20.78±0.03

Table D.1: Continued; Photometric Properties of Candidate Leo II Members

α_{J2000} (hh:mm:ss.ss)	δ_{J2000} (dd:mm:ss.ss)	g (mag)	i (mag)
11:13:34.73	22:11:02.10	19.46±0.03	20.79±0.03
11:13:30.41	22:08:05.00	19.53±0.03	20.78±0.03
11:13:23.69	22:09:12.80	19.44±0.03	20.79±0.03
11:13:35.77	22:08:36.50	19.48±0.03	20.79±0.03
11:13:18.47	22:08:31.70	19.56±0.03	20.78±0.03
11:13:20.71	22:13:34.30	19.57±0.03	20.81±0.03
11:13:30.45	22:08:25.00	19.49±0.03	20.83±0.03
11:13:32.34	22:06:55.90	19.52±0.03	20.82±0.03
11:13:33.82	22:10:03.50	19.58±0.03	20.81±0.03
11:14:23.87	22:19:37.20	19.57±0.03	20.82±0.03
11:13:50.91	22:12:27.90	19.50±0.03	20.83±0.03
11:13:23.31	22:05:23.30	19.47±0.03	20.84±0.03
11:13:23.35	22:08:13.60	19.69±0.03	20.81±0.03
11:13:20.12	22:06:06.60	19.59±0.03	20.83±0.03
11:13:21.93	22:08:19.70	19.52±0.03	20.84±0.03
11:13:33.00	22:09:47.40	19.56±0.03	20.85±0.03
11:13:11.54	22:11:27.50	19.52±0.03	20.85±0.03
11:13:17.06	22:05:16.30	19.62±0.03	20.84±0.03
11:13:24.20	22:06:15.40	19.59±0.03	20.84±0.03
11:13:36.22	22:08:51.30	19.42±0.03	20.87±0.03
11:13:23.43	22:06:18.10	19.50±0.03	20.87±0.03
11:13:30.15	22:09:31.60	19.57±0.03	20.87±0.03
11:13:26.10	22:06:48.20	19.62±0.03	20.87±0.03
11:13:20.64	22:09:33.90	19.62±0.03	20.89±0.03
11:13:34.45	22:11:05.70	19.63±0.03	20.89±0.03
11:13:34.28	22:08:20.40	19.77±0.03	20.87±0.03
11:13:46.44	22:07:09.10	19.72±0.03	20.88±0.03
11:13:31.24	22:11:04.00	19.64±0.03	20.90±0.03
11:13:23.46	22:08:51.20	19.66±0.03	20.91±0.03
11:13:36.80	22:06:48.50	19.68±0.03	20.91±0.03
11:13:15.57	22:08:26.60	19.65±0.03	20.92±0.03
11:13:33.76	22:09:50.00	19.69±0.03	20.91±0.03
11:13:32.16	22:08:30.70	19.64±0.03	20.92±0.03
11:13:13.68	22:10:35.80	19.67±0.03	20.93±0.03
11:13:42.41	22:10:02.90	19.76±0.03	20.92±0.03
11:13:33.91	22:00:51.40	19.81±0.03	20.91±0.03
11:12:31.54	22:03:00.00	19.74±0.04	20.92±0.04

Table D.1: Continued; Photometric Properties of Candidate Leo II Members

α_{J2000} (hh:mm:ss.ss)	δ_{J2000} (dd:mm:ss.ss)	g (mag)	i (mag)
11:13:37.90	22:08:13.40	19.60±0.03	20.94±0.03
11:13:28.60	22:08:38.00	19.67±0.03	20.94±0.03
11:13:25.54	22:09:15.60	19.68±0.03	20.94±0.03
11:13:34.44	22:09:32.00	19.69±0.03	20.94±0.03
11:13:26.93	22:06:21.30	19.71±0.03	20.94±0.03
11:13:21.48	22:08:46.30	19.67±0.03	20.95±0.03
11:13:29.42	22:10:31.60	19.70±0.03	20.94±0.03
11:13:27.76	22:07:46.00	19.70±0.03	20.95±0.03
11:13:27.50	22:13:41.70	19.71±0.03	20.95±0.03
11:13:33.00	22:08:01.70	19.72±0.03	20.95±0.03
11:13:31.43	22:08:43.10	19.79±0.03	20.94±0.03
11:13:38.32	22:09:08.60	19.69±0.03	20.96±0.03
11:13:27.85	22:09:04.50	19.71±0.03	20.96±0.03
11:13:24.71	22:08:08.50	19.70±0.03	20.97±0.03
11:13:07.60	22:09:30.40	19.75±0.03	20.97±0.03
11:13:19.45	22:11:06.20	19.69±0.03	20.97±0.03
11:13:22.56	22:07:31.30	19.73±0.03	20.97±0.03
11:13:31.52	22:11:25.60	19.70±0.03	20.98±0.03
11:13:18.71	22:10:30.40	19.67±0.03	20.98±0.03
11:13:19.54	22:06:11.50	19.77±0.03	20.98±0.03
11:13:39.13	22:09:52.70	19.71±0.03	20.99±0.03
11:13:42.88	22:13:55.80	19.75±0.03	20.99±0.03
11:13:24.28	22:09:05.10	19.72±0.03	21.00±0.03
11:13:39.14	22:09:20.50	19.80±0.03	20.99±0.03
11:13:22.57	22:10:07.70	19.74±0.03	21.01±0.03
11:13:27.96	22:07:23.30	19.77±0.03	21.00±0.03
11:13:44.66	22:08:25.40	19.73±0.03	21.01±0.03
11:12:53.12	22:00:25.70	19.86±0.03	21.00±0.03
11:13:28.89	22:10:42.20	19.92±0.03	20.99±0.03
11:13:26.95	22:11:50.10	19.78±0.03	21.01±0.03
11:13:12.95	22:08:09.70	19.80±0.03	21.01±0.03
11:13:30.83	22:09:13.90	19.81±0.03	21.01±0.03
11:13:07.48	22:06:26.40	19.93±0.03	21.00±0.03
11:13:14.50	22:08:50.70	19.78±0.03	21.02±0.03
11:14:20.03	22:20:09.60	19.86±0.03	21.01±0.03
11:13:30.47	22:08:14.70	19.82±0.03	21.02±0.03
11:13:24.55	22:12:48.60	19.73±0.03	21.04±0.03

Table D.1: Continued; Photometric Properties of Candidate Leo II Members

α_{J2000} (hh:mm:ss.ss)	δ_{J2000} (dd:mm:ss.ss)	g (mag)	i (mag)
11:13:18.95	22:07:13.80	19.70±0.03	21.05±0.03
11:13:23.79	22:08:49.80	19.80±0.03	21.04±0.03
11:13:23.12	22:08:02.70	19.83±0.03	21.04±0.03
11:13:33.03	22:07:22.50	19.93±0.03	21.03±0.03
11:13:23.32	22:13:17.30	19.82±0.03	21.05±0.03
11:13:36.34	22:11:32.90	19.80±0.03	21.05±0.03
11:13:08.30	22:10:31.00	19.85±0.03	21.04±0.03
11:13:23.42	22:05:38.60	19.76±0.03	21.05±0.03
11:13:13.77	22:04:19.30	19.79±0.03	21.05±0.03
11:13:35.49	22:09:27.90	19.77±0.03	21.06±0.03
11:13:34.20	22:09:07.40	19.85±0.03	21.06±0.03
11:13:30.44	22:07:03.70	19.82±0.03	21.07±0.03
11:13:38.88	22:09:47.10	19.78±0.03	21.07±0.03
11:13:34.85	22:06:17.70	19.78±0.03	21.08±0.03
11:13:14.24	22:14:17.80	19.93±0.03	21.06±0.03
11:13:31.40	22:09:14.20	19.94±0.03	21.06±0.03
11:13:21.55	22:10:52.70	19.86±0.03	21.07±0.03
11:13:16.06	22:06:57.50	19.92±0.03	21.07±0.04
11:13:18.57	22:07:58.40	19.88±0.03	21.08±0.03
11:12:41.24	22:12:06.40	19.92±0.03	21.08±0.04
11:13:19.06	22:06:45.20	19.98±0.03	21.08±0.03
11:13:18.86	22:10:19.10	19.84±0.03	21.10±0.03
11:14:18.96	22:11:08.20	19.81±0.03	21.11±0.03
11:13:19.30	22:07:44.90	19.86±0.03	21.10±0.03
11:13:22.36	22:11:02.80	19.90±0.03	21.10±0.03
11:13:42.44	22:04:22.20	19.77±0.03	21.12±0.03
11:13:18.68	22:09:22.40	19.80±0.03	21.12±0.03
11:13:21.99	22:11:32.10	19.92±0.03	21.11±0.03
11:13:17.36	22:06:04.10	19.91±0.03	21.12±0.03
11:13:39.93	22:07:16.40	19.90±0.03	21.12±0.03
11:12:35.98	22:03:23.60	19.94±0.04	21.11±0.04
11:13:27.28	22:07:05.80	19.85±0.03	21.13±0.03
11:13:40.26	22:06:28.90	19.91±0.03	21.12±0.03
11:13:42.34	22:07:40.50	19.80±0.03	21.14±0.03
11:13:21.55	22:06:29.90	19.96±0.03	21.12±0.04
11:13:28.68	22:08:26.60	19.84±0.03	21.13±0.04
11:13:44.39	22:14:37.00	19.92±0.03	21.12±0.03

Table D.1: Continued; Photometric Properties of Candidate Leo II Members

α_{J2000} (hh:mm:ss.ss)	δ_{J2000} (dd:mm:ss.ss)	g (mag)	i (mag)
11:13:17.97	22:09:53.50	19.90±0.03	21.13±0.03
11:13:15.86	22:04:51.40	19.93±0.03	21.13±0.03
11:13:15.72	22:09:05.70	19.88±0.03	21.14±0.03
11:13:27.06	22:09:13.20	19.86±0.03	21.15±0.03
11:13:20.44	22:10:17.60	19.91±0.03	21.14±0.03
11:13:32.04	22:07:51.50	19.95±0.03	21.15±0.03
11:13:26.17	22:08:45.60	19.89±0.03	21.16±0.04
11:13:26.51	22:07:57.40	19.95±0.03	21.15±0.03
11:13:30.84	22:07:46.10	19.90±0.03	21.16±0.04
11:13:30.17	22:07:46.40	19.99±0.03	21.16±0.04
11:13:27.22	22:10:59.70	20.03±0.03	21.16±0.03
11:13:34.83	22:03:10.70	19.96±0.03	21.17±0.03
11:13:23.84	22:04:58.10	19.91±0.03	21.18±0.03
11:13:36.83	22:11:24.80	19.93±0.03	21.18±0.03
11:13:06.41	22:12:05.50	19.94±0.03	21.17±0.03
11:13:26.73	22:08:32.40	20.07±0.03	21.16±0.04
11:13:20.45	22:07:15.60	20.02±0.04	21.16±0.04
11:13:32.87	22:09:53.20	19.96±0.03	21.18±0.03
11:13:34.10	22:13:01.10	19.97±0.03	21.18±0.03
11:13:31.98	22:09:04.40	19.99±0.03	21.18±0.03
11:13:44.49	22:08:04.00	19.83±0.04	21.20±0.04
11:12:29.76	22:08:47.80	19.81±0.04	21.20±0.04
11:13:20.97	22:07:01.30	19.90±0.03	21.19±0.03
11:13:23.75	22:08:10.50	19.95±0.03	21.19±0.03
11:13:30.43	22:10:43.30	19.95±0.03	21.19±0.03
11:13:29.79	22:11:18.90	19.92±0.03	21.20±0.03
11:13:32.01	22:07:39.50	19.94±0.03	21.20±0.03
11:13:35.60	22:07:53.50	19.99±0.03	21.19±0.04
11:13:43.15	22:07:57.40	19.98±0.03	21.20±0.03
11:13:25.06	22:07:13.50	19.96±0.03	21.20±0.04
11:13:24.25	22:07:49.00	19.93±0.03	21.21±0.03
11:13:34.57	22:06:52.60	19.98±0.03	21.20±0.04
11:13:03.81	22:05:47.10	20.00±0.03	21.20±0.03
11:13:23.20	22:08:17.90	20.10±0.03	21.19±0.03
11:13:22.90	22:10:18.80	19.96±0.03	21.21±0.03
11:13:34.72	22:10:07.50	20.01±0.03	21.20±0.04
11:13:43.08	22:08:14.20	20.08±0.03	21.21±0.04

Table D.1: Continued; Photometric Properties of Candidate Leo II Members

α_{J2000} (hh:mm:ss.ss)	δ_{J2000} (dd:mm:ss.ss)	g (mag)	i (mag)
11:13:57.06	22:12:16.60	20.01±0.03	21.22±0.03
11:13:28.80	22:11:10.70	20.02±0.03	21.22±0.04
11:13:26.16	22:08:12.90	19.97±0.03	21.22±0.04
11:13:23.63	22:08:25.10	20.19±0.03	21.21±0.04
11:13:31.74	22:07:51.30	20.00±0.03	21.23±0.03
11:13:21.13	22:07:57.60	20.05±0.03	21.23±0.04
11:13:16.66	22:06:26.20	20.04±0.03	21.24±0.03
11:13:36.43	22:10:06.50	20.03±0.03	21.24±0.03
11:13:37.22	22:09:07.50	20.05±0.03	21.24±0.04
11:13:52.85	22:08:42.60	20.00±0.03	21.25±0.03
11:13:19.64	22:09:12.00	20.14±0.03	21.24±0.04
11:13:18.83	22:11:15.00	20.00±0.03	21.25±0.04
11:13:53.79	22:10:45.60	20.07±0.03	21.25±0.03
11:13:32.65	22:10:11.30	20.13±0.03	21.25±0.04
11:13:22.92	22:10:02.30	20.00±0.04	21.26±0.04
11:13:20.54	22:12:12.00	20.02±0.03	21.26±0.03
11:13:25.67	22:08:23.10	20.25±0.04	21.24±0.05
11:14:01.86	22:03:08.50	20.24±0.03	21.25±0.04
11:13:32.76	22:08:14.00	19.99±0.04	21.28±0.05
11:13:23.20	22:09:28.30	20.03±0.04	21.27±0.04
11:13:34.66	22:08:19.60	20.07±0.03	21.28±0.04
11:13:20.39	22:10:02.70	20.06±0.04	21.29±0.04
11:13:28.38	22:10:15.90	20.13±0.03	21.28±0.04
11:13:12.23	22:16:09.20	20.09±0.03	21.29±0.04
11:13:52.52	22:07:13.20	20.10±0.03	21.29±0.03
11:13:23.91	22:11:19.20	20.04±0.03	21.30±0.03
11:13:19.53	22:08:48.90	20.12±0.03	21.29±0.04
11:13:20.81	22:10:32.30	20.07±0.03	21.30±0.04
11:13:35.93	22:08:29.40	20.12±0.03	21.29±0.04
11:13:28.43	22:11:09.90	20.10±0.03	21.30±0.04
11:13:32.76	22:10:31.40	20.06±0.03	21.31±0.04
11:13:19.99	22:07:11.90	20.08±0.04	21.30±0.04
11:13:22.86	22:08:23.70	20.13±0.04	21.30±0.04
11:13:40.41	22:05:29.70	20.21±0.04	21.29±0.04
11:13:24.96	22:09:16.30	20.14±0.04	21.30±0.04
11:13:51.52	22:09:02.30	20.09±0.03	21.31±0.03
11:13:26.82	22:11:58.30	20.20±0.03	21.30±0.04

Table D.1: Continued; Photometric Properties of Candidate Leo II Members

α_{J2000} (hh:mm:ss.ss)	δ_{J2000} (dd:mm:ss.ss)	g (mag)	i (mag)
11:13:25.61	22:10:50.80	20.12±0.03	21.32±0.04
11:13:29.62	22:09:19.80	20.15±0.03	21.32±0.04
11:13:47.59	22:11:15.00	20.15±0.03	21.32±0.04
11:13:40.25	22:10:44.00	20.04±0.03	21.34±0.03
11:13:15.89	22:10:10.10	20.26±0.04	21.31±0.04
11:13:23.84	22:09:11.30	20.16±0.03	21.32±0.04
11:13:12.07	22:03:24.10	20.12±0.04	21.33±0.04
11:13:37.32	22:09:58.90	20.05±0.03	21.34±0.03
11:13:22.32	22:07:22.00	20.23±0.04	21.32±0.04
11:13:32.34	22:07:34.40	20.13±0.04	21.33±0.04
11:13:51.00	22:08:36.00	20.19±0.03	21.33±0.03
11:13:30.68	22:12:19.80	20.13±0.03	21.34±0.04
11:13:42.44	22:10:51.30	20.14±0.03	21.34±0.03
11:13:21.96	22:08:56.70	20.20±0.04	21.33±0.04
11:13:28.02	22:09:08.30	20.12±0.03	21.35±0.04
11:13:19.91	22:06:11.10	20.22±0.04	21.34±0.04
11:13:44.80	22:09:36.90	20.16±0.03	21.35±0.04
11:13:30.52	22:09:02.60	20.13±0.04	21.36±0.04
11:13:29.14	22:06:04.80	20.11±0.03	21.36±0.04
11:13:22.46	22:07:05.80	20.32±0.04	21.34±0.04
11:12:25.80	22:05:27.70	20.27±0.04	21.35±0.05
11:13:31.88	22:04:56.20	20.17±0.04	21.37±0.04
11:13:25.84	22:06:14.00	20.24±0.04	21.36±0.04
11:13:09.28	22:07:02.80	20.29±0.03	21.35±0.04
11:13:37.87	22:04:38.60	20.14±0.03	21.38±0.03
11:13:42.26	22:09:26.10	20.22±0.03	21.37±0.04
11:13:27.66	22:11:57.00	20.20±0.03	21.37±0.04
11:13:23.70	22:08:54.30	20.15±0.03	21.38±0.03
11:13:24.35	22:10:58.50	20.15±0.03	21.39±0.03
11:13:32.89	22:06:48.40	20.24±0.03	21.38±0.04
11:13:26.05	22:03:00.90	20.20±0.03	21.38±0.04
11:13:41.64	22:08:52.50	20.14±0.04	21.39±0.04
11:13:02.74	22:07:14.50	20.21±0.03	21.39±0.04
11:13:48.62	22:17:23.50	20.29±0.04	21.38±0.04
11:13:23.35	22:10:00.80	20.17±0.03	21.39±0.03
11:13:19.35	22:10:30.00	20.20±0.03	21.39±0.04
11:13:27.99	22:11:47.30	20.18±0.04	21.40±0.04

Table D.1: Continued; Photometric Properties of Candidate Leo II Members

α_{J2000} (hh:mm:ss.ss)	δ_{J2000} (dd:mm:ss.ss)	g (mag)	i (mag)
11:13:42.53	22:15:02.90	20.42±0.03	21.37±0.04
11:13:36.69	22:08:10.90	20.29±0.03	21.39±0.04
11:13:28.63	22:12:05.20	20.15±0.04	21.41±0.04
11:13:28.05	22:10:06.50	20.17±0.04	21.41±0.04
11:13:28.66	22:10:14.50	20.24±0.04	21.40±0.04
11:14:06.54	22:19:22.30	20.28±0.04	21.40±0.04
11:13:33.76	22:09:23.60	20.26±0.04	21.40±0.04
11:13:30.40	22:03:58.20	20.25±0.03	21.41±0.04
11:13:25.40	22:07:18.00	20.26±0.04	21.41±0.04
11:13:03.98	22:07:15.30	20.23±0.03	21.42±0.04
11:13:13.62	22:08:20.70	20.19±0.04	21.43±0.04
11:13:30.20	22:08:14.00	20.22±0.04	21.43±0.04
11:12:54.90	22:22:04.90	20.19±0.13	21.44±0.12
11:13:37.58	22:04:42.20	20.24±0.03	21.43±0.04
11:13:20.65	22:09:53.30	20.36±0.04	21.42±0.04
11:13:32.37	22:08:49.60	20.30±0.04	21.44±0.04
11:13:26.99	22:10:45.00	20.31±0.04	21.44±0.04
11:13:31.43	22:07:34.10	20.30±0.04	21.44±0.04
11:13:17.30	22:13:34.00	20.29±0.04	21.44±0.04
11:13:28.57	22:08:07.40	20.32±0.04	21.45±0.04
11:13:55.87	21:55:15.50	20.42±0.03	21.44±0.04
11:13:36.83	22:09:10.40	20.39±0.04	21.45±0.05
11:13:29.73	22:08:27.20	20.27±0.04	21.46±0.04
11:13:11.78	22:11:50.90	20.37±0.03	21.45±0.04
11:13:07.05	22:09:27.20	20.30±0.03	21.47±0.04
11:13:24.93	22:11:32.10	20.29±0.04	21.47±0.04
11:13:33.04	22:10:12.00	20.24±0.04	21.48±0.04
11:13:19.19	22:09:01.30	20.36±0.04	21.46±0.04
11:13:24.86	22:06:37.40	20.29±0.04	21.47±0.04
11:13:18.14	22:07:54.90	20.28±0.04	21.47±0.04
11:13:14.47	22:14:02.90	20.22±0.04	21.48±0.04
11:13:33.46	22:09:54.50	20.28±0.03	21.48±0.04
11:13:31.04	22:08:15.80	20.35±0.04	21.48±0.04
11:13:24.55	22:10:16.70	20.53±0.04	21.45±0.05
11:13:30.50	22:10:00.50	20.38±0.04	21.47±0.04
11:13:24.61	22:10:53.00	20.40±0.03	21.48±0.04
11:13:28.36	22:10:25.70	20.21±0.04	21.50±0.04

Table D.1: Continued; Photometric Properties of Candidate Leo II Members

α_{J2000} (hh:mm:ss.ss)	δ_{J2000} (dd:mm:ss.ss)	g (mag)	i (mag)
11:13:40.20	22:10:35.10	20.29±0.04	21.50±0.04
11:13:37.49	22:07:40.60	20.37±0.04	21.49±0.04
11:13:25.21	22:06:13.80	20.33±0.03	21.50±0.04
11:13:38.62	22:08:23.30	20.40±0.04	21.49±0.04
11:13:10.32	22:09:05.60	20.38±0.03	21.50±0.04
11:13:20.60	22:05:58.10	20.42±0.04	21.50±0.04
11:13:25.95	22:06:28.60	20.42±0.04	21.50±0.04
11:13:05.46	22:06:57.00	20.32±0.04	21.52±0.04
11:13:03.68	22:08:24.00	20.45±0.03	21.50±0.04
11:13:42.01	22:10:14.50	20.35±0.04	21.52±0.04
11:13:18.78	22:13:13.40	20.39±0.04	21.51±0.04
11:13:28.64	22:08:43.20	20.30±0.04	21.53±0.04
11:13:58.84	22:12:17.30	20.37±0.04	21.52±0.05
11:13:30.71	22:10:08.50	20.28±0.04	21.54±0.04
11:13:34.54	22:08:04.00	20.37±0.04	21.53±0.04
11:13:11.05	22:09:37.40	20.34±0.04	21.53±0.04
11:13:17.73	22:06:48.00	20.38±0.04	21.53±0.04
11:13:29.13	22:08:25.00	20.27±0.04	21.54±0.04
11:13:31.97	22:07:37.00	20.35±0.04	21.54±0.04
11:13:39.33	22:09:18.60	20.46±0.04	21.52±0.04
11:13:32.76	22:14:33.80	20.41±0.04	21.53±0.04
11:13:28.60	22:05:37.10	20.39±0.03	21.54±0.03

APPENDIX E

Spectroscopic Properties of Leo II Stars

We measured spectroscopic properties of 336 stars in Leo II. 222 of these stars passed our quality cuts (described in Section 2.2.4) and are listed in the following table. Many of the stars were observed on more than one observing run. For these cases we report the average measurements as the first entry for the star and the individual measurements immediately below that. The right ascension, declination, number of observations, and membership status for multiply-observed stars are only listed on the first line with the average spectroscopic measurements. Column 1 lists the right ascension; column 2 lists the declination; column 3 lists the heliocentric Julian date; column 4 lists the radial velocity and error; column 5 lists the effective temperature and error; column 6 lists the surface gravity and error; column 7 lists the metallicity and error; column 8 lists the number of observations; column 9 lists our determination of membership status. 'Y' indicates it is a Leo II member. 'N' indicates it is not a Leo II member.

Table E.1: Spectroscopic properties of stars in the direction of Leo II

α_{J2000}	δ_{J2000}	HJD	v	T_{eff}	$\log(g)$	[Fe/H]	N_{obs}	Mem
(deg)	(deg)	(-2450000 days)	(km s^{-1})	(K)	(dex)	(dex)		
168.228745	22.368030	5059.35	208.67 ± 0.87	5209 ± 223	3.15 ± 0.43	-1.78 ± 0.26	2	N
		4526.81	208.87 ± 1.00	5153 ± 238	3.31 ± 0.46	-1.89 ± 0.29		
		5591.90	208.07 ± 1.77	5621 ± 644	2.19 ± 1.13	-1.22 ± 0.64		
168.332825	22.139639	4526.81	71.08 ± 2.19	6347 ± 601	1.46 ± 0.68	0.17 ± 0.53	1	Y
168.361542	22.140249	4526.81	76.11 ± 2.64	5636 ± 438	4.65 ± 0.75	-0.73 ± 0.51	1	N
168.331375	22.146915	5591.90	75.00 ± 0.91	4800 ± 167	0.98 ± 0.27	-1.26 ± 0.22	1	Y
168.392960	22.153250	5591.90	71.64 ± 0.78	4622 ± 147	0.92 ± 0.24	-2.11 ± 0.18	1	Y
168.353699	22.122332	5969.43	78.11 ± 0.90	4946 ± 173	1.02 ± 0.23	-0.96 ± 0.23	2	Y
		5597.94	79.17 ± 2.17	5492 ± 714	2.81 ± 0.92	-2.38 ± 0.73		
		6340.91	77.89 ± 0.99	4912 ± 179	0.90 ± 0.23	-0.80 ± 0.24		
168.325912	22.141500	5969.43	75.30 ± 0.87	4699 ± 185	2.28 ± 0.43	-1.63 ± 0.24	2	Y
		5597.94	67.90 ± 1.28	5120 ± 435	2.94 ± 0.66	-1.71 ± 0.51		
		6340.91	81.64 ± 1.19	4607 ± 204	1.80 ± 0.56	-1.61 ± 0.28		
168.368866	22.138166	5599.80	75.43 ± 1.85	4792 ± 363	1.70 ± 0.84	0.29 ± 0.52	1	Y
168.341370	22.138805	6340.91	84.19 ± 2.35	5133 ± 508	1.05 ± 0.36	0.64 ± 0.57	1	Y
168.326935	22.142139	6341.92	76.27 ± 1.81	6174 ± 704	3.43 ± 0.95	-1.48 ± 0.56	1	Y
168.172203	21.969577	5124.19	70.77 ± 0.17	5604 ± 22	4.47 ± 0.04	-0.23 ± 0.02	8	N
		3850.66	70.69 ± 0.51	5301 ± 90	3.92 ± 0.23	0.18 ± 0.10		
		4212.78	70.81 ± 0.47	5636 ± 54	4.49 ± 0.11	-0.24 ± 0.06		
		4522.71	70.81 ± 0.50	5591 ± 80	4.32 ± 0.15	-0.54 ± 0.09		
		4526.81	71.30 ± 0.46	5646 ± 54	4.56 ± 0.10	-0.21 ± 0.06		
		5597.94	71.18 ± 0.46	5547 ± 68	4.39 ± 0.14	-0.29 ± 0.07		
		5599.80	70.55 ± 0.48	5638 ± 71	4.48 ± 0.15	-0.14 ± 0.07		
		6340.91	70.41 ± 0.46	5649 ± 54	4.57 ± 0.10	-0.23 ± 0.06		
		6341.92	70.36 ± 0.46	5618 ± 57	4.47 ± 0.12	-0.23 ± 0.06		
		6341.92	70.36 ± 0.46	5618 ± 57	4.47 ± 0.12	-0.23 ± 0.06		
168.232233	21.913524	5123.20	14.46 ± 0.17	5627 ± 23	4.25 ± 0.04	-0.48 ± 0.03	8	N
		3850.66	14.90 ± 0.88	5580 ± 202	4.64 ± 0.43	0.64 ± 0.17		
		4212.78	14.69 ± 0.48	5668 ± 74	4.30 ± 0.13	-0.42 ± 0.08		
		4522.71	14.74 ± 0.49	5561 ± 101	4.03 ± 0.19	-0.74 ± 0.11		
		4526.81	14.39 ± 0.47	5670 ± 63	4.30 ± 0.11	-0.50 ± 0.07		
		5591.90	14.18 ± 0.46	5631 ± 48	4.28 ± 0.09	-0.50 ± 0.05		
		5597.94	14.75 ± 0.46	5570 ± 76	4.11 ± 0.14	-0.56 ± 0.08		
		6340.91	14.06 ± 0.46	5626 ± 55	4.27 ± 0.11	-0.49 ± 0.06		
6341.92	14.38 ± 0.46	5619 ± 59	4.21 ± 0.11	-0.51 ± 0.07				
168.319920	21.971185	5458.28	42.55 ± 0.19	5442 ± 22	4.77 ± 0.05	-0.33 ± 0.02	7	N
		4212.78	42.54 ± 0.48	5443 ± 57	4.80 ± 0.12	-0.40 ± 0.06		
		4522.71	42.09 ± 0.64	5458 ± 110	4.87 ± 0.25	0.33 ± 0.12		

Table E.1: Continued; Spectroscopic properties of stars in the direction of Leo II

α_{J2000}	δ_{J2000}	HJD	v	T_{eff}	$\log(g)$	[Fe/H]	N_{obs}	Mem
(deg)	(deg)	(-2450000 days)	(km s ⁻¹)	(K)	(dex)	(dex)		
		5591.90	42.44 ± 0.46	5444 ± 52	4.77 ± 0.11	-0.41 ± 0.06		
		5597.94	43.43 ± 0.47	5456 ± 53	4.82 ± 0.11	-0.33 ± 0.06		
		5599.80	42.19 ± 0.52	5486 ± 81	4.72 ± 0.17	-0.19 ± 0.08		
		6340.91	42.45 ± 0.46	5414 ± 53	4.74 ± 0.11	-0.39 ± 0.06		
		6341.92	42.44 ± 0.47	5427 ± 56	4.70 ± 0.12	-0.34 ± 0.06		
168.407975	21.905901	5119.04	51.73 ± 0.22	5625 ± 28	4.21 ± 0.05	-0.47 ± 0.03	5	N
		3850.66	51.84 ± 0.69	5461 ± 133	3.72 ± 0.29	-0.55 ± 0.15		
		4212.78	51.57 ± 0.48	5628 ± 68	4.17 ± 0.13	-0.53 ± 0.07		
		5591.90	51.39 ± 0.46	5635 ± 51	4.30 ± 0.10	-0.45 ± 0.06		
		5597.94	52.21 ± 0.46	5647 ± 56	4.26 ± 0.10	-0.46 ± 0.06		
		6341.92	51.70 ± 0.46	5617 ± 64	4.13 ± 0.12	-0.45 ± 0.07		
168.300224	22.056662	5966.91	81.22 ± 1.33	5236 ± 416	2.92 ± 0.56	-1.78 ± 0.43	2	Y
		5591.90	79.12 ± 1.91	6123 ± 753	4.33 ± 0.83	-0.93 ± 0.70		
		6341.92	83.21 ± 1.86	4845 ± 499	1.75 ± 0.76	-2.27 ± 0.54		
168.342695	22.060175	5435.88	80.63 ± 0.43	4433 ± 54	1.26 ± 0.17	-2.74 ± 0.06	4	Y
		4212.78	79.73 ± 1.05	4446 ± 124	1.23 ± 0.38	-2.84 ± 0.15		
		5591.90	80.46 ± 0.63	4472 ± 108	1.31 ± 0.30	-2.73 ± 0.12		
		5597.94	79.89 ± 1.10	4684 ± 227	2.01 ± 0.55	-2.39 ± 0.29		
		6340.91	82.07 ± 0.88	4381 ± 76	1.05 ± 0.27	-2.74 ± 0.10		
168.355033	22.057600	5062.37	85.28 ± 0.45	4587 ± 86	0.81 ± 0.12	-1.44 ± 0.11	2	Y
		4526.81	84.78 ± 0.62	4613 ± 113	0.89 ± 0.20	-1.59 ± 0.14		
		5597.94	85.87 ± 0.67	4551 ± 132	0.77 ± 0.15	-1.23 ± 0.17		
168.358483	22.050218	6091.58	79.50 ± 0.82	4685 ± 163	1.31 ± 0.30	-1.23 ± 0.21	3	Y
		5591.90	79.01 ± 1.30	4553 ± 184	1.10 ± 0.36	-1.09 ± 0.25		
		6340.91	79.33 ± 1.43	5189 ± 499	1.39 ± 0.61	-1.43 ± 0.52		
		6341.92	80.38 ± 1.54	5165 ± 508	2.60 ± 0.98	-1.77 ± 0.59		
168.391767	21.980727	5268.84	-3.68 ± 0.22	4798 ± 22	5.29 ± 0.06	-0.05 ± 0.03	5	N
		3850.66	-3.92 ± 0.60	4725 ± 74	5.27 ± 0.23	0.18 ± 0.10		
		4212.78	-3.64 ± 0.47	4841 ± 45	5.19 ± 0.12	-0.14 ± 0.06		
		5597.94	-2.99 ± 0.47	4778 ± 47	5.28 ± 0.13	-0.03 ± 0.05		
		6340.91	-4.28 ± 0.46	4797 ± 47	5.44 ± 0.13	0.01 ± 0.05		
		6341.92	-3.65 ± 0.48	4802 ± 49	5.27 ± 0.14	-0.15 ± 0.06		
168.391210	22.014251	5591.90	-34.68 ± 1.81	5159 ± 370	4.79 ± 0.59	-2.53 ± 0.40	1	N
168.395083	22.052944	4902.34	84.99 ± 0.93	4770 ± 209	1.21 ± 0.33	-1.44 ± 0.27	2	Y
		4212.78	83.43 ± 2.20	5508 ± 843	2.45 ± 1.20	-1.40 ± 0.83		
		5591.90	85.33 ± 1.03	4721 ± 216	1.10 ± 0.35	-1.44 ± 0.28		
168.407826	22.062301	4724.30	76.08 ± 1.25	5534 ± 246	3.39 ± 0.39	-0.95 ± 0.31	2	Y

Table E.1: Continued; Spectroscopic properties of stars in the direction of Leo II

α_{J2000}	δ_{J2000}	HJD	v	T_{eff}	$\log(g)$	[Fe/H]	N_{obs}	Mem
(deg)	(deg)	(-2450000 days)	(km s ⁻¹)	(K)	(dex)	(dex)		
		3850.66	76.95 ± 1.84	5690 ± 286	4.99 ± 0.52	-0.82 ± 0.37		
		5597.94	75.34 ± 1.70	5091 ± 483	1.36 ± 0.58	-1.23 ± 0.54		
168.376635	22.066142	5059.35	78.52 ± 0.94	4815 ± 207	1.29 ± 0.34	-1.21 ± 0.26	2	Y
		4526.81	78.57 ± 1.27	4812 ± 261	1.18 ± 0.41	-1.22 ± 0.34		
		5591.90	78.46 ± 1.41	4821 ± 339	1.52 ± 0.59	-1.19 ± 0.41		
168.521288	21.913347	5617.09	113.02 ± 0.21	5348 ± 24	5.00 ± 0.05	-0.50 ± 0.03	5	N
		4212.78	114.15 ± 0.47	5389 ± 58	5.14 ± 0.13	-0.59 ± 0.06		
		5591.90	107.67 ± 0.46	5392 ± 48	5.11 ± 0.10	-0.45 ± 0.06		
		5597.94	103.01 ± 0.48	5331 ± 61	4.98 ± 0.15	-0.39 ± 0.07		
		6340.91	116.94 ± 0.46	5308 ± 51	4.88 ± 0.11	-0.49 ± 0.06		
		6341.92	123.59 ± 0.48	5307 ± 60	4.85 ± 0.14	-0.59 ± 0.07		
168.559307	22.067029	6341.42	-22.54 ± 0.40	6005 ± 101	3.81 ± 0.15	-1.69 ± 0.09	2	N
		6340.91	-22.50 ± 0.54	6107 ± 132	4.04 ± 0.19	-1.63 ± 0.12		
		6341.92	-22.60 ± 0.60	5861 ± 157	3.41 ± 0.26	-1.80 ± 0.15		
168.576972	21.952827	6341.42	22.56 ± 0.33	5465 ± 42	4.69 ± 0.09	-0.89 ± 0.04	2	N
		6340.91	22.59 ± 0.46	5484 ± 58	4.73 ± 0.12	-0.90 ± 0.06		
		6341.92	22.53 ± 0.48	5442 ± 62	4.65 ± 0.13	-0.88 ± 0.07		
168.507724	22.052319	5591.90	129.11 ± 1.86	5026 ± 351	3.80 ± 1.06	-1.25 ± 0.40	1	N
168.614502	22.076345	5511.16	77.83 ± 0.67	4706 ± 88	4.41 ± 0.23	-1.73 ± 0.11	3	N
		3850.66	77.18 ± 1.47	4822 ± 265	3.44 ± 0.49	-2.24 ± 0.34		
		6340.91	76.96 ± 1.06	4517 ± 131	4.23 ± 0.38	-2.56 ± 0.16		
		6341.92	79.02 ± 1.05	4868 ± 132	5.07 ± 0.35	-0.66 ± 0.17		
168.206646	22.338805	5375.66	48.83 ± 0.20	4718 ± 21	5.12 ± 0.06	-0.32 ± 0.03	6	N
		3850.66	49.41 ± 0.50	4743 ± 51	4.85 ± 0.17	-0.47 ± 0.07		
		4522.71	48.52 ± 0.53	4844 ± 57	4.92 ± 0.20	-0.74 ± 0.07		
		5597.94	49.38 ± 0.47	4676 ± 49	5.07 ± 0.13	-0.31 ± 0.05		
		5599.80	48.77 ± 0.51	4620 ± 59	4.92 ± 0.18	-0.25 ± 0.07		
		6340.91	48.39 ± 0.46	4755 ± 44	5.41 ± 0.12	-0.11 ± 0.06		
		6341.92	48.54 ± 0.47	4663 ± 50	5.19 ± 0.13	-0.23 ± 0.06		
168.215025	22.350828	5341.85	7.81 ± 0.22	5943 ± 59	3.42 ± 0.12	-2.22 ± 0.06	8	N
		4212.78	8.72 ± 0.57	6129 ± 156	3.60 ± 0.28	-2.02 ± 0.14		
		4522.71	5.74 ± 1.08	6532 ± 368	4.05 ± 0.59	-2.04 ± 0.29		
		4526.81	7.02 ± 0.53	5898 ± 144	3.37 ± 0.37	-2.20 ± 0.15		
		5591.90	6.02 ± 0.50	5909 ± 109	3.35 ± 0.22	-2.23 ± 0.11		
		5597.94	7.07 ± 0.55	5806 ± 159	2.58 ± 0.41	-2.43 ± 0.16		
		5599.80	6.95 ± 0.94	5986 ± 359	4.10 ± 0.58	-2.22 ± 0.32		
		6340.91	10.05 ± 0.58	5918 ± 176	3.58 ± 0.33	-2.27 ± 0.17		

Table E.1: Continued; Spectroscopic properties of stars in the direction of Leo II

α_{J2000} (deg)	δ_{J2000} (deg)	HJD (-2450000 days)	v (km s ⁻¹)	T_{eff} (K)	$\log(g)$ (dex)	[Fe/H] (dex)	N_{obs}	Mem
		6341.92	10.40 ± 0.67	5896 ± 197	3.29 ± 0.40	-2.30 ± 0.19		
168.225234	22.298736	5374.34	76.58 ± 0.25	5875 ± 63	4.38 ± 0.09	-1.96 ± 0.06	6	N
		3850.66	76.87 ± 1.06	6242 ± 311	4.83 ± 0.41	-2.06 ± 0.25		
		4522.71	75.23 ± 1.18	6716 ± 327	5.14 ± 0.36	-1.72 ± 0.25		
		5591.90	76.06 ± 0.48	5737 ± 105	4.27 ± 0.14	-2.03 ± 0.10		
		5597.94	77.37 ± 0.54	5752 ± 142	4.29 ± 0.21	-2.11 ± 0.13		
		6340.91	76.44 ± 0.53	5861 ± 123	4.25 ± 0.17	-1.94 ± 0.12		
		6341.92	76.89 ± 0.63	6280 ± 229	4.64 ± 0.28	-1.58 ± 0.18		
168.264771	22.296952	5432.31	13.97 ± 0.38	5077 ± 45	4.94 ± 0.11	-0.56 ± 0.05	2	N
		4522.71	14.54 ± 0.66	5144 ± 107	4.61 ± 0.27	-1.34 ± 0.12		
		6341.92	13.68 ± 0.47	5062 ± 49	5.00 ± 0.12	-0.36 ± 0.06		
168.381129	22.316702	5181.40	27.99 ± 0.26	5422 ± 45	4.39 ± 0.08	-2.15 ± 0.05	5	N
		3850.66	28.72 ± 0.54	5786 ± 151	4.93 ± 0.22	-2.03 ± 0.14		
		4522.71	28.23 ± 0.66	5151 ± 138	3.78 ± 0.26	-2.40 ± 0.16		
		5591.90	27.38 ± 0.48	5413 ± 58	4.36 ± 0.11	-2.12 ± 0.06		
		5599.80	28.21 ± 0.74	5386 ± 207	4.10 ± 0.37	-2.18 ± 0.22		
		6341.92	27.74 ± 0.57	5452 ± 124	4.46 ± 0.19	-2.19 ± 0.13		
168.256153	22.389621	5515.11	-20.21 ± 0.38	4471 ± 47	4.91 ± 0.15	-0.46 ± 0.06	4	N
		4526.81	-19.38 ± 0.68	4407 ± 83	5.12 ± 0.30	-0.61 ± 0.12		
		5591.90	-20.72 ± 0.57	4508 ± 76	4.75 ± 0.22	-0.31 ± 0.09		
		5599.80	-18.62 ± 1.66	4467 ± 137	4.80 ± 0.59	-1.18 ± 0.35		
		6341.92	-20.89 ± 0.89	4515 ± 119	5.04 ± 0.35	-0.50 ± 0.15		
168.271675	22.319749	5167.33	-0.52 ± 0.25	4761 ± 25	5.20 ± 0.07	-0.18 ± 0.03	4	N
		4212.78	-0.80 ± 0.47	4785 ± 48	5.35 ± 0.14	0.07 ± 0.06		
		4522.71	-1.17 ± 0.65	4777 ± 62	4.50 ± 0.27	-1.41 ± 0.11		
		5591.90	-0.13 ± 0.46	4756 ± 44	5.29 ± 0.12	-0.02 ± 0.05		
		6341.92	-0.28 ± 0.48	4731 ± 51	5.05 ± 0.16	-0.23 ± 0.06		
168.476538	22.381918	5345.82	36.12 ± 0.25	5366 ± 31	4.88 ± 0.07	-0.86 ± 0.03	4	N
		3850.66	51.64 ± 0.49	5326 ± 58	4.82 ± 0.13	-1.13 ± 0.06		
		5591.90	34.31 ± 0.46	5269 ± 56	4.59 ± 0.13	-0.65 ± 0.06		
		5599.80	42.01 ± 0.57	5436 ± 84	4.96 ± 0.19	-0.76 ± 0.09		
		6340.91	19.20 ± 0.47	5488 ± 61	5.19 ± 0.13	-0.87 ± 0.07		
168.405048	22.289645	4906.29	-9.92 ± 0.35	4797 ± 36	5.15 ± 0.10	0.22 ± 0.05	2	N
		4212.78	-9.59 ± 0.47	4799 ± 48	5.23 ± 0.13	0.34 ± 0.06		
		5599.80	-10.32 ± 0.52	4795 ± 53	5.01 ± 0.16	0.05 ± 0.07		
168.431276	22.401918	5614.21	9.31 ± 0.23	4459 ± 30	5.35 ± 0.06	-0.77 ± 0.03	6	N
		4212.78	6.76 ± 0.53	4469 ± 71	5.55 ± 0.10	-0.57 ± 0.07		

Table E.1: Continued; Spectroscopic properties of stars in the direction of Leo II

α_{J2000}	δ_{J2000}	HJD	v	T_{eff}	$\log(g)$	[Fe/H]	N_{obs}	Mem
(deg)	(deg)	(-2450000 days)	(km s ⁻¹)	(K)	(dex)	(dex)		
		5591.90	6.47 ± 0.50	4435 ± 74	5.23 ± 0.15	-0.80 ± 0.06		
		5597.94	62.97 ± 1.01	5297 ± 332	2.44 ± 0.57	-2.00 ± 0.37		
		5599.80	6.77 ± 0.59	4378 ± 70	5.13 ± 0.23	-0.84 ± 0.09		
		6340.91	6.37 ± 0.49	4479 ± 62	5.39 ± 0.15	-0.78 ± 0.06		
		6341.92	5.95 ± 0.52	4488 ± 68	5.21 ± 0.18	-0.89 ± 0.08		
168.452489	22.289828	5591.90	280.15 ± 1.64	5008 ± 298	4.62 ± 0.66	-1.87 ± 0.38	1	N
168.468538	22.333068	4902.34	16.58 ± 0.49	4586 ± 63	4.41 ± 0.19	-0.38 ± 0.08	2	N
		4212.78	16.68 ± 0.94	4462 ± 138	4.36 ± 0.49	0.73 ± 0.23		
		5591.90	16.54 ± 0.58	4618 ± 70	4.42 ± 0.21	-0.55 ± 0.09		
168.583376	22.335966	5276.84	142.63 ± 1.34	4603 ± 159	4.20 ± 0.47	-0.02 ± 0.28	2	N
		4212.78	144.24 ± 1.80	4523 ± 170	3.96 ± 0.63	0.97 ± 0.34		
		6340.91	140.63 ± 2.01	5179 ± 457	4.52 ± 0.71	-2.22 ± 0.50		
168.582646	22.365862	5160.08	-10.86 ± 0.30	4328 ± 24	5.09 ± 0.10	-1.58 ± 0.04	4	N
		3850.66	-10.73 ± 0.58	4322 ± 46	4.96 ± 0.18	-1.73 ± 0.07		
		5591.90	-11.03 ± 0.57	4321 ± 46	5.23 ± 0.18	-1.39 ± 0.08		
		5597.94	-9.97 ± 0.59	4338 ± 53	5.12 ± 0.20	-1.55 ± 0.07		
		5599.80	-11.83 ± 0.63	4336 ± 52	5.03 ± 0.26	-1.62 ± 0.09		
168.599362	22.326965	5966.91	86.22 ± 0.91	4960 ± 134	4.83 ± 0.32	-1.61 ± 0.16	2	N
		5591.90	86.46 ± 1.52	5184 ± 179	5.02 ± 0.41	-1.48 ± 0.21		
		6341.92	86.09 ± 1.14	4672 ± 203	4.52 ± 0.52	-1.78 ± 0.23		
168.123920	22.146578	6341.42	115.81 ± 1.04	4565 ± 117	4.46 ± 0.44	-0.24 ± 0.27	2	N
		6340.91	118.64 ± 1.93	4583 ± 183	4.36 ± 0.84	-0.22 ± 0.64		
		6341.92	114.65 ± 1.24	4552 ± 153	4.49 ± 0.51	-0.24 ± 0.30		
168.107426	22.091015	5966.91	-93.73 ± 1.08	5166 ± 138	4.92 ± 0.33	-0.36 ± 0.22	2	N
		5591.90	-93.05 ± 1.32	5243 ± 157	5.06 ± 0.37	-0.52 ± 0.25		
		6341.92	-95.17 ± 1.91	4906 ± 288	4.40 ± 0.71	0.38 ± 0.52		
168.167794	22.056836	5055.38	-3.42 ± 0.19	5273 ± 22	5.15 ± 0.05	-0.15 ± 0.02	7	N
		3850.66	-3.50 ± 1.03	5013 ± 177	4.37 ± 0.57	1.36 ± 0.11		
		4212.78	-3.40 ± 0.48	5302 ± 56	5.19 ± 0.14	-0.07 ± 0.06		
		4522.71	-3.27 ± 0.64	5023 ± 88	4.15 ± 0.22	-1.48 ± 0.12		
		4526.81	-2.78 ± 0.47	5317 ± 51	5.27 ± 0.12	-0.08 ± 0.06		
		5591.90	-3.27 ± 0.46	5292 ± 49	5.21 ± 0.11	-0.19 ± 0.06		
		6340.91	-3.75 ± 0.47	5268 ± 50	5.13 ± 0.12	-0.25 ± 0.05		
		6341.92	-3.94 ± 0.46	5295 ± 49	5.31 ± 0.12	-0.22 ± 0.05		
168.178024	22.089599	6091.58	83.03 ± 0.46	4640 ± 83	1.03 ± 0.17	-1.66 ± 0.11	3	Y
		5591.90	83.09 ± 0.67	4703 ± 131	0.98 ± 0.27	-1.65 ± 0.18		
		6340.91	82.95 ± 1.03	4463 ± 132	0.97 ± 0.26	-1.80 ± 0.19		

Table E.1: Continued; Spectroscopic properties of stars in the direction of Leo II

α_{J2000}	δ_{J2000}	HJD	v	T_{eff}	$\log(g)$	[Fe/H]	N_{obs}	Mem
(deg)	(deg)	(-2450000 days)	(km s ⁻¹)	(K)	(dex)	(dex)		
		6341.92	82.98 ± 0.83	4860 ± 186	1.27 ± 0.40	-1.44 ± 0.25		
168.227179	22.103762	6093.59	63.81 ± 1.15	4764 ± 233	1.54 ± 0.40	-2.77 ± 0.25	3	Y
		5597.94	58.85 ± 2.91	4654 ± 313	1.27 ± 0.52	-2.92 ± 0.34		
		6340.91	65.52 ± 1.72	5225 ± 793	1.88 ± 0.92	-2.02 ± 0.69		
		6341.92	63.85 ± 1.84	4822 ± 391	1.94 ± 0.83	-2.82 ± 0.44		
168.240740	22.180602	5701.90	78.41 ± 0.59	4846 ± 123	1.17 ± 0.18	-1.45 ± 0.16	4	Y
		4526.81	77.78 ± 1.47	4650 ± 229	1.64 ± 0.48	-1.85 ± 0.31		
		5597.94	80.23 ± 1.25	5111 ± 307	1.71 ± 0.64	-1.73 ± 0.34		
		6340.91	78.10 ± 1.16	5072 ± 251	0.88 ± 0.22	-0.29 ± 0.34		
		6341.92	77.77 ± 0.99	4711 ± 223	1.81 ± 0.51	-1.80 ± 0.30		
168.264708	22.192902	5265.07	49.82 ± 0.33	4493 ± 38	4.84 ± 0.13	0.01 ± 0.05	4	N
		3850.66	51.04 ± 1.53	4462 ± 130	4.75 ± 0.49	0.73 ± 0.30		
		4526.81	50.59 ± 0.64	4369 ± 66	4.71 ± 0.22	0.21 ± 0.11		
		6340.91	49.22 ± 0.57	4443 ± 76	4.64 ± 0.24	0.06 ± 0.10		
		6341.92	49.65 ± 0.57	4672 ± 68	5.15 ± 0.22	-0.20 ± 0.08		
168.273713	22.118336	5062.37	91.30 ± 0.86	5176 ± 215	0.97 ± 0.22	0.08 ± 0.27	2	Y
		4526.81	97.85 ± 1.07	5158 ± 239	0.89 ± 0.23	0.52 ± 0.31		
		5597.94	79.08 ± 1.46	5250 ± 492	1.94 ± 0.78	-1.50 ± 0.58		
168.281640	22.158394	5597.94	70.10 ± 1.09	5200 ± 445	1.86 ± 0.73	-1.11 ± 0.52	1	Y
168.303913	22.135978	5486.54	83.02 ± 0.60	4923 ± 128	1.24 ± 0.26	-1.12 ± 0.17	3	Y
		4526.81	84.61 ± 2.23	5289 ± 607	1.90 ± 0.96	0.28 ± 0.62		
		5591.90	82.83 ± 0.75	4833 ± 152	1.15 ± 0.33	-1.43 ± 0.20		
		6340.91	83.03 ± 1.10	5118 ± 261	1.28 ± 0.49	-0.67 ± 0.33		
168.304767	22.131270	5597.94	79.65 ± 0.68	4684 ± 122	1.10 ± 0.33	-1.46 ± 0.16	1	Y
168.298067	22.190933	6341.42	74.96 ± 0.79	4531 ± 126	1.07 ± 0.24	-1.63 ± 0.17	2	Y
		6340.91	77.77 ± 2.09	5042 ± 369	1.00 ± 0.33	0.26 ± 0.48		
		6341.92	74.50 ± 0.85	4463 ± 135	1.13 ± 0.34	-1.90 ± 0.18		
168.303779	22.154937	5598.87	75.01 ± 0.67	4656 ± 119	1.12 ± 0.22	-1.31 ± 0.16	2	Y
		5597.94	75.20 ± 0.79	4674 ± 146	1.30 ± 0.33	-1.57 ± 0.19		
		5599.80	74.50 ± 1.29	4621 ± 204	0.97 ± 0.30	-0.75 ± 0.29		
168.171762	22.201726	5434.36	2.35 ± 1.40	4523 ± 132	3.09 ± 0.57	0.39 ± 0.30	2	N
		4526.81	2.92 ± 1.91	4589 ± 226	2.65 ± 0.86	0.89 ± 0.41		
		6341.92	1.69 ± 2.06	4488 ± 163	3.43 ± 0.77	-0.18 ± 0.44		
168.261342	22.120660	6341.92	75.44 ± 1.20	5937 ± 715	2.29 ± 1.02	-0.09 ± 0.72	1	Y
168.265818	22.096370	4526.81	70.11 ± 2.43	4802 ± 386	1.22 ± 0.53	-1.02 ± 0.53	1	Y
168.272724	22.115792	5591.90	65.50 ± 1.22	4989 ± 411	1.62 ± 0.62	-1.52 ± 0.51	1	Y
168.276658	22.201502	6341.42	74.15 ± 1.24	4962 ± 295	1.73 ± 0.56	-1.52 ± 0.34	2	Y

Table E.1: Continued; Spectroscopic properties of stars in the direction of Leo II

α_{J2000}	δ_{J2000}	HJD	v	T_{eff}	$\log(g)$	[Fe/H]	N_{obs}	Mem
(deg)	(deg)	(-2450000 days)	(km s ⁻¹)	(K)	(dex)	(dex)		
		6340.91	73.18 ± 2.06	5466 ± 668	1.63 ± 0.85	-0.59 ± 0.67		
		6341.92	74.70 ± 1.55	4839 ± 329	1.80 ± 0.74	-1.85 ± 0.40		
168.307310	22.071999	6341.92	77.97 ± 1.29	4764 ± 285	1.52 ± 0.51	-2.48 ± 0.34	1	Y
168.265289	22.139937	5591.90	84.51 ± 2.42	5799 ± 975	2.08 ± 1.08	-0.82 ± 0.94	1	Y
168.279338	22.157528	6341.92	77.14 ± 1.71	5145 ± 449	1.66 ± 0.78	-1.41 ± 0.51	1	Y
168.292953	22.151511	5591.90	71.45 ± 1.67	5168 ± 532	1.83 ± 0.77	-1.94 ± 0.59	1	Y
168.365346	22.170285	3850.66	83.43 ± 1.43	4732 ± 218	2.17 ± 0.57	-2.51 ± 0.26	1	Y
168.336710	22.142885	4212.78	75.73 ± 0.87	4581 ± 146	0.79 ± 0.16	-0.72 ± 0.19	1	Y
168.383543	22.149615	3850.66	70.98 ± 0.86	4655 ± 155	1.62 ± 0.38	-1.73 ± 0.20	1	Y
168.365372	22.177712	4212.78	80.39 ± 0.73	4602 ± 138	0.84 ± 0.19	-0.83 ± 0.18	1	Y
168.372743	22.163738	4212.78	85.57 ± 0.77	4754 ± 148	1.38 ± 0.35	-1.20 ± 0.20	1	Y
168.380019	22.140152	4212.78	69.81 ± 0.99	4429 ± 106	1.67 ± 0.33	-2.18 ± 0.15	1	Y
168.373341	22.149361	4526.81	82.94 ± 1.39	4749 ± 225	1.75 ± 0.61	-1.74 ± 0.30	1	Y
168.369883	22.146404	5591.90	87.07 ± 0.59	4514 ± 107	0.78 ± 0.15	-1.47 ± 0.12	1	Y
168.379041	22.145726	5966.41	80.30 ± 0.48	4621 ± 87	0.99 ± 0.18	-1.58 ± 0.10	2	Y
		5591.90	80.16 ± 0.66	4594 ± 120	0.97 ± 0.22	-1.44 ± 0.14		
		6340.91	80.44 ± 0.68	4652 ± 127	1.03 ± 0.28	-1.75 ± 0.16		
168.383842	22.153266	6341.92	82.17 ± 0.78	5124 ± 176	1.45 ± 0.43	-1.27 ± 0.22	1	Y
168.383543	22.153729	5970.36	60.99 ± 0.74	4644 ± 129	1.72 ± 0.39	-1.37 ± 0.20	2	Y
		5599.80	60.06 ± 1.76	4494 ± 164	1.70 ± 0.51	-0.96 ± 0.29		
		6340.91	61.19 ± 0.82	4894 ± 212	1.74 ± 0.60	-1.75 ± 0.28		
168.424703	22.093107	3850.66	70.57 ± 1.09	4835 ± 280	2.32 ± 0.51	-2.17 ± 0.36	1	Y
168.408103	22.252007	4212.78	-28.20 ± 0.46	4935 ± 50	5.23 ± 0.11	-0.60 ± 0.06	1	N
168.418470	22.205108	5014.12	81.39 ± 0.48	4625 ± 72	1.18 ± 0.18	-1.88 ± 0.08	3	Y
		3850.66	81.84 ± 1.38	4821 ± 396	2.71 ± 0.63	-3.35 ± 0.43		
		5591.90	81.19 ± 0.54	4595 ± 75	0.93 ± 0.20	-1.85 ± 0.09		
		5599.80	82.41 ± 1.50	5342 ± 416	2.59 ± 0.69	-0.98 ± 0.50		
168.422588	22.208965	5276.84	59.04 ± 0.33	5358 ± 38	4.49 ± 0.09	-0.43 ± 0.04	2	N
		4212.78	56.44 ± 0.47	5375 ± 55	4.52 ± 0.12	-0.33 ± 0.06		
		6340.91	61.61 ± 0.47	5341 ± 54	4.46 ± 0.13	-0.52 ± 0.06		
168.307823	22.147241	4212.78	67.04 ± 0.94	4406 ± 90	0.80 ± 0.16	-1.82 ± 0.12	1	Y
168.324119	22.151826	6340.91	78.71 ± 0.69	4562 ± 128	0.77 ± 0.14	-1.13 ± 0.16	1	Y
168.314674	22.150231	4526.81	79.39 ± 1.16	5044 ± 207	0.97 ± 0.29	-0.13 ± 0.29	1	Y
168.315467	22.151526	6341.92	68.67 ± 1.25	4905 ± 384	2.86 ± 0.76	-1.88 ± 0.43	1	Y
168.320595	22.100961	4526.81	80.78 ± 1.22	5088 ± 283	1.22 ± 0.45	-0.45 ± 0.39	1	Y
168.326167	22.112404	5591.90	78.56 ± 0.64	4752 ± 116	0.73 ± 0.12	-0.79 ± 0.15	1	Y
168.332535	22.096383	4212.78	76.73 ± 1.25	4826 ± 220	1.48 ± 0.57	-0.79 ± 0.31	1	Y

Table E.1: Continued; Spectroscopic properties of stars in the direction of Leo II

α_{J2000}	δ_{J2000}	HJD	v	T_{eff}	$\log(g)$	[Fe/H]	N_{obs}	Mem
(deg)	(deg)	(-2450000 days)	(km s ⁻¹)	(K)	(dex)	(dex)		
168.333801	22.101774	5969.43	71.84 ± 0.79	4763 ± 173	1.09 ± 0.25	-1.09 ± 0.23	2	Y
		5597.94	71.95 ± 1.23	4680 ± 254	0.99 ± 0.29	-1.42 ± 0.33		
		6340.91	71.76 ± 1.02	4835 ± 236	1.37 ± 0.49	-0.76 ± 0.33		
168.323001	22.202270	5591.90	75.59 ± 0.67	4424 ± 94	1.02 ± 0.23	-2.03 ± 0.11	1	Y
168.332447	22.155648	4526.81	84.45 ± 0.81	4434 ± 109	1.00 ± 0.27	-1.11 ± 0.16	1	Y
168.332647	22.162751	4212.78	71.84 ± 0.78	4811 ± 104	0.76 ± 0.14	-0.07 ± 0.14	1	Y
168.335991	22.159365	6340.91	79.97 ± 1.43	4776 ± 295	1.40 ± 0.49	-1.89 ± 0.36	1	Y
168.339449	22.087781	5599.80	75.56 ± 1.98	4831 ± 290	1.16 ± 0.40	-0.33 ± 0.39	1	Y
168.335836	22.120783	4212.78	71.28 ± 1.07	5250 ± 281	1.55 ± 0.58	-1.44 ± 0.32	1	Y
168.341818	22.074613	5969.93	97.24 ± 0.76	4537 ± 125	1.26 ± 0.30	-2.34 ± 0.17	2	Y
		5597.94	97.86 ± 1.19	4618 ± 208	1.45 ± 0.52	-1.90 ± 0.29		
		6341.92	96.81 ± 0.99	4490 ± 157	1.16 ± 0.37	-2.55 ± 0.21		
168.343937	22.125318	5966.41	68.31 ± 0.71	4795 ± 176	1.52 ± 0.33	-2.01 ± 0.21	2	Y
		5591.90	67.72 ± 0.85	4745 ± 217	1.61 ± 0.44	-2.01 ± 0.27		
		6340.91	69.69 ± 1.31	4892 ± 300	1.40 ± 0.50	-2.01 ± 0.34		
168.344921	22.098423	4526.81	64.82 ± 0.75	4651 ± 144	0.93 ± 0.24	-1.94 ± 0.18	1	Y
168.349274	22.082756	5434.36	82.94 ± 0.90	5150 ± 305	1.50 ± 0.35	-1.07 ± 0.33	2	Y
		4526.81	84.56 ± 1.26	4927 ± 365	1.14 ± 0.40	-0.84 ± 0.43		
		6341.92	81.29 ± 1.27	5666 ± 554	2.67 ± 0.73	-1.42 ± 0.54		
168.347091	22.089747	5969.43	66.72 ± 0.90	4609 ± 152	0.97 ± 0.20	-1.53 ± 0.19	2	Y
		5597.94	69.80 ± 1.72	4644 ± 274	1.17 ± 0.41	-1.30 ± 0.36		
		6340.91	65.56 ± 1.05	4593 ± 182	0.91 ± 0.24	-1.63 ± 0.23		
168.336875	22.191882	5599.80	73.71 ± 1.30	4591 ± 213	1.17 ± 0.41	-1.16 ± 0.33	1	Y
168.339014	22.177162	4212.78	61.23 ± 0.99	4594 ± 157	0.79 ± 0.15	-0.94 ± 0.21	1	Y
168.351373	22.092882	5591.90	74.77 ± 0.77	4454 ± 116	0.96 ± 0.24	-1.92 ± 0.14	1	Y
168.347429	22.148418	4522.71	84.91 ± 1.76	6834 ± 511	4.67 ± 0.56	-1.23 ± 0.35	1	N
168.342671	22.148342	4526.81	94.94 ± 0.70	4437 ± 104	1.19 ± 0.28	-1.75 ± 0.13	1	Y
168.345948	22.172960	5059.35	86.13 ± 0.44	4498 ± 75	0.87 ± 0.14	-1.34 ± 0.09	2	Y
		4526.81	86.29 ± 0.75	4463 ± 118	1.04 ± 0.27	-1.38 ± 0.15		
		5591.90	86.04 ± 0.54	4523 ± 98	0.80 ± 0.16	-1.31 ± 0.11		
168.353465	22.154679	5591.90	71.94 ± 0.59	5018 ± 119	0.71 ± 0.10	-0.87 ± 0.17	1	Y
168.348635	22.153514	5597.94	62.13 ± 1.15	5016 ± 301	1.59 ± 0.55	-1.54 ± 0.37	1	Y
168.346721	22.163973	5591.90	75.71 ± 0.59	4591 ± 113	1.03 ± 0.23	-1.62 ± 0.13	1	Y
168.347707	22.147494	6341.92	61.64 ± 1.08	5011 ± 272	2.04 ± 0.64	-1.75 ± 0.35	1	Y
168.347566	22.121425	4212.78	80.15 ± 0.66	4513 ± 125	1.07 ± 0.26	-1.49 ± 0.14	1	Y
168.348467	22.118636	5591.90	81.19 ± 0.62	4763 ± 112	1.02 ± 0.25	-1.25 ± 0.14	1	Y
168.351946	22.103707	4212.78	78.67 ± 0.72	4636 ± 144	1.66 ± 0.30	-2.05 ± 0.18	1	Y

Table E.1: Continued; Spectroscopic properties of stars in the direction of Leo II

α_{J2000}	δ_{J2000}	HJD	v	T_{eff}	$\log(g)$	[Fe/H]	N_{obs}	Mem
(deg)	(deg)	(-2450000 days)	(km s ⁻¹)	(K)	(dex)	(dex)		
168.350775	22.104231	5969.93	93.59 ± 0.66	5087 ± 169	1.77 ± 0.39	-1.41 ± 0.21	2	Y
		5597.94	92.50 ± 0.91	5103 ± 265	1.71 ± 0.52	-1.46 ± 0.31		
		6341.92	94.80 ± 0.96	5076 ± 220	1.85 ± 0.59	-1.37 ± 0.28		
168.341306	22.201801	3850.66	72.50 ± 2.00	6660 ± 770	2.35 ± 1.00	-1.95 ± 0.54	1	Y
168.349861	22.141484	4212.78	80.92 ± 1.06	5062 ± 212	0.79 ± 0.16	0.20 ± 0.26	1	Y
168.350324	22.159308	6340.91	89.74 ± 0.97	4575 ± 183	1.17 ± 0.36	-1.75 ± 0.25	1	Y
168.356523	22.128904	4212.78	80.16 ± 1.23	4970 ± 252	1.60 ± 0.57	-1.44 ± 0.34	1	Y
168.360670	22.123947	3850.66	85.07 ± 1.30	5603 ± 280	4.72 ± 0.57	-0.73 ± 0.31	1	N
168.354593	22.209850	4212.78	83.62 ± 2.57	5073 ± 360	1.12 ± 0.42	0.68 ± 0.36	1	Y
168.356646	22.203513	5591.90	83.64 ± 1.42	5851 ± 508	4.00 ± 0.64	-1.08 ± 0.50	1	Y
168.360468	22.185403	4212.78	83.41 ± 0.75	4829 ± 147	0.87 ± 0.20	-0.83 ± 0.19	1	Y
168.356143	22.223920	5095.78	91.24 ± 0.58	4556 ± 111	0.94 ± 0.18	-2.15 ± 0.13	2	Y
		3850.66	91.57 ± 0.87	4557 ± 202	1.35 ± 0.50	-3.12 ± 0.23		
		6340.91	90.98 ± 0.78	4555 ± 133	0.87 ± 0.20	-1.70 ± 0.16		
168.373208	22.121111	4526.81	83.59 ± 0.86	4506 ± 136	0.86 ± 0.20	-1.40 ± 0.17	1	Y
168.380500	22.073602	4212.78	85.01 ± 0.80	4902 ± 147	1.03 ± 0.29	-1.54 ± 0.19	1	Y
168.376071	22.115956	4212.78	87.15 ± 1.29	4787 ± 273	1.78 ± 0.54	-2.54 ± 0.34	1	Y
168.379537	22.108393	3850.66	86.23 ± 0.77	4538 ± 128	1.04 ± 0.27	-1.30 ± 0.15	1	Y
168.378516	22.136512	3850.66	100.72 ± 2.00	4876 ± 225	1.58 ± 0.78	0.13 ± 0.33	1	N
168.376682	22.134689	5434.36	59.51 ± 0.73	5421 ± 226	2.17 ± 0.42	-1.34 ± 0.24	2	Y
		4526.81	63.77 ± 1.35	5287 ± 449	1.79 ± 0.80	-1.63 ± 0.46		
		6341.92	57.71 ± 0.88	5467 ± 262	2.32 ± 0.50	-1.23 ± 0.29		
168.376933	22.137381	6340.91	79.23 ± 1.52	5206 ± 472	1.65 ± 0.71	-1.45 ± 0.54	1	Y
168.394371	22.138740	6340.91	84.65 ± 1.85	7317 ± 664	4.00 ± 0.74	-0.86 ± 0.50	1	Y
168.393857	22.134419	5591.90	68.95 ± 1.80	4889 ± 449	2.66 ± 1.04	-1.62 ± 0.56	1	Y
168.372524	22.175408	5591.90	89.24 ± 0.82	4771 ± 173	1.17 ± 0.35	-1.16 ± 0.24	1	Y
168.369798	22.219940	3850.66	72.61 ± 1.36	5917 ± 372	4.29 ± 0.62	-1.88 ± 0.30	1	N
168.379188	22.189434	4212.78	74.23 ± 0.80	4920 ± 170	1.34 ± 0.40	-0.90 ± 0.23	1	Y
168.373550	22.188914	5966.41	77.71 ± 0.61	4832 ± 123	1.14 ± 0.25	-1.40 ± 0.16	2	Y
		5591.90	78.36 ± 0.71	4836 ± 133	1.04 ± 0.29	-1.30 ± 0.17		
		6340.91	75.75 ± 1.23	4814 ± 311	1.47 ± 0.55	-1.91 ± 0.38		
168.374080	22.188551	6341.92	82.71 ± 1.54	5268 ± 332	1.42 ± 0.57	-1.26 ± 0.37	1	Y
168.383560	22.124923	3850.66	79.41 ± 0.66	4415 ± 88	0.81 ± 0.16	-1.04 ± 0.11	1	Y
168.381927	22.129646	4212.78	69.32 ± 1.16	6147 ± 497	3.07 ± 0.56	-1.21 ± 0.40	1	Y
168.383300	22.127610	6340.91	76.90 ± 1.85	4610 ± 214	2.15 ± 0.56	-2.36 ± 0.28	1	Y
168.378052	22.180874	3850.66	78.52 ± 1.29	5021 ± 230	2.78 ± 0.45	-2.21 ± 0.27	1	Y
168.380113	22.184423	6340.91	73.65 ± 1.46	4993 ± 427	2.92 ± 0.99	-2.42 ± 0.46	1	Y

Table E.1: Continued; Spectroscopic properties of stars in the direction of Leo II

α_{J2000}	δ_{J2000}	HJD	v	T_{eff}	$\log(g)$	[Fe/H]	N_{obs}	Mem
(deg)	(deg)	(-2450000 days)	(km s ⁻¹)	(K)	(dex)	(dex)		
168.386005	22.117952	4212.78	75.25 ± 0.77	4830 ± 195	1.65 ± 0.45	-2.03 ± 0.25	1	Y
168.381981	22.162453	4212.78	81.40 ± 1.97	4685 ± 242	2.74 ± 0.67	-1.13 ± 0.35	1	Y
168.391124	22.102234	5095.78	80.08 ± 0.46	4493 ± 77	0.84 ± 0.13	-1.46 ± 0.09	2	Y
		3850.66	79.76 ± 0.68	4566 ± 130	0.83 ± 0.18	-0.95 ± 0.16		
		6340.91	80.33 ± 0.61	4454 ± 96	0.85 ± 0.17	-1.68 ± 0.10		
168.392378	22.108066	6341.92	74.08 ± 1.04	4912 ± 168	1.22 ± 0.40	-1.54 ± 0.21	1	Y
168.397612	22.080946	4212.78	72.02 ± 1.55	5125 ± 439	2.66 ± 0.72	-2.24 ± 0.51	1	Y
168.387447	22.163132	5591.90	81.77 ± 0.66	4840 ± 131	1.63 ± 0.35	-1.60 ± 0.18	1	Y
168.382364	22.237312	5095.78	87.17 ± 0.49	4794 ± 96	1.09 ± 0.15	-1.33 ± 0.11	2	Y
		3850.66	89.67 ± 0.78	5525 ± 228	3.06 ± 0.43	-1.80 ± 0.22		
		6340.91	85.57 ± 0.62	4636 ± 106	0.80 ± 0.16	-1.17 ± 0.13		
168.394768	22.161791	3850.66	89.38 ± 0.84	5074 ± 210	1.96 ± 0.36	-1.64 ± 0.28	1	Y
168.404620	22.159210	5059.35	77.42 ± 0.60	4583 ± 108	0.90 ± 0.18	-2.23 ± 0.12	2	Y
		4526.81	101.16 ± 1.50	5267 ± 471	2.51 ± 1.00	-2.37 ± 0.48		
		5591.90	72.92 ± 0.65	4545 ± 110	0.85 ± 0.18	-2.22 ± 0.12		
168.401499	22.156571	3850.66	72.61 ± 0.95	4641 ± 169	1.24 ± 0.35	-1.84 ± 0.21	1	Y
168.390860	22.167593	5433.86	88.81 ± 0.88	5341 ± 261	2.78 ± 0.52	-1.72 ± 0.28	2	Y
		4526.81	86.52 ± 1.50	5638 ± 953	2.60 ± 1.14	-1.27 ± 0.88		
		6340.91	90.02 ± 1.09	5317 ± 271	2.83 ± 0.59	-1.77 ± 0.30		
168.390259	22.177559	6340.91	88.12 ± 1.31	5928 ± 508	3.98 ± 0.72	-1.10 ± 0.44	1	Y
168.399008	22.143442	4212.78	72.68 ± 1.10	5294 ± 413	2.59 ± 0.70	-2.13 ± 0.45	1	Y
168.393524	22.195150	4725.23	83.28 ± 0.72	4888 ± 157	2.04 ± 0.33	-1.84 ± 0.21	2	Y
		3850.66	83.52 ± 0.88	4812 ± 175	2.16 ± 0.37	-2.07 ± 0.23		
		5599.80	82.79 ± 1.25	5197 ± 353	1.59 ± 0.73	-0.85 ± 0.48		
168.404546	22.118717	5276.84	69.71 ± 0.52	4621 ± 98	1.05 ± 0.20	-1.46 ± 0.12	2	Y
		4212.78	69.60 ± 0.85	4783 ± 173	1.60 ± 0.46	-1.97 ± 0.22		
		6340.91	69.78 ± 0.67	4544 ± 119	0.92 ± 0.22	-1.25 ± 0.14		
168.395942	22.192990	6340.91	88.24 ± 1.65	4882 ± 384	3.07 ± 0.96	-2.69 ± 0.40	1	Y
168.394219	22.247911	5591.90	73.85 ± 0.69	4684 ± 134	1.38 ± 0.36	-1.64 ± 0.17	1	Y
168.400093	22.205788	5277.35	83.34 ± 0.56	4834 ± 122	1.46 ± 0.29	-1.19 ± 0.17	2	Y
		4212.78	84.02 ± 0.82	4721 ± 194	1.13 ± 0.39	-0.82 ± 0.28		
		6341.92	82.78 ± 0.75	4907 ± 157	1.91 ± 0.45	-1.43 ± 0.22		
168.410476	22.163128	5591.90	76.27 ± 0.65	4917 ± 103	1.11 ± 0.30	-1.47 ± 0.14	1	Y
168.413001	22.164606	6340.91	96.26 ± 1.85	6728 ± 944	2.76 ± 1.10	-1.12 ± 0.63	1	Y
168.408419	22.188178	4212.78	68.92 ± 0.99	4862 ± 242	1.30 ± 0.42	-0.95 ± 0.33	1	Y
168.414429	22.154657	4212.78	82.94 ± 0.69	4515 ± 131	1.25 ± 0.30	-1.63 ± 0.16	1	Y
168.413035	22.155662	5433.86	80.19 ± 1.29	5426 ± 477	2.12 ± 0.68	-1.87 ± 0.44	2	Y

Table E.1: Continued; Spectroscopic properties of stars in the direction of Leo II

α_{J2000}	δ_{J2000}	HJD	v	T_{eff}	$\log(g)$	[Fe/H]	N_{obs}	Mem
(deg)	(deg)	(-2450000 days)	(km s ⁻¹)	(K)	(dex)	(dex)		
		4526.81	81.62 ± 1.60	5124 ± 593	1.82 ± 0.85	-1.88 ± 0.59		
		6340.91	77.55 ± 2.17	5977 ± 802	2.65 ± 1.14	-1.86 ± 0.65		
168.421817	22.128119	3850.66	73.78 ± 0.94	4700 ± 156	0.89 ± 0.23	-0.58 ± 0.24	1	Y
168.423364	22.127127	4526.81	79.22 ± 1.51	4706 ± 256	1.71 ± 0.63	-1.94 ± 0.33	1	Y
168.427980	22.124331	5594.92	77.44 ± 0.58	4669 ± 105	1.00 ± 0.21	-2.15 ± 0.13	2	Y
		5591.90	77.15 ± 0.67	4630 ± 114	0.92 ± 0.22	-2.12 ± 0.14		
		5597.94	78.38 ± 1.18	4872 ± 260	1.51 ± 0.59	-2.30 ± 0.32		
168.316018	22.080891	6341.92	83.28 ± 1.92	6148 ± 780	3.91 ± 1.08	-1.36 ± 0.72	1	Y
168.316861	22.115910	5591.90	87.52 ± 1.33	4854 ± 381	1.26 ± 0.47	-2.17 ± 0.41	1	Y
168.300912	22.269158	5591.90	83.24 ± 1.44	4512 ± 187	1.42 ± 0.58	-2.07 ± 0.27	1	Y
168.316177	22.169413	5591.90	49.99 ± 1.35	4691 ± 235	1.07 ± 0.34	-1.63 ± 0.29	1	N
168.329372	22.112509	6341.92	76.94 ± 1.36	5122 ± 273	1.11 ± 0.39	-1.76 ± 0.30	1	Y
168.328423	22.187452	5591.90	66.48 ± 1.16	4575 ± 192	1.15 ± 0.36	-2.28 ± 0.25	1	Y
168.347533	22.093999	6341.92	82.29 ± 1.44	4628 ± 247	1.32 ± 0.52	-2.34 ± 0.31	1	Y
168.341596	22.192213	5966.91	84.18 ± 0.83	4726 ± 171	1.28 ± 0.32	-1.70 ± 0.21	2	Y
		5591.90	84.67 ± 0.98	4647 ± 195	1.28 ± 0.42	-1.61 ± 0.25		
		6341.92	82.87 ± 1.61	4984 ± 353	1.28 ± 0.49	-1.91 ± 0.39		
168.358687	22.113342	6340.91	83.51 ± 0.92	4647 ± 184	0.85 ± 0.21	-1.22 ± 0.24	1	Y
168.347123	22.221428	5966.91	72.28 ± 0.94	4623 ± 173	1.19 ± 0.32	-1.81 ± 0.20	2	Y
		5591.90	72.53 ± 1.05	4572 ± 180	1.11 ± 0.36	-1.80 ± 0.22		
		6341.92	71.27 ± 2.10	5189 ± 601	1.50 ± 0.68	-1.89 ± 0.50		
168.363610	22.118247	4212.78	83.72 ± 1.47	5187 ± 484	1.97 ± 0.71	-2.13 ± 0.51	1	Y
168.365603	22.129396	4526.81	70.03 ± 1.30	5019 ± 247	0.92 ± 0.27	-0.94 ± 0.33	1	Y
168.366421	22.123087	5966.41	78.51 ± 0.69	4788 ± 146	1.02 ± 0.22	-1.35 ± 0.17	2	Y
		5591.90	78.20 ± 0.86	4734 ± 194	1.17 ± 0.37	-1.15 ± 0.23		
		6340.91	79.04 ± 1.14	4859 ± 221	0.94 ± 0.27	-1.61 ± 0.27		
168.369941	22.186285	5597.94	86.10 ± 2.38	6325 ± 746	3.52 ± 0.99	-1.35 ± 0.57	1	Y
168.364535	22.228195	5591.90	84.69 ± 1.01	4531 ± 174	1.32 ± 0.41	-2.28 ± 0.22	1	Y
168.382802	22.082248	6341.42	87.97 ± 1.03	4653 ± 205	1.86 ± 0.51	-2.13 ± 0.26	2	Y
		6340.91	88.56 ± 1.42	4595 ± 229	2.11 ± 0.73	-2.11 ± 0.31		
		6341.92	87.30 ± 1.49	4884 ± 457	1.61 ± 0.72	-2.16 ± 0.47		
168.369268	22.201402	5591.90	59.67 ± 2.00	5017 ± 312	1.14 ± 0.48	-1.74 ± 0.39	1	Y
168.384699	22.115485	5591.90	69.71 ± 1.12	4617 ± 192	1.10 ± 0.36	-1.33 ± 0.26	1	Y
168.377773	22.205481	5591.90	72.17 ± 1.25	5267 ± 485	2.12 ± 0.78	-1.03 ± 0.57	1	Y
168.395187	22.104883	5059.35	75.51 ± 0.62	4655 ± 131	0.98 ± 0.21	-1.25 ± 0.17	2	Y
		4526.81	75.58 ± 1.15	4636 ± 244	1.17 ± 0.44	-1.28 ± 0.35		
		5591.90	75.48 ± 0.74	4663 ± 156	0.93 ± 0.24	-1.24 ± 0.19		

Table E.1: Continued; Spectroscopic properties of stars in the direction of Leo II

α_{J2000}	δ_{J2000}	HJD	v	T_{eff}	$\log(g)$	[Fe/H]	N_{obs}	Mem
(deg)	(deg)	(-2450000 days)	(km s ⁻¹)	(K)	(dex)	(dex)		
168.394005	22.114571	6341.92	69.47 ± 1.52	5259 ± 490	2.15 ± 0.90	-1.99 ± 0.50	1	Y
168.398312	22.131495	6341.92	73.05 ± 1.78	5343 ± 388	1.88 ± 0.81	-1.78 ± 0.39	1	Y
168.394658	22.183880	5966.91	85.38 ± 0.61	4828 ± 128	1.15 ± 0.26	-1.48 ± 0.17	2	Y
		5591.90	86.01 ± 0.73	4785 ± 147	1.06 ± 0.30	-1.37 ± 0.20		
		6341.92	83.87 ± 1.12	4966 ± 263	1.43 ± 0.53	-1.79 ± 0.33		
168.407727	22.077355	4212.78	85.06 ± 1.43	5421 ± 614	2.37 ± 0.95	-1.72 ± 0.60	1	Y
168.406514	22.078363	5591.90	77.27 ± 1.34	4624 ± 238	1.37 ± 0.55	-1.98 ± 0.31	1	Y
168.409612	22.152349	5597.94	75.81 ± 1.93	5935 ± 814	2.40 ± 1.19	-1.61 ± 0.65	1	Y
168.401758	22.168451	5591.90	88.15 ± 1.21	4952 ± 260	2.49 ± 0.57	-1.90 ± 0.33	1	Y
168.407867	22.136993	5591.90	85.27 ± 0.89	4569 ± 166	1.01 ± 0.28	-1.99 ± 0.21	1	Y
168.417672	22.108010	4526.81	74.40 ± 2.30	4966 ± 506	1.57 ± 0.81	-1.52 ± 0.55	1	Y
168.417680	22.178869	4212.78	65.59 ± 0.96	4597 ± 202	1.56 ± 0.50	-1.61 ± 0.29	1	Y
168.423418	22.147864	5597.94	72.66 ± 1.52	5401 ± 509	4.77 ± 0.74	-1.90 ± 0.60	1	N
168.429763	22.132577	5591.90	83.86 ± 0.99	5185 ± 254	1.55 ± 0.59	-1.35 ± 0.31	1	Y
168.426824	22.180893	5591.90	72.15 ± 1.06	5566 ± 497	2.36 ± 0.80	-0.82 ± 0.53	1	Y
168.428609	22.232123	4212.78	89.71 ± 1.75	4846 ± 379	1.83 ± 0.83	-0.86 ± 0.52	1	Y
168.428379	22.235459	5062.37	86.20 ± 1.09	4738 ± 182	1.53 ± 0.43	-2.45 ± 0.22	2	Y
		4526.81	86.45 ± 1.64	4671 ± 226	1.56 ± 0.62	-2.44 ± 0.27		
		5597.94	85.99 ± 1.47	4862 ± 308	1.51 ± 0.58	-2.45 ± 0.37		
168.434929	22.243589	5591.90	79.23 ± 1.53	5115 ± 523	1.92 ± 0.85	-2.36 ± 0.53	1	Y
168.464637	22.150594	5591.90	82.80 ± 1.85	5117 ± 404	1.66 ± 0.66	-1.91 ± 0.42	1	Y
168.462098	22.207720	5134.21	76.73 ± 0.63	4821 ± 138	1.42 ± 0.31	-1.86 ± 0.18	3	Y
		4212.78	79.75 ± 1.36	4898 ± 363	1.48 ± 0.60	-1.78 ± 0.44		
		5591.90	75.72 ± 0.78	4747 ± 153	1.26 ± 0.37	-1.94 ± 0.20		
		5597.94	76.91 ± 1.79	6285 ± 754	3.13 ± 1.32	-1.13 ± 0.67		
168.328238	22.220353	5591.90	85.45 ± 1.83	4845 ± 407	1.90 ± 0.71	-2.37 ± 0.49	1	Y
168.323824	22.113282	6340.91	82.05 ± 2.14	5385 ± 840	2.30 ± 1.16	-0.38 ± 0.81	1	Y
168.310269	22.234085	4526.81	78.76 ± 1.57	4660 ± 288	2.19 ± 0.78	-1.22 ± 0.42	1	Y
168.355007	22.103800	6340.91	74.02 ± 2.19	5096 ± 520	1.83 ± 0.85	-0.81 ± 0.60	1	Y
168.386460	22.242679	5591.90	98.08 ± 1.29	5161 ± 604	1.82 ± 0.83	-2.06 ± 0.61	1	Y
168.425033	22.170671	5591.90	73.34 ± 1.54	5565 ± 421	1.67 ± 0.64	-1.63 ± 0.37	1	Y
168.565569	22.206052	5594.92	211.66 ± 0.33	5200 ± 42	2.83 ± 0.08	-1.38 ± 0.05	2	N
		5591.90	211.28 ± 0.46	5152 ± 51	2.76 ± 0.10	-1.40 ± 0.06		
		5597.94	212.06 ± 0.48	5300 ± 73	2.99 ± 0.14	-1.34 ± 0.09		
168.472271	22.246066	5969.43	83.32 ± 0.81	5173 ± 230	1.85 ± 0.39	-2.41 ± 0.24	2	Y
		5597.94	85.34 ± 1.36	5186 ± 375	1.32 ± 0.55	-2.54 ± 0.33		
		6340.91	82.20 ± 1.01	5164 ± 292	2.44 ± 0.57	-2.28 ± 0.34		

Table E.1: Continued; Spectroscopic properties of stars in the direction of Leo II

α_{J2000}	δ_{J2000}	HJD	v	T_{eff}	$\log(g)$	[Fe/H]	N_{obs}	Mem
(deg)	(deg)	(-2450000 days)	(km s^{-1})	(K)	(dex)	(dex)		
168.498916	22.113254	5511.16	78.63 ± 0.44	4909 ± 78	1.35 ± 0.21	-1.18 ± 0.11	3	Y
		3850.66	73.68 ± 1.82	5056 ± 234	1.38 ± 0.55	0.29 ± 0.37		
		6340.91	78.77 ± 0.64	5058 ± 122	1.52 ± 0.32	-1.28 ± 0.16		
		6341.92	79.12 ± 0.65	4745 ± 113	1.18 ± 0.31	-1.34 ± 0.15		
168.516204	22.174784	5544.67	85.45 ± 0.36	4531 ± 58	0.98 ± 0.12	-2.74 ± 0.07	5	Y
		3850.66	85.88 ± 1.29	4507 ± 166	1.22 ± 0.39	-2.72 ± 0.21		
		5591.90	84.79 ± 0.58	4415 ± 82	0.80 ± 0.16	-2.70 ± 0.09		
		5597.94	87.77 ± 0.97	4543 ± 180	1.12 ± 0.37	-3.21 ± 0.20		
		6340.91	85.82 ± 0.78	4706 ± 147	1.26 ± 0.40	-2.73 ± 0.18		
		6341.92	84.64 ± 0.79	4837 ± 178	1.74 ± 0.52	-2.49 ± 0.23		
168.513952	22.211801	5597.94	82.42 ± 0.82	4716 ± 247	1.37 ± 0.52	-2.36 ± 0.30	1	Y
168.470146	22.145110	6340.91	77.93 ± 1.81	5043 ± 475	2.73 ± 1.07	-2.14 ± 0.56	1	Y
168.578968	22.185577	3850.66	-31.85 ± 2.60	4592 ± 309	4.34 ± 0.91	-3.51 ± 0.36	1	N
168.630780	22.301546	5621.88	-0.27 ± 0.23	5236 ± 25	4.79 ± 0.06	-0.14 ± 0.03	4	N
		4212.78	-0.51 ± 0.46	5277 ± 51	4.95 ± 0.12	-0.02 ± 0.05		
		5591.90	-0.39 ± 0.46	5224 ± 47	4.81 ± 0.10	-0.10 ± 0.05		
		6340.91	0.13 ± 0.46	5238 ± 53	4.74 ± 0.13	-0.25 ± 0.06		
		6341.92	-0.30 ± 0.47	5203 ± 53	4.66 ± 0.12	-0.18 ± 0.06		
168.648723	22.117923	6341.42	37.92 ± 0.33	4647 ± 36	4.92 ± 0.10	-0.02 ± 0.04	2	N
		6340.91	37.83 ± 0.47	4644 ± 49	4.92 ± 0.14	-0.04 ± 0.06		
		6341.92	38.01 ± 0.47	4650 ± 51	4.93 ± 0.15	-0.00 ± 0.06		
168.647602	22.132710	5095.78	-32.88 ± 1.25	4460 ± 105	4.31 ± 0.32	-2.82 ± 0.14	2	N
		3850.66	-31.64 ± 1.55	4443 ± 106	4.46 ± 0.34	-2.82 ± 0.14		
		6340.91	-35.21 ± 2.13	5382 ± 784	2.87 ± 1.05	-2.67 ± 0.79		
168.655068	22.248906	5966.41	78.13 ± 0.67	4728 ± 84	4.96 ± 0.25	-1.56 ± 0.11	2	N
		5591.90	78.22 ± 0.75	4855 ± 109	5.00 ± 0.32	-0.95 ± 0.14		
		6340.91	77.80 ± 1.48	4533 ± 134	4.89 ± 0.40	-2.89 ± 0.20		

APPENDIX F

Velocities of Stars in Leo II

We collected velocity data for 196 stars in Leo II that had more than one epoch of observations. This amounted to 596 velocity measurements. We applied offsets to these velocity data to put them all on the same velocity standard as Chapter II (Spencer et al., 2017a). As such, the velocities we report in the following table will not match the values listed in the original papers. Column 1 lists the identifier that we assign to the star; column 2 lists the number of observations; column 3 lists the right ascension; column 4 lists the declination; column 5 lists the heliocentric Julian date; column 6 lists the radial velocity and error; and column 7 lists the paper where the velocity measurement originated from. “S17a” is in reference to Chapter II (Spencer et al., 2017a); “KG10” is Kirby et al. (2010); “KK07” is Koch et al. (2007b); and “V95” is Vogt et al. (1995).

Table F.1: Velocities of RGB stars in Leo II

Star ID	n	α_{J2000} (hh:mm:ss.ss)	δ_{J2000} (dd:mm:ss.ss)	HJD (days)	v (km s ⁻¹)	Ref.
LeoII-001	4	11:13:34.31	22:09:11.70	2455591.9	71.64 ± 0.78	S17a
LeoII-001	4	11:13:34.32	22:09:11.59	2452704.2	72.84 ± 2.55	KK07
LeoII-001	4	11:13:34.32	22:09:11.59	2453061.2	75.24 ± 2.21	KK07
LeoII-001	4	11:13:34.30	22:09:11.70	2453770.0	68.81 ± 2.36	KG10

Table F.1: Continued; Velocities of RGB stars in Leo II

Star ID	n	α_{J2000} (hh:mm:ss.ss)	δ_{J2000} (dd:mm:ss.ss)	HJD (days)	v (km s ⁻¹)	Ref.
LeoII-002	3	11:13:18.22	22:08:29.40	2455597.9	67.90± 1.28	S17a
LeoII-002	3	11:13:18.22	22:08:29.40	2456340.9	81.64± 1.19	S17a
LeoII-002	3	11:13:18.23	22:08:29.29	2452704.2	74.99± 28.67	KK07
LeoII-003	2	11:13:28.53	22:08:17.40	2455599.8	75.43± 1.85	S17a
LeoII-003	2	11:13:28.53	22:08:17.30	2453061.2	80.03± 1.43	KK07
LeoII-004	7	11:13:22.25	22:03:36.63	2454212.8	79.73± 1.05	S17a
LeoII-004	7	11:13:22.25	22:03:36.63	2455591.9	80.46± 0.63	S17a
LeoII-004	7	11:13:22.25	22:03:36.63	2455597.9	79.89± 1.10	S17a
LeoII-004	7	11:13:22.25	22:03:36.63	2456340.9	82.07± 0.88	S17a
LeoII-004	7	11:13:22.27	22:03:36.61	2452693.2	88.23± 13.09	KK07
LeoII-004	7	11:13:22.27	22:03:36.61	2452704.2	82.24± 2.10	KK07
LeoII-004	7	11:13:22.25	22:03:36.70	2453770.0	83.20± 2.32	KG10
LeoII-005	5	11:13:37.88	22:03:44.28	2453850.7	76.95± 1.84	S17a
LeoII-005	5	11:13:37.88	22:03:44.28	2455597.9	75.34± 1.70	S17a
LeoII-005	5	11:13:37.90	22:03:44.32	2452693.2	92.82± 20.11	KK07
LeoII-005	5	11:13:37.90	22:03:44.32	2453061.2	72.91± 2.28	KK07
LeoII-005	5	11:13:37.89	22:03:44.30	2453770.0	74.47± 2.52	KG10
LeoII-006	4	11:13:30.39	22:03:58.11	2454526.8	78.57± 1.27	S17a
LeoII-006	4	11:13:30.39	22:03:58.11	2455591.9	78.46± 1.41	S17a
LeoII-006	4	11:13:30.41	22:03:58.10	2452693.2	96.61± 17.90	KK07
LeoII-006	4	11:13:30.41	22:03:58.10	2452704.2	74.82± 2.73	KK07
LeoII-007	4	11:12:42.72	22:05:22.56	2455591.9	83.09± 0.67	S17a
LeoII-007	4	11:12:42.72	22:05:22.56	2456340.9	82.95± 1.03	S17a
LeoII-007	4	11:12:42.72	22:05:22.56	2456341.9	82.98± 0.83	S17a
LeoII-007	4	11:12:42.72	22:05:22.49	2452704.2	81.58± 21.65	KK07
LeoII-008	6	11:12:57.78	22:10:50.17	2454526.8	77.78± 1.47	S17a
LeoII-008	6	11:12:57.78	22:10:50.17	2455597.9	80.23± 1.25	S17a
LeoII-008	6	11:12:57.78	22:10:50.17	2456340.9	78.10± 1.16	S17a
LeoII-008	6	11:12:57.78	22:10:50.17	2456341.9	77.77± 0.99	S17a
LeoII-008	6	11:12:57.79	22:10:50.20	2452704.2	78.46± 3.81	KK07
LeoII-008	6	11:12:57.78	22:10:50.30	2453770.0	78.23± 2.43	KG10
LeoII-009	5	11:13:12.94	22:08:09.52	2454526.8	84.61± 2.23	S17a
LeoII-009	5	11:13:12.94	22:08:09.52	2455591.9	82.83± 0.75	S17a
LeoII-009	5	11:13:12.94	22:08:09.52	2456340.9	83.03± 1.10	S17a
LeoII-009	5	11:13:12.96	22:08:09.60	2452704.2	84.27± 16.85	KK07
LeoII-009	5	11:13:12.94	22:08:09.60	2453770.0	85.94± 2.33	KG10
LeoII-010	2	11:13:13.14	22:07:52.57	2455597.9	79.65± 0.68	S17a

Table F.1: Continued; Velocities of RGB stars in Leo II

Star ID	n	α_{J2000} (hh:mm:ss.ss)	δ_{J2000} (dd:mm:ss.ss)	HJD (days)	v (km s ⁻¹)	Ref.
LeoII-010	2	11:13:13.16	22:07:52.61	2452704.2	81.32± 3.04	KK07
LeoII-011	4	11:13:11.54	22:11:27.36	2456340.9	77.77± 2.09	S17a
LeoII-011	4	11:13:11.54	22:11:27.36	2456341.9	74.50± 0.85	S17a
LeoII-011	4	11:13:11.55	22:11:27.38	2452704.2	74.24± 6.49	KK07
LeoII-011	4	11:13:11.54	22:11:27.40	2453770.0	76.97± 2.23	KG10
LeoII-012	4	11:13:12.91	22:09:17.77	2455597.9	75.20± 0.79	S17a
LeoII-012	4	11:13:12.91	22:09:17.77	2455599.8	74.50± 1.29	S17a
LeoII-012	4	11:13:12.92	22:09:17.78	2452693.2	77.62± 29.60	KK07
LeoII-012	4	11:13:12.91	22:09:17.80	2453770.0	72.97± 2.16	KG10
LeoII-013	4	11:13:06.40	22:12:05.41	2456340.9	73.18± 2.06	S17a
LeoII-013	4	11:13:06.40	22:12:05.41	2456341.9	74.70± 1.55	S17a
LeoII-013	4	11:13:06.40	22:12:05.51	2452704.2	73.60± 11.24	KK07
LeoII-013	4	11:13:06.40	22:12:05.50	2453770.0	75.06± 2.72	KG10
LeoII-014	3	11:13:27.68	22:10:13.03	2453850.7	83.43± 1.43	S17a
LeoII-014	3	11:13:27.69	22:10:13.12	2452693.2	82.32± 11.95	KK07
LeoII-014	3	11:13:27.66	22:10:12.57	2449432.8	80.64± 1.90	V95
LeoII-015	3	11:13:20.81	22:08:34.39	2454212.8	75.73± 0.87	S17a
LeoII-015	3	11:13:20.82	22:08:34.51	2452704.2	74.50± 2.84	KK07
LeoII-015	3	11:13:20.83	22:08:34.37	2449431.9	73.24± 3.30	V95
LeoII-016	4	11:13:32.05	22:08:58.61	2453850.7	70.98± 0.86	S17a
LeoII-016	4	11:13:32.07	22:08:58.70	2452693.2	71.80± 4.21	KK07
LeoII-016	4	11:13:32.07	22:08:58.70	2453061.2	69.19± 1.07	KK07
LeoII-016	4	11:13:32.01	22:08:58.40	2449431.9	70.04± 1.60	V95
LeoII-017	5	11:13:27.69	22:10:39.76	2454212.8	80.39± 0.73	S17a
LeoII-017	5	11:13:27.70	22:10:39.90	2452693.2	72.77± 7.36	KK07
LeoII-017	5	11:13:27.70	22:10:39.90	2453061.2	79.13± 1.68	KK07
LeoII-017	5	11:13:27.69	22:10:39.90	2453770.0	81.09± 2.14	KG10
LeoII-017	5	11:13:27.67	22:10:39.27	2449432.1	81.84± 4.00	V95
LeoII-018	4	11:13:29.46	22:09:49.46	2454212.8	85.57± 0.77	S17a
LeoII-018	4	11:13:29.47	22:09:49.61	2452693.2	77.83± 12.32	KK07
LeoII-018	4	11:13:29.46	22:09:49.60	2453770.0	87.22± 2.15	KG10
LeoII-018	4	11:13:29.43	22:09:49.04	2449432.0	82.34± 3.40	V95
LeoII-019	4	11:13:28.77	22:08:47.05	2455591.9	87.07± 0.59	S17a
LeoII-019	4	11:13:28.79	22:08:47.11	2452693.2	91.70± 11.25	KK07
LeoII-019	4	11:13:28.79	22:08:47.11	2453061.2	82.93± 1.42	KK07
LeoII-019	4	11:13:28.75	22:08:46.95	2449430.8	89.94± 3.70	V95
LeoII-020	5	11:13:30.97	22:08:44.61	2455591.9	80.16± 0.66	S17a

Table F.1: Continued; Velocities of RGB stars in Leo II

Star ID	n	α_{J2000} (hh:mm:ss.ss)	δ_{J2000} (dd:mm:ss.ss)	HJD (days)	v (km s ⁻¹)	Ref.
LeoII-020	5	11:13:30.97	22:08:44.61	2456340.9	80.44± 0.68	S17a
LeoII-020	5	11:13:30.98	22:08:44.70	2452693.2	84.43± 14.22	KK07
LeoII-020	5	11:13:30.98	22:08:44.70	2453061.2	80.72± 1.31	KK07
LeoII-020	5	11:13:30.94	22:08:44.42	2449432.0	78.74± 3.30	V95
LeoII-021	3	11:13:32.12	22:09:11.76	2456341.9	82.17± 0.78	S17a
LeoII-021	3	11:13:32.14	22:09:11.92	2452693.2	89.44± 16.29	KK07
LeoII-021	3	11:13:32.09	22:09:11.50	2449431.8	83.84± 3.00	V95
LeoII-022	4	11:13:32.05	22:09:13.42	2455599.8	60.06± 1.76	S17a
LeoII-022	4	11:13:32.05	22:09:13.42	2456340.9	61.19± 0.82	S17a
LeoII-022	4	11:13:32.06	22:09:13.50	2453061.2	63.17± 1.05	KK07
LeoII-022	4	11:13:32.01	22:09:13.10	2449430.9	62.84± 1.80	V95
LeoII-023	4	11:13:41.93	22:05:35.19	2453850.7	70.57± 1.09	S17a
LeoII-023	4	11:13:41.95	22:05:35.20	2452704.2	70.84± 2.30	KK07
LeoII-023	4	11:13:41.95	22:05:35.20	2453061.2	72.33± 1.40	KK07
LeoII-023	4	11:13:41.94	22:05:35.30	2453770.0	68.21± 2.31	KG10
LeoII-024	3	11:13:13.88	22:08:50.07	2454212.8	67.04± 0.94	S17a
LeoII-024	3	11:13:13.89	22:08:50.21	2452704.2	66.81± 20.06	KK07
LeoII-024	3	11:13:13.88	22:08:50.20	2453770.0	70.12± 2.12	KG10
LeoII-025	3	11:13:15.71	22:09:05.49	2456341.9	68.67± 1.25	S17a
LeoII-025	3	11:13:15.73	22:09:05.62	2453061.2	74.97± 2.44	KK07
LeoII-025	3	11:13:15.72	22:09:05.70	2453770.0	61.58± 16.13	KG10
LeoII-026	3	11:13:16.94	22:06:03.46	2454526.8	80.78± 1.22	S17a
LeoII-026	3	11:13:16.96	22:06:03.49	2453061.2	84.21± 1.71	KK07
LeoII-026	3	11:13:16.95	22:06:03.60	2453770.0	80.13± 2.23	KG10
LeoII-027	2	11:13:18.28	22:06:44.65	2455591.9	78.55± 0.64	S17a
LeoII-027	2	11:13:18.30	22:06:44.71	2453061.2	79.75± 1.50	KK07
LeoII-028	3	11:13:19.81	22:05:46.98	2454212.8	76.73± 1.25	S17a
LeoII-028	3	11:13:19.83	22:05:47.11	2453061.2	76.12± 1.32	KK07
LeoII-028	3	11:13:19.81	22:05:47.00	2453770.0	78.81± 2.41	KG10
LeoII-029	5	11:13:20.11	22:06:06.39	2455597.9	71.95± 1.23	S17a
LeoII-029	5	11:13:20.11	22:06:06.39	2456340.9	71.76± 1.02	S17a
LeoII-029	5	11:13:20.13	22:06:06.41	2452704.2	79.41± 2.84	KK07
LeoII-029	5	11:13:20.13	22:06:06.41	2453061.2	71.53± 1.70	KK07
LeoII-029	5	11:13:20.12	22:06:06.50	2453770.0	75.88± 2.75	KG10
LeoII-030	3	11:13:17.52	22:12:08.17	2455591.9	75.59± 0.67	S17a
LeoII-030	3	11:13:17.53	22:12:08.32	2452704.2	77.00± 3.58	KK07
LeoII-030	3	11:13:17.52	22:12:08.30	2453770.0	74.90± 2.23	KG10

Table F.1: Continued; Velocities of RGB stars in Leo II

Star ID	n	α_{J2000} (hh:mm:ss.ss)	δ_{J2000} (dd:mm:ss.ss)	HJD (days)	v (km s ⁻¹)	Ref.
LeoII-031	5	11:13:19.79	22:09:20.33	2454526.8	84.45± 0.81	S17a
LeoII-031	5	11:13:19.80	22:09:20.41	2452693.2	81.46± 11.37	KK07
LeoII-031	5	11:13:19.80	22:09:20.41	2452704.2	83.83± 2.59	KK07
LeoII-031	5	11:13:19.79	22:09:20.50	2453770.0	82.06± 2.15	KG10
LeoII-031	5	11:13:19.81	22:09:20.18	2449430.9	83.14± 2.10	V95
LeoII-032	4	11:13:19.84	22:09:45.90	2454212.8	71.85± 0.78	S17a
LeoII-032	4	11:13:19.84	22:09:46.01	2452693.2	66.11± 24.96	KK07
LeoII-032	4	11:13:19.84	22:09:46.00	2453770.0	68.70± 2.14	KG10
LeoII-032	4	11:13:19.85	22:09:45.58	2449432.0	72.14± 2.40	V95
LeoII-033	2	11:13:21.47	22:05:16.01	2455599.8	75.56± 1.98	S17a
LeoII-033	2	11:13:21.48	22:05:16.12	2453061.2	76.62± 2.36	KK07
LeoII-034	4	11:13:20.60	22:07:14.82	2454212.8	71.28± 1.07	S17a
LeoII-034	4	11:13:20.62	22:07:14.92	2452704.2	75.90± 2.67	KK07
LeoII-034	4	11:13:20.62	22:07:14.92	2453061.2	75.40± 1.26	KK07
LeoII-034	4	11:13:20.62	22:07:14.97	2449432.9	74.24± 3.20	V95
LeoII-035	4	11:13:22.04	22:04:28.61	2455597.9	97.86± 1.19	S17a
LeoII-035	4	11:13:22.04	22:04:28.61	2456341.9	96.81± 0.99	S17a
LeoII-035	4	11:13:22.05	22:04:28.70	2453061.2	94.09± 2.69	KK07
LeoII-035	4	11:13:22.04	22:04:28.70	2453770.0	97.16± 2.73	KG10
LeoII-036	4	11:13:22.55	22:07:31.14	2455591.9	67.72± 0.85	S17a
LeoII-036	4	11:13:22.55	22:07:31.14	2456340.9	69.69± 1.31	S17a
LeoII-036	4	11:13:22.56	22:07:31.30	2452704.2	65.07± 21.17	KK07
LeoII-036	4	11:13:22.56	22:07:31.30	2453061.2	70.80± 2.20	KK07
LeoII-037	3	11:13:22.78	22:05:54.32	2454526.8	64.82± 0.75	S17a
LeoII-037	3	11:13:22.80	22:05:54.38	2453061.2	63.88± 2.69	KK07
LeoII-037	3	11:13:22.79	22:05:54.30	2453770.0	67.49± 2.38	KG10
LeoII-038	5	11:13:23.82	22:04:57.92	2454526.8	84.56± 1.26	S17a
LeoII-038	5	11:13:23.82	22:04:57.92	2456341.9	81.29± 1.27	S17a
LeoII-038	5	11:13:23.84	22:04:58.01	2452693.2	93.52± 31.61	KK07
LeoII-038	5	11:13:23.84	22:04:58.01	2452704.2	85.60± 2.97	KK07
LeoII-038	5	11:13:23.83	22:04:58.00	2453770.0	88.38± 3.35	KG10
LeoII-039	4	11:13:23.30	22:05:23.09	2455597.9	69.80± 1.72	S17a
LeoII-039	4	11:13:23.30	22:05:23.09	2456340.9	65.56± 1.05	S17a
LeoII-039	4	11:13:23.32	22:05:23.10	2452704.2	72.56± 2.50	KK07
LeoII-039	4	11:13:23.32	22:05:23.10	2453061.2	63.68± 2.66	KK07
LeoII-040	3	11:13:20.85	22:11:30.78	2455599.8	73.71± 1.30	S17a
LeoII-040	3	11:13:20.86	22:11:30.91	2453061.2	75.01± 1.34	KK07

Table F.1: Continued; Velocities of RGB stars in Leo II

Star ID	n	α_{J2000} (hh:mm:ss.ss)	δ_{J2000} (dd:mm:ss.ss)	HJD (days)	v (km s ⁻¹)	Ref.
LeoII-040	3	11:13:20.85	22:11:30.90	2453770.0	67.05 ± 2.16	KG10
LeoII-041	3	11:13:22.24	22:08:54.03	2454526.8	94.94 ± 0.70	S17a
LeoII-041	3	11:13:22.26	22:08:54.10	2452693.2	84.77 ± 15.79	KK07
LeoII-041	3	11:13:22.25	22:08:53.85	2449432.8	88.44 ± 4.20	V95
LeoII-042	6	11:13:23.03	22:10:22.66	2454526.8	86.29 ± 0.75	S17a
LeoII-042	6	11:13:23.03	22:10:22.66	2455591.9	86.04 ± 0.54	S17a
LeoII-042	6	11:13:23.04	22:10:22.69	2452693.2	82.52 ± 29.10	KK07
LeoII-042	6	11:13:23.04	22:10:22.69	2453061.2	85.51 ± 1.11	KK07
LeoII-042	6	11:13:23.03	22:10:22.70	2453770.0	86.25 ± 2.17	KG10
LeoII-042	6	11:13:23.02	22:10:22.24	2449432.0	80.84 ± 4.40	V95
LeoII-043	3	11:13:23.42	22:07:17.13	2454212.8	80.15 ± 0.66	S17a
LeoII-043	3	11:13:23.43	22:07:17.18	2453061.2	79.36 ± 1.08	KK07
LeoII-043	3	11:13:23.42	22:07:17.30	2453770.0	81.11 ± 2.15	KG10
LeoII-044	2	11:13:23.63	22:07:07.09	2455591.9	81.19 ± 0.62	S17a
LeoII-044	2	11:13:23.65	22:07:07.21	2453061.2	84.48 ± 1.32	KK07
LeoII-045	2	11:13:24.47	22:06:13.35	2454212.8	78.67 ± 0.72	S17a
LeoII-045	2	11:13:24.48	22:06:13.39	2452704.2	69.68 ± 1.34	KK07
LeoII-046	3	11:13:21.91	22:12:06.48	2453850.7	72.50 ± 2.00	S17a
LeoII-046	3	11:13:21.93	22:12:06.59	2453061.2	74.16 ± 1.51	KK07
LeoII-046	3	11:13:21.91	22:12:06.60	2453770.0	73.30 ± 2.13	KG10
LeoII-047	2	11:13:24.08	22:09:33.51	2456340.9	89.74 ± 0.97	S17a
LeoII-047	2	11:13:24.09	22:09:33.59	2453061.2	81.45 ± 1.29	KK07
LeoII-048	5	11:13:25.56	22:07:44.05	2454212.8	80.16 ± 1.23	S17a
LeoII-048	5	11:13:25.59	22:07:44.11	2452693.2	78.03 ± 9.31	KK07
LeoII-048	5	11:13:25.59	22:07:44.11	2452704.2	80.54 ± 2.46	KK07
LeoII-048	5	11:13:25.57	22:07:44.20	2453770.0	82.81 ± 2.15	KG10
LeoII-048	5	11:13:25.56	22:07:44.10	2449432.9	82.14 ± 2.90	V95
LeoII-049	2	11:13:25.60	22:12:12.65	2455591.9	83.64 ± 1.42	S17a
LeoII-049	2	11:13:25.61	22:12:12.82	2453061.2	94.95 ± 1.73	KK07
LeoII-050	3	11:13:26.51	22:11:07.45	2454212.8	83.41 ± 0.75	S17a
LeoII-050	3	11:13:26.52	22:11:07.51	2453061.2	68.21 ± 1.26	KK07
LeoII-050	3	11:13:26.49	22:11:06.88	2449432.8	66.24 ± 2.30	V95
LeoII-051	4	11:13:29.57	22:07:16.00	2454526.8	83.59 ± 0.86	S17a
LeoII-051	4	11:13:29.59	22:07:16.00	2452704.2	81.57 ± 23.03	KK07
LeoII-051	4	11:13:29.59	22:07:16.00	2453061.2	84.17 ± 1.13	KK07
LeoII-051	4	11:13:29.57	22:07:16.10	2453770.0	85.61 ± 2.15	KG10
LeoII-052	4	11:13:31.32	22:04:24.97	2454212.8	85.01 ± 0.80	S17a

Table F.1: Continued; Velocities of RGB stars in Leo II

Star ID	n	α_{J2000} (hh:mm:ss.ss)	δ_{J2000} (dd:mm:ss.ss)	HJD (days)	v (km s ⁻¹)	Ref.
LeoII-052	4	11:13:31.34	22:04:25.00	2452693.2	73.02± 10.08	KK07
LeoII-052	4	11:13:31.34	22:04:25.00	2452704.2	84.00± 1.40	KK07
LeoII-052	4	11:13:31.33	22:04:25.00	2453770.0	82.96± 2.27	KG10
LeoII-053	3	11:13:30.26	22:06:57.44	2454212.8	87.15± 1.29	S17a
LeoII-053	3	11:13:30.28	22:06:57.49	2452693.2	96.54± 12.01	KK07
LeoII-053	3	11:13:30.23	22:06:57.53	2449432.8	86.04± 2.10	V95
LeoII-054	4	11:13:31.09	22:06:30.21	2453850.7	86.23± 0.77	S17a
LeoII-054	4	11:13:31.11	22:06:30.31	2452693.2	80.49± 5.03	KK07
LeoII-054	4	11:13:31.11	22:06:30.31	2452704.2	84.88± 1.01	KK07
LeoII-054	4	11:13:31.09	22:06:30.30	2453770.0	84.02± 2.17	KG10
LeoII-055	4	11:13:30.40	22:08:04.88	2454526.8	63.77± 1.35	S17a
LeoII-055	4	11:13:30.40	22:08:04.88	2456341.9	57.71± 0.88	S17a
LeoII-055	4	11:13:30.42	22:08:04.99	2453061.2	68.08± 2.92	KK07
LeoII-055	4	11:13:30.40	22:08:05.00	2453770.0	70.72± 2.24	KG10
LeoII-056	4	11:13:31.01	22:11:21.96	2454212.8	74.23± 0.80	S17a
LeoII-056	4	11:13:31.02	22:11:22.09	2452693.2	82.33± 12.11	KK07
LeoII-056	4	11:13:31.01	22:11:22.10	2453770.0	74.43± 2.17	KG10
LeoII-056	4	11:13:30.96	22:11:21.32	2449432.8	78.04± 2.50	V95
LeoII-057	4	11:13:32.05	22:07:29.72	2453850.7	79.41± 0.66	S17a
LeoII-057	4	11:13:32.07	22:07:29.78	2452693.2	75.30± 7.34	KK07
LeoII-057	4	11:13:32.06	22:07:29.80	2453770.0	77.16± 2.15	KG10
LeoII-057	4	11:13:32.02	22:07:29.70	2449430.8	85.74± 3.80	V95
LeoII-058	5	11:13:31.66	22:07:46.73	2454212.8	69.32± 1.16	S17a
LeoII-058	5	11:13:31.68	22:07:46.81	2452693.2	57.26± 12.25	KK07
LeoII-058	5	11:13:31.68	22:07:46.81	2453061.2	66.88± 1.38	KK07
LeoII-058	5	11:13:31.66	22:07:46.80	2453770.0	65.22± 2.24	KG10
LeoII-058	5	11:13:31.63	22:07:46.61	2449432.0	64.54± 3.10	V95
LeoII-059	4	11:13:30.73	22:10:51.15	2453850.7	78.52± 1.29	S17a
LeoII-059	4	11:13:30.75	22:10:51.20	2452693.2	77.50± 5.11	KK07
LeoII-059	4	11:13:30.73	22:10:51.30	2453770.0	78.95± 2.13	KG10
LeoII-059	4	11:13:30.69	22:10:50.52	2449431.9	81.24± 3.20	V95
LeoII-060	2	11:13:31.23	22:11:03.92	2456340.9	73.65± 1.46	S17a
LeoII-060	2	11:13:31.24	22:11:04.09	2453061.2	78.72± 2.46	KK07
LeoII-061	3	11:13:31.68	22:09:44.83	2454212.8	81.40± 1.97	S17a
LeoII-061	3	11:13:31.69	22:09:44.89	2452693.2	85.66± 17.65	KK07
LeoII-061	3	11:13:31.69	22:09:44.89	2452704.2	80.38± 2.97	KK07
LeoII-062	7	11:13:33.87	22:06:08.04	2453850.7	79.76± 0.68	S17a

Table F.1: Continued; Velocities of RGB stars in Leo II

Star ID	n	α_{J2000} (hh:mm:ss.ss)	δ_{J2000} (dd:mm:ss.ss)	HJD (days)	v (km s ⁻¹)	Ref.
LeoII-062	7	11:13:33.87	22:06:08.04	2456340.9	80.33± 0.61	S17a
LeoII-062	7	11:13:33.89	22:06:08.10	2452693.2	81.63± 6.40	KK07
LeoII-062	7	11:13:33.89	22:06:08.10	2452704.2	78.59± 2.41	KK07
LeoII-062	7	11:13:33.89	22:06:08.10	2453061.2	79.36± 1.00	KK07
LeoII-062	7	11:13:33.87	22:06:08.10	2453770.0	82.28± 2.21	KG10
LeoII-062	7	11:13:33.83	22:06:08.17	2449432.0	81.34± 3.00	V95
LeoII-063	4	11:13:35.43	22:04:51.41	2454212.8	72.02± 1.55	S17a
LeoII-063	4	11:13:35.45	22:04:51.38	2452693.2	65.72± 15.46	KK07
LeoII-063	4	11:13:35.45	22:04:51.38	2452704.2	74.32± 2.45	KK07
LeoII-063	4	11:13:35.44	22:04:51.50	2453770.0	72.62± 2.53	KG10
LeoII-064	4	11:13:31.77	22:14:14.32	2453850.7	89.67± 0.78	S17a
LeoII-064	4	11:13:31.77	22:14:14.32	2456340.9	85.57± 0.62	S17a
LeoII-064	4	11:13:31.78	22:14:14.39	2452704.2	80.38± 2.96	KK07
LeoII-064	4	11:13:31.78	22:14:14.40	2453770.0	86.12± 2.13	KG10
LeoII-065	2	11:13:33.66	22:10:39.21	2456340.9	88.12± 1.31	S17a
LeoII-065	2	11:13:33.68	22:10:39.29	2452693.2	85.71± 20.81	KK07
LeoII-066	5	11:13:37.09	22:07:07.38	2454212.8	69.60± 0.85	S17a
LeoII-066	5	11:13:37.09	22:07:07.38	2456340.9	69.78± 0.67	S17a
LeoII-066	5	11:13:37.11	22:07:07.50	2452704.2	70.46± 1.42	KK07
LeoII-066	5	11:13:37.11	22:07:07.50	2453061.2	69.50± 1.11	KK07
LeoII-066	5	11:13:37.10	22:07:07.50	2453770.0	67.34± 2.16	KG10
LeoII-067	3	11:13:35.03	22:11:34.76	2456340.9	88.24± 1.65	S17a
LeoII-067	3	11:13:35.04	22:11:34.80	2452704.2	89.35± 5.44	KK07
LeoII-067	3	11:13:35.04	22:11:34.80	2453061.2	84.26± 1.46	KK07
LeoII-068	5	11:13:36.02	22:12:20.84	2454212.8	84.02± 0.82	S17a
LeoII-068	5	11:13:36.02	22:12:20.84	2456341.9	82.78± 0.75	S17a
LeoII-068	5	11:13:36.04	22:12:20.99	2452693.2	89.25± 3.17	KK07
LeoII-068	5	11:13:36.04	22:12:20.99	2452704.2	84.47± 2.58	KK07
LeoII-068	5	11:13:36.03	22:12:20.90	2453770.0	89.03± 2.20	KG10
LeoII-069	4	11:13:38.02	22:11:17.44	2454212.8	68.92± 0.99	S17a
LeoII-069	4	11:13:38.04	22:11:17.59	2452693.2	80.84± 19.67	KK07
LeoII-069	4	11:13:38.04	22:11:17.59	2452704.2	75.86± 5.37	KK07
LeoII-069	4	11:13:38.03	22:11:17.60	2453770.0	68.90± 2.29	KG10
LeoII-070	4	11:13:39.13	22:09:20.38	2454526.8	81.62± 1.60	S17a
LeoII-070	4	11:13:39.13	22:09:20.38	2456340.9	77.55± 2.17	S17a
LeoII-070	4	11:13:39.15	22:09:20.48	2452704.2	85.43± 6.17	KK07
LeoII-070	4	11:13:39.14	22:09:20.50	2453770.0	80.33± 2.37	KG10

Table F.1: Continued; Velocities of RGB stars in Leo II

Star ID	n	α_{J2000} (hh:mm:ss.ss)	δ_{J2000} (dd:mm:ss.ss)	HJD (days)	v (km s ⁻¹)	Ref.
LeoII-071	3	11:13:41.24	22:07:41.23	2453850.7	73.78± 0.94	S17a
LeoII-071	3	11:13:41.25	22:07:41.30	2452704.2	73.62± 2.03	KK07
LeoII-071	3	11:13:41.24	22:07:41.30	2453770.0	72.78± 2.19	KG10
LeoII-072	4	11:13:42.72	22:07:27.59	2455591.9	77.15± 0.67	S17a
LeoII-072	4	11:13:42.72	22:07:27.59	2455597.9	78.38± 1.18	S17a
LeoII-072	4	11:13:42.73	22:07:27.59	2452704.2	77.15± 2.76	KK07
LeoII-072	4	11:13:42.73	22:07:27.70	2453770.0	79.28± 2.18	KG10
LeoII-073	3	11:13:15.84	22:04:51.21	2456341.9	83.28± 1.92	S17a
LeoII-073	3	11:13:15.86	22:04:51.31	2452704.2	82.10± 2.84	KK07
LeoII-073	3	11:13:15.86	22:04:51.31	2453061.2	80.40± 2.73	KK07
LeoII-074	3	11:13:16.05	22:06:57.28	2455591.9	87.52± 1.33	S17a
LeoII-074	3	11:13:16.06	22:06:57.38	2453061.2	84.79± 2.61	KK07
LeoII-074	3	11:13:16.05	22:06:57.40	2453770.0	89.43± 3.32	KG10
LeoII-075	4	11:13:12.22	22:16:08.97	2455591.9	83.24± 1.44	S17a
LeoII-075	4	11:13:12.23	22:16:09.30	2452693.2	74.55± 4.97	KK07
LeoII-075	4	11:13:12.23	22:16:09.30	2453061.2	80.13± 2.47	KK07
LeoII-075	4	11:13:12.23	22:16:09.20	2453770.0	78.16± 2.52	KG10
LeoII-076	3	11:13:18.82	22:11:14.83	2455591.9	66.48± 1.16	S17a
LeoII-076	3	11:13:18.83	22:11:15.00	2453061.2	66.70± 2.17	KK07
LeoII-076	3	11:13:18.82	22:11:15.00	2453770.0	65.26± 2.61	KG10
LeoII-077	2	11:13:23.41	22:05:38.40	2456341.9	82.29± 1.44	S17a
LeoII-077	2	11:13:23.42	22:05:38.40	2452704.2	79.16± 10.48	KK07
LeoII-078	4	11:13:21.98	22:11:31.97	2455591.9	84.67± 0.98	S17a
LeoII-078	4	11:13:21.98	22:11:31.97	2456341.9	82.87± 1.61	S17a
LeoII-078	4	11:13:22.00	22:11:32.10	2452704.2	86.90± 12.20	KK07
LeoII-078	4	11:13:22.00	22:11:32.10	2453061.2	82.22± 2.35	KK07
LeoII-079	4	11:13:23.31	22:13:17.14	2455591.9	72.53± 1.05	S17a
LeoII-079	4	11:13:23.31	22:13:17.14	2456341.9	71.27± 2.10	S17a
LeoII-079	4	11:13:23.32	22:13:17.18	2452704.2	72.40± 11.70	KK07
LeoII-079	4	11:13:23.32	22:13:17.30	2453770.0	72.55± 2.40	KG10
LeoII-080	4	11:13:27.74	22:07:45.83	2454526.8	70.03± 1.30	S17a
LeoII-080	4	11:13:27.76	22:07:45.91	2452704.2	73.36± 12.71	KK07
LeoII-080	4	11:13:27.76	22:07:45.91	2453061.2	76.76± 2.31	KK07
LeoII-080	4	11:13:27.75	22:07:46.00	2453770.0	73.67± 2.24	KG10
LeoII-081	3	11:13:27.49	22:13:41.50	2455591.9	84.69± 1.01	S17a
LeoII-081	3	11:13:27.50	22:13:41.59	2452704.2	82.86± 2.32	KK07
LeoII-081	3	11:13:27.50	22:13:41.60	2453770.0	85.08± 2.37	KG10

Table F.1: Continued; Velocities of RGB stars in Leo II

Star ID	n	α_{J2000} (hh:mm:ss.ss)	δ_{J2000} (dd:mm:ss.ss)	HJD (days)	v (km s ⁻¹)	Ref.
LeoII-082	3	11:13:31.87	22:04:56.09	2456340.9	88.56± 1.42	S17a
LeoII-082	3	11:13:31.87	22:04:56.09	2456341.9	87.30± 1.49	S17a
LeoII-082	3	11:13:31.89	22:04:56.10	2452704.2	85.18± 2.67	KK07
LeoII-083	3	11:13:32.33	22:06:55.75	2455591.9	69.71± 1.12	S17a
LeoII-083	3	11:13:32.34	22:06:55.80	2453061.2	72.09± 1.51	KK07
LeoII-083	3	11:13:32.33	22:06:55.80	2453770.0	73.62± 2.64	KG10
LeoII-084	2	11:13:30.66	22:12:19.73	2455591.9	72.17± 1.25	S17a
LeoII-084	2	11:13:30.68	22:12:19.80	2453061.2	69.80± 1.78	KK07
LeoII-085	5	11:13:34.85	22:06:17.58	2454526.8	75.58± 1.15	S17a
LeoII-085	5	11:13:34.85	22:06:17.58	2455591.9	75.48± 0.74	S17a
LeoII-085	5	11:13:34.86	22:06:17.60	2452704.2	80.95± 2.51	KK07
LeoII-085	5	11:13:34.86	22:06:17.60	2453061.2	75.28± 1.32	KK07
LeoII-085	5	11:13:34.85	22:06:17.70	2453770.0	74.74± 2.99	KG10
LeoII-086	3	11:13:34.56	22:06:52.46	2456341.9	69.47± 1.52	S17a
LeoII-086	3	11:13:34.58	22:06:52.60	2452704.2	76.91± 10.99	KK07
LeoII-086	3	11:13:34.56	22:06:52.60	2453770.0	68.48± 4.14	KG10
LeoII-087	3	11:13:35.59	22:07:53.38	2456341.9	73.05± 1.78	S17a
LeoII-087	3	11:13:35.61	22:07:53.51	2452704.2	97.38± 11.33	KK07
LeoII-087	3	11:13:35.61	22:07:53.51	2453061.2	79.89± 1.30	KK07
LeoII-088	3	11:13:37.56	22:04:42.11	2455591.9	77.27± 1.34	S17a
LeoII-088	3	11:13:37.58	22:04:42.10	2452704.2	72.91± 4.96	KK07
LeoII-088	3	11:13:37.58	22:04:42.10	2453061.2	81.78± 2.14	KK07
LeoII-089	3	11:13:37.89	22:08:13.17	2455591.9	85.27± 0.89	S17a
LeoII-089	3	11:13:37.90	22:08:13.42	2452704.2	85.44± 3.17	KK07
LeoII-089	3	11:13:37.89	22:08:13.30	2453770.0	79.45± 2.43	KG10
LeoII-090	4	11:13:40.24	22:06:28.84	2454526.8	74.40± 2.30	S17a
LeoII-090	4	11:13:40.26	22:06:28.91	2452704.2	82.26± 2.79	KK07
LeoII-090	4	11:13:40.26	22:06:28.91	2453061.2	78.88± 2.04	KK07
LeoII-090	4	11:13:40.25	22:06:28.90	2453770.0	76.89± 2.81	KG10
LeoII-091	4	11:13:43.14	22:07:57.28	2455591.9	83.86± 0.99	S17a
LeoII-091	4	11:13:43.15	22:07:57.40	2452693.2	52.40± 17.15	KK07
LeoII-091	4	11:13:43.15	22:07:57.40	2452704.2	82.66± 9.76	KK07
LeoII-091	4	11:13:43.15	22:07:57.30	2453770.0	84.48± 2.53	KG10
LeoII-092	3	11:13:42.87	22:13:55.64	2454212.8	89.71± 1.75	S17a
LeoII-092	3	11:13:42.87	22:13:55.81	2452704.2	96.21± 11.17	KK07
LeoII-092	3	11:13:42.87	22:13:55.81	2453061.2	85.89± 2.66	KK07
LeoII-093	4	11:13:42.81	22:14:07.65	2454526.8	86.45± 1.64	S17a

Table F.1: Continued; Velocities of RGB stars in Leo II

Star ID	n	α_{J2000} (hh:mm:ss.ss)	δ_{J2000} (dd:mm:ss.ss)	HJD (days)	v (km s ⁻¹)	Ref.
LeoII-093	4	11:13:42.81	22:14:07.65	2455597.9	85.99± 1.47	S17a
LeoII-093	4	11:13:42.82	22:14:07.69	2452693.2	87.22± 15.96	KK07
LeoII-093	4	11:13:42.83	22:14:07.70	2453770.0	86.83± 2.25	KG10
LeoII-094	4	11:13:50.90	22:12:27.79	2454212.8	79.75± 1.36	S17a
LeoII-094	4	11:13:50.90	22:12:27.79	2455591.9	75.72± 0.78	S17a
LeoII-094	4	11:13:50.90	22:12:27.79	2455597.9	76.91± 1.79	S17a
LeoII-094	4	11:13:50.91	22:12:27.90	2453061.2	72.21± 1.55	KK07
LeoII-095	5	11:13:59.74	22:06:47.71	2453850.7	73.68± 1.82	S17a
LeoII-095	5	11:13:59.74	22:06:47.71	2456340.9	78.77± 0.64	S17a
LeoII-095	5	11:13:59.74	22:06:47.71	2456341.9	79.12± 0.65	S17a
LeoII-095	5	11:13:59.75	22:06:47.81	2452693.2	75.86± 13.07	KK07
LeoII-095	5	11:13:59.75	22:06:47.81	2452704.2	80.17± 2.84	KK07
LeoII-096	4	11:14:03.35	22:12:42.48	2455597.9	82.42± 0.82	S17a
LeoII-096	4	11:14:03.35	22:12:42.52	2452704.2	80.96± 10.38	KK07
LeoII-096	4	11:14:03.35	22:12:42.52	2453061.2	76.82± 1.59	KK07
LeoII-096	4	11:14:03.35	22:12:42.60	2453770.0	76.19± 2.21	KG10
LeoII-097	4	11:13:52.84	22:08:42.40	2456340.9	77.93± 1.81	S17a
LeoII-097	4	11:13:52.86	22:08:42.61	2452693.2	99.26± 22.73	KK07
LeoII-097	4	11:13:52.86	22:08:42.61	2452704.2	72.83± 8.12	KK07
LeoII-097	4	11:13:52.85	22:08:42.70	2453770.0	78.65± 2.50	KG10
LeoII-098	2	11:13:19.53	22:08:48.89	2455591.9	75.00± 0.91	S17a
LeoII-098	2	11:13:19.52	22:08:48.90	2453770.0	72.27± 3.09	KG10
LeoII-099	3	11:13:24.89	22:07:20.40	2455597.9	79.17± 2.17	S17a
LeoII-099	3	11:13:24.89	22:07:20.40	2456340.9	77.89± 0.99	S17a
LeoII-099	3	11:13:24.88	22:07:20.40	2453770.0	65.68± 2.79	KG10
LeoII-100	3	11:13:25.21	22:03:27.36	2454526.8	84.78± 0.62	S17a
LeoII-100	3	11:13:25.21	22:03:27.36	2455597.9	85.87± 0.67	S17a
LeoII-100	3	11:13:25.21	22:03:27.50	2453770.0	86.14± 2.33	KG10
LeoII-101	3	11:13:34.82	22:03:10.60	2454212.8	83.43± 2.20	S17a
LeoII-101	3	11:13:34.82	22:03:10.60	2455591.9	85.33± 1.03	S17a
LeoII-101	3	11:13:34.83	22:03:10.70	2453770.0	82.92± 2.95	KG10
LeoII-102	4	11:12:54.52	22:06:13.54	2455597.9	58.85± 2.91	S17a
LeoII-102	4	11:12:54.52	22:06:13.54	2456340.9	65.52± 1.72	S17a
LeoII-102	4	11:12:54.52	22:06:13.54	2456341.9	63.85± 1.84	S17a
LeoII-102	4	11:12:54.54	22:06:13.70	2453770.0	64.10± 3.00	KG10
LeoII-103	2	11:13:07.59	22:09:30.22	2455597.9	70.10± 1.09	S17a
LeoII-103	2	11:13:07.60	22:09:30.30	2453770.0	67.80± 2.49	KG10

Table F.1: Continued; Velocities of RGB stars in Leo II

Star ID	n	α_{J2000} (hh:mm:ss.ss)	δ_{J2000} (dd:mm:ss.ss)	HJD (days)	v (km s ⁻¹)	Ref.
LeoII-104	2	11:13:03.80	22:05:46.93	2454526.8	70.11± 2.43	S17a
LeoII-104	2	11:13:03.81	22:05:46.90	2453770.0	73.37± 3.67	KG10
LeoII-105	2	11:13:13.75	22:04:19.20	2456341.9	77.97± 1.29	S17a
LeoII-105	2	11:13:13.76	22:04:19.20	2453770.0	80.19± 3.33	KG10
LeoII-106	2	11:13:07.04	22:09:27.10	2456341.9	77.14± 1.71	S17a
LeoII-106	2	11:13:07.05	22:09:27.20	2453770.0	83.55± 4.72	KG10
LeoII-107	2	11:13:31.20	22:08:24.55	2454212.8	69.81± 0.99	S17a
LeoII-107	2	11:13:31.21	22:08:24.70	2453770.0	68.43± 2.18	KG10
LeoII-108	3	11:13:29.60	22:08:57.70	2454526.8	82.94± 1.39	S17a
LeoII-108	3	11:13:29.60	22:08:57.80	2453770.0	84.39± 2.14	KG10
LeoII-108	3	11:13:29.57	22:08:57.44	2449432.0	85.14± 2.40	V95
LeoII-109	4	11:13:40.43	22:12:18.39	2453850.7	81.84± 1.38	S17a
LeoII-109	4	11:13:40.43	22:12:18.39	2455591.9	81.19± 0.54	S17a
LeoII-109	4	11:13:40.43	22:12:18.39	2455599.8	82.41± 1.50	S17a
LeoII-109	4	11:13:40.44	22:12:18.50	2453770.0	81.48± 2.13	KG10
LeoII-110	2	11:13:17.79	22:09:06.57	2456340.9	78.71± 0.69	S17a
LeoII-110	2	11:13:17.79	22:09:06.70	2453770.0	79.17± 2.15	KG10
LeoII-111	2	11:13:15.52	22:09:00.83	2454526.8	79.39± 1.16	S17a
LeoII-111	2	11:13:15.53	22:09:01.00	2453770.0	80.99± 2.18	KG10
LeoII-112	2	11:13:23.67	22:09:12.65	2455597.9	62.13± 1.15	S17a
LeoII-112	2	11:13:23.67	22:09:12.80	2453770.0	62.15± 2.33	KG10
LeoII-113	2	11:13:23.21	22:09:50.30	2455591.9	75.71± 0.59	S17a
LeoII-113	2	11:13:23.21	22:09:50.40	2453770.0	76.99± 2.20	KG10
LeoII-114	3	11:13:24.19	22:06:15.23	2455597.9	92.50± 0.91	S17a
LeoII-114	3	11:13:24.19	22:06:15.23	2456341.9	94.80± 0.96	S17a
LeoII-114	3	11:13:24.19	22:06:15.40	2453770.0	94.48± 2.68	KG10
LeoII-115	2	11:13:25.10	22:12:35.46	2454212.8	83.62± 2.57	S17a
LeoII-115	2	11:13:25.10	22:12:35.60	2453770.0	83.22± 2.21	KG10
LeoII-116	3	11:13:25.47	22:13:26.11	2453850.7	91.57± 0.87	S17a
LeoII-116	3	11:13:25.47	22:13:26.11	2456340.9	90.98± 0.78	S17a
LeoII-116	3	11:13:25.48	22:13:26.20	2453770.0	96.65± 2.14	KG10
LeoII-117	2	11:13:30.46	22:08:14.57	2456340.9	79.23± 1.52	S17a
LeoII-117	2	11:13:30.46	22:08:14.60	2453770.0	81.19± 2.93	KG10
LeoII-118	2	11:13:29.78	22:11:18.78	2456341.9	82.71± 1.54	S17a
LeoII-118	2	11:13:29.78	22:11:19.00	2453770.0	76.25± 2.50	KG10
LeoII-119	2	11:13:31.99	22:07:39.40	2456340.9	76.90± 1.85	S17a
LeoII-119	2	11:13:32.00	22:07:39.50	2453770.0	75.16± 3.13	KG10

Table F.1: Continued; Velocities of RGB stars in Leo II

Star ID	n	α_{J2000} (hh:mm:ss.ss)	δ_{J2000} (dd:mm:ss.ss)	HJD (days)	v (km s ⁻¹)	Ref.
LeoII-120	2	11:13:32.64	22:07:04.63	2454212.8	75.25 ± 0.77	S17a
LeoII-120	2	11:13:32.64	22:07:04.70	2453770.0	79.32 ± 2.19	KG10
LeoII-121	2	11:13:36.36	22:09:23.66	2453850.7	72.61 ± 0.95	S17a
LeoII-121	2	11:13:36.36	22:09:23.80	2453770.0	66.58 ± 2.19	KG10
LeoII-122	2	11:13:38.52	22:09:47.26	2455591.9	76.27 ± 0.65	S17a
LeoII-122	2	11:13:38.52	22:09:47.40	2453770.0	76.30 ± 2.33	KG10
LeoII-123	2	11:13:39.46	22:09:16.77	2454212.8	82.94 ± 0.69	S17a
LeoII-123	2	11:13:39.47	22:09:16.90	2453770.0	87.72 ± 2.13	KG10
LeoII-124	2	11:13:41.61	22:07:37.66	2454526.8	79.22 ± 1.51	S17a
LeoII-124	2	11:13:41.62	22:07:37.70	2453770.0	78.92 ± 2.21	KG10
LeoII-125	2	11:13:19.05	22:06:45.03	2456341.9	76.94 ± 1.36	S17a
LeoII-125	2	11:13:19.05	22:06:45.20	2453770.0	80.18 ± 2.34	KG10
LeoII-126	2	11:13:27.27	22:07:05.69	2454212.8	83.72 ± 1.47	S17a
LeoII-126	2	11:13:27.27	22:07:05.80	2453770.0	66.70 ± 2.24	KG10
LeoII-127	3	11:13:27.94	22:07:23.11	2455591.9	78.20 ± 0.86	S17a
LeoII-127	3	11:13:27.94	22:07:23.11	2456340.9	79.04 ± 1.14	S17a
LeoII-127	3	11:13:27.95	22:07:23.30	2453770.0	77.58 ± 3.52	KG10
LeoII-128	2	11:13:38.31	22:09:08.46	2455597.9	75.81 ± 1.93	S17a
LeoII-128	2	11:13:38.31	22:09:08.60	2453770.0	78.29 ± 2.30	KG10
LeoII-129	2	11:13:40.24	22:10:43.93	2454212.8	65.60 ± 0.96	S17a
LeoII-129	2	11:13:40.25	22:10:44.10	2453770.0	66.65 ± 2.52	KG10
LeoII-130	2	11:13:42.44	22:10:51.21	2455591.9	72.15 ± 1.06	S17a
LeoII-130	2	11:13:42.45	22:10:51.40	2453770.0	64.01 ± 2.71	KG10
LeoII-131	2	11:13:51.51	22:09:02.14	2455591.9	82.80 ± 1.85	S17a
LeoII-131	2	11:13:51.53	22:09:02.20	2453770.0	82.15 ± 2.59	KG10
LeoII-132	2	11:13:14.46	22:14:02.71	2454526.8	78.76 ± 1.57	S17a
LeoII-132	2	11:13:14.47	22:14:02.90	2453770.0	79.87 ± 2.61	KG10
LeoII-133	2	11:13:42.01	22:10:14.42	2455591.9	73.34 ± 1.54	S17a
LeoII-133	2	11:13:42.01	22:10:14.50	2453770.0	75.88 ± 2.65	KG10
LeoII-134	3	11:13:53.34	22:14:45.84	2455597.9	85.34 ± 1.36	S17a
LeoII-134	3	11:13:53.34	22:14:45.84	2456340.9	82.20 ± 1.01	S17a
LeoII-134	3	11:13:53.35	22:14:45.80	2453770.0	77.66 ± 2.19	KG10
LeoII-135	6	11:14:03.89	22:10:29.22	2453850.7	85.88 ± 1.29	S17a
LeoII-135	6	11:14:03.89	22:10:29.22	2455591.9	84.79 ± 0.58	S17a
LeoII-135	6	11:14:03.89	22:10:29.22	2455597.9	87.77 ± 0.97	S17a
LeoII-135	6	11:14:03.89	22:10:29.22	2456340.9	85.82 ± 0.78	S17a
LeoII-135	6	11:14:03.89	22:10:29.22	2456341.9	84.64 ± 0.79	S17a

Table F.1: Continued; Velocities of RGB stars in Leo II

Star ID	n	α_{J2000} (hh:mm:ss.ss)	δ_{J2000} (dd:mm:ss.ss)	HJD (days)	v (km s ⁻¹)	Ref.
LeoII-135	6	11:14:03.90	22:10:29.40	2453770.0	83.70± 2.25	KG10
LeoII-136	2	11:13:12.05	22:03:23.98	2455591.9	79.12± 1.91	S17a
LeoII-136	2	11:13:12.05	22:03:23.98	2456341.9	83.21± 1.86	S17a
LeoII-137	3	11:13:26.04	22:03:00.78	2455591.9	79.01± 1.30	S17a
LeoII-137	3	11:13:26.04	22:03:00.78	2456340.9	79.33± 1.43	S17a
LeoII-137	3	11:13:26.04	22:03:00.78	2456341.9	80.38± 1.54	S17a
LeoII-138	2	11:13:05.69	22:07:06.01	2454526.8	97.85± 1.07	S17a
LeoII-138	2	11:13:05.69	22:07:06.01	2455597.9	79.08± 1.46	S17a
LeoII-139	2	11:13:29.65	22:11:20.09	2455591.9	78.36± 0.71	S17a
LeoII-139	2	11:13:29.65	22:11:20.09	2456340.9	75.75± 1.23	S17a
LeoII-140	2	11:13:37.11	22:09:33.16	2454526.8	101.16± 1.50	S17a
LeoII-140	2	11:13:37.11	22:09:33.16	2455591.9	72.92± 0.65	S17a
LeoII-141	2	11:13:33.81	22:10:03.33	2454526.8	86.52± 1.50	S17a
LeoII-141	2	11:13:33.81	22:10:03.33	2456340.9	90.02± 1.09	S17a
LeoII-142	2	11:13:34.44	22:11:42.54	2453850.7	83.52± 0.88	S17a
LeoII-142	2	11:13:34.44	22:11:42.54	2455599.8	82.79± 1.25	S17a
LeoII-143	2	11:13:34.72	22:11:01.97	2455591.9	86.01± 0.73	S17a
LeoII-143	2	11:13:34.72	22:11:01.97	2456341.9	83.87± 1.12	S17a
LeoII-144	3	11:13:33.27	22:11:23.60	2452693.2	103.01± 13.67	KK07
LeoII-144	3	11:13:33.27	22:11:23.60	2452704.2	84.05± 2.79	KK07
LeoII-144	3	11:13:33.26	22:11:23.70	2453770.0	84.01± 2.24	KG10
LeoII-145	3	11:13:36.18	22:10:18.80	2452693.2	81.56± 16.42	KK07
LeoII-145	3	11:13:36.18	22:10:18.80	2453061.2	82.12± 1.45	KK07
LeoII-145	3	11:13:36.17	22:10:18.80	2453770.0	83.93± 2.19	KG10
LeoII-146	2	11:13:40.68	22:08:46.90	2452704.2	81.34± 6.24	KK07
LeoII-146	2	11:13:40.67	22:08:46.90	2453770.0	83.89± 2.33	KG10
LeoII-147	2	11:13:35.82	22:09:35.32	2453061.2	84.87± 1.10	KK07
LeoII-147	2	11:13:35.80	22:09:35.30	2453770.0	79.69± 2.13	KG10
LeoII-148	3	11:13:23.43	22:06:18.00	2452704.2	92.52± 2.75	KK07
LeoII-148	3	11:13:23.43	22:06:18.00	2453061.2	86.24± 2.21	KK07
LeoII-148	3	11:13:23.42	22:06:18.00	2453770.0	88.84± 2.26	KG10
LeoII-149	3	11:13:17.07	22:05:16.12	2452704.2	73.90± 2.79	KK07
LeoII-149	3	11:13:17.07	22:05:16.12	2453061.2	81.46± 1.87	KK07
LeoII-149	3	11:13:17.06	22:05:16.10	2453770.0	75.31± 2.80	KG10
LeoII-150	2	11:13:34.46	22:11:05.71	2452693.2	78.34± 17.65	KK07
LeoII-150	2	11:13:34.44	22:11:05.70	2453770.0	72.88± 2.27	KG10
LeoII-151	2	11:13:28.60	22:08:38.00	2453061.2	89.75± 2.57	KK07

Table F.1: Continued; Velocities of RGB stars in Leo II

Star ID	n	α_{J2000} (hh:mm:ss.ss)	δ_{J2000} (dd:mm:ss.ss)	HJD (days)	v (km s ⁻¹)	Ref.
LeoII-151	2	11:13:28.59	22:08:38.00	2453770.0	92.02± 2.42	KG10
LeoII-152	3	11:13:36.81	22:06:48.38	2452704.2	75.72± 2.71	KK07
LeoII-152	3	11:13:36.81	22:06:48.38	2453061.2	71.35± 1.31	KK07
LeoII-152	3	11:13:36.80	22:06:48.50	2453770.0	81.01± 2.52	KG10
LeoII-153	2	11:13:18.96	22:07:13.69	2453061.2	97.33± 1.65	KK07
LeoII-153	2	11:13:18.95	22:07:13.80	2453770.0	82.96± 2.84	KG10
LeoII-154	3	11:13:28.76	22:13:11.89	2452693.2	71.12± 2.66	KK07
LeoII-154	3	11:13:28.76	22:13:11.89	2452704.2	71.13± 2.85	KK07
LeoII-154	3	11:13:28.76	22:13:11.90	2453770.0	69.18± 2.12	KG10
LeoII-155	2	11:13:44.66	22:08:25.40	2453061.2	71.37± 1.38	KK07
LeoII-155	2	11:13:44.66	22:08:25.40	2453770.0	67.53± 2.30	KG10
LeoII-156	2	11:13:24.55	22:12:48.49	2452704.2	83.34± 4.60	KK07
LeoII-156	2	11:13:24.54	22:12:48.60	2453770.0	81.77± 2.29	KG10
LeoII-157	2	11:13:46.45	22:07:09.08	2452704.2	85.78± 2.63	KK07
LeoII-157	2	11:13:46.45	22:07:09.10	2453770.0	82.63± 2.37	KG10
LeoII-158	3	11:13:36.34	22:11:32.89	2452693.2	68.73± 13.01	KK07
LeoII-158	3	11:13:36.34	22:11:32.89	2453061.2	85.43± 2.32	KK07
LeoII-158	3	11:13:36.33	22:11:32.90	2453770.0	86.76± 2.51	KG10
LeoII-159	2	11:13:38.89	22:09:47.02	2453061.2	68.76± 1.16	KK07
LeoII-159	2	11:13:38.87	22:09:47.00	2453770.0	66.72± 2.31	KG10
LeoII-160	3	11:13:17.36	22:06:04.00	2452704.2	70.51± 11.82	KK07
LeoII-160	3	11:13:17.36	22:06:04.00	2453061.2	71.05± 1.91	KK07
LeoII-160	3	11:13:17.35	22:06:04.00	2453770.0	70.39± 2.49	KG10
LeoII-161	3	11:13:39.94	22:07:16.28	2452693.2	57.09± 20.71	KK07
LeoII-161	3	11:13:39.94	22:07:16.28	2452704.2	84.68± 3.05	KK07
LeoII-161	3	11:13:39.93	22:07:16.30	2453770.0	84.46± 2.37	KG10
LeoII-162	2	11:13:57.05	22:12:16.60	2453061.2	84.70± 2.82	KK07
LeoII-162	2	11:13:57.05	22:12:16.50	2453770.0	89.31± 2.54	KG10
LeoII-163	3	11:13:28.43	22:11:09.82	2452704.2	80.51± 10.91	KK07
LeoII-163	3	11:13:28.43	22:11:09.82	2453061.2	80.51± 1.87	KK07
LeoII-163	3	11:13:28.42	22:11:09.90	2453770.0	80.36± 2.64	KG10
LeoII-164	2	11:13:20.54	22:12:11.92	2452704.2	81.33± 12.16	KK07
LeoII-164	2	11:13:20.53	22:12:12.00	2453770.0	77.39± 2.44	KG10
LeoII-165	3	11:13:44.81	22:09:36.90	2452704.2	90.60± 11.18	KK07
LeoII-165	3	11:13:44.81	22:09:36.90	2453061.2	83.56± 2.21	KK07
LeoII-165	3	11:13:44.80	22:09:36.80	2453770.0	87.62± 2.65	KG10
LeoII-166	3	11:13:35.94	22:08:29.40	2452704.2	84.69± 4.45	KK07

Table F.1: Continued; Velocities of RGB stars in Leo II

Star ID	n	α_{J2000} (hh:mm:ss.ss)	δ_{J2000} (dd:mm:ss.ss)	HJD (days)	v (km s ⁻¹)	Ref.
LeoII-166	3	11:13:35.94	22:08:29.40	2453061.2	85.84± 2.46	KK07
LeoII-166	3	11:13:35.93	22:08:29.40	2453770.0	91.42± 3.95	KG10
LeoII-167	2	11:13:27.99	22:11:47.18	2452704.2	77.19± 10.67	KK07
LeoII-167	2	11:13:27.99	22:11:47.30	2453770.0	73.74± 2.47	KG10
LeoII-168	3	11:13:36.70	22:08:10.79	2452704.2	74.69± 28.33	KK07
LeoII-168	3	11:13:36.70	22:08:10.79	2453061.2	84.30± 2.30	KK07
LeoII-168	3	11:13:36.68	22:08:10.80	2453770.0	87.96± 3.39	KG10
LeoII-169	2	11:13:18.54	22:04:47.10	2452704.2	84.04± 1.54	KK07
LeoII-169	2	11:13:18.53	22:04:47.20	2453770.0	85.52± 2.23	KG10
LeoII-170	4	11:13:25.70	22:06:37.69	2452693.2	57.09± 10.85	KK07
LeoII-170	4	11:13:25.70	22:06:37.69	2453061.2	63.77± 1.70	KK07
LeoII-170	4	11:13:25.69	22:06:37.80	2453770.0	65.04± 2.22	KG10
LeoII-170	4	11:13:25.68	22:06:37.80	2449431.9	64.44± 3.70	V95
LeoII-171	3	11:13:19.26	22:07:41.59	2452704.2	84.61± 2.19	KK07
LeoII-171	3	11:13:19.25	22:07:41.60	2453770.0	83.68± 2.14	KG10
LeoII-171	3	11:13:19.28	22:07:41.59	2449432.1	77.24± 3.40	V95
LeoII-172	2	11:13:16.15	22:11:47.18	2452704.2	68.17± 3.46	KK07
LeoII-172	2	11:13:16.14	22:11:47.30	2453770.0	69.66± 2.15	KG10
LeoII-173	3	11:13:22.19	22:06:10.19	2452693.2	89.78± 9.01	KK07
LeoII-173	3	11:13:22.19	22:06:10.19	2452704.2	85.28± 2.21	KK07
LeoII-173	3	11:13:22.18	22:06:10.30	2453770.0	84.12± 2.15	KG10
LeoII-174	3	11:13:13.14	22:09:59.11	2452704.2	86.03± 2.57	KK07
LeoII-174	3	11:13:13.14	22:09:59.11	2453061.2	85.32± 1.35	KK07
LeoII-174	3	11:13:13.12	22:09:59.10	2453770.0	85.36± 2.17	KG10
LeoII-175	3	11:13:19.00	22:13:47.71	2452693.2	71.92± 10.40	KK07
LeoII-175	3	11:13:19.00	22:13:47.71	2453061.2	72.90± 1.20	KK07
LeoII-175	3	11:13:19.00	22:13:47.80	2453770.0	75.27± 2.14	KG10
LeoII-176	2	11:13:33.10	22:07:37.60	2453061.2	92.75± 1.14	KK07
LeoII-176	2	11:13:33.09	22:07:37.60	2453770.0	92.87± 2.14	KG10
LeoII-177	3	11:13:13.37	22:07:26.00	2452693.2	75.93± 15.38	KK07
LeoII-177	3	11:13:13.37	22:07:26.00	2453061.2	72.46± 0.98	KK07
LeoII-177	3	11:13:13.36	22:07:26.10	2453770.0	71.81± 2.42	KG10
LeoII-178	2	11:13:22.67	22:06:58.00	2453061.2	83.50± 1.14	KK07
LeoII-178	2	11:13:22.65	22:06:58.10	2453770.0	83.13± 2.15	KG10
LeoII-179	2	11:13:32.48	22:11:22.99	2453061.2	73.64± 1.28	KK07
LeoII-179	2	11:13:32.47	22:11:23.00	2453770.0	73.86± 2.24	KG10
LeoII-180	3	11:13:35.56	22:09:06.19	2452693.2	75.67± 8.59	KK07

Table F.1: Continued; Velocities of RGB stars in Leo II

Star ID	n	α_{J2000} (hh:mm:ss.ss)	δ_{J2000} (dd:mm:ss.ss)	HJD (days)	v (km s ⁻¹)	Ref.
LeoII-180	3	11:13:35.54	22:09:06.30	2453770.0	84.27± 2.14	KG10
LeoII-180	3	11:13:35.48	22:09:05.95	2449431.8	82.64± 1.80	V95
LeoII-181	4	11:13:25.93	22:08:58.88	2452693.2	67.36± 3.76	KK07
LeoII-181	4	11:13:25.93	22:08:58.88	2452704.2	70.43± 2.70	KK07
LeoII-181	4	11:13:25.93	22:08:58.88	2453061.2	70.65± 1.11	KK07
LeoII-181	4	11:13:25.90	22:08:58.59	2449430.9	70.64± 1.80	V95
LeoII-182	3	11:13:29.68	22:06:46.51	2452704.2	72.34± 2.39	KK07
LeoII-182	3	11:13:29.68	22:06:46.51	2453061.2	72.74± 0.99	KK07
LeoII-182	3	11:13:29.64	22:06:46.54	2449432.8	76.44± 1.80	V95
LeoII-183	2	11:13:24.07	22:09:02.81	2452693.2	72.01± 14.31	KK07
LeoII-183	2	11:13:24.06	22:09:02.42	2449432.9	75.14± 2.10	V95
LeoII-184	2	11:13:34.45	22:09:32.00	2452704.2	80.78± 4.48	KK07
LeoII-184	2	11:13:34.45	22:09:32.00	2453061.2	75.40± 2.25	KK07
LeoII-185	2	11:13:26.95	22:11:50.10	2452704.2	75.92± 4.53	KK07
LeoII-185	2	11:13:26.95	22:11:50.10	2453061.2	70.15± 2.21	KK07
LeoII-186	2	11:13:23.00	22:09:22.72	2452693.2	77.31± 3.71	KK07
LeoII-186	2	11:13:23.00	22:09:22.72	2452704.2	78.81± 9.36	KK07
LeoII-187	2	11:13:20.98	22:08:00.89	2452704.2	79.69± 3.76	KK07
LeoII-187	2	11:13:20.98	22:08:00.89	2453061.2	78.30± 2.02	KK07
LeoII-188	2	11:13:17.97	22:09:53.39	2452704.2	75.92± 20.36	KK07
LeoII-188	2	11:13:17.97	22:09:53.39	2453061.2	73.43± 2.16	KK07
LeoII-189	2	11:13:18.57	22:07:58.30	2452704.2	93.18± 27.84	KK07
LeoII-189	2	11:13:18.57	22:07:58.30	2453061.2	92.42± 2.19	KK07
LeoII-190	2	11:13:34.11	22:13:00.98	2452693.2	75.79± 12.94	KK07
LeoII-190	2	11:13:34.11	22:13:00.98	2452704.2	80.80± 10.90	KK07
LeoII-191	2	11:13:34.73	22:10:07.50	2452704.2	78.83± 3.62	KK07
LeoII-191	2	11:13:34.73	22:10:07.50	2453061.2	90.75± 2.29	KK07
LeoII-192	2	11:13:29.14	22:06:04.72	2452704.2	66.63± 6.69	KK07
LeoII-192	2	11:13:29.14	22:06:04.72	2453061.2	68.22± 2.34	KK07
LeoII-193	2	11:13:41.63	22:08:52.40	2452704.2	69.45± 8.94	KK07
LeoII-193	2	11:13:41.63	22:08:52.40	2453061.2	68.49± 2.28	KK07
LeoII-194	2	11:13:24.36	22:10:58.51	2452693.2	82.52± 23.34	KK07
LeoII-194	2	11:13:24.36	22:10:58.51	2453061.2	89.95± 2.41	KK07
LeoII-195	2	11:13:30.89	22:09:32.80	2452704.2	71.71± 2.77	KK07
LeoII-195	2	11:13:30.89	22:09:32.80	2453061.2	72.58± 1.50	KK07
LeoII-196	2	11:13:31.58	22:08:34.20	2453770.0	70.95± 2.19	KG10
LeoII-196	2	11:13:31.54	22:08:33.91	2449432.0	67.34± 3.30	V95

APPENDIX G

Velocities of Stars in Draco

We collected velocity data for 341 stars in Draco that had more than one epoch of observations. This amounted to 1204 velocity measurements. We applied offsets to these velocity data to put them all on the same velocity standard as Walker et al. (2015b). As such, the velocities we report in the following table will not match the values listed in the original papers. Column 1 lists the identifier that we assign to the star; column 2 lists the number of observations; column 3 lists the right ascension; column 4 lists the declination; column 5 lists the heliocentric Julian date; column 6 lists the radial velocity and error; and column 7 lists the paper where the velocity measurement originated from. “W15” is in reference to Walker et al. (2015b); “K10” is Kirby et al. (2010); “W04” is Wilkinson et al. (2004); “K02” is Kleyana et al. (2002); “A95” is Armandroff et al. (1995); and “O95” is Olszewski et al. (1995).

Table G.1: Velocities of RGB stars in Draco

Star ID	n	α_{J2000} (hh:mm:ss.ss)	δ_{J2000} (dd:mm:ss.ss)	HJD (days)	v (km s ⁻¹)	Ref.
Draco-001	2	17:15:36.04	57:48:34.40	2455707.8	-287.1± 1.4	W15
Draco-001	2	17:15:36.04	57:48:34.40	2455712.8	-289.2± 1.4	W15
Draco-002	2	17:15:41.94	57:37:05.50	2455707.8	-299.5± 2.2	W15
Draco-002	2	17:15:41.94	57:37:05.50	2455712.8	-299.0± 1.7	W15

Table G.1: Continued. Velocities of RGB stars in Draco

Star ID	n	α_{J2000} (hh:mm:ss.ss)	δ_{J2000} (dd:mm:ss.ss)	HJD (days)	v (km s ⁻¹)	Ref.
Draco-003	2	17:16:01.59	57:59:19.10	2455707.8	-282.9± 0.8	W15
Draco-003	2	17:16:01.59	57:59:19.10	2452813.0	-285.2± 3.0	W04
Draco-004	2	17:16:27.79	57:48:08.59	2455332.7	-283.6± 0.9	W15
Draco-004	2	17:16:27.81	57:48:08.64	2452813.0	-284.4± 0.8	W04
Draco-005	3	17:16:40.45	57:55:08.00	2454912.0	-276.3± 0.6	W15
Draco-005	3	17:16:40.45	57:55:08.00	2454914.9	-275.6± 0.7	W15
Draco-005	3	17:16:40.45	57:55:07.97	2452813.0	-275.9± 1.4	W04
Draco-006	2	17:16:55.62	57:47:16.79	2454524.0	-306.9± 1.6	W15
Draco-006	2	17:16:55.61	57:47:16.73	2452813.0	-297.9± 1.6	W04
Draco-007	3	17:16:59.67	57:49:33.60	2454159.0	-300.3± 2.0	W15
Draco-007	3	17:16:59.67	57:49:33.60	2454170.9	-298.1± 2.2	W15
Draco-007	3	17:16:59.67	57:49:33.60	2455707.2	-300.6± 1.2	W15
Draco-008	4	17:17:05.97	57:59:33.50	2454159.0	-275.6± 1.6	W15
Draco-008	4	17:17:05.97	57:59:33.50	2454170.9	-276.5± 1.5	W15
Draco-008	4	17:17:05.97	57:59:33.50	2455707.3	-274.2± 0.8	W15
Draco-008	4	17:17:05.98	57:59:33.47	2452813.0	-273.4± 3.8	W04
Draco-009	4	17:17:14.11	58:10:48.50	2454165.9	-282.5± 1.1	W15
Draco-009	4	17:17:14.11	58:10:48.50	2455332.9	-282.7± 1.5	W15
Draco-009	4	17:17:14.11	58:10:48.50	2455591.0	-282.4± 1.5	W15
Draco-009	4	17:17:14.11	58:10:48.50	2455707.1	-284.6± 0.6	W15
Draco-010	2	17:17:19.80	57:57:39.40	2455331.8	-279.7± 1.6	W15
Draco-010	2	17:17:19.80	57:57:39.40	2455707.3	-281.7± 0.6	W15
Draco-011	4	17:17:20.93	58:01:57.31	2454524.0	-277.7± 1.5	W15
Draco-011	4	17:17:20.93	58:01:57.31	2454912.0	-275.3± 0.5	W15
Draco-011	4	17:17:20.93	58:01:57.31	2454914.9	-276.6± 0.5	W15
Draco-011	4	17:17:20.93	58:01:57.25	2452813.0	-269.7± 3.6	W04
Draco-012	5	17:17:22.24	58:07:25.40	2454165.9	-285.0± 0.6	W15
Draco-012	5	17:17:22.24	58:07:25.40	2455331.7	-286.4± 0.8	W15
Draco-012	5	17:17:22.24	58:07:25.40	2455707.6	-285.7± 0.2	W15
Draco-012	5	17:17:22.24	58:07:25.40	2455711.8	-285.9± 0.4	W15
Draco-012	5	17:17:22.24	58:07:25.43	2452813.0	-283.8± 2.1	W04
Draco-013	5	17:17:33.65	57:41:01.99	2454168.9	-295.6± 1.3	W15
Draco-013	5	17:17:33.65	57:41:01.99	2455332.9	-298.1± 1.5	W15
Draco-013	5	17:17:33.65	57:41:01.99	2455707.8	-296.1± 1.6	W15
Draco-013	5	17:17:33.65	57:41:01.99	2455710.8	-298.6± 3.4	W15
Draco-013	5	17:17:33.65	57:41:02.00	2452813.0	-290.6± 7.4	W04
Draco-014	2	17:17:38.58	58:04:39.09	2454165.9	-265.6± 0.5	W15

Table G.1: Continued. Velocities of RGB stars in Draco

Star ID	n	α_{J2000} (hh:mm:ss.ss)	δ_{J2000} (dd:mm:ss.ss)	HJD (days)	v (km s ⁻¹)	Ref.
Draco-014	2	17:17:38.58	58:04:38.40	2451720.5	-266.9± 0.8	K02
Draco-015	5	17:17:38.60	57:58:54.60	2454524.0	-288.7± 1.5	W15
Draco-015	5	17:17:38.60	57:58:54.60	2455332.7	-292.5± 1.8	W15
Draco-015	5	17:17:38.60	57:58:54.60	2455707.8	-290.8± 0.6	W15
Draco-015	5	17:17:38.60	57:58:54.59	2451720.5	-285.4± 3.4	K02
Draco-015	5	17:17:38.60	57:58:54.59	2452813.0	-290.3± 1.4	W04
Draco-016	8	17:17:46.16	57:42:21.91	2454155.0	-300.0± 0.8	W15
Draco-016	8	17:17:46.16	57:42:21.91	2454159.0	-298.3± 0.7	W15
Draco-016	8	17:17:46.16	57:42:21.91	2454170.9	-299.5± 0.6	W15
Draco-016	8	17:17:46.16	57:42:21.91	2454168.9	-298.8± 0.6	W15
Draco-016	8	17:17:46.16	57:42:21.91	2455332.8	-299.4± 0.6	W15
Draco-016	8	17:17:46.16	57:42:21.91	2455707.8	-299.2± 0.5	W15
Draco-016	8	17:17:46.17	57:42:21.89	2451720.5	-298.9± 0.9	K02
Draco-016	8	17:17:46.17	57:42:21.89	2452813.0	-295.3± 1.6	W04
Draco-017	4	17:17:55.37	57:55:59.10	2455708.4	-289.8± 0.4	W15
Draco-017	4	17:17:55.37	57:55:59.10	2455712.9	-289.6± 0.7	W15
Draco-017	4	17:17:55.37	57:55:59.12	2451720.5	-291.3± 1.3	K02
Draco-017	4	17:17:55.37	57:55:59.12	2452813.0	-293.4± 2.5	W04
Draco-018	2	17:17:56.48	57:54:00.71	2454912.0	-287.7± 1.0	W15
Draco-018	2	17:17:56.48	57:54:00.71	2454914.9	-287.5± 1.1	W15
Draco-019	5	17:17:58.39	58:05:59.20	2454165.9	-298.1± 0.6	W15
Draco-019	5	17:17:58.39	58:05:59.20	2455332.3	-297.7± 0.6	W15
Draco-019	5	17:17:58.39	58:05:59.20	2455707.1	-298.2± 0.3	W15
Draco-019	5	17:17:58.38	58:05:59.21	2451720.5	-297.7± 3.4	K02
Draco-019	5	17:17:58.38	58:05:59.21	2452813.0	-298.3± 1.3	W04
Draco-020	2	17:17:59.93	57:56:41.70	2455591.0	-301.5± 2.5	W15
Draco-020	2	17:17:59.93	57:56:41.70	2455706.9	-303.3± 1.9	W15
Draco-021	2	17:18:04.17	58:06:07.70	2454914.9	-290.7± 1.6	W15
Draco-021	2	17:18:04.17	58:06:07.70	2455707.2	-292.8± 1.0	W15
Draco-022	8	17:18:05.76	58:11:22.50	2454155.0	-288.0± 0.9	W15
Draco-022	8	17:18:05.76	58:11:22.50	2454159.0	-288.9± 0.7	W15
Draco-022	8	17:18:05.76	58:11:22.50	2454170.9	-290.1± 0.5	W15
Draco-022	8	17:18:05.76	58:11:22.50	2454165.9	-289.4± 0.6	W15
Draco-022	8	17:18:05.76	58:11:22.50	2455707.6	-289.4± 0.3	W15
Draco-022	8	17:18:05.76	58:11:22.50	2455712.9	-289.2± 0.9	W15
Draco-022	8	17:18:05.74	58:11:22.45	2451720.5	-286.4± 1.9	K02
Draco-022	8	17:18:05.74	58:11:22.45	2452813.0	-286.6± 2.8	W04

Table G.1: Continued. Velocities of RGB stars in Draco

Star ID	n	α_{J2000} (hh:mm:ss.ss)	δ_{J2000} (dd:mm:ss.ss)	HJD (days)	v (km s ⁻¹)	Ref.
Draco-023	4	17:18:06.28	58:01:55.40	2454155.0	-299.2± 1.1	W15
Draco-023	4	17:18:06.28	58:01:55.40	2454159.0	-299.0± 0.9	W15
Draco-023	4	17:18:06.28	58:01:55.40	2454165.9	-298.7± 0.6	W15
Draco-023	4	17:18:06.28	58:01:55.40	2454170.9	-298.8± 0.7	W15
Draco-024	6	17:18:08.07	58:01:46.90	2454912.0	-309.4± 0.5	W15
Draco-024	6	17:18:08.07	58:01:46.90	2454914.9	-308.9± 0.5	W15
Draco-024	6	17:18:08.07	58:01:46.90	2455706.9	-309.3± 0.4	W15
Draco-024	6	17:18:08.07	58:01:46.88	2451720.5	-310.2± 0.5	K02
Draco-024	6	17:18:08.07	58:01:46.88	2452813.0	-309.3± 1.4	W04
Draco-024	6	17:18:08.02	58:01:46.10	2449457.9	-305.6± 4.5	A95
Draco-025	4	17:18:10.39	57:52:09.00	2455332.7	-309.2± 0.8	W15
Draco-025	4	17:18:10.39	57:52:09.00	2455706.8	-308.6± 0.4	W15
Draco-025	4	17:18:10.34	57:52:08.49	2449130.9	-306.2± 3.3	A95
Draco-025	4	17:18:10.34	57:52:08.49	2449457.9	-309.9± 1.5	A95
Draco-026	3	17:18:10.75	57:50:31.01	2455331.8	-298.2± 1.5	W15
Draco-026	3	17:18:10.75	57:50:31.01	2455707.8	-299.0± 1.1	W15
Draco-026	3	17:18:10.75	57:50:31.01	2455710.8	-296.4± 1.2	W15
Draco-027	5	17:18:13.01	57:42:46.60	2455331.8	-283.3± 0.9	W15
Draco-027	5	17:18:13.01	57:42:46.60	2455708.4	-283.1± 0.5	W15
Draco-027	5	17:18:13.01	57:42:46.60	2455712.9	-284.8± 0.8	W15
Draco-027	5	17:18:13.01	57:42:46.58	2451720.5	-286.8± 2.3	K02
Draco-027	5	17:18:13.01	57:42:46.58	2452813.0	-280.9± 1.6	W04
Draco-028	2	17:18:22.32	57:53:47.00	2454159.0	-283.7± 1.2	W15
Draco-028	2	17:18:22.32	57:53:47.00	2454170.9	-285.7± 1.3	W15
Draco-029	4	17:18:30.56	57:51:46.70	2455331.7	-286.9± 0.9	W15
Draco-029	4	17:18:30.56	57:51:46.70	2455710.8	-287.1± 0.6	W15
Draco-029	4	17:18:30.55	57:51:46.69	2451720.5	-282.9± 2.5	K02
Draco-029	4	17:18:30.55	57:51:46.69	2452813.0	-287.6± 2.6	W04
Draco-030	5	17:18:32.86	57:50:56.30	2454912.0	-285.2± 0.5	W15
Draco-030	5	17:18:32.86	57:50:56.30	2454914.9	-286.3± 0.5	W15
Draco-030	5	17:18:32.85	57:50:56.29	2451720.5	-289.7± 1.2	K02
Draco-030	5	17:18:32.85	57:50:56.29	2452813.0	-285.7± 1.2	W04
Draco-030	5	17:18:32.80	57:50:55.90	2449457.9	-284.4± 4.7	A95
Draco-031	2	17:18:33.63	57:58:36.81	2454912.0	-292.9± 0.9	W15
Draco-031	2	17:18:33.63	57:58:36.81	2454914.9	-293.4± 0.9	W15
Draco-032	2	17:18:35.69	58:00:50.40	2455707.3	-289.8± 0.5	W15
Draco-032	2	17:18:35.67	58:00:50.10	2451720.5	-289.4± 3.3	K02

Table G.1: Continued. Velocities of RGB stars in Draco

Star ID	n	α_{J2000} (hh:mm:ss.ss)	δ_{J2000} (dd:mm:ss.ss)	HJD (days)	v (km s ⁻¹)	Ref.
Draco-033	2	17:18:40.48	57:54:39.29	2455591.0	-290.3± 1.8	W15
Draco-033	2	17:18:40.48	57:54:39.29	2455706.9	-288.0± 1.2	W15
Draco-034	8	17:18:42.24	57:59:10.00	2454165.9	-289.2± 0.5	W15
Draco-034	8	17:18:42.24	57:59:10.00	2455332.9	-287.6± 0.5	W15
Draco-034	8	17:18:42.24	57:59:10.00	2455591.0	-288.1± 0.5	W15
Draco-034	8	17:18:42.24	57:59:10.00	2455707.5	-290.6± 0.2	W15
Draco-034	8	17:18:42.24	57:59:10.00	2455712.9	-290.8± 0.5	W15
Draco-034	8	17:18:42.24	57:59:09.96	2451720.5	-290.3± 0.8	K02
Draco-034	8	17:18:42.24	57:59:09.96	2452813.0	-289.7± 1.0	W04
Draco-034	8	17:18:42.18	57:59:09.30	2449457.9	-291.1± 4.2	A95
Draco-035	4	17:18:42.96	57:38:49.71	2454155.0	-301.5± 0.6	W15
Draco-035	4	17:18:42.96	57:38:49.71	2454168.9	-301.0± 0.5	W15
Draco-035	4	17:18:42.95	57:38:49.63	2451720.5	-296.3± 0.8	K02
Draco-035	4	17:18:42.95	57:38:49.63	2452813.0	-300.7± 1.5	W04
Draco-036	3	17:18:44.51	57:54:38.20	2455706.8	-285.1± 0.8	W15
Draco-036	3	17:18:44.52	57:54:38.16	2451720.5	-284.3± 1.2	K02
Draco-036	3	17:18:44.52	57:54:38.16	2452813.0	-282.4± 1.1	W04
Draco-037	3	17:18:45.55	58:04:56.30	2455591.0	-301.1± 2.0	W15
Draco-037	3	17:18:45.55	58:04:56.30	2455707.9	-300.3± 0.6	W15
Draco-037	3	17:18:45.55	58:04:56.30	2455712.9	-299.7± 1.1	W15
Draco-038	5	17:18:45.85	58:07:32.90	2454165.9	-275.5± 1.1	W15
Draco-038	5	17:18:45.85	58:07:32.90	2454912.0	-276.4± 0.9	W15
Draco-038	5	17:18:45.85	58:07:32.90	2454914.9	-277.2± 0.8	W15
Draco-038	5	17:18:45.85	58:07:32.90	2455707.8	-276.2± 0.7	W15
Draco-038	5	17:18:45.84	58:07:32.84	2451720.5	-265.5± 4.6	K02
Draco-039	2	17:18:49.58	57:55:00.70	2454159.0	-289.0± 1.5	W15
Draco-039	2	17:18:49.58	57:55:00.70	2454170.9	-292.9± 1.4	W15
Draco-040	4	17:18:50.86	57:41:37.40	2454168.9	-276.7± 1.2	W15
Draco-040	4	17:18:50.86	57:41:37.40	2455591.0	-280.5± 1.6	W15
Draco-040	4	17:18:50.86	57:41:37.40	2455707.7	-281.5± 0.6	W15
Draco-040	4	17:18:50.86	57:41:37.40	2455712.9	-279.2± 1.4	W15
Draco-041	2	17:18:51.31	57:42:16.00	2454912.0	-288.2± 0.8	W15
Draco-041	2	17:18:51.31	57:42:16.00	2454914.9	-288.1± 0.6	W15
Draco-042	5	17:18:52.10	58:04:12.90	2454912.0	-293.1± 0.4	W15
Draco-042	5	17:18:52.10	58:04:12.90	2454914.9	-293.0± 0.4	W15
Draco-042	5	17:18:52.11	58:04:12.94	2451720.5	-295.3± 0.8	K02
Draco-042	5	17:18:52.11	58:04:12.94	2452813.0	-296.1± 1.5	W04

Table G.1: Continued. Velocities of RGB stars in Draco

Star ID	n	α_{J2000} (hh:mm:ss.ss)	δ_{J2000} (dd:mm:ss.ss)	HJD (days)	v (km s ⁻¹)	Ref.
Draco-042	5	17:18:52.04	58:04:12.21	2449130.9	-292.1± 2.3	A95
Draco-043	4	17:18:53.47	57:58:26.00	2454155.0	-291.2± 1.1	W15
Draco-043	4	17:18:53.47	57:58:26.00	2454159.0	-291.9± 0.7	W15
Draco-043	4	17:18:53.47	57:58:26.00	2454170.9	-290.8± 0.6	W15
Draco-043	4	17:18:53.47	57:58:26.00	2454975.5	-289.9± 2.1	K10
Draco-044	2	17:18:54.51	57:50:05.50	2455706.9	-283.8± 1.5	W15
Draco-044	2	17:18:54.51	57:50:05.50	2455710.8	-284.8± 2.0	W15
Draco-045	4	17:18:56.08	57:43:45.31	2454168.9	-283.2± 0.8	W15
Draco-045	4	17:18:56.08	57:43:45.31	2455332.9	-285.2± 1.0	W15
Draco-045	4	17:18:56.07	57:43:45.26	2451720.5	-281.5± 3.7	K02
Draco-045	4	17:18:56.07	57:43:45.26	2452813.0	-284.4± 3.0	W04
Draco-046	3	17:18:56.14	58:10:07.30	2454914.9	-304.7± 1.9	W15
Draco-046	3	17:18:56.14	58:10:07.30	2455708.9	-304.1± 1.2	W15
Draco-046	3	17:18:56.14	58:10:07.30	2455710.8	-305.6± 1.6	W15
Draco-047	4	17:18:56.88	57:46:28.50	2454159.0	-293.4± 1.4	W15
Draco-047	4	17:18:56.88	57:46:28.50	2454168.9	-295.5± 1.1	W15
Draco-047	4	17:18:56.88	57:46:28.50	2454170.9	-292.9± 1.2	W15
Draco-047	4	17:18:56.87	57:46:28.45	2452813.0	-297.4± 4.1	W04
Draco-048	5	17:18:57.59	57:54:14.21	2454168.9	-278.3± 0.5	W15
Draco-048	5	17:18:57.59	57:54:14.21	2455332.7	-280.1± 0.9	W15
Draco-048	5	17:18:57.60	57:54:14.18	2451720.5	-278.4± 1.1	K02
Draco-048	5	17:18:57.60	57:54:14.18	2452813.0	-280.3± 1.5	W04
Draco-048	5	17:18:57.54	57:54:13.30	2449457.9	-272.6± 4.0	A95
Draco-049	5	17:18:58.27	57:48:57.61	2454155.0	-300.9± 0.5	W15
Draco-049	5	17:18:58.27	57:48:57.61	2454168.9	-300.5± 0.5	W15
Draco-049	5	17:18:58.27	57:48:57.56	2451720.5	-299.8± 0.7	K02
Draco-049	5	17:18:58.27	57:48:57.56	2452813.0	-298.5± 2.7	W04
Draco-049	5	17:18:58.24	57:48:56.80	2449130.9	-301.7± 4.8	A95
Draco-050	2	17:18:58.38	57:37:27.50	2455707.9	-289.5± 0.7	W15
Draco-050	2	17:18:58.38	57:37:27.50	2455710.8	-289.3± 1.1	W15
Draco-051	4	17:18:59.84	58:06:29.30	2454165.9	-286.7± 1.0	W15
Draco-051	4	17:18:59.84	58:06:29.30	2455331.8	-288.0± 1.0	W15
Draco-051	4	17:18:59.84	58:06:29.30	2455591.0	-287.4± 1.4	W15
Draco-051	4	17:18:59.84	58:06:29.30	2455706.8	-286.8± 0.8	W15
Draco-052	2	17:19:00.52	57:59:35.80	2455331.8	-305.4± 1.3	W15
Draco-052	2	17:19:00.51	57:59:35.80	2454975.5	-306.6± 2.4	K10
Draco-053	5	17:19:03.58	57:46:42.41	2454168.9	-289.2± 0.5	W15

Table G.1: Continued. Velocities of RGB stars in Draco

Star ID	n	α_{J2000} (hh:mm:ss.ss)	δ_{J2000} (dd:mm:ss.ss)	HJD (days)	v (km s ⁻¹)	Ref.
Draco-053	5	17:19:03.58	57:46:42.41	2455591.0	-289.8± 0.5	W15
Draco-053	5	17:19:03.57	57:46:42.42	2451720.5	-282.3± 1.9	K02
Draco-053	5	17:19:03.57	57:46:42.42	2452813.0	-289.6± 1.1	W04
Draco-053	5	17:19:03.54	57:46:41.60	2449130.9	-290.7± 3.4	A95
Draco-054	3	17:19:05.58	57:53:58.21	2454155.0	-290.7± 1.5	W15
Draco-054	3	17:19:05.58	57:53:58.21	2454168.9	-287.4± 0.8	W15
Draco-054	3	17:19:05.57	57:53:58.30	2454975.5	-286.6± 2.1	K10
Draco-055	5	17:19:07.73	58:00:19.71	2455332.1	-290.9± 0.6	W15
Draco-055	5	17:19:07.73	58:00:19.71	2455707.5	-290.2± 0.3	W15
Draco-055	5	17:19:07.73	58:00:19.71	2455711.8	-290.8± 0.7	W15
Draco-055	5	17:19:07.73	58:00:19.69	2451720.5	-287.3± 3.3	K02
Draco-055	5	17:19:07.73	58:00:19.71	2454975.5	-288.3± 2.2	K10
Draco-056	3	17:19:08.32	57:57:50.59	2454159.0	-294.0± 0.7	W15
Draco-056	3	17:19:08.32	57:57:50.59	2454170.9	-293.5± 0.8	W15
Draco-056	3	17:19:08.32	57:57:50.59	2454975.5	-291.1± 2.1	K10
Draco-057	3	17:19:09.86	57:57:10.70	2454912.0	-288.5± 1.4	W15
Draco-057	3	17:19:09.86	57:57:10.70	2454914.9	-289.3± 0.8	W15
Draco-057	3	17:19:09.85	57:57:10.70	2454975.5	-287.5± 2.2	K10
Draco-058	3	17:19:10.14	58:08:06.60	2454165.9	-294.9± 1.1	W15
Draco-058	3	17:19:10.14	58:08:06.60	2455707.6	-296.8± 0.4	W15
Draco-058	3	17:19:10.15	58:08:06.58	2452813.0	-293.6± 6.1	W04
Draco-059	4	17:19:10.26	57:54:37.50	2455591.0	-297.0± 1.0	W15
Draco-059	4	17:19:10.26	57:54:37.50	2455707.4	-298.9± 0.4	W15
Draco-059	4	17:19:10.26	57:54:37.50	2455711.8	-297.7± 0.7	W15
Draco-059	4	17:19:10.27	57:54:37.55	2451720.5	-295.6± 2.4	K02
Draco-060	5	17:19:10.82	57:59:17.30	2454155.0	-299.3± 0.5	W15
Draco-060	5	17:19:10.82	57:59:17.30	2454165.9	-298.6± 0.5	W15
Draco-060	5	17:19:10.82	57:59:17.30	2451720.5	-297.0± 0.7	K02
Draco-060	5	17:19:10.77	57:59:16.40	2449457.9	-296.5± 1.6	A95
Draco-060	5	17:19:10.81	57:59:17.40	2454975.5	-296.3± 2.1	K10
Draco-061	2	17:19:11.87	57:54:27.99	2454159.0	-296.9± 0.9	W15
Draco-061	2	17:19:11.87	57:54:27.99	2454170.9	-296.2± 0.7	W15
Draco-062	5	17:19:12.26	58:02:57.80	2455708.4	-281.7± 0.3	W15
Draco-062	5	17:19:12.26	58:02:57.80	2455712.9	-282.2± 0.5	W15
Draco-062	5	17:19:12.26	58:02:57.77	2451720.5	-290.9± 1.1	K02
Draco-062	5	17:19:12.26	58:02:57.77	2452813.0	-291.7± 1.0	W04
Draco-062	5	17:19:12.22	58:02:57.00	2449130.9	-285.1± 2.1	A95

Table G.1: Continued. Velocities of RGB stars in Draco

Star ID	n	α_{J2000} (hh:mm:ss.ss)	δ_{J2000} (dd:mm:ss.ss)	HJD (days)	v (km s ⁻¹)	Ref.
Draco-063	5	17:19:12.45	57:56:22.89	2455331.8	-262.3± 1.1	W15
Draco-063	5	17:19:12.45	57:56:22.89	2455591.0	-262.9± 1.8	W15
Draco-063	5	17:19:12.45	57:56:22.89	2455707.5	-287.4± 0.5	W15
Draco-063	5	17:19:12.45	57:56:22.89	2455711.8	-290.1± 0.9	W15
Draco-063	5	17:19:12.45	57:56:23.01	2454975.5	-283.0± 2.2	K10
Draco-064	5	17:19:13.88	57:51:54.99	2455331.8	-298.4± 1.0	W15
Draco-064	5	17:19:13.88	57:51:54.99	2455591.0	-299.1± 1.1	W15
Draco-064	5	17:19:13.88	57:51:54.99	2455707.6	-299.6± 0.6	W15
Draco-064	5	17:19:13.88	57:51:54.99	2455711.8	-299.1± 0.8	W15
Draco-064	5	17:19:13.88	57:51:55.04	2451720.5	-297.8± 2.3	K02
Draco-065	2	17:19:14.90	57:56:51.80	2455331.8	-282.5± 1.3	W15
Draco-065	2	17:19:14.89	57:56:51.80	2454975.5	-281.1± 2.2	K10
Draco-066	2	17:19:16.58	57:59:20.20	2455706.9	-292.8± 1.3	W15
Draco-066	2	17:19:16.58	57:59:20.20	2454975.5	-292.9± 2.5	K10
Draco-067	3	17:19:16.61	57:58:08.80	2454912.0	-288.4± 0.9	W15
Draco-067	3	17:19:16.61	57:58:08.80	2454914.9	-289.2± 0.7	W15
Draco-067	3	17:19:16.62	57:58:08.80	2452813.0	-280.4± 4.4	W04
Draco-068	5	17:19:16.93	58:15:50.89	2454155.0	-298.1± 0.9	W15
Draco-068	5	17:19:16.93	58:15:50.89	2454165.9	-296.2± 0.8	W15
Draco-068	5	17:19:16.93	58:15:50.89	2454524.0	-297.1± 1.2	W15
Draco-068	5	17:19:16.92	58:15:50.90	2451720.5	-290.0± 1.8	K02
Draco-068	5	17:19:16.92	58:15:50.90	2452813.0	-299.5± 1.6	W04
Draco-069	4	17:19:17.60	57:54:32.10	2454912.0	-290.5± 0.5	W15
Draco-069	4	17:19:17.61	57:54:32.15	2451720.5	-289.3± 1.4	K02
Draco-069	4	17:19:17.61	57:54:32.15	2452813.0	-289.8± 3.3	W04
Draco-069	4	17:19:17.59	57:54:32.19	2454975.5	-290.6± 2.1	K10
Draco-070	5	17:19:18.64	57:51:03.50	2455332.2	-297.8± 0.6	W15
Draco-070	5	17:19:18.64	57:51:03.50	2455591.0	-297.5± 0.9	W15
Draco-070	5	17:19:18.64	57:51:03.50	2455707.5	-296.6± 0.3	W15
Draco-070	5	17:19:18.64	57:51:03.50	2455711.5	-297.0± 0.5	W15
Draco-070	5	17:19:18.62	57:51:03.50	2454975.5	-296.2± 2.2	K10
Draco-071	3	17:19:20.00	57:49:04.90	2454912.0	-294.9± 0.7	W15
Draco-071	3	17:19:20.00	57:49:04.87	2451720.5	-295.3± 1.3	K02
Draco-071	3	17:19:20.00	57:49:04.87	2452813.0	-290.0± 1.9	W04
Draco-072	5	17:19:20.00	57:59:43.09	2454912.0	-307.1± 0.6	W15
Draco-072	5	17:19:20.00	57:59:43.09	2454914.9	-307.7± 0.5	W15
Draco-072	5	17:19:20.00	57:59:43.12	2451720.5	-306.4± 2.1	K02

Table G.1: Continued. Velocities of RGB stars in Draco

Star ID	n	α_{J2000} (hh:mm:ss.ss)	δ_{J2000} (dd:mm:ss.ss)	HJD (days)	v (km s ⁻¹)	Ref.
Draco-072	5	17:19:20.00	57:59:43.12	2452813.0	-311.2± 2.3	W04
Draco-072	5	17:19:20.00	57:59:43.21	2454975.5	-306.7± 2.1	K10
Draco-073	3	17:19:20.34	57:28:50.00	2455331.7	-306.8± 2.1	W15
Draco-073	3	17:19:20.34	57:28:50.00	2455708.9	-303.8± 1.4	W15
Draco-073	3	17:19:20.34	57:28:50.00	2455710.8	-305.6± 1.1	W15
Draco-074	2	17:19:21.20	57:45:29.80	2454168.9	-309.0± 1.2	W15
Draco-074	2	17:19:21.20	57:45:29.80	2454170.9	-308.1± 1.6	W15
Draco-075	5	17:19:21.45	57:55:37.61	2454155.0	-303.8± 1.0	W15
Draco-075	5	17:19:21.45	57:55:37.61	2454168.9	-304.2± 0.7	W15
Draco-075	5	17:19:21.45	57:55:37.61	2455591.0	-303.4± 0.8	W15
Draco-075	5	17:19:21.45	57:55:37.61	2455706.9	-304.8± 0.6	W15
Draco-075	5	17:19:21.45	57:55:37.61	2454975.5	-303.0± 2.1	K10
Draco-076	2	17:19:21.71	58:00:40.50	2454165.9	-271.8± 0.5	W15
Draco-076	2	17:19:21.71	58:00:40.50	2451720.5	-275.3± 1.5	K02
Draco-077	2	17:19:21.82	58:01:52.20	2455707.3	-296.7± 0.4	W15
Draco-077	2	17:19:21.82	58:01:52.21	2451720.5	-295.6± 1.2	K02
Draco-078	2	17:19:22.02	57:59:02.71	2455331.8	-295.5± 1.8	W15
Draco-078	2	17:19:22.01	57:59:02.80	2454975.5	-294.6± 2.3	K10
Draco-079	5	17:19:22.53	57:50:13.00	2455331.7	-293.0± 1.6	W15
Draco-079	5	17:19:22.53	57:50:13.00	2455591.0	-294.6± 0.9	W15
Draco-079	5	17:19:22.53	57:50:13.00	2455707.5	-294.5± 0.3	W15
Draco-079	5	17:19:22.53	57:50:13.00	2455711.5	-294.6± 0.4	W15
Draco-079	5	17:19:22.53	57:50:13.02	2451720.5	-300.1± 2.2	K02
Draco-080	5	17:19:22.91	58:23:41.10	2455331.7	-266.4± 1.0	W15
Draco-080	5	17:19:22.91	58:23:41.10	2455591.0	-266.9± 0.7	W15
Draco-080	5	17:19:22.91	58:23:41.10	2455707.8	-266.6± 0.4	W15
Draco-080	5	17:19:22.91	58:23:41.10	2455710.9	-266.5± 0.6	W15
Draco-080	5	17:19:22.91	58:23:41.03	2452813.0	-266.2± 2.9	W04
Draco-081	3	17:19:22.92	57:55:30.60	2455331.7	-277.3± 1.2	W15
Draco-081	3	17:19:22.93	57:55:30.65	2451720.5	-279.9± 1.7	K02
Draco-081	3	17:19:22.93	57:55:30.65	2452813.0	-283.6± 3.3	W04
Draco-082	2	17:19:23.72	57:47:22.79	2454155.0	-295.8± 1.2	W15
Draco-082	2	17:19:23.72	57:47:22.79	2454168.9	-293.9± 1.0	W15
Draco-083	3	17:19:24.93	58:02:29.30	2455708.9	-285.1± 1.7	W15
Draco-083	3	17:19:24.93	58:02:29.30	2455712.9	-287.8± 2.0	W15
Draco-083	3	17:19:24.93	58:02:29.33	2452813.0	-275.6± 7.6	W04
Draco-084	2	17:19:25.66	57:57:05.61	2454912.0	-308.5± 1.4	W15

Table G.1: Continued. Velocities of RGB stars in Draco

Star ID	n	α_{J2000} (hh:mm:ss.ss)	δ_{J2000} (dd:mm:ss.ss)	HJD (days)	v (km s ⁻¹)	Ref.
Draco-084	2	17:19:25.65	57:57:05.70	2454975.5	-306.4± 2.2	K10
Draco-085	3	17:19:25.69	58:01:00.09	2454165.9	-285.1± 1.0	W15
Draco-085	3	17:19:25.69	58:01:00.09	2455331.8	-286.6± 1.0	W15
Draco-085	3	17:19:25.69	58:01:00.09	2455707.8	-286.3± 0.9	W15
Draco-086	2	17:19:29.67	57:54:35.40	2455331.8	-295.7± 1.8	W15
Draco-086	2	17:19:29.66	57:54:35.40	2454975.5	-296.1± 2.3	K10
Draco-087	3	17:19:29.88	57:48:16.70	2454912.0	-281.2± 0.7	W15
Draco-087	3	17:19:29.88	57:48:16.70	2455591.0	-281.9± 0.9	W15
Draco-087	3	17:19:29.88	57:48:16.70	2455706.9	-281.4± 0.6	W15
Draco-088	5	17:19:31.87	57:33:34.70	2454168.9	-309.1± 1.0	W15
Draco-088	5	17:19:31.87	57:33:34.70	2455708.2	-309.9± 0.5	W15
Draco-088	5	17:19:31.87	57:33:34.70	2455710.8	-310.7± 0.8	W15
Draco-088	5	17:19:31.86	57:33:34.70	2451720.5	-308.8± 1.8	K02
Draco-088	5	17:19:31.86	57:33:34.70	2452813.0	-309.6± 2.0	W04
Draco-089	4	17:19:32.81	57:49:48.80	2455332.4	-286.9± 0.6	W15
Draco-089	4	17:19:32.81	57:49:48.80	2455591.0	-288.0± 0.9	W15
Draco-089	4	17:19:32.81	57:49:48.80	2455706.9	-287.2± 0.8	W15
Draco-089	4	17:19:32.80	57:49:48.79	2451720.5	-288.8± 3.3	K02
Draco-090	4	17:19:34.17	58:00:31.20	2455332.1	-270.0± 0.8	W15
Draco-090	4	17:19:34.17	58:00:31.20	2455591.0	-271.0± 1.2	W15
Draco-090	4	17:19:34.17	58:00:31.20	2455707.5	-271.7± 0.3	W15
Draco-090	4	17:19:34.17	58:00:31.20	2455711.8	-271.8± 0.8	W15
Draco-091	3	17:19:34.37	57:46:11.60	2454155.0	-289.7± 1.0	W15
Draco-091	3	17:19:34.36	57:46:11.57	2451720.5	-286.3± 1.5	K02
Draco-091	3	17:19:34.36	57:46:11.57	2452813.0	-292.3± 1.8	W04
Draco-092	3	17:19:34.69	57:48:05.00	2454168.9	-289.1± 0.6	W15
Draco-092	3	17:19:34.74	57:48:05.30	2451720.5	-294.3± 2.4	K02
Draco-092	3	17:19:34.66	57:48:05.00	2454975.5	-288.6± 2.1	K10
Draco-093	2	17:19:37.09	58:05:20.10	2454165.9	-283.8± 1.2	W15
Draco-093	2	17:19:37.10	58:05:20.08	2451720.5	-274.2± 2.6	K02
Draco-094	4	17:19:37.70	57:49:18.49	2454155.0	-297.0± 1.8	W15
Draco-094	4	17:19:37.70	57:49:18.49	2454168.9	-295.3± 0.8	W15
Draco-094	4	17:19:37.70	57:49:18.49	2455331.8	-294.9± 1.1	W15
Draco-094	4	17:19:37.70	57:49:18.48	2451720.5	-292.5± 5.1	K02
Draco-095	7	17:19:38.58	57:58:01.20	2454155.0	-271.9± 1.9	W15
Draco-095	7	17:19:38.58	57:58:01.20	2454159.0	-267.8± 1.6	W15
Draco-095	7	17:19:38.58	57:58:01.20	2454170.9	-267.2± 1.3	W15

Table G.1: Continued. Velocities of RGB stars in Draco

Star ID	n	α_{J2000} (hh:mm:ss.ss)	δ_{J2000} (dd:mm:ss.ss)	HJD (days)	v (km s ⁻¹)	Ref.
Draco-095	7	17:19:38.58	57:58:01.20	2455331.8	-279.5± 2.5	W15
Draco-095	7	17:19:38.58	57:58:01.20	2455591.0	-266.4± 1.9	W15
Draco-095	7	17:19:38.58	57:58:01.20	2455707.8	-267.2± 0.5	W15
Draco-095	7	17:19:38.58	57:58:01.20	2455711.8	-268.9± 1.0	W15
Draco-096	2	17:19:41.80	57:54:45.41	2454912.0	-275.3± 1.3	W15
Draco-096	2	17:19:41.80	57:54:45.41	2454914.9	-274.6± 1.1	W15
Draco-097	6	17:19:41.85	57:52:19.21	2454155.0	-294.8± 0.5	W15
Draco-097	6	17:19:41.85	57:52:19.21	2454168.9	-294.7± 0.5	W15
Draco-097	6	17:19:41.80	57:52:18.40	2446918.9	-296.5± 1.6	O95
Draco-097	6	17:19:41.80	57:52:18.40	2448774.9	-296.0± 5.6	A95
Draco-097	6	17:19:41.80	57:52:18.40	2449130.9	-293.5± 1.5	A95
Draco-097	6	17:19:41.84	57:52:19.21	2454975.5	-293.3± 2.1	K10
Draco-098	3	17:19:42.39	57:58:37.70	2454912.0	-296.3± 0.6	W15
Draco-098	3	17:19:42.39	57:58:37.70	2454914.9	-296.1± 0.6	W15
Draco-098	3	17:19:42.38	57:58:37.70	2451720.5	-293.2± 3.1	K02
Draco-099	2	17:19:43.16	57:53:01.20	2454168.9	-289.3± 1.3	W15
Draco-099	2	17:19:43.15	57:53:01.10	2454975.5	-284.6± 2.4	K10
Draco-100	6	17:19:43.19	57:52:34.70	2454159.0	-274.8± 1.3	W15
Draco-100	6	17:19:43.19	57:52:34.70	2454170.9	-284.2± 2.1	W15
Draco-100	6	17:19:43.19	57:52:34.70	2455332.4	-290.1± 1.1	W15
Draco-100	6	17:19:43.19	57:52:34.70	2455707.4	-285.0± 0.5	W15
Draco-100	6	17:19:43.19	57:52:34.70	2455712.9	-288.4± 1.8	W15
Draco-100	6	17:19:43.19	57:52:34.70	2454975.5	-280.0± 2.2	K10
Draco-101	3	17:19:44.36	58:00:58.29	2454159.0	-287.0± 1.6	W15
Draco-101	3	17:19:44.36	58:00:58.29	2454170.9	-286.9± 1.3	W15
Draco-101	3	17:19:44.35	58:00:58.20	2454975.5	-284.1± 2.4	K10
Draco-102	2	17:19:44.45	57:47:27.30	2455331.8	-282.1± 1.8	W15
Draco-102	2	17:19:44.45	57:47:27.30	2455707.8	-283.7± 1.4	W15
Draco-103	3	17:19:46.88	57:59:56.10	2454912.0	-301.8± 1.0	W15
Draco-103	3	17:19:46.88	57:59:56.10	2454914.9	-303.8± 0.9	W15
Draco-103	3	17:19:46.88	57:59:56.00	2454975.5	-303.2± 2.2	K10
Draco-104	11	17:19:47.70	57:48:36.59	2454912.0	-281.6± 0.5	W15
Draco-104	11	17:19:47.70	57:48:36.59	2454914.9	-281.4± 0.4	W15
Draco-104	11	17:19:47.69	57:48:36.54	2451720.5	-280.3± 0.8	K02
Draco-104	11	17:19:47.69	57:48:36.54	2452813.0	-282.7± 1.7	W04
Draco-104	11	17:19:47.65	57:48:35.70	2446964.8	-281.5± 1.9	O95
Draco-104	11	17:19:47.65	57:48:35.70	2446965.8	-279.6± 2.0	O95

Table G.1: Continued. Velocities of RGB stars in Draco

Star ID	n	α_{J2000} (hh:mm:ss.ss)	δ_{J2000} (dd:mm:ss.ss)	HJD (days)	v (km s ⁻¹)	Ref.
Draco-104	11	17:19:47.65	57:48:35.70	2448774.9	-285.5± 3.8	A95
Draco-104	11	17:19:47.65	57:48:35.70	2448776.9	-284.1± 3.3	A95
Draco-104	11	17:19:47.65	57:48:35.70	2449130.9	-280.0± 1.6	A95
Draco-104	11	17:19:47.65	57:48:35.70	2449457.9	-280.2± 1.2	A95
Draco-104	11	17:19:47.67	57:48:36.59	2454975.5	-280.3± 2.1	K10
Draco-105	6	17:19:49.80	58:00:26.70	2454155.0	-280.0± 1.2	W15
Draco-105	6	17:19:49.80	58:00:26.70	2454159.0	-280.5± 0.9	W15
Draco-105	6	17:19:49.80	58:00:26.70	2454170.9	-280.6± 1.0	W15
Draco-105	6	17:19:49.80	58:00:26.70	2455331.7	-279.1± 1.6	W15
Draco-105	6	17:19:49.80	58:00:26.70	2455707.2	-281.1± 0.5	W15
Draco-105	6	17:19:49.80	58:00:26.60	2454975.5	-278.4± 2.2	K10
Draco-106	4	17:19:50.04	57:56:40.69	2454912.0	-274.4± 0.5	W15
Draco-106	4	17:19:50.03	57:56:40.60	2451720.5	-280.9± 2.5	K02
Draco-106	4	17:19:50.03	57:56:40.60	2452813.0	-276.7± 3.0	W04
Draco-106	4	17:19:50.03	57:56:40.60	2454975.5	-274.4± 2.1	K10
Draco-107	3	17:19:50.11	57:57:10.40	2454912.0	-285.2± 1.5	W15
Draco-107	3	17:19:50.11	57:57:10.40	2454914.9	-283.9± 1.7	W15
Draco-107	3	17:19:50.11	57:57:10.30	2454975.5	-281.9± 2.2	K10
Draco-108	3	17:19:50.28	57:55:20.20	2454912.0	-296.0± 1.3	W15
Draco-108	3	17:19:50.28	57:55:20.20	2454914.9	-296.8± 0.8	W15
Draco-108	3	17:19:50.27	57:55:20.10	2454975.5	-295.7± 2.2	K10
Draco-109	3	17:19:53.80	57:59:59.70	2455591.0	-297.3± 1.6	W15
Draco-109	3	17:19:53.80	57:59:59.70	2455706.9	-296.9± 0.9	W15
Draco-109	3	17:19:53.80	57:59:59.60	2454975.5	-292.6± 2.3	K10
Draco-110	4	17:19:53.84	58:06:44.10	2455591.0	-279.6± 0.7	W15
Draco-110	4	17:19:53.84	58:06:44.10	2455707.1	-280.2± 0.3	W15
Draco-110	4	17:19:53.85	58:06:44.10	2451720.5	-277.5± 1.5	K02
Draco-110	4	17:19:53.85	58:06:44.10	2452813.0	-279.1± 1.1	W04
Draco-111	2	17:19:54.19	57:57:44.59	2455708.9	-296.8± 1.6	W15
Draco-111	2	17:19:54.18	57:57:44.59	2454975.5	-294.4± 2.5	K10
Draco-112	3	17:19:54.58	57:57:06.70	2454155.0	-299.2± 1.0	W15
Draco-112	3	17:19:54.58	57:57:06.70	2454912.0	-300.2± 1.4	W15
Draco-112	3	17:19:54.58	57:57:06.70	2454914.9	-300.6± 0.7	W15
Draco-113	2	17:19:55.91	57:51:24.49	2455707.8	-289.9± 0.7	W15
Draco-113	2	17:19:55.91	57:51:24.49	2455712.9	-289.7± 1.3	W15
Draco-114	4	17:19:56.39	57:59:16.00	2454912.0	-288.4± 0.6	W15
Draco-114	4	17:19:56.39	57:59:16.00	2454914.9	-288.7± 0.6	W15

Table G.1: Continued. Velocities of RGB stars in Draco

Star ID	n	α_{J2000} (hh:mm:ss.ss)	δ_{J2000} (dd:mm:ss.ss)	HJD (days)	v (km s ⁻¹)	Ref.
Draco-114	4	17:19:56.39	57:59:16.01	2451720.5	-294.3± 3.1	K02
Draco-114	4	17:19:56.39	57:59:16.00	2454975.5	-285.4± 2.1	K10
Draco-115	2	17:19:56.59	57:52:42.90	2455331.7	-296.2± 0.9	W15
Draco-115	2	17:19:56.58	57:52:42.85	2451720.5	-295.3± 1.4	K02
Draco-116	2	17:19:57.66	57:50:05.50	2454912.0	-294.2± 0.8	W15
Draco-116	2	17:19:57.66	57:50:05.50	2454914.9	-294.9± 0.8	W15
Draco-117	2	17:19:57.81	58:00:51.50	2455707.9	-279.0± 1.1	W15
Draco-117	2	17:19:57.81	58:00:51.50	2455711.8	-277.5± 1.1	W15
Draco-118	2	17:19:57.90	58:01:20.10	2455331.7	-306.9± 3.5	W15
Draco-118	2	17:19:57.90	58:01:20.00	2454975.5	-307.8± 2.2	K10
Draco-119	10	17:19:58.89	57:57:20.91	2454524.0	-271.2± 0.5	W15
Draco-119	10	17:19:58.88	57:57:20.88	2452813.0	-275.3± 1.0	W04
Draco-119	10	17:19:58.86	57:57:20.00	2445847.9	-274.7± 2.0	O95
Draco-119	10	17:19:58.86	57:57:20.00	2446208.9	-271.2± 1.6	O95
Draco-119	10	17:19:58.86	57:57:20.00	2446329.6	-268.5± 2.5	O95
Draco-119	10	17:19:58.86	57:57:20.00	2447419.7	-269.9± 2.0	O95
Draco-119	10	17:19:58.86	57:57:20.00	2448161.7	-277.5± 2.0	O95
Draco-119	10	17:19:58.86	57:57:20.00	2448774.9	-271.5± 5.3	A95
Draco-119	10	17:19:58.86	57:57:20.00	2449130.9	-276.6± 2.4	A95
Draco-119	10	17:19:58.89	57:57:20.91	2454975.5	-272.6± 2.1	K10
Draco-120	5	17:19:59.74	57:55:05.89	2454155.0	-294.1± 1.1	W15
Draco-120	5	17:19:59.74	57:55:05.89	2454168.9	-294.8± 1.0	W15
Draco-120	5	17:19:59.74	57:55:05.89	2454912.0	-292.6± 0.7	W15
Draco-120	5	17:19:59.74	57:55:05.89	2454914.9	-294.4± 0.6	W15
Draco-120	5	17:19:59.73	57:55:05.89	2454975.5	-294.0± 2.2	K10
Draco-121	5	17:20:00.53	57:52:56.60	2455331.8	-294.8± 1.1	W15
Draco-121	5	17:20:00.53	57:52:56.60	2455591.0	-290.4± 1.9	W15
Draco-121	5	17:20:00.53	57:52:56.60	2455707.4	-291.4± 0.5	W15
Draco-121	5	17:20:00.53	57:52:56.60	2455712.9	-294.5± 1.0	W15
Draco-121	5	17:20:00.52	57:52:56.60	2454975.5	-289.0± 2.2	K10
Draco-122	3	17:20:00.69	57:53:46.60	2454912.0	-301.4± 0.6	W15
Draco-122	3	17:20:00.69	57:53:46.60	2454914.9	-301.4± 0.6	W15
Draco-122	3	17:20:00.68	57:53:46.54	2452813.0	-298.3± 5.9	W04
Draco-123	2	17:20:01.52	58:01:33.40	2455710.8	-280.1± 0.9	W15
Draco-123	2	17:20:01.52	58:01:33.38	2451720.5	-295.1± 1.2	K02
Draco-124	5	17:20:01.59	57:57:04.60	2454912.0	-296.4± 0.5	W15
Draco-124	5	17:20:01.59	57:57:04.54	2451720.5	-296.4± 1.2	K02

Table G.1: Continued. Velocities of RGB stars in Draco

Star ID	n	α_{J2000} (hh:mm:ss.ss)	δ_{J2000} (dd:mm:ss.ss)	HJD (days)	v (km s ⁻¹)	Ref.
Draco-124	5	17:20:01.59	57:57:04.54	2452813.0	-283.5± 2.3	W04
Draco-124	5	17:20:01.56	57:57:03.81	2449457.9	-298.1± 3.4	A95
Draco-124	5	17:20:01.59	57:57:04.60	2454975.5	-297.7± 2.1	K10
Draco-125	3	17:20:01.76	57:46:46.60	2454155.0	-296.0± 1.2	W15
Draco-125	3	17:20:01.76	57:46:46.60	2455331.8	-296.3± 1.0	W15
Draco-125	3	17:20:01.76	57:46:46.60	2455710.8	-296.9± 0.7	W15
Draco-126	5	17:20:01.96	57:51:30.40	2455331.7	-308.0± 1.5	W15
Draco-126	5	17:20:01.96	57:51:30.40	2455707.5	-310.0± 0.4	W15
Draco-126	5	17:20:01.96	57:51:30.40	2455711.8	-310.2± 0.6	W15
Draco-126	5	17:20:01.94	57:51:30.35	2451720.5	-312.6± 1.7	K02
Draco-126	5	17:20:01.93	57:51:30.40	2454975.5	-310.0± 2.1	K10
Draco-127	2	17:20:01.98	57:54:22.29	2455331.8	-278.7± 1.4	W15
Draco-127	2	17:20:01.97	57:54:22.29	2454975.5	-279.8± 2.2	K10
Draco-128	2	17:20:02.76	57:48:57.19	2455331.7	-294.1± 2.6	W15
Draco-128	2	17:20:02.76	57:48:57.17	2451720.5	-284.1± 2.7	K02
Draco-129	5	17:20:05.33	57:50:18.20	2454155.0	-290.9± 0.7	W15
Draco-129	5	17:20:05.32	57:50:18.17	2451720.5	-288.8± 1.3	K02
Draco-129	5	17:20:05.32	57:50:18.17	2452813.0	-282.9± 2.3	W04
Draco-129	5	17:20:05.31	57:50:17.39	2448776.9	-289.8± 5.6	A95
Draco-129	5	17:20:05.31	57:50:17.39	2449457.9	-291.3± 5.4	A95
Draco-130	2	17:20:05.65	57:57:58.50	2455591.0	-294.0± 1.7	W15
Draco-130	2	17:20:05.64	57:57:58.40	2454975.5	-290.4± 2.3	K10
Draco-131	3	17:20:05.67	57:53:03.70	2454168.9	-292.2± 0.9	W15
Draco-131	3	17:20:05.67	57:53:03.70	2454912.0	-292.8± 0.8	W15
Draco-131	3	17:20:05.67	57:53:03.70	2454914.9	-292.9± 0.9	W15
Draco-132	4	17:20:06.07	58:02:50.10	2455332.9	-293.0± 1.0	W15
Draco-132	4	17:20:06.07	58:02:50.10	2455707.9	-292.7± 0.6	W15
Draco-132	4	17:20:06.07	58:02:50.06	2452813.0	-290.4± 6.2	W04
Draco-132	4	17:20:06.07	58:02:50.00	2454975.5	-292.4± 2.3	K10
Draco-133	6	17:20:06.90	57:52:37.10	2455332.9	-288.5± 0.5	W15
Draco-133	6	17:20:06.90	57:52:37.09	2452813.0	-285.5± 4.1	W04
Draco-133	6	17:20:06.87	57:52:36.19	2448774.9	-283.1± 8.3	A95
Draco-133	6	17:20:06.87	57:52:36.19	2449130.9	-291.5± 3.8	A95
Draco-133	6	17:20:06.87	57:52:36.19	2449457.9	-285.6± 4.1	A95
Draco-133	6	17:20:06.89	57:52:37.10	2454975.5	-287.2± 2.1	K10
Draco-134	2	17:20:07.22	58:01:04.60	2454912.0	-302.4± 1.5	W15
Draco-134	2	17:20:07.22	58:01:04.60	2454914.9	-305.7± 1.7	W15

Table G.1: Continued. Velocities of RGB stars in Draco

Star ID	n	α_{J2000} (hh:mm:ss.ss)	δ_{J2000} (dd:mm:ss.ss)	HJD (days)	v (km s ⁻¹)	Ref.
Draco-135	2	17:20:07.41	57:53:12.11	2455331.8	-296.2± 1.1	W15
Draco-135	2	17:20:07.40	57:53:12.11	2454975.5	-297.3± 2.2	K10
Draco-136	3	17:20:07.46	57:54:32.70	2454912.0	-304.9± 0.7	W15
Draco-136	3	17:20:07.44	57:54:32.65	2451720.5	-298.9± 1.9	K02
Draco-136	3	17:20:07.44	57:54:32.70	2454975.5	-305.5± 2.2	K10
Draco-137	2	17:20:07.97	57:53:52.60	2455706.8	-308.9± 1.1	W15
Draco-137	2	17:20:07.97	57:53:52.70	2454975.5	-310.5± 2.3	K10
Draco-138	6	17:20:09.72	57:46:29.40	2454155.0	-292.9± 0.5	W15
Draco-138	6	17:20:09.72	57:46:29.40	2455710.8	-287.7± 0.5	W15
Draco-138	6	17:20:09.72	57:46:29.39	2451720.5	-293.7± 0.8	K02
Draco-138	6	17:20:09.72	57:46:29.39	2452813.0	-288.0± 1.6	W04
Draco-138	6	17:20:09.67	57:46:28.50	2449130.9	-293.4± 4.2	A95
Draco-138	6	17:20:09.67	57:46:28.50	2449457.9	-289.6± 2.0	A95
Draco-139	3	17:20:10.37	57:53:12.50	2454159.0	-299.4± 0.9	W15
Draco-139	3	17:20:10.37	57:53:12.50	2454170.9	-300.9± 0.9	W15
Draco-139	3	17:20:10.36	57:53:12.50	2454975.5	-300.9± 2.1	K10
Draco-140	2	17:20:10.46	58:02:39.40	2454912.0	-306.2± 1.8	W15
Draco-140	2	17:20:10.46	58:02:39.40	2454914.9	-307.3± 1.2	W15
Draco-141	2	17:20:10.48	57:58:20.79	2455331.8	-287.5± 0.7	W15
Draco-141	2	17:20:10.48	57:58:20.78	2451720.5	-272.6± 1.2	K02
Draco-142	3	17:20:10.85	57:52:57.49	2454168.9	-278.9± 1.3	W15
Draco-142	3	17:20:10.85	57:52:57.49	2455331.7	-281.5± 1.4	W15
Draco-142	3	17:20:10.84	57:52:57.49	2454975.5	-281.1± 2.2	K10
Draco-143	2	17:20:11.02	57:56:45.71	2455331.7	-294.7± 1.7	W15
Draco-143	2	17:20:11.02	57:56:45.64	2451720.5	-278.6± 2.3	K02
Draco-144	5	17:20:11.63	57:49:36.40	2453850.8	-290.4± 1.6	W15
Draco-144	5	17:20:11.63	57:49:36.40	2455331.7	-292.2± 0.7	W15
Draco-144	5	17:20:11.63	57:49:36.44	2451720.5	-293.9± 1.4	K02
Draco-144	5	17:20:11.60	57:49:35.50	2448776.9	-298.7± 7.6	A95
Draco-144	5	17:20:11.60	57:49:35.50	2449457.9	-290.8± 5.0	A95
Draco-145	2	17:20:11.97	57:56:29.20	2454914.9	-290.1± 0.9	W15
Draco-145	2	17:20:11.95	57:56:29.20	2454975.5	-288.5± 2.6	K10
Draco-146	3	17:20:12.93	57:54:03.00	2454168.9	-286.7± 1.1	W15
Draco-146	3	17:20:12.93	57:54:03.00	2455332.9	-290.2± 0.7	W15
Draco-146	3	17:20:12.92	57:54:03.10	2454975.5	-288.6± 2.2	K10
Draco-147	6	17:20:13.52	57:51:59.20	2454155.0	-292.9± 0.5	W15
Draco-147	6	17:20:13.52	57:51:59.22	2451720.5	-294.0± 1.1	K02

Table G.1: Continued. Velocities of RGB stars in Draco

Star ID	n	α_{J2000} (hh:mm:ss.ss)	δ_{J2000} (dd:mm:ss.ss)	HJD (days)	v (km s ⁻¹)	Ref.
Draco-147	6	17:20:13.48	57:51:58.40	2448774.9	-293.6± 4.5	A95
Draco-147	6	17:20:13.48	57:51:58.40	2448776.9	-293.7± 2.4	A95
Draco-147	6	17:20:13.48	57:51:58.40	2449130.9	-293.3± 2.6	A95
Draco-147	6	17:20:13.51	57:51:59.29	2454975.5	-294.2± 2.1	K10
Draco-148	5	17:20:14.52	58:12:51.40	2454165.9	-301.0± 0.6	W15
Draco-148	5	17:20:14.52	58:12:51.40	2455591.0	-302.0± 1.0	W15
Draco-148	5	17:20:14.52	58:12:51.40	2455708.9	-301.2± 0.4	W15
Draco-148	5	17:20:14.52	58:12:51.40	2455712.9	-301.8± 0.6	W15
Draco-148	5	17:20:14.53	58:12:51.41	2451720.5	-301.0± 2.1	K02
Draco-149	3	17:20:14.81	57:56:25.50	2455708.9	-280.3± 1.0	W15
Draco-149	3	17:20:14.81	57:56:25.50	2455712.9	-283.2± 0.9	W15
Draco-149	3	17:20:14.80	57:56:25.44	2451720.5	-286.1± 3.4	K02
Draco-150	2	17:20:15.22	58:00:35.01	2453850.8	-289.3± 2.1	W15
Draco-150	2	17:20:15.23	58:00:34.99	2451720.5	-296.4± 1.6	K02
Draco-151	2	17:20:15.73	57:54:27.59	2454914.9	-287.2± 1.9	W15
Draco-151	2	17:20:15.72	57:54:27.59	2454975.5	-290.2± 2.4	K10
Draco-152	6	17:20:16.13	57:52:56.00	2454912.0	-296.9± 0.6	W15
Draco-152	6	17:20:16.13	57:52:56.00	2454914.9	-296.6± 0.5	W15
Draco-152	6	17:20:16.08	57:52:55.20	2448774.9	-299.6± 8.4	A95
Draco-152	6	17:20:16.08	57:52:55.20	2449130.9	-289.0± 5.8	A95
Draco-152	6	17:20:16.08	57:52:55.20	2449457.9	-296.7± 4.4	A95
Draco-152	6	17:20:16.12	57:52:56.11	2454975.5	-297.6± 2.1	K10
Draco-153	8	17:20:16.16	58:04:04.80	2454155.0	-297.8± 0.7	W15
Draco-153	8	17:20:16.16	58:04:04.80	2454165.9	-297.6± 0.5	W15
Draco-153	8	17:20:16.16	58:04:04.80	2455331.8	-298.2± 0.5	W15
Draco-153	8	17:20:16.16	58:04:04.80	2455591.0	-298.9± 0.7	W15
Draco-153	8	17:20:16.16	58:04:04.80	2455706.9	-298.0± 0.5	W15
Draco-153	8	17:20:16.16	58:04:04.80	2455710.8	-298.8± 0.6	W15
Draco-153	8	17:20:16.17	58:04:04.80	2452813.0	-297.2± 1.3	W04
Draco-153	8	17:20:16.16	58:04:04.80	2454975.5	-297.6± 2.2	K10
Draco-154	3	17:20:16.98	57:53:12.30	2455331.7	-292.4± 0.6	W15
Draco-154	3	17:20:16.98	57:53:12.23	2451720.5	-289.9± 1.1	K02
Draco-154	3	17:20:16.98	57:53:12.23	2452813.0	-289.9± 1.8	W04
Draco-155	7	17:20:17.01	57:56:12.30	2454912.0	-294.1± 0.5	W15
Draco-155	7	17:20:17.01	57:56:12.30	2454914.9	-293.3± 0.5	W15
Draco-155	7	17:20:17.01	57:56:12.30	2455710.8	-295.2± 0.5	W15
Draco-155	7	17:20:17.01	57:56:12.30	2451720.5	-294.8± 1.1	K02

Table G.1: Continued. Velocities of RGB stars in Draco

Star ID	n	α_{J2000} (hh:mm:ss.ss)	δ_{J2000} (dd:mm:ss.ss)	HJD (days)	v (km s ⁻¹)	Ref.
Draco-155	7	17:20:17.01	57:56:12.30	2452813.0	-292.8± 2.3	W04
Draco-155	7	17:20:16.97	57:56:11.50	2448774.9	-296.1± 7.5	A95
Draco-155	7	17:20:16.97	57:56:11.50	2449130.9	-288.7± 4.7	A95
Draco-156	6	17:20:17.01	57:59:02.01	2454912.0	-307.5± 0.5	W15
Draco-156	6	17:20:17.01	57:59:02.01	2454914.9	-307.5± 0.5	W15
Draco-156	6	17:20:17.02	57:59:01.97	2451720.5	-304.8± 1.4	K02
Draco-156	6	17:20:17.02	57:59:01.97	2452813.0	-309.7± 2.0	W04
Draco-156	6	17:20:16.97	57:59:01.31	2448774.9	-309.0± 3.2	A95
Draco-156	6	17:20:16.97	57:59:01.31	2449457.9	-306.9± 1.9	A95
Draco-157	2	17:20:17.95	57:59:47.81	2455707.8	-281.9± 1.3	W15
Draco-157	2	17:20:17.95	57:59:47.81	2454975.5	-280.5± 2.5	K10
Draco-158	6	17:20:18.00	58:01:11.91	2454912.0	-288.5± 0.7	W15
Draco-158	6	17:20:18.00	58:01:11.91	2454914.9	-288.3± 0.6	W15
Draco-158	6	17:20:18.00	58:01:11.91	2455708.9	-289.8± 0.8	W15
Draco-158	6	17:20:18.00	58:01:11.91	2455712.9	-288.6± 0.7	W15
Draco-158	6	17:20:17.99	58:01:11.82	2451720.5	-287.5± 2.7	K02
Draco-158	6	17:20:17.98	58:01:11.79	2454975.5	-287.9± 2.2	K10
Draco-159	4	17:20:18.60	57:46:01.10	2455331.8	-303.2± 1.1	W15
Draco-159	4	17:20:18.60	57:46:01.10	2455707.9	-302.7± 0.5	W15
Draco-159	4	17:20:18.60	57:46:01.13	2451720.5	-303.9± 1.6	K02
Draco-159	4	17:20:18.60	57:46:01.13	2452813.0	-302.0± 3.8	W04
Draco-160	2	17:20:19.32	57:51:19.49	2455332.9	-277.5± 1.1	W15
Draco-160	2	17:20:19.30	57:51:19.61	2454975.5	-277.7± 2.2	K10
Draco-161	2	17:20:19.64	57:54:02.20	2454168.9	-297.3± 1.2	W15
Draco-161	2	17:20:19.62	57:54:02.20	2454975.5	-303.5± 2.2	K10
Draco-162	4	17:20:19.92	57:59:17.40	2455591.0	-308.1± 1.4	W15
Draco-162	4	17:20:19.92	57:59:17.40	2455707.4	-307.4± 0.4	W15
Draco-162	4	17:20:19.92	57:59:17.40	2455711.8	-308.1± 0.7	W15
Draco-162	4	17:20:19.92	57:59:17.40	2454975.5	-306.6± 2.2	K10
Draco-163	2	17:20:20.21	57:56:55.50	2454912.0	-297.4± 0.7	W15
Draco-163	2	17:20:20.21	57:56:55.50	2454914.9	-296.3± 0.6	W15
Draco-164	3	17:20:21.12	57:49:27.20	2453850.8	-293.6± 0.7	W15
Draco-164	3	17:20:21.12	57:49:27.20	2455332.9	-295.5± 0.5	W15
Draco-164	3	17:20:21.12	57:49:27.23	2451720.5	-294.2± 0.8	K02
Draco-165	4	17:20:23.63	57:59:08.10	2454912.0	-298.1± 0.8	W15
Draco-165	4	17:20:23.63	57:59:08.10	2455708.9	-296.8± 0.7	W15
Draco-165	4	17:20:23.63	57:59:08.10	2455712.9	-297.4± 0.7	W15

Table G.1: Continued. Velocities of RGB stars in Draco

Star ID	n	α_{J2000} (hh:mm:ss.ss)	δ_{J2000} (dd:mm:ss.ss)	HJD (days)	v (km s ⁻¹)	Ref.
Draco-165	4	17:20:23.62	57:59:08.10	2454975.5	-298.2± 2.2	K10
Draco-166	3	17:20:23.72	58:05:24.21	2455331.8	-305.2± 0.7	W15
Draco-166	3	17:20:23.72	58:05:24.21	2455706.8	-305.3± 0.6	W15
Draco-166	3	17:20:23.73	58:05:24.18	2451720.5	-308.9± 2.5	K02
Draco-167	5	17:20:24.10	57:55:15.40	2455331.8	-295.6± 0.8	W15
Draco-167	5	17:20:24.10	57:55:15.40	2455591.0	-294.3± 0.8	W15
Draco-167	5	17:20:24.10	57:55:15.40	2455707.4	-294.0± 0.4	W15
Draco-167	5	17:20:24.10	57:55:15.40	2455711.8	-294.0± 0.5	W15
Draco-167	5	17:20:24.10	57:55:15.42	2451720.5	-289.5± 2.1	K02
Draco-168	2	17:20:24.16	57:53:52.40	2455706.8	-293.0± 1.1	W15
Draco-168	2	17:20:24.14	57:53:52.40	2454975.5	-293.1± 2.3	K10
Draco-169	2	17:20:24.18	57:56:25.90	2455331.8	-298.5± 0.6	W15
Draco-169	2	17:20:24.16	57:56:25.90	2454975.5	-299.0± 2.2	K10
Draco-170	2	17:20:24.20	58:11:20.40	2455331.7	-293.9± 1.9	W15
Draco-170	2	17:20:24.20	58:11:20.40	2455707.3	-294.9± 0.6	W15
Draco-171	3	17:20:24.62	57:55:14.79	2454912.0	-300.4± 0.6	W15
Draco-171	3	17:20:24.62	57:55:14.79	2454914.9	-299.8± 0.6	W15
Draco-171	3	17:20:24.62	57:55:14.79	2455707.8	-300.1± 0.6	W15
Draco-172	3	17:20:24.91	57:48:42.80	2454912.0	-312.2± 1.4	W15
Draco-172	3	17:20:24.91	57:48:42.80	2454914.9	-309.6± 1.4	W15
Draco-172	3	17:20:24.89	57:48:42.80	2454975.5	-291.1± 2.3	K10
Draco-173	3	17:20:27.24	57:56:12.00	2454912.0	-288.1± 0.5	W15
Draco-173	3	17:20:27.24	57:56:11.94	2452813.0	-288.0± 1.9	W04
Draco-173	3	17:20:27.23	57:56:12.00	2454975.5	-288.2± 2.1	K10
Draco-174	4	17:20:27.38	57:56:52.39	2455331.7	-294.5± 0.6	W15
Draco-174	4	17:20:27.37	57:56:52.33	2451720.5	-291.2± 0.8	K02
Draco-174	4	17:20:27.33	57:56:51.50	2448774.9	-298.1± 9.8	A95
Draco-174	4	17:20:27.33	57:56:51.50	2449457.9	-294.8± 2.7	A95
Draco-175	2	17:20:28.75	58:03:58.99	2455708.9	-303.6± 2.1	W15
Draco-175	2	17:20:28.75	58:03:58.99	2455712.9	-305.9± 1.9	W15
Draco-176	2	17:20:30.41	57:58:05.40	2455331.8	-298.7± 1.1	W15
Draco-176	2	17:20:30.40	57:58:05.49	2454975.5	-293.2± 2.2	K10
Draco-177	3	17:20:30.94	57:57:53.70	2455708.9	-292.5± 2.0	W15
Draco-177	3	17:20:30.94	57:57:53.70	2455712.9	-290.7± 1.4	W15
Draco-177	3	17:20:30.93	57:57:53.79	2454975.5	-290.8± 2.3	K10
Draco-178	4	17:20:31.66	57:50:55.10	2454168.9	-290.1± 0.5	W15
Draco-178	4	17:20:31.66	57:50:55.07	2451720.5	-285.1± 1.1	K02

Table G.1: Continued. Velocities of RGB stars in Draco

Star ID	n	α_{J2000} (hh:mm:ss.ss)	δ_{J2000} (dd:mm:ss.ss)	HJD (days)	v (km s ⁻¹)	Ref.
Draco-178	4	17:20:31.66	57:50:55.07	2452813.0	-283.0± 7.8	W04
Draco-178	4	17:20:31.65	57:50:55.10	2454975.5	-290.1± 2.1	K10
Draco-179	3	17:20:32.13	58:05:39.90	2454165.9	-287.6± 1.3	W15
Draco-179	3	17:20:32.16	58:05:39.90	2451720.5	-280.6± 3.6	K02
Draco-179	3	17:20:32.13	58:05:40.00	2454975.5	-286.3± 2.3	K10
Draco-180	8	17:20:32.83	57:51:43.90	2454912.0	-300.2± 0.5	W15
Draco-180	8	17:20:32.83	57:51:43.90	2454914.9	-301.3± 0.4	W15
Draco-180	8	17:20:32.81	57:51:43.10	2445503.8	-300.8± 1.2	O95
Draco-180	8	17:20:32.81	57:51:43.10	2445848.9	-302.0± 2.6	O95
Draco-180	8	17:20:32.81	57:51:43.10	2446208.9	-300.8± 1.5	O95
Draco-180	8	17:20:32.81	57:51:43.10	2446593.9	-300.6± 1.7	O95
Draco-180	8	17:20:32.81	57:51:43.10	2448774.9	-302.6± 2.3	A95
Draco-180	8	17:20:32.81	57:51:43.10	2449130.9	-299.4± 0.8	A95
Draco-181	4	17:20:33.53	57:50:19.60	2454912.0	-276.5± 0.5	W15
Draco-181	4	17:20:33.53	57:50:19.60	2454914.9	-276.3± 0.5	W15
Draco-181	4	17:20:33.53	57:50:19.61	2451720.5	-276.8± 2.2	K02
Draco-181	4	17:20:33.53	57:50:19.61	2452813.0	-275.5± 4.2	W04
Draco-182	9	17:20:34.19	57:53:31.89	2454912.0	-287.2± 0.4	W15
Draco-182	9	17:20:34.19	57:53:31.89	2454914.9	-286.7± 0.4	W15
Draco-182	9	17:20:34.19	57:53:31.92	2451720.5	-286.0± 0.9	K02
Draco-182	9	17:20:34.12	57:53:31.10	2446210.9	-287.1± 1.6	O95
Draco-182	9	17:20:34.12	57:53:31.10	2448774.9	-283.3± 5.0	A95
Draco-182	9	17:20:34.12	57:53:31.10	2448776.9	-295.5± 5.6	A95
Draco-182	9	17:20:34.12	57:53:31.10	2449130.9	-284.9± 1.8	A95
Draco-182	9	17:20:34.12	57:53:31.10	2449457.9	-287.7± 1.5	A95
Draco-182	9	17:20:34.17	57:53:32.00	2454975.5	-288.2± 2.1	K10
Draco-183	2	17:20:34.57	57:58:12.59	2454155.0	-288.0± 1.1	W15
Draco-183	2	17:20:34.55	57:58:12.59	2454975.5	-287.1± 2.2	K10
Draco-184	2	17:20:34.65	58:00:38.20	2454914.9	-303.0± 1.3	W15
Draco-184	2	17:20:34.65	58:00:38.20	2454975.5	-284.6± 2.8	K10
Draco-185	4	17:20:34.77	57:59:56.80	2454155.0	-298.0± 0.5	W15
Draco-185	4	17:20:34.77	57:59:56.80	2451720.5	-297.5± 0.7	K02
Draco-185	4	17:20:34.73	57:59:56.00	2448776.9	-303.1± 2.6	A95
Draco-185	4	17:20:34.73	57:59:56.00	2449459.9	-294.6± 5.6	A95
Draco-186	4	17:20:35.32	57:54:07.39	2455332.2	-293.4± 0.4	W15
Draco-186	4	17:20:35.32	57:54:07.39	2455591.0	-291.9± 0.8	W15
Draco-186	4	17:20:35.32	57:54:07.39	2455707.4	-292.2± 0.3	W15

Table G.1: Continued. Velocities of RGB stars in Draco

Star ID	n	α_{J2000} (hh:mm:ss.ss)	δ_{J2000} (dd:mm:ss.ss)	HJD (days)	v (km s ⁻¹)	Ref.
Draco-186	4	17:20:35.32	57:54:07.39	2455711.8	-293.3± 0.5	W15
Draco-187	3	17:20:35.51	57:53:14.00	2455708.9	-302.9± 2.2	W15
Draco-187	3	17:20:35.51	57:53:14.00	2455712.9	-302.9± 1.6	W15
Draco-187	3	17:20:35.49	57:53:13.91	2454975.5	-301.9± 2.6	K10
Draco-188	2	17:20:36.87	57:58:55.70	2455706.8	-297.3± 1.6	W15
Draco-188	2	17:20:36.85	57:58:55.70	2454975.5	-290.8± 2.9	K10
Draco-189	4	17:20:37.41	57:59:12.50	2454912.0	-278.8± 0.5	W15
Draco-189	4	17:20:37.41	57:59:12.50	2454914.9	-278.6± 0.4	W15
Draco-189	4	17:20:37.41	57:59:12.52	2452813.0	-284.8± 1.3	W04
Draco-189	4	17:20:37.39	57:59:12.60	2454975.5	-282.5± 2.1	K10
Draco-190	2	17:20:37.67	57:52:16.60	2454155.0	-302.8± 1.7	W15
Draco-190	2	17:20:37.66	57:52:16.60	2454975.5	-303.8± 2.2	K10
Draco-191	3	17:20:38.25	57:54:48.30	2455707.8	-294.1± 0.9	W15
Draco-191	3	17:20:38.25	57:54:48.30	2455710.8	-291.4± 1.0	W15
Draco-191	3	17:20:38.24	57:54:48.30	2454975.5	-289.4± 2.3	K10
Draco-192	2	17:20:38.33	57:55:32.30	2455706.8	-288.3± 0.8	W15
Draco-192	2	17:20:38.32	57:55:32.40	2454975.5	-287.4± 2.3	K10
Draco-193	3	17:20:38.54	58:00:24.50	2454165.9	-299.7± 1.3	W15
Draco-193	3	17:20:38.54	58:00:24.50	2455331.8	-298.9± 1.0	W15
Draco-193	3	17:20:38.54	58:00:24.50	2455706.8	-298.3± 0.7	W15
Draco-194	2	17:20:39.19	57:55:57.50	2455706.8	-291.7± 2.3	W15
Draco-194	2	17:20:39.18	57:55:57.50	2454975.5	-294.0± 2.9	K10
Draco-195	3	17:20:39.21	57:52:34.81	2454159.0	-292.3± 1.3	W15
Draco-195	3	17:20:39.21	57:52:34.81	2454170.9	-294.1± 1.3	W15
Draco-195	3	17:20:39.21	57:52:34.81	2455706.8	-293.1± 0.7	W15
Draco-196	2	17:20:39.23	57:57:26.70	2454159.0	-276.7± 1.4	W15
Draco-196	2	17:20:39.23	57:57:26.70	2454170.9	-274.8± 1.5	W15
Draco-197	2	17:20:39.71	57:50:50.11	2455331.8	-293.1± 0.9	W15
Draco-197	2	17:20:39.71	57:50:50.06	2451720.5	-301.5± 3.5	K02
Draco-198	5	17:20:39.84	57:51:15.31	2454912.0	-282.9± 0.5	W15
Draco-198	5	17:20:39.84	57:51:15.31	2454914.9	-283.1± 0.5	W15
Draco-198	5	17:20:39.84	57:51:15.30	2451720.5	-282.8± 1.3	K02
Draco-198	5	17:20:39.80	57:51:14.40	2448776.9	-281.5± 6.9	A95
Draco-198	5	17:20:39.83	57:51:15.31	2454975.5	-282.3± 2.1	K10
Draco-199	4	17:20:40.20	57:47:07.00	2455331.7	-296.3± 0.6	W15
Draco-199	4	17:20:40.19	57:47:06.97	2451720.5	-299.4± 2.4	K02
Draco-199	4	17:20:40.16	57:47:06.21	2448774.9	-298.6± 3.9	A95

Table G.1: Continued. Velocities of RGB stars in Draco

Star ID	n	α_{J2000} (hh:mm:ss.ss)	δ_{J2000} (dd:mm:ss.ss)	HJD (days)	v (km s ⁻¹)	Ref.
Draco-199	4	17:20:40.16	57:47:06.21	2449457.9	-292.3± 3.2	A95
Draco-200	2	17:20:40.31	57:56:18.10	2455331.7	-293.4± 0.8	W15
Draco-200	2	17:20:40.31	57:56:18.13	2451720.5	-291.9± 1.5	K02
Draco-201	4	17:20:41.06	57:58:25.60	2455591.0	-294.1± 1.8	W15
Draco-201	4	17:20:41.06	57:58:25.60	2455706.9	-293.7± 0.6	W15
Draco-201	4	17:20:41.06	57:58:25.57	2451720.5	-295.5± 2.2	K02
Draco-201	4	17:20:41.05	57:58:25.69	2454975.5	-294.0± 2.2	K10
Draco-202	2	17:20:41.51	57:47:56.80	2455331.8	-288.2± 0.9	W15
Draco-202	2	17:20:41.51	57:47:56.80	2455706.8	-288.0± 0.9	W15
Draco-203	7	17:20:41.82	58:00:24.80	2454912.0	-301.6± 0.6	W15
Draco-203	7	17:20:41.82	58:00:24.80	2454914.9	-301.4± 0.4	W15
Draco-203	7	17:20:41.82	58:00:24.80	2455710.9	-304.7± 0.5	W15
Draco-203	7	17:20:41.79	58:00:23.90	2446595.0	-305.5± 2.5	O95
Draco-203	7	17:20:41.79	58:00:23.90	2446595.8	-305.4± 2.1	O95
Draco-203	7	17:20:41.79	58:00:23.90	2447333.9	-304.1± 2.0	O95
Draco-203	7	17:20:41.79	58:00:23.90	2448776.9	-305.5± 5.0	A95
Draco-204	4	17:20:42.10	57:49:29.50	2454912.0	-305.5± 0.8	W15
Draco-204	4	17:20:42.10	57:49:29.50	2454914.9	-305.6± 0.7	W15
Draco-204	4	17:20:42.10	57:49:29.50	2455591.0	-305.4± 1.0	W15
Draco-204	4	17:20:42.10	57:49:29.50	2455706.9	-306.2± 0.7	W15
Draco-205	6	17:20:43.37	57:50:42.80	2453850.8	-296.8± 1.6	W15
Draco-205	6	17:20:43.37	57:50:42.80	2455331.7	-299.9± 1.5	W15
Draco-205	6	17:20:43.37	57:50:42.80	2455591.0	-299.1± 0.8	W15
Draco-205	6	17:20:43.37	57:50:42.80	2455707.4	-298.3± 0.3	W15
Draco-205	6	17:20:43.37	57:50:42.80	2455711.8	-298.8± 0.4	W15
Draco-205	6	17:20:43.36	57:50:42.80	2454975.5	-299.2± 2.2	K10
Draco-206	6	17:20:43.67	57:48:44.20	2455331.7	-284.1± 0.5	W15
Draco-206	6	17:20:43.64	57:48:43.30	2446919.0	-283.0± 1.3	O95
Draco-206	6	17:20:43.64	57:48:43.30	2447328.9	-282.1± 2.8	O95
Draco-206	6	17:20:43.64	57:48:43.30	2447421.7	-283.1± 1.5	O95
Draco-206	6	17:20:43.64	57:48:43.30	2448776.9	-286.7± 1.4	A95
Draco-206	6	17:20:43.64	57:48:43.30	2449457.9	-286.2± 1.0	A95
Draco-207	2	17:20:43.93	57:51:45.30	2454168.9	-291.0± 1.0	W15
Draco-207	2	17:20:43.93	57:51:45.30	2455707.8	-291.7± 0.7	W15
Draco-208	2	17:20:44.49	57:55:11.60	2454912.0	-295.7± 2.0	W15
Draco-208	2	17:20:44.49	57:55:11.60	2454914.9	-294.4± 1.9	W15
Draco-209	2	17:20:44.54	57:51:39.60	2454912.0	-288.4± 0.9	W15

Table G.1: Continued. Velocities of RGB stars in Draco

Star ID	n	α_{J2000} (hh:mm:ss.ss)	δ_{J2000} (dd:mm:ss.ss)	HJD (days)	v (km s ⁻¹)	Ref.
Draco-209	2	17:20:44.54	57:51:39.60	2454914.9	-287.9± 0.7	W15
Draco-210	4	17:20:44.73	57:54:59.40	2454155.0	-285.3± 1.2	W15
Draco-210	4	17:20:44.73	57:54:59.40	2455706.9	-291.2± 0.7	W15
Draco-210	4	17:20:44.73	57:54:59.36	2451720.5	-293.5± 3.9	K02
Draco-210	4	17:20:44.71	57:54:59.50	2454975.5	-290.4± 2.3	K10
Draco-211	3	17:20:45.43	57:49:00.11	2453850.8	-290.3± 1.5	W15
Draco-211	3	17:20:45.43	57:49:00.08	2451720.5	-282.8± 1.1	K02
Draco-211	3	17:20:45.43	57:49:00.08	2452813.0	-289.0± 1.4	W04
Draco-212	7	17:20:47.57	57:54:08.51	2454170.9	-290.2± 0.9	W15
Draco-212	7	17:20:47.57	57:54:08.51	2455331.8	-288.2± 0.8	W15
Draco-212	7	17:20:47.57	57:54:08.51	2455591.0	-288.9± 0.8	W15
Draco-212	7	17:20:47.57	57:54:08.51	2455707.4	-288.7± 0.3	W15
Draco-212	7	17:20:47.57	57:54:08.51	2455710.8	-290.2± 0.9	W15
Draco-212	7	17:20:47.57	57:54:08.46	2452813.0	-284.4± 3.2	W04
Draco-212	7	17:20:47.55	57:54:08.51	2454975.5	-287.2± 2.2	K10
Draco-213	3	17:20:47.78	57:53:24.21	2455708.9	-291.1± 1.6	W15
Draco-213	3	17:20:47.78	57:53:24.21	2455712.9	-291.6± 1.6	W15
Draco-213	3	17:20:47.76	57:53:24.21	2454975.5	-292.6± 2.7	K10
Draco-214	8	17:20:47.78	57:59:55.50	2454912.0	-297.5± 0.5	W15
Draco-214	8	17:20:47.78	57:59:55.50	2454914.9	-296.9± 0.4	W15
Draco-214	8	17:20:47.78	57:59:55.50	2451720.5	-294.1± 0.9	K02
Draco-214	8	17:20:47.73	57:59:54.70	2446595.9	-298.3± 1.9	O95
Draco-214	8	17:20:47.73	57:59:54.70	2447632.0	-298.3± 2.7	O95
Draco-214	8	17:20:47.73	57:59:54.70	2448774.9	-297.0± 1.9	A95
Draco-214	8	17:20:47.73	57:59:54.70	2449130.9	-297.6± 1.3	A95
Draco-214	8	17:20:47.73	57:59:54.70	2449457.9	-294.7± 1.2	A95
Draco-215	2	17:20:47.92	57:51:38.10	2455707.8	-295.8± 1.0	W15
Draco-215	2	17:20:47.90	57:51:38.10	2454975.5	-294.1± 2.3	K10
Draco-216	2	17:20:48.12	57:54:56.50	2454159.0	-289.7± 0.8	W15
Draco-216	2	17:20:48.12	57:54:56.50	2454170.9	-289.9± 1.4	W15
Draco-217	2	17:20:48.76	57:57:14.60	2455706.8	-294.9± 1.4	W15
Draco-217	2	17:20:48.74	57:57:14.70	2454975.5	-294.7± 2.4	K10
Draco-218	5	17:20:50.93	57:51:09.70	2453850.8	-282.1± 1.3	W15
Draco-218	5	17:20:50.94	57:51:09.72	2451720.5	-282.0± 1.0	K02
Draco-218	5	17:20:50.94	57:51:09.72	2452813.0	-278.3± 2.6	W04
Draco-218	5	17:20:50.89	57:51:09.10	2449130.9	-289.3± 5.3	A95
Draco-218	5	17:20:50.89	57:51:09.10	2449457.9	-278.0± 7.3	A95

Table G.1: Continued. Velocities of RGB stars in Draco

Star ID	n	α_{J2000} (hh:mm:ss.ss)	δ_{J2000} (dd:mm:ss.ss)	HJD (days)	v (km s ⁻¹)	Ref.
Draco-219	3	17:20:50.98	58:04:49.20	2454165.9	-294.4± 2.6	W15
Draco-219	3	17:20:50.98	58:04:49.20	2455707.3	-292.5± 1.0	W15
Draco-219	3	17:20:50.97	58:04:49.30	2454975.5	-288.7± 2.4	K10
Draco-220	3	17:20:51.16	57:38:14.21	2455331.8	-301.4± 0.7	W15
Draco-220	3	17:20:51.16	57:38:14.17	2451720.5	-306.2± 2.0	K02
Draco-220	3	17:20:51.16	57:38:14.17	2452813.0	-299.3± 3.2	W04
Draco-221	2	17:20:51.34	58:05:40.50	2455712.9	-293.9± 1.8	W15
Draco-221	2	17:20:51.33	58:05:40.50	2454975.5	-286.8± 2.7	K10
Draco-222	6	17:20:52.06	57:59:47.81	2453850.8	-295.1± 0.8	W15
Draco-222	6	17:20:52.06	57:59:47.76	2451720.5	-294.2± 0.9	K02
Draco-222	6	17:20:52.03	57:59:46.99	2448439.9	-293.0± 2.2	O95
Draco-222	6	17:20:52.03	57:59:46.99	2448774.9	-298.5± 3.4	A95
Draco-222	6	17:20:52.03	57:59:46.99	2449130.9	-296.1± 1.6	A95
Draco-222	6	17:20:52.05	57:59:47.90	2454975.5	-293.1± 2.1	K10
Draco-223	2	17:20:52.51	57:55:10.61	2455707.9	-287.7± 1.2	W15
Draco-223	2	17:20:52.51	57:55:10.61	2455712.9	-283.6± 3.3	W15
Draco-224	8	17:20:52.99	57:55:57.81	2454912.0	-295.7± 0.5	W15
Draco-224	8	17:20:52.99	57:55:57.81	2454914.9	-296.2± 0.5	W15
Draco-224	8	17:20:52.95	57:55:57.10	2445846.9	-296.2± 1.8	O95
Draco-224	8	17:20:52.95	57:55:57.10	2447057.6	-294.0± 3.1	O95
Draco-224	8	17:20:52.95	57:55:57.10	2447058.7	-295.2± 1.7	O95
Draco-224	8	17:20:52.95	57:55:57.10	2448774.9	-296.6± 5.1	A95
Draco-224	8	17:20:52.95	57:55:57.10	2449130.9	-294.1± 0.9	A95
Draco-224	8	17:20:52.97	57:55:57.90	2454975.5	-294.7± 2.1	K10
Draco-225	6	17:20:52.99	57:56:27.70	2454155.0	-287.1± 1.5	W15
Draco-225	6	17:20:52.99	57:56:27.70	2454168.9	-283.9± 0.9	W15
Draco-225	6	17:20:52.99	57:56:27.70	2455332.3	-284.4± 0.7	W15
Draco-225	6	17:20:52.99	57:56:27.70	2455591.0	-284.5± 0.8	W15
Draco-225	6	17:20:52.99	57:56:27.70	2455707.4	-284.0± 0.4	W15
Draco-225	6	17:20:52.99	57:56:27.70	2455710.8	-283.9± 0.7	W15
Draco-226	6	17:20:53.72	57:58:12.59	2455706.9	-284.6± 0.5	W15
Draco-226	6	17:20:53.72	57:58:12.50	2451720.5	-288.4± 1.4	K02
Draco-226	6	17:20:53.68	57:58:11.70	2448774.9	-285.2± 8.0	A95
Draco-226	6	17:20:53.68	57:58:11.70	2449130.9	-283.5± 5.4	A95
Draco-226	6	17:20:53.68	57:58:11.70	2449457.9	-284.2± 2.0	A95
Draco-226	6	17:20:53.71	57:58:12.59	2454975.5	-285.1± 2.1	K10
Draco-227	2	17:20:53.73	57:49:30.10	2455706.8	-296.4± 1.4	W15

Table G.1: Continued. Velocities of RGB stars in Draco

Star ID	n	α_{J2000} (hh:mm:ss.ss)	δ_{J2000} (dd:mm:ss.ss)	HJD (days)	v (km s ⁻¹)	Ref.
Draco-227	2	17:20:53.73	57:49:30.10	2455710.8	-297.1± 1.1	W15
Draco-228	2	17:20:53.96	57:47:59.30	2455591.0	-298.8± 1.9	W15
Draco-228	2	17:20:53.96	57:47:59.30	2455710.8	-301.4± 1.5	W15
Draco-229	2	17:20:55.52	57:44:34.40	2455331.7	-302.1± 1.2	W15
Draco-229	2	17:20:55.53	57:44:34.37	2451720.5	-304.0± 2.8	K02
Draco-230	2	17:20:56.25	58:00:26.60	2455707.8	-292.2± 0.9	W15
Draco-230	2	17:20:56.25	58:00:26.60	2455712.9	-292.8± 1.3	W15
Draco-231	4	17:20:56.58	58:02:35.10	2454165.9	-283.6± 1.2	W15
Draco-231	4	17:20:56.58	58:02:35.10	2455332.9	-282.2± 0.9	W15
Draco-231	4	17:20:56.58	58:02:35.05	2451720.5	-283.0± 2.5	K02
Draco-231	4	17:20:56.56	58:02:35.10	2454975.5	-280.7± 2.2	K10
Draco-232	2	17:20:58.49	57:51:02.40	2454168.9	-281.9± 1.7	W15
Draco-232	2	17:20:58.47	57:51:02.40	2454975.5	-279.6± 2.7	K10
Draco-233	2	17:20:59.19	57:47:41.31	2454168.9	-296.2± 1.0	W15
Draco-233	2	17:20:59.19	57:47:41.31	2455591.0	-296.0± 1.1	W15
Draco-234	2	17:21:00.18	57:46:37.70	2455332.4	-304.7± 0.5	W15
Draco-234	2	17:21:00.18	57:46:37.74	2451720.5	-303.2± 1.7	K02
Draco-235	3	17:21:00.59	57:49:21.30	2454155.0	-293.9± 0.9	W15
Draco-235	3	17:21:00.59	57:49:21.30	2454912.0	-292.7± 0.6	W15
Draco-235	3	17:21:00.58	57:49:21.20	2454975.5	-299.0± 2.2	K10
Draco-236	2	17:21:01.28	57:57:43.40	2455331.8	-295.0± 0.6	W15
Draco-236	2	17:21:01.25	57:57:43.50	2454975.5	-294.5± 2.1	K10
Draco-237	2	17:21:01.77	57:49:59.40	2454170.9	-285.2± 1.7	W15
Draco-237	2	17:21:01.77	57:49:59.40	2455332.9	-288.5± 1.2	W15
Draco-238	6	17:21:02.24	58:15:38.30	2454912.0	-276.8± 0.5	W15
Draco-238	6	17:21:02.24	58:15:38.30	2454914.9	-276.5± 0.4	W15
Draco-238	6	17:21:02.24	58:15:38.30	2455707.9	-276.4± 0.3	W15
Draco-238	6	17:21:02.23	58:15:38.30	2451720.5	-277.2± 0.9	K02
Draco-238	6	17:21:02.23	58:15:38.30	2452813.0	-276.1± 1.1	W04
Draco-238	6	17:21:02.19	58:15:37.50	2448776.9	-292.4± 6.5	A95
Draco-239	5	17:21:02.63	57:52:44.70	2454155.0	-296.1± 1.4	W15
Draco-239	5	17:21:02.63	57:52:44.70	2454159.0	-296.3± 1.5	W15
Draco-239	5	17:21:02.63	57:52:44.70	2454168.9	-295.3± 0.9	W15
Draco-239	5	17:21:02.63	57:52:44.70	2454170.9	-296.2± 1.7	W15
Draco-239	5	17:21:02.63	57:52:44.70	2455706.8	-295.6± 0.9	W15
Draco-240	5	17:21:02.86	57:50:00.11	2455331.7	-279.7± 1.7	W15
Draco-240	5	17:21:02.86	57:50:00.11	2455591.0	-279.2± 0.8	W15

Table G.1: Continued. Velocities of RGB stars in Draco

Star ID	n	α_{J2000} (hh:mm:ss.ss)	δ_{J2000} (dd:mm:ss.ss)	HJD (days)	v (km s ⁻¹)	Ref.
Draco-240	5	17:21:02.86	57:50:00.11	2455707.4	-280.5± 0.4	W15
Draco-240	5	17:21:02.86	57:50:00.11	2455711.8	-279.1± 0.7	W15
Draco-240	5	17:21:02.85	57:50:00.11	2454975.5	-280.8± 2.2	K10
Draco-241	3	17:21:03.21	57:55:59.30	2453850.8	-289.4± 1.2	W15
Draco-241	3	17:21:03.21	57:55:59.30	2455332.3	-291.0± 0.4	W15
Draco-241	3	17:21:03.21	57:55:59.34	2451720.5	-290.3± 0.8	K02
Draco-242	8	17:21:03.55	57:57:08.20	2453850.8	-290.3± 0.7	W15
Draco-242	8	17:21:03.55	57:57:08.20	2455331.8	-289.6± 0.5	W15
Draco-242	8	17:21:03.55	57:57:08.21	2451720.5	-287.6± 0.7	K02
Draco-242	8	17:21:03.52	57:57:07.41	2446965.7	-290.3± 1.7	O95
Draco-242	8	17:21:03.52	57:57:07.41	2448774.9	-284.2± 7.4	A95
Draco-242	8	17:21:03.52	57:57:07.41	2449130.9	-287.6± 4.9	A95
Draco-242	8	17:21:03.52	57:57:07.41	2449457.9	-288.2± 2.7	A95
Draco-242	8	17:21:03.52	57:57:07.41	2449459.9	-285.0± 5.5	A95
Draco-243	5	17:21:03.69	57:39:54.19	2455331.8	-292.3± 1.6	W15
Draco-243	5	17:21:03.69	57:39:54.19	2455591.0	-292.8± 2.3	W15
Draco-243	5	17:21:03.69	57:39:54.19	2455707.2	-290.0± 0.8	W15
Draco-243	5	17:21:03.69	57:39:54.19	2455711.8	-290.1± 0.8	W15
Draco-243	5	17:21:03.70	57:39:54.25	2451720.5	-284.1± 3.4	K02
Draco-244	3	17:21:04.50	57:50:47.80	2454170.9	-299.0± 2.3	W15
Draco-244	3	17:21:04.50	57:50:47.80	2455708.9	-290.5± 2.0	W15
Draco-244	3	17:21:04.50	57:50:47.80	2455712.9	-301.0± 1.9	W15
Draco-245	7	17:21:04.83	58:02:01.10	2454165.9	-294.7± 0.5	W15
Draco-245	7	17:21:04.83	58:02:01.10	2455332.9	-294.9± 0.6	W15
Draco-245	7	17:21:04.83	58:02:01.10	2455707.1	-295.2± 0.3	W15
Draco-245	7	17:21:04.84	58:02:01.10	2451720.5	-298.1± 1.3	K02
Draco-245	7	17:21:04.84	58:02:01.10	2452813.0	-294.0± 1.9	W04
Draco-245	7	17:21:04.80	58:02:00.30	2448776.9	-300.3± 8.1	A95
Draco-245	7	17:21:04.80	58:02:00.30	2449457.9	-299.5± 4.5	A95
Draco-246	2	17:21:05.79	58:04:54.90	2454165.9	-293.4± 1.3	W15
Draco-246	2	17:21:05.85	58:04:55.00	2451720.5	-289.9± 3.9	K02
Draco-247	5	17:21:10.39	57:47:53.30	2455591.0	-305.9± 0.6	W15
Draco-247	5	17:21:10.39	57:47:53.30	2455708.9	-306.1± 0.6	W15
Draco-247	5	17:21:10.40	57:47:53.30	2451720.5	-307.3± 1.4	K02
Draco-247	5	17:21:10.40	57:47:53.30	2452813.0	-307.2± 1.6	W04
Draco-247	5	17:21:10.35	57:47:52.59	2449459.9	-310.6± 8.1	A95
Draco-248	2	17:21:12.79	58:04:41.00	2454165.9	-290.4± 1.5	W15

Table G.1: Continued. Velocities of RGB stars in Draco

Star ID	n	α_{J2000} (hh:mm:ss.ss)	δ_{J2000} (dd:mm:ss.ss)	HJD (days)	v (km s ⁻¹)	Ref.
Draco-248	2	17:21:12.79	58:04:41.00	2455706.8	-289.5± 0.8	W15
Draco-249	4	17:21:13.83	57:52:45.81	2455331.8	-287.4± 1.0	W15
Draco-249	4	17:21:13.83	57:52:45.81	2455706.8	-288.4± 0.6	W15
Draco-249	4	17:21:13.83	57:52:45.80	2451720.5	-280.7± 3.4	K02
Draco-249	4	17:21:13.81	57:52:45.81	2454975.5	-285.0± 2.3	K10
Draco-250	4	17:21:14.58	57:52:13.90	2454159.0	-287.9± 0.8	W15
Draco-250	4	17:21:14.58	57:52:13.90	2454170.9	-286.0± 0.9	W15
Draco-250	4	17:21:14.58	57:52:13.90	2454912.0	-286.6± 0.7	W15
Draco-250	4	17:21:14.58	57:52:13.90	2454914.9	-286.7± 0.5	W15
Draco-251	5	17:21:14.69	57:52:10.29	2455331.8	-286.9± 0.6	W15
Draco-251	5	17:21:14.70	57:52:10.31	2452813.0	-284.2± 2.8	W04
Draco-251	5	17:21:14.64	57:52:09.50	2448776.9	-293.2± 8.2	A95
Draco-251	5	17:21:14.64	57:52:09.50	2449130.9	-276.6± 7.0	A95
Draco-251	5	17:21:14.69	57:52:10.29	2454975.5	-287.1± 2.1	K10
Draco-252	2	17:21:17.49	57:59:49.30	2454912.0	-291.7± 1.5	W15
Draco-252	2	17:21:17.49	57:59:49.30	2454914.9	-290.8± 1.3	W15
Draco-253	3	17:21:17.89	57:56:21.19	2455331.7	-292.0± 0.7	W15
Draco-253	3	17:21:17.90	57:56:21.30	2451720.5	-291.2± 1.8	K02
Draco-253	3	17:21:17.90	57:56:21.30	2452813.0	-297.7± 5.6	W04
Draco-254	4	17:21:21.58	58:06:08.30	2454155.0	-306.1± 2.0	W15
Draco-254	4	17:21:21.58	58:06:08.30	2455332.3	-301.2± 0.9	W15
Draco-254	4	17:21:21.58	58:06:08.30	2455707.9	-302.4± 0.8	W15
Draco-254	4	17:21:21.58	58:06:08.30	2455712.9	-305.9± 1.3	W15
Draco-255	6	17:21:22.28	58:02:15.50	2454912.0	-303.2± 1.1	W15
Draco-255	6	17:21:22.28	58:02:15.50	2454914.9	-303.6± 0.7	W15
Draco-255	6	17:21:22.28	58:02:15.50	2455707.5	-303.1± 0.4	W15
Draco-255	6	17:21:22.29	58:02:15.54	2451720.5	-307.6± 2.3	K02
Draco-255	6	17:21:22.29	58:02:15.54	2452813.0	-300.1± 7.2	W04
Draco-255	6	17:21:22.27	58:02:15.50	2454975.5	-298.8± 2.3	K10
Draco-256	2	17:21:24.66	58:05:48.10	2454912.0	-295.6± 2.3	W15
Draco-256	2	17:21:24.66	58:05:48.10	2454914.9	-297.8± 1.4	W15
Draco-257	5	17:21:30.29	57:50:16.30	2453850.8	-300.5± 0.9	W15
Draco-257	5	17:21:30.29	57:50:16.30	2455331.7	-302.2± 0.6	W15
Draco-257	5	17:21:30.33	57:50:16.40	2451720.5	-304.6± 1.1	K02
Draco-257	5	17:21:30.23	57:50:15.60	2448774.9	-303.1± 3.1	A95
Draco-257	5	17:21:30.23	57:50:15.60	2449130.9	-305.4± 3.8	A95
Draco-258	3	17:21:35.39	57:54:59.19	2455332.3	-308.4± 0.8	W15

Table G.1: Continued. Velocities of RGB stars in Draco

Star ID	n	α_{J2000} (hh:mm:ss.ss)	δ_{J2000} (dd:mm:ss.ss)	HJD (days)	v (km s ⁻¹)	Ref.
Draco-258	3	17:21:35.39	57:54:59.19	2455707.8	-303.2± 1.0	W15
Draco-258	3	17:21:35.39	57:54:59.22	2451720.5	-296.2± 2.9	K02
Draco-259	3	17:21:36.80	57:58:37.00	2455331.7	-292.9± 1.8	W15
Draco-259	3	17:21:36.81	57:58:37.02	2451720.5	-303.6± 3.0	K02
Draco-259	3	17:21:36.77	57:58:37.10	2454975.5	-294.5± 2.2	K10
Draco-260	6	17:21:37.76	58:00:52.20	2455331.8	-277.4± 0.9	W15
Draco-260	6	17:21:37.76	58:00:52.20	2455591.0	-277.2± 1.9	W15
Draco-260	6	17:21:37.76	58:00:52.20	2455707.4	-277.7± 0.4	W15
Draco-260	6	17:21:37.76	58:00:52.20	2455711.5	-279.0± 0.5	W15
Draco-260	6	17:21:37.79	58:00:52.31	2451720.5	-282.5± 3.4	K02
Draco-260	6	17:21:37.76	58:00:52.29	2454975.5	-280.0± 2.2	K10
Draco-261	2	17:21:38.65	57:55:39.99	2454912.0	-274.1± 0.9	W15
Draco-261	2	17:21:38.65	57:55:39.99	2454914.9	-276.2± 0.9	W15
Draco-262	2	17:21:39.02	57:57:55.20	2455706.8	-298.6± 1.6	W15
Draco-262	2	17:21:38.99	57:57:55.31	2454975.5	-302.2± 2.3	K10
Draco-263	5	17:21:39.37	57:46:40.10	2455332.9	-307.1± 0.5	W15
Draco-263	5	17:21:39.42	57:46:40.40	2451720.5	-310.4± 1.3	K02
Draco-263	5	17:21:39.43	57:46:39.89	2448774.9	-311.9± 5.3	A95
Draco-263	5	17:21:39.43	57:46:39.89	2449130.9	-295.9± 5.5	A95
Draco-263	5	17:21:39.43	57:46:39.89	2449457.9	-303.8± 2.3	A95
Draco-264	5	17:21:40.36	57:47:32.00	2453850.8	-288.3± 0.8	W15
Draco-264	5	17:21:40.36	57:47:32.00	2455332.8	-282.0± 0.5	W15
Draco-264	5	17:21:40.36	57:47:32.00	2455707.3	-279.5± 0.4	W15
Draco-264	5	17:21:40.41	57:47:32.30	2451720.5	-293.0± 0.8	K02
Draco-264	5	17:21:40.32	57:47:31.41	2449130.9	-286.9± 2.8	A95
Draco-265	4	17:21:41.80	57:55:50.71	2455331.8	-294.4± 1.0	W15
Draco-265	4	17:21:41.80	57:55:50.71	2455706.8	-295.5± 0.7	W15
Draco-265	4	17:21:41.80	57:55:50.74	2451720.5	-283.0± 2.9	K02
Draco-265	4	17:21:41.78	57:55:50.80	2454975.5	-295.6± 2.2	K10
Draco-266	5	17:21:42.55	58:14:33.00	2453850.8	-287.2± 1.4	W15
Draco-266	5	17:21:42.55	58:14:33.00	2454165.9	-288.2± 0.6	W15
Draco-266	5	17:21:42.55	58:14:33.00	2455332.9	-288.2± 0.7	W15
Draco-266	5	17:21:42.55	58:14:33.00	2455707.9	-288.2± 0.4	W15
Draco-266	5	17:21:42.55	58:14:33.04	2452813.0	-285.2± 1.3	W04
Draco-267	4	17:21:49.18	57:53:37.10	2454912.0	-293.6± 0.6	W15
Draco-267	4	17:21:49.18	57:53:37.10	2454914.9	-293.6± 0.5	W15
Draco-267	4	17:21:49.22	57:53:37.20	2451720.5	-291.3± 2.0	K02

Table G.1: Continued. Velocities of RGB stars in Draco

Star ID	n	α_{J2000} (hh:mm:ss.ss)	δ_{J2000} (dd:mm:ss.ss)	HJD (days)	v (km s ⁻¹)	Ref.
Draco-267	4	17:21:49.17	57:53:37.19	2454975.5	-293.6± 2.1	K10
Draco-268	2	17:21:49.94	57:58:17.10	2455706.8	-310.8± 1.5	W15
Draco-268	2	17:21:49.93	57:58:17.19	2454975.5	-311.1± 2.6	K10
Draco-269	3	17:21:50.93	57:54:38.10	2455707.3	-289.0± 1.0	W15
Draco-269	3	17:21:50.93	57:54:38.10	2455710.8	-293.1± 1.2	W15
Draco-269	3	17:21:50.93	57:54:38.31	2454975.5	-289.9± 2.3	K10
Draco-270	5	17:21:52.47	57:52:36.80	2454155.0	-316.7± 0.8	W15
Draco-270	5	17:21:52.47	57:52:36.80	2454168.9	-316.3± 0.8	W15
Draco-270	5	17:21:52.47	57:52:36.80	2455707.8	-281.6± 0.6	W15
Draco-270	5	17:21:52.47	57:52:36.80	2455710.8	-285.9± 0.6	W15
Draco-270	5	17:21:52.46	57:52:36.89	2454975.5	-292.6± 2.1	K10
Draco-271	2	17:21:53.31	57:55:59.80	2455707.3	-297.1± 1.1	W15
Draco-271	2	17:21:53.31	57:55:59.80	2455710.8	-299.8± 1.1	W15
Draco-272	2	17:21:55.22	57:56:59.30	2455706.8	-304.9± 0.9	W15
Draco-272	2	17:21:55.20	57:56:59.40	2454975.5	-305.5± 2.3	K10
Draco-273	6	17:21:56.95	57:59:33.80	2453850.8	-297.7± 1.2	W15
Draco-273	6	17:21:56.95	57:59:33.80	2455331.7	-299.2± 0.6	W15
Draco-273	6	17:21:56.95	57:59:33.80	2455591.0	-300.2± 0.5	W15
Draco-273	6	17:21:56.96	57:59:33.86	2451720.5	-314.0± 5.4	K02
Draco-273	6	17:21:56.96	57:59:33.86	2452813.0	-299.1± 1.4	W04
Draco-273	6	17:21:56.94	57:59:33.89	2454975.5	-299.7± 2.1	K10
Draco-274	3	17:22:02.29	58:01:17.30	2455591.0	-300.0± 1.6	W15
Draco-274	3	17:22:02.30	58:01:17.33	2451720.5	-295.8± 5.3	K02
Draco-274	3	17:22:02.30	58:01:17.33	2452813.0	-302.3± 11.4	W04
Draco-275	3	17:22:02.87	58:08:35.60	2454165.9	-283.7± 1.3	W15
Draco-275	3	17:22:02.87	58:08:35.60	2455708.9	-284.0± 1.7	W15
Draco-275	3	17:22:02.87	58:08:35.60	2455712.9	-280.3± 2.6	W15
Draco-276	4	17:22:03.60	57:45:07.20	2455332.5	-286.8± 0.4	W15
Draco-276	4	17:22:03.60	57:45:07.20	2455707.5	-286.7± 0.3	W15
Draco-276	4	17:22:03.60	57:45:07.20	2451720.5	-287.7± 1.9	K02
Draco-276	4	17:22:03.60	57:45:07.20	2452813.0	-286.4± 3.9	W04
Draco-277	5	17:22:03.76	57:41:28.60	2454912.0	-292.3± 0.5	W15
Draco-277	5	17:22:03.76	57:41:28.60	2454914.9	-291.9± 0.5	W15
Draco-277	5	17:22:03.76	57:41:28.60	2455331.8	-291.8± 0.5	W15
Draco-277	5	17:22:03.75	57:41:28.64	2451720.5	-294.0± 2.3	K02
Draco-277	5	17:22:03.75	57:41:28.64	2452813.0	-291.3± 2.8	W04
Draco-278	3	17:22:04.51	57:57:15.00	2454155.0	-306.2± 0.8	W15

Table G.1: Continued. Velocities of RGB stars in Draco

Star ID	n	α_{J2000} (hh:mm:ss.ss)	δ_{J2000} (dd:mm:ss.ss)	HJD (days)	v (km s ⁻¹)	Ref.
Draco-278	3	17:22:04.51	57:57:15.00	2454912.0	-305.8± 0.6	W15
Draco-278	3	17:22:04.51	57:57:15.00	2454914.9	-306.1± 0.6	W15
Draco-279	2	17:22:05.31	58:01:46.90	2455332.5	-302.8± 0.6	W15
Draco-279	2	17:22:05.31	58:01:46.90	2455710.9	-303.8± 1.6	W15
Draco-280	5	17:22:06.07	58:00:11.80	2455332.3	-285.5± 0.8	W15
Draco-280	5	17:22:06.07	58:00:11.80	2455706.9	-285.8± 0.8	W15
Draco-280	5	17:22:06.07	58:00:11.80	2455710.8	-285.6± 1.2	W15
Draco-280	5	17:22:06.08	58:00:11.81	2451720.5	-289.0± 3.2	K02
Draco-280	5	17:22:06.08	58:00:11.81	2452813.0	-290.0±11.8	W04
Draco-281	2	17:22:06.54	57:56:10.19	2455332.8	-304.6± 1.4	W15
Draco-281	2	17:22:06.54	57:56:10.21	2451720.5	-302.6± 4.2	K02
Draco-282	4	17:22:11.21	57:56:33.10	2453850.8	-305.0± 1.6	W15
Draco-282	4	17:22:11.21	57:56:33.10	2455331.7	-307.8± 0.9	W15
Draco-282	4	17:22:11.21	57:56:33.18	2451720.5	-311.1± 1.9	K02
Draco-282	4	17:22:11.21	57:56:33.18	2452813.0	-316.5± 4.3	W04
Draco-283	3	17:22:27.12	57:45:54.40	2454168.9	-294.6± 1.0	W15
Draco-283	3	17:22:27.12	57:45:54.40	2455332.9	-294.3± 0.8	W15
Draco-283	3	17:22:27.12	57:45:54.36	2451720.5	-294.5± 2.1	K02
Draco-284	4	17:22:29.19	58:05:10.20	2455332.9	-306.4± 2.4	W15
Draco-284	4	17:22:29.19	58:05:10.20	2455707.2	-307.4± 0.9	W15
Draco-284	4	17:22:29.19	58:05:10.18	2452813.0	-307.1± 6.8	W04
Draco-284	4	17:22:29.18	58:05:10.20	2454975.5	-307.0± 2.4	K10
Draco-285	7	17:22:32.22	58:17:46.90	2453850.8	-279.9± 1.3	W15
Draco-285	7	17:22:32.22	58:17:46.90	2454165.9	-281.5± 0.6	W15
Draco-285	7	17:22:32.22	58:17:46.90	2455332.3	-282.6± 0.5	W15
Draco-285	7	17:22:32.22	58:17:46.90	2455591.0	-282.7± 1.2	W15
Draco-285	7	17:22:32.22	58:17:46.90	2455707.8	-282.6± 0.4	W15
Draco-285	7	17:22:32.22	58:17:46.90	2455712.9	-282.5± 0.8	W15
Draco-285	7	17:22:32.22	58:17:46.90	2452813.0	-283.9± 2.6	W04
Draco-286	7	17:22:33.51	57:48:03.80	2454168.9	-277.4± 1.0	W15
Draco-286	7	17:22:33.51	57:48:03.80	2455332.3	-276.8± 0.7	W15
Draco-286	7	17:22:33.51	57:48:03.80	2455591.0	-278.0± 0.9	W15
Draco-286	7	17:22:33.51	57:48:03.80	2455707.6	-277.0± 0.4	W15
Draco-286	7	17:22:33.51	57:48:03.80	2455712.9	-276.8± 0.9	W15
Draco-286	7	17:22:33.51	57:48:03.74	2451720.5	-275.2± 3.1	K02
Draco-286	7	17:22:33.51	57:48:03.74	2452813.0	-276.0± 1.5	W04
Draco-287	4	17:22:36.47	58:03:03.50	2455332.5	-301.7± 0.9	W15

Table G.1: Continued. Velocities of RGB stars in Draco

Star ID	n	α_{J2000} (hh:mm:ss.ss)	δ_{J2000} (dd:mm:ss.ss)	HJD (days)	v (km s ⁻¹)	Ref.
Draco-287	4	17:22:36.47	58:03:03.50	2455708.3	-301.2± 0.9	W15
Draco-287	4	17:22:36.47	58:03:03.50	2455712.9	-300.9± 1.6	W15
Draco-287	4	17:22:36.47	58:03:03.50	2454975.5	-300.2± 2.3	K10
Draco-288	7	17:22:43.68	57:57:30.70	2455332.3	-282.1± 0.5	W15
Draco-288	7	17:22:43.68	57:57:30.70	2455591.0	-281.6± 0.7	W15
Draco-288	7	17:22:43.68	57:57:30.70	2455707.8	-282.2± 0.6	W15
Draco-288	7	17:22:43.68	57:57:30.70	2455710.8	-281.7± 0.6	W15
Draco-288	7	17:22:43.68	57:57:30.71	2451720.5	-279.6± 1.8	K02
Draco-288	7	17:22:43.68	57:57:30.71	2452813.0	-280.7± 2.7	W04
Draco-288	7	17:22:43.67	57:57:30.81	2454975.5	-280.4± 2.2	K10
Draco-289	5	17:23:01.23	57:46:56.10	2455332.8	-292.7± 1.8	W15
Draco-289	5	17:23:01.23	57:46:56.10	2455591.0	-296.7± 1.9	W15
Draco-289	5	17:23:01.23	57:46:56.10	2455707.3	-292.1± 0.8	W15
Draco-289	5	17:23:01.23	57:46:56.10	2455710.8	-292.1± 2.9	W15
Draco-289	5	17:23:01.21	57:46:56.03	2452813.0	-286.1± 2.4	W04
Draco-290	4	17:23:02.91	57:27:29.30	2453850.8	-289.9± 1.4	W15
Draco-290	4	17:23:02.91	57:27:29.30	2454168.9	-291.5± 0.6	W15
Draco-290	4	17:23:02.91	57:27:29.30	2455332.9	-291.2± 0.7	W15
Draco-290	4	17:23:02.91	57:27:29.34	2452813.0	-292.8± 1.5	W04
Draco-291	3	17:24:53.57	58:17:27.79	2455332.8	-298.7± 1.4	W15
Draco-291	3	17:24:53.57	58:17:27.79	2455711.4	-297.8± 1.0	W15
Draco-291	3	17:24:53.58	58:17:27.85	2452813.0	-288.2± 8.1	W04
Draco-292	2	17:27:38.35	58:15:47.10	2454213.8	-288.7± 0.5	W15
Draco-292	2	17:27:38.35	58:15:47.10	2455712.4	-287.8± 0.5	W15
Draco-293	2	17:18:41.37	57:59:52.08	2451720.5	-262.8± 1.9	K02
Draco-293	2	17:18:41.37	57:59:52.08	2452813.0	-252.4± 2.4	W04
Draco-294	2	17:19:24.35	57:52:20.28	2452813.0	-281.8± 2.5	W04
Draco-294	2	17:19:24.29	57:52:19.50	2449457.9	-279.8± 9.0	A95
Draco-295	2	17:18:57.75	57:55:46.24	2451720.5	-296.5± 1.2	K02
Draco-295	2	17:18:57.75	57:55:46.24	2452813.0	-296.3± 1.6	W04
Draco-296	2	17:19:43.48	57:56:33.22	2452813.0	-270.2± 2.1	W04
Draco-296	2	17:19:43.42	57:56:32.50	2449130.9	-274.6± 5.5	A95
Draco-297	4	17:20:31.18	57:58:05.45	2451720.5	-302.4± 1.3	K02
Draco-297	4	17:20:31.18	57:58:05.45	2452813.0	-305.7± 2.0	W04
Draco-297	4	17:20:31.13	57:58:04.60	2449130.9	-312.5± 5.6	A95
Draco-297	4	17:20:31.13	57:58:04.60	2449457.9	-297.2± 3.4	A95
Draco-298	3	17:19:53.44	57:56:16.37	2451720.5	-295.7± 1.4	K02

Table G.1: Continued. Velocities of RGB stars in Draco

Star ID	n	α_{J2000} (hh:mm:ss.ss)	δ_{J2000} (dd:mm:ss.ss)	HJD (days)	v (km s ⁻¹)	Ref.
Draco-298	3	17:19:53.44	57:56:16.37	2452813.0	-293.4± 2.0	W04
Draco-298	3	17:19:53.44	57:56:16.40	2454975.5	-295.6± 2.1	K10
Draco-299	3	17:20:15.71	57:53:43.26	2451720.5	-298.1± 1.3	K02
Draco-299	3	17:20:15.71	57:53:43.26	2452813.0	-311.0± 3.1	W04
Draco-299	3	17:20:15.66	57:53:42.60	2449457.9	-306.2± 6.9	A95
Draco-300	2	17:19:56.90	57:52:22.91	2451720.5	-272.7± 1.9	K02
Draco-300	2	17:19:56.90	57:52:22.91	2452813.0	-277.8± 6.5	W04
Draco-301	4	17:20:53.73	57:54:40.43	2451720.5	-284.3± 1.1	K02
Draco-301	4	17:20:53.73	57:54:40.43	2452813.0	-286.2± 1.4	W04
Draco-301	4	17:20:53.67	57:54:39.69	2448774.9	-288.4± 6.8	A95
Draco-301	4	17:20:53.67	57:54:39.69	2449457.9	-282.6± 3.4	A95
Draco-302	2	17:19:53.04	57:51:37.84	2451720.5	-303.5± 1.1	K02
Draco-302	2	17:19:53.04	57:51:37.84	2452813.0	-302.7± 2.8	W04
Draco-303	2	17:20:20.37	57:51:58.25	2451720.5	-292.1± 1.1	K02
Draco-303	2	17:20:20.37	57:51:58.25	2452813.0	-290.9± 2.1	W04
Draco-304	2	17:21:14.22	57:52:22.37	2451720.5	-290.7± 1.3	K02
Draco-304	2	17:21:14.22	57:52:22.37	2452813.0	-287.6± 2.7	W04
Draco-305	2	17:21:15.46	57:57:28.69	2452813.0	-296.7± 2.1	W04
Draco-305	2	17:21:15.39	57:57:28.10	2449457.9	-290.6± 5.5	A95
Draco-306	2	17:19:35.51	57:58:46.60	2451720.5	-282.4± 1.0	K02
Draco-306	2	17:19:35.45	57:58:46.60	2454975.5	-271.9± 2.1	K10
Draco-307	2	17:22:18.61	57:57:19.33	2451720.5	-281.7± 2.5	K02
Draco-307	2	17:22:18.61	57:57:19.33	2452813.0	-292.4± 3.5	W04
Draco-308	2	17:22:10.71	57:53:57.37	2451720.5	-324.2± 0.6	K02
Draco-308	2	17:22:10.71	57:53:57.37	2452813.0	-323.7± 1.0	W04
Draco-309	3	17:20:05.66	57:57:52.74	2451720.5	-284.1± 0.8	K02
Draco-309	3	17:20:05.64	57:57:52.39	2449457.9	-283.5± 3.9	A95
Draco-309	3	17:20:05.66	57:57:52.80	2454975.5	-284.3± 2.1	K10
Draco-310	2	17:20:24.57	57:57:08.20	2451720.5	-290.6± 1.5	K02
Draco-310	2	17:20:24.51	57:57:08.20	2454975.5	-288.8± 2.1	K10
Draco-311	3	17:19:57.91	57:56:58.34	2451720.5	-292.5± 1.1	K02
Draco-311	3	17:19:57.87	57:56:57.39	2449457.9	-289.5± 2.4	A95
Draco-311	3	17:19:57.91	57:56:58.39	2454975.5	-289.6± 2.1	K10
Draco-312	8	17:19:36.00	57:56:28.90	2451720.5	-288.3± 0.7	K02
Draco-312	8	17:19:35.96	57:56:28.20	2445253.6	-284.6± 2.0	O95
Draco-312	8	17:19:35.96	57:56:28.20	2445504.9	-292.9± 1.5	O95
Draco-312	8	17:19:35.96	57:56:28.20	2446256.9	-289.0± 2.9	O95

Table G.1: Continued. Velocities of RGB stars in Draco

Star ID	n	α_{J2000} (hh:mm:ss.ss)	δ_{J2000} (dd:mm:ss.ss)	HJD (days)	v (km s ⁻¹)	Ref.
Draco-312	8	17:19:35.96	57:56:28.20	2447334.9	-291.6± 2.4	O95
Draco-312	8	17:19:35.96	57:56:28.20	2447421.7	-287.2± 1.8	O95
Draco-312	8	17:19:35.96	57:56:28.20	2448774.9	-304.2± 9.2	A95
Draco-312	8	17:19:35.96	57:56:28.20	2449130.9	-288.5± 2.1	A95
Draco-313	2	17:19:45.12	57:55:14.20	2451720.5	-296.8± 0.9	K02
Draco-313	2	17:19:45.09	57:55:13.39	2449130.9	-301.5± 2.7	A95
Draco-314	2	17:19:57.37	57:55:04.80	2451720.5	-306.1± 1.9	K02
Draco-314	2	17:19:57.29	57:55:04.61	2454975.5	-302.6± 2.1	K10
Draco-315	2	17:22:13.68	57:53:06.70	2451720.5	-300.0± 0.8	K02
Draco-315	2	17:22:13.63	57:53:06.50	2454975.5	-304.6± 2.1	K10
Draco-316	2	17:19:57.02	57:52:57.83	2451720.5	-272.3± 1.7	K02
Draco-316	2	17:19:57.01	57:52:57.80	2454975.5	-279.5± 2.1	K10
Draco-317	2	17:19:13.46	57:52:33.35	2451720.5	-286.5± 1.0	K02
Draco-317	2	17:19:13.44	57:52:33.41	2454975.5	-281.8± 2.1	K10
Draco-318	2	17:20:56.66	57:51:57.35	2451720.5	-292.5± 2.4	K02
Draco-318	2	17:20:56.65	57:51:57.40	2454975.5	-294.2± 2.2	K10
Draco-319	2	17:19:36.31	57:51:24.84	2451720.5	-280.2± 0.8	K02
Draco-319	2	17:19:36.30	57:51:24.90	2454975.5	-279.3± 2.1	K10
Draco-320	2	17:19:49.01	58:04:30.90	2449130.9	-295.6± 5.2	A95
Draco-320	2	17:19:49.01	58:04:30.90	2449457.9	-292.9± 2.7	A95
Draco-321	7	17:19:17.46	58:01:06.10	2446593.9	-311.7± 1.9	O95
Draco-321	7	17:19:17.46	58:01:06.10	2446594.8	-316.5± 1.7	O95
Draco-321	7	17:19:17.46	58:01:06.10	2446703.6	-313.1± 1.7	O95
Draco-321	7	17:19:17.46	58:01:06.10	2446920.0	-319.9± 1.8	O95
Draco-321	7	17:19:17.46	58:01:06.10	2446920.9	-318.3± 1.6	O95
Draco-321	7	17:19:17.46	58:01:06.10	2447420.6	-316.5± 1.4	O95
Draco-321	7	17:19:17.46	58:01:06.10	2449457.9	-316.8± 1.2	A95
Draco-322	3	17:21:56.91	57:59:32.79	2448774.9	-298.5± 7.8	A95
Draco-322	3	17:21:56.91	57:59:32.79	2448776.9	-302.0± 2.8	A95
Draco-322	3	17:21:56.91	57:59:32.79	2449130.9	-297.0± 3.4	A95
Draco-323	2	17:19:51.78	57:59:16.61	2448776.9	-305.0± 2.5	A95
Draco-323	2	17:19:51.78	57:59:16.61	2449130.9	-306.0± 3.5	A95
Draco-324	5	17:20:37.36	57:59:11.40	2445846.9	-283.2± 2.2	O95
Draco-324	5	17:20:37.36	57:59:11.40	2446209.9	-282.6± 1.2	O95
Draco-324	5	17:20:37.36	57:59:11.40	2446594.9	-280.8± 1.6	O95
Draco-324	5	17:20:37.36	57:59:11.40	2448776.9	-286.8± 3.3	A95
Draco-324	5	17:20:37.36	57:59:11.40	2449457.9	-281.5± 1.0	A95

Table G.1: Continued. Velocities of RGB stars in Draco

Star ID	n	α_{J2000} (hh:mm:ss.ss)	δ_{J2000} (dd:mm:ss.ss)	HJD (days)	v (km s ⁻¹)	Ref.
Draco-325	5	17:20:03.93	57:59:07.10	2445503.9	-295.2± 1.1	O95
Draco-325	5	17:20:03.93	57:59:07.10	2446256.8	-292.6± 2.1	O95
Draco-325	5	17:20:03.93	57:59:07.10	2448774.9	-286.7± 4.3	A95
Draco-325	5	17:20:03.93	57:59:07.10	2448776.9	-282.6± 4.9	A95
Draco-325	5	17:20:03.93	57:59:07.10	2449130.9	-287.6± 2.0	A95
Draco-326	5	17:19:35.40	57:58:45.60	2446966.7	-279.0± 1.2	O95
Draco-326	5	17:19:35.40	57:58:45.60	2447333.9	-279.0± 2.5	O95
Draco-326	5	17:19:35.40	57:58:45.60	2447419.7	-279.0± 1.7	O95
Draco-326	5	17:19:35.40	57:58:45.60	2448776.9	-279.8± 2.9	A95
Draco-326	5	17:19:35.40	57:58:45.60	2449130.9	-277.3± 2.0	A95
Draco-327	2	17:20:07.54	57:58:24.20	2448776.9	-298.3± 6.1	A95
Draco-327	2	17:20:07.54	57:58:24.20	2449457.9	-292.4± 4.7	A95
Draco-328	6	17:19:44.70	57:57:36.11	2445504.8	-290.4± 1.2	O95
Draco-328	6	17:19:44.70	57:57:36.11	2445847.9	-288.2± 3.0	O95
Draco-328	6	17:19:44.70	57:57:36.11	2446210.9	-290.9± 1.7	O95
Draco-328	6	17:19:44.70	57:57:36.11	2448774.9	-293.0± 2.6	A95
Draco-328	6	17:19:44.70	57:57:36.11	2449130.9	-292.2± 0.8	A95
Draco-328	6	17:19:44.73	57:57:37.00	2454975.5	-291.8± 2.1	K10
Draco-329	2	17:20:40.20	57:57:31.40	2448776.9	-300.2± 1.9	A95
Draco-329	2	17:20:40.20	57:57:31.40	2449457.9	-300.1± 0.7	A95
Draco-330	2	17:19:46.51	57:56:55.00	2448774.9	-335.9± 2.0	A95
Draco-330	2	17:19:46.51	57:56:55.00	2449130.9	-333.7± 1.3	A95
Draco-331	2	17:20:05.75	57:56:22.40	2448776.9	-290.3± 2.3	A95
Draco-331	2	17:20:05.75	57:56:22.40	2449130.9	-288.3± 1.7	A95
Draco-332	4	17:21:58.17	57:56:03.40	2448774.9	-303.4± 4.6	A95
Draco-332	4	17:21:58.17	57:56:03.40	2448776.9	-302.3± 2.3	A95
Draco-332	4	17:21:58.17	57:56:03.40	2449130.9	-306.1± 2.8	A95
Draco-332	4	17:21:58.20	57:56:04.21	2454975.5	-304.7± 2.1	K10
Draco-333	3	17:18:57.71	57:55:45.30	2448774.9	-296.5± 9.0	A95
Draco-333	3	17:18:57.71	57:55:45.30	2449130.9	-292.1± 5.7	A95
Draco-333	3	17:18:57.71	57:55:45.30	2449457.9	-292.9± 3.2	A95
Draco-334	2	17:19:41.10	57:54:55.59	2448774.9	-281.7± 6.1	A95
Draco-334	2	17:19:41.10	57:54:55.59	2449130.9	-289.9± 4.1	A95
Draco-335	2	17:19:39.92	57:54:23.80	2448774.9	-305.8± 7.8	A95
Draco-335	2	17:19:39.92	57:54:23.80	2449130.9	-303.4± 1.5	A95
Draco-336	2	17:22:10.67	57:53:56.10	2449130.9	-325.0± 4.2	A95
Draco-336	2	17:22:10.67	57:53:56.10	2449459.9	-324.1± 4.4	A95

Table G.1: Continued. Velocities of RGB stars in Draco

Star ID	n	α_{J2000} (hh:mm:ss.ss)	δ_{J2000} (dd:mm:ss.ss)	HJD (days)	v (km s ⁻¹)	Ref.
Draco-337	5	17:22:13.62	57:53:05.40	2446965.8	-300.2± 1.5	O95
Draco-337	5	17:22:13.62	57:53:05.40	2447420.7	-299.4± 1.7	O95
Draco-337	5	17:22:13.62	57:53:05.40	2448774.9	-298.7± 6.8	A95
Draco-337	5	17:22:13.62	57:53:05.40	2448776.9	-299.8± 4.8	A95
Draco-337	5	17:22:13.62	57:53:05.40	2449130.9	-301.3± 2.7	A95
Draco-338	3	17:19:13.40	57:52:32.40	2446966.8	-284.0± 2.2	O95
Draco-338	3	17:19:13.40	57:52:32.40	2447421.6	-282.1± 2.1	O95
Draco-338	3	17:19:13.40	57:52:32.40	2449130.9	-282.1± 1.6	A95
Draco-339	2	17:21:26.35	57:52:03.30	2448776.9	-295.1± 3.9	A95
Draco-339	2	17:21:26.35	57:52:03.30	2449459.9	-289.6± 6.4	A95
Draco-340	4	17:19:36.25	57:51:23.70	2446594.9	-277.4± 2.1	O95
Draco-340	4	17:19:36.25	57:51:23.70	2447329.9	-279.4± 1.6	O95
Draco-340	4	17:19:36.25	57:51:23.70	2448776.9	-286.4± 7.5	A95
Draco-340	4	17:19:36.25	57:51:23.70	2449457.9	-281.8± 1.4	A95
Draco-341	2	17:20:13.35	57:50:50.70	2448776.9	-295.8± 4.7	A95
Draco-341	2	17:20:13.35	57:50:50.70	2449457.9	-280.4± 6.8	A95

APPENDIX H

Velocities of Stars in Ursa Minor

We collected velocity data for 284 stars in Ursa Minor that had more than one epoch of observations. This amounted to 875 velocity measurements. We applied offsets to these velocity data to put them all on the same velocity standard as Walker et al. (2017). As such, the velocities we report in the following table will not match the values listed in the original papers. Column 1 lists the identifier that we assign to the star; column 2 lists the number of observations; column 3 lists the right ascension; column 4 lists the declination; column 5 lists the heliocentric Julian date; column 6 lists the radial velocity and error; and column 7 lists the paper where the velocity measurement originated from. “W17” is in reference to Walker et al. (2017); “K10” is Kirby et al. (2010); “W04” is Wilkinson et al. (2004); “K03” is Kleyna et al. (2003); “A95” is Armandroff et al. (1995); and “O95” is Olszewski et al. (1995).

Table H.1: Velocities of RGB stars in Ursa Minor

Star ID	n	α_{J2000} (hh:mm:ss.ss)	δ_{J2000} (dd:mm:ss.ss)	HJD (days)	v (km s ⁻¹)	Ref.
UrsaMinor-001	2	15:04:55.74	66:28:39.91	2454616.8	-235.5± 0.8	W15
UrsaMinor-001	2	15:04:55.74	66:28:39.91	2455232.9	-234.9± 1.3	W15
UrsaMinor-002	2	15:05:29.84	67:12:43.69	2455659.7	-245.9± 1.9	W15
UrsaMinor-002	2	15:05:29.92	67:12:43.52	2452769.0	-263.9± 7.8	W04

Table H.1: Continued. Velocities of RGB stars in Ursa Minor

Star ID	n	α_{J2000} (hh:mm:ss.ss)	δ_{J2000} (dd:mm:ss.ss)	HJD (days)	v (km s ⁻¹)	Ref.
UrsaMinor-003	2	15:05:44.64	67:03:11.11	2454615.3	-250.5± 0.5	W15
UrsaMinor-003	2	15:05:44.70	67:03:11.12	2452769.0	-260.9± 2.1	W04
UrsaMinor-004	2	15:05:53.65	67:22:31.70	2454616.9	-254.5± 0.6	W15
UrsaMinor-004	2	15:05:53.62	67:22:31.26	2452769.0	-264.5± 3.3	W04
UrsaMinor-005	2	15:05:57.37	66:27:22.59	2454616.8	-251.3± 0.6	W15
UrsaMinor-005	2	15:05:57.37	66:27:22.59	2455232.9	-249.6± 1.4	W15
UrsaMinor-006	6	15:05:57.46	67:16:37.89	2454614.9	-250.5± 0.5	W15
UrsaMinor-006	6	15:05:57.46	67:16:37.89	2454913.7	-248.5± 0.6	W15
UrsaMinor-006	6	15:05:57.46	67:16:37.89	2455659.7	-249.6± 0.8	W15
UrsaMinor-006	6	15:05:57.48	67:16:37.88	2452401.0	-240.1± 5.1	K03
UrsaMinor-006	6	15:05:57.48	67:16:37.88	2452769.0	-246.9± 1.2	W04
UrsaMinor-006	6	15:05:57.44	67:16:37.80	2448776.7	-258.5± 8.8	A95
UrsaMinor-007	4	15:05:59.36	67:18:02.51	2454614.9	-249.5± 1.4	W15
UrsaMinor-007	4	15:05:59.36	67:18:02.51	2454915.9	-248.8± 0.8	W15
UrsaMinor-007	4	15:05:59.38	67:18:02.48	2452401.0	-240.5± 8.4	K03
UrsaMinor-007	4	15:05:59.38	67:18:02.48	2452769.0	-251.7± 1.4	W04
UrsaMinor-008	2	15:06:07.12	66:52:57.99	2454913.7	-247.6± 1.6	W15
UrsaMinor-008	2	15:06:07.12	66:52:57.99	2455232.9	-247.9± 1.6	W15
UrsaMinor-009	3	15:06:11.79	67:24:00.01	2454913.7	-241.4± 2.6	W15
UrsaMinor-009	3	15:06:11.79	67:24:00.01	2455659.7	-241.7± 1.3	W15
UrsaMinor-009	3	15:06:11.81	67:23:59.57	2452769.0	-253.5± 5.9	W04
UrsaMinor-010	4	15:06:15.99	66:54:07.50	2454614.9	-245.6± 0.7	W15
UrsaMinor-010	4	15:06:15.99	66:54:07.50	2455232.9	-228.2± 0.6	W15
UrsaMinor-010	4	15:06:16.01	66:54:07.52	2452401.0	-226.9± 6.5	K03
UrsaMinor-010	4	15:06:16.01	66:54:07.52	2452769.0	-230.7± 1.5	W04
UrsaMinor-011	3	15:06:20.85	67:04:04.09	2454615.8	-252.5± 0.4	W15
UrsaMinor-011	3	15:06:20.85	67:04:04.20	2449128.8	-248.5± 3.4	A95
UrsaMinor-011	3	15:06:20.85	67:04:04.20	2449130.8	-252.4± 2.9	A95
UrsaMinor-012	4	15:06:22.18	67:01:12.29	2454614.9	-244.5± 1.3	W15
UrsaMinor-012	4	15:06:22.22	67:01:11.96	2452401.0	-237.2± 5.2	K03
UrsaMinor-012	4	15:06:22.22	67:01:11.96	2452769.0	-249.8± 1.3	W04
UrsaMinor-012	4	15:06:22.17	67:01:12.40	2449128.8	-240.0± 9.5	A95
UrsaMinor-013	3	15:06:27.76	67:11:46.50	2454615.8	-247.5± 0.9	W15
UrsaMinor-013	3	15:06:27.81	67:11:46.25	2452401.0	-237.3± 6.9	K03
UrsaMinor-013	3	15:06:27.81	67:11:46.25	2452769.0	-259.3± 3.7	W04
UrsaMinor-014	4	15:06:30.38	66:56:41.09	2454615.8	-244.5± 0.3	W15
UrsaMinor-014	4	15:06:30.38	66:56:41.09	2455659.7	-243.9± 0.6	W15

Table H.1: Continued. Velocities of RGB stars in Ursa Minor

Star ID	n	α_{J2000} (hh:mm:ss.ss)	δ_{J2000} (dd:mm:ss.ss)	HJD (days)	v (km s ⁻¹)	Ref.
UrsaMinor-014	4	15:06:30.42	66:56:40.99	2452769.0	-245.1± 1.0	W04
UrsaMinor-014	4	15:06:30.36	66:56:41.09	2449128.8	-242.4± 4.5	A95
UrsaMinor-015	4	15:06:30.42	66:53:32.10	2454615.8	-245.6± 0.7	W15
UrsaMinor-015	4	15:06:30.42	66:53:32.10	2455232.9	-246.0± 1.3	W15
UrsaMinor-015	4	15:06:30.42	66:53:32.10	2455659.7	-247.5± 1.1	W15
UrsaMinor-015	4	15:06:30.46	66:53:32.03	2452769.0	-229.2± 4.6	W04
UrsaMinor-016	2	15:06:30.54	66:58:48.40	2454913.7	-255.2± 1.5	W15
UrsaMinor-016	2	15:06:30.57	66:58:48.29	2452769.0	-256.7± 1.2	W04
UrsaMinor-017	2	15:06:35.55	67:05:15.69	2454615.8	-245.3± 0.9	W15
UrsaMinor-017	2	15:06:35.57	67:05:15.43	2452769.0	-259.4± 5.2	W04
UrsaMinor-018	4	15:06:36.09	67:04:22.30	2454615.8	-249.0± 0.6	W15
UrsaMinor-018	4	15:06:36.14	67:04:21.90	2452401.0	-256.5± 9.8	K03
UrsaMinor-018	4	15:06:36.14	67:04:21.90	2452769.0	-234.7± 1.4	W04
UrsaMinor-018	4	15:06:36.08	67:04:22.30	2449130.8	-253.7± 9.4	A95
UrsaMinor-019	4	15:06:38.69	66:58:39.61	2454615.8	-246.7± 0.4	W15
UrsaMinor-019	4	15:06:38.74	66:58:39.50	2452401.0	-248.0± 2.7	K03
UrsaMinor-019	4	15:06:38.74	66:58:39.50	2452769.0	-246.4± 1.6	W04
UrsaMinor-019	4	15:06:38.66	66:58:39.80	2449128.8	-248.6± 5.1	A95
UrsaMinor-020	2	15:06:39.24	67:07:12.81	2454615.8	-252.7± 0.6	W15
UrsaMinor-020	2	15:06:39.30	67:07:12.54	2452401.0	-269.1± 4.9	K03
UrsaMinor-021	3	15:06:40.16	66:52:05.39	2454913.7	-251.1± 1.0	W15
UrsaMinor-021	3	15:06:40.16	66:52:05.39	2455232.9	-250.7± 1.0	W15
UrsaMinor-021	3	15:06:40.16	66:52:05.39	2455659.7	-252.2± 1.3	W15
UrsaMinor-022	2	15:06:43.14	67:06:00.60	2454615.8	-231.3± 0.5	W15
UrsaMinor-022	2	15:06:43.13	67:06:00.71	2449130.8	-237.9± 7.3	A95
UrsaMinor-023	7	15:06:43.34	67:09:12.61	2454615.8	-253.4± 0.4	W15
UrsaMinor-023	7	15:06:43.34	67:09:12.61	2454913.7	-252.6± 0.4	W15
UrsaMinor-023	7	15:06:43.34	67:09:12.61	2446918.7	-252.2± 1.2	O95
UrsaMinor-023	7	15:06:43.34	67:09:12.61	2447672.7	-255.5± 1.9	O95
UrsaMinor-023	7	15:06:43.34	67:09:12.61	2448774.8	-251.7± 3.2	A95
UrsaMinor-023	7	15:06:43.34	67:09:12.61	2449128.8	-251.3± 2.1	A95
UrsaMinor-023	7	15:06:43.34	67:09:12.61	2449130.8	-252.7± 0.6	A95
UrsaMinor-024	2	15:06:47.69	67:00:22.30	2454915.9	-256.7± 2.0	W15
UrsaMinor-024	2	15:06:47.72	67:00:21.96	2452769.0	-261.3± 4.2	W04
UrsaMinor-025	3	15:06:52.57	67:12:03.70	2454614.9	-224.0± 1.0	W15
UrsaMinor-025	3	15:06:52.57	67:12:03.70	2454913.7	-221.7± 1.4	W15
UrsaMinor-025	3	15:06:52.59	67:12:03.42	2452769.0	-206.7± 2.8	W04

Table H.1: Continued. Velocities of RGB stars in Ursa Minor

Star ID	n	α_{J2000} (hh:mm:ss.ss)	δ_{J2000} (dd:mm:ss.ss)	HJD (days)	v (km s ⁻¹)	Ref.
UrsaMinor-026	3	15:06:57.55	66:54:38.70	2454614.9	-264.7± 1.5	W15
UrsaMinor-026	3	15:06:57.60	66:54:38.66	2452401.0	-259.2± 5.6	K03
UrsaMinor-026	3	15:06:57.60	66:54:38.66	2452769.0	-267.1± 2.0	W04
UrsaMinor-027	2	15:06:58.55	67:12:48.19	2454615.8	-253.3± 1.8	W15
UrsaMinor-027	2	15:06:58.55	67:12:48.19	2454913.7	-252.8± 1.7	W15
UrsaMinor-028	2	15:07:12.29	67:20:23.00	2454614.9	-246.5± 0.7	W15
UrsaMinor-028	2	15:07:12.37	67:20:22.67	2452401.0	-243.7± 7.3	K03
UrsaMinor-029	2	15:07:12.57	66:51:37.40	2454615.8	-243.8± 1.4	W15
UrsaMinor-029	2	15:07:12.62	66:51:37.37	2452769.0	-226.8± 7.6	W04
UrsaMinor-030	2	15:07:14.31	66:56:48.40	2454615.8	-259.1± 0.9	W15
UrsaMinor-030	2	15:07:14.33	66:56:48.19	2452769.0	-257.4± 4.1	W04
UrsaMinor-031	4	15:07:17.32	67:12:52.31	2454615.8	-247.6± 0.5	W15
UrsaMinor-031	4	15:07:17.37	67:12:51.84	2452401.0	-245.1± 4.6	K03
UrsaMinor-031	4	15:07:17.37	67:12:51.84	2452769.0	-250.3± 1.4	W04
UrsaMinor-031	4	15:07:17.35	67:12:52.39	2449130.8	-248.6± 9.5	A95
UrsaMinor-032	3	15:07:22.54	67:12:01.20	2454615.8	-259.6± 0.5	W15
UrsaMinor-032	3	15:07:22.54	67:12:01.00	2448776.7	-261.6± 9.9	A95
UrsaMinor-032	3	15:07:22.54	67:12:01.00	2449130.8	-265.1± 9.0	A95
UrsaMinor-033	2	15:07:26.30	66:58:18.40	2454913.7	-260.4± 1.5	W15
UrsaMinor-033	2	15:07:26.30	66:58:18.40	2455659.7	-260.7± 2.5	W15
UrsaMinor-034	5	15:07:26.40	67:16:25.61	2454913.7	-240.7± 0.8	W15
UrsaMinor-034	5	15:07:26.40	67:16:25.61	2455659.7	-241.4± 1.1	W15
UrsaMinor-034	5	15:07:26.43	67:16:25.39	2452401.0	-237.8± 4.9	K03
UrsaMinor-034	5	15:07:26.43	67:16:25.39	2452769.0	-243.7± 1.5	W04
UrsaMinor-034	5	15:07:26.37	67:16:25.69	2449130.8	-250.3± 7.4	A95
UrsaMinor-035	2	15:07:27.19	67:02:31.50	2454915.9	-252.6± 1.3	W15
UrsaMinor-035	2	15:07:27.21	67:02:31.31	2455329.0	-257.9± 2.2	K10
UrsaMinor-036	2	15:07:28.74	67:10:53.00	2454615.8	-264.4± 1.3	W15
UrsaMinor-036	2	15:07:28.75	67:10:52.75	2452769.0	-276.1± 4.2	W04
UrsaMinor-037	2	15:07:31.91	67:02:15.10	2454615.8	-248.2± 1.1	W15
UrsaMinor-037	2	15:07:31.93	67:02:14.91	2455329.0	-251.6± 2.3	K10
UrsaMinor-038	4	15:07:36.27	66:48:21.00	2454913.7	-236.6± 1.7	W15
UrsaMinor-038	4	15:07:36.27	66:48:21.00	2455232.9	-239.5± 1.4	W15
UrsaMinor-038	4	15:07:36.34	66:48:20.84	2452401.0	-233.9± 5.2	K03
UrsaMinor-038	4	15:07:36.34	66:48:20.84	2452769.0	-227.3± 4.5	W04
UrsaMinor-039	2	15:07:38.79	66:56:06.79	2454615.3	-262.2± 0.9	W15
UrsaMinor-039	2	15:07:38.79	66:56:06.79	2455232.9	-256.4± 1.4	W15

Table H.1: Continued. Velocities of RGB stars in Ursa Minor

Star ID	n	α_{J2000} (hh:mm:ss.ss)	δ_{J2000} (dd:mm:ss.ss)	HJD (days)	v (km s ⁻¹)	Ref.
UrsaMinor-040	3	15:07:42.61	67:03:09.90	2454614.9	-235.6± 0.9	W15
UrsaMinor-040	3	15:07:42.56	67:03:09.61	2452401.0	-230.4± 7.0	K03
UrsaMinor-040	3	15:07:42.66	67:03:09.49	2455329.0	-240.5± 2.2	K10
UrsaMinor-041	2	15:07:42.73	66:54:11.40	2454615.8	-243.3± 0.7	W15
UrsaMinor-041	2	15:07:42.78	66:54:11.30	2452769.0	-243.8± 2.6	W04
UrsaMinor-042	2	15:07:46.61	67:02:20.21	2454615.8	-245.9± 2.9	W15
UrsaMinor-042	2	15:07:46.65	67:02:19.91	2455329.0	-240.7± 2.3	K10
UrsaMinor-043	3	15:07:48.44	67:13:04.50	2454615.8	-252.1± 0.5	W15
UrsaMinor-043	3	15:07:48.53	67:13:04.29	2448774.8	-249.9± 9.0	A95
UrsaMinor-043	3	15:07:48.52	67:13:04.20	2454885.0	-250.2± 2.1	K10
UrsaMinor-044	3	15:07:49.91	67:08:06.89	2454913.7	-245.2± 1.2	W15
UrsaMinor-044	3	15:07:49.92	67:08:06.72	2452769.0	-258.4± 2.9	W04
UrsaMinor-044	3	15:07:49.90	67:08:07.00	2449128.8	-225.8± 9.4	A95
UrsaMinor-045	2	15:07:50.63	67:00:40.90	2454615.8	-242.8± 1.3	W15
UrsaMinor-045	2	15:07:50.64	67:00:40.79	2455329.0	-251.9± 2.5	K10
UrsaMinor-046	5	15:07:50.80	67:11:13.30	2454615.8	-249.7± 0.5	W15
UrsaMinor-046	5	15:07:50.83	67:11:12.84	2452769.0	-251.5± 1.1	W04
UrsaMinor-046	5	15:07:50.78	67:11:13.11	2448774.8	-253.9± 8.6	A95
UrsaMinor-046	5	15:07:50.78	67:11:13.11	2449128.8	-247.1± 6.4	A95
UrsaMinor-046	5	15:07:50.88	67:11:12.91	2454885.0	-246.2± 2.1	K10
UrsaMinor-047	2	15:07:52.57	67:02:18.70	2454615.8	-231.1± 0.8	W15
UrsaMinor-047	2	15:07:52.60	67:02:18.40	2455329.0	-235.6± 2.2	K10
UrsaMinor-048	2	15:07:54.62	67:10:44.71	2454614.9	-257.4± 0.5	W15
UrsaMinor-048	2	15:07:54.59	67:10:44.51	2449128.8	-261.6± 3.6	A95
UrsaMinor-049	4	15:07:55.09	67:07:18.41	2454614.9	-244.4± 0.4	W15
UrsaMinor-049	4	15:07:55.12	67:07:18.12	2452401.0	-242.3± 3.5	K03
UrsaMinor-049	4	15:07:55.08	67:07:18.49	2448774.8	-241.8± 5.3	A95
UrsaMinor-049	4	15:07:55.08	67:07:18.49	2449128.8	-244.1± 3.0	A95
UrsaMinor-050	2	15:07:55.64	67:06:26.09	2454615.8	-245.7± 0.8	W15
UrsaMinor-050	2	15:07:55.69	67:06:25.89	2455329.0	-246.4± 2.2	K10
UrsaMinor-051	2	15:07:56.37	67:16:29.90	2454615.8	-249.5± 1.5	W15
UrsaMinor-051	2	15:07:56.40	67:16:29.59	2454885.0	-248.1± 2.6	K10
UrsaMinor-052	2	15:07:59.71	67:11:41.81	2454615.8	-256.3± 1.0	W15
UrsaMinor-052	2	15:07:59.77	67:11:41.40	2454885.0	-258.2± 2.2	K10
UrsaMinor-053	2	15:08:00.42	67:05:25.31	2454615.8	-248.0± 1.4	W15
UrsaMinor-053	2	15:08:00.47	67:05:25.11	2455329.0	-247.8± 2.2	K10
UrsaMinor-054	4	15:08:02.00	67:20:39.39	2454615.8	-252.9± 0.4	W15

Table H.1: Continued. Velocities of RGB stars in Ursa Minor

Star ID	n	α_{J2000} (hh:mm:ss.ss)	δ_{J2000} (dd:mm:ss.ss)	HJD (days)	v (km s ⁻¹)	Ref.
UrsaMinor-054	4	15:08:02.00	67:20:39.39	2454915.9	-252.2± 0.6	W15
UrsaMinor-054	4	15:08:01.97	67:20:39.31	2449130.8	-258.4± 3.8	A95
UrsaMinor-054	4	15:08:01.97	67:20:39.31	2449457.8	-254.1± 3.2	A95
UrsaMinor-055	2	15:08:02.91	67:05:01.99	2454615.8	-261.0± 1.1	W15
UrsaMinor-055	2	15:08:02.90	67:05:01.60	2454885.0	-265.8± 2.8	K10
UrsaMinor-056	3	15:08:04.31	67:06:50.39	2454614.9	-243.9± 1.7	W15
UrsaMinor-056	3	15:08:04.34	67:06:50.15	2452769.0	-242.8± 2.9	W04
UrsaMinor-056	3	15:08:04.36	67:06:50.31	2455329.0	-246.2± 2.1	K10
UrsaMinor-057	7	15:08:04.94	67:14:00.70	2454615.8	-256.8± 0.4	W15
UrsaMinor-057	7	15:08:04.95	67:14:00.90	2445848.7	-253.1± 2.4	O95
UrsaMinor-057	7	15:08:04.95	67:14:00.90	2448774.8	-255.1± 2.3	A95
UrsaMinor-057	7	15:08:04.95	67:14:00.90	2449128.8	-253.4± 1.8	A95
UrsaMinor-057	7	15:08:04.95	67:14:00.90	2449130.8	-253.4± 2.5	A95
UrsaMinor-057	7	15:08:04.95	67:14:00.90	2449457.8	-255.4± 1.2	A95
UrsaMinor-057	7	15:08:04.99	67:14:00.70	2455329.0	-262.2± 2.1	K10
UrsaMinor-058	4	15:08:06.17	66:58:47.41	2454615.8	-234.1± 0.6	W15
UrsaMinor-058	4	15:08:06.17	66:58:47.41	2454913.7	-233.2± 1.4	W15
UrsaMinor-058	4	15:08:06.19	66:58:47.17	2452401.0	-227.3± 4.6	K03
UrsaMinor-058	4	15:08:06.19	66:58:47.17	2452769.0	-223.8± 1.4	W04
UrsaMinor-059	2	15:08:06.74	67:12:55.99	2454615.8	-245.8± 1.3	W15
UrsaMinor-059	2	15:08:06.79	67:12:55.80	2455329.0	-246.2± 2.2	K10
UrsaMinor-060	4	15:08:06.78	67:03:10.80	2454614.9	-244.7± 0.7	W15
UrsaMinor-060	4	15:08:06.78	67:03:10.58	2452401.0	-239.7± 4.1	K03
UrsaMinor-060	4	15:08:06.78	67:03:10.58	2452769.0	-248.4± 1.8	W04
UrsaMinor-060	4	15:08:06.78	67:03:10.61	2454885.0	-247.3± 2.3	K10
UrsaMinor-061	4	15:08:06.96	66:46:37.20	2454615.8	-237.8± 0.8	W15
UrsaMinor-061	4	15:08:06.96	66:46:37.20	2454915.9	-235.9± 1.3	W15
UrsaMinor-061	4	15:08:06.96	66:46:37.20	2455232.9	-236.0± 1.0	W15
UrsaMinor-061	4	15:08:06.96	66:46:37.20	2455659.7	-235.7± 1.2	W15
UrsaMinor-062	2	15:08:08.95	67:11:42.71	2454913.7	-245.7± 1.4	W15
UrsaMinor-062	2	15:08:08.99	67:11:42.41	2455329.0	-247.0± 2.1	K10
UrsaMinor-063	3	15:08:08.96	67:09:21.81	2454614.9	-248.4± 0.6	W15
UrsaMinor-063	3	15:08:08.90	67:09:21.70	2449130.8	-250.0± 5.9	A95
UrsaMinor-063	3	15:08:09.06	67:09:21.59	2454885.0	-246.2± 2.1	K10
UrsaMinor-064	8	15:08:10.02	67:17:25.29	2454614.9	-266.1± 0.4	W15
UrsaMinor-064	8	15:08:10.02	67:17:25.29	2454913.7	-265.4± 0.4	W15
UrsaMinor-064	8	15:08:10.03	67:17:25.10	2445847.7	-265.6± 3.3	O95

Table H.1: Continued. Velocities of RGB stars in Ursa Minor

Star ID	n	α_{J2000} (hh:mm:ss.ss)	δ_{J2000} (dd:mm:ss.ss)	HJD (days)	v (km s ⁻¹)	Ref.
UrsaMinor-064	8	15:08:10.03	67:17:25.10	2446122.0	-264.0± 1.4	O95
UrsaMinor-064	8	15:08:10.03	67:17:25.10	2446208.8	-265.5± 1.8	O95
UrsaMinor-064	8	15:08:10.03	67:17:25.10	2446479.0	-263.6± 1.8	O95
UrsaMinor-064	8	15:08:10.03	67:17:25.10	2448774.8	-260.1± 6.3	A95
UrsaMinor-064	8	15:08:10.03	67:17:25.10	2449128.8	-266.3± 1.5	A95
UrsaMinor-065	6	15:08:10.49	67:17:07.50	2454615.8	-257.7± 0.5	W15
UrsaMinor-065	6	15:08:10.49	67:17:07.50	2454915.9	-257.1± 0.6	W15
UrsaMinor-065	6	15:08:10.46	67:17:07.30	2448776.7	-261.6± 4.8	A95
UrsaMinor-065	6	15:08:10.46	67:17:07.30	2449130.8	-259.3± 2.6	A95
UrsaMinor-065	6	15:08:10.46	67:17:07.30	2449457.8	-255.5± 3.0	A95
UrsaMinor-065	6	15:08:10.51	67:17:07.11	2454885.0	-257.1± 2.2	K10
UrsaMinor-066	2	15:08:11.60	67:03:25.80	2454615.8	-242.0± 0.9	W15
UrsaMinor-066	2	15:08:11.61	67:03:25.50	2454885.0	-239.2± 3.1	K10
UrsaMinor-067	5	15:08:15.45	67:11:51.80	2454615.8	-256.8± 0.5	W15
UrsaMinor-067	5	15:08:15.47	67:11:51.58	2452401.0	-255.0± 5.6	K03
UrsaMinor-067	5	15:08:15.47	67:11:51.58	2452769.0	-257.8± 1.5	W04
UrsaMinor-067	5	15:08:15.45	67:11:51.69	2449128.8	-261.2± 9.1	A95
UrsaMinor-067	5	15:08:15.52	67:11:51.50	2454885.0	-257.4± 2.1	K10
UrsaMinor-068	3	15:08:16.55	67:02:53.50	2454615.4	-238.1± 0.4	W15
UrsaMinor-068	3	15:08:16.55	67:02:53.27	2452769.0	-230.4± 1.8	W04
UrsaMinor-068	3	15:08:16.58	67:02:53.31	2455329.0	-242.8± 2.1	K10
UrsaMinor-069	4	15:08:17.14	67:08:21.69	2454915.9	-247.1± 1.1	W15
UrsaMinor-069	4	15:08:17.14	67:08:21.52	2452401.0	-243.8± 5.5	K03
UrsaMinor-069	4	15:08:17.14	67:08:21.52	2452769.0	-251.3± 2.5	W04
UrsaMinor-069	4	15:08:17.26	67:08:21.61	2454885.0	-247.9± 2.2	K10
UrsaMinor-070	3	15:08:19.09	67:06:52.10	2454913.7	-229.2± 0.8	W15
UrsaMinor-070	3	15:08:19.11	67:06:51.84	2452769.0	-225.0± 2.0	W04
UrsaMinor-070	3	15:08:19.20	67:06:51.90	2454885.0	-229.2± 2.1	K10
UrsaMinor-071	2	15:08:20.52	67:15:42.19	2454913.7	-238.2± 1.4	W15
UrsaMinor-071	2	15:08:20.56	67:15:41.69	2454885.0	-240.7± 2.3	K10
UrsaMinor-072	4	15:08:20.88	67:07:50.49	2454615.8	-241.1± 0.6	W15
UrsaMinor-072	4	15:08:20.88	67:07:50.23	2452769.0	-241.4± 2.0	W04
UrsaMinor-072	4	15:08:20.83	67:07:50.41	2449130.8	-254.1± 9.7	A95
UrsaMinor-072	4	15:08:21.04	67:07:50.41	2454885.0	-240.5± 2.2	K10
UrsaMinor-073	2	15:08:22.85	67:20:36.10	2454614.9	-249.6± 0.8	W15
UrsaMinor-073	2	15:08:22.88	67:20:35.91	2454886.0	-250.9± 2.1	K10
UrsaMinor-074	3	15:08:23.70	67:18:22.40	2454616.9	-240.5± 0.7	W15

Table H.1: Continued. Velocities of RGB stars in Ursa Minor

Star ID	n	α_{J2000} (hh:mm:ss.ss)	δ_{J2000} (dd:mm:ss.ss)	HJD (days)	v (km s ⁻¹)	Ref.
UrsaMinor-074	3	15:08:23.70	67:18:22.40	2455659.7	-242.6± 2.2	W15
UrsaMinor-074	3	15:08:23.73	67:18:22.01	2454886.0	-238.1± 2.2	K10
UrsaMinor-075	4	15:08:24.34	67:05:44.50	2454615.8	-241.6± 0.6	W15
UrsaMinor-075	4	15:08:24.35	67:05:44.16	2452769.0	-243.5± 2.0	W04
UrsaMinor-075	4	15:08:24.31	67:05:44.39	2449128.8	-227.3± 7.9	A95
UrsaMinor-075	4	15:08:24.43	67:05:44.31	2454885.0	-241.3± 2.1	K10
UrsaMinor-076	2	15:08:24.99	67:15:03.10	2454614.9	-236.7± 1.4	W15
UrsaMinor-076	2	15:08:25.01	67:15:02.69	2455329.0	-238.7± 2.2	K10
UrsaMinor-077	2	15:08:25.30	67:02:10.49	2454615.8	-245.3± 0.9	W15
UrsaMinor-077	2	15:08:25.42	67:02:10.41	2454885.0	-244.6± 2.7	K10
UrsaMinor-078	4	15:08:25.95	67:17:24.80	2454614.9	-252.0± 0.5	W15
UrsaMinor-078	4	15:08:25.95	67:17:24.80	2454914.8	-251.2± 0.5	W15
UrsaMinor-078	4	15:08:25.98	67:17:24.32	2452769.0	-259.2± 2.0	W04
UrsaMinor-078	4	15:08:25.98	67:17:24.31	2454886.0	-250.9± 2.1	K10
UrsaMinor-079	10	15:08:27.13	67:10:07.79	2454614.9	-235.6± 0.4	W15
UrsaMinor-079	10	15:08:27.12	67:10:07.71	2445504.7	-233.2± 1.1	O95
UrsaMinor-079	10	15:08:27.12	67:10:07.71	2445848.8	-230.6± 1.9	O95
UrsaMinor-079	10	15:08:27.12	67:10:07.71	2446208.7	-233.1± 1.4	O95
UrsaMinor-079	10	15:08:27.12	67:10:07.71	2446478.9	-235.3± 1.4	O95
UrsaMinor-079	10	15:08:27.12	67:10:07.71	2448774.8	-232.8± 2.6	A95
UrsaMinor-079	10	15:08:27.12	67:10:07.71	2448776.7	-235.1± 1.6	A95
UrsaMinor-079	10	15:08:27.12	67:10:07.71	2449128.8	-234.2± 1.6	A95
UrsaMinor-079	10	15:08:27.12	67:10:07.71	2449130.8	-231.1± 1.2	A95
UrsaMinor-079	10	15:08:27.23	67:10:07.71	2454885.0	-232.6± 2.1	K10
UrsaMinor-080	2	15:08:28.03	67:10:19.11	2454913.7	-236.2± 1.5	W15
UrsaMinor-080	2	15:08:28.13	67:10:18.89	2454885.0	-238.1± 2.2	K10
UrsaMinor-081	3	15:08:28.43	67:21:35.01	2454615.8	-241.4± 0.8	W15
UrsaMinor-081	3	15:08:28.43	67:21:35.01	2455659.7	-243.5± 1.9	W15
UrsaMinor-081	3	15:08:28.48	67:21:34.79	2454886.0	-234.7± 2.2	K10
UrsaMinor-082	2	15:08:28.64	67:06:17.90	2454913.7	-247.3± 1.7	W15
UrsaMinor-082	2	15:08:28.72	67:06:17.60	2454885.0	-247.4± 2.2	K10
UrsaMinor-083	6	15:08:29.92	66:52:20.19	2454615.4	-247.7± 0.8	W15
UrsaMinor-083	6	15:08:29.92	66:52:20.19	2454915.9	-247.0± 1.4	W15
UrsaMinor-083	6	15:08:29.92	66:52:20.19	2455232.9	-245.5± 1.2	W15
UrsaMinor-083	6	15:08:29.92	66:52:20.19	2455659.7	-245.7± 1.2	W15
UrsaMinor-083	6	15:08:29.99	66:52:19.99	2452401.0	-243.1± 5.1	K03
UrsaMinor-083	6	15:08:29.99	66:52:19.99	2452769.0	-243.0± 2.0	W04

Table H.1: Continued. Velocities of RGB stars in Ursa Minor

Star ID	n	α_{J2000} (hh:mm:ss.ss)	δ_{J2000} (dd:mm:ss.ss)	HJD (days)	v (km s ⁻¹)	Ref.
UrsaMinor-084	2	15:08:33.42	67:13:59.79	2454615.8	-240.0± 1.5	W15
UrsaMinor-084	2	15:08:33.46	67:13:59.81	2452769.0	-236.5± 3.4	W04
UrsaMinor-085	2	15:08:33.56	67:12:28.61	2454915.9	-252.0± 1.7	W15
UrsaMinor-085	2	15:08:33.60	67:12:28.31	2455329.0	-258.0± 2.3	K10
UrsaMinor-086	8	15:08:34.38	67:10:34.41	2454614.9	-249.1± 0.4	W15
UrsaMinor-086	8	15:08:34.38	67:10:34.21	2445848.9	-250.9± 1.9	O95
UrsaMinor-086	8	15:08:34.38	67:10:34.21	2446210.7	-251.6± 1.3	O95
UrsaMinor-086	8	15:08:34.38	67:10:34.21	2448774.8	-246.4± 3.7	A95
UrsaMinor-086	8	15:08:34.38	67:10:34.21	2448776.7	-248.9± 6.6	A95
UrsaMinor-086	8	15:08:34.38	67:10:34.21	2449128.8	-247.5± 1.7	A95
UrsaMinor-086	8	15:08:34.38	67:10:34.21	2449130.8	-250.6± 1.1	A95
UrsaMinor-086	8	15:08:34.48	67:10:34.29	2454885.0	-244.2± 2.1	K10
UrsaMinor-087	6	15:08:35.65	67:03:41.29	2454614.9	-234.5± 0.5	W15
UrsaMinor-087	6	15:08:35.65	67:03:41.29	2454913.7	-234.8± 0.4	W15
UrsaMinor-087	6	15:08:35.63	67:03:41.29	2446919.9	-237.9± 1.4	O95
UrsaMinor-087	6	15:08:35.63	67:03:41.29	2447334.8	-235.6± 2.0	O95
UrsaMinor-087	6	15:08:35.63	67:03:41.29	2448774.8	-230.9± 3.7	A95
UrsaMinor-087	6	15:08:35.63	67:03:41.29	2449128.8	-238.9± 2.0	A95
UrsaMinor-088	2	15:08:36.15	67:16:59.70	2454616.9	-265.8± 1.0	W15
UrsaMinor-088	2	15:08:36.19	67:16:59.20	2454886.0	-265.0± 2.2	K10
UrsaMinor-089	4	15:08:36.49	67:17:08.51	2454615.8	-239.8± 0.6	W15
UrsaMinor-089	4	15:08:36.49	67:17:08.51	2454915.9	-237.7± 1.0	W15
UrsaMinor-089	4	15:08:36.53	67:17:08.09	2452401.0	-235.5± 4.9	K03
UrsaMinor-089	4	15:08:36.49	67:17:08.40	2449457.8	-242.5± 6.3	A95
UrsaMinor-090	2	15:08:36.93	67:12:40.39	2454913.7	-245.3± 0.9	W15
UrsaMinor-090	2	15:08:36.99	67:12:40.09	2454886.1	-245.9± 2.1	K10
UrsaMinor-091	2	15:08:40.06	67:28:57.10	2454615.8	-248.3± 0.8	W15
UrsaMinor-091	2	15:08:40.06	67:28:57.10	2454913.7	-245.3± 1.5	W15
UrsaMinor-092	5	15:08:41.39	67:08:45.01	2454614.9	-233.1± 0.8	W15
UrsaMinor-092	5	15:08:41.40	67:08:44.66	2452769.0	-229.5± 1.5	W04
UrsaMinor-092	5	15:08:41.37	67:08:44.90	2449128.8	-235.6± 7.4	A95
UrsaMinor-092	5	15:08:41.37	67:08:44.90	2449130.8	-217.9± 6.2	A95
UrsaMinor-092	5	15:08:41.37	67:08:44.90	2449457.8	-237.2± 4.9	A95
UrsaMinor-093	6	15:08:42.25	67:13:13.30	2454614.9	-242.5± 0.4	W15
UrsaMinor-093	6	15:08:42.25	67:13:13.21	2448774.8	-242.3± 5.8	A95
UrsaMinor-093	6	15:08:42.25	67:13:13.21	2448776.7	-249.5± 4.3	A95
UrsaMinor-093	6	15:08:42.25	67:13:13.21	2449130.8	-242.6± 2.6	A95

Table H.1: Continued. Velocities of RGB stars in Ursa Minor

Star ID	n	α_{J2000} (hh:mm:ss.ss)	δ_{J2000} (dd:mm:ss.ss)	HJD (days)	v (km s ⁻¹)	Ref.
UrsaMinor-093	6	15:08:42.25	67:13:13.21	2449457.8	-241.5± 2.5	A95
UrsaMinor-093	6	15:08:42.31	67:13:12.99	2454886.1	-244.4± 2.1	K10
UrsaMinor-094	3	15:08:42.80	67:19:12.00	2454614.9	-241.0± 0.8	W15
UrsaMinor-094	3	15:08:42.80	67:19:12.00	2455659.7	-241.0± 1.3	W15
UrsaMinor-094	3	15:08:42.87	67:19:11.59	2454886.0	-240.5± 2.2	K10
UrsaMinor-095	2	15:08:44.04	67:02:59.19	2454615.8	-243.5± 1.5	W15
UrsaMinor-095	2	15:08:44.09	67:02:59.00	2454885.0	-240.8± 3.0	K10
UrsaMinor-096	2	15:08:44.55	66:59:28.00	2454614.9	-256.6± 1.1	W15
UrsaMinor-096	2	15:08:44.55	66:59:28.00	2454915.9	-255.0± 2.0	W15
UrsaMinor-097	3	15:08:44.62	67:17:00.49	2454615.8	-247.3± 1.0	W15
UrsaMinor-097	3	15:08:44.62	67:17:00.49	2454914.8	-246.5± 1.1	W15
UrsaMinor-097	3	15:08:44.62	67:17:00.49	2455659.7	-249.0± 1.7	W15
UrsaMinor-098	7	15:08:44.62	67:20:03.20	2454614.9	-227.8± 0.7	W15
UrsaMinor-098	7	15:08:44.62	67:20:03.20	2454915.9	-230.0± 1.0	W15
UrsaMinor-098	7	15:08:44.66	67:20:02.90	2452401.0	-217.8± 5.3	K03
UrsaMinor-098	7	15:08:44.66	67:20:02.90	2452769.0	-230.0± 2.0	W04
UrsaMinor-098	7	15:08:44.59	67:20:03.00	2448776.7	-225.2± 9.8	A95
UrsaMinor-098	7	15:08:44.59	67:20:03.00	2449457.8	-222.8± 9.5	A95
UrsaMinor-098	7	15:08:44.70	67:20:02.81	2454886.0	-230.3± 2.2	K10
UrsaMinor-099	2	15:08:45.17	67:11:39.00	2454913.7	-230.0± 1.4	W15
UrsaMinor-099	2	15:08:45.22	67:11:38.70	2455329.0	-234.5± 2.2	K10
UrsaMinor-100	2	15:08:46.11	67:02:14.99	2454615.8	-230.4± 1.0	W15
UrsaMinor-100	2	15:08:46.11	67:02:14.99	2454915.9	-228.3± 1.1	W15
UrsaMinor-101	2	15:08:49.11	67:21:21.91	2454616.9	-252.4± 0.6	W15
UrsaMinor-101	2	15:08:49.11	67:21:21.91	2454915.9	-252.9± 1.4	W15
UrsaMinor-102	2	15:08:49.45	67:31:32.51	2454615.3	-244.9± 0.8	W15
UrsaMinor-102	2	15:08:49.45	67:31:32.51	2454913.7	-242.8± 2.9	W15
UrsaMinor-103	5	15:08:50.24	67:10:10.21	2454615.8	-252.5± 0.4	W15
UrsaMinor-103	5	15:08:50.23	67:10:10.40	2448776.7	-250.7± 4.3	A95
UrsaMinor-103	5	15:08:50.23	67:10:10.40	2449128.8	-249.3± 3.4	A95
UrsaMinor-103	5	15:08:50.23	67:10:10.40	2449130.8	-253.6± 6.3	A95
UrsaMinor-103	5	15:08:50.23	67:10:10.40	2449457.8	-255.5± 2.7	A95
UrsaMinor-104	3	15:08:50.59	67:00:52.21	2454615.8	-248.0± 0.9	W15
UrsaMinor-104	3	15:08:50.59	67:00:52.21	2455659.7	-246.6± 1.5	W15
UrsaMinor-104	3	15:08:50.60	67:00:51.55	2452769.0	-236.3± 4.0	W04
UrsaMinor-105	3	15:08:51.36	67:18:46.29	2454913.7	-261.0± 2.2	W15
UrsaMinor-105	3	15:08:51.36	67:18:46.29	2455659.7	-260.7± 2.8	W15

Table H.1: Continued. Velocities of RGB stars in Ursa Minor

Star ID	n	α_{J2000} (hh:mm:ss.ss)	δ_{J2000} (dd:mm:ss.ss)	HJD (days)	v (km s ⁻¹)	Ref.
UrsaMinor-105	3	15:08:51.42	67:18:45.91	2454886.1	-258.8± 2.3	K10
UrsaMinor-106	2	15:08:51.56	67:21:52.10	2454615.8	-259.5± 0.7	W15
UrsaMinor-106	2	15:08:51.56	67:21:52.10	2455659.7	-259.2± 1.6	W15
UrsaMinor-107	2	15:08:51.60	67:14:52.61	2454616.9	-242.4± 0.9	W15
UrsaMinor-107	2	15:08:51.64	67:14:52.09	2454886.1	-242.5± 2.2	K10
UrsaMinor-108	6	15:08:52.16	67:12:46.90	2454615.8	-243.9± 0.4	W15
UrsaMinor-108	6	15:08:52.14	67:12:46.90	2446595.7	-242.8± 2.1	O95
UrsaMinor-108	6	15:08:52.14	67:12:46.90	2448774.8	-245.5± 2.4	A95
UrsaMinor-108	6	15:08:52.14	67:12:46.90	2449128.8	-240.1± 1.9	A95
UrsaMinor-108	6	15:08:52.14	67:12:46.90	2449457.8	-246.8± 1.9	A95
UrsaMinor-108	6	15:08:52.21	67:12:46.60	2454886.1	-245.0± 2.1	K10
UrsaMinor-109	2	15:08:53.23	67:17:52.71	2454615.8	-250.2± 0.8	W15
UrsaMinor-109	2	15:08:53.28	67:17:52.21	2454886.1	-250.8± 2.2	K10
UrsaMinor-110	4	15:08:53.33	67:01:53.41	2454615.8	-259.3± 0.7	W15
UrsaMinor-110	4	15:08:53.33	67:01:53.41	2454915.9	-258.8± 0.9	W15
UrsaMinor-110	4	15:08:53.41	67:01:52.86	2452401.0	-255.7± 5.0	K03
UrsaMinor-110	4	15:08:53.41	67:01:52.86	2452769.0	-260.5± 2.4	W04
UrsaMinor-111	4	15:08:54.89	66:56:25.71	2454615.8	-243.9± 0.8	W15
UrsaMinor-111	4	15:08:54.89	66:56:25.71	2455659.7	-243.2± 1.5	W15
UrsaMinor-111	4	15:08:54.90	66:56:25.62	2452401.0	-239.3± 6.9	K03
UrsaMinor-111	4	15:08:54.90	66:56:25.62	2452769.0	-237.5± 3.3	W04
UrsaMinor-112	2	15:08:55.44	67:15:16.51	2454615.4	-256.7± 0.3	W15
UrsaMinor-112	2	15:08:55.47	67:15:16.01	2454886.0	-249.9± 2.1	K10
UrsaMinor-113	2	15:08:55.46	67:24:00.09	2454615.8	-247.6± 1.3	W15
UrsaMinor-113	2	15:08:55.46	67:24:00.09	2454915.9	-245.9± 1.8	W15
UrsaMinor-114	4	15:08:55.98	67:12:46.60	2454615.8	-251.8± 0.6	W15
UrsaMinor-114	4	15:08:56.08	67:12:46.22	2452401.0	-255.1± 6.2	K03
UrsaMinor-114	4	15:08:56.08	67:12:46.22	2452769.0	-255.1± 2.0	W04
UrsaMinor-114	4	15:08:56.03	67:12:46.41	2454886.1	-251.7± 2.1	K10
UrsaMinor-115	2	15:08:57.84	66:58:20.19	2454614.9	-246.1± 1.3	W15
UrsaMinor-115	2	15:08:57.84	66:58:20.19	2454913.7	-246.2± 2.3	W15
UrsaMinor-116	2	15:08:57.98	67:10:40.31	2454614.9	-245.2± 0.6	W15
UrsaMinor-116	2	15:08:58.02	67:10:39.90	2452401.0	-242.1± 5.3	K03
UrsaMinor-117	2	15:09:00.18	67:13:39.61	2454615.8	-241.5± 1.1	W15
UrsaMinor-117	2	15:09:00.22	67:13:39.19	2454886.1	-247.3± 2.3	K10
UrsaMinor-118	2	15:09:05.44	67:14:53.71	2454615.8	-245.2± 0.7	W15
UrsaMinor-118	2	15:09:05.50	67:14:53.45	2452769.0	-242.0± 2.4	W04

Table H.1: Continued. Velocities of RGB stars in Ursa Minor

Star ID	n	α_{J2000} (hh:mm:ss.ss)	δ_{J2000} (dd:mm:ss.ss)	HJD (days)	v (km s ⁻¹)	Ref.
UrsaMinor-119	3	15:09:05.63	67:16:15.20	2454615.8	-267.2± 0.5	W15
UrsaMinor-119	3	15:09:05.69	67:16:14.84	2452769.0	-269.7± 1.1	W04
UrsaMinor-119	3	15:09:05.65	67:16:14.60	2454886.1	-268.2± 2.2	K10
UrsaMinor-120	7	15:09:06.44	67:17:07.61	2454615.8	-245.6± 0.4	W15
UrsaMinor-120	7	15:09:06.49	67:17:07.22	2452401.0	-241.9± 3.8	K03
UrsaMinor-120	7	15:09:06.49	67:17:07.22	2452769.0	-245.9± 2.3	W04
UrsaMinor-120	7	15:09:06.42	67:17:07.50	2448774.8	-260.8± 7.2	A95
UrsaMinor-120	7	15:09:06.42	67:17:07.50	2449128.8	-254.6± 6.3	A95
UrsaMinor-120	7	15:09:06.42	67:17:07.50	2449130.8	-244.3± 4.3	A95
UrsaMinor-120	7	15:09:06.46	67:17:07.11	2454886.1	-247.0± 2.1	K10
UrsaMinor-121	3	15:09:07.36	66:59:09.90	2454615.8	-241.3± 0.7	W15
UrsaMinor-121	3	15:09:07.36	66:59:09.90	2454915.9	-239.7± 1.3	W15
UrsaMinor-121	3	15:09:07.38	66:59:09.49	2452769.0	-241.6± 2.0	W04
UrsaMinor-122	2	15:09:07.97	67:13:54.11	2454615.8	-247.8± 1.0	W15
UrsaMinor-122	2	15:09:07.99	67:13:53.70	2454886.0	-248.4± 2.2	K10
UrsaMinor-123	5	15:09:08.22	67:21:10.90	2454615.8	-248.3± 0.4	W15
UrsaMinor-123	5	15:09:08.21	67:21:10.79	2448776.7	-251.2± 6.0	A95
UrsaMinor-123	5	15:09:08.21	67:21:10.79	2449130.8	-256.2± 5.7	A95
UrsaMinor-123	5	15:09:08.21	67:21:10.79	2449457.8	-245.3± 3.1	A95
UrsaMinor-123	5	15:09:08.32	67:21:10.49	2454886.1	-248.9± 2.1	K10
UrsaMinor-124	2	15:09:10.44	67:14:32.10	2454615.8	-246.5± 0.9	W15
UrsaMinor-124	2	15:09:10.46	67:14:31.71	2454886.0	-246.8± 2.2	K10
UrsaMinor-125	3	15:09:12.24	67:13:27.99	2454913.7	-256.3± 2.3	W15
UrsaMinor-125	3	15:09:12.28	67:13:27.55	2452769.0	-249.6± 5.5	W04
UrsaMinor-125	3	15:09:12.26	67:13:27.61	2454886.0	-255.3± 2.3	K10
UrsaMinor-126	3	15:09:12.78	67:16:08.91	2454913.7	-255.3± 0.8	W15
UrsaMinor-126	3	15:09:12.78	67:16:08.91	2455659.7	-257.1± 2.4	W15
UrsaMinor-126	3	15:09:12.79	67:16:08.39	2454886.1	-256.1± 2.2	K10
UrsaMinor-127	6	15:09:12.82	67:33:11.71	2454616.9	-261.6± 0.4	W15
UrsaMinor-127	6	15:09:12.92	67:33:11.56	2452401.0	-258.2± 6.0	K03
UrsaMinor-127	6	15:09:12.92	67:33:11.56	2452769.0	-259.3± 1.9	W04
UrsaMinor-127	6	15:09:12.81	67:33:11.49	2448776.7	-249.9± 6.9	A95
UrsaMinor-127	6	15:09:12.81	67:33:11.49	2449130.8	-260.6± 4.8	A95
UrsaMinor-127	6	15:09:12.81	67:33:11.49	2449457.8	-263.7± 4.6	A95
UrsaMinor-128	2	15:09:13.10	67:20:28.60	2454614.9	-241.1± 1.6	W15
UrsaMinor-128	2	15:09:13.18	67:20:28.19	2454886.1	-254.3± 2.2	K10
UrsaMinor-129	2	15:09:13.65	67:16:11.71	2454615.8	-252.1± 0.5	W15

Table H.1: Continued. Velocities of RGB stars in Ursa Minor

Star ID	n	α_{J2000} (hh:mm:ss.ss)	δ_{J2000} (dd:mm:ss.ss)	HJD (days)	v (km s ⁻¹)	Ref.
UrsaMinor-129	2	15:09:13.66	67:16:11.11	2454886.0	-250.7± 2.1	K10
UrsaMinor-130	3	15:09:13.72	67:05:10.91	2454614.9	-245.9± 1.0	W15
UrsaMinor-130	3	15:09:13.69	67:05:10.82	2452401.0	-241.6± 4.9	K03
UrsaMinor-130	3	15:09:13.69	67:05:10.82	2452769.0	-243.3± 4.0	W04
UrsaMinor-131	2	15:09:14.02	67:11:18.30	2455659.7	-248.1± 1.7	W15
UrsaMinor-131	2	15:09:14.07	67:11:18.30	2454886.1	-249.6± 2.2	K10
UrsaMinor-132	6	15:09:14.84	67:17:45.29	2454614.9	-248.1± 0.4	W15
UrsaMinor-132	6	15:09:14.84	67:17:45.29	2454915.9	-247.5± 0.5	W15
UrsaMinor-132	6	15:09:14.81	67:17:45.21	2448776.7	-255.1± 6.3	A95
UrsaMinor-132	6	15:09:14.81	67:17:45.21	2449128.8	-246.7± 2.9	A95
UrsaMinor-132	6	15:09:14.81	67:17:45.21	2449130.8	-243.9± 3.1	A95
UrsaMinor-132	6	15:09:14.88	67:17:44.79	2454886.0	-255.8± 2.1	K10
UrsaMinor-133	2	15:09:15.80	67:15:43.39	2454615.8	-237.8± 1.3	W15
UrsaMinor-133	2	15:09:15.81	67:15:42.90	2454886.1	-240.5± 2.3	K10
UrsaMinor-134	2	15:09:17.04	67:20:08.30	2454616.9	-257.0± 1.3	W15
UrsaMinor-134	2	15:09:17.12	67:20:07.81	2454886.1	-258.8± 2.2	K10
UrsaMinor-135	2	15:09:18.31	66:26:32.69	2454616.8	-256.8± 0.5	W15
UrsaMinor-135	2	15:09:18.31	66:26:32.69	2455232.9	-256.5± 0.5	W15
UrsaMinor-136	2	15:09:19.71	67:14:56.29	2454915.9	-261.2± 1.8	W15
UrsaMinor-136	2	15:09:19.72	67:14:55.80	2454886.0	-258.3± 2.2	K10
UrsaMinor-137	6	15:09:20.78	67:17:56.00	2454614.9	-246.7± 0.7	W15
UrsaMinor-137	6	15:09:20.78	67:17:56.00	2454913.7	-246.5± 1.0	W15
UrsaMinor-137	6	15:09:20.75	67:17:55.89	2448774.8	-229.9± 8.2	A95
UrsaMinor-137	6	15:09:20.75	67:17:55.89	2449128.8	-250.8± 8.7	A95
UrsaMinor-137	6	15:09:20.75	67:17:55.89	2449130.8	-249.4± 6.8	A95
UrsaMinor-137	6	15:09:20.75	67:17:55.89	2449457.8	-241.0± 8.1	A95
UrsaMinor-138	2	15:09:25.48	67:05:48.90	2454914.8	-251.3± 1.0	W15
UrsaMinor-138	2	15:09:25.49	67:05:48.48	2452401.0	-252.0± 5.6	K03
UrsaMinor-139	4	15:09:28.36	67:20:12.51	2454615.8	-246.8± 0.4	W15
UrsaMinor-139	4	15:09:28.36	67:20:12.51	2454915.9	-245.8± 0.5	W15
UrsaMinor-139	4	15:09:28.34	67:20:12.51	2449128.8	-246.4± 4.3	A95
UrsaMinor-139	4	15:09:28.34	67:20:12.51	2449130.8	-240.4± 3.2	A95
UrsaMinor-140	4	15:09:28.58	67:17:05.60	2454614.9	-240.3± 0.4	W15
UrsaMinor-140	4	15:09:28.58	67:17:05.60	2448774.8	-242.5± 3.4	A95
UrsaMinor-140	4	15:09:28.58	67:17:05.60	2449128.8	-236.2± 3.2	A95
UrsaMinor-140	4	15:09:28.58	67:17:05.60	2449130.8	-237.9± 2.2	A95
UrsaMinor-141	9	15:09:29.45	67:09:29.01	2454913.7	-259.9± 0.5	W15

Table H.1: Continued. Velocities of RGB stars in Ursa Minor

Star ID	n	α_{J2000} (hh:mm:ss.ss)	δ_{J2000} (dd:mm:ss.ss)	HJD (days)	v (km s ⁻¹)	Ref.
UrsaMinor-141	9	15:09:29.49	67:09:28.55	2452401.0	-260.0± 1.4	K03
UrsaMinor-141	9	15:09:29.49	67:09:28.55	2452769.0	-261.2± 0.6	W04
UrsaMinor-141	9	15:09:29.44	67:09:29.01	2445506.8	-261.3± 2.2	O95
UrsaMinor-141	9	15:09:29.44	67:09:29.01	2448774.8	-265.1± 2.5	A95
UrsaMinor-141	9	15:09:29.44	67:09:29.01	2448776.7	-265.9± 3.8	A95
UrsaMinor-141	9	15:09:29.44	67:09:29.01	2449128.8	-263.1± 3.4	A95
UrsaMinor-141	9	15:09:29.44	67:09:29.01	2449130.8	-261.0± 2.2	A95
UrsaMinor-141	9	15:09:29.44	67:09:29.01	2449457.8	-257.5± 2.9	A95
UrsaMinor-142	6	15:09:29.72	67:12:58.60	2454615.8	-247.5± 0.5	W15
UrsaMinor-142	6	15:09:29.75	67:12:58.28	2452769.0	-248.7± 1.6	W04
UrsaMinor-142	6	15:09:29.69	67:12:58.71	2448776.7	-250.1± 6.9	A95
UrsaMinor-142	6	15:09:29.69	67:12:58.71	2449128.8	-254.7± 6.9	A95
UrsaMinor-142	6	15:09:29.69	67:12:58.71	2449130.8	-252.3± 4.5	A95
UrsaMinor-142	6	15:09:29.73	67:12:58.41	2454885.0	-247.5± 2.1	K10
UrsaMinor-143	2	15:09:30.94	67:18:06.60	2454615.8	-257.9± 0.9	W15
UrsaMinor-143	2	15:09:30.98	67:18:06.19	2454886.1	-258.1± 2.2	K10
UrsaMinor-144	4	15:09:32.78	67:03:15.01	2454615.8	-225.8± 0.5	W15
UrsaMinor-144	4	15:09:32.78	67:03:15.01	2454914.8	-223.6± 0.6	W15
UrsaMinor-144	4	15:09:32.86	67:03:14.90	2452769.0	-229.9± 1.5	W04
UrsaMinor-144	4	15:09:32.74	67:03:15.09	2449128.8	-220.5± 6.6	A95
UrsaMinor-145	2	15:09:33.10	67:22:32.69	2454615.8	-249.8± 0.8	W15
UrsaMinor-145	2	15:09:33.19	67:22:32.31	2454886.1	-251.5± 2.5	K10
UrsaMinor-146	2	15:09:33.44	67:09:19.59	2454615.8	-256.0± 2.2	W15
UrsaMinor-146	2	15:09:33.45	67:09:19.40	2455328.9	-240.7± 2.6	K10
UrsaMinor-147	2	15:09:34.45	67:15:57.10	2454615.8	-250.8± 1.0	W15
UrsaMinor-147	2	15:09:34.46	67:15:56.69	2454886.0	-249.4± 2.3	K10
UrsaMinor-148	2	15:09:35.56	67:13:52.90	2454913.7	-237.5± 1.3	W15
UrsaMinor-148	2	15:09:35.57	67:13:52.60	2454886.0	-233.0± 2.2	K10
UrsaMinor-149	2	15:09:36.66	67:06:36.31	2454615.8	-252.3± 1.7	W15
UrsaMinor-149	2	15:09:36.68	67:06:36.11	2455328.9	-248.5± 2.4	K10
UrsaMinor-150	2	15:09:37.06	66:38:14.00	2454616.8	-251.0± 0.7	W15
UrsaMinor-150	2	15:09:37.06	66:38:14.00	2455232.9	-251.4± 1.1	W15
UrsaMinor-151	3	15:09:39.14	67:21:21.91	2454615.8	-254.3± 0.5	W15
UrsaMinor-151	3	15:09:39.10	67:21:22.00	2449130.8	-254.0± 3.2	A95
UrsaMinor-151	3	15:09:39.10	67:21:22.00	2449457.8	-256.2± 7.6	A95
UrsaMinor-152	4	15:09:39.63	67:17:38.70	2454614.9	-253.9± 0.4	W15
UrsaMinor-152	4	15:09:39.61	67:17:38.70	2448774.8	-257.1± 6.3	A95

Table H.1: Continued. Velocities of RGB stars in Ursa Minor

Star ID	n	α_{J2000} (hh:mm:ss.ss)	δ_{J2000} (dd:mm:ss.ss)	HJD (days)	v (km s ⁻¹)	Ref.
UrsaMinor-152	4	15:09:39.61	67:17:38.70	2449128.8	-254.5± 3.7	A95
UrsaMinor-152	4	15:09:39.61	67:17:38.70	2449130.8	-254.0± 1.9	A95
UrsaMinor-153	2	15:09:39.74	67:12:25.01	2454913.7	-251.5± 1.9	W15
UrsaMinor-153	2	15:09:39.76	67:12:24.79	2454885.0	-248.2± 2.3	K10
UrsaMinor-154	2	15:09:41.99	67:05:08.11	2454615.8	-248.2± 0.9	W15
UrsaMinor-154	2	15:09:42.02	67:05:07.89	2455328.9	-248.5± 2.2	K10
UrsaMinor-155	2	15:09:44.65	67:09:10.39	2454615.8	-250.6± 0.6	W15
UrsaMinor-155	2	15:09:44.67	67:09:10.20	2455328.9	-249.3± 2.2	K10
UrsaMinor-156	2	15:09:46.37	67:17:35.29	2454615.8	-250.8± 1.7	W15
UrsaMinor-156	2	15:09:46.37	67:17:35.29	2454913.7	-248.2± 1.5	W15
UrsaMinor-157	2	15:09:48.17	67:20:18.49	2454615.8	-243.2± 0.5	W15
UrsaMinor-157	2	15:09:48.26	67:20:18.11	2454885.0	-239.6± 2.1	K10
UrsaMinor-158	2	15:09:48.93	67:15:08.71	2454615.8	-236.3± 0.6	W15
UrsaMinor-158	2	15:09:48.96	67:15:08.29	2454885.0	-235.5± 2.2	K10
UrsaMinor-159	2	15:09:49.10	67:08:17.79	2454614.9	-240.9± 0.8	W15
UrsaMinor-159	2	15:09:49.13	67:08:17.49	2455328.9	-240.4± 2.1	K10
UrsaMinor-160	3	15:09:51.60	67:12:17.59	2454615.8	-247.9± 0.4	W15
UrsaMinor-160	3	15:09:51.64	67:12:17.32	2452769.0	-253.8± 5.7	W04
UrsaMinor-160	3	15:09:51.56	67:12:17.79	2449128.8	-241.0± 4.3	A95
UrsaMinor-161	2	15:09:52.41	67:13:55.29	2455659.7	-238.3± 2.2	W15
UrsaMinor-161	2	15:09:52.46	67:13:54.90	2454885.0	-235.6± 2.3	K10
UrsaMinor-162	5	15:09:53.56	67:07:40.19	2454615.8	-248.7± 0.7	W15
UrsaMinor-162	5	15:09:53.62	67:07:39.76	2452769.0	-246.0± 4.1	W04
UrsaMinor-162	5	15:09:53.55	67:07:40.41	2448776.7	-249.6± 6.5	A95
UrsaMinor-162	5	15:09:53.55	67:07:40.41	2449130.8	-237.3± 7.1	A95
UrsaMinor-162	5	15:09:53.61	67:07:40.00	2455328.9	-245.8± 2.1	K10
UrsaMinor-163	2	15:09:54.09	67:12:17.51	2454615.8	-242.6± 1.3	W15
UrsaMinor-163	2	15:09:54.16	67:12:17.21	2454886.0	-242.0± 2.6	K10
UrsaMinor-164	5	15:09:54.24	67:12:03.31	2454614.9	-248.9± 0.4	W15
UrsaMinor-164	5	15:09:54.24	67:12:03.31	2454915.9	-248.7± 0.5	W15
UrsaMinor-164	5	15:09:54.21	67:12:03.51	2448774.8	-250.1± 3.2	A95
UrsaMinor-164	5	15:09:54.21	67:12:03.51	2449130.8	-252.4± 1.9	A95
UrsaMinor-164	5	15:09:54.21	67:12:03.51	2449457.8	-249.7± 1.4	A95
UrsaMinor-165	3	15:09:55.14	67:21:37.59	2454913.7	-249.5± 1.2	W15
UrsaMinor-165	3	15:09:55.15	67:21:37.33	2452769.0	-225.4± 4.3	W04
UrsaMinor-165	3	15:09:55.23	67:21:37.21	2454885.0	-242.5± 2.2	K10
UrsaMinor-166	3	15:09:57.44	67:09:27.80	2454614.9	-245.5± 1.2	W15

Table H.1: Continued. Velocities of RGB stars in Ursa Minor

Star ID	n	α_{J2000} (hh:mm:ss.ss)	δ_{J2000} (dd:mm:ss.ss)	HJD (days)	v (km s ⁻¹)	Ref.
UrsaMinor-166	3	15:09:57.48	67:09:27.36	2452769.0	-243.7± 5.8	W04
UrsaMinor-166	3	15:09:57.47	67:09:27.50	2455328.9	-248.5± 2.1	K10
UrsaMinor-167	6	15:09:58.59	67:16:20.20	2454614.9	-246.9± 0.4	W15
UrsaMinor-167	6	15:09:58.56	67:16:20.20	2445736.9	-250.5± 2.0	O95
UrsaMinor-167	6	15:09:58.56	67:16:20.20	2446209.8	-246.4± 1.3	O95
UrsaMinor-167	6	15:09:58.56	67:16:20.20	2448775.8	-243.4± 2.7	A95
UrsaMinor-167	6	15:09:58.56	67:16:20.20	2448776.7	-252.5± 2.9	A95
UrsaMinor-167	6	15:09:58.56	67:16:20.20	2449130.8	-248.9± 2.9	A95
UrsaMinor-168	3	15:10:01.46	67:00:20.11	2454615.8	-257.3± 0.9	W15
UrsaMinor-168	3	15:10:01.49	67:00:19.73	2452401.0	-244.6± 6.3	K03
UrsaMinor-168	3	15:10:01.49	67:00:19.73	2452769.0	-253.4± 7.8	W04
UrsaMinor-169	2	15:10:01.48	67:11:39.09	2454614.9	-240.6± 1.0	W15
UrsaMinor-169	2	15:10:01.56	67:11:38.81	2454886.0	-246.2± 2.6	K10
UrsaMinor-170	3	15:10:01.65	67:12:09.30	2454615.8	-243.6± 0.9	W15
UrsaMinor-170	3	15:10:01.69	67:12:09.00	2452769.0	-228.8± 9.8	W04
UrsaMinor-170	3	15:10:01.72	67:12:09.11	2454886.0	-251.4± 2.5	K10
UrsaMinor-171	2	15:10:03.13	67:12:05.51	2454615.8	-249.5± 1.1	W15
UrsaMinor-171	2	15:10:03.20	67:12:05.21	2454886.0	-240.6± 6.1	K10
UrsaMinor-172	2	15:10:04.71	67:21:47.51	2454615.8	-249.2± 0.6	W15
UrsaMinor-172	2	15:10:04.80	67:21:47.10	2454885.0	-245.3± 2.2	K10
UrsaMinor-173	2	15:10:04.76	67:20:51.81	2454615.8	-258.9± 1.1	W15
UrsaMinor-173	2	15:10:04.79	67:20:51.51	2455327.9	-260.0± 2.2	K10
UrsaMinor-174	3	15:10:07.01	67:22:53.81	2454614.9	-241.2± 0.8	W15
UrsaMinor-174	3	15:10:07.02	67:22:53.33	2452769.0	-240.2± 2.0	W04
UrsaMinor-174	3	15:10:07.09	67:22:53.29	2454885.0	-237.7± 2.1	K10
UrsaMinor-175	2	15:10:08.14	67:19:25.51	2455659.7	-241.4± 2.0	W15
UrsaMinor-175	2	15:10:08.17	67:19:25.21	2455327.9	-243.5± 2.2	K10
UrsaMinor-176	2	15:10:08.67	67:18:38.19	2454615.8	-246.3± 0.5	W15
UrsaMinor-176	2	15:10:08.74	67:18:38.11	2454885.0	-244.8± 2.1	K10
UrsaMinor-177	10	15:10:09.01	67:12:52.50	2454614.9	-234.6± 0.4	W15
UrsaMinor-177	10	15:10:09.01	67:12:52.61	2445737.0	-230.3± 2.3	O95
UrsaMinor-177	10	15:10:09.01	67:12:52.61	2445846.8	-235.7± 2.1	O95
UrsaMinor-177	10	15:10:09.01	67:12:52.61	2446209.7	-237.5± 1.8	O95
UrsaMinor-177	10	15:10:09.01	67:12:52.61	2446593.7	-232.0± 1.7	O95
UrsaMinor-177	10	15:10:09.01	67:12:52.61	2446594.7	-236.4± 2.2	O95
UrsaMinor-177	10	15:10:09.01	67:12:52.61	2448776.7	-233.6± 1.7	A95
UrsaMinor-177	10	15:10:09.01	67:12:52.61	2449128.8	-231.9± 1.3	A95

Table H.1: Continued. Velocities of RGB stars in Ursa Minor

Star ID	n	α_{J2000} (hh:mm:ss.ss)	δ_{J2000} (dd:mm:ss.ss)	HJD (days)	v (km s ⁻¹)	Ref.
UrsaMinor-177	10	15:10:09.01	67:12:52.61	2449130.8	-232.4± 1.4	A95
UrsaMinor-177	10	15:10:09.07	67:12:52.09	2454885.0	-232.7± 2.1	K10
UrsaMinor-178	2	15:10:09.88	67:13:21.40	2454615.8	-243.2± 1.3	W15
UrsaMinor-178	2	15:10:09.94	67:13:21.10	2454885.0	-241.2± 2.2	K10
UrsaMinor-179	7	15:10:10.11	67:10:37.81	2454615.4	-231.6± 0.4	W15
UrsaMinor-179	7	15:10:10.11	67:10:37.81	2454915.9	-232.0± 0.6	W15
UrsaMinor-179	7	15:10:10.14	67:10:37.45	2452401.0	-233.9± 2.5	K03
UrsaMinor-179	7	15:10:10.14	67:10:37.45	2452769.0	-232.6± 1.2	W04
UrsaMinor-179	7	15:10:10.08	67:10:37.89	2448774.8	-233.0± 4.5	A95
UrsaMinor-179	7	15:10:10.08	67:10:37.89	2448776.7	-239.5± 8.3	A95
UrsaMinor-179	7	15:10:10.20	67:10:37.59	2454885.0	-230.3± 2.1	K10
UrsaMinor-180	7	15:10:11.66	67:08:29.19	2454615.4	-245.9± 0.4	W15
UrsaMinor-180	7	15:10:11.66	67:08:29.19	2454915.9	-244.5± 0.7	W15
UrsaMinor-180	7	15:10:11.63	67:08:29.41	2448774.8	-246.8± 7.7	A95
UrsaMinor-180	7	15:10:11.63	67:08:29.41	2449128.8	-245.8± 8.5	A95
UrsaMinor-180	7	15:10:11.63	67:08:29.41	2449130.8	-247.3± 4.4	A95
UrsaMinor-180	7	15:10:11.63	67:08:29.41	2449457.8	-245.0± 5.7	A95
UrsaMinor-180	7	15:10:11.68	67:08:28.89	2455328.9	-243.7± 2.1	K10
UrsaMinor-181	2	15:10:12.64	67:22:42.30	2454615.8	-250.6± 0.7	W15
UrsaMinor-181	2	15:10:12.67	67:22:42.19	2454885.0	-244.2± 2.2	K10
UrsaMinor-182	2	15:10:13.12	67:23:16.91	2454616.9	-239.6± 0.6	W15
UrsaMinor-182	2	15:10:13.20	67:23:16.50	2454885.0	-238.5± 2.2	K10
UrsaMinor-183	4	15:10:13.60	67:06:17.30	2454615.8	-255.5± 0.5	W15
UrsaMinor-183	4	15:10:13.55	67:06:17.49	2449130.8	-274.2± 6.6	A95
UrsaMinor-183	4	15:10:13.55	67:06:17.49	2449457.8	-254.9± 9.4	A95
UrsaMinor-183	4	15:10:13.63	67:06:17.00	2455328.9	-253.6± 2.1	K10
UrsaMinor-184	3	15:10:16.91	67:13:42.90	2454615.8	-251.2± 0.9	W15
UrsaMinor-184	3	15:10:16.96	67:13:42.60	2452401.0	-249.4± 2.7	K03
UrsaMinor-184	3	15:10:16.96	67:13:42.49	2454885.0	-244.6± 2.2	K10
UrsaMinor-185	5	15:10:17.58	67:15:53.50	2454913.7	-242.3± 0.6	W15
UrsaMinor-185	5	15:10:17.55	67:15:53.61	2448776.7	-239.1± 6.6	A95
UrsaMinor-185	5	15:10:17.55	67:15:53.61	2449128.8	-239.0± 6.9	A95
UrsaMinor-185	5	15:10:17.55	67:15:53.61	2449130.8	-242.7± 6.9	A95
UrsaMinor-185	5	15:10:17.55	67:15:53.61	2449457.8	-251.2± 5.5	A95
UrsaMinor-186	2	15:10:17.62	67:20:15.69	2454615.8	-246.7± 0.6	W15
UrsaMinor-186	2	15:10:17.58	67:20:15.99	2449457.8	-243.9± 6.9	A95
UrsaMinor-187	3	15:10:17.86	67:25:25.89	2454615.8	-253.2± 0.4	W15

Table H.1: Continued. Velocities of RGB stars in Ursa Minor

Star ID	n	α_{J2000} (hh:mm:ss.ss)	δ_{J2000} (dd:mm:ss.ss)	HJD (days)	v (km s ⁻¹)	Ref.
UrsaMinor-187	3	15:10:17.83	67:25:26.30	2449130.8	-262.9± 6.6	A95
UrsaMinor-187	3	15:10:17.83	67:25:26.30	2449457.8	-252.9± 3.3	A95
UrsaMinor-188	4	15:10:19.37	67:05:32.80	2454615.3	-241.2± 0.4	W15
UrsaMinor-188	4	15:10:19.36	67:05:33.00	2449128.8	-233.5± 4.5	A95
UrsaMinor-188	4	15:10:19.36	67:05:33.00	2449457.8	-244.4± 5.7	A95
UrsaMinor-188	4	15:10:19.42	67:05:32.50	2455328.9	-243.0± 2.1	K10
UrsaMinor-189	2	15:10:20.15	67:22:10.31	2454614.9	-242.9± 2.2	W15
UrsaMinor-189	2	15:10:20.20	67:22:09.89	2454885.0	-243.7± 2.2	K10
UrsaMinor-190	2	15:10:21.55	67:20:01.80	2454913.7	-240.0± 1.8	W15
UrsaMinor-190	2	15:10:21.61	67:20:01.60	2454885.0	-256.6± 2.2	K10
UrsaMinor-191	2	15:10:21.73	67:19:56.99	2454615.8	-248.0± 0.6	W15
UrsaMinor-191	2	15:10:21.76	67:19:56.71	2455327.9	-252.5± 2.1	K10
UrsaMinor-192	4	15:10:23.90	67:20:37.99	2454615.8	-246.1± 0.4	W15
UrsaMinor-192	4	15:10:23.86	67:20:38.10	2449130.8	-249.1± 5.2	A95
UrsaMinor-192	4	15:10:23.86	67:20:38.10	2449457.8	-254.5± 6.9	A95
UrsaMinor-192	4	15:10:23.95	67:20:37.69	2454885.0	-243.9± 2.1	K10
UrsaMinor-193	3	15:10:24.93	67:06:42.51	2454615.8	-238.1± 0.9	W15
UrsaMinor-193	3	15:10:24.96	67:06:42.19	2452769.0	-238.1± 5.1	W04
UrsaMinor-193	3	15:10:24.96	67:06:42.21	2455328.9	-235.4± 2.2	K10
UrsaMinor-194	6	15:10:27.06	67:24:36.21	2454914.8	-254.6± 0.3	W15
UrsaMinor-194	6	15:10:27.07	67:24:36.51	2448774.8	-258.9± 3.0	A95
UrsaMinor-194	6	15:10:27.07	67:24:36.51	2449128.8	-255.8± 1.7	A95
UrsaMinor-194	6	15:10:27.07	67:24:36.51	2449130.8	-255.5± 0.7	A95
UrsaMinor-194	6	15:10:27.07	67:24:36.51	2449457.8	-252.1± 2.0	A95
UrsaMinor-194	6	15:10:27.10	67:24:35.79	2454885.0	-252.8± 2.1	K10
UrsaMinor-195	2	15:10:31.54	67:20:29.40	2454915.9	-250.3± 2.6	W15
UrsaMinor-195	2	15:10:31.57	67:20:29.26	2452769.0	-239.9± 9.5	W04
UrsaMinor-196	2	15:10:31.56	67:19:06.81	2454615.8	-243.1± 0.5	W15
UrsaMinor-196	2	15:10:31.57	67:19:06.59	2455327.9	-242.0± 2.1	K10
UrsaMinor-197	2	15:10:35.03	67:19:35.59	2454615.8	-262.0± 2.0	W15
UrsaMinor-197	2	15:10:35.05	67:19:35.40	2455327.9	-265.7± 2.2	K10
UrsaMinor-198	4	15:10:38.16	67:13:39.50	2454615.8	-251.4± 0.4	W15
UrsaMinor-198	4	15:10:38.12	67:13:39.61	2448774.8	-251.8± 2.5	A95
UrsaMinor-198	4	15:10:38.12	67:13:39.61	2449130.8	-253.0± 3.7	A95
UrsaMinor-198	4	15:10:38.12	67:13:39.61	2449457.8	-253.3± 3.0	A95
UrsaMinor-199	2	15:10:40.65	67:17:14.69	2454615.8	-246.4± 1.0	W15
UrsaMinor-199	2	15:10:40.65	67:17:14.69	2454915.9	-247.2± 1.4	W15

Table H.1: Continued. Velocities of RGB stars in Ursa Minor

Star ID	n	α_{J2000} (hh:mm:ss.ss)	δ_{J2000} (dd:mm:ss.ss)	HJD (days)	v (km s ⁻¹)	Ref.
UrsaMinor-200	4	15:10:43.00	67:03:47.50	2454615.8	-233.2± 0.4	W15
UrsaMinor-200	4	15:10:42.96	67:03:47.80	2449130.8	-233.7± 9.3	A95
UrsaMinor-200	4	15:10:42.96	67:03:47.80	2449457.8	-240.0± 9.8	A95
UrsaMinor-200	4	15:10:43.02	67:03:47.31	2455328.9	-233.5± 2.1	K10
UrsaMinor-201	5	15:10:43.67	67:12:51.90	2454615.8	-247.5± 0.4	W15
UrsaMinor-201	5	15:10:43.67	67:12:51.90	2454913.7	-247.5± 0.6	W15
UrsaMinor-201	5	15:10:43.62	67:12:52.01	2448776.7	-251.9± 2.7	A95
UrsaMinor-201	5	15:10:43.62	67:12:52.01	2449128.8	-232.8± 6.9	A95
UrsaMinor-201	5	15:10:43.62	67:12:52.01	2449130.8	-253.4± 4.1	A95
UrsaMinor-202	4	15:10:45.31	67:11:39.50	2454615.8	-242.2± 0.6	W15
UrsaMinor-202	4	15:10:45.34	67:11:39.30	2452401.0	-247.4± 4.7	K03
UrsaMinor-202	4	15:10:45.34	67:11:39.30	2452769.0	-239.9± 2.0	W04
UrsaMinor-202	4	15:10:45.28	67:11:39.50	2449457.8	-242.8± 6.4	A95
UrsaMinor-203	3	15:10:46.15	67:16:41.10	2454615.8	-247.8± 0.4	W15
UrsaMinor-203	3	15:10:46.12	67:16:41.21	2449130.8	-246.5± 1.7	A95
UrsaMinor-203	3	15:10:46.12	67:16:41.21	2449457.8	-248.4± 2.7	A95
UrsaMinor-204	2	15:10:46.70	67:25:00.21	2454616.9	-249.5± 0.8	W15
UrsaMinor-204	2	15:10:46.74	67:25:00.08	2452769.0	-243.2± 2.9	W04
UrsaMinor-205	2	15:10:50.63	67:18:46.21	2454614.9	-239.6± 1.3	W15
UrsaMinor-205	2	15:10:50.64	67:18:45.99	2455327.9	-244.5± 2.2	K10
UrsaMinor-206	2	15:10:51.83	66:55:11.31	2455659.7	-242.9± 1.3	W15
UrsaMinor-206	2	15:10:51.83	66:55:11.17	2452769.0	-223.5± 6.0	W04
UrsaMinor-207	2	15:10:52.14	67:03:13.99	2454614.9	-241.8± 1.2	W15
UrsaMinor-207	2	15:10:52.16	67:03:13.80	2455328.9	-240.1± 2.2	K10
UrsaMinor-208	2	15:10:52.22	67:18:57.50	2454615.8	-254.0± 1.9	W15
UrsaMinor-208	2	15:10:52.24	67:18:57.30	2455327.9	-255.2± 2.4	K10
UrsaMinor-209	2	15:10:52.97	67:22:20.69	2454616.9	-232.4± 0.8	W15
UrsaMinor-209	2	15:10:53.01	67:22:20.39	2455327.9	-237.5± 2.2	K10
UrsaMinor-210	2	15:10:54.45	67:22:49.99	2454913.7	-245.7± 0.8	W15
UrsaMinor-210	2	15:10:54.45	67:22:49.58	2452769.0	-248.3± 2.0	W04
UrsaMinor-211	2	15:10:56.27	67:25:14.41	2454615.8	-242.9± 1.0	W15
UrsaMinor-211	2	15:10:56.29	67:25:14.30	2452769.0	-246.8± 5.9	W04
UrsaMinor-212	2	15:10:57.43	67:18:56.40	2454614.9	-233.0± 0.8	W15
UrsaMinor-212	2	15:10:57.45	67:18:56.27	2452769.0	-233.3± 1.3	W04
UrsaMinor-213	2	15:10:58.49	67:21:29.41	2454615.8	-243.9± 1.1	W15
UrsaMinor-213	2	15:10:58.51	67:21:29.00	2455327.9	-246.3± 2.2	K10
UrsaMinor-214	4	15:11:00.90	66:53:04.50	2454915.9	-256.3± 0.5	W15

Table H.1: Continued. Velocities of RGB stars in Ursa Minor

Star ID	n	α_{J2000} (hh:mm:ss.ss)	δ_{J2000} (dd:mm:ss.ss)	HJD (days)	v (km s ⁻¹)	Ref.
UrsaMinor-214	4	15:11:00.88	66:53:04.24	2452401.0	-254.3± 3.5	K03
UrsaMinor-214	4	15:11:00.82	66:53:04.61	2448776.7	-267.1± 9.1	A95
UrsaMinor-214	4	15:11:00.89	66:53:04.20	2455328.9	-259.5± 2.1	K10
UrsaMinor-215	2	15:11:02.49	67:23:46.90	2454615.8	-256.7± 0.8	W15
UrsaMinor-215	2	15:11:02.49	67:23:46.90	2455659.7	-255.1± 2.0	W15
UrsaMinor-216	7	15:11:05.70	67:13:15.71	2454614.9	-240.6± 0.4	W15
UrsaMinor-216	7	15:11:05.61	67:13:15.11	2446594.7	-238.1± 2.8	O95
UrsaMinor-216	7	15:11:05.61	67:13:15.11	2446595.7	-242.8± 2.2	O95
UrsaMinor-216	7	15:11:05.61	67:13:15.11	2448774.8	-244.1± 5.7	A95
UrsaMinor-216	7	15:11:05.61	67:13:15.11	2449128.8	-240.4± 1.7	A95
UrsaMinor-216	7	15:11:05.61	67:13:15.11	2449130.8	-240.7± 3.2	A95
UrsaMinor-216	7	15:11:05.61	67:13:15.11	2449457.8	-240.3± 1.3	A95
UrsaMinor-217	2	15:11:08.42	67:10:05.82	2454615.8	-235.5± 0.6	W15
UrsaMinor-217	2	15:11:08.46	67:10:05.70	2452769.0	-234.6± 1.6	W04
UrsaMinor-218	2	15:11:11.13	66:54:23.71	2454615.8	-230.7± 0.6	W15
UrsaMinor-218	2	15:11:11.14	66:54:23.41	2455328.9	-230.1± 2.1	K10
UrsaMinor-219	3	15:11:17.79	67:19:20.51	2454614.9	-246.1± 0.5	W15
UrsaMinor-219	3	15:11:17.79	67:19:20.51	2454915.9	-246.1± 0.6	W15
UrsaMinor-219	3	15:11:17.78	67:19:20.60	2449130.8	-252.1± 6.6	A95
UrsaMinor-220	5	15:11:19.57	67:22:35.41	2454914.8	-248.2± 0.3	W15
UrsaMinor-220	5	15:11:19.57	67:22:35.41	2455659.7	-238.8± 0.5	W15
UrsaMinor-220	5	15:11:19.56	67:22:35.41	2448774.8	-238.3± 7.5	A95
UrsaMinor-220	5	15:11:19.56	67:22:35.41	2449457.8	-243.2± 1.4	A95
UrsaMinor-220	5	15:11:19.61	67:22:35.11	2455327.9	-242.2± 2.1	K10
UrsaMinor-221	5	15:11:25.53	67:13:49.61	2454615.8	-251.1± 0.3	W15
UrsaMinor-221	5	15:11:25.49	67:13:49.80	2448776.7	-252.1± 2.6	A95
UrsaMinor-221	5	15:11:25.49	67:13:49.80	2449128.8	-246.1± 3.1	A95
UrsaMinor-221	5	15:11:25.49	67:13:49.80	2449130.8	-254.7± 1.4	A95
UrsaMinor-221	5	15:11:25.49	67:13:49.80	2449457.8	-253.2± 1.2	A95
UrsaMinor-222	4	15:11:27.07	67:16:16.71	2454615.8	-249.1± 0.4	W15
UrsaMinor-222	4	15:11:27.02	67:16:16.71	2446918.8	-246.6± 2.5	O95
UrsaMinor-222	4	15:11:27.02	67:16:16.71	2449128.8	-249.7± 3.8	A95
UrsaMinor-222	4	15:11:27.02	67:16:16.71	2449457.8	-246.6± 3.6	A95
UrsaMinor-223	6	15:11:28.38	67:14:42.59	2454614.9	-246.5± 0.4	W15
UrsaMinor-223	6	15:11:28.32	67:14:42.69	2446919.7	-246.5± 1.5	O95
UrsaMinor-223	6	15:11:28.32	67:14:42.69	2448774.8	-242.5± 4.6	A95
UrsaMinor-223	6	15:11:28.32	67:14:42.69	2449128.8	-245.2± 3.3	A95

Table H.1: Continued. Velocities of RGB stars in Ursa Minor

Star ID	n	α_{J2000} (hh:mm:ss.ss)	δ_{J2000} (dd:mm:ss.ss)	HJD (days)	v (km s ⁻¹)	Ref.
UrsaMinor-223	6	15:11:28.32	67:14:42.69	2449130.8	-250.4± 0.7	A95
UrsaMinor-223	6	15:11:28.32	67:14:42.69	2449457.8	-242.2± 1.6	A95
UrsaMinor-224	4	15:11:36.38	67:18:07.89	2454614.9	-246.3± 0.4	W15
UrsaMinor-224	4	15:11:36.34	67:18:07.89	2448774.8	-256.2± 4.5	A95
UrsaMinor-224	4	15:11:36.34	67:18:07.89	2449128.8	-244.4± 3.4	A95
UrsaMinor-224	4	15:11:36.34	67:18:07.89	2449130.8	-247.3± 1.6	A95
UrsaMinor-225	3	15:11:42.50	67:02:26.89	2454614.9	-235.3± 0.8	W15
UrsaMinor-225	3	15:11:42.50	67:02:26.89	2455659.7	-236.4± 1.4	W15
UrsaMinor-225	3	15:11:42.55	67:02:26.81	2452401.0	-235.7± 6.3	K03
UrsaMinor-226	2	15:11:51.98	67:06:41.80	2454615.8	-246.6± 1.9	W15
UrsaMinor-226	2	15:11:51.98	67:06:41.80	2455659.7	-244.5± 2.7	W15
UrsaMinor-227	2	15:11:53.25	67:18:29.40	2454615.8	-236.7± 1.3	W15
UrsaMinor-227	2	15:11:53.25	67:18:29.40	2455659.7	-238.2± 2.3	W15
UrsaMinor-228	2	15:11:53.87	66:49:52.21	2454615.4	-252.6± 0.5	W15
UrsaMinor-228	2	15:11:53.87	66:49:51.99	2455328.9	-255.0± 2.1	K10
UrsaMinor-229	2	15:11:55.23	67:10:47.81	2454615.8	-249.6± 0.6	W15
UrsaMinor-229	2	15:11:55.23	67:10:47.81	2455659.7	-251.3± 1.0	W15
UrsaMinor-230	4	15:12:02.97	67:12:18.01	2454615.8	-255.1± 0.5	W15
UrsaMinor-230	4	15:12:03.04	67:12:17.71	2452401.0	-259.5± 4.7	K03
UrsaMinor-230	4	15:12:03.04	67:12:17.71	2452769.0	-255.1± 1.3	W04
UrsaMinor-230	4	15:12:02.92	67:12:18.09	2449457.8	-260.0± 6.4	A95
UrsaMinor-231	2	15:12:16.06	67:17:12.00	2454615.8	-238.5± 0.8	W15
UrsaMinor-231	2	15:12:16.18	67:17:11.76	2452769.0	-237.5± 4.4	W04
UrsaMinor-232	2	15:12:17.35	67:01:44.70	2454615.8	-244.5± 0.9	W15
UrsaMinor-232	2	15:12:17.41	67:01:44.83	2452769.0	-239.3± 8.3	W04
UrsaMinor-233	2	15:12:22.15	67:14:06.80	2454615.8	-248.1± 1.1	W15
UrsaMinor-233	2	15:12:22.25	67:14:06.61	2452769.0	-246.8± 4.5	W04
UrsaMinor-234	3	15:12:44.75	67:18:42.39	2454615.8	-230.6± 0.4	W15
UrsaMinor-234	3	15:12:44.87	67:18:42.16	2452401.0	-229.7± 3.7	K03
UrsaMinor-234	3	15:12:44.71	67:18:42.31	2449457.8	-229.0± 7.3	A95
UrsaMinor-235	3	15:12:54.38	67:21:08.70	2454913.7	-267.1± 0.6	W15
UrsaMinor-235	3	15:12:54.38	67:21:08.70	2455234.0	-267.9± 1.8	W15
UrsaMinor-235	3	15:12:54.38	67:21:08.70	2455659.7	-267.2± 1.7	W15
UrsaMinor-236	2	15:13:07.14	67:03:15.39	2454615.8	-236.5± 1.6	W15
UrsaMinor-236	2	15:13:07.06	67:03:15.88	2452769.0	-239.4± 7.3	W04
UrsaMinor-237	3	15:13:26.04	67:16:22.40	2454615.4	-249.5± 0.4	W15
UrsaMinor-237	3	15:13:26.13	67:16:22.73	2452401.0	-251.3± 4.0	K03

Table H.1: Continued. Velocities of RGB stars in Ursa Minor

Star ID	n	α_{J2000} (hh:mm:ss.ss)	δ_{J2000} (dd:mm:ss.ss)	HJD (days)	v (km s ⁻¹)	Ref.
UrsaMinor-237	3	15:13:26.01	67:16:22.89	2449457.8	-236.8± 6.8	A95
UrsaMinor-238	4	15:13:30.26	67:06:37.10	2454615.5	-229.6± 0.2	W15
UrsaMinor-238	4	15:13:30.34	67:06:37.12	2452769.0	-231.6± 1.1	W04
UrsaMinor-238	4	15:13:30.22	67:06:37.29	2449457.8	-233.7± 6.8	A95
UrsaMinor-238	4	15:13:30.28	67:06:36.80	2455328.0	-228.8± 2.1	K10
UrsaMinor-239	4	15:13:39.48	67:19:18.70	2454913.7	-253.2± 0.8	W15
UrsaMinor-239	4	15:13:39.48	67:19:18.70	2455234.0	-251.9± 1.1	W15
UrsaMinor-239	4	15:13:39.56	67:19:19.27	2452401.0	-245.2± 7.0	K03
UrsaMinor-239	4	15:13:39.56	67:19:19.27	2452769.0	-256.6± 2.6	W04
UrsaMinor-240	2	15:13:48.96	67:58:22.00	2455234.0	-245.5± 1.2	W15
UrsaMinor-240	2	15:13:48.96	67:58:22.00	2455332.6	-244.6± 1.0	W15
UrsaMinor-241	2	15:14:34.11	67:40:20.29	2454615.9	-257.9± 2.5	W15
UrsaMinor-241	2	15:14:34.15	67:40:20.10	2455328.0	-258.6± 2.5	K10
UrsaMinor-242	3	15:14:52.99	67:48:46.59	2455234.0	-253.7± 1.6	W15
UrsaMinor-242	3	15:14:52.99	67:48:46.59	2455332.6	-250.7± 1.2	W15
UrsaMinor-242	3	15:14:53.04	67:48:46.48	2452769.0	-222.5±11.4	W04
UrsaMinor-243	2	15:14:58.78	67:43:22.61	2454615.9	-249.9± 0.5	W15
UrsaMinor-243	2	15:14:58.86	67:43:22.26	2452769.0	-226.5± 7.2	W04
UrsaMinor-244	3	15:15:14.00	67:44:38.61	2455234.0	-243.6± 1.8	W15
UrsaMinor-244	3	15:15:14.00	67:44:38.61	2455332.6	-243.9± 1.1	W15
UrsaMinor-244	3	15:15:14.06	67:44:38.33	2452769.0	-244.5± 5.4	W04
UrsaMinor-245	2	15:15:48.43	67:44:36.49	2454615.9	-252.7± 1.3	W15
UrsaMinor-245	2	15:15:48.44	67:44:36.41	2455328.0	-263.5± 2.4	K10
UrsaMinor-246	3	15:16:12.82	67:58:27.61	2454615.9	-247.7± 0.6	W15
UrsaMinor-246	3	15:16:12.82	67:58:27.61	2455234.0	-247.2± 0.9	W15
UrsaMinor-246	3	15:16:12.82	67:58:27.61	2455332.6	-244.9± 0.7	W15
UrsaMinor-247	3	15:16:30.68	67:57:52.80	2454615.9	-250.8± 0.6	W15
UrsaMinor-247	3	15:16:30.68	67:57:52.80	2455234.0	-250.2± 1.2	W15
UrsaMinor-247	3	15:16:30.68	67:57:52.80	2455332.6	-249.6± 1.5	W15
UrsaMinor-248	3	15:16:52.51	67:51:21.61	2454615.9	-245.4± 0.5	W15
UrsaMinor-248	3	15:16:52.51	67:51:21.61	2455234.0	-245.7± 0.6	W15
UrsaMinor-248	3	15:16:52.51	67:51:21.61	2455332.6	-244.5± 0.5	W15
UrsaMinor-249	2	15:17:32.90	67:52:27.20	2454615.9	-246.6± 1.5	W15
UrsaMinor-249	2	15:17:32.90	67:52:27.20	2455234.0	-248.7± 1.7	W15
UrsaMinor-250	3	15:17:43.28	68:03:23.41	2454615.9	-244.9± 0.5	W15
UrsaMinor-250	3	15:17:43.28	68:03:23.41	2455234.0	-244.1± 1.0	W15
UrsaMinor-250	3	15:17:43.28	68:03:23.41	2455332.1	-244.0± 0.5	W15

Table H.1: Continued. Velocities of RGB stars in Ursa Minor

Star ID	n	α_{J2000} (hh:mm:ss.ss)	δ_{J2000} (dd:mm:ss.ss)	HJD (days)	v (km s ⁻¹)	Ref.
UrsaMinor-251	2	15:13:35.58	67:18:15.88	2452769.0	-258.8± 4.7	W04
UrsaMinor-251	2	15:13:35.52	67:18:15.80	2455328.0	-257.8± 2.2	K10
UrsaMinor-252	2	15:13:07.21	67:20:35.41	2452769.0	-253.1± 1.2	W04
UrsaMinor-252	2	15:13:07.08	67:20:35.49	2449457.8	-258.6± 5.9	A95
UrsaMinor-253	2	15:12:54.45	67:21:10.30	2452769.0	-266.1± 2.2	W04
UrsaMinor-253	2	15:12:54.34	67:21:10.29	2449457.8	-257.6± 4.4	A95
UrsaMinor-254	2	15:12:42.35	67:24:07.63	2452769.0	-252.9± 1.0	W04
UrsaMinor-254	2	15:12:42.19	67:24:07.70	2449457.8	-257.6± 5.2	A95
UrsaMinor-255	2	15:12:23.69	67:24:05.62	2452401.0	-271.2± 4.2	K03
UrsaMinor-255	2	15:12:23.69	67:24:05.62	2452769.0	-258.5± 1.9	W04
UrsaMinor-256	2	15:09:44.55	67:20:55.57	2452769.0	-267.4± 4.2	W04
UrsaMinor-256	2	15:09:44.63	67:20:55.49	2454885.0	-271.3± 2.2	K10
UrsaMinor-257	2	15:09:24.22	67:19:10.88	2452401.0	-273.8± 5.1	K03
UrsaMinor-257	2	15:09:24.22	67:19:10.88	2452769.0	-262.0± 6.4	W04
UrsaMinor-258	2	15:09:19.11	67:27:34.38	2452401.0	-236.5± 6.6	K03
UrsaMinor-258	2	15:09:19.11	67:27:34.38	2452769.0	-234.8± 2.6	W04
UrsaMinor-259	8	15:09:13.78	67:15:33.30	2452769.0	-224.8± 1.0	W04
UrsaMinor-259	8	15:09:13.72	67:15:33.70	2445414.8	-274.9± 2.5	O95
UrsaMinor-259	8	15:09:13.72	67:15:33.70	2445503.7	-243.5± 1.4	O95
UrsaMinor-259	8	15:09:13.72	67:15:33.70	2445736.9	-249.1± 1.9	O95
UrsaMinor-259	8	15:09:13.72	67:15:33.70	2445846.7	-246.5± 1.8	O95
UrsaMinor-259	8	15:09:13.72	67:15:33.70	2446124.0	-235.8± 1.7	O95
UrsaMinor-259	8	15:09:13.72	67:15:33.70	2448774.8	-239.2± 2.3	A95
UrsaMinor-259	8	15:09:13.72	67:15:33.70	2449128.8	-246.0± 2.2	A95
UrsaMinor-260	2	15:08:30.82	67:10:58.62	2452401.0	-244.1± 9.7	K03
UrsaMinor-260	2	15:08:30.89	67:10:58.80	2454885.0	-245.8± 2.2	K10
UrsaMinor-261	5	15:08:22.26	67:15:50.80	2452401.0	-222.7± 5.1	K03
UrsaMinor-261	5	15:08:22.26	67:15:50.80	2452769.0	-223.0± 1.6	W04
UrsaMinor-261	5	15:08:22.21	67:15:51.09	2449128.8	-222.3± 7.4	A95
UrsaMinor-261	5	15:08:22.21	67:15:51.09	2449457.8	-221.1± 3.8	A95
UrsaMinor-261	5	15:08:22.28	67:15:50.59	2454885.0	-221.9± 2.1	K10
UrsaMinor-262	2	15:10:22.32	67:33:21.82	2452401.0	-238.5± 5.1	K03
UrsaMinor-262	2	15:10:22.32	67:33:21.82	2452769.0	-230.2± 1.0	W04
UrsaMinor-263	2	15:10:05.50	67:40:43.50	2452401.0	-268.5± 5.5	K03
UrsaMinor-263	2	15:10:05.50	67:40:43.50	2452769.0	-268.8± 1.3	W04
UrsaMinor-264	2	15:12:18.49	67:25:34.72	2452769.0	-235.6± 3.5	W04
UrsaMinor-264	2	15:12:18.41	67:25:34.60	2455327.9	-238.5± 2.2	K10

Table H.1: Continued. Velocities of RGB stars in Ursa Minor

Star ID	n	α_{J2000} (hh:mm:ss.ss)	δ_{J2000} (dd:mm:ss.ss)	HJD (days)	v (km s ⁻¹)	Ref.
UrsaMinor-265	2	15:11:09.96	67:30:30.67	2452401.0	-234.1± 3.8	K03
UrsaMinor-265	2	15:11:09.96	67:30:30.67	2452769.0	-237.8± 2.0	W04
UrsaMinor-266	3	15:13:12.32	67:33:20.59	2452769.0	-250.6± 1.2	W04
UrsaMinor-266	3	15:13:12.27	67:33:20.80	2449457.8	-252.2± 4.1	A95
UrsaMinor-266	3	15:13:12.33	67:33:20.61	2455327.9	-244.4± 2.1	K10
UrsaMinor-267	3	15:12:28.96	67:30:46.19	2452401.0	-250.9± 6.2	K03
UrsaMinor-267	3	15:12:28.96	67:30:46.19	2452769.0	-257.6± 2.6	W04
UrsaMinor-267	3	15:12:28.91	67:30:46.31	2455327.9	-258.5± 2.1	K10
UrsaMinor-268	2	15:11:52.95	67:36:10.98	2452769.0	-271.0± 1.8	W04
UrsaMinor-268	2	15:11:52.90	67:36:11.09	2455328.1	-265.3± 2.2	K10
UrsaMinor-269	2	15:11:52.49	67:33:55.44	2452769.0	-237.4± 6.5	W04
UrsaMinor-269	2	15:11:52.51	67:33:55.49	2455328.1	-243.9± 2.2	K10
UrsaMinor-270	2	15:11:36.64	67:31:31.08	2452769.0	-237.1± 6.7	W04
UrsaMinor-270	2	15:11:36.62	67:31:31.19	2455328.1	-251.7± 2.2	K10
UrsaMinor-271	2	15:05:52.04	66:41:30.05	2452401.0	-231.2± 1.9	K03
UrsaMinor-271	2	15:05:52.04	66:41:30.05	2452769.0	-234.3± 1.4	W04
UrsaMinor-272	2	15:05:36.38	66:40:48.40	2452401.0	-237.4± 6.6	K03
UrsaMinor-272	2	15:05:36.38	66:40:48.40	2452769.0	-243.2± 4.2	W04
UrsaMinor-273	2	15:04:15.33	66:51:09.29	2452401.0	-236.1± 5.4	K03
UrsaMinor-273	2	15:04:15.33	66:51:09.29	2452769.0	-224.5± 2.1	W04
UrsaMinor-274	2	15:12:10.76	67:26:02.00	2452401.0	-243.1± 4.7	K03
UrsaMinor-274	2	15:12:10.76	67:26:02.00	2452769.0	-244.3± 3.4	W04
UrsaMinor-275	2	15:11:55.61	67:25:09.34	2452769.0	-253.3± 4.5	W04
UrsaMinor-275	2	15:11:55.54	67:25:09.19	2455327.9	-251.6± 2.1	K10
UrsaMinor-276	5	15:11:48.46	67:19:37.78	2452401.0	-249.7± 1.7	K03
UrsaMinor-276	5	15:11:48.46	67:19:37.78	2452769.0	-247.0± 1.2	W04
UrsaMinor-276	5	15:11:48.31	67:19:37.90	2448774.8	-232.2± 5.3	A95
UrsaMinor-276	5	15:11:48.31	67:19:37.90	2449128.8	-247.8± 4.4	A95
UrsaMinor-276	5	15:11:48.31	67:19:37.90	2449130.8	-250.4± 1.8	A95
UrsaMinor-277	2	15:11:38.97	67:20:14.82	2452769.0	-244.4± 0.7	W04
UrsaMinor-277	2	15:11:38.87	67:20:15.01	2448776.7	-250.9± 4.9	A95
UrsaMinor-278	2	15:11:29.52	67:21:42.37	2452769.0	-239.6± 5.4	W04
UrsaMinor-278	2	15:11:29.42	67:21:42.40	2455327.9	-249.2± 2.1	K10
UrsaMinor-279	2	15:11:14.09	67:27:16.85	2452401.0	-242.0± 5.8	K03
UrsaMinor-279	2	15:11:14.09	67:27:16.85	2452769.0	-237.3± 3.1	W04
UrsaMinor-280	2	15:10:45.20	67:28:34.32	2452401.0	-249.7± 6.7	K03
UrsaMinor-280	2	15:10:45.20	67:28:34.32	2452769.0	-255.6± 2.4	W04

Table H.1: Continued. Velocities of RGB stars in Ursa Minor

Star ID	n	α_{J2000} (hh:mm:ss.ss)	δ_{J2000} (dd:mm:ss.ss)	HJD (days)	v (km s ⁻¹)	Ref.
UrsaMinor-281	8	15:10:37.56	67:27:38.99	2452401.0	-246.4± 2.0	K03
UrsaMinor-281	8	15:10:37.56	67:27:38.99	2452769.0	-246.4± 1.5	W04
UrsaMinor-281	8	15:10:37.50	67:27:39.21	2446593.8	-247.1± 1.8	O95
UrsaMinor-281	8	15:10:37.50	67:27:39.21	2446920.8	-247.7± 1.5	O95
UrsaMinor-281	8	15:10:37.50	67:27:39.21	2448774.8	-246.1± 3.7	A95
UrsaMinor-281	8	15:10:37.50	67:27:39.21	2449128.8	-249.7± 2.1	A95
UrsaMinor-281	8	15:10:37.50	67:27:39.21	2449130.8	-247.6± 1.0	A95
UrsaMinor-281	8	15:10:37.50	67:27:39.21	2449457.8	-246.8± 0.9	A95
UrsaMinor-282	2	15:11:24.23	67:33:50.41	2449457.8	-249.1± 1.9	A95
UrsaMinor-282	2	15:11:24.29	67:33:50.19	2455328.1	-245.2± 2.1	K10
UrsaMinor-283	2	15:12:20.01	67:20:16.90	2449130.8	-263.2± 9.1	A95
UrsaMinor-283	2	15:12:20.01	67:20:16.90	2449457.8	-267.8± 4.3	A95
UrsaMinor-284	8	15:09:36.21	67:04:19.99	2446919.8	-222.5± 1.1	O95
UrsaMinor-284	8	15:09:36.21	67:04:19.99	2447328.9	-219.3± 2.0	O95
UrsaMinor-284	8	15:09:36.21	67:04:19.99	2447672.7	-224.1± 2.0	O95
UrsaMinor-284	8	15:09:36.21	67:04:19.99	2448774.8	-223.3± 7.8	A95
UrsaMinor-284	8	15:09:36.21	67:04:19.99	2448776.7	-219.9± 4.5	A95
UrsaMinor-284	8	15:09:36.21	67:04:19.99	2449128.8	-221.0± 2.7	A95
UrsaMinor-284	8	15:09:36.21	67:04:19.99	2449130.8	-220.7± 3.0	A95
UrsaMinor-284	8	15:09:36.21	67:04:19.99	2449457.8	-225.6± 2.8	A95

BIBLIOGRAPHY

BIBLIOGRAPHY

- Aaronson, M. 1983, *ApJ*, 266, L11
- Aaronson, M., & Olszewski, E. 1987, in *IAU Symposium*, Vol. 117, *Dark matter in the universe*, ed. J. Kormendy & G. R. Knapp, 153–158
- Ackermann, M., Ajello, M., Albert, A., et al. 2011, *Physical Review Letters*, 107, 241302
- Aparicio, A., Carrera, R., & Martínez-Delgado, D. 2001, *AJ*, 122, 2524
- Armandroff, T. E., & Da Costa, G. S. 1986, *AJ*, 92, 777
- Armandroff, T. E., Olszewski, E. W., & Pryor, C. 1995, *AJ*, 110, 2131
- Assmann, P., Fellhauer, M., Wilkinson, M. I., & Smith, R. 2013, *MNRAS*, 432, 274
- Bahcall, J. N., & Tremaine, S. 1981, *ApJ*, 244, 805
- Battaglia, G., Helmi, A., Tolstoy, E., et al. 2008, *ApJ*, 681, L13
- Battaglia, G., Tolstoy, E., Helmi, A., et al. 2011, *MNRAS*, 411, 1013
- . 2006, *A&A*, 459, 423
- Bellazzini, M., Ferraro, F. R., Origlia, L., et al. 2002, *AJ*, 124, 3222
- Bellazzini, M., Gennari, N., & Ferraro, F. R. 2005, *MNRAS*, 360, 185
- Belokurov, V., Zucker, D. B., Evans, N. W., et al. 2006, *ApJ*, 642, L137

- Bonanos, A. Z., Stanek, K. Z., Szentgyorgyi, A. H., Sasselov, D. D., & Bakos, G. Á. 2004, *AJ*, 127, 861
- Bosler, T. L., Smecker-Hane, T. A., & Stetson, P. B. 2007, *MNRAS*, 378, 318
- Carrera, R., Aparicio, A., Martínez-Delgado, D., & Alonso-García, J. 2002, *AJ*, 123, 3199
- Casas, R. A., Arias, V., Peña Ramírez, K., & Kroupa, P. 2012, *MNRAS*, 424, 1941
- Chabrier, G. 2001, *ApJ*, 554, 1274
- Cohen, J. G. 1983, *ApJ*, 270, L41
- Coleman, M., Da Costa, G. S., Bland-Hawthorn, J., et al. 2004, *AJ*, 127, 832
- Coleman, M. G., Jordi, K., Rix, H.-W., Grebel, E. K., & Koch, A. 2007, *AJ*, 134, 1938
- Cottaar, M., & Hénault-Brunet, V. 2014, *A&A*, 562, A20
- Cottaar, M., Meyer, M. R., & Parker, R. J. 2012, *A&A*, 547, A35
- Dabringhausen, J., Kroupa, P., Famaey, B., & Fellhauer, M. 2016, *MNRAS*, 463, 1865
- Demers, S., & Harris, W. E. 1983, *AJ*, 88, 329
- Duchêne, G., & Kraus, A. 2013, *ARA&A*, 51, 269
- Duquennoy, A., & Mayor, M. 1991, *A&A*, 248, 485
- Evans, N. W., Wilkinson, M. I., Perrett, K. M., & Bridges, T. J. 2003, *ApJ*, 583, 752
- Feroz, F., & Hobson, M. P. 2008, *MNRAS*, 384, 449
- Feroz, F., Hobson, M. P., & Bridges, M. 2009, *MNRAS*, 398, 1601

- Fischer, D. A., & Marcy, G. W. 1992, *ApJ*, 396, 178
- Frebel, A., Simon, J. D., Geha, M., & Willman, B. 2010, *ApJ*, 708, 560
- Geha, M., Willman, B., Simon, J. D., et al. 2009, *ApJ*, 692, 1464
- Geringer-Sameth, A., Koushiappas, S. M., & Walker, M. G. 2015, *Phys. Rev. D*, 91, 083535
- Goodwin, S. P., Kroupa, P., Goodman, A., & Burkert, A. 2007, *Protostars and Planets V*, 133
- Gullieuszik, M., Held, E. V., Rizzi, L., et al. 2008, *MNRAS*, 388, 1185
- Hargreaves, J. C., Gilmore, G., & Annan, J. D. 1996a, *MNRAS*, 279, 108
- Hargreaves, J. C., Gilmore, G., Irwin, M. J., & Carter, D. 1994a, *MNRAS*, 269, 957
- . 1994b, *MNRAS*, 271, 693
- . 1996b, *MNRAS*, 282, 305
- Harrington, R. G., & Wilson, A. G. 1950, *PASP*, 62, 118
- Helmi, A., White, S. D. M., de Zeeuw, P. T., & Zhao, H. 1999, *Nature*, 402, 53
- Iben, Jr., I., & Livio, M. 1993, *PASP*, 105, 1373
- Jardel, J. R., Gebhardt, K., Fabricius, M. H., Drory, N., & Williams, M. J. 2013, *ApJ*, 763, 91
- Kaplinghat, M., & Strigari, L. E. 2008, *ApJ*, 682, L93
- Kimmig, B., Seth, A., Ivans, I. I., et al. 2015, *AJ*, 149, 53
- Kirby, E. N., Cohen, J. G., Guhathakurta, P., et al. 2013, *ApJ*, 779, 102

- Kirby, E. N., Cohen, J. G., Simon, J. D., et al. 2017, *ApJ*, 838, 83
- Kirby, E. N., Lanfranchi, G. A., Simon, J. D., Cohen, J. G., & Guhathakurta, P. 2011, *ApJ*, 727, 78
- Kirby, E. N., Guhathakurta, P., Simon, J. D., et al. 2010, *ApJS*, 191, 352
- Klessen, R. S., & Kroupa, P. 1998, *ApJ*, 498, 143
- Kleyna, J., Wilkinson, M. I., Evans, N. W., Gilmore, G., & Frayn, C. 2002, *MNRAS*, 330, 792
- Kleyna, J. T., Wilkinson, M. I., Gilmore, G., & Evans, N. W. 2003, *ApJ*, 588, L21
- Klypin, A., Kravtsov, A. V., Valenzuela, O., & Prada, F. 1999, *ApJ*, 522, 82
- Koch, A., Grebel, E. K., Kleyna, J. T., et al. 2007a, *AJ*, 133, 270
- Koch, A., Kleyna, J. T., Wilkinson, M. I., et al. 2007b, *AJ*, 134, 566
- Komiyama, Y., Doi, M., Furusawa, H., et al. 2007, *AJ*, 134, 835
- Koposov, S. E., Gilmore, G., Walker, M. G., et al. 2011, *ApJ*, 736, 146
- Kounkel, M., Megeath, S. T., Poteet, C. A., Fischer, W. J., & Hartmann, L. 2016, *ApJ*, 821, 52
- Kroupa, P. 1997, *New A*, 2, 139
- Kroupa, P., Tout, C. A., & Gilmore, G. 1993, *MNRAS*, 262, 545
- Law, D. R., & Majewski, S. R. 2010, *ApJ*, 714, 229
- Lee, Y. S., Beers, T. C., Sivarani, T., et al. 2008a, *AJ*, 136, 2022
- . 2008b, *AJ*, 136, 2050

- Lépine, S., Koch, A., Rich, R. M., & Kuijken, K. 2011, *ApJ*, 741, 100
- Little, B., & Tremaine, S. 1987, *ApJ*, 320, 493
- Marks, M., & Kroupa, P. 2011, *MNRAS*, 417, 1702
- Martin, N. F., Ibata, R. A., Chapman, S. C., Irwin, M., & Lewis, G. F. 2007, *MNRAS*, 380, 281
- Martinez, G. D., Minor, Q. E., Bullock, J., et al. 2011, *ApJ*, 738, 55
- Mateo, M., Olszewski, E., Welch, D. L., Fischer, P., & Kunkel, W. 1991, *AJ*, 102, 914
- Mateo, M., Olszewski, E. W., Pryor, C., Welch, D. L., & Fischer, P. 1993, *AJ*, 105, 510
- Mateo, M., Olszewski, E. W., & Walker, M. G. 2008, *ApJ*, 675, 201
- Mateo, M. L. 1998, *ARA&A*, 36, 435
- Mayor, M., Benz, W., Imbert, M., et al. 1984, *A&A*, 134, 118
- McClure, R. D. 1984, *ApJ*, 280, L31
- McConnachie, A. W. 2012, *AJ*, 144, 4
- McConnachie, A. W., & Côté, P. 2010, *ApJ*, 722, L209
- Mighell, K. J., & Rich, R. M. 1996, *AJ*, 111, 777
- Minor, Q. E. 2013, *ApJ*, 779, 116
- Minor, Q. E., Martinez, G., Bullock, J., Kaplinghat, M., & Trainor, R. 2010, *ApJ*, 721, 1142
- Moore, B., Ghigna, S., Governato, F., et al. 1999, *ApJ*, 524, L19

Muñoz, R. R., Carlin, J. L., Frinchaboy, P. M., et al. 2006a, ApJ, 650, L51

Muñoz, R. R., Frinchaboy, P. M., Majewski, S. R., et al. 2005, ApJ, 631, L137

Muñoz, R. R., Majewski, S. R., Zaggia, S., et al. 2006b, ApJ, 649, 201

Nie, J. D., Wood, P. R., & Nicholls, C. P. 2012, MNRAS, 423, 2764

Oldham, L. J., & Auger, M. W. 2016, MNRAS, 457, 421

Olszewski, E. W., Aaronson, M., & Hill, J. M. 1995, AJ, 110, 2120

Olszewski, E. W., Pryor, C., & Armandroff, T. E. 1996, AJ, 111, 750

Peñarrubia, J., Ludlow, A. D., Chanamé, J., & Walker, M. G. 2016, MNRAS, 461, L72

Piatek, S., & Pryor, C. 1995, AJ, 109, 1071

Piatek, S., Pryor, C., & Olszewski, E. W. 2016, AJ, 152, 166

Pryor, C. 1996, in Astronomical Society of the Pacific Conference Series, Vol. 92, Formation of the Galactic Halo...Inside and Out, ed. H. L. Morrison & A. Sarajedini, 424

Queloz, D., Dubath, P., & Pasquini, L. 1995, A&A, 300, 31

Raghavan, D., McAlister, H. A., Henry, T. J., et al. 2010, ApJS, 190, 1

Reid, I. N., & Gizis, J. E. 1997, AJ, 113, 2246

Robin, A. C., Reylé, C., Derrière, S., & Picaud, S. 2003, A&A, 409, 523

Schechter, P. L., Mateo, M., & Saha, A. 1993, PASP, 105, 1342

Searle, L., & Zinn, R. 1978, ApJ, 225, 357

- Seitzer, P., & Frogel, J. A. 1985, *AJ*, 90, 1796
- Simon, J. D., & Geha, M. 2007, *ApJ*, 670, 313
- Simon, J. D., Geha, M., Minor, Q. E., et al. 2011, *ApJ*, 733, 46
- Simon, J. D., Drlica-Wagner, A., Li, T. S., et al. 2015, *ApJ*, 808, 95
- Spencer, M., Loebman, S., & Yoachim, P. 2014, *ApJ*, 788, 146
- Spencer, M. E., Mateo, M., Walker, M. G., & Olszewski, E. W. 2017a, *ApJ*, 836, 202
- Spencer, M. E., Mateo, M., Walker, M. G., et al. 2017b, *AJ*, 153, 254
- Strader, J., Caldwell, N., & Seth, A. C. 2011, *AJ*, 142, 8
- Strigari, L. E., Bullock, J. S., Kaplinghat, M., et al. 2008, *Nature*, 454, 1096
- Suntzeff, N. B., Aaronson, M., Olszewski, E. W., & Cook, K. H. 1986, *AJ*, 91, 1091
- Suntzeff, N. B., Mateo, M., Terndrup, D. M., et al. 1993, *ApJ*, 418, 208
- Szentgyorgyi, A. H., Cheimets, P., Eng, R., et al. 1998, in *SPIE Conference Series*, Vol. 3355, *Optical Astronomical Instrumentation*, ed. S. D’Odorico, 242–252
- Tolstoy, E., Hill, V., & Tosi, M. 2009, *ARA&A*, 47, 371
- Torrealba, G., Kuposov, S. E., Belokurov, V., & Irwin, M. 2016, *MNRAS*, 459, 2370
- Vogt, S. S., Mateo, M., Olszewski, E. W., & Keane, M. J. 1995, *AJ*, 109, 151
- Walker, M. G. 2007, PhD thesis, University of Michigan
- Walker, M. G., Mateo, M., & Olszewski, E. W. 2008, *ApJ*, 688, L75
- . 2009a, *AJ*, 137, 3100
- Walker, M. G., Mateo, M., Olszewski, E. W., et al. 2015a, *ApJ*, 808, 108

—. 2006, *AJ*, 131, 2114

—. 2009b, *ApJ*, 704, 1274

Walker, M. G., Olszewski, E. W., & Mateo, M. 2015b, *MNRAS*, 448, 2717

—. 2017, in prep.

Watkins, L. L., Evans, N. W., & An, J. H. 2010, *MNRAS*, 406, 264

Weisz, D. R., Dolphin, A. E., Skillman, E. D., et al. 2014, *ApJ*, 789, 147

Wilkinson, M. I., Kleyna, J. T., Evans, N. W., et al. 2004, *ApJ*, 611, L21

Williams, G. G., Olszewski, E., Lesser, M. P., & Burge, J. H. 2004, in *Proc. SPIE*, Vol. 5492, *Ground-based Instrumentation for Astronomy*, ed. A. F. M. Moorwood & M. Iye, 787–798

Willman, B., & Strader, J. 2012, *AJ*, 144, 76

Zaritsky, D., Olszewski, E. W., Schommer, R. A., Peterson, R. C., & Aaronson, M. 1989, *ApJ*, 345, 759